IMEKO JOINT CONFERENCE
TC8-TC11-TC24
PHILIPPINES 2026

“Leveraging INNOVATION for Future-Ready MEASUREMENTS for Industry, Health and Environment”

CONFERENCE PROCEEDINGS

IMEKO

DOST-ITDI
INDUSTRIAL TECHNOLOGY DEVELOPMENT INSTITUTE
OneDOST4U: Solutions & Opportunities for All

27th to 29th AUGUST 2026

ACACIA HOTEL MANILA, Alabang,
Muntinlupa City, Metro Manila, PHILIPPINES

IMEKO WORLD CONGRESS

PALACONGRESSI DI RIMINI, ITALY

30 AUGUST - 3 SEPTEMBER, 2027

IMEKO XXV World Congress will be held in **Rimini**, certainly among the most welcoming Italian places, from **30 August to 3 September 2027**.

We have lined up an exciting programme that will include industry-based workshops, distinguished plenary and keynote speakers, industry led concurrent sessions, applied research presentations and a plethora of networking opportunities. The congress aims to outline the new challenges that the metrology will face and for these reason the multi- and interdisciplinary meeting of all the scientific communities will be welcome.

Stay tuned and save the dates….see you in Rimini!





SAVE THE DATE



www.imeko2027.org



FOLLOW US

MESSAGE

MICHELA SEGA, PhD
Senior Researcher,
Istituto Nazionale di Ricerca Metrologica – INRiM (Italy)
CHAIRPERSON, IMEKO TC8



On behalf of the IMEKO TC8 “Traceability in Metrology”, it is my great pleasure and honor to welcome you to the 2026 IMEKO TC8, TC11 and TC24 Joint Conference, held in the beautiful city of Manila, Philippines, from 26th to 29th August 2026.

The conference represents a further step in the close collaboration among the three IMEKO Technical Committees, that share common transversal topics and interests. In a rapidly evolving landscape, this event serves as a premier platform to discuss cutting-edge trends, address pressing challenges, and spark new ideas and will provide networking opportunities. We have lined up an exciting program featuring outstanding keynote speakers and technical sessions to explore the latest developments in traceability, measurement standards and metrological infrastructure.

We would like to express our sincere appreciation to all the authors who submitted their work, and to the reviewers whose insights maintained the high standard of this event. A special thank to our local organizers and sponsors for making this conference a reality. Please take full advantage of the sessions, connect with old colleagues, meet new ones, and enjoy everything that Manila has to offer.

Have a wonderful and inspiring conference!

MESSAGE

ÁLVARO SILVA RIBEIRO, PhD
Head of Metrology Division and Quality Manager
National Laboratory for Civil Engineering (Portugal)
CHAIRPERSON, IMEKO TC11



On behalf of IMEKO Technical Committee 11 – Measurement in Testing, Inspection and Certification (TC11), it is my pleasure to welcome you to the IMEKO Joint Conference of TC8,TC11 and TC24, held in Manila, Philippines, in 2026.

This conference highlights the scientific and technical importance of IMEKO as a forum for advancing measurement science through international and interdisciplinary collaboration. The longstanding cooperation among TC8, TC11 and TC24, together with the valuable contributions of EUROLAB and other stakeholders, continues to strengthen the links between research, industry and conformity assessment. Holding this event in the Asia-Pacific region further reinforces IMEKO's global commitment to knowledge exchange and international cooperation. Testing, inspection and certification are essential for ensuring safety, quality and confidence in products and services. Reliable conformity assessment depends on accurate measurements, validated methods, advanced technologies and competent personnel, supporting laboratories, inspection bodies, certification organizations and industry while generating significant economic and societal benefits.

I sincerely hope that this conference will inspire stimulating discussions, foster new scientific collaborations, strengthen existing partnerships and provide valuable opportunities for networking among all participants. May the presentations, technical sessions and informal exchanges contribute to new ideas, future joint initiatives and lasting friendships. I would also like to express my sincere appreciation to the Local Organizing Committee, the sponsors, and all supporting organizations for their dedication, commitment, and invaluable contributions to the successful organization of this conference. I wish you all a productive, successful and enjoyable conference, a rewarding stay in Manila, and every success in your future scientific and professional endeavors.

Welcome to the IMEKO Joint Conference TC8, TC11 and TC24!

MESSAGE

TATJANA TOMIĆ, PhD
R&D Laboratory Senior Expert Coordinator,
INA Oil Industry (Croatia)
CHAIRPERSON, IMEKO TC24



On behalf of the IMEKO TC24 dedicate to Chemical Measurements, I welcome you to the IMEKO TC8, TC11 and TC24 Joint Conference, which is held from 26th to 29th August 2026, in Manila, Philippines.

IMEKO is an organization that promotes cooperation of the scientists in the different field of measurements. In TC24, we encourage connection of experts in the field of chemistry and chemical metrology as well as international exchange of expert's work, results, problems and solutions. Chemical metrology is a field that plays a crucial role in science, industry and everyday life. Without reliable chemical measurements, there is no scientific progress, no fair exchange of goods, no protection of health and the environment. Conference brings together experts from different areas and all participants have an opportunity to exchange knowledge, experiences but also their challenges – from the method development and validations, through the role of reference materials in chemical measurements, to the application of international standards and impact on everyday quality assurance issues.

This conference represents a continuation of the excellent cooperation between the three IMEKO technical committees but also it is a major step forward. We are honored to have colleagues from the Philippine scientific community in our committees; they represent a great contribution to metrology, and they are the driving force of this conference. I would like to thank the organizers for their hard work and sponsors for their support.

Also, I would like to thank the authors for their willingness to share papers, results and knowledge, to the reviewers who significantly contributed to the conference high quality and all the participants for interest and contribution.
I wish all participants successful work, enjoying new experiences and a pleasant stay in Manila.

MESSAGE

ADMER REY C. DABLIO, RCh, CCPQM
Supervising Science Research Specialist
DOST-Industrial Technology Development Institute
CHAIRPERSON, Local Organizing Committee



Warmest greetings to all delegates, distinguished guests, speakers, and participants!
Maligayang pagdating sa Pilipinas at malugod na pagtanggap sa inyong lahat!
*(*A warm welcome to the Philippines and a heartfelt welcome to you all!)

On behalf of the Local Organizing Committee and the Department of Science and Technology – Industrial Technology Development Institute (DOST-ITDI), it is my absolute privilege to welcome you to Metro Manila for the 2026 IMEKO Joint Conference, bringing together TC8 (Traceability in Metrology), TC11 (Measurement in Testing, Inspection and Certification), and TC24 (Chemical Measurements).

This gathering unites key pillars of the global measurement infrastructure. Over the next three (3) days, we will address emerging challenges and opportunities—from digital traceability and certified reference materials to quality management, chemical sensing, and environmental sustainability. Beyond the technical exchange, we invite you to experience the rich heritage and genuine warmth of Filipino hospitality. Our sincere thanks go to the IMEKO leadership, TC officers, partners, and sponsors whose dedication made this event possible.

Nawa'y maging makabuluhan at matagumpay ang ating pagsasama-sama para sa ikauunlad ng agham at teknolohiya.
(May our gathering be meaningful and successful for the advancement of science and technology.)

Maraming salamat at mabuhay! (Thank you very much and welcome!)

ANNABELLE V. BRIONES, PhD, CESO III
Director IV / Scientist I
DOST-Industrial Technology Development Institute
Head of Host Member Organization



MESSAGE

To our distinguished guests, renowned keynote and plenary speakers, local and international delegates, and colleagues in the scientific community,

On behalf of the Industrial Technology Development Institute of the Department of Science and Technology (DOST-ITDI), it is my distinct honor and great pleasure to welcome all of you to the IMEKO TC8-TC11-TC24 Joint Conference 2026.

To our international participants who have traveled from around the world, a warm welcome to the beautiful shores of the Philippines! We are excited to host you not only amid our rich cultural heritage and legendary hospitality but also in a thriving environment of scientific discovery and forward-thinking collaboration.

This joint conference marks a significant, historic milestone for our country. By bringing together the world's leading experts in measurement science, this event strongly positions the Philippines within the global scientific community. It highlights our nation's rapidly growing capabilities and unwavering dedication to precise measurements, scientific metrology, and advanced analytical testing—disciplines that form the unseen foundation of international trade, industrial quality, safety, and sustainable technological progress.

This gathering holds a deeply meaningful connection for us at DOST-ITDI. As an institute, our main goal is to conduct multidisciplinary research and development, provide specialized technical services, and oversee the country's national metrology infrastructure to promote industrial growth and economic advancement. Every aspect of this conference—from traceability in testing to environmental and food analysis—directly reflects our mission to establish the fundamental measurement systems that help local industries stay competitive and scientifically reliable.

As you browse through this Program Book, you will find an agenda carefully designed to challenge assumptions, inspire innovative discussion, and promote international collaborations. I encourage each of you to actively participate, share groundbreaking ideas, and create networks that will go beyond geographic boundaries long after our stay in Manila ends.

Thank you for sharing your expertise and passion at this historic event. I hope you all have a deeply fulfilling, productive, and inspiring conference.

Mabuhay and welcome to the Philippines!

IMEKO TC Chairpersons

MICHELA SEGA, PhD
Instituto Nazionale di Ricerca Metrologica (INRiM), Italy
IMEKO TC8

ÁLVARO SILVA RIBEIRO, PhD
National Laboratory for Civil Engineering, Portugal
IMEKO TC11

TATJANA TOMIC, PhD
INA Industrija nafte d.d., Croatia
IMEKO TC24

IMEKO TC Officers
(involved in the preparation of the conference)

IMEKO TC8
SERGIO OLIVEIRA
THOMAS WIEDENHOEFER

IMEKO TC11
MARIJA ČUNDEVA-BLAJER
MLADEN JAKOVČIĆ
ADMER REY C. DABLIO

IMEKO TC24
LEONARDO IANNUCCI

LOCAL ORGANIZING COMMITTEE

OVER-ALL COORDINATION
Over-all Chairperson: ANNABELLE V. BRIONES, PhD
Chairperson: ADMER REY C. DABLIO
Co-Chairpersons: MA. RACHEL V. PARCON
MICHAEL JASON A. SOLIS

WELCOME RECEPTION
ADMER REY C. DABLIO (Head)
CYRIL C. RAMIL
PERSIA ADA N. DE YRO

PROGRAM
ADMER REY C. DABLIO (Head)
BIANCA J. BARING
MA. RACHEL V. PARCON

REGISTRATION (On-site)
CYRIL C. RAMIL (Head)
MARLON S.A. AGUINALDO
HAROLD E. ARMARIO
AGNES P. DE ASIS
JHON RUIZ C. NUEVA
MARIANNE D. POMARIN
ANNA MARIE A. UMALI

LOGISTICS
JAN-ERVIN C. GUERRERO (Head)
KENNETH EDWARD EUGENIO D. PEDRES

CONFERENCE PROGRAM BOOK, BAG, KIT, AND SOUVENIRS
JOHANNA ANDREA V. VALDUEZA (Head)
HAROLD E. ARMARIO

FOOD
RUTH L. DAMIAN (Head)
GRACE V. AMANDY
JOHANNA ANDREA C. VALDUEZA

WAYS AND MEANS
PERSIA ADA N. DE YRO (Head)
ADMER REY C. DABLIO
RAY NOEL DELDA
MICHAEL S. LAGMAY
HAROLD E. ARMARIO

AWARDS AND TOKENS
GRACE V. AMANDY (Head)
HAROLD E. ARMARIO

SESSION MODERATION
ADMER REY C. DABLIO (Head)
LEAH C. DAJAY
CHRISTY S. DANIEL
ERISH T. DARANCIANG
PERSIA ADA N. DE YRO
ALLENI T. JUNSAY
MA. RACHEL V. PARCON
MARYNESS I. SALAZAR
MICHAEL JASON A. SOLIS

DOCUMENTATION
CHRISTY S. DANIEL (Head)
JHON RUIZ C. NUEVA
MARIANNE D. POMARIN
ANNA MARIE A. UMALI

CONFERENCE WEBSITE
ADMER REY C. DABLIO (Head)
JEFREY G. PAGUINTO

INFORMATION TECHNOLOGY
ADMER REY C. DABLIO (Head)
ELLIARD ROSWELL S. YANZA

INTERNATIONAL PROGRAM COMMITTEE

IMEKO TC8
Traceability in Metrology

- Sergio Oliveira, Brazil
  Chairperson
- Giovanni Battista Rossi, Italy
- Marco Di Luzio, Italy
- Oleksandr Samoilenko, Ukraine
- Michela Sega, Italy
- Thomas Wiedenhoefer, Germany
- Antoaneta Yovcheva, Bulgaria
- Zoltan Zelenka, Hungary

IMEKO TC11
Measurement in Testing, Inspection and Certification (TIC)

- Marija Čundeva-Blajer, North Macedonia
  Chairperson
- Gorana Baršić, Croatia
- Agne Bertasiene, Lithuania
- Rola Bou Khozam, Lebanon
- Rama Dasu Pittala, India
- Kiril Demerdziev, North Macedonia
- Maria do Ceu Lopes de Sousa Ferreira, Portugal
- Mladen Jakovčić, Croatia
- Ivana Ljevaković-Musladin, Croatia
- Gertrud Mamiya, Rwanda
- Kruno Milicevic, Croatia
- Jose Luis Prieto Calviño, Spain
- Admer Rey C. Dablio, Philippines
- Paolo Emilio Roccato, Italy
- Annette Röttger, Germany
- Alvaro Silva Ribeiro, Portugal
- Vedran Šimunovic, Croatia
- Bodan Velkovski, North Macedonia
- Honglei Yang, China

IMEKO TC24
Chemical Measurements

- Leonardo Iannucci, Italy
  Chairperson
- Aleksandra Aleksić, Serbia
- Emma Angelini, Italy
- Sandra Babić, Croatia
- Admer Rey C. Dablio, Philippines
- Florbela Dias, Portugal
- Francesca Durbiano, Italy
- Erinc Engin, UK
- Leila Es Sebar, Italy
- Sabrina Grassini, Italy
- Pavel Gurikov, Germany
- Alleni T. Junsay, Philippines
- Boryana Koleva, Bulgaria
- Luca Lombardo, Italy
- Jaroslav Otta, Estonia
- Zhechao Qu, Germany
- Valnei Smarcaro da Cunha, Brazil
- Christabel Tan, United Kingdom
- Tatjana Tomić, Croatia

This page is intentionally left blank.

2026 IMEKO Joint Conference
TC8 - TC11 - TC24
Metro Manila, Philippines, August 26-29, 2026

Audit-Ready and Explainable Machine Learning for Chemical Measurements: A Case Study on Ceramic Oxide Profiles

David Jaucian Alcarde Jr.[1]

[1]*Packaging Technology Division, Industrial Technolgy Development Institute, Department of Science and Technology (DOST-ITDI), Bicutan, Taguig, Metro Manila, Philippines 1631*

Corresponding email: da6914@rit.edu

***Abstract* – Interpretation of high-dimensional chemical composition measurements remains a challenge in materials characterization and conformity assessment. This study presents an audit-ready and explainable machine learning workflow for classifying ceramic body and glaze samples based on multivariate oxide composition data from the UCI Machine Learning Repository (n = 88; 17 variables). Interpretable linear and nonlinear models achieved perfect classification performance under stratified cross-validation (accuracy and ROC-AUC = 1.00). Robustness analysis using Monte Carlo perturbation demonstrated invariant classification stability (100%) under realistic analytical variability up to ±5%. Feature importance analysis identified chemically meaningful drivers, including Al_2O_3, CaO, and SrO. The results show that explainable machine learning can provide a transparent and reproducible framework for interpreting chemical measurements, supporting reliable decision-making in chemical metrology and testing applications.**

I. INTRODUCTION

Chemical composition measurements are fundamental to materials characterization, quality control, and conformity assessment across a wide range of industrial and laboratory applications. In ceramic systems, multivariate oxide composition data are routinely used to distinguish between functional components such as bodies and glazes, which differ in structural role, processing conditions, and chemical formulation [1], [2]. However, interpretation of such high-dimensional chemical measurement data remains analytically demanding, often relying on expert knowledge and heuristic reasoning [3], [4]. This introduces variability in decision-making and limits reproducibility, particularly in contexts requiring traceable and auditable analytical outcomes [5], [6].

Recent advances in machine learning (ML) have enabled data-driven approaches for interpreting complex measurement datasets, offering the ability to uncover latent patterns and improve classification accuracy [7]–[10]. In chemical measurement domains, ML has been applied to tasks such as compositional analysis, process monitoring, and anomaly detection [11]–[13]. Despite these advances, the integration of ML into measurement science and testing, inspection, and certification (TIC) workflows remains limited by concerns regarding transparency, robustness, and traceability [14]–[16]. Black-box models, in particular, pose challenges for auditability and regulatory acceptance, where decisions must be explainable and defensible [17].

Within the framework of modern metrology, there is increasing emphasis on digitalization and traceability in data-driven systems, including the role of artificial intelligence in supporting measurement interpretation [18]. In this context, traceability extends beyond calibration chains to include reproducibility of data processing pipelines, transparency of decision logic, and robustness to measurement variability. For chemical measurements, where analytical uncertainty and sampling effects are inherent, it is essential that ML-based approaches demonstrate not only predictive performance but also stability under plausible perturbations and alignment with known physicochemical behavior [19], [20].

This study addresses these challenges by developing an audit-ready and explainable ML workflow for the interpretation of ceramic oxide composition measurements. Using a publicly available dataset from the UCI Machine Learning Repository, the work evaluates the capability of both interpretable linear models and nonlinear ensemble methods to classify ceramic body and glaze samples based on measured oxide components [21]. Emphasis is placed on three key aspects: (i) validated classification performance under cross-validation, (ii) robustness of decisions under simulated analytical variability using Monte Carlo perturbation, and (iii) chemical interpretability of model outputs through feature importance analysis. By integrating performance validation, robustness assessment, and explainability within a reproducible digital pipeline, the study demonstrates how ML can function as a traceable and

audit-ready interpretation layer for chemical measurement data. The findings contribute to the emerging field of AI-driven chemical metrology, supporting the use of digital analytical tools for reliable, transparent, and defensible decision-making in testing and inspection environments.

.

II. MATERIALS AND METHODS

A. Dataset and Chemical Measurement Variables

The study utilized a publicly available dataset obtained from the UCI Machine Learning Repository, comprising 88 ceramic samples categorized as ceramic body (n = 44) and glaze (n = 44). The key characteristics of the dataset and chemical measurement variables are summarized in Table 1.

Table 1. Dataset description and chemical measurement variables used for classification of ceramic body and glaze samples.

Parameter	Description
Data source	UCI Machine Learning Repository
Total samples	88
Class labels	Ceramic Body (n = 44); Glaze (n = 44)
Class balance	Balanced dataset (50% per class)
Measurement type	Oxide composition (multivariate chemical measurements)
Number of features	17 oxide variables
Oxide components	Na_2O, MgO, Al_2O_3, SiO_2, K_2O, CaO, TiO_2, Fe_2O_3, MnO, CuO, ZnO, PbO_2, Rb_2O, SrO, Y_2O_3, ZrO_2, P_2O_5
Feature representation	Continuous numerical values (composition data)
Target variable	Binary classification (Body = 0; Glaze = 1)
Preprocessing	No feature engineering; all variables retained
Data splitting	Stratified 5-fold cross-validation
Analytical context	Composition-based differentiation of ceramic components

As shown in Table 1, each sample was described by seventeen oxide composition variables representing measured chemical constituents, including Na_2O, MgO, Al_2O_3, SiO_2, K_2O, CaO, TiO_2, Fe_2O_3, MnO, CuO, ZnO, PbO_2, Rb_2O, SrO, Y_2O_3, ZrO_2, and P_2O_5. Sample identifiers were retained for traceability but excluded from model training. The oxide composition vectors were treated as multivariate chemical measurement results forming the input space for data-driven classification. No additional feature engineering was applied, and all variables were used in their original form to preserve the integrity of the measurement data.

B. Machine Learning Framework for Measurement Interpretation

A tiered machine learning framework was implemented to balance interpretability and predictive capability. A logistic regression classifier was employed as an interpretable linear baseline, while a random forest classifier was used to capture nonlinear relationships among oxide variables. Model performance was evaluated using stratified five-fold cross-validation to ensure balanced representation of body and glaze classes in each fold. Classification accuracy and receiver operating characteristic area under the curve (ROC-AUC) were used as performance metrics. All modeling steps were conducted within a reproducible computational workflow to ensure transparency and repeatability of results. Data processing, model development, Monte Carlo simulations, and visualization procedures were implemented in Python 3.11 using the Google Colaboratory (Colab) environment. Major libraries included pandas, NumPy, scikit-learn, and Matplotlib.

C. Monte Carlo Perturbation for Robustness Assessment

To evaluate the stability of classification decisions under plausible analytical variability, Monte Carlo perturbation was applied to the oxide composition measurements. For each simulation, relative Gaussian noise was introduced independently to each oxide variable, scaled proportionally to its measured value. Noise levels ranging from 0% to ±5% were applied to represent typical ranges of variability in compositional measurements. For each perturbation level, multiple simulated datasets were generated and classified using the trained model. Classification stability was quantified as the proportion of samples retaining their original class assignment across all simulations. Additional simulations with higher perturbation levels (up to ±50%) were conducted to explore the breakdown behavior of the classification model under extreme variability conditions. This approach provides a robustness assessment of ML-based decisions without requiring explicit measurement uncertainty budgets, focusing instead on sensitivity to plausible perturbations in chemical measurements.

D. Explainability Analysis

Explainability of the classification model was assessed using feature importance derived from the random forest algorithm. Importance scores were computed based on the contribution of each oxide variable to the reduction of classification impurity across decision trees. The resulting importance values were normalized

and ranked to identify dominant chemical drivers of classification. This analysis enables interpretation of ML decisions in terms of underlying chemical composition, facilitating alignment with known material behavior and supporting the transparency of the analytical workflow.

E. Reproducibility and Auditability

All data processing, model training, and evaluation procedures were implemented within a reproducible digital pipeline using fixed random seeds and documented computational steps. The use of a publicly accessible dataset, combined with transparent modeling procedures and robustness testing, supports auditability of the analytical workflow. While the dataset does not include calibration traceability or explicit measurement uncertainty information, the methodology emphasizes traceability of the data-processing and decision-making pipeline, consistent with emerging practices in digital metrology and AI-assisted measurement interpretation. This ensures transparency and reproducibility of the analytical workflow in alignment with digital metrology practices. Taken together, the methodological steps described above are consolidated in the workflow diagram shown in Figure 1.

The complete workflow of the audit-ready machine learning pipeline, integrating data preprocessing, model training, validation, robustness assessment, and explainability analysis, is summarized in Figure 1. This structured workflow supports transparent and reproducible interpretation of multivariate chemical measurement data.

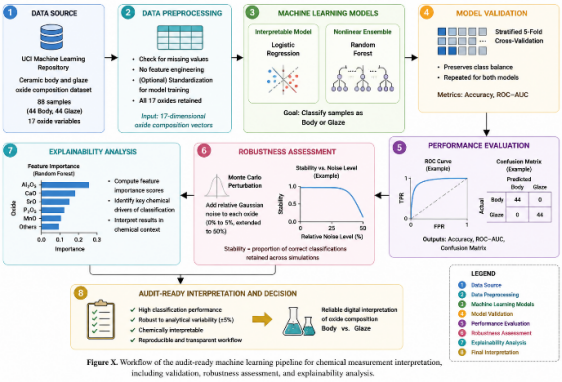


Figure 1. Workflow of the audit-ready machine learning pipeline for chemical measurement interpretation, including data preprocessing, model training, validation, robustness assessment, and explainability analysis.

III. RESULTS AND DISCUSSIONS

A. Classification Performance of Chemical Measurement Data

Machine learning models were applied to multivariate oxide composition measurements to classify ceramic samples as body or glaze. The performance of both the interpretable linear model (logistic regression) and the nonlinear ensemble model (random forest) is summarized in Table 2.

Table 2. Cross-validated classification performance metrics (mean ± standard deviation) using stratified five-fold cross-validation.

	Model	Accuracy	ROC-AUC
0	Logistic Regression	1.00 ± 0.00	1.00 ± 0.00
1	Random Forest	1.00 ± 0.00	1.00 ± 0.00

As can be seen in Table 2, both models achieved error-free classification performance, with accuracy and ROC-AUC values of 1.00 across all validation folds. This indicates complete separability between the two classes under the evaluated conditions. To further visualize classification performance, the receiver operating characteristic (ROC) curve is shown in Figure 2.

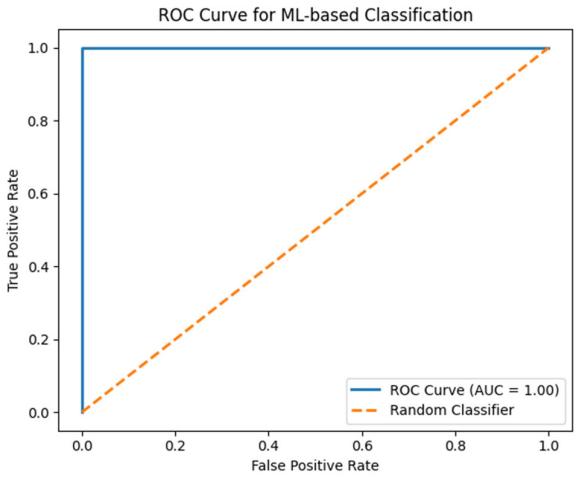


Figure 2. Receiver operating characteristic (ROC) curve for ML-based classification of ceramic body and glaze samples. The dashed diagonal line represents the performance of a random classifier, while the solid curve represents the classification model (AUC = 1.00).

The ROC curve demonstrates perfect discrimination between body and glaze samples, confirming the robustness of classification performance. The agreement between linear and nonlinear models suggests that the separability is inherent to the chemical measurement data rather than dependent on model complexity.

B. Multivariate Structure of Oxide Composition Data

To examine the structure of the oxide composition measurements, principal component analysis

(PCA) was performed. The resulting projection is presented in Figure 3.

.

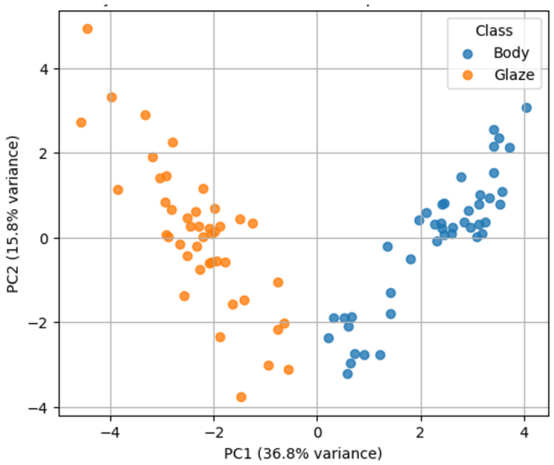


Figure 3. PCA projection of oxide composition measurements showing body–glaze separability

Figure 3 shows a clear separation between body and glaze samples is observed in the principal component space, indicating that the dominant sources of variance correspond to class distinctions. This result supports the classification findings and confirms that the dataset exhibits intrinsic multivariate structure suitable for data-driven interpretation.

C. Robustness to Simulated Analytical Variability

The robustness of classification decisions was evaluated using Monte Carlo perturbation to simulate analytical variability in oxide measurements. The stability results for perturbation levels up to ±5% are summarized in Table 3.

Table 3. Monte Carlo robustness results across perturbation levels

Relative Noise (±%)	Classification Stability
0.0%	1.000000
0.5%	1.000000
1.0%	1.000000
2.0%	1.000000
5.0%	1.000000
10.0%	1.000000
20.0%	0.999356
30.0%	0.995152
40.0%	0.985076
50.0%	0.970379

Table 3 shows that the Classification stability remained at 100% across all perturbation levels up to ±5%, indicating that no class reversals occurred under realistic measurement variability conditions. The robustness behavior across extended perturbation levels is further illustrated in Figure 4.

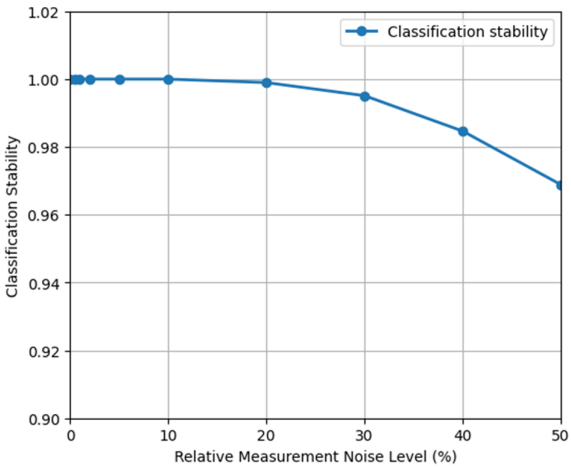


Figure 4. Monte Carlo robustness curve showing classification stability versus noise level

The stability curve in Figure 4 shows that classification performance remains invariant within realistic variability ranges and begins to degrade only under extreme perturbations exceeding typical analytical conditions. Stability remains above 0.99 up to approximately ±10% noise and decreases to 0.968 at ±50% perturbation, indicating a gradual breakdown of classification reliability. These results demonstrate that the ML-based decision boundary is well separated from class overlap regions and is therefore robust to plausible measurement fluctuations.

D. Explainability and Chemical Interpretation

To interpret the classification results, feature importance analysis was conducted using the random forest model. The ranked importance values are summarized in Table 4.

Table 4. Ranked oxide feature importance values derived from the random forest model for classification of ceramic body and glaze samples.

Rank	**Oxide**	**Importance Score**
1	Al_2O_3	0.2469
2	SrO	0.2156
3	CaO	0.2151
4	P_2O_5	0.1503
5	MnO	0.0763
6	Rb_2O	0.0306
7	ZrO_2	0.0198
8	Fe_2O_3	0.0151
9	Y_2O_3	0.0141
10	Na_2O	0.0056
11	MgO	0.0036

12	TiO_2	0.0026
13	SiO_2	0.0015
14	K_2O	0.0013
15	ZnO	0.0007
16	PbO_2	0.0005

The most influential variables were identified in Table 4 as alumina (Al_2O_3; importance = 0.247), strontium oxide (SrO; 0.216), and calcium oxide (CaO; 0.215), followed by phosphorus pentoxide (P_2O_5; 0.150) and manganese oxide (MnO; 0.076). The distribution of feature importance values is further illustrated in Figure 5.

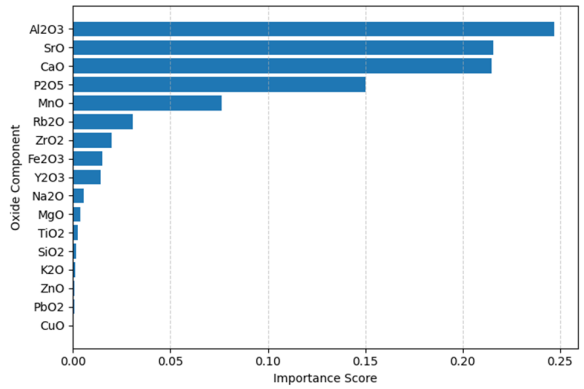


Figure 5. Explainability plot showing ranked oxide feature importance derived from the random forest model for classification of ceramic body and glaze samples.

The results shown in Figure 5 are consistent with established ceramic chemistry. Alumina is a primary structural component of ceramic bodies, while CaO and SrO act as fluxing agents in glaze formulations. Network modifiers such as P_2O_5 and MnO contribute to glass structure and surface properties. The alignment between ML-derived drivers and known compositional roles supports the chemical validity of the classification model.

E. Implications for Chemical Metrology and TIC Applications

The combined results demonstrate that explainable machine learning can transform multivariate chemical composition measurements into robust, transparent, and reproducible classification decisions. The integration of cross-validation, Monte Carlo robustness assessment, and explainability analysis provides a comprehensive evaluation framework aligned with modern requirements in chemical metrology. From a testing, inspection, and certification (TIC) perspective, the proposed workflow supports conformity assessment decision-making, where classification outcomes must be both accurate and defensible. The demonstrated robustness to analytical variability ensures reliability under realistic measurement conditions, while explainability enables interpretation in chemically meaningful terms.

Although the present study utilizes secondary data without explicit calibration traceability, the methodology is transferable to laboratory-generated datasets. Integration with certified reference materials and formal uncertainty evaluation frameworks could further enhance applicability in regulated environments.

IV. CONCLUSIONS

This study demonstrated that explainable machine learning can be used as a reliable and audit-ready interpretation layer for multivariate chemical composition measurements. Using a publicly available ceramic oxide dataset (n = 88; 17 variables), both interpretable linear and nonlinear ensemble models achieved error-free classification performance under stratified cross-validation (accuracy and ROC-AUC = 1.00), indicating complete separability between ceramic body and glaze compositions. Robustness analysis based on Monte Carlo perturbation showed that classification stability remained at 100% for perturbations up to ±5%, with gradual degradation only under unrealistically high variability (e.g., ~0.969 stability at ±50%). These results confirm that the learned decision boundary lies well within chemically separable regions of the measurement space and is insensitive to plausible analytical variability. Explainability analysis further identified chemically meaningful drivers—notably Al_2O_3, CaO, and SrO—consistent with established roles of structural oxides and fluxes in ceramic systems, supporting the physical credibility of the model.

Taken together, the integration of cross-validated performance, robustness assessment, and explainability within a reproducible pipeline provides a transparent and defensible framework for data-driven interpretation of chemical measurements. This aligns with emerging needs in chemical metrology and the TIC sector for digitalized workflows that support traceable, reproducible, and conformity-relevant decisions. While the present work is based on secondary data without explicit calibration traceability or uncertainty budgets, the methodology is directly transferable to laboratory-generated datasets. Future work may incorporate certified reference materials, uncertainty quantification, and interlaboratory validation to further strengthen metrological traceability. Overall, the proposed approach highlights the potential of AI-driven chemical measurements to enhance decision confidence in modern analytical practice.

REFERENCES

[1] L. Zhao and Y. Zhang, “Revealing the Individual Effects of Firing Temperature and Chemical Composition on Raman Parameters of Celadon Glaze,” *Ceramics*, vol. 6, no. 2. pp. 1263–1276,

2023. doi: 10.3390/ceramics6020077.

[2] S. Conte, C. Molinari, S. Javed, M. Dondi, and C. Zanelli, “Compositional diversity of vitrified silicate ceramics: Delimiting the chemical perimeter of industrial bodies,” *Ceram. Int.*, vol. 50, no. 22, Part B, pp. 46157–46165, 2024, doi: https://doi.org/10.1016/j.ceramint.2024.09.024.

[3] Y. E. Cho, S. Sim, J. Choi, and S. Ahn, “Explainable machine learning-based classification of traditional Korean ceramics using XRF chemical composition data,” *npj Herit. Sci.*, vol. 14, no. 1, p. 28, 2026, doi: 10.1038/s40494-026-02301-4.

[4] J. V Lisboa, F. Rocha, and D. P. S. de Oliveira, “Application of Multivariate Analysis in the Assessment of Ceramic Raw Materials,” *Clays Clay Miner.*, vol. 64, no. 6, pp. 767–787, 2016, doi: DOI: 10.1346/CCMN.2016.064040.

[5] I. G. Zenkevich, D. A. Nikitina, and A. S. Kushakova, “Processing and Interpretation of Analytical Data with a High Degree of Uncertainty,” *J. Anal. Chem.*, vol. 77, no. 11, pp. 1399–1412, 2022, doi: 10.1134/S1061934822090143.

[6] R. K. Cross *et al.*, “Reproducibility of methods required to identify and characterize nanoforms of substances,” *NanoImpact*, vol. 27, p. 100410, 2022, doi: https://doi.org/10.1016/j.impact.2022.100410.

[7] J. Crossa *et al.*, “Machine learning algorithms translate big data into predictive breeding accuracy,” *Trends Plant Sci.*, vol. 30, no. 2, pp. 167–184, 2025, doi: https://doi.org/10.1016/j.tplants.2024.09.011.

[8] L. Oneto *et al.*, “Informed machine learning for complex data,” *Neurocomputing*, vol. 669, p. 132505, 2026, doi: https://doi.org/10.1016/j.neucom.2025.132505.

[9] D. Sharma, “Artificial intelligence, machine learning and omic data integration in osteoarthritis,” *Osteoarthr. Cartil.*, vol. 34, no. 3, pp. 311–320, 2026, doi: https://doi.org/10.1016/j.joca.2025.10.012.

[10] J. K. Paul, M. Azmal, O. F. Talukder, A. N. M. S. N. B. Haque, M. Meem, and A. Ghosh, “Harnessing machine learning for improved diagnosis, drug discovery, and patient care,” *Comput. Struct. Biotechnol. Reports*, vol. 2, p. 100051, 2025, doi: https://doi.org/10.1016/j.csbr.2025.100051.

[11] M. Kanan and G. Latafat, “Modern Anomaly Detection Methods in Industry: A Comparative Analysis of Machine Learning Algorithms and Their Application to Improve the Efficiency of Manufacturing Processes,” *Prem. J. Sci.*, vol. 14, 2025, doi: https://doi.org/10.70389/PJS.100154.

[12] P. Özdemir and R. Yıldırım, “ML@ChemE: Past, Present, and Future of Machine Learning in Chemical Engineering,” *ChemBioEng Rev.*, vol. 12, no. 4, p. e70012, Aug. 2025, doi: https://doi.org/10.1002/cben.70012.

[13] O. R. Ojo, O. E. Elesho, A. Adeniyi, and O. J. Oluwadamilola, “Applying Machine Learning Models for Real-Time Process Monitoring and Anomaly Detection in Pharma Manufacturing,” *GSC Biol. Pharm. Sci.*, vol. 27, no. 1, pp. 315–341, 2024, doi: https://doi.org/10.30574/gscbps.2024.27.1.0153.

[14] V. Aschepkov, “METHODS OF MACHINE LEARNING IN MODERN METROLOGY,” *Meas. Equip. Metrol.*, 2024, [Online]. Available: https://api.semanticscholar.org/CorpusID:268593955

[15] M. Mora-Cantallops, S. Sánchez-Alonso, E. García-Barriocanal, and M.-A. Sicilia, “Traceability for Trustworthy AI: A Review of Models and Tools,” *Big Data and Cognitive Computing*, vol. 5, no. 2. p. 20, 2021. doi: 10.3390/bdcc5020020.

[16] N. Lorde, S. Mahapatra, and T. Kalaria, “Machine Learning for Patient-Based Real-Time Quality Control (PBRTQC), Analytical and Preanalytical Error Detection in Clinical Laboratory.,” *Diagnostics (Basel, Switzerland)*, vol. 14, no. 16, Aug. 2024, doi: 10.3390/diagnostics14161808.

[17] M. A. Camilleri, “Opening the black box: Operational principles, tools and frameworks that advance explainable artificial intelligence (XAI) models,” *Technol. Forecast. Soc. Change*, vol. 229, p. 124710, 2026, doi: https://doi.org/10.1016/j.techfore.2026.124710.

[18] R. Benyon Puig, J. G. Gallegos, I. Mohino Herranz, F. J. Pérez Sanz, and T. Vicente Mussons, “Digital transformation: Ensuring metrological traceability,” *Meas. Sensors*, vol. 38, p. 101801, 2025, doi: https://doi.org/10.1016/j.measen.2024.101801.

[19] B. C. Garain, M. J. Pinheiro, M. de O. Bispo, and M. Barbatti, “Uncertainty Calibration in Molecular Machine Learning: Comparing Evidential and Ensemble Approaches.,” *Chemistry*, vol. 32, no. 15, p. e03299, Apr. 2026, doi: 10.1002/chem.202503299.

[20] S. Seal *et al.*, “Machine Learning for Toxicity Prediction Using Chemical Structures: Pillars for Success in the Real World.,” *Chem. Res. Toxicol.*, vol. 38, no. 5, pp. 759–807, May 2025, doi: 10.1021/acs.chemrestox.5c00033.

[21] UCI Machine Learning Repository, “Chemical Composition of Ceramic Samples [Dataset].” 2019. doi: https://doi.org/10.24432/C54P5X.

2026 IMEKO Joint Conference
TC8 - TC11 - TC24
Metro Manila, Philippines, August 26-29, 2026

Elemental Fingerprinting of Reinforcing Steel Bars Using Portable EDXRF and Chemometric Analysis for Origin Discrimination

Mary Joy M. Bautista[1], Morris D. Pioquinto[2], George Catague[3] & Jo Marie Venus T. Agad[4]

[1]*Department of Science and Technology- Metals Industry Research and Development Center, Taguig City, 1631, Philippines, mmbautista@mirdc.dost.gov.ph*
[2]*Department of Science and Technology- Metals Industry Research and Development Center, Taguig City, 1631, Philippines, mdpioquinto@mirdc.dost.gov.ph*
[3]*QES Technology, Philippines, Inc., Muntinlupa City 1770, Philippines, george.catague@qesnet.com*
[4]*Department of Science and Technology- Metals Industry Research and Development Center, Taguig City, 1631, Philippines, jtagad@mirdc.dost.gov.ph*

Abstract. **Elemental fingerprinting provides a robust approach for determining the origin of reinforcing steel bars and strengthening quality control in construction materials through the evaluation of alloying and trace elements. In this study, Energy Dispersive X-ray Fluorescence (EDXRF) coupled with multivariate chemometric techniques was employed to characterize and discriminate locally manufactured and imported reinforcing steel bars.**

Unsupervised methods, including Principal Component Analysis (PCA) and Hierarchical Cluster Analysis (HCA), were used to explore data structure and assess compositional similarities. Significant differences in Cr, Cu, Mn, Mo, Ni, and Sn were identified as key discriminating variables. PCA showed clear separation between local and imported samples, while HCA confirmed consistent clustering patterns.

Supervised classification models, namely Linear Discriminant Analysis (LDA) and Decision Tree (DT), further validated the discrimination performance, achieving high and consistent classification accuracy under leave-one-out cross-validation. The Decision Tree identified Ni as the primary splitting variable, providing a simple and interpretable classification rule.

The agreement between unsupervised and supervised chemometric approaches confirms the reliability of EDXRF-derived elemental fingerprints for provenance identification. The proposed method offers a rapid, non-destructive, and effective tool for traceability, quality assurance, and regulatory monitoring of reinforcing steel bars in the construction industry.

Keywords: EDXRF, deformed steel bars, PCA, HCA, LDA, Decision Tree

I. INTRODUCTION

Reinforcing steel bars (rebars) are essential components in reinforced concrete structures, directly affecting the safety, durability, and mechanical performance of civil infrastructure. In rapidly developing countries such as the Philippines, the increasing demand for infrastructure has led to a mixed supply chain of locally produced and imported rebars. Although the Philippine National Standard (PNS 49:2020) sets requirements for chemical composition and mechanical properties, ensuring consistent compliance remains challenging, particularly for unmarked or undocumented imported materials that pose risks to structural integrity.

Traditional verification methods such as visual inspection, mechanical testing, and documentation review are insufficient for determining material provenance or detecting subtle compositional differences [1]. Energy Dispersive X-ray Fluorescence (EDXRF) offers a rapid, non-destructive, multi-elemental analysis technique suitable for metallic materials and has been widely validated for industrial applications [2]. When integrated with chemometric tools, EDXRF data enables robust pattern recognition and sample discrimination. In particular, Principal Component Analysis (PCA) and Hierarchical Cluster Analysis (HCA) are effective for reducing data dimensionality and identifying mm compositional groupings based on the elemental similarities [3], [4]. Previous studies have demonstrated the effectiveness of EDXRF combined with multivariate analysis for provenance determination in complex materials, including archaeological samples and other heterogeneous systems, where elemental fingerprints successfully distinguish compositional groups [5]. Similar approaches have been applied in elemental fingerprinting studies across fields such as archaeometry [6], and food authentication

highlighting their robustness in origin discrimination [7]. Elemental fingerprinting using trace elements has been widely applied in provenance studies, demonstrating strong capability in distinguishing material origins across various fields [6], [8]. However, its application to modern reinforcing steel bars for origin classification and regulatory traceability remains limited, particularly in developing countries with complex import systems.

In this study, an elemental fingerprinting approach integrating portable EDXRF with statistical and chemometric analyses is proposed to differentiate locally produced and imported reinforcing steel bars. Key alloying and trace elements (Cr, Cu, Mn, Mo, Ni, Pb, and Sn) were evaluated using descriptive statistics, PCA, HCA, Linear Discriminant Analysis (LDA), and Decision Tree classification [9]. The novelty of this work lies in the use of portable, non-destructive instrumentation combined with exploratory and supervised chemometric techniques for rapid origin discrimination and supply-chain traceability of reinforcing steel bars. The proposed methodology offers a practical tool for regulatory monitoring, quality assurance, and materials authentication within the steel industry.

II. METHODOLOGY

A. Sample description and collection

The samples analyzed in this study consisted of thirty (30) weldable deformed reinforcing steel bars obtained from various local suppliers and import sources in the Philippines. According to supplier documentation and inventory records submitted to the Metals Industry Research and Development Center – Department of Science and Technology (MIRDC–DOST), the samples represent both locally manufactured rebars and imported materials originating from countries such as Oman, Indonesia, Vietnam, Kuwait, and Russia.

The selected reinforcing steel bars (Figure 1) varied in diameter and grade but conformed to commercially available construction materials used in infrastructure projects. Each sample was assigned a unique identification code based on origin to facilitate traceability throughout the analysis.

B. EDXRF instrumentation and measurement

Elemental analysis was performed using a portable SciAps X-200 EDXRF analyzer equipped with a silicon drift detector (SDD) and Fundamental Parameters (FP) quantification algorithm. Prior to analysis, sample surfaces were ground and cleaned to remove corrosion products and contaminants. Five measurements were collected from different locations on each steel bar, and the average concentration was used for subsequent analysis.

C. Analytical quality assurance and validation



Fig 1. Cut-out samples of deformed steel bars from selected local and imported suppliers.

The analytical performance of the EDXRF spectrometer was assessed through calibration and validation using certified reference materials (CRMs) representative of carbon steel alloy compositions. The CRMs utilized in this study were obtained from accredited suppliers, namely Bureau of Analysed Samples, Ltd., Brammer Standards Co., Inc., and MBH Analytical Ltd., with traceability to National Institute of Standards and Technology (NIST) reference materials. Accuracy was assessed through recovery studies, while precision was evaluated using replicate measurements. Recovery (%), relative error (%), and relative standard deviation (RSD, %) were calculated using Equations (1)–(3).

$$\%Recovery = \frac{Measured\ Value}{Certified\ Value}\ x\ 100 \quad (1)$$

$$Relative\ Error\ = \frac{Measured\ Value - Certified}{Certified\ Value}\ x\ 100 \quad (2)$$

$$\%RSD = \frac{SD}{Mean}\ x\ 100 \quad (3)$$

D. Data processing and exploratory analysis

EDXRF elemental data were processed using Microsoft Excel and XLSTAT. Descriptive statistics were used to assess data consistency, while exploratory analysis examined compositional trends. Prior to multivariate analysis, Fe was excluded because of its dominant concentration and limited discriminatory power. The remaining variables (Cr, Cu, Mn, Mo, Ni, Pb and Sn) were mean-centered without variance scaling using the default XLSTAT preprocessing procedure. PCA was performed using the covariance matrix because all variables were measured in the same unit (wt.%). HCA was performed using Euclidean distance and Ward's minimum variance linkage. Instrument-reported values of 0.000 wt.% do not indicate concentrations below the analytical detection limit. Rather, they represent concentrations that were below the instrument's quantitative reporting resolution after Fundamental Parameters (FP) quantification and numerical rounding by the SciAps X-200 software. These values were therefore retained as reported by the instrument and treated

Table 1. Quality assurance results using CRMs of EDXRF analysis

CRMs	Element	Certified Value	Measured Value	SD	RSD (%)	% Recovery	Relative Error
401/1	Cr	0.055	0.055	0.005	8.27	100.18	0.18
454/1	Cr	0.062	0.057	0.003	4.68	91.61	-8.39
455/1	Cr	0.21	0.203	0.006	2.76	96.48	-3.52
455/1	Cu	0.038	0.042	0.005	10.82	109.47	9.47
454/1	Cu	0.051	0.050	0.004	7.90	98.63	-1.37
401/1	Cu	0.088	0.088	0.009	10.14	100.23	0.23
1264	Cu	0.249	0.246	0.012	4.70	98.67	-1.33
455/1	Mn	0.4	0.397	0.011	2.88	99.33	-0.68
454/1	Mn	0.8	0.784	0.013	1.68	97.96	-2.04
12X357	Mo	0.0122	0.013	0.001	10.36	105.19	5.19
451/1	Mo	0.039	0.040	0.003	6.52	102.31	2.31
401/1	Ni	0.031	0.030	0.003	10.89	96.77	-3.23
454/1	Ni	0.069	0.065	0.007	11.14	94.64	-5.36
455/1	Ni	0.35	0.355	0.011	3.09	101.40	1.40
12X12747	Ni	0.391	0.371	0.026	7.13	94.76	-5.24
1264	Pb	0.024	0.025	0.002	7.95	102.08	2.08

Table 2. Elemental composition in weight percent of Reinforcing Steel Bars using EDXRF

Test #	Lab Sample ID	Source	Size, Ø	%Cr	%Cu	%Fe	%Mn	%Mo	%Ni	%Pb	%Sn
1	PCL-2023-0552	Philippines	20 mm	0.130	0.156	99.022	0.592	0.013	0.081	0.026	0.029
2	PCL-2023-0553	Philippines	25 mm	0.220	0.195	98.858	0.629	0.012	0.079	0.025	0.028
3	PCL-2023-0554	Philippines	10 mm	0.142	0.209	98.534	0.913	0.011	0.127	0	0.039
4	PCL-2023-0555	Philippines	16 mm	0.168	0.191	98.284	1.260	0.012	0.079	0.023	0.036
5	PCL-2023-0556	Philippines	20 mm	0.167	0.206	98.316	1.212	0.009	0.088	0	0.009
6	PCL-2023-0557	Philippines	32 mm	0.252	0.205	98.126	1.304	0.012	0.080	0.024	0.035
7	PCL-2023-0558	Philippines	36 mm	0.170	0.188	98.300	1.236	0.010	0.079	0.025	0.013
8	PCL-2023-0559	Philippines	40 mm	0.253	0.152	98.222	1.254	0.014	0.075	0.028	0.037
9	PCL-2023-0560	Philippines	50 mm	0.157	0.234	98.272	1.180	0.013	0.121	0.025	0.016
10	PCL-2023-0563	Philippines	16 mm	0.114	0.155	98.804	0.836	0.012	0.080	0.017	0.038
11	PCL-2023-0564	Philippines	20 mm	0.142	0.209	98.574	0.911	0.012	0.122	0.028	0.038
12	PCL-2023-0565	Philippines	25 mm	0.116	0.169	98.764	0.880	0.010	0.063	0	0.042
13	PCL-2023-0566	Philippines	28 mm	0.109	0.272	98.692	0.827	0.013	0.090	0.015	0.041
14	PCL-2023-0567	Philippines	32 mm	0.080	0.137	98.818	0.874	0.011	0.071	0.014	0.034
15	PCL-2023-0568	Philippines	36 mm	0.127	0.172	98.752	0.856	0.013	0.082	0	0.033
16	PCL-2023-0573	Philippines	16 mm	0.143	0.161	98.450	0.907	0.007	0.065	0	0.038
17	PCL-2023-0574	Philippines	20 mm	0.152	0.174	98.700	0.875	0.011	0.079	0.017	0.034
18	PCL-2023-0575	Philippines	25 mm	0.191	0.171	98.314	0.898	0.011	0.074	0.017	0.032
19	PCL-2023-0577	Philippines	25 mm	0.251	0.201	98.158	1.262	0.028	0.091	0.018	0.040
20	PCL-2023-1108	Oman	10 mm	0	0.013	98.436	0.575	0	0	0	0
21	PCL-2023-1109	Oman	12 mm	0.348	0.107	98.902	0.520	0.009	0.002	0	0
22	PCL-2023-0341	Indonesia	16 mm	0.052	0.024	98.746	0.794	0	0.033	0	0.012
23	PCL-2023-0349	Vietnam	10 mm	0.037	0.038	98.708	0.814	0	0	0.021	0
24	PCL-2023-0348	Kuwait	50 mm	0.073	0.106	98.498	1.004	0.006	0.038	0.018	0
25	PCL-2023-0347	Russia	40 mm	0.025	0.018	98.744	0.798	0	0	0	0.012
26	PCL-2023-0346	Russia	36 mm	0.028	0.030	98.560	0.793	0	0	0.023	0
27	PCL-2023-0345	Indonesia	32 mm	0.073	0.023	98.744	0.809	0	0.031	0.020	0.014
28	PCL-2023-0344	Indonesia	28 mm	0.017	0.022	98.360	0.813	0	0	0.021	0.014
29	PCL-2023-0343	Russia	25 mm	0.033	0.027	98.784	0.769	0.002	0	0.021	0
30	PCL-2023-0342	Indonesia	20 mm	0.073	0.023	98.508	0.798	0	0.029	0.020	0.013

as valid observations during all statistical and chemometric analyses. No values were excluded or replaced by imputation.

Multivariate analysis was performed using PCA and HCA for dimensionality reduction and pattern recognition. PCA identified the main sources of variability, while HCA evaluated sample clustering. Supervised classification was performed using Linear Discriminant Analysis (LDA) and Decision Tree (DT) models with leave-one-out cross-validation (LOOCV). LDA was developed using Cr, Cu, Fe, Mn, Mo, Ni, Pb, and Sn with equal class priors. The Decision Tree employed the Gini impurity criterion and generated a single, unpruned split. During LOOCV, one sample was excluded at each iteration, the classification model was rebuilt using the remaining 29 samples, and the excluded sample was subsequently classified. This procedure was repeated until every sample had served once as the validation sample [9].

III. RESULTS AND DISCUSSION

A. EDXRF Performance and Elemental Composition

Prior to chemometric analysis, the analytical performance of the portable EDXRF instrument was evaluated using CRMs as seen on **Table 1.** Recoveries ranged from 91.61% to 109.47 %, while RSD values ranged from 1.68% to 11.14%, demonstrating acceptable accuracy and precision for alloying and trace element determination. Minor deviations observed for Cu and Ni at low concentration levels are consistent with the expected uncertainty of EDXRF measurements and do not affect the suitability of the method for elemental fingerprinting of reinforcing steel bars summarized in **Table 2.**

The statistical comparison of local and imported reinforcing steel bars presented in **Table 3** revealed significant differences ($p < 0.05$) for Cr, Cu, Mn, Mo, Ni, and Sn. Among these variables, Cu and Ni exhibited the largest compositional differences, suggesting their importance as elemental markers for origin discrimination. In contrast, Pb showed no statistically significant difference ($p > 0.05$). These findings indicate that the elemental dataset contains sufficient discriminatory information to support subsequent chemometric and classification analyses.

Table 3. Statistical Comparison of Local and Imported Reinforcing Steel Bars

Element	Local (n = 19) Mean ± SD (%)	Imported (n= 11) Mean ± SD (%)	p-value
Cr	0.163 ± 0.050	0.091 ± 0.118	0.0022
Cu	0.187 ± 0.032	0.047 ± 0.042	<0.00001
Fe	98.523± 0.270	98.619 ± 0.172	0.2342
Mn	0.985 ± 0.221	0.760 ± 0.128	0.0007
Mo	0.012 ± 0.004	0.003 ± 0.005	0.00013
Ni	0.086 ± 0.018	0.016 ± 0.021	<0.00001
Pb	0.017 ± 0.010	0.014 ± 0.010	0.5260
Sn	0.032 ± 0.009	0.007 ± 0.008	0.000025

Fe was excluded from PCA and HCA because it exhibited limited discriminatory power ($p = 0.2342$) and dominated the dataset due to its high abundance. However, it was retained in the supervised classification models to evaluate the predictive performance of the complete elemental dataset. Initial statistical inspection of the dataset (mean and standard deviation) revealed measurable variability across samples, particularly in trace elements such as Pb and Sn. Alloying elements (Cr, Mn, Ni, Mo, Cu) showed relatively controlled ranges, consistent with standard steelmaking practices. However, the presence of variability even within nominally similar grades suggests underlying differences in raw material sourcing and metallurgical processing routes. Such complexity is typical in XRF-derived multielement datasets, where direct interpretation is limited due to inter-element correlations and overlapping compositional domains. Recent studies emphasize that chemometric tools are essential for extracting meaningful patterns and enabling classification in such systems [9], [10].

B. Chemometric Analysis

PCA was employed to reduce dataset dimensionality and extract dominant compositional patterns. The first three principal components (F1, F2, F3) accounted for a cumulative variance of 84.092%, with F1 contributing 59.366% (**Table 4**) summarizes the PCA loadings, eigenvalues, explained variance, and cumulative variance of the first three principal components. This level of variance retention confirms that the PCA model sufficiently captures the underlying structure of the dataset, consistent with modern chemometric standards [8], [11].

Table 4. PCA factor loadings, eigenvalues, and explained variance of EDXRF-derived elemental variables.

	F1	F2	F3
Cr	0.728	-0.073	0.615
Cu	0.941	-0.110	-0.044
Mn	0.614	0.425	0.132
Mo	0.923	-0.065	0.110
Ni	0.912	-0.064	-0.253
Pb	0.223	0.899	-0.136
Sn	0.795	-0.235	-0.412
	F1	F2	F3
Eigenvalue	4.156	1.069	0.662
Variability (%)	59.366	15.270	9.457
Cumulative %	59.366	74.636	84.092

The two-dimensional PCA biplot (Figure 2), combining both sample scores and elemental loadings, reveals a clear

and well-defined separation into two distinct groups, demonstrating the effectiveness of PCA in discriminating reinforcing steel bars based on elemental composition. With the first two principal components (F1 = 59.37% and F2 = 15.27%) explaining a cumulative variance of 74.64%, the model adequately represents the dataset.

The separation was primarily driven by Cr, Cu, Mn, Mo, Ni, and Sn, which exhibited strong positive loadings and were identified as key elemental fingerprinting markers. In contrast, Pb contributed mainly to variability among imported samples. The observed clustering patterns confirm the suitability of portable EDXRF-derived elemental

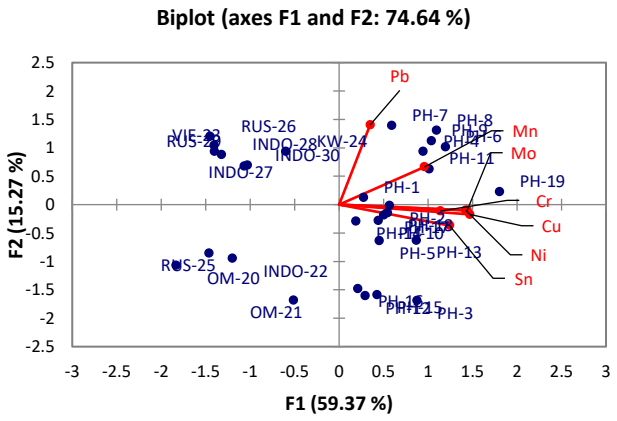


Fig. 2. Biplot obtained from 2D PCA with all the elements contributing to the separation of reinforcing steel bars.

fingerprints for origin discrimination. This suggests more controlled metallurgical practices and consistent alloying strategies in local production, forming a potential elemental fingerprint [6]-[9].

HCA was performed using Euclidean distance and Ward's linkage method to evaluate sample similarity. The dendrogram (Figure 3) produced two major clusters

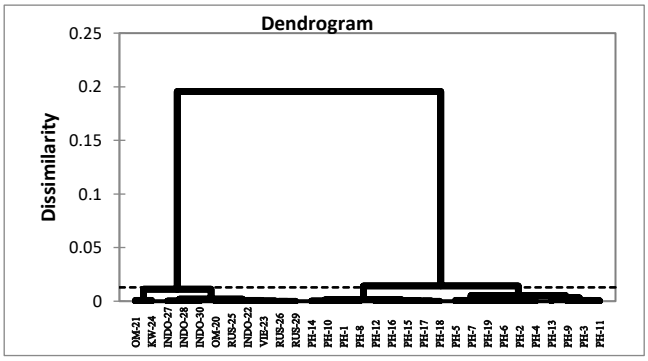


Fig. 3. Hierarchical cluster dendrogram of reinforcing steel bars generated using Euclidean distance and Ward's linkage method.

corresponding to local and imported reinforcing steel bars, consistent with the PCA results. Local samples exhibited shorter branch lengths, indicating greater compositional similarity, whereas imported samples showed broader dispersion, reflecting greater variability in raw materials and production processes. The agreement between PCA and HCA demonstrates consistent compositional discrimination between sample groups.

Table 5. Performance of supervised classification models for origin discrimination of reinforcing steel bars using EDXRF-derived elemental fingerprints.

Model	Accuracy (%)	Sensitivity (%)a	Specificity (%)b	Validation Method
Linear Discriminant Analysis (LDA)	100.0	100.00	100.00	LOOCV
Decision Tree (DT)	100.0	100.00	100.00	LOOCV

a Sensitivity = proportion of locally manufactured reinforcing steel bars correctly classified.
b Specificity = proportion of imported reinforcing steel bars correctly classified.

To further validate the discriminatory capability of the elemental fingerprints identified by PCA and HCA, supervised classification models were developed. The results presented in **Table 5** further confirmed that portable EDXRF-derived elemental fingerprints provide a reliable approach for discriminating the origin of reinforcing steel bars. As an alternative supervised classification method, Decision Tree analysis was emp loyed because of its simplicity and ease of interpretation.

Table 6. Summary of supervised classification models for origin discrimination of reinforcing steel bars

Method	Key Variables	Classification Rule / Function	Output
LDA	Cr, Cu, Fe, Mn, Mo, Ni, Pb, Sn	Linear discriminant function (LD1) derived from the elemental dataset	LOOCV accuracy = 100%
Decision Tree	Ni	IF–THEN rule	Ni ≤ 0.060 wt.% → Imported; Ni > 0.060 wt.% → Local; LOOCV accuracy = 100%

The concentrations of Cr, Cu, Fe, Mn, Mo, Ni, Pb, and Sn obtained from all samples (n = 30) as presented in **Table 6** were used to determine whether a reinforcing steel bar originated from local manufacturers or imported sources. The optimal Decision Tree consisted of a single terminal split based on Ni concentration, yielding an overall leave-one-out

cross-validation (LOOCV) accuracy of 100%. The model correctly classified all locally manufactured samples (19/19) and all imported samples (11/11). The resulting classification rule assigned samples with Ni concentrations ≤ 0.060 wt.% as imported and those with Ni concentrations > 0.060 wt.% as locally manufactured. The simplicity of this single-node decision rule, together with its high predictive performance, highlights the potential of Ni as a practical marker for reinforcing steel provenance determination.

IV. CONCLUSION

This study demonstrated the capability of portable EDXRF combined with chemometric techniques for the provenance determination of reinforcing steel bars. Significant differences in elemental composition were observed for Cr, Cu, Mn, Mo, Ni, and Sn, contributing to the discrimination between locally manufactured and imported reinforcing steel bars. Exploratory analyses using PCA and HCA revealed distinct clustering according to origin, indicating that elemental fingerprints can effectively discriminate between the two groups.

The robustness of these fingerprints was further confirmed through supervised classification. Both Linear Discriminant Analysis and Decision Tree models achieved an identical leave-one-out cross-validation accuracy of 100.00%, correctly classifying all locally manufactured and imported reinforcing steel bars. While LDA utilized the combined multivariate elemental information, the Decision Tree identified Ni as the most influential variable, yielding a simple classification rule in which samples with Ni concentrations ≤ 0.060 wt.% were classified as imported and those with higher concentrations as local.

The convergence of exploratory (PCA and HCA) and supervised (LDA and Decision Tree) chemometric approaches demonstrates that portable EDXRF-derived elemental fingerprints provide a rapid, non-destructive, and robust tool for reinforcing steel provenance determination, with potential applications in quality assurance, supply-chain traceability, and regulatory monitoring.

REFERENCES

[1] M.Bautista, M.Pioquinto, V.Agad, and G.Catalan, “Rapid Monitoring of Key Alloying Elements in Deformed Steel Bars Using Portable EDXRF and LIBS : A Strategy Against Substandard Quality,” in Joint conference of the TCs ‘Traceability in Metrology’ (IMEKO TC8, TC11, TC24), Torino, Italy, 2025, pp. 1–6. doi: 10.21014/tc24-2025.001.

[2] M.Gajic-Kvascev, V.Andric, R.Jancic-Heinemann, O. Mladenovic, and A. Bulatovic, “Comparison of Quantitative and Qualitative EDXRF Analysis for Provenance Study of Archaeological Ceramics,” Materials (Basel)., vol. 17, no. 15, 2024, doi: 10.3390/ma17153725.

[3] Z.Selivanovs, V.Panchuk, and D.Kirsanov, “On the Possibility of Universal Chemometric Calibration in X-ray Fluorescence Spectrometry: Case Study with Ore and Steel Samples,” Appl. Sci., vol. 13, no. 9, 2023, doi: 10.3390/app13095415.

[4] M.Bautista and F.Sevilla, “Compositional Analysis of Ancient Philippine Swivel Cannon Using Portable Energy Dispersive X-ray Fluorescence Spectrometry Coupled with Chemometric Analysis,” Philipp. J. Sci., vol. 154, no. 4, pp. 867–881, 2025, doi: 10.56899/154.04.07.

[5] E.Mohammed, A.Mitwally and B.Yu, “Geochemical studies and resource potential of magnetite in Taiwanese beach sands and related source rocks: Implications for geochemical fingerprinting of ore minerals,” Ore Geol. Rev., vol. 162, no. 1, p. 105649, 2023, doi: 10.1016/j.oregeorev.2023.105649.

[6] A.Maltsev, N.Umarova, G.Pashkova,M. Mukhamedova, D.Shergin, V.Panchuk, D. Kirsanov, and E.Demonterova “Combination of Total-Reflection X-Ray Fluorescence Method and Chemometric Techniques for Provenance Study of Archaeological Ceramics,” Molecules, vol. 28, no. 3, 2023, doi: 10.3390/molecules28031099.

[7] D.Galvan, J.Craveiro, L.Effting, CAparecida, F. Melquiades, E.Bona, C.Conte-Jinior, “Energy-dispersive X-ray fluorescence combined with chemometric tools applied to tomato and sweet pepper classification,” Food Control, vol. 143, no. July 2022, 2023, doi: 10.1016/j.foodcont.2022.109326.

[8] V.Andrić, M.Gajić-Kvaščev, D..Crkvenjakov, M. Marić-Stojanović, and S.Gadžurić, “Evaluation of pattern recognition techniques for the attribution of cultural heritage objects based on the qualitative XRF data,” Microchem. J., vol. 167, Aug. 2021, doi: 10.1016/j.microc.2021.106267.

[9] M.Grainger, H.Klaus, N.Hewitt, H.Gan, and A. French, “Graphical Discrimination of New Zealand Honey from International Honey Using Elemental Analysis,” Biol. Trace Elem. Res., vol. 202, no. 2, pp. 754–764, Feb. 2024, doi: 10.1007/s12011-023-03680-6.

[10] A.Ari and M.Budi, “Application of elemental fingerprinting for the authentication of tea : A review,” vol. 12, no. 03, pp. 45–54, 2022, doi: 10.7324/JAPS.2022.120305.

[11] F.Figueiredo, J.Carretas, J.Leal, and J.Sardinha, “Fast, accessible and reliable method for elemental analysis of metals in solution by ED-XRF spectroscopy,” J. Anal. Sci. Technol., vol. 15, no. 1, Dec. 2024, doi: 10.1186/s40543-024-00442-4.

2026 IMEKO Joint Conference
TC8 - TC11 - TC24
Metro Manila, Philippines, August 26-29, 2026

Chemometric Evaluation of Philippine FDA Migration Screening Parameters in Commercial Polyethylene Food Packaging using Aqueous Food Simulant

Winnie Alejandro[1], Elyson Keith Encarnacion[1], Anne Alcantara[1], Agaseve Del Rosario[1], David Alcarde[1], Rizel Marie Ting[1], Josefino Antonio Mendoza[1], Darylle Jerome Ortiz[1], Alliyah Gahle Enriquez[2], Maria Jelo Mantile[3]

[1] Industrial Technology Development Institute – Department of Science and Technology, General Santos Avenue, Bicutan, Taguig City, Philippines, winpalejandro@gmail.com

[2] Pamantasan ng Lungsod ng Maynila, General Luna Street, Intramuros, Manila, Philippines, alliyahgahleenriquez@gmail.com

[3] Adamson University, San Marcelino Street, Ermita, Manila, Philippines, maria.jelo.mantile@adamson.edu.ph

***Abstract* – This study investigated migration behavior in commercial polyethylene (PE) food packaging using the Philippine FDA migration screening parameters and chemometric analysis under aqueous simulant conditions and chemometric analysis under aqueous simulant conditions. Fourteen PE brands collected from retail markets in Metro Manila were evaluated for Total Residual Contaminants (TRC), Total Oxidizable Contaminants (TOCs), and Total UV-Absorbing Contaminants (TACs). Migration testing was performed using distilled water as the food simulant at 60 °C for 30 min. Statistical analyses included descriptive statistics, Shapiro–Wilk normality testing, inferential comparison against FDA screening limits, Spearman correlation, and Principal Component Analysis (PCA). All measured migration values were significantly below regulatory reference limits, indicating acceptable safety performance among tested samples. TACs showed non-normal distribution, while TRC and TOCs were normally distributed. Weak and non-significant correlations among parameters suggested that each indicator reflected different migration characteristics. PCA demonstrated that the first two principal components explained most dataset variability, enabling differentiation of migration patterns among polyethylene brands.**

I. INTRODUCTION

Chemical migration from packaging materials into food is a key safety issue in the evaluation of food contact materials [1], [2]. Packaging materials may contain residual monomers, additives, processing aids, stabilizers, oligomers, and degradation by-products that can transfer into food during storage or use [3], [4]. The extent of migration is influenced by factors such as polymer composition, food type, temperature, contact duration, and physicochemical interactions between packaging and food matrices [5], [6]. As a result, understanding the migration behavior of contaminants is critical in the safety evaluation and regulatory compliance of food contact materials.

Among food-contact materials made of polymers, polyethylene (PE) is widely used in flexible packaging applications [7] and is therefore frequently evaluated in migration studies [8], [9]. Although PE is generally regarded as chemically stable [10], migration may still occur due to incomplete polymerization, oxidative degradation, thermal processing, or the incorporation of additives during manufacturing [11].

Regulatory agencies commonly apply migration testing as a screening approach to assess food-contact safety [12], [13]. Rather than identifying individual compounds, screening methods quantify broad contamination indicators that collectively reflect extractable or reactive chemical species [14]. In the Philippines, the Food and Drug Administration (FDA) recommends voluntary testing of polyethylene food-contact materials using Total

Residual Contaminants (TRC), Total Oxidizable Contaminants (TOCs), and Total UV-Absorbing Contaminants (TACs). These parameters provide complementary information on migration behavior and support regulatory evaluation [12].

Despite their routine application, the statistical relationship among TRC, TOCs, and TACs remains insufficiently explored [15], [16], [17]. It is unclear whether these indicators represent overlapping contamination pathways or independent measurement domains. Understanding these relationships is important because correlated indicators may provide redundant information, whereas independent indicators may justify multi-parameter migration assessment [18].

Chemometric analysis offers an effective framework for interpreting migration datasets containing multiple analytical variables [19]. Statistical tools such as correlation analysis and Principal Component Analysis (PCA) allow evaluation of multidimensional relationships and contamination patterns [20], [21]. This study evaluates migration screening parameters among commercially available PE packaging materials using inferential statistics and chemometric tools to examine compliance, interrelationships, and multivariate behavior across commercial brands.

II. MATERIALS AND METHODS

A. Sample Collection

Different brands of polyethylene bags were purchased from various retail markets across Metro Manila. Samples were purposively selected to represent commercially available products from different retailers. For each acquired sample, retailer information were recorded to document the sampling location. Representitative samples were subject to Fourier-Transform Infrared Spectroscopy to verify polyethylene composition of each brand. Fourteen unique polyethylene brands were identified and assigned a coded identifier to maintain confidentiality of results. The samples were subsequently analyzed for TACs, TOCs and TRC.

B. Sample Extraction

Samples were prepared by cutting polyethylene films into 10 cm × 10 cm sections and gently wiping both surfaces with lint-free paper to minimize contamination. Two replicate samples were prepared for each brand. To facilitate extraction, the cut samples were placed in glass beakers containing 200 mL of distilled water as the aqueous simulant. Method reagent blanks consisting of distilled water without samples were prepared in parallel. Beakers were covered with aluminum foil and incubated at 60 °C for 30 min under controlled conditions. After extraction, the samples were removed using tweezers, and the migration extracts were retained for subsequent analysis.

C. Total Absorbing Contaminants Analysis

The extraction solutions were analyzed using a Shimadzu UV-1800 over a wavelength range of 220–360 nm using a 5 cm quartz cuvette. This analysis was conducted to evaluate UV-absorbing contaminants present in the migration extracts.

D. Total Residual Contaminants Analysis

A 50 mL aliquot of the extraction solution was transferred into a corresponding pre-weighed beaker and evaporated to dryness on a hot plate. The beakers containing the residue were then dried in a pre-heated oven at 105 °C for 2 h, cooled in a desiccator for 1 h, and weighed using Metler Toledo XSR 105 analytical balance. The drying, cooling, and weighing procedure was repeated by reheating the beakers at 105 °C for an additional 1 h, followed by desiccation and reweighing, until constant mass was obtained. Total residue was determined from the difference between the mass of the beaker containing residue and the pre-weighed beaker, multiplied by 1,000,000 and divided by the aliquot volume (50 mL), refer to equation 1. Precision was assessed using percent relative standard deviation (%RSD) calculated from replicate measurements.

$$TRC\ (mg/L) = \frac{(W_2 + W_1) \times 1{,}000{,}000}{50} \quad (1)$$

E. Total Oxidizable Contaminants Analysis

100 mL of the extraction solution was transferred into a cleaned Erlenmeyer flask, followed by the addition of 5 mL of (1→3) sulfuric acid and 5 mL of 0.002 mol/L potassium permanganate solution. The mixture was heated to boiling and maintained for 5 min. After heating, 10 mL of 0.005 mol/L sodium oxalate solution was added, and the solution was titrated with 0.002 mol/L potassium permanganate until a persistent slight pink color was obtained. The volume of potassium permanganate consumed was recorded. A blank determination was performed under identical conditions using distilled water instead of the extraction solution.

F. Statistical Analysis

Descriptive statistics were calculated for TRC, TOCs, and TACs to summarize migration behavior across polyethylene brands. Data normality was assessed using the Shapiro–Wilk test. One-sample t-tests were applied to normally distributed TRC and TOCs data to compare mean values against the FDA screening limit of 10 mg/L, while the Wilcoxon signed-rank test was used for TACs to compare the median value against the FDA screening limit of 0.300 AU at a significance level of $\alpha = 0.05$. Due to the non-normal distribution of TACs, Spearman correlation analysis was performed to evaluate relationships among migration parameters. PCA using standardized variables

was conducted to examine multivariate relationships and differentiate polyethylene brands based on migration characteristics. All statistical analyses were performed using appropriate statistical software at a 95% confidence level.

III. RESULTS AND DISCUSSION

A. Analysis Results and Descriptive Statistics

Each identified PE brand was subjected to analysis for TACs, TRC and TOCs. A summary of the results is presented in Table 1.

Table 1. Summarized Results of Tested PE Samples

Code	TACs (AU)	TRC (mg/L)	TOCs (mg/L)
PE-0001	0.010	4.40	0.02
PE-0002	0.012	6.60	0.03
PE-0003	0.006	3.60	0.76
PE-0004	0.007	0.70	0.52
PE-0005	0.010	3.90	0.69
PE-0006	0.010	3.40	0.12
PE-0007	0.027	7.40	0.45
PE-0008	0.006	7.60	0.20
PE-0010	0.005	3.80	0.13
PE-0011	0.006	5.50	0.16
PE-0012	0.006	4.50	0.31
PE-0013	0.006	4.80	0.22
PE-0014	0.005	7.80	0.22
PE-0015	0.017	9.70	0.87

Table 2 presents the descriptive statistics for TACs, TRC and TOCs across the tested PE samples. TACs are expressed in absorbance units (AU), while TRC and TOCs are reported in mg/L; therefore, direct comparison of their magnitudes is not appropriate.

For TACs, the mean value was 0.0095 AU, with a relatively small standard deviation (SD = 0.0061), indicating low absolute variability. However, the coefficient of variation (CV = 63.80%) suggests considerable relative variability among brands, implying differences in the presence of UV-absorbing compounds, potentially associated with additives such as stabilizers or degradation products.

In contrast, TRC showed a mean of 5.2643 mg/L and moderate variability (SD = 2.3303; CV = 44.27%). The range (0.700–9.700 mg/L) indicates noticeable variation among samples, although the lower CV suggests that TRC values are relatively more consistent compared to the other parameters. This may reflect similar baseline levels of extractable residual substances across PE materials.

TOCs exhibited the highest variability among the parameters, with a mean of 0.3357 mg/L, SD of 0.2769, and CV of 82.48%. The wide range (0.020–0.870 mg/L) indicates substantial heterogeneity in oxidizable contaminants, which may be influenced by differences in polymer composition, additive content, and processing conditions among brands.

Overall, the observed variability across all parameters highlights inter-brand differences in migration behavior. The combined evaluation of TACs, TRC, and TOCs provides a more comprehensive understanding of the types and extent of contaminants present in polyethylene packaging materials.

Table 2. Descriptive Statistics of Tested PE Samples

Variable	Mean	Median	SD	Variance	Min	Max	Range	CV percent
TACs	0.0095	0.0065	0.0061	3.6731e-05	0.005	0.027	0.022	63.7957
TRC	5.2643	4.6500	2.3303	5.430165e+00	0.700	9.700	9.000	44.2657
TOCs	0.3357	0.2200	0.2769	7.66733e-02	0.020	0.870	0.850	82.4803

B. Shapiro-Wilk Test for Normality

The Shapiro–Wilk test was conducted to evaluate the normality of TACs, TRC, and TOCs distributions. TRC values showed no significant deviation from normality (W = 0.962, p = 0.753), indicating an approximately normal distribution. Similarly, TOCs did not significantly deviate from normality (W = 0.892, p = 0.087), suggesting acceptable normality. In contrast, TACs significantly deviated from a normal distribution (W = 0.720, p = < 0.05), indicating non-normality. These findings suggest that parametric analyses may be appropriate for TRC and TOCs, whereas non-parametric methods are more suitable for TACs. This result is summarized in Table 3.

Table 3. Normality Test Result

Variable	W Statistic	p-value	Distribution
TACs	0.720	< 0.05	Non-normal
TRC	0.962	0.753	Normal
TOCs	0.892	0.087	Normal

C. Statistical comparison of TACs, TRC, and TOCs against each respective regulatory reference values.

Table 4 presents the statistical comparison of TACs,

TRC, and TOCs against their respective FDA screening limits. For the normally distributed TRC and TOCs datasets, one-sample t-tests showed that the mean values were significantly lower than the regulatory reference value of 10 mg/L. TRC exhibited a mean concentration of 5.264 mg/L ($t = -7.604$, $p < 0.001$), while TOCs showed a substantially lower mean of 0.336 mg/L ($t = -130.59$, $p < 0.001$). These results indicate that both migration parameters remained well below the screening threshold.

For TACs, which did not meet the assumption of normality, a Wilcoxon signed-rank test was performed. The pseudomedian TACs value of 0.0080 AU was significantly lower than the FDA reference value of 0.300 AU ($V = 0$, $p = 0.0005$). This result confirms that UV-absorbing contaminant levels were substantially below the regulatory limit.

Overall, all measured migration parameters were significantly lower than their corresponding FDA screening limits, indicating that the analyzed polyethylene samples complied with the established reference values for contaminant migration

Table 4. Statistical comparison of TACs, TRC, and TOCs against their respective regulatory reference values.

Variable	Test Used	Reference Value	Sample Estimate	Test Statistic	p-value
TACs	Wilcoxon Signed-Rank	0.300 AU	0.0080 AU (Pseudo) median		< 0.05
TRC	One-Sample t-test	10 mg/L	5.264 mg/L (Mean)	$t = -7.604$	< 0.05
TOCs	One-Sample t-test	10 mg/L	0.336 mg/L (Mean)	$t = -130.59$	< 0.05

D. Evaluation of relationships among migration parameters

Spearman correlation analysis results are summarized in Table 5. Weak and non-significant positive correlations were observed among all migration parameter pairs ($\rho = 0.062–0.122$, $p > 0.05$), indicating limited monotonic relationships among TACs, TRC, and TOCs.

Table 5. Spearman correlation analysis among TRC, TACs, and TOCs for polyethylene samples.

Variable Pair	Spearman's rho (ρ)	p-value
TACs vs TRC	0.122	0.678
TACs vs TOCs	0.119	0.686
TRC vs TOCs	0.062	0.834

The weak associations may be attributed to differences in polymer composition, additive formulation, thermal history, oxidation state, and manufacturing conditions among commercial polyethylene products. In addition, each migration parameter reflects different contaminant characteristics. TACs primarily represent UV-absorbing compounds such as antioxidants and degradation products [22], [23], TRC measures extractable non-volatile residues [24], while TOCs reflects oxidizable substances [25]. Because these parameters evaluate distinct chemical behaviors, increases in one parameter may not necessarily correspond to proportional increases in another.

The limited sample size, purposive sampling approach, and use of only aqueous simulant conditions may have also contributed to the observed variability [26]. Temperature is another important factor influencing contaminant migration from polymeric food-contact materials because elevated temperatures generally increase molecular mobility and diffusion rates within the polymer matrix, thereby enhancing the migration of extractable substances into food simulants [2], [5], [6]. In the present study, all polyethylene samples were evaluated under identical extraction conditions (60 °C for 30 min) using the analytical procedure adopted for the Philippine FDA-voluntary certification of food-contact articles. Consequently, temperature was intentionally maintained as a controlled experimental variable to ensure a consistent basis for comparing migration behavior among polyethylene samples. Accordingly, the influence of temperature could not be evaluated independently in the present study because it was deliberately held constant throughout all experiments. Therefore, the observed differences among samples are more likely attributable to material-related factors, including polymer composition, additive formulation, and manufacturing conditions, rather than differences in extraction temperature. Future studies should evaluate migration behavior under multiple temperature conditions, incorporate different food simulants, increase the sample size, and perform targeted identification of specific migrants to improve chemometric interpretation and broaden the applicability of migration assessment under realistic food-contact scenarios.

E. Principal Component Analysis (PCA)

PCA was performed to evaluate multivariate relationships among TACs, TRC, and TOCs and to assess variability among polyethylene brands. As summarized in

Table 6, the first two principal components explained 83.0% of the total dataset variability, indicating that migration behavior could be adequately interpreted within a two-dimensional multivariate space.

Table 6. PCA summary for TRC, TACs, and TOCs

Principal Component	Variance Explained (%)	Cumulative Variance (%)
PC1 (Dim1)	51.8	51.8
PC2 (Dim2)	31.2	83.0
Total (PC1 + PC2)	83.0	–

As shown in Figure 1, TACs and TRC vectors were oriented in a similar direction, suggesting partial association between these parameters, whereas the TOCs vector was positioned separately, indicating a more independent contribution to sample variability. These observations are consistent with the weak correlations obtained from Spearman analysis and suggest that each migration parameter reflects distinct aspects of contaminant migration behavior.

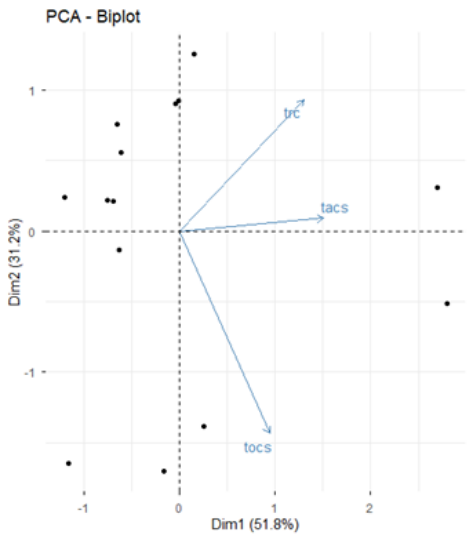


Figure 1. Principal Component Analysis (PCA) biplot

From a chemometric perspective, PCA was used to evaluate whether migration assessment could be simplified through dimensional reduction. However, the weak relationships among parameters indicate that substantial simplification may not yet be appropriate under the evaluated conditions. Although some overlap between TACs and TRC was observed, each parameter still contributed unique analytical information, supporting the continued use of multi-parameter migration assessment for polyethylene food packaging materials.

The partial overlap between TACs and TRC may be associated with migrated compounds such as antioxidants, stabilizers, oligomers, and degradation by-products that contribute both UV-absorbing and extractable residual characteristics. Nevertheless, these shared contributions were insufficient to establish strong redundancy among migration parameters across the evaluated commercial samples.

IV. CONCLUSION

In conclusion, commercially available polyethylene food packaging materials exhibited acceptable migration performance under aqueous simulant conditions based on the Philippine FDA migration screening parameters. Chemometric evaluation showed that TRC, TOCs, and TACs behaved largely independently, indicating that each parameter reflects different aspects of contaminant migration rather than redundant information. Although PCA reduced the dataset into two principal components explaining most of the variability, the weak correlations among parameters suggest that simplification of migration testing through parameter reduction may not yet be appropriate. The observed variability among brands highlights the influence of manufacturing-related factors such as additive composition, processing conditions, and polymer characteristics on migration behavior. Since all migration experiments were performed under identical extraction conditions, the effect of temperature was intentionally controlled and therefore could not be evaluated independently in the present study. Future studies should evaluate migration behavior under multiple temperature conditions, incorporate different food simulants, increase the sample size, and perform targeted identification of specific migrants to improve chemometric interpretation and provide a more comprehensive understanding of contaminant migration under realistic food-contact scenarios. Overall, the study supports the continued use of multi-parameter migration assessment and demonstrates the value of chemometric tools in evaluating food packaging safety.

REFERENCES

[1] Q. Zhang, Y. Huo, Q. Yang, F. Zhao, M. Li, and J. Ju, “Migration of chemical substances from packaging materials to food,” *Food Chem.*, vol. 485, p. 144544, Sep. 2025, doi: 10.1016/j.foodchem.2025.144544.

[2] R. K. Gupta *et al.*, “Migration of Chemical Compounds from Packaging Materials into Packaged Foods: Interaction, Mechanism, Assessment, and Regulations,” *Foods*, vol. 13, no. 19, p. 3125, Jan. 2024, doi: 10.3390/foods13193125.

[3] P. Khokhar and K. Pawar, “Chemical migration from packaging materials into consumable food matrices: A mini review,” *Int. J. Agric. Food Sci.*, vol. 7, no. 1, pp. 21–25, Jan. 2025, doi: 10.33545/2664844X.2025.v7.i1a.233.

[4] W. Meng, H. Sun, and G. Su, “Plastic packaging-associated chemicals and their hazards – An overview of reviews,” *Chemosphere*, vol. 331, p. 138795, Aug. 2023, doi: 10.1016/j.chemosphere.2023.138795.
[5] N. Seref and G. Cufaoglu, “Food Packaging and Chemical Migration: A Food Safety Perspective,” *J. Food Sci.*, vol. 90, no. 5, p. e70265, 2025, doi: 10.1111/1750-3841.70265.
[6] C. Muzeza, V. Ngole-Jeme, and T. A. M. Msagati, “The Mechanisms of Plastic Food-Packaging Monomers’ Migration into Food Matrix and the Implications on Human Health,” *Foods*, vol. 12, no. 18, p. 3364, Jan. 2023, doi: 10.3390/foods12183364.
[7] S. S. Ali *et al.*, “Degradation of conventional plastic wastes in the environment: A review on current status of knowledge and future perspectives of disposal,” *Sci. Total Environ.*, vol. 771, p. 144719, Jun. 2021, doi: 10.1016/j.scitotenv.2020.144719.
[8] S. Gerassimidou *et al.*, “Unpacking the complexity of the polyethylene food contact articles value chain: A chemicals perspective,” *J. Hazard. Mater.*, vol. 454, p. 131422, Jul. 2023, doi: 10.1016/j.jhazmat.2023.131422.
[9] R. M. Ting *et al.*, “Method validation and profiling of total UV-absorbing contaminants migrating from monolayered low-density polyethylene used for aqueous foods in the Philippines,” *Polyolefins J.*, no. Online First, Oct. 2025, doi: 10.22063/poj.2025.35740.1367.
[10] Z. Yao, H. J. Seong, and Y.-S. Jang, “Environmental toxicity and decomposition of polyethylene,” *Ecotoxicol. Environ. Saf.*, vol. 242, p. 113933, Sep. 2022, doi: 10.1016/j.ecoenv.2022.113933.
[11] R. Yang, “Chapter 7 - Polymer degradation and stability,” in *Polymer Science and Nanotechnology*, R. Narain, Ed., Elsevier, 2020, pp. 125–148. doi: 10.1016/B978-0-12-816806-6.00007-8.
[12] “FDA Circular No.2022-0011|| Guidelines on the Application and Issuance of Voluntary Certification of Food Contact Articles (FCA) Used for Prepackaged Processed Food Products - Food and Drug Administration.” Accessed: Apr. 29, 2026. [Online]. Available: https://www.fda.gov.ph/fda-circular-no-2022-0011-guidelines-on-the-application-and-issuance-of-voluntary-certification-of-food-contact-articles-fca-used-for-prepackaged-processed-food-products/
[13] H. F. Program, “Guidance for Industry: Preparation of Premarket Submissions for Food Contact Substances (Chemistry Recommendations).” Accessed: Apr. 29, 2026. [Online]. Available: https://www.fda.gov/regulatory-information/search-fda-guidance-documents/guidance-industry-preparation-premarket-submissions-food-contact-substances-chemistry
[14] A. S. Tsagkaris *et al.*, “Critical assessment of recent trends related to screening and confirmatory analytical methods for selected food contaminants and allergens,” *TrAC Trends Anal. Chem.*, vol. 121, p. 115688, Dec. 2019, doi: 10.1016/j.trac.2019.115688.
[15] H. E. Armario *et al.*, “Preliminary Screening and Method Comparison of Total Residual Contaminants Migrating to Fatty and Oily Foods from Low-Density Polyethylene (LDPE) Food Contact Articles Sold in the Philippines,” vol. 14, 2025.
[16] H. Ohno, M. Suzuki, M. Mutsuga, and Y. Kawamura, “Study of Relationship between Consumption of Potassium Permanganate and Total Organic Carbon on Plastic Kitchen Utensils, Food Packages and Toys,” *Shokuhin Eiseigaku Zasshi J. Food Hyg. Soc. Jpn.*, vol. 50, pp. 230–6, Oct. 2009, doi: 10.3358/shokueishi.50.230.
[17] W. P. Alejandro, E. K. P. Encarnacion, A. C. Alcantara, D. J. A. Jr, H. E. Armario, and A. F. D. Rosario, “Assessment of Total UV-Absorbing Contaminants in LDPE Food Packaging from Philippine Markets,” *Curr. Res. Nutr. Food Sci. J.*, vol. 13, no. 2, pp. 913–925, 2010, doi: 10.12944/CRNFSJ.13.2.26.
[18] H. Atmanspacher and M. Martin, “Correlations and How to Interpret Them,” *Information*, vol. 10, p. 272, Aug. 2019, doi: 10.3390/info10090272.
[19] M. Guembe-Garcia, L. R. Magnaghi, G. E. Franceschi, A. Bova, and R. Biesuz, “Multi-Way Data Analysis Nowadays: Taking Advanced Chemometric Tools to Everyday Analytical Chemistry Applications,” *Chemosensors*, vol. 14, no. 2, p. 37, Feb. 2026, doi: 10.3390/chemosensors14020037.
[20] O. Rodionova, S. Kucheryavskiy, and A. Pomerantsev, “Efficient tools for principal component analysis of complex data— a tutorial,” *Chemom. Intell. Lab. Syst.*, vol. 213, p. 104304, Jun. 2021, doi: 10.1016/j.chemolab.2021.104304.
[21] R. Todeschini, “Data correlation, number of significant principal components and shape of molecules. The *K* correlation index,” *Anal. Chim. Acta*, vol. 348, no. 1, pp. 419–430, Aug. 1997, doi: 10.1016/S0003-2670(97)00290-0.
[22] L. Cuadros-Rodríguez, M. Lazúen-Muros, C. Ruiz-Samblás, and N. Navas-Iglesias, “Leachables from plastic materials in contact with drugs. State of the art and review of current analytical approaches,” *Int. J. Pharm.*, vol. 583, p. 119332, Jun. 2020, doi: 10.1016/j.ijpharm.2020.119332.
[23] G. A. El-Hiti, D. S. Ahmed, E. Yousif, O. S. A. Al-Khazrajy, M. Abdallh, and S. A. Alanazi, “Modifications of Polymers through the Addition of Ultraviolet Absorbers to Reduce the Aging Effect of Accelerated and Natural Irradiation,” *Polymers*, vol.

14, no. 1, p. 20, Jan. 2022, doi: 10.3390/polym14010020.
[24] R. Paiva, I. Veroneze, M. Wrona, C. Nerín, and S. Cruz, *The Role of Residual Contaminants and Recycling Steps on Rheological Properties of Recycled Polypropylene*. 2021. doi: 10.21203/rs.3.rs-476987/v1.
[25] L.-X. Zhu *et al.*, "Sources of potassium permanganate consumption for food contact paper," *Food Packag. Shelf Life*, vol. 20, p. 100319, Jun. 2019, doi: 10.1016/j.fpsl.2019.100319.
[26] P. G. C. Nayanathara Thathsarani Pilapitiya and A. S. Ratnayake, "The world of plastic waste: A review," *Clean. Mater.*, vol. 11, p. 100220, Mar. 2024, doi: 10.1016/j.clema.2024.100220.

2026 IMEKO Joint Conference
TC8 - TC11 - TC24
Metro Manila, Philippines, August 26-29, 2026

PFOA and PFOS migration from food-contact materials (FCMs) using LC-MS/MS

Agaseve F. Del Rosario[1], Elyson Keith P. Encarnacion[1], Rizel Marie S.M. Ting[1], Aaron C. Dacuya[2], Johnree Omar Delos Santos[1,3], Harold E. Armario[1], and Jeric B. Bañadera[1]

[1] *Department of Science and Technology, Industrial Technology Development Institute, Packaging Safety Laboratory, agasevedelrosario@gmail.com*
[2] *Department of Science and Technology, Industrial Technology Development Institute, National Metrology Division, acdacuya@itdi.dost.gov.ph*
[3] *Pamantasan ng Lungsod ng Maynila, College of Science, Chemistry Department, joadelossantos2022@plm.edu.ph*

***Abstract* – PFAS, including PFOA and PFOS, can migrate from food contact materials (FCMs) into food and are known for their toxicity and bioaccumulation. This study screened 10 FCMs used in the Philippines using 95% ethanol as oily food simulant to determine the extent of migration. UHPLC-MS/MS was employed to assess method performance and quantify migrating PFAS. The modified method did not show any losses from both the heating and modified SPE method. Limit of detections (LODs) for both PFOA and PFOS (0.007 ng/g and 0.003 ng/g, respectively), and repeatability at low and high levels met relevant limits and guidelines. PFOS repeatability at high concentrations could not be measured due to the lack of representative samples. PFOS was below the detection levels, while migrating PFOA above LOQ ranged from 0.03 to 0.69 ng/g. Higher PFOA migration was found in printed representative sample compared to the non-printed part, suggesting potential contamination from printing inks.**

I. INTRODUCTION

Per- and polyfluoroalkyl substances (PFAS) are synthetic chemicals used provide resistance against thermal and chemical degradation in commercial and industrial products, owing to their strong carbon-fluorine bonds. As a result, PFAS are widely used to reinforce paper FCMs against oil and water. However, these chemicals were found to bioaccumulate and exert toxic effects in humans such as endocrine disruption, hepatotoxicity, developmental effects, and cancer. PFAS were also found to migrate from FCMs to food and food simulants, which, upon ingestion, serves as a potential exposure route [1], [2].

Recent literature found that long-chain PFAS such as Perfluorooctanoic acid (PFOA) and Perfluorooctane sulfonate (PFOS), migrate more towards lipophilic substances such as 50% ethanol [3]. Moreover, migration conditions such as elevated temperature and contact time increase the rate of migration. Such factors could be found in fast-food take-outs, where foods with oily surfaces are placed in FCMs at a relatively high temperatures to maintain acceptable quality upon the time of delivery and consumption [4]. Moreover, undocumented local practices such as storing and re-heating in take-out containers lengthen the contact duration. The combination of such factors increases the risk from PFAS exposure, especially for legacy PFAS such as PFOA and PFOS which are still detected in local FCMs [5].

Using UHPLC-MS/MS-based method, this study aims to determine the extent of PFOA and PFOS migration from commercially available FCMs to 95% ethanol as a fatty food simulant. The data generated could support exposure and risk assessments for health research and policy development.

II. METHOD

A. Chemicals and Materials

Native-standards were purchased from LGC Standards (Teddington, Middlesex, UK). Ammonium acetate, AR grade Ethanol, and LCMS grade solvents (water, acetonitrile, and methanol) were purchased from Fisher Scientific (Pittsburgh, PA, USA). SUPELCO EN-VI-Carb solid phase extraction (SPE) cartridge was purchased from UCT (Bristol, PA, USA). All the materials that will be in contact with the sample or solution were rinsed with methanol before use, if applicable. Packaging samples were obtained from the manufacturers.

B. Migration assay

The migration assay was designed using the EU regulation No. 10/2011, specifically mimicking the OM no. 3 conditions to represent food-contact time of 15

minutes and 120 minutes at 100ºC and 70ºC, respectively [6]. Since Tenax® underestimates PFAS migration, 95% (v/v) ethanol was used to represent migration to fatty foods. CEN standards listed the use of the simulant for migration analysis of paper. Moreover, Zabaleta et al. (2020) and Sonego et al. (2023) utilized the simulant to represent worst-case scenario migration to fatty food [7], [8].

Sample preparation and clean-up are based on the methods of Schaider et al. (2017) and EPA 537.1 with some modifications while the migration assay was conducted using the principles and simulant conditions listed in EU regulation No. 10/2011 [9], [10]. Briefly, sample areas of 5 cm x 10 cm were cut into identical strips and added into polypropylene (PP) centrifuge tubes with 12.5 mL 95% ethanol. The mixture was heated at 70ºC for 2 hours, conditions representing contact conditions of 100ºC for 15 mins and the testing condition. Samples were removed after the assay and the solution was sonicated for 30 minutes. Four milliliter aliquots were passed through pre-conditioned SPE cartridges, evaporated, and reconstituted with 1 mL 96:4 MeOH:water. The solution was then filtered through a 0.21 µm syring filter into a PP LC vial.

C. Instrumentation

Instrumentation was conducted using a Triple Quadrupole LC-MS. The LC-MS/MS system is composed of Agilent 6470 triple-quadrupole mass spectrometer and Agilent Infinity 2490 LC pump. Chromatographic separation was achieved using a ZORBAX Eclipse Plus C18 Rapid Resolution HD column (3.0 × 50 mm, 1.8 µm) fitted with a Zorbax Stable Bond C18 (4.5 × 75 mm, 3.5µm) maintained at 40°C. The mobile phase consisted of 95:5 water: methanol with 2 mM ammonium acetate (Phase A) and ACN (Phase B). The injection volume was 10 µL and was separated using the gradient condition outlined in Table 1.

Mass spectrometer conditions are as follows: electrospray ion source (ESI), capillary voltage 2500 V, Gas temperature 230ºC, and Sheath gas temperature 350ºC. The sheath gas and atomizing gas were nitrogen at flow rates of 10 $L \cdot min^{-1}$ and 6.0 $L \cdot min^{-1}$ respectively. Nitrogen gas (N_2) was supplied by a nitrogen generator. The collision gas was argon. Multiple reaction monitoring (MRM) mode was used for tandem mass spectrometry. The mass spectrometry parameters of the two analytes are shown in Table 1.

Table 1*. UHPLC-MS/MS Parameters*

Parameters	**Optimized Setting**
Injection Volume	10 µL
Needle Wash, Flush Port	3 secs
Draw Speed	200 µL / min
Eject Speed	400 µL / min
Wait Time after Draw	1.2 secs
LC Flow Rate	0.45 mL / min
Run Time	12 mins
Autosampler Temperature	10 °C
Column Oven Temperature	40 °C
Pump Mode	Binary Gradient
Gradient Conditions	%A / %B
	0.00 — 98 — 2
	0.20 — 98 — 2
	4.00 — 70 — 30
	7.00 — 45 — 55
	9.00 — 25 — 75
	10.00 — 5 — 95
	10.40 — 98 — 2
	11.80 — 98 — 2
	12.00 — 98 — 2
Ion Source	Electrospray Ionization
Gas Temperature	230 °C
Gas Flow	6.0 L / min
Nebulizer Pressure	20 psi
Capillary Voltage	2500 V

Compound	PFOA		PFOS	
Time Segment (mins)	7-7.8		7.8-12	
Precursor Ion (units)	413		498.9	
Product Ion (units)	369	169	99	80.1
Dwell	200	200	200	200
Fragmentor	69	69	195	195
Collision Energy	3	9	40	65
Cell Accelerator	7	7	7	7

D. Method performance assessment

The method used for the migration assay was a validated in-house method developed, with modifications. As such, recoveries for the modified steps were assessed by statistically comparing triplicate spiked solvents for each modified steps against the original method. Analysis of Variance (ANOVA) at 95% confidence level was used for the statistical treatment.

Minimum performance parameters such as the Limit of detection (LOD), Limit of quantitation (LOQ), and repeatability at low and high concentrations were assessed

using six replicates of representative samples. Calculations were done according to the Eurachem: The Fitness for Purpose of Analytical Methods (2025) guideline [11].

III. RESULTS AND DISCUSSION

A. Method Performance

Recoveries of the modified steps did not show any significant difference with the previously validated method ($p<0.05$). The calibration curve range and estimates of the LOD, LOQ, and precision of the method are summarized in in Table 2. Calibration curves for both PFAS were linear, with R^2 values ranging from 0.999 to 0.997. LODs were comparable to those reported by Lerch et al. (2022) but were lower compared to Vera et al. (2024), likely due to the difference in working range and method of limit estimation [12], [13]. Repeatability was also within the acceptable limits of the AOAC SMPR® 2025.001.

Table 2. Method performance assessment

	PFOA	PFOS
Working Range	0.01 – 5 ng/g	0.01 – 5 ng/g
LOD	0.007 ng/g	0.003 ng/g
LOQ	0.022 ng/g	0.010 ng/g
Repeatability (0.4 ng/g of sx)	28.94%	27.00%
Repeatability (36.01 ng/g of sx)	9.11%	-

B. Concentrations of migrating PFOA and PFOS

Migrated PFOA were detected in 100% of the samples, while PFOS was undetected (<LOD), which is in agreement with reported detection frequency of PFAS on commercial food packaging materials in the Philippines [5]. Moreover, earlier literature reports similar trend on the occurrence of PFOA and PFOS in globally-sourced FCMs, reflecting the effect of earlier set ban and voluntary phase-out of PFOS as compared to PFOA [14], [15], [16].

In agreement with the results of this study, migration studies failed to obtain measurable migrating PFOS likely due to the low concentrations initially present in the materials. Recent reports on PFOS concentrations of globally-sourced FCMs ranged from ND-0.93 ng/g. Additionally, migration assays conducted in comparable conditions with present study had migration percentages ranging from 0.4%-18.0% [14], [16], [17]. On the other hand, migrating PFOA concentrations in this study is consistent with the potential levels that could migrate (~10% migration) from the FCMs in the Philippines analyzed by Encarnacion et al [5].

Table 3. Average concentration of migrated PFOA and PFOS

Sample code	Average (ng PFOA/g of sx)	Average (ng PFOS/g of sx)
S1	<LOQ	ND
S2	<LOQ	ND
S3	0.19	ND
S4	0.025	ND
S5	<LOQ	ND
S6	<LOQ	ND
S7	<LOQ	ND
S8	<LOQ	ND
S9	<LOQ	ND
S10	0.69	ND

ND = Not detected07

The non-negligible levels in present study could be attributed to contaminated additives and/or recycled raw materials. Since virgin pulp contain no PFAS or have negligible levels, PFAS addition either intentional or non-intentional occur upstream [13], [14], [16], [18]. Moreover, PFAS is added to the paper pulp to impart chemical resistance or for surface treatment. Curtzwiler et al. (2021) argued that PFOA levels below 337 ppm posed no economic advantage and concentrations below could be considered as Non-Intentionally Added Substance (NIAS), which could be argued for the measured levels in this study [19].

C. Exposure risk

The PFAS concentrations measured in this study are comparable to those reported in recent migration studies, suggesting a potentially elevated contribution of FCMs to dietary exposure[13], [14], [16], [18]. Although FCMs are not typically the dominant exposure pathway compared to drinking water or other food sources, they represent a non-negligible and preventable source of intake [20].

Assuming a weekly intake of fast-food, the estimated weekly intake of PFAS from FCM exposure remains

below the tolerable weekly intake (TWI) established by the European Food Safety Authority, which is 4.4 ng/kg body weight per week for the sum of selected PFAS [21]. However, exposure at low levels does not necessarily indicate negligible risk. PFAS are highly persistent, bioaccumulative, and have long biological half-lives in humans, leading to gradual accumulation even at low exposure levels [20].

Chronic exposure to PFAS has been associated with a range of adverse health outcomes, including immunotoxicity, endocrine disruption, and developmental effects[22], [23]. Importantly, recent evidence suggests that even low-level, long-term exposure may contribute to subtle but clinically relevant effects, particularly in sensitive populations such as children [24]. Therefore, while the estimated intake from FCMs alone may fall below regulatory thresholds, the cumulative contribution from multiple exposure pathways warrants concern.

D. Difference of migrating PFOA in printed and non-printed pieces

Five replicates of the printed and the non-printed parts of the representative sample had average concentrations of 0.013 and 0.004 ng PFOA per gram of simulant, respectively. Analysis of variance (ANOVA) revealed a significant difference ($p<0.05$) between the tested groups. On the other hand, migrated PFOS concentrations did not exhibit a significant difference.

This aligns with the reports of PFAS use in printer ink cartridges [25], [26]. Other paper additives such as coatings, laminates, and adhesives could also impart low concentrations as these chemicals can also be contaminated from their respective manufacturing processes. As such, the development of an encompassing regulatory framework and analytical methods encompassing various materials is imperative.

IV. CONCLUSION

This study demonstrated the migration of PFOA from commercially available paper-based food-contact materials into 95% ethanol under conditions simulating fatty food contact, while PFOS remained below detectable levels. The developed UHPLC-MS/MS method showed acceptable linearity, sensitivity, and repeatability for PFAS migration analysis. The detected PFOA concentrations were consistent with recent reports on PFAS occurrence in food packaging materials and may be associated with contaminated additives and recycled raw materials. Although the estimated exposure levels remained below current tolerable intake thresholds, the persistence and bioaccumulative nature of PFAS highlight the potential risk from chronic low-level exposure. Furthermore, significantly higher migration from printed areas suggests that inks and related additives may contribute to PFAS contamination. Overall, the findings emphasize the need for continued monitoring, improved regulatory frameworks, and broader assessment of PFAS sources in food-contact materials.

V. REFERENCES

[1] A. Yashwanth *et al.*, “Food packaging solutions in the post-per- and polyfluoroalkyl substances (PFAS) and microplastics era: A review of functions, materials, and bio-based alternatives,” *Compr. Rev. Food Sci. Food Saf.*, vol. 24, no. 1, p. e70079, 2025, doi: 10.1111/1541-4337.70079.

[2] A. F. Peritore, E. Gugliandolo, S. Cuzzocrea, R. Crupi, and D. Britti, “Current Review of Increasing Animal Health Threat of Per- and Polyfluoroalkyl Substances (PFAS): Harms, Limitations, and Alternatives to Manage Their Toxicity,” *Int. J. Mol. Sci.*, vol. 24, no. 14, p. 11707, Jan. 2023, doi: 10.3390/ijms241411707.

[3] Y. Yang *et al.*, “Per- and Polyfluoroalkyl Substances (PFAS) in Consumer Products: An Overview of the Occurrence, Migration, and Exposure Assessment,” *Molecules*, vol. 30, no. 5, p. 994, Jan. 2025, doi: 10.3390/molecules30050994.

[4] D. W. Phelps, L. V. Parkinson, J. M. Boucher, J. Muncke, and B. Geueke, “Per- and Polyfluoroalkyl Substances in Food Packaging: Migration, Toxicity, and Management Strategies,” *Environ. Sci. Technol.*, vol. 58, no. 13, pp. 5670–5684, Apr. 2024, doi: 10.1021/acs.est.3c03702.

[5] E. K. P. Encarnacion, A. C. Alcantara, H. E. Armario, W. P. Alejandro, Z. Zhan, and Z. Sun, “Preliminary Screening of Per- and Polyfluoroalkyl Substances (PFAS) in Philippine Fast Food Packaging Using Liquid Chromatography–Mass Spectrometry (LC-MS),” *Curr. Res. Nutr. Food Sci. J.*, vol. 12, no. 1, pp. 423–436, Apr. 2024.

[6] *Commission Regulation (EU) No 10/2011 of 14 January 2011 on plastic materials and articles intended to come into contact with food Text with EEA relevance*, vol. 012. 2011. Accessed: May 07, 2026. [Online]. Available: http://data.europa.eu/eli/reg/2011/10/oj

[7] I. Zabaleta *et al.*, “Occurrence of per- and polyfluorinated compounds in paper and board packaging materials and migration to food simulants and foodstuffs,” *Food Chem.*, vol. 321, p. 126746, Aug. 2020, doi: 10.1016/j.foodchem.2020.126746.

[8] E. Sonego *et al.*, “Occurrence and migration study

of chemicals from baking paper and aluminium foil," *Food Chem.*, vol. 409, p. 135260, May 2023, doi: 10.1016/j.foodchem.2022.135260.

[9] L. A. Schaider *et al.*, "Fluorinated Compounds in U.S. Fast Food Packaging," *Environ. Sci. Technol. Lett.*, vol. 4, no. 3, pp. 105–111, 2017, doi: 10.1021/acs.estlett.6b00435.

[10] O. of R. & Development, "Method 537.1 Determination of Selected Per- and Polyflourinated Alkyl Substances in Drinking Water by Solid Phase Extraction and Liquid Chromatography/Tandem Mass Spectrometry (LC/MS/MS)." Accessed: May 07, 2026. [Online]. Available: https://cfpub.epa.gov/si/si_public_record_report.cfm?dirEntryId=348508&Lab=CESER&simpleSearch=0&showCriteria=2&searchAll=537.1&TIMSType=&dateBeginPublishedPresented=03%2F24%2F2018

[11] "The Fitness for Purpose of Analytical Methods (2025)." Accessed: May 07, 2026. [Online]. Available: https://www.eurachem.org/index.php/3-publications/guides/144-gdmv2014

[12] M. Lerch, K. H. Nguyen, and K. Granby, "Is the use of paper food contact materials treated with per- and polyfluorinated alkyl substances safe for high-temperature applications? – Migration study in real food and food simulants," *Food Chem.*, vol. 393, p. 133375, Nov. 2022, doi: 10.1016/j.foodchem.2022.133375.

[13] P. Vera, E. Canellas, N. Dreolin, J. Goshawk, and C. Nerín, "The analysis of the migration of per and poly fluoroalkyl substances (PFAS) from food contact materials using ultrahigh performance liquid chromatography coupled to ion-mobility quadrupole time-of-flight mass spectrometry (UPLC- IMS-QTOF)," *Talanta*, vol. 266, p. 124999, Jan. 2024, doi: 10.1016/j.talanta.2023.124999.

[14] K. Stroski and Y. Sapozhnikova, "Assessment of per- and polyfluoroalkyl substances (PFAS) in consumer food packaging," *Chemosphere*, vol. 395, p. 144824, Feb. 2026, doi: 10.1016/j.chemosphere.2026.144824.

[15] M. Jovanović, V. Müller, J. Feldmann, and E. Leitner, "Analysis of per- and polyfluoroalkyl substances (PFAS) in raw materials intended for the production of paper-based food contact materials – evaluating LC-MS/MS versus total fluorine and extractable organic fluorine," *Food Addit. Contam. Part A*, vol. 41, no. 5, pp. 525–536, May 2024, doi: 10.1080/19440049.2024.2332334.

[16] Y. Sapozhnikova, R. B. Taylor, M. Bedi, and C. Ng, "Assessing per- and polyfluoroalkyl substances in globally sourced food packaging," *Chemosphere*, vol. 337, p. 139381, Oct. 2023, doi: 10.1016/j.chemosphere.2023.139381.

[17] M. J. Dueñas-Mas, A. Ballesteros-Gómez, and J. de Boer, "Determination of several PFAS groups in food packaging material from fast-food restaurants in France," *Chemosphere*, vol. 339, p. 139734, Oct. 2023, doi: 10.1016/j.chemosphere.2023.139734.

[18] P. Vázquez Loureiro, K.-H. Nguyen, A. Rodríguez Bernaldo de Quirós, R. Sendón, K. Granby, and A. A. Niklas, "Identification and quantification of per- and polyfluorinated alkyl substances (PFAS) migrating from food contact materials (FCM)," *Chemosphere*, vol. 360, p. 142360, Jul. 2024, doi: 10.1016/j.chemosphere.2024.142360.

[19] G. W. Curtzwiler, P. Silva, A. Hall, A. Ivey, and K. Vorst, "Significance of Perfluoroalkyl Substances (PFAS) in Food Packaging," *Integr. Environ. Assess. Manag.*, vol. 17, no. 1, pp. 7–12, Jan. 2021, doi: 10.1002/ieam.4346.

[20] M. Di Mario *et al.*, "Risks associated with the presence of PFAS in FCM: An investigation of the Belgian market," *Chemosphere*, vol. 363, p. 142907, Sep. 2024, doi: 10.1016/j.chemosphere.2024.142907.

[21] "Contaminants in the Food Chain | EFSA." Accessed: May 07, 2026. [Online]. Available: https://www.efsa.europa.eu/en/science/scientific-committee-and-panels/contam

[22] J. C. DeWitt, S. J. Blossom, and L. A. Schaider, "Exposure to per-fluoroalkyl and polyfluoroalkyl substances leads to immunotoxicity: epidemiological and toxicological evidence," *J. Expo. Sci. Environ. Epidemiol.*, vol. 29, no. 2, pp. 148–156, Mar. 2019, doi: 10.1038/s41370-018-0097-y.

[23] V. Ehrlich *et al.*, "Consideration of pathways for immunotoxicity of per- and polyfluoroalkyl substances (PFAS)," *Environ. Health*, vol. 22, no. 1, p. 19, Feb. 2023, doi: 10.1186/s12940-022-00958-5.

[24] E. E. Antoniou and W. Dekant, "Childhood PFAS exposure and immunotoxicity: a systematic review and meta-analysis of human studies," *Syst. Rev.*, vol. 13, no. 1, p. 176, Jul. 2024, doi: 10.1186/s13643-024-02596-z.

[25] L. G. T. Gaines, "Historical and current usage of per- and polyfluoroalkyl substances (PFAS): A literature review," *Am. J. Ind. Med.*, vol. 66, no. 5, pp. 353–378, 2023, doi: 10.1002/ajim.23362.

[26] L. Zimmermann *et al.*, "Implementing the EU Chemicals Strategy for Sustainability: The case of food contact chemicals of concern," *J. Hazard. Mater.*, vol. 437, p. 129167, Sep. 2022, doi: 10.1016/j.jhazmat.2022.129167.

2026 IMEKO Joint Conference
TC8 - TC11 - TC24
Metro Manila, Philippines, August 26-29, 2026

Homogeneity Assessment of Nylon/LDPE Flexible Packaging Films Based on Oxygen Transmission Rate Measurements

Anne C. Alcantara[1], Vince Z. Tabao[12], Elyson Keith P. Encarnacion[1], Agaseve F. Del Rosario[1], Rizel Marie S.M. Ting[1], Winnie P. Alejandro[1], Josefino Antonio T. Mendoza[1], David J. Alcarde Jr.[1]

[1]*Department of Science and Technology, Industrial Technology Development Institute, Packaging Technology Division, Packaging Safety Laboratory, Bicutan, Taguig City, Philippines, acalcantara@itdi.dost.gov.ph*

[2]*Pamantasan ng Lungsod ng Maynila (PLM), Gen. Luna Cor. Muralla Street, Intramuros, Manila, Philippines, vztabao2022@plm.edu.ph*

***Abstract* – Consistency of barrier performance is critical for multilayer flexible packaging used for oxygen-sensitive products. This study evaluated the homogeneity of nylon/LDPE films using oxygen transmission rate (OTR) measurements. Twenty units from a single production batch were randomly selected and measured in duplicate under repeatability conditions to separate measurement variation from intrinsic unit-to-unit differences. Polymer composition was verified by Fourier Transform Infrared Spectroscopy (FTIR) and Differential Scanning Calorimetry (DSC). Unit mean OTR values ranged from 51.9 to 59.6 $cm^3 \cdot m^{-2} \cdot day^{-1}$, with an overall mean of 56.8 $cm^3 \cdot m^{-2} \cdot day^{-1}$. One-way ANOVA revealed statistically significant between-unit differences (s_{bb}) ($F(19,20) = 189.7$, $p < 0.001$). Variance component analysis estimated s_{bb} of 2.50 $cm^3 \cdot m^{-2} \cdot day^{-1}$ (4.4%), and a repeatability standard deviation was 0.26 $cm^3 \cdot m^{-2} \cdot day^{-1}$. The 95% confidence interval for s_{bb} was 1.59–3.96 $cm^3 \cdot m^{-2} \cdot day^{-1}$ (2.8%–7.0% relative variability). Results indicate measurable intrinsic variability within the sampled production batch emphasizing that statistical significance should be interpreted alongside magnitude of variation.**

Keywords* – *Oxygen Transmission Rate, Homogeneity Assessment, Variance Component Analysis, Repeatabilty

I. INTRODUCTION

Among the functional properties of flexible packaging materials, the ability to restrict oxygen transmission is arguably the most important — particularly when the contents are susceptible to oxidative degradation [1]–[3] [1], [2], [3]. Of the many multilayer film structures employed in commercial flexible packaging, combinations of nylon and low-density polyethylene (LDPE) have been widely used owing to their ability to provide oxygen barrier protection, mechanical durability, and reliable heat-sealing properties all at once [4]. In large-scale manufacturing environments, production systems are designed to maintain consistent barrier performance across every unit produced within a given batch. Yet, even when processing conditions are maintained within narrow tolerances, minor variation in layer thickness, polymer distribution, and processing parameters may introduce measurable differences between individual units. Such variability may influence barrier performance and contribute to differences in product quality and shelf-life performance [4], [5].

In routine practice, evaluation of barrier performance is commonly represented using average oxygen transmission rate (OTR) values, while variability among units within a production lot is less frequently characterized despite its importance for assessing material homogeneity and measurement uncertainty [5], [6]. While such differences may be statistically detectable, their practical significance in terms of material performance and quality control is not always clearly established [6],[7]. This highlights the need for approaches that go beyond merely identifying differences and instead measure the magnitude of variability in ways that are meaningful to industrial contexts.

From a measurement perspective, OTR results reflect both analytical repeatability and inherent variability of the material itself. Separating these contributing factors is essential for meaningful interpretation of barrier performance, most notably in context where consistency of multilayer films is subjected to evaluation[8], [9], [10]. Observed moderate variability has been attributed from manufacturing-related differences in film morphology, layer distribution, crystallinity, and dimensional thickness without necessarily compromising functional barrier performance [8], [11]. In light of this, it is held that the interpretation of OTR variability should consider both statistical significance and practical relevance within the intended application.

Variance component analysis (VCA) provides a structured framework for addressing this problem by partitioning

total variability into within-unit (repeatability) and between-unit (intrinsic) components [5], [12], [13], [14], [15] . Using one-way analysis of variance (ANOVA), it becomes possible to estimate the between-unit standard deviation and evaluate its associated uncertainty [9], [12]. This enables a magnitude-based interpretation of variability, supporting more informed assessment of material consistency.

The present study evaluates the homogeneity of a nylon/LDPE flexible packaging film batch using OTR measurements. The study examines the presence of unit-to-unit differences, quantifies intrinsic variability through variance component estimation, and assesses the contribution of homogeneity to overall measurement uncertainty.

By integrating ANOVA, confidence interval estimation, and uncertainty analysis, this work provides a quantitative framework for interpreting barrier performance variability in multilayer packaging materials. The approach emphasizes the importance of considering both statistical significance and practical relevance. This has implications for quality control and specification development in industrial settings.

II. MATERIALS AND METHODS

A. Sample Description and Sampling

Flexible packaging films composed of nylon and LDPE were obtained from a single production batch manufactured under standard industrial conditions. Samples were supplied in the form of finished flexible packaging bags representative of commercially produced food packaging materials. Flat sections were cut from the central body region of each bag to obtain specimens suitable for OTR analysis**.** The sampling area was selected to avoid seams, folds, printed regions, seals, and visibly damaged areas. Specimens were taken consistently from the same general region of each bag to minimize within-bag positional effects. Specimen dimensions were prepared according to the MOCON OTR 2/21 ML instrument and ASTM D3985-17 method requirements, with an exposed test area of 50 cm² [16].

A total of 100 individual bags were available within the production lot. All selected samples originated from the same manufacturing day and production lot.

Stratified random sampling was performed to obtain a representative subset of the production batch. Each bag was assigned a numerical identifier from 1 to 100, and twenty units were randomly selected using Microsoft Excel. The sampled units were considered representative of routine manufacturing variability within the selected lot. Prior to testing, film samples were stored in a dry laboratory cabinet to minimize exposure to uncontrolled environmental fluctuations before analysis. No formal humidity conditioning step was applied. Each unit was prepared from the flat section of the nylon/LDPE packaging bag and tested in duplicate under repeatability conditions using the same instrument, operator, and environmental settings throughout the study.

B. Polymer Confirmation

Polymer composition was verified using Fourier Transform Infrared Spectroscopy (FTIR) with a Shimadzu IR-Prestige-21 equipped with an Attenuated Total Reflectance (ATR) accessory. Spectra were collected in the range of 4000–400 cm^{-1} with a resolution of 4 cm^{-1}, averaging 32 scans per sample.

Differential Scanning Calorimetry (DSC) was additionally performed to support polymer characterization. Thermal analysis was conducted using a Shimadzu DSC-60A calorimeter under nitrogen atmosphere. Approximately 5 mg of sample, along with 10 mg of alumina was sealed in an aluminum pan and heated from 50 °C to 300 °C at a rate of 10 °C/min. Melting transitions were evaluated to support identification of polymer components within the multilayer.

C. OTR Measurement

OTR measurements were carried out using MOCON OTR2/21 ML permeability analyzer with an oxygen flow rate of 20 cm^3/min under controlled temperature of 23 ºC and 0% relative humidity (RH). Measurements were performed in accordance with ASTM D3985 [16].

Before permeability measurement, specimens were mounted in the test chamber and allowed to equilibrate under instrument-controlled conditions at 0% RH until stable transmission readings were achieved.

OTR measurements were performed in duplicate for each sampled unit. Duplicate analysis consisted of two independently prepared specimens obtained from the same bag and taken from the same general sampling region. The mean of duplicate measurements was used to represent the OTR value for subsequent statistical analysis.

D. Experimental Design

In this study, homogeneity refers to the degree of variability in OTR values among film units originating from the same production batch. A one-way random effects model was applied, treating sampled unit representative of the production lot. Variance components were estimated from duplicate OTR measurements obtained under repeatability conditions.

E. Statistical Analysis

Statistical analysis was performed. An ANOVA was applied, with sample unit treated as a random factor [6], [10].

Variance component estimation was conceptually aligned with homogeneity assessment principles described in ISO 33405:2024 for characterization of between-unit variability and uncertainty evaluation [5]. The ANOVA framework enabled partitioning of variability into repeatability-related and between-unit components [6], [15].

The between-unit variance component was estimated

using:

$$s_{bb}^2 = \frac{MS_{between} - MS_{within}}{r} \quad (1)$$

where $MS_{between}$ and MS_{within} represent the ANOVA mean squares, and r is the number of replicate measurements per unit.

The between-unit standard deviation (s_{bb}) was obtained as the square root of the estimated variance component and used. Repeatability variance (s_w^2) and repeatability standard deviation (s_w) were also calculated.

Confidence intervals (CI) for the estimated between-unit variability were calculated. Confidence intervals for the between-unit standard deviation were estimated using a chi-square distribution approach based on ANOVA variance component estimates.

Additional statistical screening included outlier assessment using Grubbs' test, normality evaluation using the Shapiro–Wilk test, and residual diagnostic plots to verify model adequacy. Statistical analyses were performed using R statistical software (version 4.5.2) with standard functions for ANOVA, variance component estimation, and confidence interval calculation.

III. RESULTS AND DISCUSSION

A. Polymer Confirmation by FTIR and DSC

FTIR spectra exhibited characteristic absorption bands associated with polyethylene and nylon. Polyethylene-related bands were observed near 2916 and 2845 cm^{-1}, while nylon-associated amide bands appeared near 1637 and 1537 cm^{-1}. DSC thermograms further supported material identification by showing distinct melting transitions near 123 °C and 221 °C, corresponding to the polyethylene and nylon layers, respectively. The combined FTIR and DSC results verified that the analyzed specimens originated from a consistent nylon/LDPE multilayer, supporting the assumption that all units shared the same polymer composition.

B. Descriptive Statistics of OTR Measurements

Table 1. Descriptive statistics of unit mean OTR values obtained from twenty nylon/LDPE film units.

Parameter	Value ($cm^3 \cdot m^{-2} \cdot day^{-1}$)
Mean OTR	56.8
Standard deviation, s	2.50
Coefficient of variation, CV	4.4 %
Unit mean range	51.9–59.6
Median	57.1
1st Quartile	55.5
3rd Quartile	59.1

Values are reported in $cm^3 \cdot m^{-2} \cdot day^{-1}$ unless otherwise stated.

Table 1 summarized the distribution of unit mean values across the sampled nylon/LDPE film units. Across twenty sampled units, the mean OTR was 56.8 $cm^3 \cdot m^{-2} \cdot day^{-1}$ with a standard deviation of 2.50 $cm^3 \cdot m^{-2} \cdot day^{-1}$ (CV = 4.4%). The relatively narrow spread suggests moderate unit-to-unit variability. The median was close to the mean, indicating approximate symmetry of the distribution. Quartile values further supported clustering of measurements around the central tendency, indicating that most sampled units exhibited similar oxygen barrier performance.

The distribution of unit mean OTR values across randomly selected film units is presented in Fig. 1.

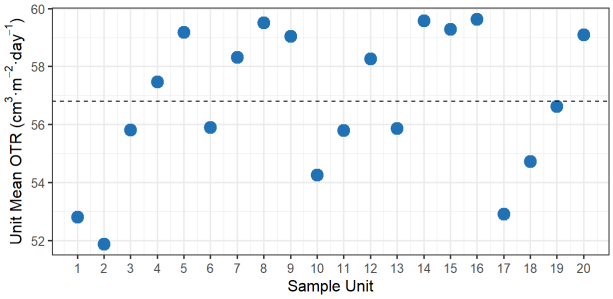


Fig. 1. Distribution of unit mean OTR values across randomly selected nylon/LDPE film units. The dashed line represents the overall mean OTR value.

Most values were clustered near the overall mean, with no isolated extreme observations. The variability appeared distributed across the batch rather than concentrated in a small number of atypical samples, supporting the interpretation of moderate unit-to-unit variation.

C. Data Screening and Assumption Checks

Grubbs' test did not identify significant outliers among the unit mean values (G = 1.96, p = 0.409), indicating that no individual sample deviated markedly from the overall distribution. Differences between duplicate measurements were generally small, with a repeatability standard deviation of 0.258 $cm^3 \cdot m^{-2} \cdot day^{-1}$, supporting good agreement between replicate measurements.

The Shapiro–Wilk test indicated mild deviation from strict normality (p-value = 0.042). However, descriptive statistics suggested that the data remained reasonably centered around the mean, and residual diagnostic plots did not reveal substantial departures from homoscedasticity or model adequacy. Slight deviations from normality were primarily observed at the tails of the distribution rather than across the full dataset. Given the balanced duplicate design and moderate sample size, one-way ANOVA was considered appropriate for variance component estimation despite minor departures from ideal normality assumptions.

These preliminary checks supported proceeding with variance partitioning to evaluate repeatability and between-unit variability.

D. One-Way ANOVA and Variance Partitioning

ANOVA revealed statistically significant between-unit effect ($F(19,20) = 189.7$, $p < 0.001$). This indicates that variability between sampled units was greater than would be expected from measurement repeatability alone.

The mean square between units ($MS_{between} = 12.581$) was substantially larger than the residual mean square ($MS_{within} = 0.066$). This difference suggests that variability within the dataset was primarily associated with intrinsic differences among film units rather than analytical noise. In practical terms, the observed variation reflects measurable unit-to-unit differences within the production batch.

ANOVA results demonstrate that variation among sampled units exceeded measurement repeatability, indicating measurable between-unit differences within the production batch. However, ANOVA alone does not describe the magnitude of variability, which requires further interpretation through variance component estimation.

These findings indicate that variance partitioning provides a more informative framework for evaluating homogeneity than significance testing alone. By separating repeatability-related variation from between-unit variability, the analysis allows a clearer interpretation of material consistency within the sampled production batch.

E. Variance Component Estimation and Homogeneity Assessment

The experimental design enabled separation of repeatability-related variation from intrinsic between-unit variability. Duplicate measurements provided estimation of within-unit variation, while differences among unit means reflected between-unit variability.

Variance component estimates are summarized in Table 2 while the relative magnitude of repeatability and between-unit variability is illustrated in Fig. 2.

Table 2. Variance component estimates for OTR homogeneity assessment.

Parameter	Value
Repeatability variance (s_w^2)	0.066
Repeatability SD (s_w)	0.258
Between-unit variance (s_{bb}^2)	6.26
Between-unit SD (s_{bb})	2.50
Relative (s_{bb}) %	4.40

The between-unit standard deviation (s_{bb}) was substantially larger than the repeatability standard deviation (s_w), indicating that unit-to-unit differences dominate the observed variation and primarily reflect material-related variability rather than analytical measurement noise. Despite statistical significance, the relative between-unit variability remained moderate (~4.4%), indicating limited variation relative to the overall mean OTR value and suggesting reasonably consistent within-lot barrier performance. Such variability is expected for multilayer films due to minor differences in layer distribution, orientation, or thickness.

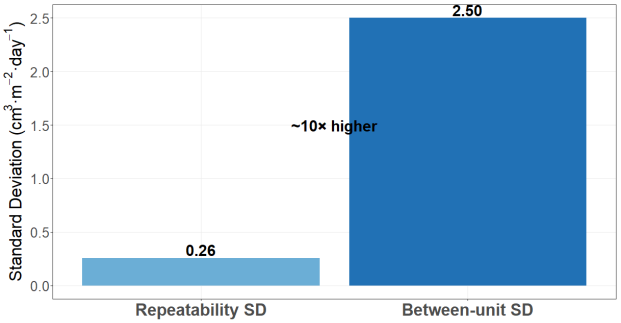


Fig. 2. Comparison of repeatability (s_w) and between-unit (s_{bb}) standard deviations. The between-unit variability is approximately one order of magnitude (~10×) greater than repeatability

The absence of universally established acceptance criteria for OTR homogeneity in multilayer flexible packaging necessitates a statistically grounded approach for evaluating material consistency. In this study, variance component analysis based on the ISO 5725-2 framework was applied to quantify repeatability within a single production batch.

The relative between-unit variability ($s_{bb}\% = 4.4\%$) provide a normalized measure of within-batch consistency. While no formal industrial specification currently defines acceptable OTR homogeneity limits, the observed value of 4.4% may serve as an empirical reference for evaluating production consistency under comparable manufacturing conditions. This interpretation is consistent with ASTM D3985, which specifies procedures for OTR determination but does not prescribe acceptance criteria for material homogeneity.

Table 3 presents an exploratory interpretation framework derived from the variability observed in the present study. Because the assessment was limited to a single production batch, the proposed framework should not be regarded as a universal acceptance criterion. Rather, it illustrates how variance component estimates and relative variability values may be interpreted to support future studies involving multiple production batches and broader industrial validation.

From a quality control perspective, variance component analysis provides information beyond average OTR values by quantifying the magnitude of intrinsic batch variability separately from measurement repeatability. Such information may support internal process monitoring, comparison of production batches, and evaluation of manufacturing consistency. Although no universally accepted homogeneity criteria currently exist for multilayer flexible packaging, variance component

estimates and their associated uncertainty provide quantitative descriptors that may assist manufacturers in establishing applications-specific quality limits.

Table 3. Exploratory interpretation framework derived from observed OTR variability for within-lot homogeneity assessment of nylon/LDPE production batch.

Parameter	Observed Result	Exploratory Interpretation
Mean OTR	56.8 $cm^3 \cdot m^{-2} \cdot day^{-1}$	Representative oxygen barrier performance of the batch
Between-unit standard deviation, s_{bb}	2.50 $cm^3 \cdot m^{-2} \cdot day^{-1}$	Indicates measurable unit-to-unit variability among units
Relative between-unit variability	4.4%	Reflects limited variability relative to the mean
Repeatability standard deviation, s_w	0.258 $cm^3 \cdot m^{-2} \cdot day^{-1}$	Measurement variability remained low relative to unit differences
Preliminary interpretive reference	~5% relative variability	May provide an exploratory reference for future within-lot homogeneity studies under comparable manufacturing conditions

F. Confidence Interval of Between-Unit Variability

The uncertainty associated with the between-unit variability estimate was evaluated using a 95% confidence interval (Table 4). The confidence interval indicates that the true level of between-unit variability within the sample production batch is statistically expected to fall within this interval under the studied conditions.

When expressed relative to the overall mean OTR value, the confidence interval provides additional context for interpreting the uncertainty associated with the homogeneity estimates. The results indicate that the estimated between-unit variability remained limited relative to the overall mean OTR value under the studied conditions.

Table 4. Confidence interval estimates for between-unit variability.

Parameter	Value
s_{bb} (95% CI)	1.59-3.96 $cm^3 \cdot m^{-2} \cdot day^{-1}$
Relative CI (%)	2.8-7.0

The confidence interval provides a more informative description of homogeneity uncertainty than reliance on a single point estimate alone, particularly when variability estimates are derived from a limited number of sampled units. Rather than relying solely on the estimated s_{bb}, the interval describes the likely range of between-unit variability that may be expected under comparable production.

G. Contribution of Homogeneity to Measurement Uncertainty

As discussed in Section E, the between-unit variability was substantially larger than repeatability, indicating that intrinsic material differences dominate short-term measurement precision.

Instrument performance was assessed using a certified reference film traceable to NIST standards. The measured OTR values showed a systematic deviation of approximately 5–6% relative to the certified value. This magnitude was comparable to the observed relative between-unit variability (~4.4%), indicating that material-related variability and calibration-related effects contribute similarly to the overall uncertainty of OTR measurements. Consequently, interpretation of barrier performance should consider both sources rather than relying solely on repeatability measurements.

Thickness variation was also evaluated based on total film thickness. Five measurements yielded a mean thickness of 89.4 μm with a coefficient of variation of approximately 0.61%, indicating high consistency in total film thickness. However, as the material consist of a multilayer nylon/LDPE structure with a nominal layer ratio of 15/70, individual layer thicknesses were not separately quantified. Therefore, while total thickness variation was small, possible variation in nylon or LDPE layer distribution cannot be ruled out as a contributor to OTR variability.

Overall, these findings indicate that while repeatability contributes minimally to measurement uncertainty, both homogeneity and calibration-related effects are significant contributors, whereas total thickness variation appears to have a relatively minor influence under the conditions studied. These findings demonstrate that homogeneity assessment is not only useful for characterizing material consistency but also for identifying the relative importance of different uncertainty sources affecting OTR measurements. Such information may support uncertainty budgeting and quality assurance activities for barrier-property testing.

IV. CONCLUSION

This study showed that VCA provides a practical framework for evaluating the homogeneity of nylon/LDPE flexible packaging films using oxygen transmission rate (OTR) measurements. Although statistically significant differences among sampled units were identified, the magnitude of variability remained moderate relative to the overall mean, indicating reasonably consistent barrier performance within a single production batch.

Between-unit variability was substantially larger than repeatability-related variation, confirming that observed differences primarily reflected intrinsic material variation rather than analytical noise. When duplicate measurements were averaged, homogeneity contributed meaningfully to overall uncertainty, emphasizing the importance of considering material variability when interpreting barrier performance.

In addition to material-related variability, calibration results indicated the presence of moderate instrument-related uncertainty. While repeatability contributed minimally, both homogeneity and calibration-related effects were found to influence the overall measurement uncertainty. These findings highlight the need to consider multiple sources of uncertainty when evaluating OTR performance.

This study was limited to a single production batch of nylon/LDPE flexible packaging film. Therefore, the findings should be interpreted as representative of with-in lot variability rather than broader manufacturing performance across multiple batches. While the observed relative variability provides a useful reference for interpreting homogeneity within the sampled lot, additional studies involving multiple production runs are needed to establish more generalizable acceptance criteria. These findings demonstrate that statistical significance should be interpreted alongside the magnitude of variability when assessing homogeneity in industrial materials. VCA offers a quantitative framework for supporting quality control activities, uncertainty evaluation, and future development of application-specific specifications for barrier consistency assessment. Further work may extend this approach to larger production batches and additional barrier properties to strengthen industrial applicability.

V. REFERENCES

[1] K. V. Lipin, I. I. Muratov, S. A. Gilfanov, A. I. Teptina, and A. R. Agafonova, "POLYMERIC BARRIER MATERIALS USED IN FLEXIBLE PACKAGING," *IVKKT*, vol. 68, no. 12, pp. 6–22, Nov. 2025, doi: 10.6060/ivkkt.20256812.7240.

[2] M. Zabihzadeh Khajavi *et al.*, "Strategies for Producing Improved Oxygen Barrier Materials Appropriate for the Food Packaging Sector," *Food Eng Rev*, vol. 12, no. 3, pp. 346–363, Sep. 2020, doi: 10.1007/s12393-020-09235-y.

[3] M. G. Jo, D. S. An, and D. S. Lee, "Characterization and Enhancement of Package O2 Barrier against Oxidative Deterioration of Powdered Infant Formula," *Journal of Packaging Technology and Research*, vol. 24, no. 1, pp. 13–16, Apr. 2018.

[4] M. Fereydoon, "Development of High Barrier Nylon Based Multilayer Films", Montréal, QC, Canada: Polytechnique Montréal, 2014.

[5] "ISO 33405:2024, Reference Materials—Guidance for Characterization and Assessment of Homogeneity and Stability." Geneva, Switzerland: ISO, 2024.

[6] "R. K. Burdick, C. M. Borror, and D. C. Mongomery, *Design and Analysis of Gauge R&R Studies*: *Making Decisions with Confidence Intervals in Random and Mixed ANOVA Models*. Philadelphia, PA, USA: Society for Industrial and Applied Mathematics, 2003.

[7] L. R. Ellison and A. Williams, *Eurachem/CITAC Guide*. *Quantifying Measurement Uncertainty in Analytical Measurement*, 4th ed. Eurachem/CITAC, 2022.

[8] M. Giacinti Baschetti and M. Minelli, "Test methods for the characterization of gas and vapor permeability in polymers for food packaging application: A review," *Polymer Testing*, vol. 89, p. 106606, Sep. 2020, doi: 10.1016/j.polymertesting.2020.106606.

[9] E. Pignères *et al.*, "How to get reliable oxygen transmission rate values for coated cardboards?" *Progress in Organic Coatings*, vol. 186, p. 108048, Jan. 2024, doi: 10.1016/j.porgcoat.2023.108048.

[10] "ISO 5725-2:2025(en), Accuracy (trueness and precision) of measurement methods and results — Part 2: Basic method for the determination of repeatability and reproducibility of a standard measurement method." International Organization for Standardization, 2025.

[11] M. Guivier, G. Almeida, S. Domenek, and C. Chevigny, "Resilient high oxygen barrier multilayer films of nanocellulose and polylactide," *Carbohydrate Polymers*, vol. 312, p. 120761, Jul. 2023, doi: 10.1016/j.carbpol.2023.120761.

[12] "*The Fitness for Purpose of Analytical Methods - A Laboratory Guide to Method Validation and Related Topics*, 3rd ed. Eurachem, 2025.

[13] D. R. Cox and P. J. Solomon, *Components of Variance*, 2019. https://www.sciencedirect.com/science/article/pii/S1756231716300640.

[14] B. Lashkari and S. Chenouri, "A Comprehensive Framework for Statistical Inference in Measurement System Assessment Studies," 2025, *arXiv*. doi: 10.48550/ARXIV.2501.18037.

[15] Evaluation Joint Committee for Guides in Metrology (JCGM). *Evaluation of measurement data — Guide to the expression of uncertainty in measurement (GUM)*, JCGM 100:2008, corrected version 2020. https://www.bipm.org/doi/10.59161/JCGM100-2008E.

[16] ASTM International, ASTM D3985-17*: Standard Test Method for Oxygen Gas Transmission Rate Through Plastic Film and Sheeting Using a Coulometric Sensor*. West Conshohocken, PA, USA: ASTM International, 2017.

2026 IMEKO Joint Conference
TC8 - TC11 - TC24
Metro Manila, Philippines, August 26-29, 2026

Accreditation and Best Practices in Meteorological Instrument Calibration: Insights from the PAGASA Instrument Calibration Laboratory

Marco Polo Ibañez[1,2*], Wilfredo Tuazon[1,2], Irwin Aguilar[1,2], Kesther Temothy Tapero[1,2], Catherine Hoseña[1,2], Jessa Padiñas[1,2], and Diether Castillo[1,2]

[1]PAGASA Instrument Calibration Laboratory
[2] DOST-PAGASA, Hydrometeorology, Tropical Meteorology, and Instrument Research and Development Section, Research & Development and Training Division, Sen. Miriam Defensor-Santiago Avenue, Quezon City, Metro Manila, Philippines 1100
*corresponding author email: marcopoloibanez@gmail.com

Abstract – **The PAGASA Instrument Calibration Laboratory (PICL) plays a critical role in ensuring the accuracy and reliability of meteorological instruments that underpin weather forecasting, climate monitoring, and disaster risk reduction in the Philippines. This paper details the laboratory's systematic transition toward nationally recognized quality infrastructure, with emphasis on how accreditation and quality management strengthens national measurement systems essential for climate resilience, disaster risk reduction, and public safety. At present, PICL is the sole accredited laboratory in the country for atmospheric pressure calibration, providing a critical link in the national traceability chain. Central to its best practices is the continuous sustainment of service quality through strict adherence to the Standard (ISO/IEC 17025:2017), equipment characterization, proficiency testing, measurement uncertainty evaluation, and continuous personnel competency development.**

I. INTRODUCTION

Accurate meteorological observations are fundamental to weather forecasting, climate monitoring, and disaster risk reduction [1]. Any deviation in instrument accuracy may propagate into forecast errors, potentially affecting public safety and decision-making processes [2]. Thus, calibration of meteorological instruments is essential to ensure measurement reliability and traceability to internationally recognized standards. The PAGASA Instrument Calibration Laboratory (PICL) (formerly known as Instrument Research and Development Unit/ IRDU) operates under the Hydrometeorology, Tropical Meteorology, Instrument Research and Development Section (HTMIRDS) of the Research & Development and Training Division. PICL is responsible for maintaining national reference standards and performing calibration of basic meteorological instruments used across PAGASA stations and external stakeholders. PICL aims to achieve a high level of quality in calibration practices through continuous improvement, adherence to World Meteorological Organization (WMO) Standards [3], and sustained personnel competency development. Its vision is to provide world-class calibration services using reference standards traceable to recognized national and international systems to ensure the accuracy and reliability in meteorological observations.

II. HISTORY AND ACCREDITATION OF PICL

PICL's foundation as a calibration authority was established in 1996 when the Philippines, through PAGASA, was designated by the WMO as a Regional Instrument Center (RIC) for the Southwest Pacific region. This mandated PICL to provide calibration standards, ensure and maintain the traceability of meteorological instruments, and support regional cooperation in meteorological instrumentation (references). Over the following years, PICL underwent significant physical and organizational expansion. PICL initiated the establishment of Local Instrument Centers (LICs) in Tuguegarao, Cebu, and Davao in 2017 to decentralize calibration services and improve accessibility nationwide. Infrastructure development followed, including the construction of an extension building in 2018 and acquisition of advanced calibration equipment such as the Westenberg wind tunnel for wind speed calibrations in 2019 and Kambic peltier climatic chamber for temperture and relative humidity calibrations in 2020 (Fig. 1).



Fig. 1. Calibration facilities at the PAGASA Instrument Calibration Laboratory (PICL): (a) Westenberg Wind Tunnel (Type 8600100-E) used for wind speed calibration, and (b) Kambic Climatic Chamber (Model PKK-125) used for temperature and relative humidity calibration.

Parallel to these developments, PICL initiated its transition toward ISO/IEC 17025:2017 compliance in 2018. The ISO/IEC 17025:2017 is the international standard specifying general requirements for the competence of testing and calibration laboratories [4,5]. The Standard implementation phase included development of quality manuals, procedures, and documentation aligned with ISO Standards requirements. Internal audit cycles commenced in 2021 to evaluate conformity, identify gaps, and guide continuous improvement efforts. These initiatives culminated in PICL's successful accreditation by the Philippine Accreditation Bureau (PAB) in August 2023. This accreditation formally recognizes the laboratory's technical competence and establishes its role within the national traceability chain. At present, PICL's accredited scope includes calibration services for temperature, relative humidity, and atmospheric pressure. Notably, PICL is currently the only accredited calibration laboratory in the Philippines with an accredited capability for atmospheric pressure calibration within the range of 800 hPa to 1050 hPa. Table 1 presents the laboratory's calibration parameters, indicating which parameters are accredited and non-accredited, together with their corresponding set points.

III. DEVELOPMENTS THROUGH QUALITY INFRASTRUCTURE

The development of the PICL into an accredited calibration laboratory is anchored on the systematic implementation of quality infrastructure aligned with ISO/IEC 17025:2017 requirements. Central to this development is the traceability to national and international standards, and strengthening of personnel competency, facilities, and equipment management. PICL maintains a structured system for personnel competency that includes continuous technical training and formal competency assessments.

Table 1. Scope of accreditation of PICL, indicating the meteorological parameters, their respective measurement range,, and accreditation status.

Parameter	Measurement Range	Scope of Accreditation
Atmospheric Pressure	800 hPa – 1050 hPa	Covered
Temperature	0°C - 50°C	Covered
Relative Humidity	30% RH – 95% RH	Covered
Precipitation	25 mm hr^{-1} – 300 mm hr^{-1}	Not Covered
Wind Speed	2 m s^{-1} to 45 m s^{-1}	Not Covered

Training programs and performance evaluations ensure that personnel possess the technical knowledge and skills necessary to conduct calibrations and maintain the laboratory's management system. PICL operates five dedicated calibration rooms designed for specific meteorological parameters, namely: pressure, temperature, relative humidity, precipitation, and wind. These facilities are equipped with environmental monitoring and control systems to maintain stable laboratory conditions, typically maintained at 22℃ ± 2℃ and relative humidity between 30% and 65%. PICL also maintains national reference standards for these parameters, which are regularly calibrated and characterized to ensure accuracy and reliability. The laboratory's traceability chain are traceable to the International System of Units (SI). Using atmospheric pressure as an example, Fig.2 illustrates how calibration activities in PICL is linked from SI units through accredited laboratoris and national reference standards down to working standards and field instruments. This traceablity is achieved through calibration linkages with the National Metrology Laboratory of the Industrial Technology Development Institute (NML-ITDI) and other recognized international institutions.

IV. BEST PRACTICES AND PERFORMANCE EVALUATION

PICL's quality management system (QMS) includes proficiency testing, measurement uncertainty assessment, and internal audits to ensure the reliability, validity, and continual improvement of its services. Through participation in proficiency testing and inter-laboratory comparison activities, PICL benchmarks its measurement

performance against peer laboratories and national metrology institutes.

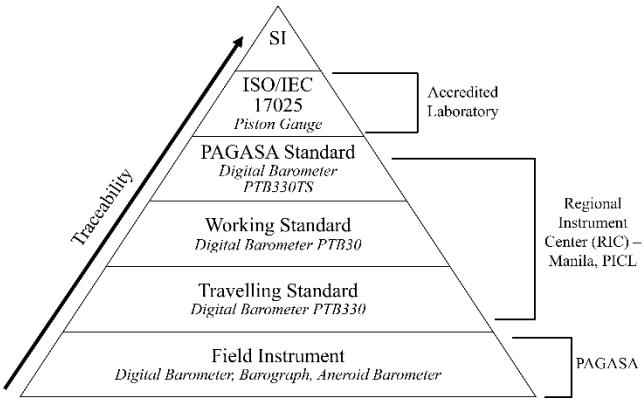


Fig. 2. Example traceability chain of PICL for atmospheric pressure, illustrating the linkage from the International System of Units (SI) to field instruments through reference and working standards.

The laboratory also maintains detailed uncertainty budgets for each calibration parameter and incorporates relevant components such as instrument resolution, environmental effects, and repeatability. Internal audits and management reviews are conducted regularly to assess compliance with ISO/IEC 17025:2017 requirements and to evaluate the effectiveness of the management system. From previous internal audits, the number of non-conformities (NCs) have fluctuated. Fig.3 shows that the number of NCs peaked in 2021, followed by a significant reduction in 2023, before rising again in 2025. This trend indicates periods of effective corrective actions and system improvement, followed by the emergence of new or recurring gaps.

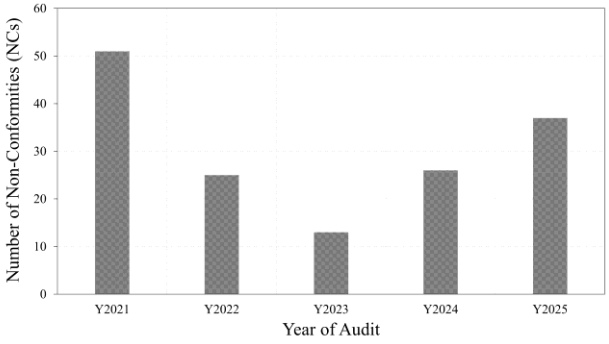


Fig. 3. Trend in the number of non-conformities (NCs) identified during PICL internal audits from 2021 to 2025.

The increase in NCs in 2025 is primarily associated with challenges in personnel competency validation, equipment management, and measurement uncertainty evaluation, indicating areas requiring attention and sustained corrective measures. Complementing the internal audit results, the First Surveillance Visit conducted by the Philippine Accreditation Bureau (PAB) on 20–21 November 2024 confirm that while the management system remains generally effective and aligned with ISO/IEC 17025:2017 requirements, further improvements are necessary to strengthen compliance to the standard and sustain long-term accreditation.

V. CHALLENGES AND FUTURE STRATEGIC DIRECTIONS

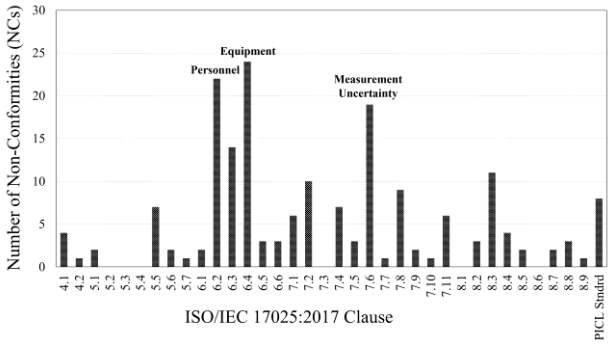


Fig. 4. Distribution of non-conformities (NCs) by ISO/IEC 17025:2017 clauses based on PICL internal audit findings from 2021 to 2025.

PICL continues to face several operational and strategic challenges. Fig. 4 presents the analysis of audit findings from 2021 to 2025 per ISO/IEC 17025:2017 Standard and PICL's own standard. Equipment management (Clause 6.4) is a persistent challenge. Delays in external characterization services have resulted in temporary suspension of calibration services, which highlights the need for alternative service providers or internal capability development. Personnel-related issues (Clause 6.2) are also another critical area, with findings related to limited internal training documentation and the absence of intra-laboratory comparison activities. Measurement uncertainty (Clause 7.6.) has also emerged as a challenge, specifically missing uncertainty components such as instrument resolution, gravity effects, and height differences in uncertainty budgets.

Despite these challenges, PICL has shown strong commitment to continuous improvement through extensive document development and revision activities to align with the requirements of the Standard. Personnel performance remains consistently high and customer satisfaction remains strong, with consistently high ratings for convenience, affordability, and overall service quality. The audits and surveillance visits also confirm that PICL maintains a management system that generally conforms to applicable standards, with demonstrated technical competence within its accredited scope. Looking forward, PICL aims to expand its accredited scope to include

precipitation and wind speed by 2028. This will enhance the laboratory's capacity to support a broader range of meteorological measurements and strengthen the national measurement infrastructure. Also, a key strategic priority is the full operationalization of Local Instrument Centers (LICs) in Tuguegarao, Cebu, and Davao to improve accessibility for stakeholders and enhance nationwide calibration capacity. Strengthening regional calibration capabilities will also reduce operational bottlenecks and improve responsiveness to national needs.

PICL will focus on strengthening competency validation, enhancing technical training documentation, and improving measurement uncertainty evaluation to address recurring audit findings. Efforts will also be made to enhance transparency in service delivery, including clearer communication of calibration timelines and improved complaint handling mechanisms. Through these initiatives, PICL aims to consolidate its role as a nationally recognized calibration facility and support climate resilience, disaster risk reduction, and public safety through reliable meteorological measurements.

VI. CONCLUSION

The development of the PAGASA Instrument Calibration Laboratory (PICL) into a nationally accredited calibration facility represents a significant milestone in strengthening the Philippines' meteorological measurement infrastructure. Through the implementation of a quality management system aligned with ISO/IEC 17025:2017, PICL has established a robust foundation for ensuring the accuracy, traceability, and reliability of meteorological measurements that support weather forecasting, climate monitoring, and disaster risk reduction. The laboratory's evolution demonstrates sustained institutional commitment to international standards, technical competence, and continual improvement. The establishment of dedicated calibration facilities and systematic implementation of quality processes have collectively enhanced the laboratory's operational capacity and credibility.

While PICL has achieved notable progress, ongoing challenges remain, particularly in the areas of measurement uncertainty evaluation, equipment management, and dependence on external service providers. Looking ahead, PICL's strategic direction focuses on expanding its accredited parameters, strengthening nationwide calibration capability through local instrument centers (LICs), and reinforcing quality practices across all operational areas. These efforts will not only enhance the reliability of meteorological measurements but also contribute to more accurate weather and climate information, improved disaster preparedness, and enhanced public safety. Ultimately, PICL's continued development reinforces the vital role of metrology in building a resilient and scientifically grounded response to environmental and societal challenges.

REFERENCES

[1] Foken. T., Beyrich, F., Wulfmeyer, V. *Introduction to Atmospheric Measurements.* In: Foken, T. (eds). Springer Handbook of Atmospheric Measurements. Springer Handbook. Springer, Cham. pp. 3-31. 2021.

[2] Kull, D., Riishojgaard, L.P., Eyre, J., Varley, R.A. *The value of surface-based meteorological observation data.* P.41. World Bank. 2021.

[3] World Meteorological Organization (WMO). *Guide to Instruments and Methods of Obsercation*. (WMO No.8). Geneva. 2021-2025.

[4] Krismastuti, F.S.H., Habibie, M.H. *Complying with the resource requirements of ISO/IEC 17025:2017 in Indonesian Calibration and Testing Laboratories: Current challenges and future directions.* Accreditation and Quality Assurance, 27(6), 359-367. 2022.

[5] International Organization for Standardization. *General requirements for the competence of testing and calibration laboratories (ISO/IEC 17025:2017).* 2017.

2026 IMEKO Joint Conference
TC8 - TC11 - TC24
Metro Manila, Philippines, August 26-29, 2026

Unsupervised Anomaly Detection in Perfluorooctane Sulfonate (PFOS) and Perfluorooctanesulfonic Acid (PFOA) Migration Measurements for Laboratory Quality Assurance and Conformity Assessment

David Jaucian Alcarde Jr.[1], Elyson Keith P. Encarnacion[2], Anne C. Alcantara[3], Harold E. Armario[4], April Star L. Canonizado[5], Agaseve F. Del Rosario[6], Winnie P. Alejandro[7], Rizel Marie S.M. Ting[8], Kim Angelene R. Tagle[9], Daniela Marie D. Barredo[10], Jeric B. Bañadera[11], Josefino Antonio T. Mendoza[12]

[1,2,3,6,7,8,9,10,11,12] *Packaging Technology Division, Industrial Technolgy Development Institute, Department of Science and Technology (DOST-ITDI), Bicutan, Taguig, Metro Manila, Philippines 1631*
[4] *Standards and Testing Division, Industrial Technolgy Development Institute, Department of Science and Technology (DOST-ITDI), Bicutan, Taguig, Metro Manila, Philippines 1631*
[5] *National Metrology Division, Industrial Technolgy Development Institute, Department of Science and Technology (DOST-ITDI), Bicutan, Taguig, Metro Manila, Philippines 1631*

Corresponding email: da6914@rit.edu

***Abstract* – Unsupervised anomaly detection provides a promising approach for the diagnostic evaluation of measurement data in laboratory quality systems. In this study, an Isolation Forest algorithm was applied to PFOS and PFOA migration measurements to identify atypical observations within a multivariate framework incorporating analyte type, analyst, and concentration regime. Out of 48 measurements, 5 observations (10.4%) were flagged as anomalous using a 10% contamination threshold. Anomalies were observed across all concentration regimes, with the highest frequency at the low concentration level, suggesting increased sensitivity to variability near detection limits. A pronounced analyst-dependent pattern was also identified, highlighting the role of intermediate precision in measurement variability. The results demonstrate that anomaly detection can serve as a useful diagnostic tool to support laboratory quality assurance and improve confidence in conformity assessment decisions.**

I. INTRODUCTION

Per- and polyfluoroalkyl substances (PFAS), including perfluorooctanoic acid (PFOA) and perfluorooctane sulfonate (PFOS), have attracted sustained regulatory and scientific attention due to their environmental persistence, bioaccumulation, and potential adverse health effects [1]–[4]. In the context of food-contact materials and packaging, migration testing of PFAS is central to demonstrating product safety and regulatory compliance. Consequently, laboratories performing such measurements operate under stringent quality systems that emphasize traceability, measurement uncertainty, and conformity assessment, as formalized in standards such as ISO/IEC 17025 and metrological guidance documents [5]–[7]. In routine practice, the evaluation of migration measurement data remains largely anchored in descriptive statistics—means, standard deviations, and repeatability/reproducibility estimates [8]. While indispensable, these summaries can obscure atypical measurement behavior arising from interactions among analyte properties, concentration regimes, and analyst-dependent effects. Such behavior, even when not attributable to gross error, is metrologically relevant because it can influence decision outcomes near regulatory limits, thereby affecting the risks of false compliance or false non-compliance. Contemporary measurement science has therefore emphasized complementing classical summaries with diagnostic analyses that make the structure of variability explicit and interpretable within an

uncertainty-aware framework [9]–[12].

For PFAS migration testing in particular—an area of growing regulatory importance—the literature is dominated by analytical method development, occurrence studies, and risk assessment, with comparatively less attention to data-centric diagnostics that support laboratory quality assurance. There is thus a clear need for approaches that leverage statistical learning to augment (not replace) established measurement-science practices by highlighting atypical behavior in a transparent, reproducible manner. In this study, we introduce an unsupervised anomaly detection framework for PFOS and PFOA migration measurements obtained under typical laboratory conditions. The approach employs Isolation Forest–based statistical learning applied to a multivariate representation of the data, incorporating analyte identity, concentration regime, analyst, and measured migration concentration. In contrast to conventional outlier rejection, the method is used diagnostically to flag measurements exhibiting atypical behavior relative to the ensemble, thereby prompting metrological review. The anticipated advantages are threefold: (i) label-free operation without predefined thresholds, (ii) sensitivity to multivariate interactions among measurement factors, and (iii) traceability-compatible transparency, enabling integration into quality systems and conformity assessment workflows.

II. MATERIALS AND DATA DESCRIPTION

A. Measurement context and measurand definition

The dataset analyzed in this study consists of laboratory-generated measurements of surface migration of perfluorooctanoic acid (PFOA) and perfluorooctane sulfonate (PFOS). The measurand is defined as the mass of analyte per unit contact area, expressed in ng/100 cm², determined under controlled experimental conditions representative of routine migration testing for food-contact materials. From a metrological perspective, each reported value represents the outcome of a measurement process influenced by multiple sources of variability, including analyte-specific behavior, sample preparation, instrumental response, and analyst-dependent effects. Consistent with the principles outlined in the Guide to the Expression of Uncertainty in Measurement [13], the observed dataset is therefore treated as a set of measurement results (an ensemble) rather than deterministic values, enabling the analysis of variability structure and identification of atypical behavior. The measurements were produced within a laboratory quality system aligned with ISO/IEC 17025, where traceability is maintained through calibrated instrumentation and standardized analytical procedures. However, as in many routine laboratory datasets, explicit uncertainty budgets for individual measurements are not directly embedded in the dataset, motivating the use of data-driven diagnostic approaches to complement traditional quality assurance practices.

B. Dataset structure and experimental factors

The dataset comprises 48 individual measurements structured across multiple experimental factors relevant to laboratory variability and measurement performance. These factors include the analyte, consisting of two PFAS compounds (PFOA and PFOS), the analyst, represented by three independent laboratory operators (ASLC, HEA, and WPA), and the concentration regime, categorized into three levels corresponding to low (L), medium (M), and high (H) surface migration conditions. Within each analyte–regime combination, replicate measurements were performed, typically in triplicate, to enable the assessment of repeatability under controlled conditions. Each observation is associated with a sample code (e.g., L1, M2, H3), which encodes both the concentration regime and the replicate index. This coding scheme reflects common laboratory practice, where replicate measurements are organized within predefined concentration levels to evaluate measurement consistency and method performance. The dataset exhibits a partially balanced structure. Low-level measurements are available for two analysts (ASLC and HEA), whereas medium- and high-level measurements are available for all three analysts. While this introduces a degree of imbalance, it remains suitable for evaluating both within-regime variability and between-analyst effects, which are critical components of laboratory quality assurance and intermediate precision assessment. From a metrological standpoint, this structure enables the dataset to be interpreted as a multilevel representation of measurement variability, supporting subsequent analysis of atypical behavior using unsupervised methods.

C. Summary of dataset characteristics

Table 1 summarizes the key characteristics of the dataset, including factor levels and total observations.

Table 1. Summary of PFOS and PFOA migration measurement dataset

Variable	Description
Analytes	PFOS, PFOA
Concentration Level	Low (L), Medium (M), High (H)
Analysts	Multiple analysts
Replicates	Repeated measurements per condition
Response Variable	Concentration (ng/100 cm²)
Data Structure	Paired PFOS–PFOA observations per replicate

Given the multivariate structure of the measurement ensemble and the lack of explicit decision

thresholds, the dataset is well-suited for unsupervised statistical analysis aimed at identifying atypical measurement behavior, as detailed in Section 3.

D. Metrological interpretation of the dataset

Within the context of measurement science, the dataset can be interpreted as a multivariate realization of a measurement system, where each observation reflects the combined influence of controlled experimental conditions and stochastic variability. The inclusion of multiple analysts introduces a component analogous to intermediate precision, while replicate measurements within concentration regimes provide information on repeatability. Importantly, the dataset does not include predefined labels for acceptable or unacceptable results, nor does it incorporate explicit decision thresholds. This reflects realistic laboratory scenarios, where conformity assessment often depends on external regulatory criteria and contextual interpretation. Consequently, the dataset is well-suited for unsupervised analytical approaches, in which atypical observations are identified relative to the internal structure of the data rather than external classification rules. In this study, the dataset is treated as a measurement ensemble embedded in a multivariate feature space, where concentration values are considered jointly with categorical factors (analyte, analyst, and regime). This representation enables the application of unsupervised anomaly detection methods to identify measurements that deviate from expected patterns of variability, thereby supporting diagnostic evaluation within laboratory quality assurance systems.

III. METHODS

A. Data representation and preprocessing

To enable multivariate analysis, each measurement was represented as a feature vector incorporating both numerical and categorical information. The primary numerical variable is the measured migration concentration $\boldsymbol{x}$ (ng/100 cm²), while categorical variables include analyte type (PFOA, PFOS), analyst identity (ASLC, HEA, WPA), and concentration regime (L, M, H). Categorical variables were encoded using integer label encoding to preserve discrete class identity without imposing artificial ordering assumptions in the modeling stage. Prior to analysis, all features were standardized to zero mean and unit variance to ensure that no single variable dominated the anomaly detection process due to differences in scale. The standardized feature vector for each observation **i** is therefore expressed as:

$$z_i = \frac{x_i - \mu}{\sigma} \quad (1)$$

where $\boldsymbol{x_i}$ is the original feature vector, and $\boldsymbol{\mu}$ and $\boldsymbol{\sigma}$ denote the vector of feature-wise means and standard deviations, respectively. This preprocessing step is consistent with multivariate statistical practice and ensures comparability across measurement dimensions.

B. Isolation Forest for unsupervised anomaly detection

Unsupervised anomaly detection was performed using the Isolation Forest (iForest) algorithm, a tree-based ensemble method designed to isolate anomalous observations through recursive partitioning [14], [15]. Unlike distance- or density-based approaches, Isolation Forest directly exploits the principle that anomalous points are more susceptible to isolation and therefore require fewer partitioning steps. Each tree in the ensemble is constructed by randomly selecting a feature and a split value within the feature range, recursively partitioning the data until each observation is isolated. The number of splits required to isolate an observation corresponds to its path length, denoted as h(x). For a dataset of size n, the expected path length for a normal observation approximates:

$$c(n) = 2H(n-1) - \frac{2(n-1)}{n} \quad (2)$$

where $H(n)$ is the harmonic number. The anomaly score for an observation $\boldsymbol{x}$ is then defined as:

$$s(x,n) = 2^{-\frac{E[h(x)]}{c(n)}} \quad (3)$$

where $E = [h(x)]$ is the average path length across all trees. Values of $s(x,n)$ approaching 1 indicate anomalous observations, while values closer to 0.5 or below correspond to normal data points. In this study, the Isolation Forest output was interpreted in terms of a decision function, producing a continuous anomaly score and a binary diagnostic classification (normal vs. anomalous). Importantly, this classification is used strictly for diagnostic purposes and not as a basis for data exclusion.

D. Model parameterization and metrological justification

The Isolation Forest model was implemented with a fixed set of parameters to ensure reproducibility and stability of the anomaly detection results. In particular, the ensemble consisted of 500 trees, with a contamination rate of 0.10, and a fixed random initialization to allow consistent comparison of outputs. A relatively large ensemble size was selected to ensure stable estimation of the average path length, which underpins the anomaly scoring mechanism. Given the modest dataset size (n = 48), increasing the number of trees reduces variance in the estimated scores and improves the robustness of the diagnostic outcome. This choice is consistent with established practices in ensemble learning, where stability is prioritized over computational efficiency, particularly in

small-sample analytical contexts. The contamination parameter, which specifies the expected proportion of anomalous observations, plays a central role in determining the threshold for binary classification. A value of 10% was adopted as a pragmatic and metrologically defensible choice. From a quality assurance perspective, it is reasonable to assume that a limited fraction of measurements may exhibit atypical behavior due to a combination of procedural variability, instrumental effects, and analyst-dependent factors. At the same time, the selected value provides a conservative diagnostic balance, ensuring sufficient sensitivity to identify potentially anomalous observations without excessive flagging of normal variability. For the present dataset, comprising 48 observations, a contamination rate of 10% corresponds to approximately four to five flagged measurements. This scale is appropriate for exploratory diagnostic analysis, allowing the identification of atypical behavior while minimizing the risk of overfitting or overinterpretation. It is important to emphasize that this parameter does not imply prior knowledge of erroneous or defective measurements; rather, it establishes a screening threshold for identifying observations that may warrant further metrological review within the laboratory quality system.

E. Role of anomaly detection in quality assurance and conformity assessment

In the context of this study, anomaly detection is not employed as a criterion for rejecting measurement results. Rather, it functions as a diagnostic support tool within laboratory quality systems. Observations flagged as anomalous are interpreted as candidates for further investigation, which may include the review of sample preparation procedures, instrument performance, calibration status, and analyst-specific practices. This approach is consistent with fundamental metrological principles, in which the integrity of measurement data is preserved and interpretation is guided by traceability and uncertainty considerations rather than automated exclusion.

IV. RESULTS AND DISCUSSIONS

A. Overview of anomaly detection results

The application of the Isolation Forest algorithm to the PFOS and PFOA migration dataset resulted in the identification of 5 anomalous observations out of a total of 48 measurements, corresponding to an anomaly rate of 10.4%. This proportion is consistent with the predefined contamination parameter and reflects the intended role of the method as a screening tool for identifying potentially atypical measurement behavior. The anomaly scores exhibited a clear separation between the majority of observations and a small subset of measurements characterized by shorter average path lengths, indicating higher susceptibility to isolation. This behavior confirms that the dataset contains a limited number of observations that deviate from the dominant multivariate structure defined by analyte type, concentration regime, and analyst. Importantly, the detected anomalies are not interpreted as erroneous measurements. Instead, they represent statistically atypical observations relative to the internal structure of the dataset, thereby serving as candidates for further metrological review. To provide a consolidated overview of the anomaly detection results across different factors, the distribution of anomalous observations is summarized in Table 2.

Table 2. Summary of anomaly detection results across analytes, analysts, and concentration

Category	Total Observations	Anomalies	(%)
Overall	48	5	10.4
Analyte			
PFOA	24	3	12.5
PFOS	24	2	8.3
Concentration Regime			
Low (L)	12	3	25.0
Medium (M)	18	1	5.6
High (H)	18	1	5.6
Analyst			
ASLC	18	1	5.6
HEA	18	0	0.0
WPA	12	4	33.3

As shown in Table 2, anomalous observations are distributed across all concentration regimes, with the highest frequency observed at the low concentration level. This pattern suggests that atypical measurement behavior is not restricted to a specific concentration range, but may arise from a combination of analytical and operational factors. The distribution of anomaly scores and the separation between normal and anomalous observations are illustrated in Figure 1.

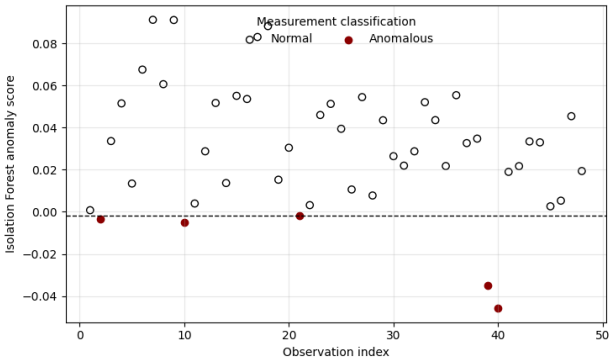


Figure 1. Distribution of Isolation Forest anomaly scores for PFOS and PFOA migration measurements. The dashed line represents the decision threshold corresponding to the

lowest 10% of anomaly scores. Observations classified as anomalous exhibit lower scores, indicating greater susceptibility to isolation within the ensemble model.

B. Distribution of anomalies across analytes and analysts

The distribution of anomalous observations across analytes and analysts provides insight into potential sources of variability. As shown in Figure 1, anomalous observations are distinctly separated from the main cluster of measurements, exhibiting lower anomaly scores that reflect their increased susceptibility to isolation within the ensemble model. This separation indicates that the method is able to identify a subset of measurements that deviate from the dominant multivariate structure of the dataset. Of the five detected anomalies, three were associated with PFOA and two with PFOS, indicating that atypical behavior is not analyte-specific but is more likely associated with measurement conditions or operational factors. This suggests that the anomalies are more likely linked to measurement conditions or operational factors rather than intrinsic chemical differences between PFOS and PFOA. A more pronounced pattern is observed when considering analyst-related effects. Four out of the five anomalous measurements were associated with a single analyst (WPA), while one anomaly was observed for analyst ASLC and none for analyst HEA. This concentration of anomalies suggests the presence of analyst-dependent variability, which may arise from differences in sample handling, procedural execution, or instrument interaction. From a quality assurance perspective, this finding is significant. While it does not imply systematic error or non-compliance, it highlights the importance of intermediate precision assessment and targeted review of analyst-specific practices. In particular, anomaly detection provides a means of identifying subtle deviations that may not be evident through conventional repeatability metrics alone.

C. Influence of concentration regime on anomalous behavior

The distribution of anomalous observations across concentration regimes is illustrated in Figure 2.

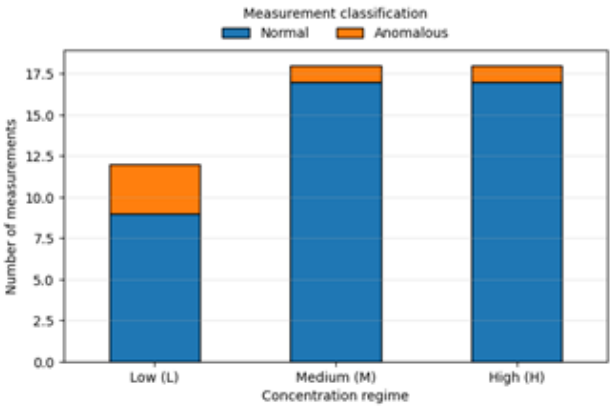


Figure 2. Distribution of normal and anomalous PFOS and PFOA migration measurements across concentration regimes. Anomalous observations are observed across all regimes, with the highest frequency at the low concentration level, indicating that atypical measurement behavior is not restricted to a specific concentration range.

The distribution of anomalous observations across concentration regimes reveals a distinct pattern. As summarized in Table 2 and illustrated in Figure 2, three of the five anomalous observations are associated with the low concentration regime, while one anomaly is observed in the medium regime and one in the high regime. This distribution indicates that atypical measurement behavior is not confined to higher concentration levels, but is instead present across the full measurement range. The higher frequency of anomalies at the low concentration level may reflect increased sensitivity to variability under conditions where signal levels are closer to detection limits, potentially amplifying the influence of background noise, minor procedural deviations, or instrumental fluctuations. At the same time, the presence of anomalies in the medium and high regimes suggests that atypical behavior may arise from a combination of factors rather than a single dominant source. From a metrological standpoint, these observations highlight the importance of evaluating measurement performance across the entire dynamic range of the method. The results suggest that variability and atypical behavior should be assessed not only at elevated concentrations, but also under low-level conditions that are often critical for compliance with regulatory limits.

V. CONCLUSIONS

This study demonstrates the applicability of unsupervised anomaly detection for the diagnostic evaluation of PFOS and PFOA migration measurements in a laboratory setting. Using an Isolation Forest approach, 5 anomalous observations out of 48 measurements (10.4%) were identified, providing a quantitative basis for detecting atypical measurement behavior within a multivariate framework. The results show that anomalous observations are distributed across analytes and concentration regimes, rather than being confined to a specific condition. In particular, the concentration of anomalies at the low concentration level (3 out of 5) highlights the importance of evaluating measurement performance near detection limits, where variability may be more pronounced. In addition, the presence of analyst-dependent patterns, with the majority of anomalies associated with a single analyst, underscores the relevance of intermediate precision in laboratory quality assessment. From a metrological perspective, the findings confirm that anomaly detection can serve as an effective screening and diagnostic tool,

complementing traditional statistical approaches without replacing established validation and uncertainty evaluation procedures. By identifying atypical observations without imposing rigid exclusion criteria, the method supports transparent data evaluation, targeted quality control interventions, and improved confidence in conformity assessment decisions.

REFERENCES

[1] V. Polychronidou and R. Nag, "Human health risk assessment of Per- and polyfluoroalkyl substances (PFAS)," *Sci. Total Environ.*, vol. 1000, p. 180428, 2025, doi: https://doi.org/10.1016/j.scitotenv.2025.180428.

[2] H. Pezeshki, S. Rajabi, M. Hashemi, S. Moradalizadeh, and H. Nasab, "Per- and poly-fluoroalkyl substances as forever chemicals in drinking water: Unraveling the nexus with obesity and endocrine disruption – A mini review," *Heliyon*, vol. 11, no. 4, p. e42782, 2025, doi: https://doi.org/10.1016/j.heliyon.2025.e42782.

[3] E. J. Itumoh, S. Data, J. L.-Y. Chen, M. Kah, L. P. Padhye, and E. M. Leitao, "Addressing the persistence of per- and poly-fluoroalkyl substances (PFAS): current challenges and potential solutions," *RSC Sustain.*, vol. 2, no. 11, pp. 3183–3201, 2024, doi: 10.1039/D4SU00152D.

[4] M. Chang *et al.*, "Perfluorooctane Sulfonate (PFOS) and Perfluorooctanoic Acid (PFOA) in the Surface Waters of China: A Meta-Analysis," *Water*, vol. 17, no. 9. p. 1275, 2025. doi: 10.3390/w17091275.

[5] F. S. H. Krismastuti and M. H. Habibie, "Complying with the resource requirements of ISO/IEC 17025:2017 in Indonesian calibration and testing laboratories: current challenges and future directions.," *Accredit. Qual. Assur. J. Qual. Comp. Reliab. Chem. Meas.*, vol. 27, no. 6, pp. 359–367, 2022, doi: 10.1007/s00769-022-01523-w.

[6] J. Monteiro Bastos da Silva, J. Chaker, A. Martail, J. Costa Moreira, A. David, and B. Le Bot, "Improving Exposure Assessment Using Non-Targeted and Suspect Screening: The ISO/IEC 17025: 2017 Quality Standard as a Guideline.," *J. xenobiotics*, vol. 11, no. 1, pp. 1–15, Jan. 2021, doi: 10.3390/jox11010001.

[7] S. Ellison and K. Tsimillis, "ISO/IEC 17025:2017 – First impressions," *Eurachem*, 2017. https://www.eurachem.org/index.php/news/newsarts/230-nws-iso17025-2017 (accessed Apr. 27, 2026).

[8] G. Simonetti *et al.*, "Studies of Potential Migration of Hazardous Chemicals from Sustainable Food Contact Materials," *Foods*, vol. 13, no. 5. p. 645, 2024. doi: 10.3390/foods13050645.

[9] C. H. H. Parimala, P. S. Varma, R. S. Kumar, A. R. Singh, B. Mohapatra, and H. K. Addis, "Uncertainty aware hybrid learning framework for fast and safe charging of lithium-ion batteries using multi-fidelity observers," *Sci. Rep.*, vol. 16, no. 1, p. 2452, 2026, doi: 10.1038/s41598-025-31976-1.

[10] E. Knar, "Integrating Scientific Readiness and Added Scientific Value: A Multiplicative Conceptual Model for Research Assessment," *Publications*, vol. 13, no. 4. p. 57, 2025. doi: 10.3390/publications13040057.

[11] X. Wang, Y. Fan, M. Yu, and F. Yuan, "Uncertainty-aware feature-weighted ensemble framework for heart disease prediction," *Sci. Rep.*, vol. 16, no. 1, p. 13321, 2026, doi: 10.1038/s41598-026-42419-w.

[12] M. Şengöz, "A Comparative Analysis of Classical Statistics and Data Science in Academic and Scientific Research TT - Akademik ve Bilimsel Araştırmalarda Klasik İstatistik ve Veri Bilimi Üzerine Mukayeseli Bir Analiz," *Eğitim ve Toplum Araştırmaları Derg.*, vol. 12, no. 2, pp. 263–289, 2025, doi: 10.51725/etad.1617560.

[13] Joint Committee for Guides in Metrology, "Guide to the expression of uncertainty in measurement." 2023. [Online]. Available: https://www.bipm.org/documents/20126/2071204/JCGM_GUM-1.pdf

[14] S. Wang, Z. Zhou, and H. Tian, "Improved Isolated Forest Algorithm and Application," in *2025 5th International Symposium on Computer Technology and Information Science (ISCTIS)*, 2025, pp. 104–108. doi: 10.1109/ISCTIS65944.2025.11064997.

[15] J. Gao, K. Ozbay, and Y. Hu, "Real-time anomaly detection of short-term traffic disruptions in urban areas through adaptive isolation forest," *J. Intell. Transp. Syst.*, vol. 29, no. 3, pp. 269–286, May 2025, doi: 10.1080/15472450.2024.2312809.

2026 IMEKO Joint Conference
TC8 - TC11 - TC24
Metro Manila, Philippines, August 26-29, 2026

Temporal studies on polyethylene's total UV-absorbing contaminants migrating to fatty and oily foods at refrigeration and ambient temperatures

Rizel Marie S.M. Ting[1], Elyson Keith P. Encarnacion[1], Anne C. Alcantara[1], Agaseve F. Del Rosario[1], Josefino Antonio T. Mendoza[1], David J. Alcarde Jr.[1], Winnie P. Alejandro[1], Jeric B. Bañadera[1]

[1] *Department of Science and Technology - Industrial Technology Development Institute (DOST-ITDI), General Santos Avenue, Bicutan, Taguig City, 1631, rizelting7@gmail.com*

ABSTRACT

Domestic households subject food and its packaging to diverse conditions, resulting in variable time-temperature exposures that differ from controlled laboratory settings. Because product-packaging surface interactions permit chemical migration, this study explores the effects of varying extraction times on a polyethylene (PE) sample made in contact with a fatty and oily food simulant at ambient (22-28 ºC) and refrigeration (0-5 ºC) temperatures. Sample PE-0009 was exposed to the intended product type and temperature conditions from 0.50 to 24 hours. Data analysis was conducted using the Shapiro-Wilk test to assess the normality of the dataset, resulting in a normally distributed data. Statistical analyses, additive two-way ANOVA and linear regression, were employed to evaluate significant differences between the absorbance units (AU) obtained under two temperatures at seven time-points. It was concluded that temperature did not significantly change AU throughout immersion times. While this suggests short-term thermal and structural stability of the sample, factor expansions are recommended to further strengthen claims and conclusions. This underscores that the Philippines' safety regulations on food packaging must be reinforced for consumer protection.

I. INTRODUCTION

Food packaging practices in the Philippines have been shaped by consumer accessibility and convenience. As a result, reliance on polyethylene (PE) plastic *labo* for food storage and distribution is seen in households and stores such as wet markets, *carenderias*, and street food stalls [1, 2]. Common food products contained are fatty and oily foods (e.g., raw fish and meat, beef stew known as *pares*, and deep-fried street foods) that are subjected to diverse time-temperature conditions.

Literature has shown that the structural integrity of polymers is preserved through the addition of intentionally added substances (IAS) such as plasticizers, additives, and antioxidants [3]. However, IAS could degrade and form products called non-intentionally added substances (NIAS) [3, 4] that result in potential toxicity, including carcinogenic and mutagenic effects [5, 6]. The migration of NIAS into food products poses consumer health risks, particularly through the exposure of food contact materials and articles (FCMs and FCAs) to prolonged contact time and varying temperatures.

Developed international standards and regulations for FCMs and FCAs are currently in place, including regulation (EU) No. 10/2011, US 21 Code of Federal Regulation (CFR) Part 170 to 199, China GB Standards, and JETRO 2009 [4, 7, 8, 9]. These standards are designed to encompass food quality, public health, and trade governance through the implementation of overall migration limits (OML) and specific migration limits (SML) on contaminants found in FCMs and FCAs. In the Philippines, the issuance of Circular No. 2022-0011 [10] strengthens the Republic Act No. 10611 or the Food Safety Act of 2013 [11] in implementing voluntary certification. While existing guidelines provide a foundation for safety assessment, reliance on voluntary testing may not ensure comprehensive compliance, highlighting the potential need for a shift to more stringent regulatory frameworks. Building evidence-based policy could be possible through recent studies in local FCMs and FCAs, comprising the assessment of total UV-absorbing contaminants (TACs) and total residual contaminants (TRCs) in monolayered PE/PP samples to fatty and oily [2, 12, 13], alcoholic [1, 13, 14], and aqueous foods [13, 15], and specific migrants to paper and paperboard packaging [16], among others.

Despite the expanding studies on chemical migration in food packaging, there is a lack of localized research

focusing on chemical migration that mimics the Philippine practices of storage and distribution. International standards provide methods for evaluating migration and material safety, but their applicability in local contexts remains untouched. In addressing these concerns, the Department of Science and Technology - Industrial Technology Development Institute (DOST - ITDI) and the FDA Philippines collaborate for the generation of data and research-to-policy advocacy. As such, the study intends to explore the assessment of TACs in monolayered PE samples in contact with fatty and oily foods subjected to time-temperature variations, determining their respective effects. It is the initial investigation of the migration of absorbing contaminants through the application of local practices, distinguishing from recent published studies locally. It will follow a non-targeted analysis, providing a basis for subsequent research, such as selective analysis of specific compounds (e.g., PFAS, phthalates, and bisphenols), microplastics analysis, and exposure assessment.

II. METHODOLOGY

A. Sample Selection and Preparation

The third lowest AU reading among the profiled samples from previously generated data [2] was selected as the sample. PE-0009 from Valenzuela City, obtaining an average of 0.049 AU, was considered the most suitable for the analysis due to its relatively low initial AU, availability, and quantity. Under conditions such as extended time and temperature, it is expected that a gradual rise in its AU will remain below 1.0 AU for reliable and optimal UV-Vis scanning.

B. Sample Extraction

Individual monolayered samples were measured and cut into 5 cm x 10 cm films, wiped with lint-free paper, and each placed in a 100 mL borosilicate glass reagent bottle. A 100 mL of n-Heptane was measured and added to each reagent bottle, ensuring the sample's total immersion. Reagent bottles were sealed with screw caps to prevent evaporation. All reagent bottles were then placed in a laboratory refrigerator (0-5 ºC) and a controlled environment at ambient temperature (22-28 ºC). Constant monitoring of environmental conditions was employed through the use of a thermohygrometer and thermocouple. After extraction, plastic films were removed using tweezers, and the extracting solutions were left to reach room temperature.

C. Preliminary Screening of Selected Sample

A UV-Vis Spectrophotometer (Shimadzu UV-1800), in the range of 220-360 nm, was used to analyze the extracting solutions. From the spectrum, the highest peak was recorded as the maximum absorbance. Seven time points were screened for both refrigeration and ambient temperature, with blanks and samples in duplicates (n = 2).

III. RESULTS AND DISCUSSION

A. Sample Comparison

Sample PE-0009 from Valenzuela City was previously profiled following the established criteria from the validation of modified 21 CFR Part 177 for fatty and oily foods [2]. The sample obtained an AU of 0.049 with a 9.6 %RSD. As the sample was used and depleted due to multiple analyses, another batch from the same location and retailer was purchased. Batches 1 and 2 were then subjected to the same conditions (25 ± 3 °C for 30 minutes) and obtained 0.034 and 0.072 AU, respectively. A decrease in the AU of batch 1 in a span of almost 8 months was observed (Table I). Without prior direct contact with a simulant, the absence of a receiving medium leads to the immobilization and loss of migrants in the FCMs and FCAs [17]. Gas-phase diffusion and condensation are also considered, as volatile compounds can be lost to the environment without direct food contact [18]. The presence of antioxidants or light stabilizers may have also delayed the onset of oxidative reactions and deterioration caused by heat [19], which may have contributed to the observed decline in TACs.

Table I. Comparison of Two Batches of the Same Sample.

Sample Code, Location	Batch	Average AU	%RSD	Date Analyzed
PE-0009, Valenzuela City	Batch 1	0.049	9.6	7 Oct 2024
	Batch 1	0.034	4.2	5 Jun 2025
	Batch 2	0.072	8.8	5 Jun 2025

In contrast to the decrease in AU from storage, the AU of batch 2 showed elevated TACs compared to batch 1. This can be attributed to batch-to-batch variability, especially in raw material sourcing and production from manufacturers. Variations in packaging are altered across production batches due to residual monomers and unintended impurities that contribute to measurable differences in migration [1]. Fluctuations in material content may result in higher observed migration and influence the structure of the polymer matrix that governs diffusivity. Polymers with lower crystallinity have more amorphous regions, making diffusion easier and more migration of additives and chemicals [20].

The variability observed in the migration behavior of both batches are attributed to the differing conditions and processes throughout production, storage, and distribution. Alterations in batch-specific quality control may either enhance diffusion or minimize measurable migration through volatilization and structural stabilization within the polymer matrix. Accordingly, these observations highlight the complexity of evaluating and interpreting migration data when considering real-world practices.

B. Comparison of a sample in different time points and temperatures

Analyzing PE-0009 from Valenzuela City at 7 time-points in ambient and refrigeration temperatures (Table II) produced a relatively small sample size. This allowed the selection of a well-suited assessment for the normality of the data, Shapiro-Wilk test, prior to statistical analysis. The test resulted in a p-value = 0.914 ($p > 0.05$) that suggests the differences between the two temperatures' AU, which did not significantly deviate from normality. This satisfied the parametric assumption, and the evaluation of the effects of 7 time-points and temperatures on AU values was conducted through an additive two-way ANOVA.

Table II. TACs of PE-0009 at 7 time-points in refrigeration and ambient temperatures.

Sample Code, Location, Batch	Time (Hour)	Average AU at Ambient (n = 2)	%RSD	Average AU at Refrigeration (n = 2)	%RSD
PE-0009, Valenzuela City, Batch 2	0.50	0.072	8.8	0.069	28.9
	1	0.053	1.3	0.077	31.4
	3	0.072	19.6	0.032	94.3
	4	0.086	18.1	0.070	10.2
	6	0.115	9.3	0.097	2.2
	12	0.063	27.2	0.066	41.0
	24	0.050	1.4	0.067	26.6

The analysis revealed that neither time nor temperature has a statistically significant effect on AU values ($p = 0.138$, $p = 0.592$). This suggests that there was no significant variation on TACs across time points and storage conditions. Induced modification in the molecular structure of the sample was not observed as short-term sample stability and possible manufacturing quality control were in place. Limited studies on plastic additives and antioxidants stability showed mixed results. While Simoneau and Hannaert [21] and Dopico-Garcia et al. [22] reported stability of selected additives and antioxidants at certain temperatures and simulants, some studies like Beldi et al.'s [23] demonstrated a migration increase. This proves that material composition stability is based on a multifaceted interactions, influenced by physicochemical properties of samples, simulants, and various handling and storage processes.

Additionally, a linear regression analysis (Fig. I) was conducted to characterize temporal behavior. It was deemed necessary to evaluate AU trends and changes over the storage duration as supplementary statistical approach. As such, the regression model for ambient temperature yielded a slope of -0.0009 ($R^2 = 0.124$, $p = 0.439$), indicating no statistically significant linear trend over time. This trend was similar to refrigeration temperature, with negligible slope at +0.0001 ($R^2 = 0.0005$, $p = 0.963$). AU values remained stable across all measured time points under refrigeration condition.

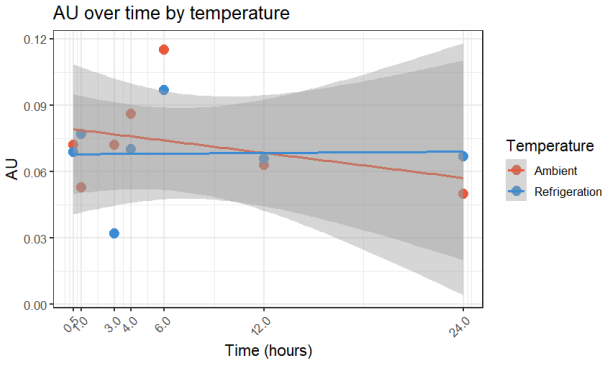


Fig. I. Linear Regression Analysis

However, the interpretation of the findings is subject to limitations that must be addressed. Observations of trends are restricted because of the limited number of samples, trials, and batch replicates. An expansion of these would capture the migration behavior of different samples and batches across various times and temperatures. Detailed information from manufacturers and retailers must be collected to account for the history of the materials, sample formulation, and other processes that may influence the compounds and additives present in the samples. Targeted based analysis (i.e., through Gas Chromatography-Tandem Mass Spectrometry/ GC-MS/MS, Liquid Chromatography Tandem Mass Spectrometry/ LC-MS/MS) is also recommended to identify specific migrants that could strengthen evidence-based data for policy recommendations.

While some international standards (i.e., US 21 CFR [7], JETRO 2009 [9], exporting country's regulation) are currently adopted by the voluntary certification of FCMs and FCAs in the Philippines [10], it is worth mentioning that not all FCMs and FCAs, contacting medium, and time, temperature, storage, handling, and distribution conditions would produce the same results using any or a combination of these standards. This statement was consistent across multiple studies, and one of which is the comparative analysis study of Armario et al. [12]. The two methods, US 21 CFR and JETRO 2009 through overall migration (TRCs), were deemed to be distinct in PE samples, having a significant difference in their average residues. Another recent study from Encarnacion et al. [13] determined that migration behavior is dependent on the nature of the simulants/foods, time, and temperature conditions in polypropylene (PP) microwavable containers. Lickly et al. [24], Goydan et al. [25], and Kang et al. [26], also confirmed that migration increases with different simulant, temperature, contact time, and composition of FCMs and FCAs.

As the Philippines experience a high year-round temperature and relative humidity due to its archipelagic location [27], it greatly influence migration kinetics and packaging performance. For instance, the US 21 CFR mimics room temperature at 21 ºC, while the typical ambient temperature in the Philippines is at around 25.5-28.3 ºC [27] depending on the season and location. Adopting international standards may underestimate actual migration occurring in the Philippine setting, considering the country's climate, abusive use of food packaging, food type, etc. With these factors mentioned, it is imperative for the local regulatory bodies and involved key actors to conclude and harmonize guidelines in such that would best fit the country's action to food and health safety.

IV. CONCLUSION

The study provides insight on the dynamic nature of PE when subjected to varying times and temperatures mimicking local practices in the Philippines. Through a series of statistical analyses, it was proven that the chemical migration between the datasets did not appear significant. Variations observed in AU were not affected by time and temperature but could be associated with the packaging's composition, storage, and production processes. Given the distinct climate of the Philippines, the adoption of international guidelines for local regulatory and storage implementations is not advisable. Locally generated, evidence-based data are therefore essential in aiming to provide research-to-policy recommendations that are appropriate and reflective of actual exposure conditions within the country.

V. REFERENCES

[1] A. K. M. Carlos, G. J. M. Manalo, E. K. P. Encarnacion, A. F. Del Rosario, J. A. T. Mendoza, A. C. Alcantara, W. P. Alejandro, and R. M. S. M. Ting, "Profiling of Total Residual Contaminants Migrating from Philippine-based Polyethylene Packaging to Fermented and Alcoholic Foods," *Curr. Res. Nutr. Food Sci. J.*, vol. 14, no. 1, pp. 460–476, 2010, doi: 10.12944/CRNFSJ.14.1.32.

[2] W. P. Alejandro, E. K. P. Encarnacion, A. C. Alcantara, D. J. Alcarde Jr., H. E. Armario, A. F. D. Rosario, and R. M. S. M. Ting, "Assessment of Total UV-Absorbing Contaminants in LDPE Food Packaging from Philippine Markets," *Curr. Res. Nutr. Food Sci. J.*, vol. 13, no. 2, pp. 913–925, Aug. 2025, doi: 10.12944/CRNFSJ.13.2.26.

[3] B. Habchi, A. Kassouf, Y. Padellec, E. Rathahao-Paris, S. Alves, D. N. Rutledge, J. Maalouly, and V. Ducruet, "An untargeted evaluation of food contact materials by flow injection analysis-mass spectrometry (FIA-MS) combined with independent components analysis (ICA)," *Anal. Chim. Acta*, vol. 1022, pp. 81–88, Aug. 2018, doi: 10.1016/j.aca.2018.03.042.

[4] *Commission Regulation (EU) No 10/2011 of 14 January 2011 on plastic materials and articles intended to come into contact with food Text with EEA relevance*, vol. 012. 2011. Accessed: May 07, 2026. [Online]. Available: http://data.europa.eu/eli/reg/2011/10/oj

[5] W. Meng, H. Sun, and G. Su, "Plastic packaging-associated chemicals and their hazards – An overview of reviews," *Chemosphere*, vol. 331, p. 138795, Aug. 2023, doi: 10.1016/j.chemosphere.2023.138795.

[6] P. Miralles, E. Fuentes-Ferragud, C. Socas-Hernández, and C. Coscollà, "Recent Trends and Challenges on the Non-Targeted Analysis and Risk Assessment of Migrant Non-Intentionally Added Substances from Plastic Food Contact Materials," *Toxics*, vol. 13, no. 7, p. 543, Jul. 2025, doi: 10.3390/toxics13070543.

[7] "CFR Part 170 -- Food Additives'. Accessed: May 07, 2026. [Online]. Available:https://www.ecfr.gov/current/title-21/part-170

[8] "China's National Food Safety Standard System:" Accessed: May 07, 2026. [Online]. Available: https://www.gbstandards.org/China_Food_Standards/#top

[9] "Japan Specifications, Standards and Testing Methods for Foodstuffs, Implements, Containers and Packaging, Toy, Detergents 2008" Accessed: May 07, 2026. [Online]. Available: https://www.dgav.pt/wp-content/uploads/2023/01/Japao-Spcs-standards-and-testing-methods.pdf

[10] "FDA Circular No.2022-0011|| Guidelines on the Application and Issuance of Voluntary Certification of Food Contact Articles (FCA) Used for Prepackaged Processed Food Products - Food and Drug Administration." Accessed: May 07, 2026. [Online]. Available: https://www.fda.gov.ph/fda-circular-no-2022-0011-guidelines-on-the-application-and-issuance-of-voluntary-certification-of-food-contact-articles-fca-used-for-prepackaged-processed-food-products/

[11] "Republic Act No. 10611" Accessed: May 07, 2026. [Online]. Available: https://icrs.gcg.gov.ph/files/ZwEcCjCRzf50gA3bTJnn.pdf

[12] H. Armario, E. K. Encarnacion, D. Alcarde Jr., A. Alcantara, W. Alejandro, A. Del Rosario, and R. M. Ting, "Preliminary Screening and Method Comparison of Total Residual Contaminants Migrating to Fatty and Oily Foods from Low-

Density Polyethylene (LDPE) Food Contact Articles Sold in the Philippines" *International Journal of Food Studies*, vol. 14, Jan. 22, 2026, doi: 10.7455//ijfs/14.01.2026.a6

[13] E. K. P. Encarnacion, S. M. J. M. Pukunum, M. J. F. Mantile, J. A. T. Mendoza, R. M. S. M. Ting, A. C. Alcantara, W. P. Alejandro, A. F. Del Rosario, and D. J. Alcarde Jr., "A Comparative Study on the Effects of Varying Simulants, Times, and Temperatures on the Total UV-Absorbing Contaminants Migrating from Philippine-based Microwavable Containers"*ACTA IMEKO*, In press

[14] A. C. Alcantara, J. T. Mendoza, V. Z. Tabao, E. K. P. Encarnacion, R. M. S. M. Ting, W. P. Alejandro, A. F. Del Rosario, and D. J. Alcarde Jr., "Structure-property-migration relaationships in polyethylene food packaging: FTIR classification, DSC crystallinity, and UV absorbing contaminants in ethanol simulants"*ACTA IMEKO*, In press

[15] R. M. S. M. Ting, E. K. P. Encarnacion, A. C. Alcantara, D. J. Alcarde Jr., H. E. Armario, W. P. Alejandro, A. F. Del Rosario, and A. S. L. Canonizado, "Method validation and profiling of total UV-absorbing contaminants migrating from monolayered low-density polyethylene used for aqueous foods in the Philippines", *Polyolefins J.*, vol. 12, no. 4, pp. 259–272, Oct. 2025, doi: 10.22063/poj.2025.35740.1367.

[16] E. K. P. Encarnacion, A. C. Alcantara, H. E. Armario, W. P. Alejandro, Z. Zhan, Z. Sun, and N. Lin, "Preliminary Screening of Per- and Polyfluoroalkyl Substances (PFAS) in Philippine Fast Food Packaging Using Liquid Chromatography–Mass Spectrometry (LC-MS) ", *Curr. Res. Nutr. Food Sci. J.*, vol. 12, no. 1, pp. 423–436, 2010, doi: 10.12944/CRNFSJ.12.1.34.

[17] R. K. Gupta, S. Pipliya, S. Karunanithi, G. M. Eswaran U, S. Kumar, S. Mandliya, P. P. Srivastav, T. Suthar, A. M. Shaikh, E. Harsanyi, and Bela Kovacs, "Migration of Chemical Compounds from Packaging Materials into Packaged Foods: Interaction, Mechanism, Assessment, and Regulations", *Foods*, vol. 13, no. 19, p. 3125, Jan. 2024, doi: 10.3390/foods13193125.

[18] P. Khokhar and K. Pawar, 'Chemical migration from packaging materials into consumable food matrices: A mini review', *Int. J. Agric. Food Sci.*, vol. 7, no. 1, pp. 21–25, 2025, doi: 10.33545/2664844X.2025.v7.i1a.233.

[19] J. H. Bridson, E. C. Gaugler, D. A. Smith, G. L. Northcott, and S. Gaw, "Leaching and extraction of additives from plastic pollution to inform environmental risk: A multidisciplinary review of analytical approaches", *J. Hazard. Mater.*, vol. 414, p. 125571, Jul. 2021, doi: 10.1016/j.jhazmat.2021.125571.

[20] D. J. Alcarde Jr., E. K. P. Encarnacion, A. C. Alcantara, H. E. Armario, A. F. Del Rosario, W. P. Alejandro, and R. M. S. M. Ting, "Gas Permeation as the Nexus of Food Safety and Sustainability in the Packaging Industry", J. Food Qual., doi: 10.1155/jfq/3278398

[21] C. Simoneau and P. Hannaert, "Stability testing of selected plastics additives for food contact in EU aqueous, fatty and alternative simulants", *Food Addit. Contam.*, vol. 16, no. 5, pp. 197–206, May 1999, doi: 10.1080/026520399284064.

[22] M. S. Dopico-Garcia, J. M. Lopez-Vilarino, and M. Gonzalez-Rodriguez, "Effect of temperature and type of food simulant on antioxidant stability", J. Applied Polymer Sci., doi: 10.1002/app.23391

[23] G. Beldì, S. Pastorelli, F. Franchini, and C. Simoneau, "Time- and temperature-dependent migration studies of Irganox 1076 from plastics into foods and food simulants", *Food Addit. Contam. Part A*, vol. 29, no. 5, pp. 836–845, May 2012, doi: 10.1080/19440049.2011.649304.

[24] T. D. Lickly, C. D. Bell, and K. M. Lehr, "The migration of Irganox 1010 antioxidant from high-density polyethylene and polypropylene into a series of potential fatty-food simulants," *Food Addit. Contam.*, vol. 7, no. 6, pp. 805–814, Nov. 1990, doi: 10.1080/02652039009373942.

[25] R. Goydan, A. D. Schwope, R. C. Reid, and G. Cramer, "High-temperature migration of antioxidants from polyolefins", *Food Addit. Contam.* vol. 7, no. 3, pp. 323–337, Apr. 1989, doi: 10.1080/02652039009373897

[26] K. Kang, Y. Chang, J. C. Choi, S. Park, and J. Han, "Migration Study of Butylated Hydroxytoluene and Irganox 1010 from Polypropylene Treated with Severe Processing Conditions", *J. Food Sci.* no. 4, pp. 1005–1010, Apr. 2018, doi: 10.1111/1750-3841.14104

[27]Philippine Atmospheric, Geophysical and Astronomical Services Administration (PAGASA), "Climate of the Philippines." DOST-PAGASA. Accessed: Jun. 8, 2026. [Online]. Available: https://www.pagasa.dost.gov.ph/information/climate-philippines

2026 IMEKO Joint Conference
TC8 - TC11 - TC24
Metro Manila, Philippines, August 26-29, 2026

Single-Laboratory Validation of a Spectrophotometric Method for the Quantitative Determination of Total UV-Absorbing Contaminants (as Bisphenol A) Migrating from Polyethylene Packaging to 8% Ethanol Food Simulant

Josefino Antonio T. Mendoza[1], Elyson Keith P. Encarnacion[1], Winnie P. Alejandro[1], Anne C. Alcantara[1], Harold E. Armario[1], David J. Alcarde Jr. [1], Agaseve F. Del Rosario[1], Rizel Marie S.M. Ting[1], Jeric B. Bañadera[1]

[1] *Department of Science and Technology, Industrial Technology Development Institute, Packaging Technology Division, General Santos Avenue, Bicutan, Taguig City, Metro Manila, Philippines, 1631, fin.mendoza19@gmail.com*

***Abstract* – Bisphenol A (BPA) is an industrial monomer widely used in polymer production to impart rigidity, transparency, and chemical resistance. The qualitative method developed by Alcantara was modified by converting TACs absorbance values into BPA concentrations through external calibration. Validation demonstrated a linear working range (R^2 = 0.9994), with an LOD of 0.0279 mg/kg and LOQ of 0.0931 mg/kg. Repeatability and trueness were satisfactory, with %RSD values ranging from 1.15% to 2.91% and mean recoveries between 97.437% and 104.528%, meeting performance criteria established by AOAC International. Ruggedness testing using polypropylene (PP) produced a mean recovery of 97.989% (%RSD = 1.42). Statistical analysis showed significant difference (p = 1.46 x 10-9) between the two polymers, indicating matrix-dependent effects and non-applicability of the method to PP. Although the method did not achieve the 0.001 mg/kg LOD for BPA referenced in European Commission Regulation (EU) 2024/3190, no criterion is currently established in the Philippine setting, supporting its use for PE films with BPA concentrations greater than 0.0279 mg/kg. Given these sensitivity limitations, higher order techniques such as GC–MS/MS or LC–MS/MS are recommended for trace-level determination and regulatory harmonization. Furthermore, inter-laboratory studies are proposed to evaluate reproducibility and strengthen method reliability.**

I. INTRODUCTION

The global expansion of plastic use is attributed to the growing demand of the market in packaging, construction, and automotive sectors among others. These are all fueled by a rapid increase in population and urbanization [1]. Polyethylene is a lightweight material, making it ideal for packaging and other applications where weight is a concern. This is further coupled by its great flexibility, elasticity, durability – for diverse shaping, chemical resistance, and electrical insulation, offering exceptional adaptability despite its affordability [2,3].

According to the World Bank Group, the Philippines contributed 2.3 billion USD to the plastic industry in 2018. For low- and middle-income households, single-use plastics provide essential low-cost goods [4]. This is supported by the data provided by Global Alliance for Incinerator Alternatives in 2019, revealing a daily consumption of approximately 45.2 million thin plastic bags [5] which are predominantly used on food-contact applications such as wrapping cooked foods, wet market products, and raw meat [6].

Given their widespread direct contact in food, concerns have been raised regarding their chemical safety, particularly the potential for contaminant migration. Previous studies have shown that absorbing contaminants can migrate from plastic bags such as polyethylene (PE) and polypropylene (PP) into a range of food simulants, including n-heptane, water, 20% ethanol, and 8% ethanol. Among these, the highest migration levels were consistently observed in fatty simulants such as n-heptane, reflecting the strong affinity of hydrophobic compounds for nonpolar media [7-11].

Bisphenol A (BPA) is a key industrial chemical utilized

as a fundamental monomer in the synthesis of polycarbonate plastics and epoxy resins to provide rigidity, transparency, and resistance [12]. Notably, due to its widespread use, BPA has the potential to inadvertently contaminate other consumer products during the manufacturing process [13,14] or through the production of plastics using recycled polyethylene terephthalate (PET) [15]. A kinetic migration study conducted by Xia and Rubino in 2015 shows that BPA could migrate from low-density polyethylene (LDPE) film to food [16]. In a related migration study, bisphenols were shown to migrate from PP-based woven bags into corn powder feed, demonstrating a potential route for BPA entry into food chain [17].

The study is a continuation of the validation study conducted by Alcantara et al. (2025) in determining the total absorbing contaminants in PE samples using 8% ethanol. Following this, the research aims to validate a proposed UV-Vis Spectrophotometry method for a rapid determination and quantification of total absorbing contaminants as Bisphenol A (BPA) migrating from polyethylene film samples to 8% ethanol, resembling slightly fermented and low-level alcoholic foods.

II. METHODOLOGY

A. *Materials*

Gravimetric approach was employed in the study. BPA stock solutions were prepared by dissolving 57.8 and 56.3 mg of the standard in 8% ethanol, yielding concentrations of 574.3 and 563.2 mg/kg, respectively. These were subsequently diluted to obtain working solutions of 10.1 and 57.9 mg/kg. Eight (8) calibration solutions, ranging from 0.06 to 3.50 mg/kg, were prepared from the 10.1 mg/kg working solution. Approximately 3.0 mg/kg quality control solution was prepared from the 57.9 mg/kg solution. Polyethylene (PE) samples sourced from Taguig market were cut into 5 x 10 cm dimensions and were placed in a clean container before further use.

B. *Extraction*

Extraction of BPA was carried out by transferring PE samples into 250 mL beakers. A 100 mL portion of 8% ethanol with accurately determined mass was added to each beaker. The beakers were covered with aluminum foil before incubation at 65.9 °C for two (2) hours. Thereafter, samples were removed from each beaker and the solutions were allowed to cool for 30 minutes to 1 hour before instrumental analysis.

C. *Ultraviolet-Visible Spectrophotometry Analysis*

The solutions were analyzed using a UV-Vis Spectrophotometer (Shimadzu Corporation). The spectrum was scanned between 220 nm and 360 nm. Nugroho et al. (2018) reported that bisphenol A absorbs light in the range of 200 - 300 nm [18]. The instrument performance was consistently monitored throughout the analysis through quality control measurements and drift checks.

D. *Method Validation*

Key performance characteristics were evaluated in the study. Linearity was assessed by constructing a curve using the eight (8) calibration solutions prepared. Limit of detection (LOD) and limit of quantification (LOQ) to assess the method's sensitivity, were determined by spiking samples at 0.35 mg/kg BPA concentration. Trueness and repeatability were determined using 10 replicates and performing recovery by spiking at low, mid, and high (0.35, 1.40, and 2.70 mg/kg, respectively) BPA concentration levels. Finally, ruggedness was assessed by applying the validated method to polypropylene (PP) samples in 10 replicates. Statistical analysis was done to evaluate the results. The equations for solving the following are as follows:

$$LOD = 3 \times \left(s \times \sqrt{\frac{1}{n1} + \frac{1}{n2}} \right) \quad (1)$$

$$LOQ = 10 \times \left(s \times \sqrt{\frac{1}{n1} + \frac{1}{n2}} \right) \quad (2)$$

$$\%\, RSD = \frac{s}{mean} \times 100 \quad (3)$$

where s is the standard deviation, n1 and n2 is equal to the number of routine sample blanks and routine sample replicates, respectively.

III. RESULTS AND DISCUSSION

A. *Linearity*

A calibration curve (y = 0.3078x - 0.0012) was established by plotting BPA concentration against absorbance at 224 nm, yielding an R^2 value of 0.9995, which meets the acceptance criterion of > 0.9900 [19,20]. Furthermore, a random distribution of residuals was observed from the residual plot indicating model adequacy [21]. This relationship was used to determine BPA concentration in the samples based on their measured absorbance [22].

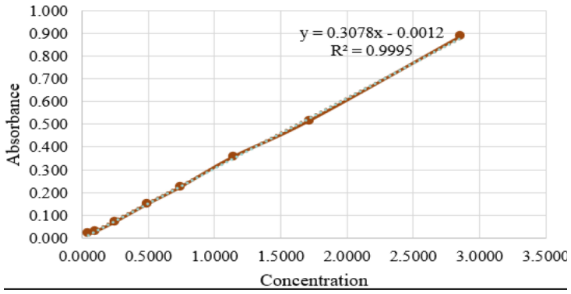


Fig 1. BPA concentration vs. absorbance at 224 nm

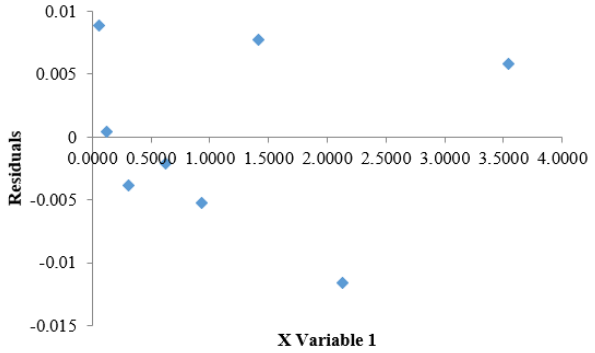


Fig 2. Residual plot of concentration vs. absorbance at 224 nm

B. *Limit of Detection and Limit of Quantification*

The LOD and LOQ of the analysis were determined to be 0.0279 and 0.0931 mg/kg, respectively. While the LOD does not meet the more stringent criterion set by EU Regulation 2024/3190 [23], it remains sufficiently sensitive for the intended analytical application. In the absence of locally established regulatory thresholds, these values provide a practical and reliable baseline for the detection and quantification of total absorbing contaminants as BPA in the Philippine context.

C. *Trueness and Repeatability*

Trueness and repeatability were evaluated at low, mid, and high BPA concentration levels. The low level yielded a mean recovery of 97.437% with a % RSD of 2.91. The mid-level showed a recovery of 104.528% and a % RSD of 1.15, while the high concentration level exhibited a recovery of 104.519% with a % RSD of 2.12%. All results satisfied the acceptance criteria established by AOAC guidelines.

A higher % RSD was observed at 2.70 mg/kg BPA concentration compared to 1.40 mg/kg, as opposed to commonly observed pattern of decreasing % RSD as concentration increases [19]. This increase in variability may be attributed to increased instrumental variability at higher absorbance values and minor deviations from the Beer-Lambert law [24,25]. In addition, matrix-related absorbance from co-extracted compounds in the polyethylene (PE) samples may have contributed to increased variability. However, due to sample inhomogeneity arising from manufacturing process, the distribution of these absorbing species may not be uniform across all replicates, leading to background contributions and inconsistent signal [25,26].

Recoveries exceeding 100% at the medium and high concentration levels indicate a slight systematic positive bias in the method. This may be explained by the presence of UV-active substances originating from the polyethylene matrix, the 8% ethanol food simulant, or trace background BPA contamination from laboratory materials and reagents. Because UV–Vis spectrophotometry measures the total absorbance of all compounds absorbing at the selected wavelength, these co-migrating or contaminating species may have contributed to the measured absorbance and been interpreted as BPA, resulting in apparent recoveries greater than 100%. These factors may explain the recoveries exceeding 100% despite identical experimental conditions among the concentration levels [10,19,20].

Nevertheless, the observed recoveries remained within the established acceptance criteria for method validation, indicating that the method demonstrates adequate accuracy and is suitable for the determination of BPA migration into the 8% ethanol food simulant [19].

D. *Ruggedness*

The preliminary validated method was applied to PP samples at the mid concentration level. The average % recovery was computed to be 97.989 with a % RSD of 1.42. An independent sample t-test was performed to compare the mean recoveries of BPA in PE and PP. The data satisfied normality (Shapiro-Wilk test, $p > 0.05$) and homogeneity of variances (F-test, $p > 0.05$). The results indicated a statistically significant difference between the mean recoveries in PE and PP ($p = 1.46 \times 10^{-9}$)

The findings support the matrix-dependent effect on extraction efficiency. PP, due to the presence of branching chains, has greater resistance to organic solvents and better hydrophobic properties [16,27,28]. Under the conditions employed, particularly with 8% ethanol as the extracting solvent, this behavior likely promotes preferential partitioning of BPA into the PP matrix at the concentration level investigated, resulting in reduced extraction efficiency and lower apparent recovery.

The observed matrix interference suggests that components co-extracted with the analyte may have influenced the analytical response under the extraction conditions employed. Since the study was designed to evaluate migration using 8% ethanol as the extraction medium, no modifications to the solvent composition or extraction temperature were investigated. Nevertheless, the findings indicate that extraction conditions may be an important factor to consider when interpreting matrix-related effects.

Table 2. Statistical analysis of BPA in PE and PP

Material	% Recovery	p-value	Remarks
PE	104.528	1.46 x 10-9	significant
PP	97.989		

IV. CONCLUSION

The study validated a method for the determination and quantification of total absorbing contaminants expressed

as Bisphenol A in PE samples using 8% ethanol as the food simulant. The method demonstrated a positive linear relationship between BPA concentrations and absorbances with an R^2 value of 0.9995. In addition, the method showed sufficient sensitivity with an LOD and LOQ of 0.0279 and 0.0931 mg/kg, respectively. Trueness and repeatability at low, mid, and high BPA concentration levels were all acceptable and within the criteria stipulated in AOAC 2016. Greater variability at high concentration level than the mid-level may be attributed to instrumental variability. In addition, recoveries exceeding 100% are attributed to matrix effects.

The validated method was applied to PP. Comparison of average recoveries of the two polymers showed that the method is not suitable for PP ($p = 1.46 \times 10^{-9}$). This is attributed to the difference in structure and properties of the two polymers, with PP exhibiting more branching and greater hydrophobicity property.

To meet the regulatory limit prescribed in the European Commission Regulation (EU) 2024/3190, further method development and optimization are recommended to enhance sensitivity and achieve lower detection limits. The use of certified reference materials (CRMs), when available, is also strongly recommended to minimize systematic bias during extraction and to improve trueness assessments. Furthermore, confirmatory analysis of bisphenol A (BPA) using advanced analytical techniques such as gas chromatography–tandem mass spectrometry (GC–MS/MS) and liquid chromatography–tandem mass spectrometry (LC–MS/MS) is encouraged to verify the presence of the analyte in the extracted solutions. As the present study focused on the use of 8% ethanol as the extraction medium, future investigations may examine the influence of alternative extraction solvents and extraction temperatures on analytical performance and matrix effects under different experimental conditions. Lastly, inter-laboratory comparison studies are recommended to evaluate method precision and reproducibility across different laboratory settings.

REFERENCES

[1] Straits Research "Plastic Market Size, Share, Trends & Forecasts by 2033." April 2026. https://straitsresearch.com/report/plastic-market.

[2] T. Kojnoková, F. Nový,L. Markovicová, T. Liptáková, "Changes of Mechanical Properties of Protective Polyethylene Films Applied in Transport Bottles and Containers for Liquid Media after Exposure to Selected Liquid Media" Transp. Res. Proc., 55, July 2021, pp. 731–736.

[3] J. Jordan, D. Casem, J. Bradley, A. Dwivedi, E. Brown, C. Jordan, "Mechanical Properties of Low-Density Polyethylene", J. dynamic behavior matter, 2, August 2016, pp. 411-420.

[4] World Bank Group, "Market Study for Philippines: Plastics Circularity Opportunities and Barriers", March 2021. https://www.worldbank.org/en/country/philippines/publication/market-study-for-philippines-plastics-circularity-opportunities-and-barriers-report-landing-page.

[5] Global Alliance for Incinerator Alternatives (GAIA), "Plastics Exposed: How Waste Assessments and Brand Audits Are Helping Philippine Cities Fight Plastic Pollution", 2019. www.no-burn.org.

[6] C. Beltran, "We're so plastic", Philstar Global, March 2019,https://www.philstar.com/opinion/2019/03/13/1900949/were-so-plastic

[7] W. Alejandro, E. Encarnacion, A. Alcantara, D. Alcarde Jr., H. Armario, A. Del Rosario, R. Ting, "Assessment of Total UV-Absorbing Contaminants in LDPE Food Packaging from Philippine Markets", Current Research in Nutrition and Food Science Journal, vol.13, No.2, May 2025.

[8] R. Ting, E. Encarnacion, A. Alcantara, D Alcarde Jr., H. Armario, W. Alejandro, A. Del Rosario, A. Canonizado, "Method Validation and Profiling of Total UV-Absorbing Contaminants Migrating from Monolayered Low-Density Polyethylene Used for Aqueous Foods in the Philippines." Polyolefins Journal, vol.12. No.4, October 2025, pp. 259-272.

[9] J. Mendoza, E. Encarnacion, M. Mantile, S. Pukunum, A. Alcantara, R. Ting, W. Alejandro, A. Del Rosario, D. Alcarde Jr., "Method Validation and Profiling of Total UV-absorbing Contaminants from Polyethylene to Alcoholic Foods in the Philippines using 20% Ethanol", Unpublished Results.

[10] A. Alcantara, E. Encarnacion, H. Armario, A. Del Rosario, Alcarde Jr., 2025, "Method Validation and Chemometric Analysis of UV-Absorbing Contaminant Migration from Low-Density Polyethylene Packaging Materials into 8% Ethanol.", Proc. of IMEKO World Congress, 2025, pp. 197-203.

[11] E. Encarnacion, W. Alejandro, R. Ting, A. Alcantara, A. Del Rosario, E. Dioso, D. Alcarde Jr., "Preliminary Assessment of Total UV-Absorbing Contaminants Migrating from Philippine-Based Microwavable Containers to Fatty / Oily Food Simulant Using Modified 21 CFR Part 177 Method.", Proc of IMEKO World Congress, pp. 204-209.

[12] S. Almeida, A. Raposo, M. Almeida-González, C. Carrascosa, "Bisphenol A: Food Exposure and Impact on Human Health." *Comprehensive Reviews in Food Science and Food Safety*, September 2018, vol.17, No.6, pp.1503–17.

[13] N. Ilaria, G. Russo, L. Grumetto, "Bisphenol A and Its Analogues: From Their Occurrence in Foodstuffs Marketed in Europe to Improved Monitoring Strategies—a Review of Published Literature from 2018 to 2023.", *Archives of Toxicology*, June 2024, vol.98, No.8, pp. 2441–61.

[14] D. Lim, S. Kwack, K. Kim, H. Kim, B. Lee,

"Potential Risk of Bisphenol A Migration from Polycarbonate Containers After Heating, Boiling and Microwaving", Journal of Toxicology and Environmental Health, Part A, December 2009, vol.72, No.21-22, pp. 1285-1291.

[15] B. Geueke, D. Phelps, L. Parkinson, J. Muncke. "Hazardous Chemicals in Recycled and Reusable Plastic Food Packaging.", Cambridge Prisms: Plastics, May 2023, vol.1, pp. 1–43.

[16] Y. Xia, M. Rubino, "Kinetic Study of Bisphenol A Migration from Low-Density Polyethylene Films into Food Simulants", Ind. Eng. Chem. Res., March 2015, vol.54, No. 14, pp. 3711-3716.

[17] R. Wang, Y. Huang, S. Dong, P. Wang, X. Su, "The Occurrence of Bisphenol Compounds in Animal Feed Plastic Packaging and Migration into Feed." Chemosphere, February 2021, vol. 265.

[18] B. Nugroho, Y. Pramudya, W. Widodo, "The Content Analysis of Bisphenol A (BPA) on Water in Plastic Glass with Varying Temperatures and Contact Times using UV-Vis Spectrophotometer", Indonesian Review of Physics, May 2019, vol.1, No.2.

[19] AOAC International, "Appendix F: Guidelines for Standard Method Performance Requirements", 2016.

[20] H. Cantwell Eurachem Guide, "The Fitness for Purpose of Analytical Methods", 3rd edition, 2025.

[21] W. Li, D. Cook, E. Tanaka, S. VanderPlas, "A Plot is Worth a Thousand Tests: Assessing Residual Diagnostics with the Lineup Protocol", Journal of Computational and Graphical Statistics, May 2024, vol.33, No.4.

[22] LibreTexts Chemistry, "Calibration Methods (Hunter). https://chem.libretexts.org/Ancillary_Materials/Worksheets/Worksheets%3A_Analytical_Chemistry_II/Calibration_Methods_(Hunter).

[23] European Union, "Commission Regulation (EU) 2024/3190 of 19 December 2024", December 2024.

[24] D. Skoog, D. West, J. Holler, S. Crouch, "Fundamentals of Analytical Chemistry", 10th edition, Cengage Learning, 2021.

[25] D. Harris, C. Lucy, "Quantitative Chemical Analysis", 11th edition, W.H. Freeman, 2025.

[26] P. Kamweru, F. Ndiritu, K. Thomas, Z. Muthui, R. Ngumbu, P. Odhiambo, "UV Absorption and Dynamic Mechanical Analysis of Polyethyelen Films', International Journal of Physical Sciences, December 2024, vol.9, No.24, pp. 545-555.

[27] A. Khoironi, H. Hadiyanto, S. Anggoro, S. Sudarno, "Evaluation of polypropylene plastic degradation and microplastic identification in sediments and Tambak Lorok coastal area, Semarang, Indonesia", Mar. Pollut. Bull., Feb 2020, vol.151.

[28] G. Braun, M. Krauss, B. Escher, "Recovery of 400 Chemicals with Three Extraction Methods for Low Volumes of Human Plasma Quantified by Instrumental Analysis and In Vitro Bioassays", Environ Sci Technol., November 2023, vol.57, No.48, pp. 19363-19373.

2026 IMEKO Joint Conference
TC8 - TC11 - TC24
Metro Manila, Philippines, August 26-29, 2026

Empirical Validation of Wringing Uncertainty Using Long-Service Gauge Blocks: Evidence-Based Replacement of Conservative Estimates in Calibration Budgets

Arvin Yan V. Pacia

Department of Science and Technology – Metals Industry Research and Development Center (DOST-MIRDC), Bicutan, Taguig City, 1631, Philippines, avpacia@dost.mirdc.gov.ph

***Abstract* - Accurate uncertainty quantification is vital for metrological traceability. This will provide a basis for empirically determined wringing errors in industrial steel gauge blocks that have been in use (i.e., 25-30 years), with an established empirical base to replace the traditional arbitrary values (0.20-0.50 microns) used today, and thereby enable calibration and measurement capability (CMC) claims that are inflated as much as 6.3 times when using conservatively determined values. The results of this study indicate that the average error per interface is 0.08 microns and therefore suggest that a 38-47 % reduction in CMC can be achieved for calibrations that serve the automotive, semiconductor, and metal fabrication industries. This methodology offers laboratories a validated approach to optimize uncertainty budgets, ensuring more competitive measurement capabilities while strictly adhering to ISO/IEC 17025 requirements and international standards.**

Keywords: Metrological Traceability, Calibration and Measurement Capability (CMC), ISO/IEC 17025, Wringing uncertainty, Uncertainty Budget optimization

I. INTRODUCTION

Measurement uncertainty assessment is a basic requirement of accreditation under ISO/IEC 17025 [1]. Laboratories performing calibration must determine all significant contributors to their total uncertainty, then evaluate and combine them to claim a Calibration and Measurement Capability (CMC). The NIST Gauge Block Handbook has identified wringing film thickness as a systematic contributor that must be quantified within the laboratory's uncertainty budget [2].

ISO-GUM, the International Organization for Standardization's Guide to the Expression of Uncertainty in Measurement, stresses that input quantities should be determined by means of actual measurement data instead of assumptions whenever possible [15]. Due to practical limitations, many calibration laboratories have adopted literature-based estimates or conservative assumptions when evaluating difficult-to-quantify uncertainty components, such as wringing film thickness.

Suga 2016 reported that wringing errors made by a novice and an expert when wringing gauge blocks were 0.04 – 0.02 microns, respectively, and that these results were obtained from the same new gauge block sets at ages 1 – 5 years [4]. The Philippine Accreditation Bureau (PAB) stated that during recent measurement audits, the most common estimate used by participating laboratories for wringing error ranged from 0.20 to 0.50 microns [1], although other calibration laboratories that offered similar services employed these values without empirical evidence to validate their accuracy.

There appears to be significant variability in how laboratories currently treat uncertainties related to wringing. Approximately sixty percent (60%) of laboratories utilize literature-based estimates of wringing uncertainties (i.e., 0.02 – 0.05 microns), thirty percent (30%) use conservative estimates (i.e., 0.10 – 0.50 microns), while ten percent (10%) actually measure wringing uncertainties. These differences between measured and estimated wringing uncertainties affect CMC claims, accredited scopes, and the outcomes of conformity assessments [11].

The use of gauge blocks in support of the maintenance of dimensional and length quality control in manufacturing, conducting applied R&D, calibrating length standards and instruments to achieve traceability to national standards, and creating and maintaining working physical reference length standards [5], [6] is supported through ISO 9001 certification and ISO/IEC 17025 accreditation. The reliability and traceability of measuring instruments are ensured through these activities. The gap between interferometric values

(~0.025 µm) and conservative Laboratory estimates (up to 0.50 µm) represents a 20-fold difference—directly impacting uncertainty budgets, CMC claims, and ultimately the Reliability of the dimensional measurement traceability chain from national standards to industrial applications.

Because of the degradation of the surface conditions of gauge blocks (such as the creation of scratches, dents, and corrosion stains) after being used for extended periods, the effectiveness of gauge blocks decreases in terms of wringing [7]. It is possible to correct this type of defect using Arkansas Stone; however, there is no guarantee that the wringing quality will be restored to its original state, as "sharp burrs" remain after deburring. Studies of gauge block wringing have shown that surface roughness may either decrease or increase after deburring [8].

This project aims to provide empirical measurements of wringing errors for aged gauge blocks, compare these empirical values with commonly used estimates, and provide guidance to assist laboratories in optimizing their uncertainty budgets in accordance with ISO/IEC 17025 requirements and enhancing metrological traceability to national standards.

II. METHODOLOGY

A. Materials and Experimental Design

The study quantified wringing error under realistic calibration laboratory conditions. Working-grade gauge blocks as seen on **Table 1** with extended service life (25-30 years) were evaluated using typical wringing procedures performed by calibration experts in a standard laboratory environment controlled per AS 1457 [12]. Surface roughness correction through deburring was implemented to minimize the influence of gauge block surface geometrical conditions accumulated during usage [7][8].

B. Equipment

Measurements utilized a GBCD-100A Automatic Gauge Block Comparator. The measuring probe measures central length, minimum length, and maximum length; however, only the measured central length was considered for this study. The comparative method of measurement compares the wrung Test Gauge Block Size Grade 0 with a standard "whole" steel gauge block with Grade 00 accuracy [12]. Surface assessment employed a Mitutoyo SJ-201 Surface Roughness Tester. Arkansas Stone was used for deburring gauge block surfaces before measurement.

C. Environmental Conditions

The study was conducted in a laboratory where environmental conditions were controlled at 20±1°C and 55±10% relative humidity as required by AS 1457 [12] using a precision air-conditioning unit. The ambient temperature fluctuation before and after each measurement was maintained within ±0.2°C only. No measurements were conducted outside the prescribed environmental conditions.

Table 1. Test configuration for wringing error evaluation

Nominal sizes	Test Gauge Block Combined Grade 0 in mm	Standard Gauge Block grade 00	Combined Gauge Block error in µm
12.9	10(SN949444)		
	1.5 (SN950614)	12.9 (SN.060501)	**-0.13**
	1.4 (SN940252)		
17.6	9 (SN944588)	17.6(SN 100170)	
	7 (SN944650)		**-0.07**
	1.6(SN 940295)		
20.2	8 (SN 945445)	20.2 (SN 100343)	
	6 (SN 946768)		
	3 (SN 940336)		**-0.26**
	2 (SN 950577)		
	1.2(SN 940356)		
22.8	20 (SN 044070)		
	1.7(SN 940857)	22.8 (SN 060210	**-0.04**
	1.1(SN 940114)		
75	40 (SN 943158)		
	30 (SN 943065)	75 (SN730166)	**-0.24**
	5 (SN 040788)		

D.. Measurement Procedure

The procedure comprised:

Surface preparation: Visual inspection, roughness measurement using Mitutoyo SJ-201, and deburring using Arkansas Stone as required (Figure1).

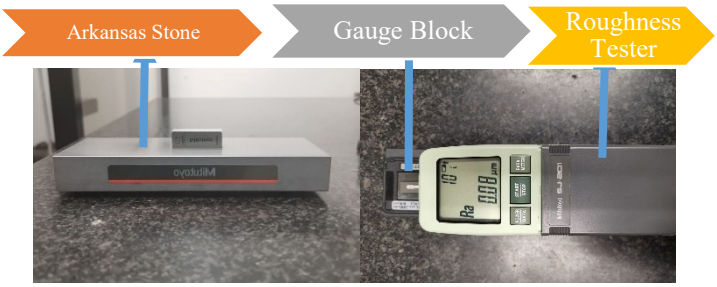


Fig 1. Surface preparation equipment: (a). Arkansas Stone for deburring ;(b)Mitutoyo SJ-201 Surface Roughness Tester

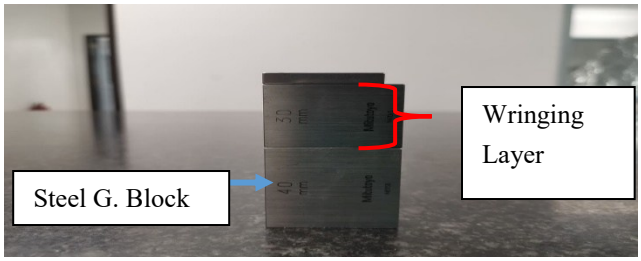


Fig 2. Combined Gage Block

Wringing: Ethyl alcohol medium directly applied on surfaces, standard sliding technique performed by a calibration expert Thermal stabilization: Wrung gauge blocks were stabilized for two hours before conducting the measurement to eliminate the effect of thermal expansion (Figure 2).

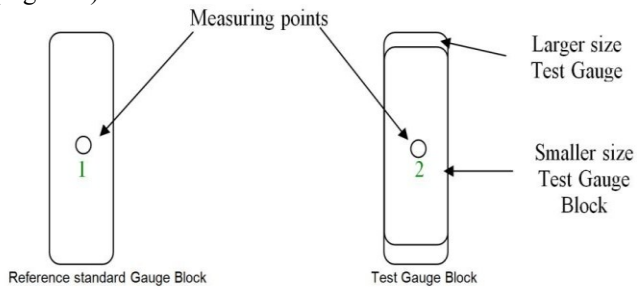


Fig 3. Measuring points of the standard and test Gauge Blocks. The comparative measurement method of GBCD-100A is governed by the following equation. The measured error at measuring point (2) is referred to as the central error of the wrung gauge block.

Measurement timing: Measurements started 30 minutes after wringing; succeeding trials were made every 3 minutes for ten trials per nominal size. Stability observation: Wrung test gauge blocks observed for 24 hours for stability to remain fixed gauge blocks were stabilized for 24 hours after cleaning and preparation before wringing [12], [13].

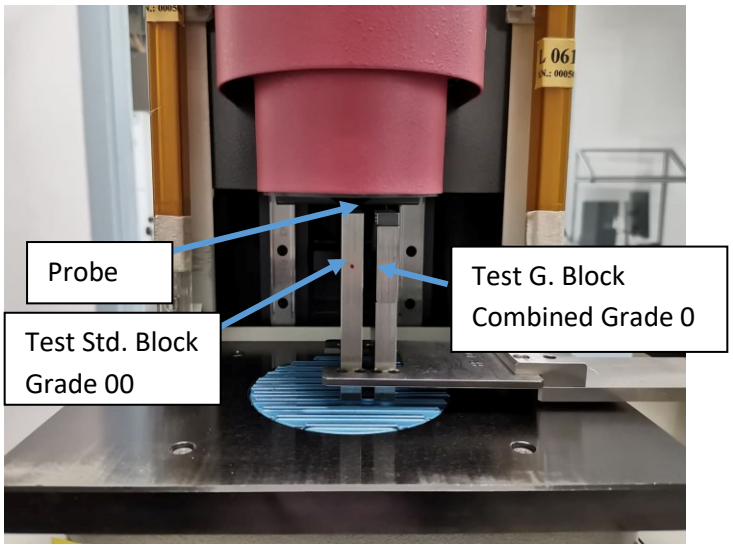


Fig 4. Set-up of measurement using Automatic Gauge Block Comparator. Gauge Blocks were stabilized for 24 hours after cleaning and preparation.

E. Wringing Error Calculation

Each test gauge block is a combination of several individual blocks wrung together. The comparator measures the central error of the whole stack relative to a single-piece (whole) standard block of the same nominal size. The total wringing contribution is therefore the difference between the measured central error of the combined stack and the sum of the individual blocks' calibrated errors:

Calculation of wringing error was done using Equation 1 shown below.

$$W_e = C_E - \sum_i^n = 1e^i \qquad (1)$$

Where:
W_e – Wringing error
C_E – Central error
∑ei - Combined Test Gauge Block Error
Computed wringing error in µm for the nth nominal size,

where the wringing error per interface is obtained by dividing the total wringing error by the number of interfaces:

$$W_c = \frac{C_E - \sum_{i}^{n=1} e^i}{n-1} \qquad (2)$$

Where:

W_c = computed wringing error for nth nominal sizes

III. RESULTS AND DISCUSSIONS

A. Surface Roughness Evaluation

Surface roughness measurements were conducted to confirm that gauge blocks were suitable for reliable wringing after deburring, with results presented in Table 2. The post-deburring surface roughness ranged from Ra 0.02 µm to Ra 0.07 µm, values considered small compared with measured wringing errors. Analysis revealed that only the nominal size of 75 mm showed significant changes before and after deburring, while other gauge blocks remained relatively unchanged [8].

B. Measured Wringing Errors

Table 3 presents the empirical wringing error results. All reported wringing statistics (mean, standard deviation, and range) are computed from the per-interface values Wc in the final column of Table 3. Statistical analysis revealed a mean wringing error per interface of 0.08 µm with a standard deviation of 0.03 µm.

Post-Measurement observation confirmed that gauge blocks remained tightly wrung to each other for more than 24 hours, indicating that the error due to loosening of wrung surfaces during measurement is negligible.

C. Uncertainty Evaluation

For each nominal length, individual contributions were combined by root-sum-of-squares to obtain the combined standard uncertainty. The effective degrees of freedom veff via the Welch–Satterthwaite equation, and the coverage factor k from the Student t-distribution at 95% confidence. The results give U95≈63U95≈63 nm (±0.063 µm) for lengths up to 22.8 mm, and U95≈122U95≈122 nm (±0.122 µm) at 75 mm. The growth with length is driven by length-dependent terms chiefly the temperature difference between gauges (∝L α ΔT∝LαΔT), which becomes the dominant contributor (≈ 50 nm) at 75 mm, and the secular change of the standard.

Table 2. Surface roughness evaluation before and after deburring.

Nominal sizes	Test Gauge Block Grade 0 in mm (Combined)	Ra Average in (µm) Before deburring	Ra Average in (µm) After deburring
12.9	10(SN949444)	0.11	0.05
	1.5 (SN950614)	0.07	0.04
	1.4 (SN940252)	0.09	0.05
17.6	9 (SN944588)	0.03	0.05
	7 (SN944650)	0.03	0.02
	1.6(SN 940295)	0.05	0.06
20.2	8 (SN 945445)	0.04	0.06
	6 (SN 946768)	0.03	0.05
	3 (SN 940336)	0.04	0.03
	2 (SN 950577)	0.04	0.06
	1.2(SN 940356)	0.06	0.06
22.8	20 (SN 044070)	0.02	0.04
	1.7(SN 940857)	0.05	0.05
	1.1(SN 940114)	0.06	0.06
75	40 (SN 943158)	0.06	0.07
	30 (SN 943065)	0.11	0.04
	5 (SN 040788)	0.17	0.05

Table 3. Computed wringing error measurement results.

Nominal Sizes in mm	Ave-Central error in µm	Measured wringing error in µm $W_e = C_E - \sum e_i$	Computed wringing error in µm for nth nominal sizes $W_c = \frac{C_E - \sum e_i}{n-1}$
12.9	0.09	0.22	0.11
17.6	0.06	0.13	0.06
20.2	-0.09	0.17	0.04
22.8	0.18	0.22	0.11
75	-0.05	0.19	0.10

Statistical analysis of the measured data revealed a mean wringing error per interface of 0.08 µm with a standard deviation of 0.03 µm, ranging from a minimum of 0.04 µm (20.2 mm nominal) to a maximum of 0.11 µm (12.9 mm and 22.8 mm nominal sizes).

Table 4. Uncertainty of measurement associated with the average wringing error

Nominal Length (mm)	Avg. Wringing (µm)	Secular Change ui(nm)	Temp. Diff. ui (nm)	Interferometric ui(nm)	Comparator ui(nm)	Combined uc (nm)	Eff. DOF veff	Coverage k	Expanded U95U95 (nm)	Reported (µm)
12.9	0.22	15.2*	15.1*	13.8*	14.4	31.1*	~32	2.04	63	±0.063
17.6	0.13	15.2*	15.1*	13.8*	14.4	31.1*	~32	2.04	63	±0.063
20.2	0.17	15.2*	15.1*	13.8*	14.4	31.1*	~32	2.04	63	±0.063
22.8	0.22	15.2	15.1	13.8	14.4	31.1	32	2.04	63	±0.063
75.0	0.19	23.7	49.8	19.8	14.4	61.3	86	1.99	122	±0.122

Notes: All uncertainties at 95% confidence, reference temperature 20 °C, steel-to-steel comparison via GBCD-100A comparator

D. Comparison with conservative Estimates

The measured mean wringing error of 0.08 µm per interface was compared against common estimation approaches used by calibration laboratories. Expert wringing values (0.02 µm) and literature typical values (0.05 µm) underestimate wringing error for aged gauge blocks, while moderate conservative estimates (0.10 µm) show reasonable agreement. Laboratories using conservative estimates of 0.20–0.50 µm (as reported in DTI-PAB measurement audits) overstate wringing uncertainty by 2.5–6.3 times compared to measured values for aged gauge blocks.

IV. CONCLUSIONS

This study establishes an empirical foundation for optimizing wringing uncertainty in gauge block calibration budgets by addressing the gap between conservative estimation practices and actual measured performance. Wringing errors for steel gauge blocks with 25-30 years of service life range from 0.04–0.11 µm per interface with a mean value of 0.08 µm, demonstrating that properly maintained gauge blocks retain wringing

performance. Wringing errors for steel gauge blocks with 25-30 years of service life range from 0.04–0.11 µm per interface with a mean value of 0.08 µm, demonstrating that properly maintained gauge blocks retain wringing performance comparable to published values for new blocks [4],[7].

Comparing measured values against current laboratory practices reveals that conservative estimates of 0.20–0.50 µm (as reported in DTI-PAB measurement audits) overstate wringing uncertainty by 2.5–6.3 times. Replacing conservative estimates with empirical values can improve reported Calibration and Measurement Capability (CMC) by 38–47% for typical dimensional calibrations while maintaining full compliance with ISO-GUM requirements for evidence-based uncertainty evaluation [3][15].

Based on experimental results, the recommended wringing quality range for 30-year gauge blocks is 0.06–0.10 µm at 1-sigma probability. Supporting measurements confirmed suitable wringing conditions with surface roughness values of Ra 0.02–0.07 µm after deburring, and stability tests showed gauge blocks remained tightly wrung for more than 24 hours, indicating negligible error due to loosening during measurement.

The measurement protocol provides a transferable methodology for laboratories to characterize their gauge block populations, while measured values offer validated Type B uncertainty estimates for blocks with similar service histories (steel, Grade 0-2, 25–30 years' industrial use, enabling immediate CMC optimization while maintaining ISO/IEC 17025 compliance. Future studies may focus on the behavior of errors up to the time of separation of wrung gauge blocks to refine further the understanding of wringing stability and long-term performance characteristics.

V. REFERENCES

[1] DTI-Bureau of Product Standards, General Requirements for the Competence of Testing and Calibration Laboratories, PNS ISO/IEC 17025

[2] T. Doiron and J. Beers, "The Gauge Block Handbook," NIST Monograph 180, National Institute of Standards and Technology, Gaithersburg, MD (25)

[3] International Organization for Standardization, "Guide to the Expression of Uncertainty of Measurement, ISO-GUM, JCGM (2008)

[4] N. Suga, "Mitutoyo Metrology Handbook – The Science of Measurement, Mitutoyo Asia Pacific Pte. Ltd., Singapore,(2016)

[5] Wade, H.. *The ASQ Metrology Handbook* (3rd ed.).(2023)

[6] R. K. Jain, *Engineering Metrology*, 21st ed. New Delhi, India: Khanna Publishers, 2014 (Reprinted 2023).

[7] C. H. Simmons, D. E. Maguire, and N. Phelps, *Manual of Engineering Drawing: Technical Product Specification and Documentation to British and International Standards*, 6th ed. Oxford, United Kingdom: Butterworth-Heinemann, 2020.

[8] R. Vegesna and R. Hocken, "A Study of Gauge Block Wringing, University of North Carolina, NC 28223-0001.

[9] R. Dieck, Measurement Uncertainty Methods and Application," Instrumentation, Systems and Automation Society, New York, 2007.

[10] R. Cook et al., Assessment of Uncertainties of Measurements for Calibration," NATA, Australia, 1999.

[11] K. Stępień, J. Świderski, and W. Makieła, "The Importance of Measurement Uncertainty During the Gauge Block Calibration in Determining Compliance with Specifications," Metrology and Measurement Systems, Vol. 32, No. 2, 2025.

[12] International Organization for Standardization, *Geometrical Product Specifications (GPS) — Length Standards — Gauge Blocks*, ISO 3650:1998, 1998.

[13] P. F. Dunn and M. P. Davis, *Measurement and Data Analysis for Engineering and Science*, 4th ed. Boca Raton, FL, USA: CRC Press, 2017.

[14] R. Figliola and D. Beasley, Theory and Design for Mechanical Measurement, John Wiley and Sons, New Jersey, 2000.

[15] JCGM, "JCGM GUM-1:2023 Guide to the Expression of Uncertainty in Measurement – Part 1: Introduction," BIPM, Sèvres, France, 2023.

2026 IMEKO Joint Conference
TC8 - TC11 - TC24
Metro Manila, Philippines, August 26-29, 2026

Development of an In-House LC-MS/MS Method for the Detection of Selected Food Allergens in Philippine Cookies

Ma. Rachel V. Parcon[1], Christy S. Daniel[1], Johanna Andrea C. Valdueza[1], Anina Marielle S.J. Medel[1], Harlene B. Cardos[1,2], Mark Nicholas L. Yow[1], Aileen C. Bidol[1], Admer Rey C. Dablio[1]
[1]Standards and Testing Division, Industrial Technology Development Institute, Department of Science and Technology, Bicutan, Taguig City, Philippines, jacvaldueza@itdi.dost.gov.ph
[2]Science Education Institute, Department of Science and Technology, Bicutan, Taguig City, Philippines

***Abstract* – Food allergies affect people globally, posing a significant public health concern. Safe food consumption depends on accurate food labelling and reliable analytical testing methods. Food allergen testing by liquid chromatography-tandem mass spectrometry (LC-MS/MS) is sensitive for detecting peptides from allergenic proteins in complex food matrices such as cookies. This study focused on optimizing protein extraction, which directly affects the recovery of allergenic proteins subjected to trypsin digestion for selective detection of unique marker peptides. Key parameters optimized included extraction buffer concentration and pH, extraction temperature and incubation time, and reduction and alkylation conditions. Protein extraction efficiency was evaluated through Bradford Assay, while customized peptide standards were used to optimize selective multiple reaction monitoring (MRM) transitions. Different sample clean-up approaches, including molecular weight cut-off filtration and C18 spin column desalting, were compared to improve peptide recovery. The optimized in-house LC-MS/MS method was sensitive, selective, and reproducible for detecting egg, peanut, and milk allergens in cookies.**

I. INTRODUCTION

Food allergy is an important food safety issue worldwide due to the increasing reported cases of allergic incidents after food consumption. Individuals with food allergy experience adverse reactions, ranging from mild to life-threatening anaphylaxis, to the specific proteins in food. Currently, there is no available treatment for preventing allergic reactions to food and the only effective way to protect affected individuals is by avoiding food with allergens [1]. Consumers can be informed of allergenic ingredients in food products through the labels in packaged food. Hence, food manufacturers are required by legislation to declare the presence of allergens in the marketed goods (e.g. Food Allergen Labeling and Consumer Protection Act (US), EU Regulation 1169/2011) [1].

In October 2019, the Philippine Food and Drug Administration (FDA) implemented Administrative Order No. 2014-0030, which requires food allergen information to be clearly declared on product labels [2]. Among the mandatory allergenic foods are cereals containing gluten, crustaceans, eggs, fish, peanuts, soybeans, milk, tree nuts, sulfite of 10 mg/kg or more, and their products. This also includes those that are manufactured in the same facility or equipment as the above-mentioned products, which may have been unintentionally contaminated with allergenic proteins. Egg, peanut, and milk were selected in this study because these are among the mandatory allergenic foods that should be declared in food labels.

The analytical method used to detect and quantify an allergen is an important aspect of food allergen management and regulatory compliance. The main analytical techniques for allergen determination are (1) immunoassays, such as enzyme-linked immunosorbent assay (ELISA) and qualitative lateral flow devices, (2) polymerase chain reaction (PCR), and (3) mass spectrometry. Immunoassays are widely-used owing to its relatively high sensitivity, short analysis time, simplicity, ease of use and accessibility of reagents and materials [3]. However, ELISA may exhibit reduced sensitivity in processed food matrices due to changes in allergenic proteins during processing, which may affect antigen–antibody interactions and lead to false-negative results [3]. PCR is a DNA-based method, or indirect determination of proteins, but could also render false positive and false negative results. Since it detects only the DNA and not the allergenic protein, correlation with the amount of allergenic proteins may not be direct, especially in processed food matrices. On the other hand, mass spectrometry offers high sensitivity and specificity that allows the simultaneous analysis of several allergens in food, including processed food products [4].

In the bottom-up mass spectrometry technique, the extracted proteins are enzyme-digested into smaller peptides and then analyzed using liquid chromatography-triple quadrupole mass spectrometry (LC-MS/MS). Through the use of tandem mass spectrometry, the mass of the peptides and the fragments derived from those peptides are measured and correctly identified. Hence, highly specific and sensitive methods can be developed through the targeted analysis of specific peptides and their fragments. This is because the target peptide, or peptide marker, used is specific for a particular food allergen.

Association of Official Analytical Collaboration (AOAC) published Standard Method Performance Requirements (SMPR) 2016.002 for the detection and quantitation of hazelnut, egg, peanut, and milk allergens using mass spectrometry-based methods [5]. The SMPR defines the scope, analytical technique, and minimum performance characteristics that candidate methods must meet to be considered fit for purpose. Based on these requirements, an LC-MS/MS method was developed and evaluated, and was subsequently granted AOAC First Action Official Method status as AOAC Method 2017.17 [6]. However, further laboratory evaluation and feedback are still needed before the method can proceed toward Final Action status.

According to the Philippine FDA verification portal, cookies constitute the majority of baked products being produced by food manufacturers in the country [7]. This is followed by biscuits, cakes and wafers. Cookies were therefore selected as the target matrix because they are widely produced in the country and represent a processed food matrix in which allergen detection may be more challenging.

This study focuses on optimizing protein extraction and efficient sample clean-up procedures for the sensitive detection of selected food allergens (egg, peanut, and milk) in Philippine cookies using a LC-MS/MS method. This method development initiative strengthens the country's capacity for food allergen testing, contributing to improved monitoring and regulatory compliance.

II. MATERIALS AND METHOD

The analytical method employed in this study was based on a modified AOAC First Action 2017.17 method and the LC–MS/MS procedure described by Tran Trung Thanh *et. al.* (2024) for the simultaneous analysis of selected tree-nut allergens in cookies [6,8]. An incurred cookie sample was used to optimize sample preparation while customized peptides were employed to optimize and confirm MRM transitions. Allergen Standard Reference Materials (NIST SRM 1845a whole egg powder, NIST SRM 1549a whole milk powder, NIST SRM 2387 peanut butter) were used to confirm the presence of egg, peanut, and milk in commercially available cookies.

A. Incurred cookie sample preparation

A blank cookie dough was first prepared by combining approximately 1 kg of flour, 4 g of salt, 5 g of baking powder, 450 g of sugar, 230 mL of virgin olive oil, and 450 mL of water, and mixing thoroughly until homogeneous. The incurred cookie sample was then prepared by adding known amounts of locally sourced egg powder, milk powder, and peanut powder into the blank cookie dough prior to baking. The dough was mixed for at least 10 minutes to ensure uniform distribution of allergens and baked for 15-20 minutes at 180 °C. The incurred cookie contained approximately 10,000 mg/kg of each allergenic protein. From this incurred cookie sample, a final concentration of approximately 240 mg/kg for each allergen (egg, peanut, and milk) was prepared by mixing appropriate amounts of the incurred cookie with the blank cookie matrix.

B. Sample preparation

Approximately 1 g of homogenized cookie sample was weighed into a centrifuge tube and defatted with hexane. This procedure was performed three times under the same conditions then residual hexane was removed using a sample concentrator.

C. Sample extraction and digestion

Extraction buffer solution made of Tris(hydroxy-methyl)-aminomethane or Tris base and urea in ammonium bicarbonate, and denaturant (Octyl β-*D*-glucopyranoside or OGS) were added to the sample followed by incubation for 1 hr. At least 1 mL aliquot of the extract was transferred to a microcentrifuge tube, centrifuged, and then 500 µL of the supernatant was transferred to a clean microcentrifuge tube. A reducing agent, Tris(2-carboxy-ethyl) phosphine hydrochloride (TCEP) or DL-Dithiothreitol (DTT), was added and the mixture was incubated at 37 °C for 1 hr. Alkylation using *S*-methyl methanethiosulfonate (MTTS) or iodoacetamide (IAA) was then performed followed by vortex mixing. Protein digestion was initiated by the addition of trypsin (Trypsin Gold, Mass spectrometry grade, Promega). The amount of trypsin used was determined by taking into consideration the amount of the protein in the sample which was quantified via Bradford Assay using bovine serum albumin (BSA) as the standard and measured on a ClarioStar Plus microplate reader (BMG Labtech). The sample was mixed and incubated at 37 °C overnight (12 ± 4 h). Digestion was quenched by the addition of 10% formic acid, after which the sample was subjected to post-digestion clean-up.

D. Post-digestion sample clean-up

Sample clean-up was performed using Pierce C18 Spin column, Monospin S Type C18 Spin column, and Amicon Ultra-0.5 Centrifugal Filter 10 kDa Molecular Weight Cut-Off (MWCO) filter units. For MWCO, the sample was loaded into a filter unit, centrifuged, and the filtrate was transferred into vials for LC–MS/MS analysis. For C18 spin columns, the column was first conditioned with 200 µL acetonitrile and equilibrated with 200 µL water containing 0.1% formic acid. Sample was loaded, centrifuged, and the eluate was reloaded onto the column prior to washing with 200 µL of the same aqueous solution. The sample was eluted with 200 µL of 60% acetonitrile containing 0.1% formic acid. The eluate was dried in a centrifugal vacuum concentrator and reconstituted in 0.5% acetonitrile with 0.1% formic acid for LC–MS/MS analysis.

E. LC-MS/MS parameters

The chromatographic separation of peptide markers was performed on a Thermo Scientific Vanquish Flex ultra-high performance liquid chromatography (uHPLC) system in the reversed phase conditions. Peptide separation was carried out on a Thermo Scientific Acclaim PepMap 100 nanoViper C18 column (1.0 mm x 15 cm, 3 µm, 100 Å). Mobile phase A was composed of 0.1% formic acid in water and mobile phase B was composed of 0.1% formic acid in acetonitrile. A flow rate of 0.1 µL/min and an injection volume of 1 µL are used. The column temperature is at 35 °C. Gradient elution program was as follows: 0-2 min constant at 5% B, linear gradient to 70% B from 2 to 13 min, constant at 70% B from 13 to 16 min, gradient to 5% B from 16 to 16.1 min, then 16.1 to 25 min constant at 5% B for column equilibration. Mass spectrometry analysis was carried out using Thermo Scientific TSQ Altis Plus Triple Quadrupole Mass Spectrometer operated in positive-ion mode. Mass spectrophotometry acquisition was set up under the following conditions: electrospray ionization (ESI positive); ion spray voltage at 4000 V, ion transfer tube temp at 325 °C, sheath gas at 50, auxiliary gas at 10, sweep gas at 1.0, vaporizer temp at 350 °C. The optimization of MRM transitions was confirmed using customized synthetic marker peptides for whole egg (GGLEPINFQTAADQAR, ≥97.3% purity), milk (YLGYLEQLLR, ≥97.3% purity), and peanut (WLGLSAEYGNLYR, ≥95.5% purity) from GenScript. The collision energy and RF lens were optimized for each peptide via syringe assisted infusion. Data processing was carried out using TraceFinder 5.2 platform

III. RESULTS AND DISCUSSION

Proper sample preparation for mass spectrometry-based analysis is a critical step in the proteomics workflow because it can be both variable and time-consuming [9]. The quality and reproducibility of sample extraction and preparation significantly impact mass spectrometry results [10]. A series of method optimization experiments were performed, with total protein concentrations quantified using the Bradford assay and results correlated with LC-MS/MS detection.

A. Effect of lipid removal and denaturation

Lipids can interfere in protein extraction since it can form complexes with proteins and cause aggregation [11]. Lipid removal is essential for more manageable sample and ensure uniformity. This step improves protein solubility in aqueous buffers by removing lipids, which can inhibit enzymes and contribute to protein degradation [12]. Denaturation means unfolding a protein to break interactions between proteins and cellular components such as membranes, nucleic acids, other proteins [13]. Unfolded proteins become more accessible to the solvent, especially in the presence of detergents or chaotropic agents, which can improve protein extraction yield [14]. Analysis was conducted with each method varied based on the use of hexane for lipid removal and addition of a denaturation step. Results in Figure 1 showed that without protein denaturation by 20 % (w/v) OGS after lipid removal by addition of hexane yields higher protein concentration. Since the cookies were baked, the proteins have likely already undergone denaturation during the baking process.

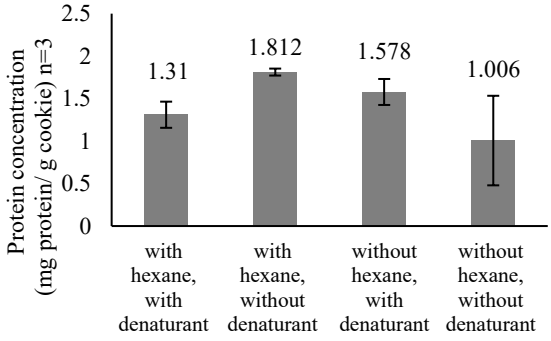


Fig. 1. Effects of denaturant and lipid removal.

B. Optimization of the protein extraction steps

Protein extraction from complex food matrices such as cookies typically requires strong denaturing agents like urea, along with buffering agents such as Tris base, to effectively solubilize proteins that have been altered by heat, fats, and sugars during baking. Urea disrupts hydrogen bonds and hydrophobic interactions, leading to protein unfolding [15], while Tris base helps maintain an optimal, usually alkaline pH range to support efficient extraction [16]. Extraction method was evaluated under different concentrations of urea and Tris base solutions to optimize the protein extraction conditions for achieving the highest protein

concentration. Results in Figure 2 showed that higher concentration of the buffer system produced higher average protein yields.

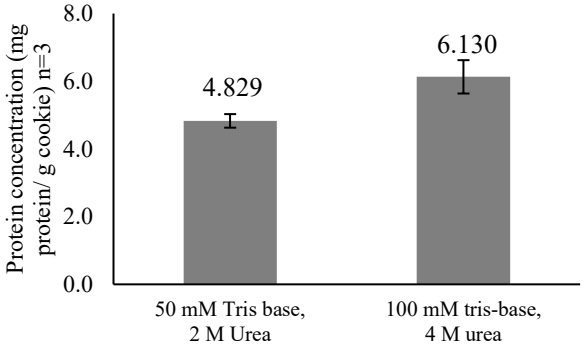


Fig. 2. Effect of different extraction buffer concentrations.

Optimal environmental conditions in protein extraction are critical, typically involving strict control over temperature, shaking condition and pH as they directly influence protein yield, stability, and integrity during the extraction process [17]. Two temperature conditions were used to compare the effect of environmental conditions during protein extraction: (a) room temperature, representing ambient laboratory conditions, and (b) 37 °C, wherein sample was incubated in a controlled environment to mimic physiological conditions. The sample incubated at 37 °C yielded a slightly higher average protein concentration and better precision compared to the sample extracted at room temperature, as shown in Figure 3. This suggests that controlled incubation at physiological temperature may enhance analytical reproducibility and mimic *in vivo* conditions. Protein extraction at 37°C is a specific, often deliberate condition used to balance high yield with the risk of protein degradation or inactivation [18].

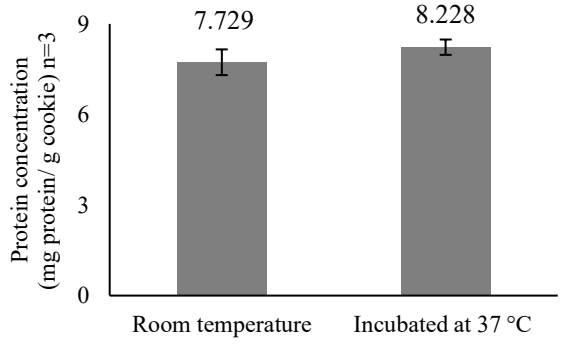


Fig. 3. Effect of environmental conditions.

Samples subjected to 1-hour incubation at 37 °C with brief shaking (10s) after 30 minutes yielded higher average protein concentrations compared to continuous 1-hour incubation with no shaking, as shown in Figure 4. Protein recovery improved under intermittent shaking conditions, suggesting enhanced matrix disruption and protein solubilization [19].

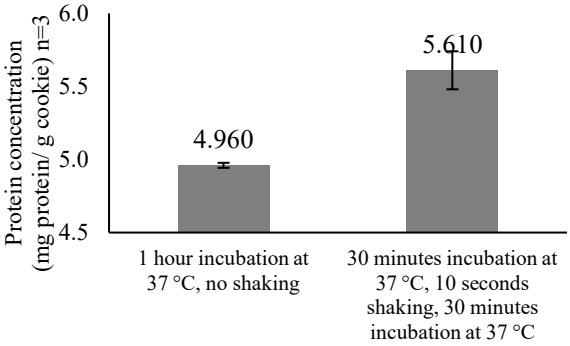


Fig. 4. Effect of shaking conditions.

The effect of the extraction buffer pH was also evaluated. Results in Figure 5 showed that an extraction buffer (100 mM tris-base, 4 M urea) with a pH of 10.6 yielded the highest protein concentration. Therefore, the pH of the prepared buffer solution was measured and adjusted to pH 10.6 prior to extraction of the defatted sample to ensure method consistency.

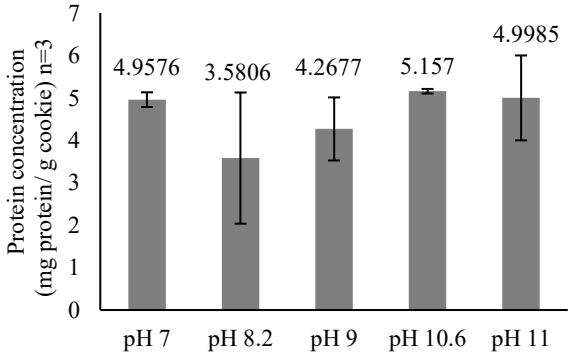


Fig. 5. Effect of different pH of the extraction buffer.

C. Comparison of reduction and alkylation techniques

Reduction involves breaking disulfide bonds between residues, which unfolds the protein and improves enzymatic access during digestion [20]. Alkylation prevents disulfide bond reformation, stabilizing the protein in a denatured state [21]. These steps increase digestion efficiency. Two different combinations of reduction-alkylation reagents were used which are 50mM TCEP-100mM MMTS and 200 mM DTT- 200 mM IAA. Protein concentration was quantified using the Bradford assay, and area response signals were obtained using LC–MS/MS for the detection of egg, milk, and peanut in samples. The results in Figure 6 indicate that the DTT-IAA method resulted in higher protein recovery compared to the TCEP-MMTS method. Similarly, LC–MS/MS results shown in Figure 7 demonstrated that the DTT-IAA method produced

higher signal responses for egg, peanut, and milk peptide markers than the TCEP-MMTS method. This further confirms that DTT-IAA method yields better protein recovery and improved peptide detectability in LC-MS/MS analyses.

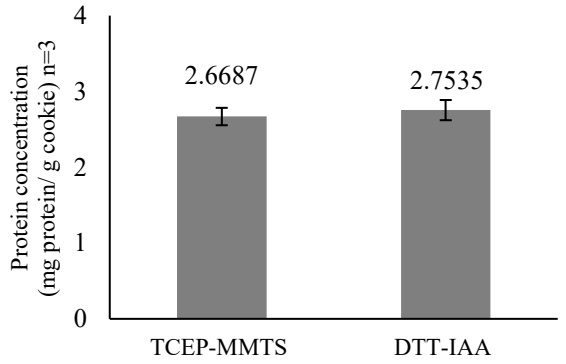


Fig. 6. Effect of different reducing-alkylating reagents.

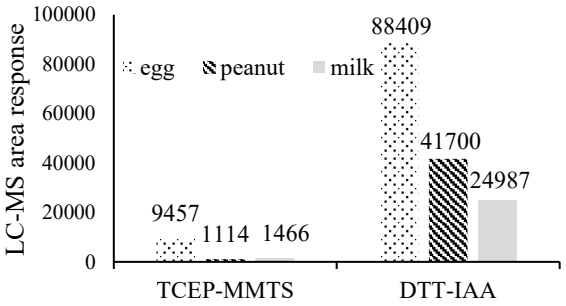


Fig. 7. Area responses egg, peanut, and milk using different reducing-alkylating reagents.

D. Estimation of trypsin-to-protein ratio for digestion

Enzymatic digestion is crucial for breaking proteins into smaller peptides that can be effectively separated by chromatography and analyzed by mass spectrometry [22]. Among proteases, trypsin is the most widely used because of its high specificity, producing peptides, which enhances their suitability for LC separation and MS analysis. Proteins undergone cleavage to produce peptides at the C-terminal side of two basic amino acids, arginine (Arg) and lysine (Lys) bonds [23]. The protein-to-trypsin ratio is a critical parameter in enzymatic digestion, as it directly influences the efficiency and completeness of protein cleavage. An appropriate ratio ensures that proteins are sufficiently digested into peptides without excessive protease activity that could lead to over digestion or nonspecific cleavage [24]. Optimizing the protein-to-trypsin ratio is essential for achieving reproducible and high-quality results in proteomic workflows. In the optimized method, 3 µL of 1 µg/ µL trypsin solution was added to a defined volume of digested sample containing 90 µg of protein to obtain a 1:30 (w/w) trypsin-to-protein ratio. The digestion was performed at 37 °C for 16 hours to achieve optimal peptide yield for LC-MS/MS. The protein concentration of the sample was determined using the Bradford assay, with milk casein solution as quality control sample (90-105 % recovery).

E. Evaluation of post-digestion sample cleanup

Effective sample cleanup following enzymatic digestion is essential for sensitive detection in LC-MS/MS as excess salts or trace amounts of detergents interfere with peptide ionization that can add to the chemical noise or background [25]. Various sample cleanup techniques were evaluated to establish an efficient cleanup protocol that maximizes the detection sensitivity and ensure reliable quantification of the target proteins. To establish the cleanup method, several approaches were conducted, including the use of MWCO, MonoSpin, Pierce C18, and their combinations.

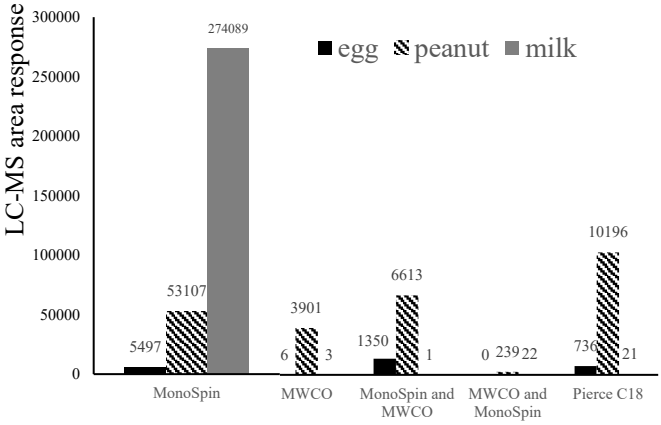


Fig. 8. Effect of different post-digestion sample clean-up.

The optimized post-digestive sample clean-up and desalting method is using GLSciences MonoSpin C18 column, as shown in Figure 8. With this method, the sample loading was controlled to avoid exceeding the capacity of the column. The results in Figure 9 showed high area responses with 100 µL sample loaded.

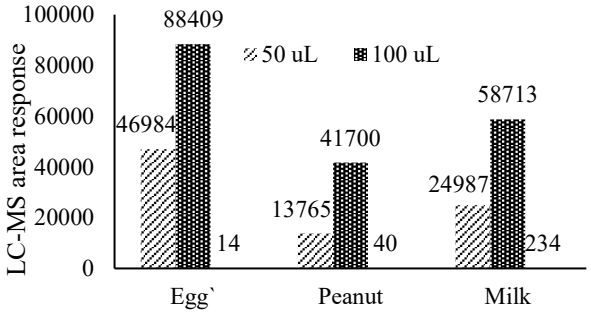


Fig. 9. Effect of different sample-loading volumes in MonoSpin.

Table 1. Optimized MRM Transitions in LC-MS/MS.

Compound (Peptide)	Polarity	Precursor (m/z)	Ion Classification	Product (m/z)	Collision Energy (V)	RF Lens (V)	Min. Dwell Time (ms)
Egg							
GGLEPINFQTAADQAR	Positive	844.533	Quantifier	666.627	29.56	107	27.168
GGLEPINFQTAADQAR	Positive	844.533	Qualifier	1121.3	36.08	107	27.168
Peanut							
WLGLSAEYGNLYR	Positive	771.45	Quantifier	1242.4	29.56	103	27.168
WLGLSAEYGNLYR	Positive	771.45	Qualifier	272.083	32.93	103	27.168
Milk							
YLGYLEQLLR	Positive	634.367	Quantifier	991.3	22.76	82	27.168
YLGYLEQLLR	Positive	634.367	Qualifier	249.05	26.84	82	27.168

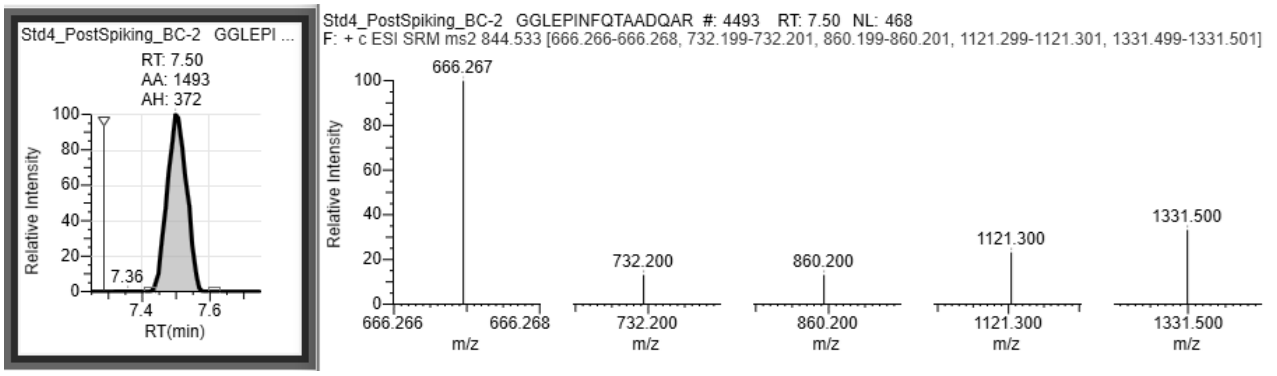


Fig. 10. EIC and mass spectrum for egg.

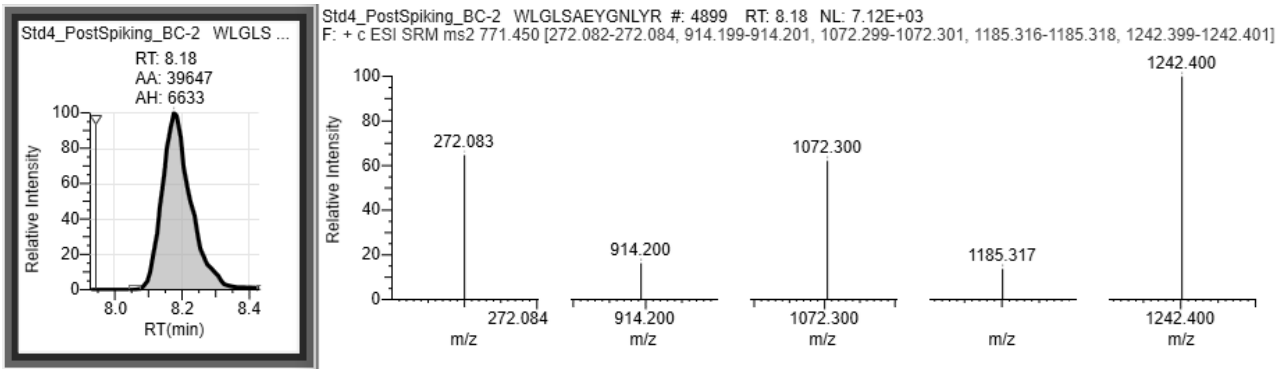


Fig. 11. EIC and mass spectrum for peanut.

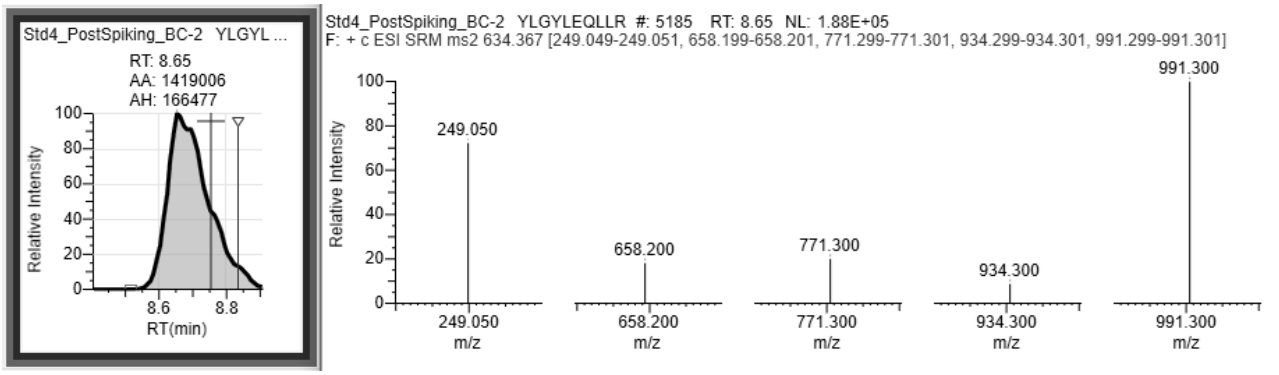


Fig. 12. EIC and mass spectrum for milk.

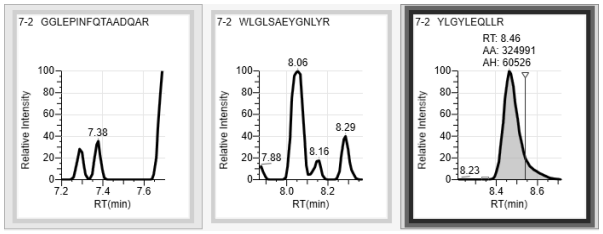


Fig. 13. EIC of Cookie 1.

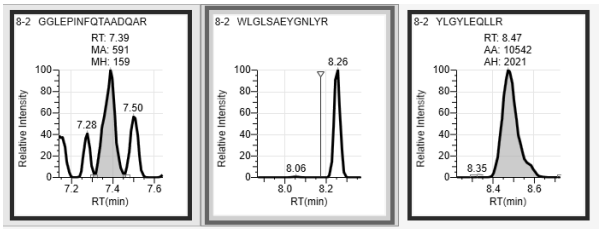


Fig. 14. EIC of Cookie 2.

F. MRM optimization in LCMSMS

The MRM transitions monitored for the mass spectrometry detection are shown in Table 1. These transitions were optimized and confirmed by using the customized peptides for each food allergen (milk, egg, peanut). The peptide sequences and precursor/product ions used were based on AOAC First Action 2017.17 [6]. One peptide sequence per allergenic protein was enough to establish the quantifier and qualifier ions for food allergen detection. The table shows the optimized quantifier ion and qualifier ions for each peptide sequence.

G. Targeted detection of food allergens using LC-MS/MS

Matrix-matched calibration standards were prepared by combining appropriate volumes of blank cookie extracts with extracts of NIST SRMs (egg, peanut, and milk) that had been processed in the same way as the samples. These standards were used to verify that the optimized sample preparation protocol enables efficient protein extraction and that the selected MRM transitions provide selective detection and reliable identification of target food allergens in cookies. The results presented in Figures 10-12 demonstrate that the expected quantifier and qualifier ions are the most abundant signals observed for each food allergen, confirming the traceability and selectivity of the optimized MRM transitions.

Two locally produced cookie samples were randomly selected from a local supermarket, then homogenized using a grinder, sieved, and extracted using the optimized sample preparation method. Using the selected MRM transitions in LC-MS/MS, the resulting extracted ion chromatogram (EIC) of Cookie 1 in Figure 13 has confirmed presence of milk the same with the indication in its food label. The same with Cookie 2 in Figure 14 wherein its food labeling and LC-MS/MS results confirmed presence of egg and milk food allergens.

IV. CONCLUSION

The laboratory has successfully developed an in-house LC-MS/MS method that is sensitive, selective, and reproducible, ensuring reliable detection of food allergens. The optimized sample preparation protocol includes lipid removal using hexane, followed by protein extraction with a Tris-base and urea buffer, reduction with dithiothreitol, alkylation with iodoacetamide, and enzymatic digestion with trypsin to generate the target peptides. Sample clean-up involved the use of a C18 MonoSpin column prior to LC–MS/MS analysis. Detection was achieved by monitoring one quantifier ion and one qualifier ion for each target allergen (egg, peanut, and milk), ensuring confident identification. The in-house developed method for the detection of selected food allergens in cookies is suitable for routine analytical testing and supports food safety and regulatory compliance of food manufacturers.

IV. CITATIONS AND REFERENCES

This work was funded by the Department of Science and Technology (DOST) under the DOST Grants-In-Aid (GIA) project entitled “Standardization and Validation of Chemical Test Methods on Allergens and Preservatives Food Safety Parameters Among DOST Laboratories” and monitored by DOST-Philippine Council for Industry, Energy and Emerging Technology Research and Development (PCIEERD).

REFERENCES

[1] A.Siragakis and D.Kizis, eds. Food Allergen Testing: Molecular, Immunochemical, and Chromatographic Techniques.1st ed. John Wiley&Sons; 2014.

[2] Department of Health – Food and Drug Administra tion, Administrative Order No. 2014-0030: “Revised Rules and Regulations Governing the Labeling of Prepackaged Food Products Distributed in the Philippines,” Philippines, 2014.

[3] A.Heick, M.Fischer, M.Kerbach, U.Timm, and M.Popping, “Application of a liquid chromatography –tandem mass spectrometry method for the simultaneous detection of seven allergenic foods in flour and bread and comparison with commercially available ELISA test kits”, Journal of AOAC Int. 2011;94(4):1060–1068.

[4] M. Planque, T. Arnould, and N. Gillard, ‘Food

Allergen Analysis: Detection, Quantification and Validation by Mass Spectrometry', Allergen. In-Tech, Oct. 04, 2017. doi: 10.5772/intechopen.693 61.

[5] AOAC INTERNATIONAL, "SMPR 2016.002: Standard Method Performance Requirements for detection and quantitation of selected food allergens," in *Official Methods of Analysis*, 20th ed., Rockville, MD, USA: AOAC INTERNATIONAL, 2016.

[6] L.S.New, J.Stahl-Zeng, A.Schreiber, M.Cafazzo, A.Liu, S.Brunelle, H.F.Liu, "Detection and quantitation of selected food allergens by liquid chromatography with tandem mass spectrometry: first action 2017.17", Journal of AOAC INTERNATIONAL, vol. 103, Issue 2, March-April 2020, pp. 570–583, doi: https://doi.org/10.5740/jaoac int.19-0112

[7] Food and Drug Administration Philippines. (n.d.). FDA Verification Portal: All food products. https://verification.fda.gov.ph/

[8] T.T.Thanh, N.T.H.Ngoc, B.C.Tien, P.C.Ly, K.V.Anh, N.H.Vo, & D.T.N. Lan, "Simultaneous analysis of certain tree-nut allergens in cookies by LC–MS/MS", Vietnam Journal of Food Control, vol. 7, No. 4, pp. 589–600, doi: https://doi.org/10.47866/ 2615-9252/vjfc.4419

[9] S. Hess, "Sample Preparation Guide for Mass Spectrometry–Based Proteomics," Current Trends in Mass Spectrometry, vol. 11, no. 3, pp. 12–17, 2013.

[10] Thermo Fisher Scientific, "Protein Sample Preparation for Mass Spectrometry." [Online].

[11] B. Krishnarjuna and A. Ramamoorthy, "Detergent-Free Isolation of Membrane Proteins and Strategies to Study Them in a Near-Native Membrane Environment," Biomolecules, vol. 12, no. 8, p. 1076, 2022, doi: 10.3390/biom12081076.

[12] W. Wang et al., "Removal of lipid contaminants by organic solvents from oilseed protein extract prior to electrophoresis," Analytical Biochemistry, vol. 329, no. 1, pp. 139–141, 2004, doi: 10.1016/j.ab.2004.02. 044.

[13] L. R. Engelking, "Protein Structure," in Textbook of Veterinary Physiological Chemistry, 3rd ed., 2015, ch. 4.

[14] S. C. Tan and B. C. Yiap, "DNA, RNA, and Protein Extraction: The Past and The Present," BioMed Research International, vol. 2009, Art. no. 574398, 2009, doi: 10.1155/2009/574398.

[15] J. W. Hsu, D. T. Wu, and S. T. Lin, "The Surprising Role of Urea in Promoting CO_2 Hydrate Formation: Enhanced Molecular Diffusivity via Weakening of the Hydrogen-Bond Network," Journal of Physical Chemistry B, vol. 129, no. 40, pp. 10440–10450, 2025, doi: 10.1021/acs.jpcb.5c04817.

[16] N. E. Good et al., "Hydrogen Ion Buffers for Biological Research," Biochemistry, vol. 5, no. 2, pp. 467–477, 1966.

[17] J. C. J. Wong et al., "Deep eutectic solvents for protein extraction: mechanisms, performance, and green metrics," Journal of Molecular Liquids, vol. 438, part A, Art. no. 128636, 2025, doi: 10.1016/j.molliq.2025.128636.

[18] O. Tas, S. G. Sumnu, and M. H. Oztop, "Effect of Extraction Methods and Preheat Treatments on the Functional Properties of Pumpkin Seed Protein Concentrate," ACS Food Science & Technology, vol. 5, no. 1, pp. 105–117, 2024, doi: 10.1021/acsfoodsci tech.4c00601.

[19] M. Ozgolet et al., "Optimization of extraction parameters of protein isolate from milk thistle seed: Physicochemical and functional characteristics," Food Science & Nutrition, vol. 12, no. 5, pp. 3346–3359, 2024, doi: 10.1002/fsn3.4001.

[20] T. Müller and D. Winter, "Systematic Evaluation of Protein Reduction and Alkylation Reveals Massive Unspecific Side Effects by Iodine-containing Reagents," Molecular & Cellular Proteomics, vol. 16, no. 7, pp. 1173–1187, 2017, doi: 10.1074/mcp.M116. 064048.

[21] BenchChem, "Assessing the completeness of disulfide bond reduction before iodoacetone treatment," 2026. [Online].

[22] M. S. Mansuri et al., "Optimal conditions for carrying out trypsin digestions on complex proteomes: From bulk samples to single cells," Journal of Proteomics, vol. 297, Art. no. 105109, 2024, doi: 10.1016/j.jprot.2024.105109.

[23] J. V. Olsen, S. E. Ong, and M. Mann, "Trypsin cleaves exclusively C-terminal to arginine and lysine residues," Molecular & Cellular Proteomics, vol. 3, no. 6, pp. 608–614, 2004, doi:10.1074/mcp.T400003-MCP200.

[24] S. V. Egeland, L. Reubsaet, and T. G. Halvorsen, "The pros and cons of increased trypsin-to-protein ratio in targeted protein analysis," Journal of Pharmaceutical and Biomedical Analysis, vol. 123, pp. 155–161, 2016, doi: 10.1016/j.jpba.2016.02.011.

[25] R. L. Gundry et al., "Preparation of proteins and peptides for mass spectrometry analysis in a bottom-up proteomics workflow," Current Protocols in Molecular Biology, vol. 90, no. 1, pp. 10.25.1–10.25.23, 2009, doi: 10.1002/0471142727.mb1025s88.

2026 IMEKO Joint Conference
TC8 - TC11 - TC24
Metro Manila, Philippines, August 26-29, 2026

Evaluating Competence of Philippine Laboratories in Testing Water Activity of Biscuit Sample through Conduct of Interlaboratory Comparison

Jan-Ervin C. Guerrero[1], Admer Rey C. Dablio[1], Nida U. Autor[2]

[1]*Standards and Testing Division, Industrial Technology Development Institute, Department of Science and Technology, Bicutan, Taguig City, Philippines, janguerrero@ymail.com*
[2] *ASCXENT Knowledge Resources, Inc., Philippine Cooperative Center, 90 Balete Drive Extension, Quezon City, Philippines*

Abstract: **Water activity (a_w) is a key factor influencing microbial growth, food safety, and product stability. This study developed and validated a biscuit-based candidate material for an interlaboratory comparison (ILC) in the Philippines. The material was prepared by pulverizing, sieving, and homogenizing commercial biscuits, then assessed for homogeneity and stability using statistical tests. Results from 11 bottles confirmed acceptable homogeneity, while short-term stability testing at 30 °C and 40 °C showed no significant changes in a_w. The material was used in an ILC following PNS ISO/IEC 17043:2023 guidelines. After removing two outliers, the consensus a_w value was 0.4040. Most participating laboratories achieved satisfactory z-scores, demonstrating good agreement and reliable performance. The study highlights the competence of local laboratories and supports harmonization and quality assurance in food testing.**

I. INTRODUCTION

Water activity (a_w) plays a vital role in determining the safety, stability, and overall quality of food products, as it governs the availability of water necessary for microbial growth and biochemical reactions [1]. By definition, water activity is the ratio of vapor pressure of water in the food substrate to the vapor pressure of pure water at the same temperature [2]. Effective control and accurate measurement of a_w are therefore essential components of food quality assurance systems. In tropical countries like the Philippines, ensuring the reliability and comparability of water activity measurements across laboratories is increasingly important in supporting food safety regulations and accreditation requirements.This study focuses on the development and validation of a biscuit-based candidate material intended for use in a local interlaboratory comparison (ILC) program. By preparing a homogeneous and stable test material and evaluating its performance through established statistical methods, the study aims to support proficiency testing initiatives aligned with national and international standards. This helped local laboratories to comply to clause 7.7.2 requirements of PNS ISO/IEC 17025:2017 on participation to proficiency testing or interlaboratory comparison, helping them sustain or gain laboratory accreditation.

II. MATERIALS AND METHODS

A. *Preparation of Candidate ILC Material;* A popular locally available biscuit brand was selected as sample for this study. The sample were the then ground, pulverized using a food processor and mortar and pestle, homogenized and pass thru No. 40 sieve. A total of 2 kgs of homogenized sample was obtained. The prepared material was subsequently bottled, labeled, sealed in individual glass jars, and stored in an incubator maintained at 25 °C. Systematic sampling of the packed material was performed to allocate samples for homogeneity testing and both short-term and long-term stability studies, including contingency reserves. On the other hand, random sampling was applied in selecting sample units to be distributed to collaborating laboratories for the interlaboratory comparison (ILC).

B. *Homogeneity Design***:** A total of 10 random samples were selected through stratified randomization and analysed using Novasina Labswift - a_w water activity meter. Three (3) replicate measurements for each bottle were carried out in a random order to determine possible analytical trend. Grubbs' tests were performed at a 95% confidence level to identify potential outliers in both individual results and sample means. Linear regression analysis was applied to evaluate any bottling trends, while homogeneity was assessed using Analysis of Variance (ANOVA). All statistical analyses were conducted in accordance with ISO Guide 35:2017 [3].

C. *Short-term Stability Design:* Short-term stability testing was conducted to evaluate the effect of transport conditions on the sample. Two test temperatures were selected: room temperature (approximately 36 °C) and an elevated temperature of 40 °C. Samples assigned to 40 °C were stored in an air oven. The study was carried out over a period of four (4) weeks. For each of weeks (1, 2, and 3), two (2) samples were exposed to each test temperature. All samples were subsequently analyzed during Week 4. Three (3) replicate measurements for each sample were made under repeatability conditions, i.e. using the same method and conditions applied during homogeneity testing. A total of 14 samples were analyzed.

D. *Long-term Stability Design:* The long-term stability of the ILC material was conducted 1, 2, 3, and 4 months after preparation and assessed using the regression analysis. Two (2) samples designated for each of the schedules were tested. The testing and reporting were made similar to the conditions of homogeneity and short-term stability.

E. *Characterization Study through Interlaboratory Comparison:* Each participating laboratory was given two (2) bottles each containing approximately 15 grams (g) of the Interlaboratory Comparison Material (ILCM) in each bottle. The samples were sent via courier while the instructions were sent via email. Participants were allowed to use the test method and equipment of their choice and were given one (1) month to analyse the sample. The results collected were then used to determine the consensus value for this interlaboratory comparison. Outlier test were performed to remove possible outlier using Grubb's test [4]. The Grubb's Statistic (G_{cal}) is calculated as:

$$G = \frac{|X_{questionable} - \bar{x}|}{SD} \quad (1)$$

where $X_{questionable}$ is the data suspected as of being an outlier, $\bar{x}$ is the sample mean (including the suspected outlier) and SD is the sample standard deviation. The calculated G will then be compared to the critical value (G_{crit}) from a Grubbs' critical value table at 95% confidence level. The criteria for the removal of the possible outlier is as follows:

- If $G_{cal} > G_{crit}$: The data point is a true outlier and can be legitimately rejected.
- If $G_{cal} \leq G_{crit}$: The data point is not considered a statistical outlier and must be kept in the dataset.

Once the outlier is gone, Grubb's test will be performed again until no more outlier is detected. The remaining values will be used for the calculation of the consensus value and will be treated as the assigned value for this scheme.

Participant's performance is primarily evaluated by their z-score calculated using the equation:

$$z = \frac{x_i - x_{pt}}{\sigma_{pt}} \quad (2)$$

where z is the z-score, x_i is the participant result, x_{pt} is the assigned value, and σ_{pt} is the standard deviation for proficiency assessment.

Table. 1 z-score criteria

z-score	Performance
$\|z\| \leq 2.0$	Satisfactory
$2.0 \leq \|z\| \leq 3.0$	Questionable
$\|z\| \geq 3.0$	Unsatisfactory

Standard deviation for proficiency assessment (σ_{pt}) is based on the Horwitz function and can be calculated using the equation below:

$$\sigma_{pt} = 0.02 * (x_{pt})^{0.8495} \quad (3)$$

where x_{pt} is a unitless mass fraction of the measurand

III. RESULTS AND DISCUSSION

A. *Production of Candidate RM material*

A total of 88 bottled samples containing approximately 15 g of the homogenized ground biscuit powder were produced for 2 kg of sample. Ten (10) bottles of candidate RMs, selected by systematic random sampling, were allotted for homogeneity, whereas six (6) bottles sampled similarly were stored in room temperature and another six (6) bottles were stored in an incubator maintained at 40 °C for stability studies. The rest of the bottled samples allotted for distribution to participating laboratories and for surplus were randomly sampled and stored in the incubator.

B. *Homogeneity Studies*

Figure 1 shows the trend plot of the homogeneity test result. Homogeneity was assessed using Cochran's test for outliers, trend analysis by linear regression (t-test), and analysis of variance (F-test). Test results are tabulated in Table 2.

Table 2. Summary of homogeneity test results of water activity in biscuit

Test	Calculated Value	Critical Value (95% C.I.)	Criteria	Remarks
Outlier Test by Cochran's Test	0.10	0.42	$C_{calc} < C_{crit}$	PASSED
Test for bottling trend by linear regression	1.21	2.31	C	PASSED; NO BOTTLING TREND
Test for homogeneity by Analysis of Variance	3.11	3.32	$F_{calc} < F_{crit}$	PASSED; SUFFICIENTLY HOMOGENEOUS

Table 5. Summary of Participants results for the water activity in biscuit Interlaboratory Comparison

Laboratory Code	**a_w Measurement**	**Expanded Uncertainty (±)**	**Confidence Level (%)**	**Coverage factor**	**z-score**	**Performance**
101	0.39	0.3	95	2	-0.45	S
102	0.406	0.012	95	1.96	0.05	S
103	0.36	0.003	95	2	-1.38	S
104	0.3879	0.0048	95	2	-0.51	S
105	0.43	0.03	95	2	0.8	S
106	0.402	0.022	95	2	-0.07	S
107	0.444	0.011	95	2	1.23	S
108	0.531	0.032	95	2	3.93	U
109	0.4	0.5	95	2	-0.14	S
110	0.46	Not reported	Not reported	Not reported	1.73	S
111	0.375	0.017	95	2	-0.91	S
112	0.0482	0.39	95	2	-11.06	U
113	0.363	0.01578	95	2	-1.28	S
114	0.391	0.015	95	2	-0.42	S
115	0.448	0.07	95	2	1.35	S

C. Stability Studies

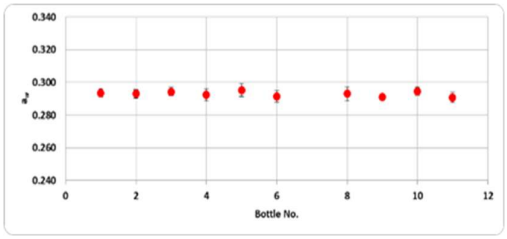


Fig 1. Trend Plot of homogeneity test of water activity in biscuit

Results of short-term stability is shown in Figure 2 and summarized in Table 3. Results showed that at elevated and accelerated temperature, the sample ILCM is stable. For the long-term stability there is no trend of significant change from day 0 to 4th month storage period of the ILCM; therefore, no instability was observed, as determined by the regression analysis and shown in Figure 3 and the summary of results tabulated in Table 4.

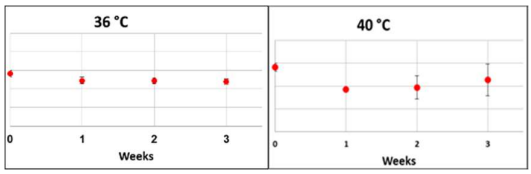


Fig 2. Short-term stability plot water activity in biscuit

Table 3. Summary of short-term test results of water activity in biscuit

Test Temp, °C	Calculated Value	Critical Value (95% C.I.)	Criteria	Remarks
40	2.10	2.31	$t_{calc} < t_{crit}$	PASSED; NO TREND
26	0.73			

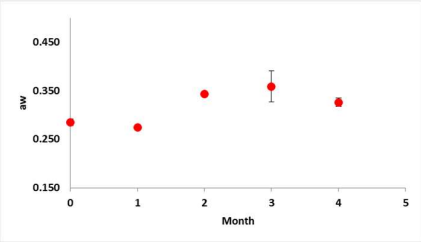


Fig 3. Long-term stability plot water activity in biscuit

Table 4. Summary of Long-term test results of water activity in biscuit

Test Temp, °C	**Calculated Value**	**Critical Value (95% C.I.)**	**Criteria**	**Remarks**
26	1.78	3.18	$t_{calc} < t_{crit}$	PASSED; NO TREND

D. *Characterization Study through Interlaboratory Comparison*

Fifteen (15) participating laboratories all over the Philippines submitted results for the characterization study. Participants labs ranges from various government office to private laboratories offering water activity analysis to local consumers. Participants z-score was calculated using equation (2). The test data were evaluated for the detection and potential removal of outliers using Grubbs' test for the mean at a 95% confidence level. Two (2) outliers were identified: one with an extremely negative z-score (−11.06) and another with a positive z-score exceeding 2.0 (3.93). Both were detected using Grubbs' test and were subsequently removed from the calculation of the consensus value. Based on the remaining valid results, the calculated consensus value is 0.4044 a_w. This consensus value serves as the assigned value against which individual laboratory performance is evaluated. The standard deviation for proficiency assessment (σ_{pt}) was determined using equation (3) to be 0.0322 a_w. All remaining participants achieved satisfactory performance scores, and is summarized in Table 5. This high level of equivalence demonstrates the robust reproducibility of the utilized a_w testing methods across diverse institutional settings in the local testing scene. Consequently, this validates that regulatory safety decisions made by these independent entities are scientifically aligned, minimizing the industry risk of discrepant product stability data.

IV. CONCLUSION

The results demonstrate the technical competence of Philippine testing laboratories in water activity measurement and strengthen confidence in the reliability and comparability of a_w data generated nationwide. Moreover, participation in interlaboratory comparisons such as this supports compliance with Clause 7.7.2 of PNS ISO/IEC 17025:2017, contributing to a stronger national quality infrastructure and promoting the harmonization of food testing practices among accredited laboratories.

REFERENCES

[1] PNS/FDA 37:2014 ICS 67.020, *Code of practice for the processing and handling of salt fermented fish and shrimps (bagoong).* Department of Trade and Industry, Filinvest Bldg., Gil J. Puyat Ave., Makati City, Philippines

[2] PNS/FDA 33:2011, ICS 67.060, *Recommended code of practice for the processing and handling of ethnic flour-based confectioneries (Polvoron, Piaya and Barquillos),* Department of Trade and Industry, Filinvest Bldg., Gil J. Puyat Ave., Makati City, Philippines

[3] ISO Guide 35:2017: *Reference materials—Guidance for characterization and assessment of homogeneity and stability*. ISO

[4] NIST Engineering Statistics Handbook, *https://www.itl.nist.gov/div898/handbook/eda/section3/eda35h1.htm*

[5] L.C. Dajay, J. C. Cotara, J.C. Laurea, M.B. Martin, M.G.Y. Parcarey, P. E. Adona Jr, *"Production and Characterization of Rice Flour as Reference Material for Chemical Analysis"* Philippine Journal of Science, 153 (3: 1151-1156, June 2024 ISSN 0031-7683

2026 IMEKO Joint Conference
TC8 - TC11 - TC24
Metro Manila, Philippines, August 26-29, 2026

Optimization and Validation of a Test Method for the Quantification of Total Mercury in Fish Tissue through Thermal Decomposition, Amalgamation, and Atomic Absorption Spectrophotometry

Kenneth Edward Eugenio D. Pedres[1]*, Theressa F. Aviles[1], Christy S. Daniel[1], Bianca Baring[1], Kurt Nowell Libante[1], Admer Rey C. Dablio[1]

[1]*Standards and Testing Division, Industrial Technology Development Institute, Department of Science and Technology, Bicutan, Taguig City, 1631, Philippines, kennethedwardpedres@gmail.com**

***Abstract* –** Mercury contamination in fish represents an ongoing public health concern that requires continuous monitoring. In the Philippines, fish is an important source of dietary protein, and fisheries contributes to local livelihoods. The Philippines Bureau of Fisheries and Aquatic Resources (BFAR) through Administrative Order No. 210-01 (s. 2001), has set a maximum permissible limit of 0.5 mg/kg total mercury in fish intended for export. Currently, limited information is available on the application of a direct mercury analyzer (DMA) for total mercury determination in freshwater fish within the Philippine setting. This study aimed to optimize analytical parameters for the quantification of total mercury in fresh fish tissue using DMA based on the US EPA Method 7473 (SW-846). This method involves thermal decomposition, amalgamation, and atomic absorption spectrophotometry for solid samples, providing enhanced operational efficiency and reduced hazardous waste generation compared to conventional methods. Method validation was performed to establish the fitness for purpose of the method prior to the analytical testing of fish samples from the local market. Performance parameters evaluated included linearity, instrument detection limit, method detection limit, method quantification limit, repeatability, intermediate precision, and trueness through recovery testing. Statistical assessment of the validation results demonstrated that the method is fit for the intended quantification of total mercury in fish tissue.

Keywords: total mercury (Hg), fish, direct mercury analyzer, method validation

I. Introduction

Mercury (Hg) is a naturally occurring heavy metal that poses significant risks to both environmental and human health. It enters the environment through a combination of natural processes—such as volcanic eruptions, forest fires, and weathering of rocks—and human activities, including mining, fossil fuel combustion, industrial discharge, and improper disposal of mercury-containing products [1], [2]. Once in the environment, mercury cycles through air, water, and soil, where it can be transformed into more toxic forms such as methylmercury, which accumulates in aquatic organisms and magnifies up the food chain [3].

Consumption of Hg contaminated aquatic lifeforms presents a pathway of Hg into the human biological system. Exposure to doses of Hg has been linked to cases of impaired neurodevelopment in the fetus of pregnant women [4], occurrence of asthma in children [5], and neurotoxicity [6], among other severely detrimental effects.

The Philippines' Bureau of Fisheries and Aquatic Resources (BFAR) under the Department of Agriculture (DA) sets a limit on fish products to be derived from specimen mercury concentrations of no more than 0.5 ppm or mg/kg, as per the BFAR Fisheries Administrative Order No. 210-01(s. 2001) [7].

Conventional methods for mercury determination in solid samples typically involve acid digestion followed by instrumental analysis using atomic absorption spectrometry (AAS), inductively coupled plasma optical emission spectrometry (ICP-OES), or inductively coupled plasma mass spectrometry (ICP-MS). While these techniques provide high sensitivity, they often require extensive sample preparation, involve the use of hazardous reagents, and are prone to contamination or analyte loss during digestion [8].

An alternative approach is direct mercury analysis based on thermal decomposition, amalgamation, and atomic absorption spectrophotometry (TDA-AAS). This technique enables the direct determination of total mercury in solid and semi-solid samples without the need for

chemical digestion. The analytical process involves sequential stages of sample drying, thermal decomposition, catalytic conversion, amalgamation, and detection. Initially, the sample is subjected to controlled heating to remove moisture, followed by high-temperature decomposition in an oxygen-rich environment to release mercury from the matrix. The liberated mercury vapor is then selectively trapped on a gold or noble metal amalgamator, effectively isolating it from potential interference. Subsequently, rapid heating of the amalgamator releases the concentrated mercury vapor into an optical cell, where its absorbance is measured at a characteristic wavelength using atomic absorption spectrophotometry [9].

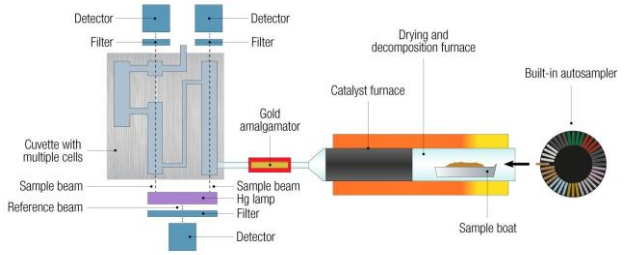


Fig. 1. Schematic on the instrumentation of DMA-80 [10].

This direct approach offers several advantages over conventional wet digestion methods, including reduced sample handling, minimized risk of contamination, shorter analysis time, and improved operational safety. Furthermore, the closed-system design enhances analytical accuracy by preventing mercury loss during sample preparation. Previous studies [8] have demonstrated that TDA-AAS provides reliable and reproducible results for a wide range of environmental and biological matrices, including fish tissue, with performance comparable to more complex instrumental techniques.

Given these advantages, direct mercury analysis has become an established method for routine determination of total mercury, particularly in food and environmental laboratories. Standardized protocols such as US EPA Method 7473 further support its application by providing validated operating conditions and quality control requirements. The adoption of this technique is therefore well-suited for studies aiming to optimize and validate analytical methods for mercury quantification in fish tissue.

This study aims to: (1) optimize the parameters for quantifying total mercury in fish using DMA based on US EPA Method 7473 (SW-846) and using fresh fish tissue as sample matrix, and (2) evaluate its fitness for the stated purpose.

II. METHODS AND PROCEDURES

The determination of total mercury was performed using DMA consistent with the principles of US EPA Method 7473 [9]. A DMA-80 evo Direct Mercury Analyzer (Milestone Srl, Italy) was employed for all measurements using nickel boats. Due to the unavailability of fish samples with detectable mercury levels, method optimization and validation were conducted using fresh fish tissue ("tilapia" or *Oreochromis niloticus*) spiked with a known amount of mercury.

A. Preparation of spiked fish tissue sample

Tilapia samples were randomly obtained from the local market, filleted, then homogenized after removal of the skin and non-edible parts. A 5.06551-gram portion of the homogenized tissue was accurately weighed and spiked with 0.21084 grams of 2.5432 mg/kg Hg solution, sourced independently from that used for calibration, yielding an expected Hg concentration of 101.6 ng/g.

B. Method Optimization

Method optimization was conducted to evaluate the effect of modifying the selected analytical parameters of the DMA in order to achieve optimal sensitivity and accuracy in the determination of total mercury in fresh fish tissue. The manufacturer-recommended operating conditions were used as the reference or default method (Table 1).

Table 1. Recommended DMA-80 evo operating parameters.

Steps/Parameter	Time (s)	Temp (°C)
Drying	90	200
Ramping	120	660
Decomposition hold	90	660
Catalyst temperature	600 °C	
Purge Time	60 s	
Amalgamation Time	12	900
Recording time	60 s	
Oxygen flow	120 mL/min	

1. Optimization of drying time

The drying step was optimized to assess the effect of moisture removal on analytical performance. The default drying time of 90 s at 200 °C was compared with extended drying times of 180 s and 265 s. The maximum drying time of 265 s was selected based on the upper range suggested in US EPA Method 7473, considering the high moisture content of the fish tissue sample (74.7 %, w/w). All other operating parameters were kept constant during this evaluation.

2. Optimization of holding time during thermal

decomposition

The effect of holding time at the maximum decomposition temperature was evaluated by comparing the default condition of 90 s with an extended duration of 180 s at 660 °C. This parameter was investigated to determine whether prolonged thermal exposure allows complete thermal breakdown of the sample matrix, enhances quantitative mercury release, or influences signal stability. Drying and ramp conditions were maintained constant throughout this experiment.

3. Optimization of sample mass

The influence of sample mass on analytical performance was evaluated at three (3) levels: 30 mg, 50 mg, and 70 mg. The minimum sample mass of 30 mg was selected based on the instrument's recommended lower limit. Increasing sample masses were investigated to assess their effect on signal intensity, precision, and recovery, as well as to determine whether higher sample loading introduces matrix-related variability or incomplete combustion. All experiments were performed in replicate under controlled conditions to ensure data reliability. The analytical responses obtained under different conditions were compared with those of the default method.

All statistical evaluations were carried out at a significance level of $\alpha = 0.05$. Bartlett's test (when three data sets were analyzed) and F-test (when two data sets were compared) were used to assess the homogeneity of variances between groups. With variances of all groups confirmed to not have any significant difference between each other, One-Way Analysis of Variance (ANOVA) and two-tailed independent t-test were performed, respectively, to compare the average results of concerned data sets.

C. Method validation

Mercury calibration standards were prepared from a 1000 mg/L Hg stock solution (Inorganic Ventures) and diluted with 10% HCl. The spiking solution for recovery studies was prepared from NIST SRM 3133 (1000 µg/ mL). No sample preparation was required for DMA-80 testing. Method validation was performed using fresh tissue of tilapia samples (previously determined to have 2.48 ng/g total Hg) spiked with mercury to obtain a final total Hg concentration of 101.6 ng/g. Mercury determination was carried out by weighing 50–60 mg of each standard and sample into the nickel boats and analyzed at 253.7 nm using compressed air combustion and a preset furnace program (optimized instrument operating parameters), with external calibration applied.

The in-house method validation study was conducted by following the Eurachem Guide in order to establish and assess the linearity and working range, repeatability, intermediate precision, trueness, limit of detection (LOD), and limit of quantification (LOQ) [11]. The fitness-for-purpose of the total mercury determination by DMA was evaluated using the information on the maximum permissible limit of Hg in fish (500 ng/g) and the acceptance criteria specified in the AOAC International SMPR® 2024.002 [12].

III. RESULTS AND DISCUSSION

A. Method Optimization

1. Optimization of Drying Time

The effect of drying time on mercury quantification was evaluated by comparing three (3) drying conditions at 200 °C: 90 s, 180 s, and 265 s. The corresponding analytical performance is summarized in Table 2.

Table 2. Effect of drying time on the total Hg in fish tissue.

	Drying time (s)		
	90	**180**	**265**
Average (ng/g)	108.6	111.8	108.6
Standard deviation (ng/g)	8.2	12.0	5.4
%RSD	7.5	10.7	5.0
n	4	4	4

To determine whether the observed differences among the three (3) drying conditions were statistically significant, one-way analysis of variance (ANOVA) was performed. The calculated F-value (F_{calc} = 0.17) was substantially lower than the critical F-value (F_{crit} = 4.26) at the 95% confidence level, indicating no statistically significant difference among the means.

These results suggest that extending the drying time up to 265 s, which is almost three (3) times the default duration, will not significantly affect mercury quantification in the fish tissue samples. Although the 265 s duration produced the lowest variability, the comparable mean concentrations and acceptable precision obtained under all conditions indicate that moisture removal was already sufficiently achieved at 90 s despite the relatively high moisture content of the fish tissue (74.7 %, w/w). Since extending the drying time did not significantly improve analytical performance and would increase total run time, the default drying time of 90 s was selected as the optimized condition.

2. Optimization of holding time during thermal decomposition

The effect of holding time during thermal decomposition at 660 °C was investigated by comparing 90 s and 180 s. The corresponding analytical performance is summarized in Table 3.

Table 3. Effect of decomposition holding time on the total Hg in fish tissue.

	Holding time (s)	
	90	**180**
Average (ng/g)	108.6	102.6
Standard deviation (ng/g)	8.2	2.8
%RSD	7.5	2.69
n	4	4

Results from the two-tailed independent t-test gave a calculated t-value (t_{calc} = 1.39) lower than the critical (t_{crit} = 2.45), demonstrating that there was no significant difference in the mean mercury concentrations obtained at 90 s and 180 s holding times. Although the extended holding time showed slightly improved precision, the lack of statistically significant improvement suggests that complete thermal decomposition and mercury release were already achieved under the default duration of 90 s. Therefore, the shorter holding time was retained for subsequent testing to maintain analytical efficiency while ensuring reliable quantification.

3. Optimization of sample mass

To identify the sufficiency of the optimized drying time and decomposition holding time in analyzing variable fish tissue masses, the sample mass was set to 30 mg, 50 mg, and 70 mg, and analyzed under the default furnace program. Results of One-way ANOVA gave a calculated F-value (F_{calc} = 3.11) lower than the critical F-value (F_{crit} = 5.14). This implies that there was no significant difference in the average total Hg measured from the fish tissues when 30 mg, 50 mg, or 70 mg of sample were used.

Although statistical evaluation showed no significant difference in mercury concentrations across the tested sample weights, using 50 to 70 mg of sample demonstrated better precision and acceptable recovery (when compared with the expected concentration of 101.6 ng/g), providing an appropriate balance between analytical sensitivity and matrix loading, while minimizing variability potentially associated with lower sample mass or incomplete combustion at higher sample mass. Accordingly, 50 mg was selected as the optimized sample mass for method validation and subsequent analyses.

Based on the optimization results, the default thermal program (Table 1) was proven suitable for analysis of total mercury content in fish tissue, while optimization of sample mass improved method precision. The selected conditions provided reliable analytical performance while minimizing total testing time.

The results further demonstrate that neither extended drying nor prolonged holding time produced a statistically significant improvement in mercury quantification compared to the standard operating conditions. While extended holding time introduced greater variability, it did not affect the accuracy of the measurement. Varying the mass of the fish tissue sample to be tested, under the default furnace program, was found to not exhibit any significant variation in terms of recovery.

These findings indicate that the manufacturer-recommended parameters for the DMA-80 evo Direct Mercury Analyzer are already optimized for fish tissue testing. Maintaining the standard conditions is therefore preferable, as they ensure reliable results while minimizing testing time and avoiding unnecessary thermal exposure.

Table 4. Effect of sample mass on the total Hg in fish tissue.

	Sample mass (mg)		
	90	**180**	**265**
Average (ng/g)	108.6	111.8	108.6
Standard deviation (ng/g)	8.2	12.0	5.4
%RSD	7.5	10.7	5.0
n	4	4	4

B. Method Validation

Linearity and calibration working range

The linearity and working range were assessed by constructing a calibration curve using different aliquots of a 1.159 ng/g Hg solution and plotting the instrument response (peak height) versus the total Hg amount (ng). The calibration curve is shown in Figure 1, while the plot of residuals is shown in Figure 2.

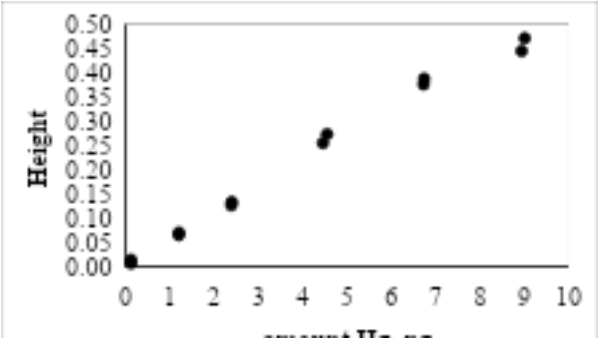


Fig. 1. Calibration curve for total Hg determination.

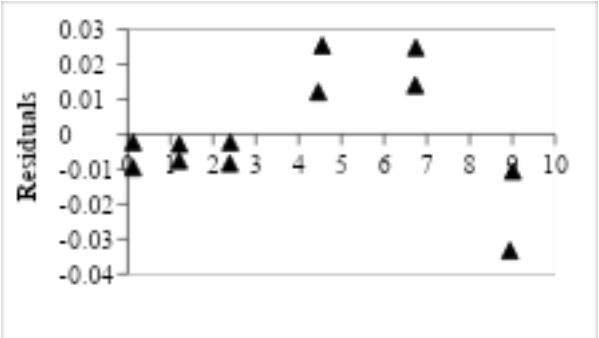


Fig. 2. Residual plot for total Hg determination.

The correlation coefficient (r = 0.9952, n = 12) confirmed a strong linear relationship between instrument response and mercury concentration, meeting the acceptance criterion (r ≥ 0.9950) and indicating good linearity across the calibration working range of 0.10-10 ng Hg. Residual analysis showed that differences between observed and predicted responses were randomly distributed around zero, with no systematic trends. Overall, method have demonstrated a good linear relationship between the amount of total Hg and the instrument response, making the linear regression model suitable for reliable quantification of total Hg.

Limit of detection and limit of quantification

At low concentration levels, the limit of detection (LOD) and limit of quantitation (LOQ) were determined to evaluate the sensitivity and regulatory suitability of the method. These parameters define the lowest concentration that can be reliably detected and quantified with acceptable accuracy. Both LOD and LOQ were estimated from eleven (11) replicate analyses of fish tissue that underwent the complete analytical procedure.

The method was developed to monitor trace levels of total Hg in fish tissue, and must therefore detect and quantify concentrations below the regulatory limits of 500 ng/g. The obtained LOD value of 0.65 ng/g and LOQ of 2.16 ng/g demonstrate that the method is sufficiently sensitive for trace-level detection and quantitation, making it suitable for assessing compliance of fresh fish tissue samples.

Repeatability and intermediate precision

Repeatability was evaluated using eleven (11) replicate measurements within a day, while intermediate precision was assessed by measurements (n=4) across three (3) different days by different analysts using the same equipment. Repeatability results showed %RSDr of 6.89, indicating good consistency under identical conditions. Intermediate precision showed higher $\%RSD_R$ value of 8.64, as expected due to increased variability over time, but remained within the acceptable limits ($\%RSD_R$ < 22%), confirming controlled analytical variability. Although the direct mercury analyzer enabled mercury determination without acid digestion, matrix effects, sample heterogeneity, mercury volatility, and potential losses during handling likely contributed to the observed variability and relatively higher %RSD values.

Trueness by recovery

Trueness was evaluated via spiking recovery of the prepared spiked sample due to the absence of a certified reference material (CRM) for Hg in fresh fish tissue. The fresh fish tissue has a native total Hg concentration of 2.48 ng/g, and was fortified with a Hg spike of 101.6 ng/g.

The results for trueness study have shown an average percent recovery of 101.6%, with %Recovery values in the range of 88.6 – 110.1. All values fall within the AOAC acceptable range of 80–110%, indicating no significant systematic bias. This demonstrates that the method provides accurate total Hg quantification in fresh fish tissue following spiking recovery assessment.

The in-house method validation results are summarized in Table 5. The direct mercury analysis method satisfied the acceptance criteria for all method validation parameters, demonstrating its suitability for the quantification of total Hg in fresh fish tissue.

Table 5. Summary of method validation.

Parameter	Acceptance Criteria	Results
Linearity and calibration working range	r > 0.9950; residuals are randomly distributed to zero	r = 0.9952; residuals are randomly distributed to zero; Working range: 0.10 – 10.0 ng *Evaluation: Passed*
Limit of detection (ng/g)	50	0.65 *Evaluation: Passed*
Limit of quantification (ng/g)	167	2.16 *Evaluation: Passed*
Repeatability	$\%RSD_r$ < 15%	$\%RSD_r$ = 6.89 (102.5 ng/g; n=11) *Evaluation: Passed*
Intermediate Precision	$\%RSD_R$ < 22%	$\%RSD_R$ = 8.64 (104.8 ng/g; n=12) *Evaluation: Passed*
Trueness by spiking	% Recovery = 80 - 110%	%Recovery = 88.6 – 110.1, n=11 *Evaluation: Passed*

IV. CONCLUSION

The study demonstrated reliable ultratrace quantification of Hg in fish tissue samples by direct mercury analysis, performing acceptably in terms of linearity, limit of detection, limit of quantification, repeatability, intermediate precision, and trueness. This method was conducted without extraction or a digestion process, proving it to be a simple, rugged, sensitive, and economical technique. Endeavors in optimization of the heating program found the default program to be sufficient in terms of trueness and precision, in regards to modified drying and holding times. The absence of pre-concentration in the methodology, and the equipment's working range, deems this method to be fit-for-purpose in testing total Hg in fish tissues, with concentrations lower than the set regulatory limit by the Philippines BFAR.

ACKNOWLEDGEMENT

The authors would like to express their gratitude for the guidance provided by the Industrial Technology Development Institute (ITDI). The authors are also grateful to the dedicated service and guidance provided by the staff of the Inorganic Chemistry Section of the Standards and Testing Division, ITDI: Ruth Damian, Michael Lagmay, Johanna Andrea C. Valdueza, Anina Marielle Medel, Leonard Montero, Andrea Tero, Mark Nicholas Yow, Mark Anthony Principe, Jason Cortez, Ryan Cortez and Nico Mangundayao.

REFERENCES

[1] Gao, X., Yuan, W., Chen, J., Huang, F., Wang, Z., Gong, Y., Zhang, Y., Liu, Y., Zhang, T., & Zheng, W. (2023). Tracing the source and transport of HG during pedogenesis in strongly weathered tropical soil using HG isotopes. *Geochimica et Cosmochimica Acta*, *361*, 101–112. https://doi.org/10.1016/j.gca.2023.10.009

[2] De Simone, F., Hedgecock, I. M., Bruno, D. E., Cinnirella, S., Sprovieri, F., & Pirrone, N. (2024). Modelling the anthropogenic HG pollution fingerprint on the Marine Fishery Production Worldwide: A preliminary exposure assessment for people living in countries having different income levels. *Environment International*, *190*, 108891. https://doi.org/10.1016/j.envint.2024.108891

[3] Fioravanti, R., Muzzioli, L., Maurel, E., Palma, G., Calabrese, G., Angioni, A., La Rocca, C., Mantovani, A., Pezzana, A., & Donini, L. M. (2025). Bioaccumulation and biomagnification of Mercury along the seafood chain in Europe: A systematic review. *Foods*, *14*(21), 3752. https://doi.org/10.3390/foods14213752

[4] Dutta, S., & Ruden, D. M. (2024). Heavy metals in umbilical cord blood: Effects on epigenetics and child development. *Cells*, *13*(21), 1775. https://doi.org/10.3390/cells13211775

[5] Kim, K.-N., Bae, S., Park, H. Y., Kwon, H.-J., & Hong, Y.-C. (2015). Low-level mercury exposure and risk of asthma in school-age children. *Epidemiology*, *26*(5), 733–739. https://doi.org/10.1097/ede.0000000000000351

[6] Bondy, S. C. (2021). Metal toxicity and neuroinflammation. *Current Opinion in Toxicology*, *26*, 8–13. https://doi.org/10.1016/j.cotox.2021.03.008

[7] Bureau of Fisheries and Aquatic Resources. (2001). Rules and regulations on the exportation of fresh, chilled and frozen fish and fishery/aquatic products. https://elibrary.judiciary.gov.ph/thebookshelf/showdocs/10/44103 and Agriculture.

[8] Liang, L., Bloom, N. S., & Horvat, M. (2003). Simultaneous determination of mercury speciation in environmental and biological samples by thermal decomposition, amalgamation, and atomic absorption spectrometry. Talanta, 60(2–3), 289–300. https://doi.org/10.1016/S0039-9140(03)00118-3

[9] U.S. Environmental Protection Agency. (1998). *Method 7473 (SW-846): Mercury in solids and solutions by thermal decomposition, amalgamation, and atomic absorption spectrophotometry (EPA-7473). U.S. EPA.* https://www.epa.gov/sites/default/files/2015-07/documents/epa-7473.pdf

[10] Milestone DMA-80 evo. (n.d.). DMA-80 evo direct mercury analyzer. Milestone Srl. Retrieved May 7, 2026, from https://www.milestonesrl.com/products/mercury-determination/dma-80-evo

[11] H. Cantwell (ed.) Eurachem Guide: The Fitness for Purpose of Analytical Methods – A Laboratory Guide to Method Validation and Related Topics, (3rd ed. 2025). Available from http://www.eurachem.org

[12] AOAC INTERNATIONAL. (2024). AOAC SMPR® 2024.002: Standard method performance requirements (SMPRs®) for determination of trace elemental contaminants in food and beverages. https://www.aoac.org/wp-content/uploads/2024/05/SMPR-2024_002.pdf

2026 IMEKO Joint Conference
TC8 - TC11 - TC24
Metro Manila, Philippines, August 26-29, 2026

Application of Multivariate Analysis in the Investigation of Microparticles Present in Philippine Milkfish, Feeds, and Marine Water

Zamantha Nadir Z. Martin [1], Len Lara H. Salvador [1], Clarisse Jasmine J. Carlos [1], Aldrin V. Palad [1], Kim Christopher C. Aganda [2], Angelene J. Alcain [1], Araceli M. Monsada [1], and Lynne Jerisa A. Castro [1]

[1] *Advanced Device and Materials Testing Laboratory (ADMATEL), Surface Engineering Section, Materials Science Division, Industrial Technology Development Institute, Department of Science & Technology, Bicutan, Taguig City 1631, Metro Manila, Philippines*
[2] *Industrial Chemical Section, Chemicals and Energy Division, Industrial Technology Development Institute, Department of Science & Technology, Bicutan, Taguig City 1631, Metro Manila, Philippines*

***Abstract* – This study investigated the characterization and distribution of microplastic (MP) contamination in cage-cultured milkfish, commercial feeds, and surrounding waters in an open-water aquaculture system. The proliferation of MPs in the aquaculture environment threatens marine environment species and poses potential risks to human health. Selected fingerlings, juveniles, and adult milkfish, along with water and feed samples, were collected in Southern Mindanao, Philippines. Samples were digested with H_2O_2 and KOH. Polypropylene (PP), polyethylene terephthalate (PET), polyamide (PA), polyethylene (PE), and cellulose fibers were detected using an ATR-FTIR technique. Principal component analysis was performed to aid in classifying the microplastic particles according to source, showing distinct separation between cellulose fibers and polymers across all sample sources. The first two principal components for fish, water, and feeds account for 88.76%, 83.89%, and 91.52% of the corresponding data set variance, respectively. Findings suggest that environmental exposure and contaminated feeds are possible pathways and factors for microplastic ingestion in milkfish.**

I. INTRODUCTION

Inexpensive, durable, and flexible, plastic has evolved from a revolutionary convenience to the most prevalent material worldwide. Due to their beneficial properties, plastics are widely used across industries such as agriculture, packaging, construction, electronics, and transportation despite their long-term environmental disposal concerns [1]. The aspects that had attracted humans to use the plastics have, nevertheless, turned out to be a problem as garbage made of plastic takes hundreds of years to decompose in nature, while people dispose of such items after a short period of time [2]. The moment plastic waste starts floating or gets washed up to rivers, lakes, and coastal areas, it is subject to the process of degradation through the action of the sun, wave motion, abrasion, and microbial activity, which results in the reduction of bigger pieces into very tiny fragments, and those very tiny pieces are known as "microplastics" [3]. Microplastics (MPs) are defined as particles smaller than five millimeters and are subdivided into two broad categories: primary microplastics, which are purposely manufactured at a small size, such as industrial pellets or cosmetic microbeads; and secondary microplastics, which come into existence when bigger plastic items become fragile and turn into smaller pieces like films, fibers, and debris [4, 5].

MPs have become a problem of great concern since the ocean has taken over as the central storage for these materials [6]. A large number of fish and other marine animals that are found in water columns take up small particles that they confuse for food, thus leading to ingestion, which can cause spoiling of tracts or, in some cases, absorption of nutrients being interfered with [7]. The chemical additives that were in the plastics, along with the contaminants that were on the surfaces of the particles, could very well be transferred into the tissue of the fish and consequently into the humans who consume the fish. Still, a lot of questions are raised about the full health impact, but nevertheless, the possible overstressing of the immune system, the causing of inflammation, and the damaging of the organs like the liver and kidneys have been some of the health effects that have been outlined [8]. In a country like the Philippines, where aquaculture is so much a part of the day-to-day lives of the people and is also the mainstay of food security [9], the pollution of the marine environment

with MPs is as much a threat to the human community as it is to the environment. Thus, the issue has to be taken with urgency rather than passing it off as a mere academic concern.

In the Philippine context, there has been a rise in studies regarding MP ingestion in fish species over the years, albeit the related literature is still limited to certain areas. Even though the Philippines is a major exporter of aquaculture products, the issue of MPs in farmed species still lacks systematic evaluation. Most of the research is still restricted to a few coastal or river areas [10, 11], which makes it less likely to compare contamination levels among different ecosystems such as marine waters, freshwater ponds, and brackish environments. Even for milkfish (*Chanos chanos*)—one of the most important fish species economically in the Philippines, farmed everywhere from coastal ponds and big cages [12]—such comparative data is limited. Consequently, previous studies typically use microplastic features such as color, size, shape, and polymer type to identify possible sources of contamination within farming areas [5, 13]. Among these characteristics, polymer type is often considered one of the most informative indicators of microplastics origin. Accordingly, polymer identification is typically performed using Fourier-transform infrared spectroscopy (FTIR), which produces characteristic spectrum for individual polymers that can be compared with reference databases to determine polymer composition [14]. Biological factors are also considered, as the size of the fish, its diet, and its growth stage seem to affect the amount and type of MPs ingested by a species. These limitations imply that larger and more coordinated research efforts are required.

The current study aimed to provide information on the characterization and quantification of MPs in milkfish, commercial feeds, and surrounding waters in an open-water aquaculture system in Southern Mindanao, Philippines. Furthermore, this study integrates vibrational spectroscopy with Principal Component Analysis (PCA) to examine patterns within each sample type, providing insights into internal FTIR spectral behavior. The evaluation will produce findings that will be used as initial data to aid monitoring, planning through regulations, and policy making for MP management grounded in science in the Philippine aquaculture sector.

II. MATERIALS AND METHODS

A. Materials

All materials utilized in the sampling preparation and analysis procedure are made of metal (stainless steel) and glass. This is done to prevent the possibility of additional plastic contamination that can be obtained during preparation. Additionally, plastic coolers are employed for sample storage. The interior linings of the storage are constructed of white polypropylene plastic, which can be easily identified due to the minuscule risk of contaminating the sample. The reagents utilized were 85% KOH and H_2O_2, both AR grade (analytical), and distilled water, which were filtered using a glass microfiber or Whatman filter paper to ensure no plastic contamination was present in the reagents used for the experiment. A vacuum pump and its manifold, along with the filtration setup, are used to filter all the reagents and actual samples. The glass microfiber filter papers are sized at 50 µm to collect microplastic particles equal to or larger than this size.

B. Sampling

The study focused on an island group in Southern Mindanao, Philippines—coded as SEM-1 for anonymity—and was undertaken in an open-water (marine) aquaculture system. The researchers worked closely with the Bureau of Fisheries and Aquatic Resources (BFAR) and Local Government Unit (LGU) to ensure full legal compliance with sampling requirements and handling protocols. From the marine cage site, milkfish samples from all life stages—fingerlings, juveniles, and adults—are collected for analysis. For the water samples, about one liter (1 L) of surface and subsurface water samples of different depths (1-4m, 5-9m, and 10m beyond) were collected from the four corners and the middle area of the cages. Representative aquafeeds from the site were also gathered for other possible sources of MPs.

C. Sample preparation: digestion

Collected adult, juvenile, and fingerling samples (n=10 each) were measured and weighed prior to analysis. The milkfish samples then underwent primary preparation, which involved deboning and gutting, before digestion. The gastrointestinal tract (GIT) of the milkfish was subjected to digestion for the extraction of MPs. Specifically, the GIT was weighed and placed in a glass container, after which the digestion procedure was carried out by adding 10% KOH to the sample and incubating it at 40°C for 48 hours. Following digestion, the samples were filtered through pre-weighed glass microfiber filters using vacuum filtration. The resulting wet filters were then oven-dried at 80°C for at least 48 hours. The collected aquafeed samples were processed using the same filtration, digestion, and drying procedures.

For the isolation of MPs in water, glass microfiber filter paper was employed during the filtration process for the removal of organic matter. The residue in the filter paper is then transferred to a beaker by periodically rinsing it with water and oven-drying it at 90°C for at least 24 hours. The oven-dried sample is then digested for 48 hours at 65°C using 10 mL of 30% H_2O_2. The sample is then filtered through a 100x100-micrometer stainless steel mesh and repeatedly cleaned with distilled water until no residue remains.

D. Profiling of microplastics

D. 1 Optical Microscopy

The filter papers containing the suspected MP samples are observed under a tabletop microscope (Carl Zeiss Stemi 2000-C Stereo Microscope) with a built-in ZEISS camera to obtain pictures of the microplastics. The optical microscope was operated via ZEN software, allowing for the measurement of MP morphology and size as well as color identification. MPs are categorized under two main types: fiber and fragment. MPs under the fiber category have a distinct thread-like shape that is long and appears as a string under the microscope [16]. Fragmented MPs, on the other hand, have no shape and are much smaller, appearing as a speck with no uniform outline [15].

D. 2 FTIR Spectroscopy

Suspected MPs obtained from the sampling area, SEM-1, are subjected to Fourier Transform Infrared (FTIR) spectroscopy. The isolated microplastics of the samples are analyzed using the PerkinElmer FT-IR Spectrometer Frontier through the Attenuated Total Reflectance (ATR) technique. The study consisted of 20 scans in the 4000-600 cm^{-1} range, with a 4 cm^{-1} resolution and a data interval of 4 cm^{-1}. The force gauge of the ATR-FTIR technique was set to a minimum of 80 Newtons to enable the best possible crystal contact with the sample.

The spectra obtained identified the microplastics and showed the peaks characterized by their functional groups. Furthermore, a search function built into the Spectrum program specifically matched the spectrum of the suspected MPs to the existing PerkinElmer library (Version 6.3.5.0176) to determine their exact identity.

E. Blank correction

A blank correction was added to the data treatment to account for MPs that may have originated from the environment or air. This was done in addition to contamination prevention measures so that any additional plastics that did not come from the samples themselves could be removed from the total concentration, and clean and accurate data were obtained. In this study, blanks per sample (milkfish, water, and feeds) were incorporated into the analysis to account for the possibility of contamination. The blank correction $(Ave\ MP/_{sample})$ was performed by subtracting the average number of MPs collected in the blanks $(\Sigma \bar{X} MP_{blank})$ from the total MPs of the actual samples to correct the concentration (ΣMP_{sample}) [17]. The equation was shown as:

$$Ave\ MP/_{sample} = (\sum MP_{sample} - \sum \bar{X} MP_{blank}) \quad (1)$$

F. Multivariate Analysis

Multivariate analysis is a means of statistical treatment often employed for large and complicated sets, with the goal of obtaining useful information without compromising data integrity. Methods such as principal component analysis (PCA) and *k*-means clustering are some of the most commonly used techniques. In principal component analysis, interrelated variables are transformed to a set of variables, referred to as principal components, while retaining essential information [16]. *K*-means clustering determines the optimal *k* number of clusters to sufficiently represent the data.

All IR spectra from the suspected microplastics were baseline-corrected before extraction and compilation in a single comma-separated values (CSV) file, after which PCA and *k*-means clustering were performed. All analyses were coded in Python using open-source libraries and processed in Google Colab.

III. Results and Discussion

A. Microplastic concentration in milkfish, feeds, and marine water

A total of 10 milkfish samples in each of the different stages (fingerling, juvenile, and adult) were analyzed for the presence of MPs. And to detect potential sources of contamination, commercial feed samples (n=3) and water samples (n=8) from the cage perimeters, center, and varying depths were gathered for analysis. Table 1 below illustrates the total average MP concentration, together with cellulose. The research included the identified cellulose because semi-synthetic cellulose fibers, such as rayon, are considered to be a major source of microfiber pollution in water bodies and are frequently used in the textile and fiber manufacturing industries [18].

Table 1. Average identified microplastics in milkfish, feeds, and water samples from the SEM-1 marine site.

Sample Type	Average microplastic with cellulose (particles g^{-1} GIT; particles L^{-1} water)
Fingerlings	0.033 ± 0.010
Juvenile	0.53 ± 0.059
Adult	8.05 ± 0.65
Feeds	1.67 ± 0.51
Water	3.87 ± 0.16

*with blank correction

Analytical data for the computed MP concentrations were reported as mean ± standard deviation. Based on the blank-corrected results obtained from Eq. 1, adult milkfish (8.05 ± 0.65) showed the highest MP concentration per 5g fish sample, based on the GIT that was analyzed, significantly higher than the juveniles (0.53 ± 0.059 per 3g of GIT) and fingerlings (0.033 ± 0.01 per 2g of GIT). This may be attributed to the high environmental baseline encountered at that site. Notably, SEM-1 water had the second-highest recorded MP concentration, at 3.87 ± 0.16

per ≤ 1 L water sample. Because fish efficiently filter and retain MPs within their gastrointestinal tract, the contamination load in adult milkfish is higher than that of the water samples [19]. Additionally, since water is a free-flowing environment, the presence of MPs is merely an instantaneous pollution [19].

While aquafarm feeds revealed a MP presence of 1.67 ± 0.51 per 5g sample, contributing to the total plastic burned observed in milkfish. Studies suggest that the use of commercial fish feed contributes to MP infiltration in cultured milkfish, which may pose a substantial threat, and these particles can arise during the manufacturing process and through environmental exposure [20]. The mean MP concentration of the various life stages and environmental media shows numerical differences, which may indicate multiple contamination pathways.

B. Physical characteristics of microplastics

The physical characterization of recovered MPs was divided into two categories based on their shapes: fiber and fragment. While fragments are irregularly shaped particles that may arise from shattered pieces of plastic bottles or plastic waste, fiber is defined as having a thread-like appearance and is primarily derived from synthetic textiles [16]. When looking at the shapes of MP particles in Table 2, it is clear that microplastic pollution is characterized mainly by the presence of fiber-shaped particles in all environmental media, and heavily so to such an extent that the latter completely dominates the former.

Table 2. Morphology (shape and size) of isolated microplastics in SEM-1.

Sample Type	Fiber, ave. length (µm)	Fragment, ave. length (µm)
Fingerlings	735.58 ± 210.57	0
Juvenile	1993.71 ± 360.56	0
Adult	1686.09 ± 1488.12	284.98 ± 108.69
Feeds	1011.35 ± 706.69	0
Water	971.79 ± 818.22	178.33 ± 47.08

Additionally, this dominance of fibers can be seen in all sources of contamination of milkfish, including water and commercial feeds. On the other hand, fragments were practically non-existent and occurred in the SEM-1's adult milkfish and water sample. It can be inferred from these variations and from the high fiber counts in the water that the local aquatic environment is a factor in MP ingestion by fish and that fibers are most probably entering the milkfish as a result of consuming contaminated food sources.

C. Distribution of identified polymer types

The study determined the polymer types across all collected milkfish, feed, and water samples using ATR-FTIR. Suspected MPs were identified based on their peak intensities, patterns, and percentage match against the database in the Spectrum Library Search Plus Software. As shown in Figure 1, cellulose is the most prevalent form of polymer, accounting for 60% of the total MP count in the samples from the marine cage-cultured system. This was followed by PET at 34%, PE at 5%, and PA and PP, which each comprised 1%. These MPs may emerge from the fragmentation of large plastic products that deteriorate due to environmental weathering or in the form of plastic pellets used in textiles [16].

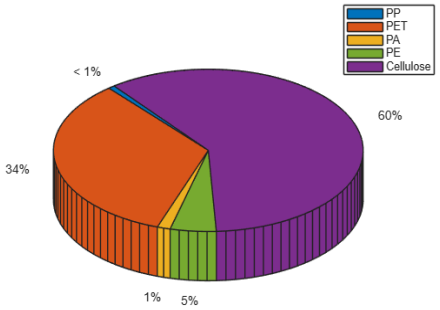


Fig. 1. Distribution of identified microplastics polymer types in milkfish, feeds, and water samples.

D. Multivariate Analysis

PCA was performed on each data set according to sample type (fish, feed, and water). The results are shown in Figs. 2A to 4A as scatter plots by plotting the first two principal components (PC 1 and PC 2), followed by their corresponding loadings plots in Figs. 2B to 4B. For the fish, water, and feed datasets, the first two principal components explain 88.76%, 83.39%, and 91.52% of the total variance, respectively. K-means clustering determined a value of k=2 for all sets to be sufficient in discriminating the samples.

Clustering across all data sets was observed to classify the samples as either cellulose-based or otherwise based on their identification via FTIR. This is very evident in the feeds group, as shown in Fig. 2A. Cluster 1 is composed entirely of data points identified as cellulose, while Cluster 2 consists of samples classified as "others." The loadings plot in Fig. 2B demonstrates that the variances in this set are influenced by O-H groups at ~3300 and 1400 cm^{-1} and C-O stretching at 1100-1000 cm^{-1}. Additionally, all samples in Cluster 2 gave weak IR signals, resulting in spectra without definite library matches, suggesting that these samples may be mixtures.

The cellulose versus non-cellulose distinction is also demonstrated in the water samples as seen in Fig. 3A. Most of the samples in Cluster 1 were designated as "others," while all samples identified as cellulose belong to Cluster 2. Some of the other samples in the same cluster were identified as PET. In fact, the majority of samples labelled

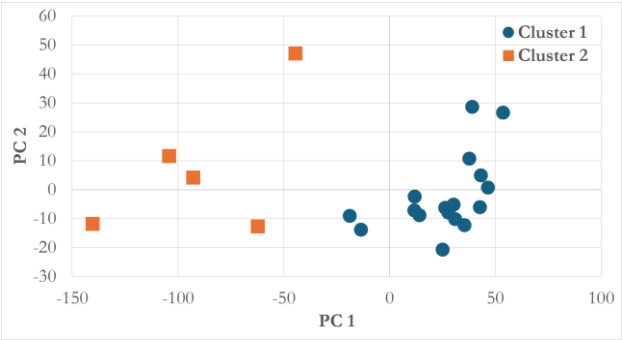


Fig. 2A. PC plot showing the clusters from feed samples.

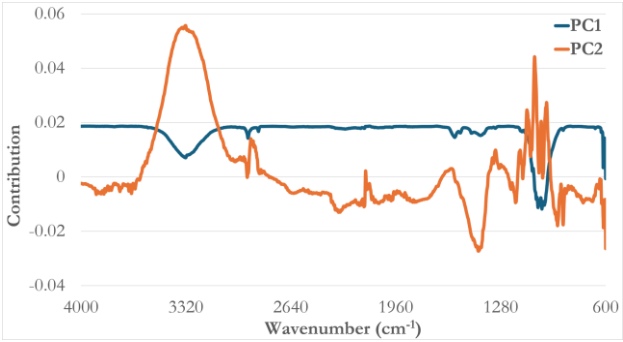


Fig. 2B. Loadings for PC1 and PC2 from feed samples.

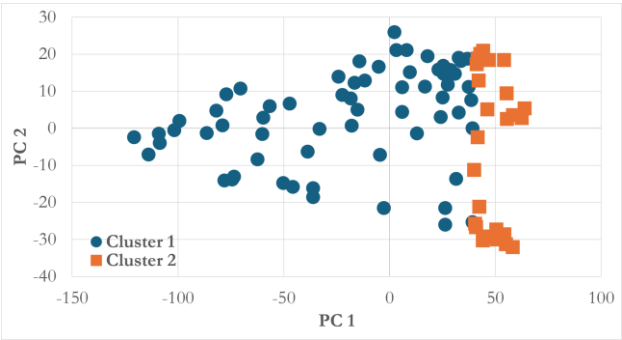


Fig. 3A. PC plot with the clusters from water samples.

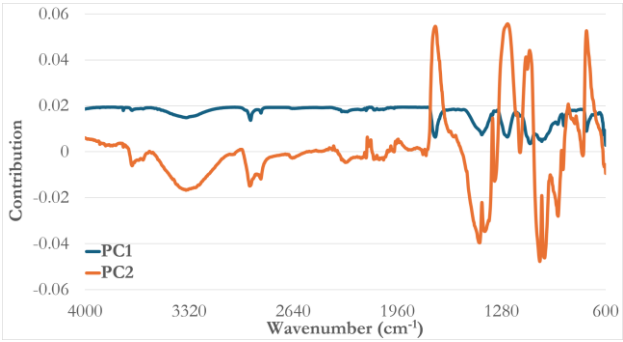


Fig. 3B. Loadings for PC1 and PC2 from water samples.

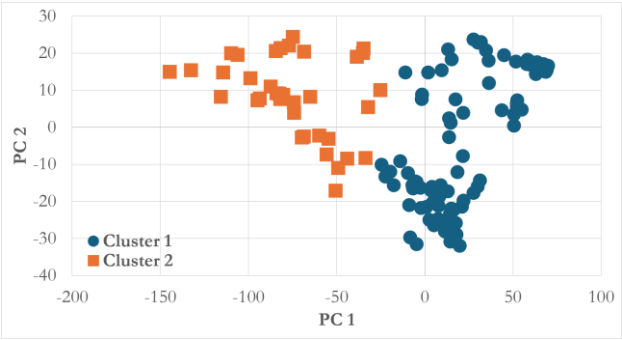


Fig. 4A. PC plot of the clusters from fish samples.

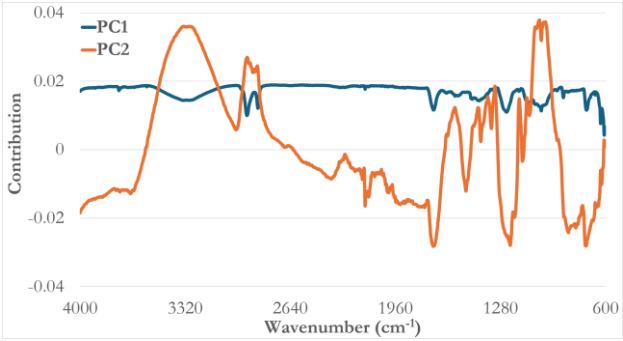


Fig. 4B. Loadings for PC1 and PC2 from fish samples.

"PET" were found in Cluster 2. This may be due to the distinct signals given by the carbonyl and alcohol groups present in cellulose and PET-based structures. This is confirmed by the loadings plot in Fig. 3B, showing that the carbonyl (~1700 cm^{-1}) and alcohol (O-H stretch at ~3300 cm^{-1}, O-H bending at ~1420-1380 cm^{-1}, and C-O stretch at 1030-1000 cm^{-1}) groups greatly contribute to the data set variance.

The PC plot for fish samples in Fig. 4A likewise highlights the cellulose/non-cellulose clustering scheme. Cellulose samples dominate Cluster 1, along with PET samples. Most of the samples in Cluster 2 were designated as "others," similar to that observed in the water samples. The loadings plot in Fig. 4B supports this pattern with the intense contributions from C=O groups at ~1700 cm^{-1} and O-H groups at ~3300 cm^{-1} and ~1220-980 cm^{-1}.

Upon closer inspection, all samples obtained from fingerlings and juvenile fish are found in Cluster 1. They are also observed to be visually tightly grouped together. Despite diverse identifications for each point, with most of them classified as "others," they may hint at a singular or similar source since these samples show little variance with respect to each other. Another possible explanation is that microplastics ingested during the fingerling stage do not, or cannot, exit the digestive tract. This is of great concern since it would imply that microplastic bioaccumulation is possible even in the early stages of the milkfish life cycle.

Overall, the multivariate analysis results highlighted the composition of microplastic samples, distinguishing between cellulose and non-cellulose origin.

IV. CONCLUSION

The presence of microplastics in Southern Mindanao, Philippines, highlights the growing issue of plastic accumulation in aquaculture settings. Different growth stages of milkfish showed varying patterns of microplastic uptake, which is indicative of direct and indirect contamination routes, such as exposure to surrounding waters and feeding on contaminated feeds. Milkfish, water, and feed samples predominantly contained fiber-shaped microplastics. The study also identified the presence of five polymer types: cellulose, PET, PE, PA, and PP. Among these, cellulose-based microplastics were the most dominant in the collected samples. Multivariate analysis further highlights the types of collected particles, distinguishing between cellulose and non-cellulose material. In conclusion, the study reveals insights into microplastic concentrations in milkfish, marine water, and feeds, highlighting the need for better-informed management strategies within the Philippine aquaculture sector.

V. ACKNOWLEDGMENT

This work is supported by the Philippine Council for Agriculture, Aquatic, and Natural Resources Research and Development (DOST-PCAARRD) and the Industrial Technology Development Institute (DOST-ITDI) of the Department of Science and Technology (DOST) of the Philippines.

REFERENCES

[1] J. Nikiema, Z. Asiedu, A review of the cost and effectiveness of solutions to address plastic pollution, Environmental Science and Pollution Research 29 (2022) 24547–24573. https://doi.org/10.1007/s11356-021-18038-5.

[2] P. Stoett, V.M. Scrich, C.I. Elliff, M.M. Andrade, N. de M. Grilli, A. Turra, Global plastic pollution, sustainable development, and plastic justice, World Development 184 (2024). https://doi.org/10.1016/j.worlddev.2024.106756.

[3] J. Dutta, M. Choudhury, Open Access Journal of Waste Management & Xenobiotics Plastic Pollution: A Global Problem from a Local Perspective J Waste Manage Xenobio Plastic Pollution: A Global Problem from a Local Perspective, n.d.

[4] M.S. Bhuyan, Effects of Microplastics on Fish and in Human Health, Frontiers Environmental Science 10 (2022). https://doi.org/10.3389/fenvs.2022.827289.

[5] H. Fakour, S.L. Lo, N.T. Yoashi, A.M. Massao, N.N. Lema, F.B. Mkhontfo, P.C. Jomalema, N.S. Jumanne, B.H. Mbuya, J.T. Mtweve, M. Imani, Quantification and analysis of microplastics in farmland soils: Characterization, sources, and pathways, Agriculture (Switzerland) 11 (2021). https://doi.org/10.3390/agriculture11040330.

[6] G. Peng, R. Bellerby, F. Zhang, X. Sun, D. Li, The ocean's ultimate trashcan: Hadal trenches as major depositories for plastic pollution, Water Research 168 (2020) 115121. https://doi.org/10.1016/J.WATRES.2019.115121.

[7] R.S. Yu, S. Singh, Microplastic Pollution: Threats and Impacts on Global Marine Ecosystems, Sustainability (Switzerland) 15 (2023). https://doi.org/10.3390/su151713252.

[8] B. Jovanović, Ingestion of microplastics by fish and its potential consequences from a physical perspective, Integrated Environmental Assessment and Management 13 (2017) 510–515. https://doi.org/10.1002/ieam.1913.

[9] A. TAHİLUDDİN, E. TERZİ, An Overview of Fisheries and Aquaculture in the Philippines, Journal of Anatolian Environmental and Animal Sciences 6 (2021) 475–486. https://doi.org/10.35229/jaes.944292.

[10] E.Q. Espiritu, R.S. Rodolfo, S.M.J. Evangelista, J.J.G. Feliciano, A.M.N. Sumaway, J.L.R. Pauco, K.V.N. Alvarez, E.P. Enriquez, Microplastics contamination in the fishes of selected sites in Pasig River and Marikina River in the Philippines, Marine Pollution Bulletin 187 (2023). https://doi.org/10.1016/j.marpolbul.2023.114573.

[11] K.M. Similatan, C.G.L.A. Arcadio, C.K.P. Navarro, R.Y. Capangpangan, H.P. Bacosa, Microplastic ingestion by adult milkfish Chanos chanos (Forsskål, 1775) in aquaculture system: The case of Butuan Bay, Philippines, Marine Pollution Bulletin 194 (2023). https://doi.org/10.1016/j.marpolbul.2023.115409.

[12] N.D. Salayo, C.L. Marte, J.D. Toledo, A.G. Gaitan, R.F. Agbayani, Developing a self-sufficient Philippine milkfish industry through value chain analysis, Ocean Coastal Management 201 (2021). https://doi.org/10.1016/j.ocecoaman.2020.105426.

[13] M. Raza, J.Y. Lee, J. Cha, Microplastics in soil and freshwater: Understanding sources, distribution, potential impacts, and regulations for management, Sci Prog 105 (2022). https://doi.org/10.1177/00368504221126676.

[14] A.G. Zea Cobos, J. Amón, E. León, P. Caballero, Standardization of FTIR-Based Methodologies for Microplastics Detection in Drinking Water: A Meta-Analysis Indeed and Practical Approach, Water (Switzerland) 16 (2024). https://doi.org/10.3390/w16223170.

[15] O. Bajt, From plastics to microplastics and organisms, FEBS Open Bio 11 (2021) 954–966. https://doi.org/10.1002/2211-5463.13120.

[16] I.T. Jolliffe and J. Cadima, Principal component analysis: a review and recent developments, Philos Trans A Math Phys Eng Sci (2016) 374 (2065): 20150202. https://doi.org/10.1098/rsta.2015.0202

[17] V.C. Shruti, G. Kutralam-Muniasamy, Blanks and bias in microplastic research: Implications for future quality assurance, Trends in Environmental Analytical Chemistry 38 (2023). https://doi.org/10.1016/j.teac.2023.e00203.

[18] S. Santonicola, M. Volgare, F. Olivieri, M. Cocca, G. Colavita, Natural and Regenerated Cellulosic Microfibers Dominate Anthropogenic Particles Ingested by Commercial Fish Species from the Adriatic Sea, Foods 14 (2025). https://doi.org/10.3390/foods14071237.

[19] A.L. Lusher, M. McHugh, R.C. Thompson, Occurrence of microplastics in the gastrointestinal tract of pelagic and demersal fish from the English Channel, Marine Pollution Bulletin 67 (2013) 94–99. https://doi.org/10.1016/J.MARPOLBUL.2012.11.02

[20] M.I. Muhib, M.M. Rahman, Microplastics contamination in fish feeds: Characterization and potential exposure risk assessment for cultivated fish of Bangladesh, Heliyon 9 (2023). https://doi.org/10.1016/j.heliyon.2023.e19789.

2026 IMEKO Joint Conference
TC8 - TC11 - TC24
Metro Manila, Philippines, August 26-29, 2026

Design and early deployment of a distributed digital environmental conditions monitoring system supporting traceability in a triple-accredited laboratory

Rossdhan L. Ramos[1]

[1] *Southern Metrology and Calibration Services, Inc., Artica Building, National Highway corner Almazora Street, Biñan, 4024 Laguna, Philippines,*
dhan.southern@gmail.com, rossdhan@southerncalibration.com

Abstract **– Environmental conditions such as thermodynamic temperature, relative humidity, and barometric pressure significantly influence calibration results and measurement uncertainties. Manual recording at discrete intervals limits temporal resolution, weakens record continuity, and introduces transcription errors that may compromise documented information integrity.**

This paper presents the design, implementation, and preliminary operational assessment of CLIMATIC, a distributed digital environmental conditions monitoring system developed in-house by a privately operated organization holding simultaneous accreditation under ISO/IEC 17025:2017, ISO/IEC 17043:2023, and ISO/IEC 17020:2012. The system acquires data at one-second intervals, applies calibration-derived correction factors, and stores traceable values as encrypted, time-stamped records. A preliminary assessment across five nodes shows improved temporal resolution, eliminated transcription errors, and reduced administrative workload, with on-going architectural refinements addressing identified performance constraints. The study demonstrates the viability of iteratively developed, laboratory-built monitoring infrastructure as a replicable alternative to commercial solutions.

I. INTRODUCTION

Calibration results and their associated measurement uncertainties are directly influenced by laboratory environmental conditions[1]. For laboratories operating under ISO/IEC 17025:2017, continuous and reliable documentation of environmental conditions is a requirement supporting the validity of results and the traceability of measurements[2, 3].

In many laboratories, environmental conditions monitoring continues to rely on manual recording: a staff member periodically reads an instrument and transcribes the value into a logbook or spreadsheet. While this satisfies minimum documentation requirements[2, 4], it introduces well-recognized limitations[5]. Manual recording is inherently discrete, and intervals between recordings constitute undocumented periods during which excursions from acceptable bounds would go undetected. Manual transcription also introduces the possibility of human error, compromising documented information integrity[6].

These limitations carry compounded significance for Southern Metrology and Calibration Services, Inc. (SMCSI), a privately operated laboratory in the Philippines holding concurrent accreditation under ISO/IEC 17025:2017 for calibration, ISO/IEC 17043:2023 for proficiency testing, and ISO/IEC 17020:2012 for inspection. The need to maintain and document adequate environmental conditions consistently across laboratory spaces serving all three accreditation scopes simultaneously introduces non-trivial risks to record completeness and integrity[2, 4 Clause 8.4].

Commercial monitoring solutions exist and similar IoT-based system have been proposed[7], but SMCSI's operational requirements, workflow-specific traceability needs, cost, and integration gap motivated in-house development. SMCSI's Research and Development Department (RDD) developed the CLimate Information Management with Automated Tracking and Integrated Control (CLIMATIC) system, the design and early deployment of which is the subject of this paper. The paper reports on a five-node pilot deployment and documents limitations and iterative refinements that inform the planned fifteen-node full deployment.

II. SYSTEM DESIGN AND IMPLEMENTATION

A. Design objectives

CLIMATIC was designed to: (1) replace discrete manual recording with continuous automated acquisition, following similar real-time design seen in recent IoT-based devices[7], but at a one-second interval for retrieving the readings of thermodynamic temperature, relative humidity, and barometric pressure; (2) ensure metrological traceability through systematic application of correction factors derived from calibration certificates[3]; (3) eliminate transcription errors by removing manual data entry from the recording process; (4) scale to fifteen nodes on existing computing infrastructure without capital expenditure on dedicated hardware; and (5) support iterative development so that operational experience could inform architectural refinements.

B. Hardware

Relative humidity is acquired using the DHT11 sensor module. Thermodynamic temperature and barometric pressure are acquired using the BMP180 sensor module; the BMP180 was selected as the primary temperature channel (stated accuracy ±1.0 °C[8]) over the DHT11 temperature channel (±2.0 °C[9]). Sensor selection prioritized low-cost commercially available modules, with the expectation that measurement quality would be validated through calibration and compensated through correction factors[1, 3] rather than sourced from higher-grade instrumentation. Both sensors are interfaced with an Arduino Uno R3, which manages digital communication and relays structured measurement data to a staff computer via USB serial. The Arduino firmware samples both sensors at a nominal one-second interval and constructs structured packets described in Section III.C.

C. System architecture

CLIMATIC follows a three-tier distributed architecture comprising the Node layer, the Base Server, and the Computerized Management System (CMS), as illustrated in Fig. 1.

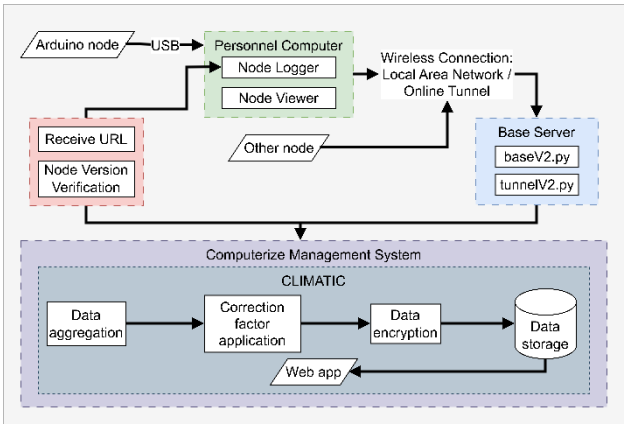


Fig. 1. Overall CLIMATIC system architecture and logic flow.

Node tier: Each node consists of an Arduino Uno connected via USB to a Windows staff computer running the Node Logger (`Node.exe`), a Python 3.13 desktop application. The Node Logger manages serial communication with the Arduino, structural packet validation, NTP-synchronized timestamping, a local API endpoint, and attempts direct transmission to the Base Server. Payloads that cannot be delivered due to network unavailability are redirected to a locally encrypted cache, from which an adaptive batching strategy retransmits data in small batches under low-cache conditions or in bulk when the cache exceeds a defined threshold. A Node Viewer (`Viewer.exe`), accessible through a system tray icon of the Node Logger, provides laboratory staff with real-time status indicators, logs, and activity controls. The Node Logger and Node Viewer are separate processes, ensuring data acquisition is uninterrupted by session events that affect only the user-facing application.

Base Server tier: A FastAPI-based `baseV2.py` script on a repurposed computer receives structured payloads from active nodes, applies structural validation, writes Fernet-encrypted local backups, and forwards valid data to the CMS. A companion `tunnelV2.py` Tunnel Manager maintains redundant public-facing access URLs through Cloudflare Tunnel, LocalTunnel, and Tailscale Funnel, with automated URL refresh, providing resilience against individual tunneling service unavailability.

CMS tier: A Django backend and React frontend on a second repurposed computer serve as the primary interface for authorized personnel. The CMS handles correction factor application, encrypted record storage, node registration and configuration, automated and on-demand PDF report generation, and a structured user access hierarchy. User and node management uses a PostgreSQL database; environmental records are retained in Fernet-encrypted flat-files organized by node identifier and date – an architectural characteristic currently under active migration, as discussed in Section IV.

D. Traceability

Traceability is established through additive correction factors derived from the calibration certificates of each deployed sensor unit[3]. Where a measurement falls between calibration reference points, linear interpolation derives the applicable correction factor:

$$CF(y) = y_1 + (x - x_1) \cdot \frac{(y_2 - y_1)}{(x_2 - x_1)} \qquad (1)$$

The corrected traceable value is then:

$$V_{\text{corrected}} = x + CF(y) \qquad (2)$$

Boundary clamping prevents extrapolation beyond the calibrated range: readings falling outside calibration reference bounds receive the correction factor of the

nearest boundary point. Correction factor configurations are restricted to supervisory-level personnel and above, preserving traceability chain integrity[1]. The complete sequence – raw acquisition, structural validation, NTP synchronization, structured transmission, correction factor application, encrypted storage – constitutes the documented chain from sensor output to traceable corrected environmental value.

E. Data security

Data at rest is protected by Fernet symmetric encryption at the Base Server's local backup and the CMS record store are all encrypted, with decryption occurring only upon authenticated retrieval. Communication security is applied selectively: USB serial communication between the Arduino and the staff computer is physically bounded and carries no encryption. Transmission over the local area network between Node and Base Server uses HTTP; tunnel-routed transmissions are HTTPS-enforced by the tunneling layer. The absence of in-flight encryption on the local network path has been identified as a current limitation, and its remediation is included in the on-going architectural refinements described in Section IV.

III. PRELIMINARY OPERATIONAL ASSESSMENT

A. Sensor proximity study

Prior to full deployment, a study was conducted to determine whether proximity to a running laptop computer – the intended operational arrangement – introduced a detectable systematic influence on sensor readings. The study was carried out on 6–8 January 2026 across four available nodes (2025RDD-005 to 2025RDD-008). Each node was calibrated under three configurations: in a climatic chamber on 6 January 2026 as a controlled-condition baseline, and on-site on 8 January 2026 under two arrangements – sensor positioned ~20 cm from a running laptop (near-laptop) and ~1.5 m away (far-from-laptop), with the reference standard thermohygrometer remaining near the laptop throughout. Three calibration certificates were issued per node, yielding twelve in total.

Correction values from calibration certificates – rather than raw sensor readings – were used as the basis for comparison to normalize out ambient differences between sessions. Direct cross-session comparison of raw readings was not practicable because controlled and on-site calibrations were conducted at different ambient conditions, yielding non-coincident test points; nearest-point selection from the chamber calibration was applied and acknowledged as an assumption.

Normalized error analysis was applied to assess whether differences between configurations were significant relative to combined measurement uncertainties:

$$E_n = \frac{x_1 - x_2}{\sqrt{U_1^2 + U_2^2}} \tag{3}$$

where x_1 and x_2 are the correction values under the two configurations being compared, and U_1 and U_2 are their respective expanded uncertainties at $k = 2$ from the calibration certificates. Values of $|E_n| < 1.0$ indicate no significant difference; values of approaching 1.0 warrant further investigation[4]. Three pairwise comparisons were evaluated per node and measurand: controlled-versus-near, controlled-versus-far, and near-versus-far. Results are presented in Table 1.

Table 1. Normalized error analysis.

Node serial number	Parameter	Normalized error, $\|E_n\|$		
		Control v. Near	Control v. Far	Near v. Far
2025RDD-005	Temperature, °C	0.36	0.47	0.20
	Humidity, % R.H.	0.037	0.13	0.063
2025RDD-006	Temperature, °C	0.36	0.088	0.30
	Humidity, % R.H.	0.66	0.17	0.52
2025RDD-007	Temperature, °C	0.10	0.054	0.054
	Humidity, % R.H.	0.058	0.10	0.031
2025RDD-008	Temperature, °C	1.0	1.0	0.011
	Humidity, % R.H.	0.16	0.17	0.0051

For three of the four nodes, all $|E_n|$ values were well within the acceptable range across both measurands and all pairwise comparisons. Node 2025RDD-008 yielded $|E_n| = 1.0$ for temperature in the controlled-versus-near and controlled-versus-far comparisons; however, the near-versus-far $|E_n|$ for the same node was 0.011 – the lowest value observed across the entire dataset – indicating near-perfect agreement between the two on-site configurations. This pattern indicates that the elevated values reflect a shift in temperature correction between the chamber and on-site sessions rather than an effect attributable to laptop proximity; no assignable cause for this shift was identified. The consistent passage of all comparisons across the remaining three nodes further supports the interpretation that this deviation is isolated to the individual sensor module. No detectable environmental influence attributable to laptop proximity was identified, supporting the suitability of the intended deployment arrangement. Node 2025RDD-008 is identified as warranting continued monitoring of its temperature correction stability.

B. Recording frequency and data completeness

A Python analysis script ingested and decrypted all CMS

record files from the five deployed nodes (VOL0, PCP0, AQD0, DIM0, HYG0), identified duplicate or repeated timestamps, and counted unique valid data points per node per day. Observed counts were compared against a theoretical maximum of 86,400 data points per 24-hour period and a system maximum of approximately 82,080, accounting for a recognized ~3-second-per-minute acquisition gap attributable to the combined timing characteristics of USB serial communication between the Arduino and host computer and Windows OS scheduling – a known constraint discussed further in Section IV. The analysis covered 174 node-day records spanning January to April 2026. Results are presented in Fig. 2.

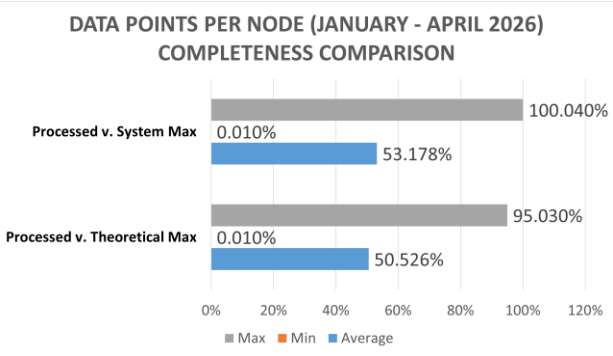


Fig. 2. Average, min, and max counted data point per node per day, across the observation period (January–April 2026).

Under manual practice, environmental conditions were recorded at approximately one-hour intervals during the working day, yielding an approximately 9 data points per day, with no monitoring outside scheduled working hours. Where CLIMATIC nodes were operated continuously, the system yielded ~82,080 monitored data points per 24-hour period – an improvement of approximately four orders of magnitude in temporal resolution – and extended coverage across the full 24-hour period. This extended coverage is directly relevant to demonstrating uninterrupted environmental compliance during overnight storage of reference standards, proficiency testing items, and units under calibration.

Departures from expected completeness were attributable to two factors. First, partial deployment status: some personnel had not yet integrated CLIMATIC into their daily workflow, resulting in host computer shutdowns or Arduino disconnections. Near-zero counts – such as 12 data points on 14 March 2026 for AQD0 and 18 data points on 24 February 2026 for PCP0 – are consistent with very brief startup operation rather than systemic failure. Second, the documented procedure for Facilities and Environmental Conditions has not yet been revised to formally require continuous node operation; personnel operating under the existing procedure had no formal obligation to maintain CLIMATIC as the primary monitoring mechanism. Procedural revision and completion of the fifteen-node rollout are expected to substantially reduce such departures.

Continuous acquisition eliminates the undocumented intervals inherent in manual practice, during which environmental excursions and their influence on measurement uncertainty would go undetected. The high-frequency record supports post-hoc evaluation of environmental stability relevant to expanded uncertainty estimation per GUM[1], and enables timely corrective action before non-conforming conditions affect conformity decisions.

C. Cross-layer integrity and transcription error analysis

Environmental data in CLIMATIC passes through a sequence of programmatic format transformations with no manual transcription at any stage:

Arduino:
`NODE_ID;T:value;H:value;P:value`

Node Logger (queued payload):
`{"node_id": ..., "date": ..., "time": ..., "T": ..., "H": ..., "P": ...}`

Base Server (encrypted record):
`NODE_ID;YYYY-MM-DD;HH:MM:ss;T:value;H:value;P:value`

CMS (encrypted record):
`NODE_ID;YYYY-MM-DD;HH:MM:ss;T:value;H:value;P:value;ACTIVE:1|0`

Structural validation is applied at the Node Logger and Base Server levels; malformed packets are discarded and logged rather than forwarded. To validate end-to-end numerical fidelity, a Python script decrypted and compared records from both the Base Server and CMS across all 174 node-day records, applying reverse correction-factor computation to recover equivalent raw values from CMS-stored corrected records. Results are presented in Fig. 3.

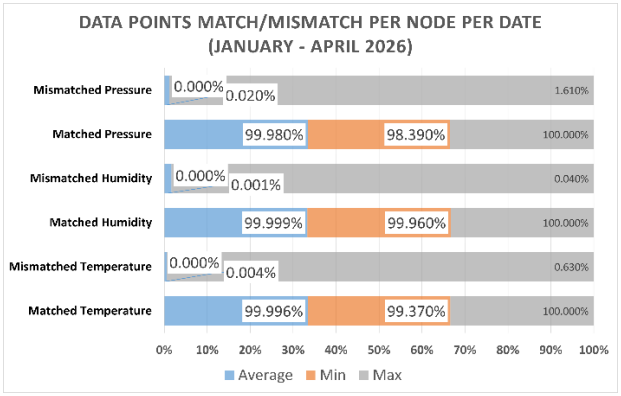


Fig. 3. Cross-layer integrity match rates (%) for

temperature, relative humidity, and barometric pressure across all five nodes.

Temperature and humidity match rates were near-perfect across all nodes, with averages ranging from 99.370% to 100.000% for thermodynamic temperature and 99.960% to 100.000% for relative humidity. Pressure match rates ranged from 98.390% (HYG0) to 100.000% (PCP0, AQD0, DIM0). Isolated mismatches on VOL0, PCP0, and HYG0 were attributable to a race condition in the data forwarding logic, resolved in commit 1cf8689afc on 24 February 2026. No discrepancy was observed in any record dated after that commit across all nodes and measurands. PDF report generation was separately validated against decrypted CMS records and introduced no further modification to the reported values. These results confirm that the programmatic data processing pipeline, in its current form, preserves full numerical fidelity from acquisition through to the CMS layer without introducing transcription errors.

D. Correction factor application accuracy

The interpolation and boundary clamping logic described in Section II.D were validated using a standalone Python script subjected to test cases covering in-range readings, boundary-coincident readings, and out-of-range readings triggering clamping behavior. In all tested cases, actual outputs matched expected outputs, and no extrapolation occurred for readings outside the calibrated range. An earlier unintended extrapolation behavior – resolved prior to the assessment period – had produced one minor humidity variance, which was documented. All post-fix evaluations passed.

E. Administrative Workload

Under CLIMATIC, data acquisition, transmission, storage, and daily report generation are performed without operator intervention, reducing reliance on manual recording and summary report preparation. At the manual practice of ~9 recordings per operational day, CLIMATIC is expected to eliminate an estimated ~18 personnel-minutes per section/laboratory per day of transcription-only activity. Attendant responsibilities are reduced to periodic dashboard review, node activity status management, and on-demand report generation. The out-of-bounds notification system enables responsive intervention without continuous active monitoring. Table 2 summarizes the key quantitative differences between the manual and CLIMATIC monitoring approaches across the five assessed nodes.

Table 2. Quantitative comparison of manual and CLIMATIC environmental monitoring.

Metric	Manual practice	CLIMATIC
Data points per day	~9	~82,080
Monitoring coverage	Working hours only	24 h
Temporal resolution	~60 min	~1 s
Transcription errors	Present	None
Recording time	~18 min/section/day	Negligible

IV. LIMITATIONS AND ITERATIVE REFINEMENTS

Operational deployment revealed several constraints documented through structured monitoring reports and addressed iteratively.

Node application stability: Early command-line-based Node Logger versions were susceptible to interruption by Windows session events including screen lock and sleep mode. Session detachment logic was implemented; subsequent monitoring confirmed uninterrupted acquisition through these events.

Acquisition gap: A timestamp handling error in an earlier serial reading implementation produced significant data gaps. A partial resolution reduced this to the residual ~3-second-per-minute gap documented in Section III.B, attributable to the combined timing behavior of the host hardware, Windows OS, and USB serial interface. This gap is not resolvable through software changes alone and is documented as a known constraint of the hybrid acquisition architecture.

Duplicate records: A race condition between the Arduino output rate and the Node Logger serial reading interval produced duplicate timestamps with marginally differing values, accounting for the isolated mismatches described in Section III.C. This was resolved in commit 1cf8689afc on 24 February 2026, with complete elimination of mismatches confirmed in all subsequent records.

Internet dependency: Tunnel-based transmission depended on internet availability, despite local data caching during outages. An internet monitoring utility was deployed at the Base Server to automate connection recovery and minimize transmission interruptions.

On-going architectural refinements: The flat-file storage architecture produced CMS record-rendering load times of approximately 5–10 seconds at one-second acquisition frequency – acceptable during the current assessment phase but not viable at full fifteen-node deployment scale. Migration to a PostgreSQL with a time-series database

architecture is currently under preliminary testing. Separately, the current HTTPS-based Node-to-Base Server transmission protocol is under evaluation for replacement with MQTTS, whose publish-subscribe architecture and lower protocol overhead are expected to provide more efficient and reliable transmission[10] under the variable network conditions encountered in laboratory environments. Both refinements are empirically motivated responses to observed operational constraints, consistent with the iterative development approach applied throughout the project.

V. CONCLUSIONS

This paper presented the design, implementation, and preliminary operational assessment of CLIMATIC, a distributed digital environmental conditions monitoring system developed entirely in-house by SMCSI's RDD. Where nodes were operated continuously, the system increased monitored data points from ~9 per day under manual practice to ~82,080 – an improvement of ~4 orders of magnitude in temporal resolution – extending coverage across the full 24-hour period and providing a substantially more complete basis for demonstrating environmental compliance during calibration activities and storage of reference standards, proficiency testing items, and units under calibration. This substantially reduces the risk of undetected out-of-compliance periods and strengthens the evidentiary basis for traceability-supporting documentation. Cross-layer integrity validation across 174 node-day records confirmed full numerical fidelity from acquisition through CMS storage, with no transcription errors at any processing stage following resolution of an identified race condition. The sensor proximity study provided no evidence of a systematic environmental influence attributable to laptop proximity across the tested nodes, supporting the suitability of the intended deployment arrangement. Correction factor application logic was verified to operate correctly across the full range of operationally plausible sensor readings, including boundary-clamped edge cases.

These results should be interpreted in the context of current deployment conditions. Data completeness varied across nodes due to inconsistent operational practices and the absence of a formally revised documented procedure integrating CLIMATIC into routine laboratory workflow. The findings are appropriately characterized as preliminary, reflecting an early-operational rather than a mature, fully integrated system. The residual ~3-second-per-minute acquisition gap is a recognized constraint of the current hybrid architecture. The file-based storage constraint is actively addressed through on-going migration to PostgreSQL with a time-series database architecture, alongside MQTTS evaluation – both empirically motivated responses to observed constraints.

Taken together, the findings establish iteratively developed, laboratory-built monitoring infrastructure as a technically and operationally viable alternative to commercial solutions for laboratories pursuing in-house digitalization of traceability-supporting processes. Beyond SMCSI's own operations, the planned fifteen-node full deployment is expected to extend these benefits organization-wide, pending completion of the on-going database migration and protocol refinements. The CLIMATIC development pathway – including its documented limitations and architectural decisions – may serve as a reference for similarly positioned laboratories, though successful adaptation will depend on the implementing organization's available technical expertise and operational context. Future work will report on database migration outcomes, MQTTS protocol evaluation, the full fifteen-node deployment, and formal revision of the relevant documented procedures.

REFERENCES

[1] JCGM 100:2008, "Evaluation of Measurement Data – Guide to the Expression of Uncertainty in Measurement (GUM)", BIPM/ISO/IEC.

[2] ISO/IEC 17025:2017 "General requirements for the competence of testing and calibration laboratories", International Organization for Standardization.

[3] JCGM 200:2012, "International Vocabulary of Metrology – Basic and General Concepts and Associated Terms (VIM), 3rd ed.", BIPM/ISO/IEC.

[4] ISO/IEC 17043:2023 "Conformity assessment – General requirements for the competence of proficiency testing providers", International Organization for Standardization.

[5] B.Ley, et al., "Analysis of erroneous data entries in paper based and electronic data collection", BMC Res Notes, vol. 12, 2019.

[6] K.Barchard, L.Pace, "Preventing human error: The impact of data entry methods on data accuracy and statistical results", Computers in Human Behavior, vol. 27, no. 5, pp. 1834-1839.

[7] M.N.M.Aashiq, et al., "An IoT-based handheld environmental and air quality monitoring station", Acta IMEKO, vol. 12 no. 3 (2023).

[8] Bosch Sensortec, "BMP180 Digital pressure sensor datasheet", Document BST-BMP180-DS000-09. (https://cdn-shop.adafruit.com/datasheets/BST-BMP180-DS000-09.pdf).

[9] Adafruit Industries, "DHT11, DHT22 and AM2302 Sensors". (https://cdn-learn.adafruit.com/downloads/pdf/dht.pdf).

[10] M.S.Rocha et al., "On the performance of OPC UA and MQTT for data exchange between industrial plants and cloud servers," Acta IMEKO, vol. 8, no. 2 (2019)

2026 IMEKO Joint Conference
TC8 - TC11 - TC24
Metro Manila, Philippines, August 26-29, 2026

Validation of AOAC official method 995.11 for total phosphorus determination in fish products

Isaiah U. Sta. Ana[1], Michael S. Lagmay[1], John Cyrus O. Alfaro[1], Jan-Ervin C. Guerrero[1], Andrea V. Tero[1], Leonard M. Montero[1], Ma. Rachel V. Parcon[1]

[1]*Standards and Testing Division, Industrial Technology Development Institute, Department of Science and Technology, Bicutan, Taguig City, 1631, Philippines, ieubando@itdi.dost.gov.ph*

Abstract **– Phosphorus is an essential nutrient necessary for skeletal integrity, cellular membrane structure, energy metabolism, and acid-base balance. However, excessive phosphorus intake has been linked to vascular calcification, impaired kidney function, and increased cardiovascular risk, particularly in individuals with chronic kidney disease. Phosphorus occurs naturally in organically-bound forms or is intentionally added as inorganic phosphate additives, the latter being more bioavailable and potentially posing greater health risks.**

This study applied AOAC 995.11 to determine total phosphorus in fish, a widely consumed dietary source of phosphorus. Although this method is established for various food matrices, its extension to fish products requires specific validation to account for the unique organic and mineral profiles of aquatic species and their processed derivatives. While the method does not distinguish between natural and added phosphorus, it quantifies total phosphorus which provides preliminary information on potential overexposure.

The method demonstrated acceptable analytical performance, characterized by good linearity ($r \geq 0.995$) across the range of 0.05-1.20 mg/L P. Method detection and quantitation limits were established at 1.60 and 5.35 mg/kg P, respectively. Precision was confirmed by Horwitz ratios (HorRat) of 0.3-1.3 for repeatability and 0.5-2.0 for intermediate precision. Trueness was verified through spike recoveries (93-108%) and the analysis of NIST SRM 1546a (Meat Homogenate), which yielded recoveries of 91-95%. Overall, the method is fit for purpose for the determination of total phosphorus in fish matrix.

I. INTRODUCTION

Phosphorus is an essential nutrient that is naturally present in the human body and required as part of a balanced diet. About 85% of phosphorus in the body is present in the bones and teeth. It helps maintain proper bone density and reduces the risk of conditions like osteoporosis and rickets. This mineral also supports the conversion of macromolecules (i.e., carbohydrates, fats, and proteins) into usable energy [1,2]. Phosphorus is abundant in many foods, making it relatively easy to meet daily requirements through a balanced diet. It can be derived from animal meat and its products, as well as plant-based sources and beverages. Phosphorus is naturally present in foodstuffs in the form of organic esters and can also be added as an additive [3].

Naturally occurring phosphates are organically-bound and only 40-60% are absorbed in the gastrointestinal tract. In contrast, inorganic phosphates are highly bioavailable, posing a significant threat, particularly to patients suffering from chronic kidney disease (CKD). High serum phosphate concentration was found to contribute to the 12% mortality of CKD patients [3]. Elevated levels also disrupt the hormonal activities of fibroblast growth factor-23 (FGF-23) and parathyroid hormone (PTH), leading to vascular calcification, bone defects, and cardiovascular-related diseases [4,5].

Food additives are chemical substances intentionally added to food to enhance their sensory qualities and improve product stability. Phosphates are one of the classes of legally permitted food additives that can act as acidity regulators, emulsifiers, sequestrants, stabilizers, and humectants. However, given the potential harmful effects of its excessive intake, the Codex Alimentarius Commission established a maximum allowable level of added phosphates, expressed as phosphorus (P), at 2200 mg/kg in various food categories, including processed, frozen, cooked, smoked, and preserved fish and seafood products [6-9].

In the Philippines, in order to protect the consumers and facilitate market access of local foods and food products, R.A. 10611, or the Food Safety Act of 2013, has been implemented. The law institutionalizes chemical testing as an essential tool for detecting contaminants and additives, verifying compliance with safety standards, and supporting risk-based food safety regulation [10]. The successful implementation of this law is anchored on the capability of chemical testing laboratories in generating accurate and reliable measurement results, as these will serve as the basis for the regulatory bodies to allow these foods to be in the market.

There is no standard method yet to measure the concentration of added phosphate. Several studies have explored different techniques to determine phosphorus

originating from additives. For instance, in the analysis of phosphate additives in instant noodles, P-31 nuclear magnetic resonance (^{31}P-NMR) was employed, allowing identification of specific phosphate types such as E450 and E451 [11]. In hake fillets, the various forms of added phosphates were analyzed using ion-exchange chromatography [12]. Similarly, polyphosphates in meat, marine, and dairy products have been detected using high-performance ion-exchange chromatography, either via conductometric detection or coupled to Q-Exactive orbitrap high-resolution mass spectrometry [13]. These methods provide accurate detection of added phosphates; however, they require sophisticated instrumentation and highly skilled personnel.

AOAC Official Method 995.11 is a colorimetric method for determining total phosphorus in food. Although it does not distinguish between naturally occurring and added phosphate, it provides useful preliminary information on potential overexposure. In this method, all phosphate species (both bound and added) are converted to orthophosphate by dry ashing followed by acid digestion. The resulting phosphate reacts with ammonium molybdate under acidic conditions to form a phosphomolybdate complex, which is then reduced by ascorbic acid to produce a blue-colored molybdenum complex, $[(MoO_2{\cdot}4MoO_3)_2{\cdot}H_3PO_4]$. The absorbance of this complex is measured at 823 nm using a UV–Vis spectrophotometer [14].

The method was already validated through an interlaboratory study for various food matrices, including potato flour, sausage, cold ham, infant formula, cheese, and skimmed milk [15], representing plant-based, meat, and dairy products. However, fish and fish products, which have distinct organic and mineral compositions, were not included in the original validation. Therefore, in-house validation is required to confirm the method's suitability for this matrix. In this study, AOAC 995.11 was validated to assess its fitness for the determination of total phosphorus in fish and fish products.

II. METHODS AND PROCEDURES

A. Chemicals and Reagents

Hydrochloric acid (HCl), 37%, and sulfuric acid (H_2SO_4), 98%, were purchased from RCl Labscan Ltd. (Thailand); zinc oxide (ZnO), 99.5%, and ascorbic acid ($C_6H_8O_6$), 99.7%, were obtained from Techno Pharmchem (India); potassium hydroxide (KOH), ≥85%, was from Himedia Laboratories Pvt. Ltd (India); and sodium molybdate dihydrate ($Na_2MoO_4{\cdot}2H_2O$) was supplied by Loba Chemie Pvt. Ltd. (India). Deionized water (DI) was used for all solution preparations.

A commercially available phosphorus standard (1000 mg/L) traceable to NIST was purchased from AccuStandard, Inc. (New Haven, CT, USA). This served as the stock solution for the preparation of intermediate and working standards. A potassium dihydrogen phosphate (KH_2PO_4) standard traceable to NIST was also used for recovery studies. A certified reference material (CRM), NIST Standard Reference Material (Gaithersburg, MD, USA) for Meat Homogenate (NIST SRM 1546a), was used to establish the trueness of the method.

B. Sample Preparation

Samples were ground and homogenized thoroughly to obtain a representative subsample. The oil in canned tuna, the tomato sauce in canned sardines, and the coating (crust) of the fish nuggets are included as part of the sample. The homogenized material was then stored in clean polyethylene containers to prevent contamination and moisture uptake prior to analysis. Samples were accurately weighed using an analytical balance in a clean 150 mL borosilicate beaker. Approximately 0.5 g of ZnO was added to the sample as an ashing aid, facilitating efficient oxidation of organic matter and recovery of inorganic constituents. The mixture was carefully homogenized using a glass rod to ensure uniform distribution of the added reagent.

The prepared samples were initially charred on a hot plate to slowly decompose organic material and minimize sample loss due to rapid combustion during ashing. After charring, the beakers were placed in a muffle furnace and the temperature was gradually increased to 525 °C. The samples were maintained at this temperature until complete ashing was achieved. After cooling, the ash residues were subjected to acid digestion by adding 5 mL of deionized water followed by 5 mL of HCl. The mixture was gently boiled for 5 minutes to ensure dissolution of soluble inorganic components and to facilitate extraction of analytes from the ash matrix.

Afterwards, the content was quantitatively filtered into a 50 mL volumetric flask using a Whatman filter paper no. 41 (or equivalent), with subsequent washing of hot DI water to ensure complete transfer of analytes. The cooled solution was then neutralized with 50% w/v KOH until it became slightly opalescent, indicating near-neutral conditions. HCl was subsequently added dropwise to redissolve any precipitates and restore clarity of the solution. Finally, the solution was diluted to the 50 mL mark with deionized water, mixed thoroughly, and transferred to high-density polyethylene containers for storage pending analysis.

C. Color Development

An appropriate volume of the sample aliquot was transferred into a 25 mL volumetric flask, with the addition of 5 mL of water and 10 mL of molybdate-ascorbic acid solution. The flasks were immersed in boiling water for 15 min to develop a blue-colored solution, indicating the formation of $[(MoO_2{\cdot}4MoO_3)_2{\cdot}H_3PO_4]$ complex. Afterward, the samples were cooled to room temperature and diluted with DI water to mark. Working standard solutions were also prepared in the same manner.

D. Instrumentation

A calibration curve was established to determine the phosphorus content in the samples. The intensity of the blue color is apparently proportional to the phosphorus concentration in the sample. Spectrophotometric measurement was performed using a Shimadzu UV-1900i UV-Visible spectrophotometer. Table 1 presents the equipment parameters for the analysis of phosphorus.

Table 1. Instrumental parameters for phosphorus determination using UV-Vis spectrophotometer

Parameter	Description/Value
Light Source	tungsten-halogen
Analytical Wavelength	823 nm
Spectral bandwidth	1 nm
Cell type	quartz
Path Length, cm	1.0
Measurement Mode	absorbance

E. Method Validation

A single-laboratory method validation was conducted by following the internationally recognized guides from Eurachem [16] and IUPAC [17]. Performance characteristics such as linearity and working range, limit of detection and quantification (LOD and LOQ), repeatability, intermediate precision, and trueness by bias using a certified reference material (CRM) and by spike recovery, were evaluated. The acceptance criteria for determining the suitability of the method were based on the laboratory's in-house protocol for method validation which were based on AOAC Peer-Verified Methods and regulatory limits.

III. RESULTS AND DISCUSSION

A. Linearity and Working Range

The working range is the interval over which the method provides results with an acceptable uncertainty [16]. In spectrophotometry, a linear mathematical model is commonly used to describe the relationship between the instrument signal and analyte concentration. Linearity is a critical performance characteristic that verifies the suitability of the calibration model and ensures accurate and reliable quantification across the established working range.

The linearity of the method was evaluated by analyzing phosphorus (P) standard solutions at various concentration levels over the range of 0.05 to 4.0 mg/L. The calibration curve (Fig. 1) was constructed by plotting absorbance against phosphorus concentration. Concentration levels above 1.20 mg/L were excluded from the calibration range because they produced absorbance values exceeding the recommended analytical limit (>0.9 A.U.), where deviations from the Beer–Lambert law become significant. At high absorbance (low transmittance), instrumental limitations such as stray light, detector noise, and limited spectral resolution introduce negative deviations from linearity. These effects arise because stray radiation and instrumental imperfections contribute additional light to the detector, compromising measurement accuracy and linearity [18,19]. The upper range is consistent with the AOAC method, while the lower limit was extended to 0.05 mg/L as supported by the calculated instrument LOQ of 0.024 mg/L. The resulting calibration curve (0.05–1.20 mg/L P) shows good linearity, with a positive slope indicating a direct relationship.

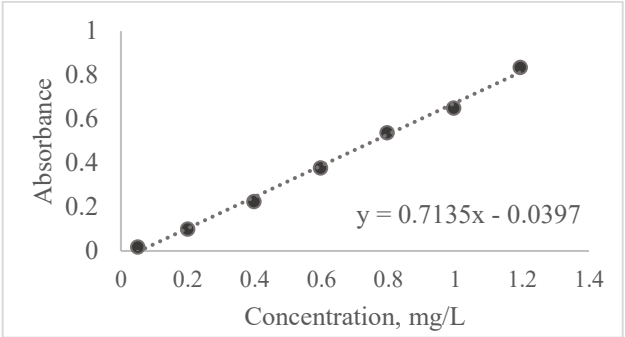


Fig. 1. Calibration curve

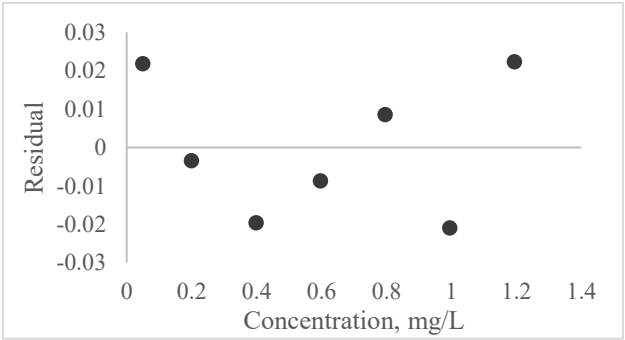


Fig. 2. Residual plot

The correlation coefficient (r = 0.998, n = 7) confirmed a strong linear relationship between absorbance and phosphorus concentration, meeting the acceptance criterion ($r \geq 0.995$). This is further supported by the residual plot, a plot of the difference between the observed instrument response and the instrument response predicted by the regression line against analyte concentration. As shown in Fig. 2, the plot demonstrates random distribution of residuals about zero, indicating the absence of systematic trends. The results collectively confirmed the linearity of the established working range. Hence, the linear calibration model is suitable for the reliable quantitation of P in the target matrix.

B. Limit of Detection and Quantification

The method's limit of detection (LOD) is the lowest concentration of the analyte that can be detected by the method at a specified level of confidence, while the

method's limit of quantification (LOQ) is the minimum concentration that can be reported with acceptable performance [14, 16, 20]. Both the LOD and LOQ were determined using ten replicates of a sample containing a low concentration of the analyte, that have undergone the whole process of the method. The LOD and LOQ were calculated using the following equation:

$$\boldsymbol{LOD = 3\,x\,s'} \quad (1)$$

$$LOQ = 10\,x\,s' \quad (2)$$

where s' is the corrected standard deviation calculated using the equation below:

$$\boldsymbol{s' = s\sqrt{\frac{1}{n} + \frac{1}{n_b}}} \quad (3)$$

where s is the standard deviation of the replicate observations, n is the number of replicate observations averaged in routine use, and n_b is the number of blank samples used in blank corrections in routine analysis. The method achieved an LOD of 1.60 mg/kg P and an LOQ of 5.35 mg/kg P.

In terms of method sensitivity, a fit-for-purpose method should be capable of detecting and quantifying phosphorus at concentration levels below relevant regulatory thresholds. No maximum allowable level (MAL) has been established yet for total phosphorus, as it is an essential and naturally occurring nutrient. However, since the method is intended as a preliminary screening tool for potential overexposure from added phosphates, the MAL of 2200 mg/kg P in fish and fish products, as specified by the Codex Alimentarius, may be used as a reference basis. The method is capable of detecting and quantifying phosphorus at levels well below this threshold, making it suitable for screening applications in fish and fish products.

C. Precision

Precision is a measure of how close the results are to one another. It can be assessed by determining the repeatability and intermediate precision of the measurement results. Repeatability refers to the extent of agreement between results when the same method is applied under identical conditions (i.e., same operator, same equipment, same location, and within a short time frame). It isolates random error under the most controlled scenario, making it the highest possible precision for a method. On the other hand, intermediate precision measures precision when some controlled variations (i.e., different days, different analysts, or different equipment) are introduced, but still within a single laboratory. The same test material is used. It reflects the method's robustness to normal day-to-day operational changes without involving multiple laboratories [14,16].

For repeatability assessment, six replicates of each test sample (canned tuna, canned sardines, and fish nuggets) were analyzed under repeatability conditions. These samples were intentionally selected to represent different matrix characteristics: canned tuna (high fat/oily), canned sardines in tomato sauce (complex), and fish nuggets (starch-rich). Such variation in composition can influence extraction efficiency and analytical response. The percent relative standard deviation, $\%RSD_r$, and the predicted relative standard deviation ($PRSD_r$) were determined to get the HorRat values for repeatability. $PRSD_r$ were calculated using the equation:

$$\boldsymbol{PRSD = 2^{1-0.5logC}} \quad (4)$$

where C is the mass fraction of the analyte. HorRat was determined using the formula:

$$\boldsymbol{HorRat = \frac{\%RSD}{PRSD}} \quad (5)$$

All three determinations achieved an acceptable HorRat value (0.3-1.3), as presented in Table 2, thereby passing the repeatability assessment [14]. This demonstrates that the method can produce consistent results regardless of differences in sample matrix composition when operated under the same conditions.

Table 2. Results of the Repeatability Test

Parameter	Canned Tuna (n=6)	Canned Sardines (n=6)	Fish Nuggets (n=6)
Mean, mg/kg	791	1399	1586
$\%RSD_r$	1.98	1.65	1.84
$PRSD_r$	5.86	5.38	5.28
HorRat	0.34	0.31	0.35
Evaluation	passed	passed	passed

Intermediate precision was evaluated, with commercially available canned tuna and NIST SRM 1546a as the test samples, using two approaches: (1) analysis of sample using different equipment (Shimadzu UV-1900i and Hitachi UH5300) on different days; and (2) analysis of sample performed by different analysts, using the same equipment, and in the same laboratory over an extended timescale. The one-way ANOVA was applied to calculate the standard deviation. The results of the intermediate precision studies, summarized in Table 3, show that both approaches passed the acceptance criteria of 0.5-2.0 for intermediate precision [21,22]. This confirms that variations in laboratory conditions, analysts, time, and other possible sources are under control.

Table 3. Results of the Intermediate Precision Test

Parameter	Approach 1 (n=6)	Approach 2 (n=12)
Mean, mg/kg	818	1498
$\%RSD_R$	2.92	5.25
$PRSD_R$	5.81	5.31
HorRat	0.50	0.99
Evaluation	passed	passed

D. Trueness

According to Eurachem, method trueness is an expression of the close agreement of the result, in terms of mean, to the reference value [16]. In this work, two approaches were employed: (1) recovery experiment using spiked samples; and (2) analysis of CRM.

For trueness by recovery, the samples were spiked with a known amount of phosphorus at the same concentration level as the native analyte present in the samples. The same test samples used in the precision study were analyzed to evaluate potential matrix effects across different fish product types. This approach allows assessment of the method's trueness under realistic sample conditions, where matrix components may influence analyte extraction, digestion efficiency, or instrumental response. The selected matrices, representing distinct product types, were used to determine whether such effects would significantly impact quantification. The percent recoveries obtained for all three sample types were within the acceptable range, as shown in Table 4, demonstrating that the method is accurate and not significantly affected by matrix interferences across the tested fish products.

Table 4. Results of the Trueness by Recovery Assessment

Parameter	**Canned Tuna** (n=6)	**Canned Sardines** (n=3)	**Fish Nuggets** (n=3)
Percent Recovery	95-103	93-107	99-108
Acceptance Criteria	90-110	90-110	90-110
Evaluation	passed	passed	passed

To evaluate trueness through the analysis of a CRM, NIST SRM 1546a for Meat Homogenate was analyzed (n=11) using the method. This CRM was selected because, at the time of validation, it was the closest available reference material in terms of matrix composition to fish. The percentage recovery achieved ranged from 91% to 95%, with respect to the reference value of 1651 mg/kg. This passed the laboratory acceptable recovery range of 90-110% at this concentration level. The slightly reduced recovery (91-95%) can be attributed to a combination of matrix differences and minor extraction or measurement inefficiencies. The CRM (meat homogenate) does not perfectly match the fish matrix in terms of fat content, protein composition, and moisture, which can influence analyte binding and extraction behavior; such matrix-related effects are well known to impact analytical recovery [23]. Consequently, a small fraction of the analyte may remain incompletely extracted. In addition, minor inefficiencies during sample preparation, such as incomplete digestion, adsorption of analytes onto glassware, and cumulative losses during transfer steps, can further reduce recovery. On the measurement side, residual matrix components may lead to signal suppression or enhancement, while slight calibration mismatches and instrument variability can introduce a small systematic bias. These combined effects, typically contributing only a few percent each, are widely reported in analytical chemistry literature as common causes of recoveries slightly below 100%, and together they reasonably explain the observed 91-95% recovery while remaining within acceptable validation criteria [16, 17].

Nevertheless, the results for trueness assessment imply that systematic errors are sufficiently controlled by the method. This also indicates that the unique organic matrix and mineral profile exhibited by fish and fish products, which could introduce interferences, did not significantly affect the analytical signal. Hence, the methods can provide accurate quantitation of phosphorus in fish matrices.

With all the method validation performance characteristics achieving results within the acceptance criteria, the method is deemed fit for its intended use.

IV. CONCLUSION

In conclusion, the use of AOAC Official Method 995.11 can be extended to fish and fish products, as demonstrated by the validation results. Although the method cannot distinguish between naturally occurring and intentionally added phosphorus, it is useful for screening fish products that may contain potentially harmful levels of phosphate additives. Because it offers a simple and straightforward approach to phosphorus determination, it is well suited for rapid screening of products in the market. When a product is found to contain excessively high phosphorus levels, i.e., exceeding regulatory limits, a more advanced method capable of specifically determining added phosphate can then be applied, providing a more cost-effective approach to regulation.

FUNDING STATEMENT

This work was supported by the Department of Science and Technology under the Grants-in-Aid Project titled "Standardization and Validation of Chemical Test Methods on Allergens and Preservatives Food Safety Parameters Among DOST Laboratories."

ACKNOWLEDGEMENT

The authors would like to express their gratitude for the guidance provided by the Philippine Council for Industry, Energy, and Emerging Technology Research and Development of the Department of Science and Technology during project implementation. The authors are also grateful to the dedicated service and assistance provided by the heads of the Chemistry Laboratory Admer Rey C. Dablio, Cyril C. Ramil, and Christy S. Daniel and the staff Theressa Aviles-Liclican, Harlene B. Cardos, Mark Anthony Principe, Edhilson Mauricio, Jason Cortez, Katherine Batis, and Ryan Garcia.

REFERENCES

[1] Office of Dietary Supplements, *Phosphorus: Fact Sheet for Health Professionals*. U.S. Department of Health and Human Services, National Institutes of Health, 2023. [Online]. Accessed: Apr. 14, 2026.

[2] Harvard T.H. Chan School of Public Health, *Phosphorus*. The Nutrition Source, 2023. [Online]. Accessed: Apr. 14, 2026.

[3] E. Ritz, K. Hahn, M. Ketteler, M. K. Kuhlmann, and J. Mann, "Phosphate additives in food—a health risk," *Deutsches Ärzteblatt International*, vol. 109, no. 4, pp. 49–55, 2012, doi:10.3238/arztebl.2012.0049.

[4] H. Komaba and M. Fukagawa, "Phosphate—a poison for humans?," *Kidney International*, vol. 90, no. 4, pp. 753–763, 2016, doi:10.1016/j.kint.2016.03.039.

[5] J. Uribarri and M. S. Calvo, "Dietary phosphorus excess: A risk factor in chronic bone, kidney, and cardiovascular disease," *Advances in Nutrition*, vol. 4, no. 5, pp. 542–544, 2013, doi:10.3945/an.113.004234.

[6] Codex Alimentarius Commission, *General Standard for Food Additives (CXS 192-1995)*. FAO/WHO, 2024. [Online]. Accessed: Apr. 14, 2026.

[7] Seafish, *Review of Polyphosphates as Additives and Testing Methods for Them in Scallops and Prawns*, 2012.

[8] W. J. F. Lemos Junior, D. Santinello, S. Mohammadzadeh, L. Treu, A. S. Sant'ana, and S. Campanaro, "Polyphosphate in food systems: Their roles and applications in foods and contribution to sustainable processing practices," *Trends in Food Science & Technology*, vol. 152, Art. no. 104696, 2024, doi:10.1016/j.tifs.2024.104696.

[9] L. E. Lampila, "Applications and functions of food-grade phosphates," *Annals of the New York Academy of Sciences*, vol. 1301, no. 1, pp. 37–44, 2013, doi:10.1111/nyas.12230.

[10] Republic of the Philippines, Republic Act No. 10611: An Act to Strengthen the Food Safety Regulatory System in the Country to Protect Consumer Health and Facilitate Market Access of Local Foods and Food Products, and for Other Purposes, Aug. 23, 2013.

[11] T. Q. Pham, L. Anh, T. Nguyen, N. T. Dao, and T. T. Ta, "Determination of phosphorus additives in instant noodle samples by phosphorus-31 nuclear magnetic resonance (^{31}P-NMR)," *Vietnam Journal of Science, Technology and Engineering*, vol. 66, no. 3, pp. 39–45, 2024, doi:10.31276/VJSTE.2023.0072.

[12] B. Teixeira and R. Mendes, "Analysis of added phosphates in hake fillets by ion-exchange chromatography: A case study of false positives induced by nucleotides coelution," *Food Chemistry*, vol. 368, p. 130841, Jan. 2022, doi: 10.1016/j.foodchem.2021.130841.

[13] R. Pavlović, F. Di Cesare, F. Longo, et al., "Undeclared (poly)phosphates detection in food of animal origin as a potential tool toward fraud prevention," *Foods*, vol. 10, no. 7, 2021.

[14] G. W. J. Latimer, *Official Methods of Analysis: 22nd Edition (2023)*. In *Official Methods of Analysis of AOAC INTERNATIONAL*. Oxford University Press, 2023.

[15] T. K. Pulliainen and H. C. Wallin, "Determination of total phosphorus in foods by colorimetric measurement of phosphorus as molybdenum blue after dry-ashing: NMKL interlaboratory study," *Journal of AOAC International*, vol. 77, no. 6, pp. 1557–1561, 1994.

[16] H. Cantwell (ed.). Eurachem Guide: The Fitness for Purpose of Analytical Methods – A Laboratory Guide to Method Validation and Related Topics. 2025;(3rd ed).

[17] International Union of Pure and Applied Chemistry, "Harmonized guidelines for single-laboratory validation of methods of analysis," Pure and Applied Chemistry, vol. 74, no. 5, pp. 835–855, 2002.

[18] I. Oshina and J. Spigulis, "Beer–Lambert law for optical tissue diagnostics: current state of the art and the main limitations," Journal of Biomedical Optics, vol. 26, no. 10, 2021.

[19] Y.-C. Yeh et al., "A novel model extended from the Bouguer–Lambert–Beer law can describe the non-linear absorbance of potassium dichromate solutions and microalgae suspensions," Frontiers in Bioengineering and Biotechnology, vol. 11, 2023.

[20] V. J. Barwick, Ed., *Eurachem Guide: Terminology in Analytical Measurement – Introduction to VIM 3*, 2nd ed., 2023.

[21] C. Daniel, A. R. Dablio, M. Lagmay, et al., "Development and validation of methods for the determination of water-soluble and acid-soluble sulphate in concrete," *Measurement Sensors*, vol. 38, 2025, doi:10.1016/j.measen.2024.101618.

[22] W. Horwitz, "The Horwitz ratio (HorRat): A useful index of method performance with respect to precision," *Journal of AOAC International*, vol. 89, no. 4, pp. 1095–1109, 2006.

[23] European Commission, Commission Decision 2002/657/EC implementing Council Directive 96/23/EC concerning the performance of analytical methods and the interpretation of results, Off. J. Eur. Communities, 2002.

2026 IMEKO Joint Conference
TC8 - TC11 - TC24
Metro Manila, Philippines, August 26-29, 2026

Bracketing or exact matching: two different approaches for $\delta^{13}C$-CO_2 value assignment to isotopic reference gas mixtures

Michela Sega[1]*, Chiara Festevole[1], Stefano Pavarelli[1], Francesca Romana Pennecchi[1], Francesca Rolle[1], Ramona Russo[1,2], Francesca Durbiano[1]

[1] *National Institute of Metrological Research – INRiM, Strada delle Cacce 91, 10135 Torino (Italy), m.sega@inrim.it, chiara.festevole@edu.unito.it, s.pavarelli@inrim.it, f.pennecchi@inrim.it, f.rolle@inrim.it, r.russo@inrim.it, f.durbiano@inrim.it*

[2] *DENERG Dipartimento Energia, Politecnico di Torino, Corso Duca degli Abruzzi 24, 10129 Torino (Italy), ramona.russo@polito.it*

***Abstract* – The production of gas mixtures of carbon dioxide (CO_2) in synthetic air at ambient level, certified for both CO_2 amount fraction and isotopic composition of the ratio of the stable isotopes $^{13}C/^{12}C$ ($\delta^{13}C$-CO_2), allows to obtain valid references for comparable and reliable measurement results to support climate change studies. The present paper describes two approaches, i.e., the bracketing and the exact marching, for assigning the $\delta^{13}C$-CO_2 values to a set of gas mixtures of CO_2 in synthetic air at ambient level via Cavity Ring-Down Spectroscopy. The results obtained with the two approaches at different $\delta^{13}C$-CO_2 values, spanning in the range from -42 ‰ to +1.3 ‰, are presented, together with the associated uncertainties. The exact matching proved to give more reliable results.**

I. INTRODUCTION

The production of gas mixtures of carbon dioxide (CO_2) in synthetic air at ambient level, certified for both CO_2 amount fraction and isotopic composition of the ratio $^{13}C/^{12}C$ ($\delta^{13}C$-CO_2), is a promising activity to obtain valid references for comparable and reliable measurement results to support climate change studies. The most valuable method to prepare gas mixtures of stable gases is the gravimetric one, a primary method described in the International Standard ISO 6142-1 [1]. While the production of gaseous Certified Reference Materials (CRMs) of CO_2 in air at atmospheric level, certified for CO_2 amount fraction is a consolidated activity [2-4], the metrological traceability of $\delta^{13}C$-CO_2 values, which lack direct traceability to SI units, relies on the link to an international primary scale, namely the Vienna Pee Dee Belemnite (VPDB) [5]. Different analytical approaches can be used to assign the $\delta^{13}C$-CO_2 values to gas mixtures, among which Isotope Ratio Mass Spectrometry (IRMS) and Cavity Ring-Down Spectrometry (CRDS). IRMS has the intrinsic advantage of high accuracy and lower uncertainty. CRDS, on the other hand, is more user friendly and less expensive. The obtained data can be processed by using different approaches. Among these, bracketing and exact matching are two valuable strategies. In the bracketing approach, two certified reference mixtures with similar CO_2 amount fraction but different $\delta^{13}C$-CO_2 values, are used as calibration standards to assign the $\delta^{13}C$-CO_2 to a mixture under test. In the exact matching approach, instead, a single certified reference mixture with both CO_2 amount fraction and $\delta^{13}C$-CO_2 values closely matching those of the mixture under test, is used as calibration standard. The present paper describes both approaches, including their pros and cons, as applied to $\delta^{13}C$-CO_2 determination via CRDS. Some results in terms of $\delta^{13}C$-CO_2 values, spanning in the range from -42 ‰ to +1.3 ‰, and their associated uncertainties are presented.

II. MATERIALS AND METHODS

Two pure gas sources of CO_2, one having an enriched value of $\delta^{13}C$-CO_2 of +1.3 ‰ and the other having a depleted value of -42 ‰ were purchased (SIAD, Italy). They were diluted in subsequent steps by applying the gravimetric method [1] using pure gases, i.e., nitrogen (N_2) 6.0 (Air Liquide Italia, Italy), argon (Ar) 7.0 (Linde, Germany), and oxygen (O_2) 6.0 (Air Liquide Italia, Italy), to obtain 4 mixtures of CO_2 at ambient amount fraction in synthetic air (SA) at nominal $\delta^{13}C$-CO_2 values of -42 ‰ and +1.3 ‰, respectively. The blending of the two sources allowed to attain 2 mixtures with intermediate $\delta^{13}C$-CO_2 nominal value of -21 ‰. The mixtures were prepared in 5 L high-pressure cylinders of aluminium alloy (Luxfer, UK). Table 1 reports the characteristics of the prepared mixtures in terms of CO_2 amount fraction and nominal $\delta^{13}C$-CO_2 values.

Aliquots of the pure CO_2 sources were sampled in 1 L glass flasks and sent to the Max Planck Institute for

Biogeochemistry (MPI-BGC, Jena, Germany) for the confirmation of the $\delta^{13}C\text{-}CO_2$ value provided by the gas supplier.

Table 1. Characteristics of the mixtures under test (MuT). CO_2 amount fraction χ_{CO2}, associated expanded uncertainties $U(\chi_{CO2})$ ($k = 2$), and nominal $\delta^{13}C\text{-}CO_2$ values are reported.

MuT	χ_{CO2} [µmol/mol]	$U(\chi_{CO2})$ [µmol/mol]	Nominal $\delta^{13}C\text{-}CO_2$ value [‰]
A1	425.87	0.40	+1,3
A2	412.60	0.40	+1,3
B1	413.56	0.40	-21
B2	412.91	0.40	-21
C1	409.46	0.40	-42
C2	417.57	0.40	-42

The gravimetrically prepared mixtures were analysed by a CRDS analyser (CRDS G2131-i, Picarro, USA) in order to determine an analytical $\delta^{13}C\text{-}CO_2$ value linked to VPDB by an independent traceability path. The CRDS was calibrated in real-time by means of CO_2 reference mixtures in SA previously prepared by gravimetry from different pure CO_2 sources, having $\delta^{13}C\text{-}CO_2$ values assigned via IRMS at MPI-BGC on the JRAS-06 scale. The analyses and data elaborations were carried out by applying both the bracketing and the exact matching approaches, as described in the following sections.

A. Bracketing approach

In the bracketing approach, two certified reference mixtures having two different $\delta^{13}C\text{-}CO_2$ values were used as calibration standards for the CRDS, thus obtaining an analysis function which was in turn used to assign the $\delta^{13}C\text{-}CO_2$ to a mixture under test, denoted as MuT. The $\delta^{13}C\text{-}CO_2$ values of the reference mixtures bracketed the expected $\delta^{13}C\text{-}CO_2$ of the MuT. In addition, in order to account for possible dependence of the CRDS response to CO_2 concentration, reference mixtures were chosen having CO_2 amount fraction close to that of the MuT. Specifically, it was ensured that the CO_2 amount fraction of the two reference mixtures did not differ by more than 10 % from the MuT. In addition, all the mixtures, namely the reference ones and the MuT, had the same matrix. An additional reference mixture, having a $\delta^{13}C\text{-}CO_2$ value within the measurement range, was used as a control mixture to validate the CRDS calibration.
The CRDS analysis curve was determined by fitting the straight-line model (1) by applying the Weighted Total Least Squares implemented by the INRiM Calibration Curves Computing (CCC) software [6]:

$$\delta_{\mathrm{MuT,calc}} = a + b\delta_{\mathrm{MuT,meas}} \quad (1)$$

where:
$\delta_{\mathrm{MuT,calc}}$ is the calculated value of $\delta^{13}C\text{-}CO_2$ in the MuT, expressed in ‰;
a is the intercept of the analysis curve (‰);
b is the slope of the analysis curve (adimensional);
$\delta_{\mathrm{MuT,meas}}$ is the average of CRDS repeated readings (n = 100) of the MuT, expressed in ‰.
The final $\delta_{\mathrm{MuT,meas}}$ was calculated as the average of the 3 measurement repetitions.
The uncertainty associated to $\delta_{\mathrm{MuT,calc}}$ was evaluated by applying the Law of propagation of uncertainty (LPU) to eq. (1). The CCC software allows to calculate the uncertainties of the coefficients a and b of the analysis curve, taking into account the uncertainty of the calibration mixtures and the repeatability of the CRDS readings. The covariance term between the coefficients a and b was also considered.

B. Exact matching approach

In the exact matching approach, a single certified reference mixture with both CO_2 amount fraction and $\delta^{13}C\text{-}CO_2$ values closely matching those of the mixture under test, was used as calibration standard for the CRDS. An additional reference mixture, having a $\delta^{13}C\text{-}CO_2$ value within the measurement range, was used as a control mixture to validate the CRDS calibration. All the mixtures met the acceptance criteria of ensuring that the CO_2 amount fraction did not differ by more than 10 % from the mixture under test and that they had the same matrix.
The analytical value $\delta_{\mathrm{MuT,calc}}$ of a MuT with respect to the reference mixture was calculated by applying the following model equation (2):

$$\delta_{\mathrm{MuT,calc}} = \left(\delta_{\mathrm{MuT,meas}} \times \delta_{\mathrm{Ref,cert}}\right)/\delta_{\mathrm{Ref,meas}} \quad (2)$$

where:
$\delta_{\mathrm{MuT,calc}}$ is the calculated $\delta^{13}C\text{-}CO_2$ value of the MuT, expressed in ‰;
$\delta_{\mathrm{MuT,meas}}$ is the measured $\delta^{13}C\text{-}CO_2$ value of the MuT, expressed in ‰;
$\delta_{\mathrm{Ref,cert}}$ is the certified $\delta^{13}C\text{-}CO_2$ value of the reference mixture, expressed in ‰;
$\delta_{\mathrm{Ref,meas}}$ is the measured $\delta^{13}C\text{-}CO_2$ value of the reference mixture, expressed in ‰.
$\delta_{\mathrm{MuT,meas}}$ and $\delta_{\mathrm{Ref,meas}}$ were calculated as the average of 3 measurement repetitions of CRDS repeated readings (n = 100 for each repetition).
The measurement uncertainty associated to $\delta_{\mathrm{MuT,calc}}$ was evaluated by applying the LPU to eq. (2).

III. RESULTS AND DISCUSSION

The results obtained by applying the two methods are reported in Figures 1-6. The squares (■) refer to the assigned values by CRDS with the bracketing approach, while the triangles (▲) refer to the values obtained via the exact matching approach. Both values are compared with the gravimetric $\delta^{13}C\text{-}CO_2$ values, represented by dots (●), that are considered as the reference values. The expanded uncertainty bars ($k = 2$) are also reported.

Figures 1 and 2 present the results obtained for MuT A1 and MuT A2, having an enriched $\delta^{13}C\text{-}CO_2$ value, close to +1.3 ‰.

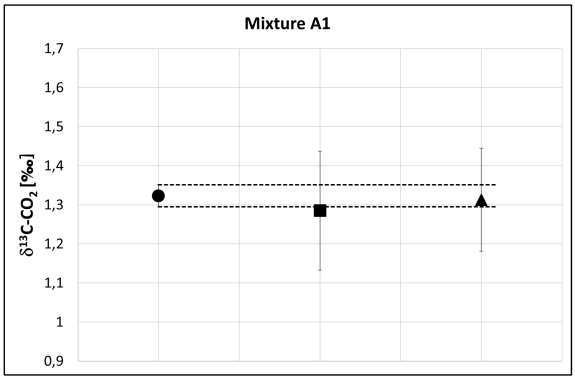


Fig. 1. $\delta^{13}C\text{-}CO_2$ values for MuT A1. ●: gravimetric value; ■ CRDS assigned values with the bracketing approach; ▲ CRDS assigned value with the exact matching approach.

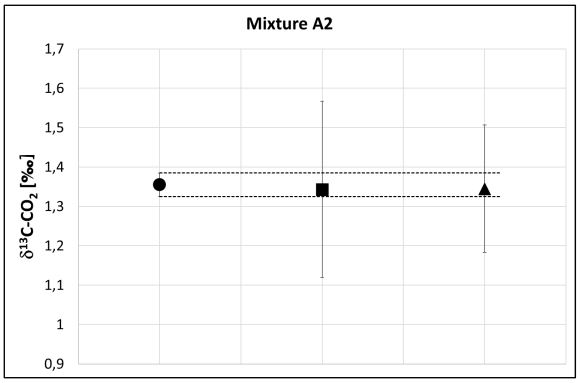


Fig. 2. $\delta^{13}C\text{-}CO_2$ values for MuT A2. ●: gravimetric value; ■ CRDS assigned values with the bracketing approach; ▲ CRDS assigned value with the exact matching approach

Figures 3 and 4 present the results obtained for MuT B1 and MuT B2, having an intermediate $\delta^{13}C\text{-}CO_2$ value, close to -21 ‰.

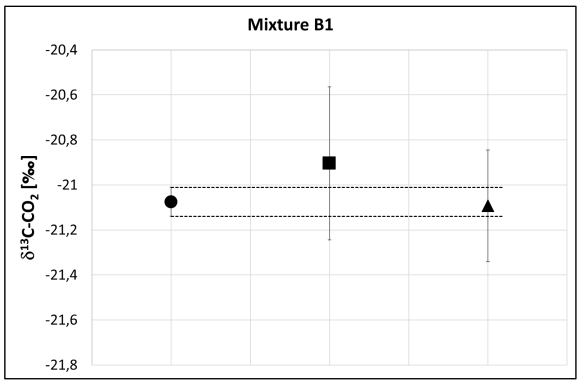


Fig. 3. $\delta^{13}C\text{-}CO_2$ values for MuT B1. ●: gravimetric value; ■ CRDS assigned values with the bracketing approach; ▲ CRDS assigned value with the exact matching approach.

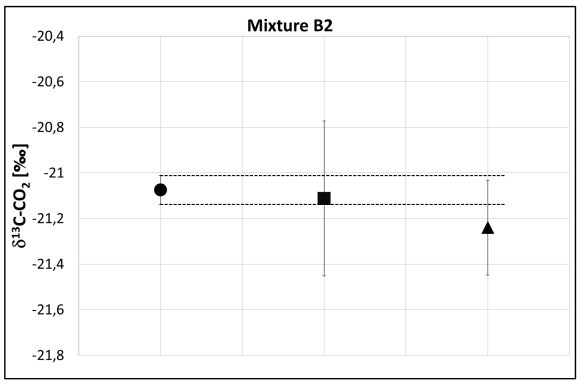


Fig. 4. $\delta^{13}C\text{-}CO_2$ values for MuT B2. ●: gravimetric value; ■ CRDS assigned values with the bracketing approach; ▲ CRDS assigned value with the exact matching approach.

Figures 5 and 6 present the results obtained for MuT C1 and MuT C2, having a depleted $\delta^{13}C\text{-}CO_2$ value, close to -42 ‰.

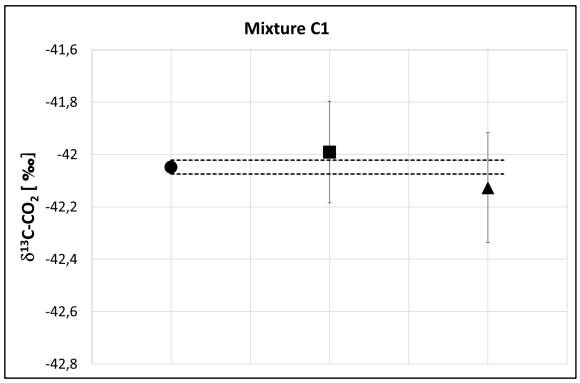


Fig. 5. $\delta^{13}C\text{-}CO_2$ values for MuT C1. ●: gravimetric value; ■ CRDS assigned values with the bracketing approach; ▲ CRDS assigned value with the exact matching approach.

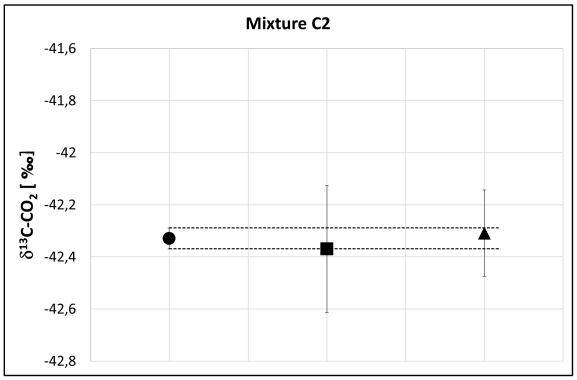


Fig. 6. $\delta^{13}C$-CO_2 values for MuT C2 ●: gravimetric value; ■ CRDS assigned values with the bracketing approach; ▲ CRDS assigned value with the exact matching approach.

The data reported in figures 1-6 show that in general the exact matching approach gives $\delta^{13}C$-CO_2 values closer to the reference one. This can be seen for MuTs A1 (Fig. 1), A2 (Fig. 2), B1 (Fig. 3), C2 (Fig. 6). MuTs B2 (Fig. 4) and C1 (Fig. 5) are the only cases in which the $\delta^{13}C$-CO_2 values assigned by bracketing result closer than the one assigned by exact matching. These results confirm the absence of a systematic bias with respect to the $\delta^{13}C$-CO_2 values. This behavior can reasonably be attributed to the contribution linked to the calibration curve of the bracketing approach, which is affected by the different values of the two reference mixtures. The exact matching approach, where the reference mixture has very similar characteristics with respect to the MuT, allows the analyzer's response to be optimized. In addition, the exact matching approach is less sensitive to instrumental drift, being the measurement sequence shorter. This influence can be further highlighted by the uncertainties obtained by applying the two methods. The exact matching approach, indeed, proved to give lower uncertainties for 5 MuTs out of 6. In the case of MuT C1 (Fig. 5), the two expanded uncertainties are anyway very close, i.e., 0.19 ‰ with the bracketing and 0.21 ‰ with the exact matching. The contribution due to repeatability within the 100 readings of each repetition remains the same for both approaches. In contrast, what varies is the repeatability among the three replicates that combine to determine the final value, which is generally better for the exact matching, and can explain the obtained results.

In addition to the positive experimental results, the exact matching approach requires shorter time for the analysis of the mixtures and only one reference mixture instead of two. Its drawback is represented by the fact that such reference mixture must be very close to the MuT in terms of CO_2 amount fraction and $\delta^{13}C$-CO_2 values.

In terms of measurement ranges, the two approaches do not show substantial differences and can be applied within the same $\delta^{13}C$-CO_2 intervals.

IV. CONCLUSIONS

The paper presented the use of two different approaches to assign $\delta^{13}C$-CO_2 values to gas mixtures of CO_2 at atmospheric amount fraction in SA. The investigation was carried out on 6 mixtures covering $\delta^{13}C$-CO_2 values from +1.3 ‰ to -42 ‰. The exact matching approach proved to give a more accurate estimate of the $\delta^{13}C$-CO_2 values in the majority of the cases examined. In addition, it generally allowed to obtain lower uncertainties. The results of the study, combined with the reduced analysis time, are very promising toward the adoption of the exact matching approach in $\delta^{13}C$-CO_2 value assignment, which might be applied also to future stability studies of the mixtures prepared by gravimetry.

V. CITATIONS AND REFERENCES

[1] International Standard ISO 6142-1, Gas analysis - Preparation of calibration gas mixtures - Part 1: Gravimetric method for Class I mixtures, International Standard Organization, Geneva (Switzerland), 2015

[2] https://www.bip.org/kcdb/. Accessed: May 3, 2026

[3] F.Durbiano, F.R.Pennecchi, F.Rolle, S.Pavarelli, M.Sega, “Stability study and uncertainty evaluation of CO_2 materials for greenhouse gases monitoring”, Measurement 232 (2024) 114653. https://doi.org/10.1016/j.measurement.2024.114653

[4] F.Rolle, F.Durbiano, S.Pavarelli, F.R.Pennecchi, M.Sega, “Comparison of gravimetry and dynamic dilution for the generation of reference gas mixtures of CO_2 at atmospheric amount fraction”, Measurement: Sensors 30 (2023) 100937. https://doi.org/10.1016/j.measen.2023.100937

[5] F.Camin, D.Besic, P.J.Brewer, C.E.Allison, T.B.Coplen, P.J.H.Dunn, M.Gehre, M.Gröning, H.A.J. Meijer, J.-F. Hélie, P.Iacumin, R.Kraft, B.Krajnc, S.Kümmel, S.Lee, J.Meija, Z.Mester, J.Mohn, H.Moossen, H.Qi, G.Skrzypek, P.Sperlich, J.Viallon, L.I.Wassenaar, R.I.Wielgosz “Stable Isotope Reference Materials and Scale Definitions—Outcomes of the 2024 IAEA Experts Meeting”, Rapid Communications in Mass Spectrometry, vol.39, No.14, 2025.

[6] CCC Software: https://www.inrim.it/en/services/software-and-databases/ccc-software. Accessed: Apr. 28, 2025.

2026 IMEKO Joint Conference
TC8 - TC11 - TC24
Metro Manila, Philippines, August 26-29, 2026

Effects of Varying Food Types and Physical Properties of Film on the Total Residual Contaminants Migrating from Monolayer Polyethylene Packaging

Maria Jelo Mantile[1,2], Sultan Muripaga Javier Pukunum[1,2], Andrea Kyla Carlos[1,3], Elyson Keith Encarnacion[1]

[1] Department of Science and Technology, Industrial Technology Development Institute (DOST-ITDI), Gen. Santos Ave, Bicutan, Taguig City, 1631, Philippines
[2] Adamson University, 900 San Marcelino St, Ermita, Manila, 1000 Metro Manila
[3]Pamantasan ng Lungsod ng Maynila, General Luna, corner Muralla St, Intramuros, Manila, 1002 Metro Manila

***Abstract* – Residual contaminants are non-volatile chemical substances that may migrate from packaging to food during contact. This study employed a modified and validated method from the Japan External Trade Organization, to quantify Total Residual Contaminants (TRCs) from monolayer polyethylene plastic bags. The average results showed the highest TRC levels in 20% ethanol > 4% acetic acid > water, suggesting enhanced extraction in semi-polar media. However, one-way analysis of variance revealed no statistically significant difference among TRCs. Principal Component (PC) Analysis showed two patterns: PC 1 showed contrasting migration behavior between aqueous and acidic food whereas the second PC 2 showed a strong association with TRC levels in alcoholic foods and film thickness with density behaving independently of the other variables. The results provide an insight into possible factors affecting chemical migration behavior and warrant further studies into applying a more comprehensive chemometric approach to better understand the underlying relationships.**

I. INTRODUCTION

Food contact materials and articles contain both intentionally added substances (IAS) and non-intentionally added substances (NIAS) originating from polymer synthesis, processing, and degradation. Under various environmental and storage conditions, these chemical constituents may migrate from packaging materials into food systems [1],[2],[3]. The resulting migrants often form complex chemical mixtures whose overall composition remains difficult to characterize using conventional targeted analytical approaches [4]. Among these substances, residual contaminants represent a group of emerging analytes that may persist during food handling and processing and contribute to dietary exposure [5]. The occurrence and measurable levels of such contaminants depend on the type of packaging material, its physicochemical stability, and the environmental stresses encountered during use [6], thereby presenting a significant challenge for comprehensive analytical characterization and reliable chemical measurement.

Polyethylene (PE) films are among the most widely used materials for food packaging applications [7], particularly in direct food contact systems [8],[9], and therefore represent a major potential pathway for human exposure to migrated chemical substances. They consist of polymerized ethylene monomers [10] produced through either high-pressure radical polymerization [11] or low-pressure catalytic processes [12]. To achieve desired mechanical performance and barrier properties, manufacturers incorporate comonomers, copolymers, and functional additives such as antioxidants, UV stabilizers, pigments, fillers, slip agents, and nucleating agents [13]. These formulations result in chemically heterogeneous materials capable of generating numerous residual contaminants. Such residues may include oligomers formed as polymerization by-products, typically composed of linear or branched hydrocarbons, as well as non-volatile additives such as fatty-amide slip agents (e.g., oleamide and erucamide) [14].

Oligomeric residues have been associated with potential adverse effects, including organ inflammation, bioaccumulation, and endocrine disruption [15]. Slip agents, although generally considered to exhibit low toxicity, are not entirely absent from migrated chemical mixtures and may still contribute to cumulative exposure [16]. In support of food safety initiatives promoted by the Food and Drug Administration (FDA) Philippines, the application of validated analytical approaches for assessing locally available packaging materials is

essential. A modified and validated method adapted from the Japan External Trade Organization (JETRO) for total residual contaminant (TRC) analysis using an evaporation-based approach provides a rapid screening technique for non-volatile chemical migrants [17].This method enables the estimation of potential real-world exposure to non-volatile migrants. Given the limited local data on residual contaminant migration and its influencing factors, this study may support the development of packaging standards and the evaluation of PE materials for different food types.

Accordingly, this study aims to compare TRC levels across different food simulants (20% ethanol, 4% acetic acid, and water), evaluate migration patterns using principal component analysis (PCA), and assess correlations among selected physicochemical parameters: density and thickness. The proposed measurement framework contributes to validated chemical measurement methodologies for emerging contaminants in food packaging, supporting regulatory decision-making, standard development, and improved assessment of PE food contact materials.

II. EXPERIMENTAL

Sample Collection and Identification. Different brands of flexible PE films were collected from public markets within the National Capital Region, Philippines, using purposive and convenience sampling. Polymer identification was performed using Fourier Transform Infrared Spectroscopy with Attenuated Total Reflectance (FTIR-ATR).

Physical Properties Determination. PE plastic films were cut into dimensions of 5 cm × 10 cm and cleaned using a lint-free cloth prior to analysis. Triplicate specimens from each sample were weighed using a semi-micro analytical balance (Mettler Toledo) and their thickness measured using a micrometer (Mitutoyo). These measurements were used to calculate the density (ρ) of the plastic films according to Equation (1).

$$\rho\ (\mathrm{g \cdot cm^{-3}}) = \frac{mass\ (g)}{0.005\ x\ thickness\ (\mu m)} \qquad (1)$$

Analysis of Total Residual Contaminants. Following a validated and adapted JETRO evaporation method for total residual contaminants migration analysis. Glass beakers were preconditioned by heating, cooling in a desiccator, and weighing until constant mass was achieved. PE film samples (50 cm²) were cleaned and immersed in 100 mL of food simulants (20% ethanol, 4% acetic acid, or distilled water) ensuring complete immersion of the film. The samples are incubated (Memmert) at 60 °C for 30 minutes, then removed, and the reaction mixture was cooled to room temperature. A 10-mL aliquot was transferred into pre-weighed beakers and evaporated to dryness. After cooling and reweighing constant mass, TRC levels were determined from the mass difference, representing the amount of non-volatile residues migrated from the plastic films.

Statistical Analysis. Statistical analyses were conducted using RStudio and JASP. Descriptive statistics summarized migration data and ranked TRC levels among samples. Data normality and homogeneity of variance were assessed using the Shapiro–Wilk and Levene's tests prior to analysis. One-way ANOVA was applied to evaluate significant differences in TRC values among food simulants. Principal Component Analysis (PCA) was performed to identify underlying data patterns, with scree plots and biplots used for visualization and interpretation. Spearman's rank correlation analysis was also conducted to determine the strength of relationships among the measured variables.

III. RESULTS AND DISCUSSION

A. TRC analysis varying food simulants

Collection of commercial flexible PE films resulted in fifteen different brand samples. Polymer identification confirmed that all samples were polyethylene, consisting of both low-density polyethylene (LDPE) and high-density polyethylene (HDPE) materials. Total residual contaminant values determined using the validated JETRO method, together with measured thickness and density parameters, are summarized in Table 1.

Table 1. Summary of TRC levels, film thickness, and density

Sample Code	Type of PE	TRC/ mg·L^{-1}			Thickness/ µm	Density/ g·cm^{-3}
		Water	20% Ethanol	4% Acetic Acid		
PE-0001	LDPE	4.63	7.58	1.35	21.8	0.901
PE-0002	LDPE	6.97	4.47	3.03	20.4	0.926
PE-0003	LDPE	3.77	4.63	2.97	25.6	0.854
PE-0004	HDPE	2.87	4.6	4.97	10.6	1.05
PE-0005	LDPE	2.27	8.1	9.1	20.2	1.00
PE-0006	LDPE	1.5	5.37	3.63	21.6	0.926
PE-0007	HDPE	7.2	5.57	4.1	13.4	0.757
PE-0008	LDPE	2	9.77	5.17	29.6	0.724
PE-0009	HDPE	3.7	3.97	3.7	7.40	0.589
PE-0010	HDPE	3.6	1.97	6.03	7.60	0.739
PE-0011	HDPE	1.63	2.43	4.37	6.20	1.15
PE-0012	HDPE	3.47	10.57	4.6	9.00	0.666
PE-0013	HDPE	1.4	4.1	11.23	10.2	0.583
PE-0014	HDPE	0.63	4.23	5.57	10.2	0.571
PE-0015	HDPE	9.7	2.3	3.9	15.4	0.821

Median TRC concentrations for the food simulants were 4.50 mg·L⁻¹ for 20% ethanol, 4.37 mg·L⁻¹ for 4% acetic acid, and 3.47 mg·L⁻¹ for distilled water. For the 20% ethanol simulant, TRC values ranged from 1.97 to 10.6 mg·L⁻¹. The 4% acetic acid simulant exhibited values between 1.35 and 11.2 mg·L⁻¹, while distilled water showed the lowest range, from 0.63 to 9.70 mg·L⁻¹. Based on mean TRC values, the migration ranking followed the order: 20% ethanol (5.31 mg·L⁻¹) > 4% acetic acid (4.92 mg·L⁻¹) > water (3.69 mg·L⁻¹).

Normality of TRC datasets was evaluated using the Shapiro–Wilk test. The distributions for 20% ethanol ($p = 0.127$) and water ($p = 0.065$) satisfied the normality assumption ($p > 0.05$), whereas the 4% acetic acid dataset deviated from normality ($p = 0.028$). Homogeneity of variance assessed using Levene's test indicated equal variances among groups ($p = 0.858$). Despite the partial deviation from normality, analysis of variance (ANOVA) was conducted due to the robustness of the test under balanced sampling conditions. The ANOVA results (Table 2) showed no statistically significant difference in TRC levels among food simulants ($p = 0.200$, $\alpha = 0.05$).

Table 2. One-way ANOVA results for of simulant and TRC values

Cases	Sum of Squares	df	Mean Square	F	p
Simulant	21.435	2	10.717	1.674	0.200
Residuals	268.911	42	6.403		

B. Partial Multivariate Analysis

Principal component analysis (PCA) was performed to examine relationships among five variables potentially influencing TRC migration: food simulant type (20% ethanol, 4% acetic acid, and water), film density, and thickness. Four principal components explained 91.92% of the total data variability.

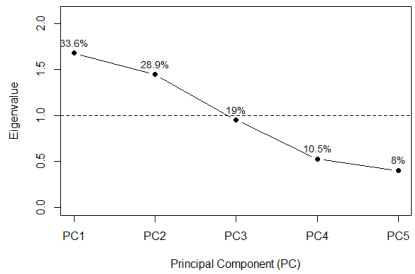


Fig. 1. Scree plot showing principal components versus eigenvalues

Following the Kaiser criterion (eigenvalue > 1) [18], two components were retained for interpretation: PC1 (eigenvalue = 1.68) and PC2 (eigenvalue = 1.44), accounting collectively for 62.5% of cumulative variance (Fig. 1). Loadings presented in Table 3 indicate that PC1 is primarily governed by food simulant effects. The negative loading associated with acetic acid suggests behavior opposite to that of water and 20% ethanol [19]. This relationship is visualized in Figure 2, where the acetic acid vector appears approximately 180° opposite to water and about 90° separated from ethanol. Similarly, the angle between ethanol and water is close to 90°, indicating weak or negligible correlation between acidic–alcoholic and alcoholic–aqueous migration behaviors [20].

These findings further support the ANOVA results presented in the previous section, indicating that TRC migration varies across food simulants, with each simulant exhibiting distinct migration mechanisms. Such behavior may be attributed to the differing affinities of food simulants toward specific groups of migrant compounds, resulting in selective extraction and distinct migration profiles. Li et al. (2016) [21] demonstrated that the migration behavior of chemical additives, including stabilizers and plasticizers, differs among food simulants, with higher migration generally observed in fatty simulants.

Moreover, acetic acid behaves differently from water because it alters the chemical environment through changes in pH. In acidic conditions, acetic acid can modify polymer–surface interactions, potentially increasing available free volume and enhancing diffusion pathways [22]. In contrast, migration in water is largely governed by diffusion-controlled transport mechanisms [23]. Considering that PE is a non-polar material, the penetration of highly polar water molecules is limited due to poor sorption affinity and weak polymer–penetrant interactions [24].

On the other hand, PC2 demonstrates a strong association between alcoholic simulant exposure and film thickness (Fig. 2). Film thickness is an important physical property of PE packaging because it influences mechanical strength, permeability, transparency, sealability, and the diffusion pathway of chemical migrants [25], [26]. Thicker films may retain larger reservoirs of extractable TRCs and, under ethanol exposure, swelling and enhanced solvent–polymer affinity may further facilitate migration, although this mechanism still requires further investigation. Previous studies have shown that, compared with thinner LDPE films, thicker films may exhibit lower distribution coefficients, indicating a greater tendency for migrant transfer into the food simulant, together with higher diffusion coefficients, suggesting faster molecular transport within the polymer matrix [27].

However, other studies have reported that the relationship between diffusion behavior and film thickness depends on both the type of food simulant and the polymer system. For instance, Goulas et al. (2001) [28] observed that specific migration into isooctane, a fatty food simulant, was influenced by film thickness, whereas migration into water did not exhibit the same dependence. This suggests that thickness alone does not directly determine the amount of residual contaminants migrated or the type of food that PE can contact. Rather, thickness affects how the film responds under specific food-contact or simulant conditions. For example, diffusivity has also been linked to polymer crystallization behavior, where thicker films may contain relatively more amorphous

regions that facilitate molecular mobility and migration processes [29]. Conversely, some studies suggest that thicker packaging can reduce migration due to decreased surface-area-to-volume ratios and longer diffusion pathways [30]. These contrasting findings indicate that the effect of thickness on migration is condition-dependent and should be interpreted together with polymer structure, simulant affinity, and the specific migrant profile of the packaging material.

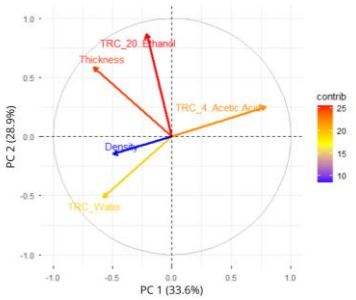


Fig. 2. Biplot of the first two principal components

Table 3. Component Loadings for Principal Components 1 and 2

	PC 1	PC 2	Uniqueness
TRC_4% Acetic Acid	-0.814	-	0.312
TRC_Water	0.759	-	0.399
Density	0.503	-	0.735
TRC_20% Ethanol	-	0.876	0.205
Thickness	-	0.814	0.225

The approximately 90° separation between ethanol and water vectors further indicates differing migration mechanisms across aqueous simulant environments (Fig.2). In support, gravimetric studies have further demonstrated that ethanol can induce swelling in polymeric materials, particularly at higher concentrations [31],[32]. Comparing the surface energy of ethanol (~22.1 mN·m-1) with that of water (~72.8 mN·m-1) and PE (~35 mN·m-1), ethanol exhibits closer surface energy compatibility with PE than water. This similarity promotes improved wettability and solvent sorption within the polymer matrix, thereby facilitating swelling-assisted migration mechanisms [33].

Spearman's rank correlation analysis was conducted to validate the relationships observed in the PCA. A moderate negative correlation was identified between migration behavior in aqueous and acidic simulants (r_s = −0.589, p = 0.023), indicating inverse migration tendencies between these environments. Additionally, a moderate positive correlation was observed between alcoholic simulant exposure and film thickness (r_s = 0.556, p = 0.031), supporting the PCA observation that thicker films exhibited increased migration in ethanol-based systems. Both correlations were statistically significant at α = 0.05.

In contrast to film thickness, film density showed high uniqueness and low loading contributions across principal components, suggesting relatively independent behavior with minimal influence on TRC variability within the studied dataset. Generally, increasing polymer density reduces permeability and consequently limits migration [34]. Density is also closely related to crystallinity, with HDPE exhibiting more tightly packed and ordered crystalline regions [35]. This may explain the weak statistical contribution of density observed in this study, particularly if only small variations in crystallinity existed among samples. Further investigation into crystallinity distribution and microstructural differences may help clarify the role of density in governing TRC migration.

IV. CONCLUSION

The JETRO-based TRC evaporation method indicated that migration levels in alcoholic food simulants were higher than in acidic and aqueous media based on average ranking. However, statistical analysis showed that these differences were not significant. Principal component analysis, together with film thickness and density, revealed two main patterns: (1) weak correlation of TRC levels across different food simulants, suggesting distinct and independent migration behaviors, and (2) a stronger association between film thickness and alcoholic simulant migration, indicating that thickness may play a more influential role under ethanol exposure and warrants further investigation. Among the variables examined, film density showed minimal contribution to the observed variability, suggesting a limited influence on TRC migration within the studied dataset. This highlights the need for more comprehensive multivariate analyses to further elucidate the interactions between polymer properties and migration behavior.

REFERENCES

[1] B. Geueke, "Non-intentionally added substances (Nias) | Food Packaging Forum", (2018, June 12)

[2] C. Shin, D.-G Kim, J.-H. Kim, J.H. Kim., M.-K. Song, & K.-S. Oh, "Migration of substances from food contact plastic materials into foodstuff and their implications for human exposure". Food and Chemical Toxicology, (2021), 154, 112373. https://doi.org/10.1016/j.fct.2021.112373

[3] K. Tumu, K. Vorst, G. Curtzwiler, "Understanding intentionally and non-intentionally added substances and associated threshold of toxicological concern in post-consumer polyolefin for use as food packaging materials," Heliyon, Vol. 10, 2024, p. e23620 https://doi.org/10.1016/j.heliyon.2023.e23620

[4] B. Geueke, D. W. Phelps, L. V. Parkinson, J. Muncke, "Hazardous chemicals in recycled and reusable plastic food packaging," Cambridge Prisms: Plastics, Vol. 1, 2023, pp. 1–43, https://doi.org/10.1017/plc.2023.7

[5] E. L. Bradley, L. Castle, S. M. Jickells, K. A.

Mountfort, W. A. Read, “Use of overall migration methodology to test for food-contact substances with specific migration limits,” Food Additives & Contaminants: Part A, Vol. 26, No. 4, 2009, pp. 574–582, https://doi.org/10.1080/02652030802477947

[6] H. Armario, E. K. Encarnacion, D. Alcarde Jr., A. Alcantara, W. Alejandro, A. Del Rosario, R. M. Ting, “Preliminary screening and method comparison of total residual contaminants migrating to fatty and oily foods from low-density polyethylene (LDPE) food contact articles sold in the Philippines,” International Journal of Food Studies, Vol. 14, No. 1, 2026, https://doi.org/10.7455//ijfs/14.01.2026.a6

[7] Bai, F., Chen, G., Hu, Y., Liu, Y., Yang, R., Liu, J., Hou, R., Li, H., Wan, X., & Cai, H. (2024). Understanding the effect of plastic food packaging materials on food flavor: A critical review. Trends in Food Science & Technology, 148, 104502. https://doi.org/10.1016/j.tifs.2024.104502

[8] W. P. Alejandro, E. K. P. Encarnacion, A. C. Alcantara, D. J. A. Jr., H. E. Armario, A. F. D. Rosario, “Assessment of total UV-absorbing contaminants in LDPE food packaging from Philippine markets,” Current Research in Nutrition and Food Science Journal, Vol. 13, No. 2, 2025, pp. 913–925,

[9] N. Sharmin, S. Bandyopadhyay, T. Radusin, K. D. Li, H. Larsen, Y. Hed, M. K. Pettersen, “An overview of enhancing polyolefin recycling in food packaging: Navigating new EU regulations and design for recycling,” Journal of Food Science, Vol. 91, No. 2, 2026, p. e70856, https://doi.org/10.1111/1750-3841.70856

[10] X. Zhong, X. Zhao, Y. Qian, Y. Zou, “Polyethylene plastic production process,” Materials Science: Materials Review, Vol. 1, No. 1, 2017, https://journal.whioce.com/index.php/msmr/article/view/200

[11] P. Knight, “Understanding the production process of low-density polyethylene (LDPE),” Chemanalyst, 2025, choihttps://www.chemanalyst.com/NewsAndDeals/NewsDetails/understanding-the-production-process-of-low-density-polyethylene-ldpe-37715

[12] L. Chen, Z. Lin, “Polyethylene: Properties, production and applications,” Proceedings of the 3rd International Academic Exchange Conference on Science and Technology Innovation (IAECST), 2021, pp. 1191–1196, https://doi.org/10.1109/IAECST54258.2021.9695646

[13] T. I. Butler, “PE processes,” in Multilayer Flexible Packaging, Elsevier, 2010, pp. 15–30, https://doi.org/10.1016/B978-0-8155-2021-4.10002-4

[14] Á. Garrido-López, V. Esquiu, M. T. Tena, “Comparison of three gas chromatography methods for the determination of slip agents in polyethylene films,” Journal of Chromatography A, Vol. 1150, No. 1–2, 2007, pp. 178–182, https://doi.org/10.1016/j.chroma.2006.11.090

[15] L. Hu, Y. Zhou, Z. Chen, D. Zhang, X. Pan, “Oligomers and monomers from biodegradable plastics: An important but neglected threat to ecosystems,” Environmental Science & Technology, Vol. 57, No. 27, 2023, pp. 9895–9897,https://doi.org/10.1021/acs.est.3c04423

[16] R. Höfer, “Processing and performance additives for plastics,” in Polymer Science: A Comprehensive Reference, Elsevier, 2012, pp. 369–381 https://doi.org/10.1016/B978-0-444-53349-4.00272-7

[17] JETRO, Specifications, Standards and Testing Methods for Foodstuffs, Implements, Containers and Packaging, 2009.

[18] D. Goretzko, M. Bühner, “Factor retention using machine learning with ordinal data,” Applied Psychological Measurement, Vol. 46, No. 5, 2022, pp. 406–421, https://doi.org/10.1177/01466216221089345

[19] S. Holland, “Data analysis in the geosciences,” Stratigrafia, n.d., Retrieved May 7, 2026, from http://stratigrafia.org/8370/lecturenotes/principalComponents.html

[20] U. Kohler, M. Luniak, “Data inspection using biplots,” The Stata Journal, Vol. 5, No. 2, 2005, pp. 208–223, https://doi.org/10.1177/1536867X0500500206

[21] B. Li, Z.-W. Wang, Q.-B. Lin, C.-Y. Hu, “Study of the migration of stabilizer and plasticizer from polyethylene terephthalate into food simulants,” Journal of Chromatographic Science, Vol. 54, No. 6, 2016, pp. 939–951, https://doi.org/10.1093/chromsci/bmw025

[22] P. Dawson, A. C. Seydim, D. Hirt, “Styrene monomer migration from expanded polystyrene into food acids and ethanol,” Journal of Food Research, Vol. 9, No. 3, 2020, p. 39, https://doi.org/10.5539/jfr.v9n3p39

[23] S. Renzetti, J. A. Voogt, L. Oliver, M. B. J. Meinders, “Water migration mechanisms in amorphous powder material and related agglomeration propensity,” Journal of Food Engineering, Vol. 110, No. 2, 2012, pp. 160–168, https://doi.org/10.1016/j.jfoodeng.2011.07.005

[24] S. Chen, X. Bao, Z. Wang, X. Rong, X. Zhang, C. Li, X. Wang, L. Wei, “Comparative study on the effects of water pressure on water absorption of ultra-high molecular weight polyethylene and polyformaldehyde,” Journal of Applied Polymer Science, Vol. 139, No. 33, 2022, p. E52783, https://doi.org/10.1002/app.52783

[25] J.O. Choi, F. Jitsunari, F. Asakawa, H.J. Park & D.S. Lee, “ Migration of surrogate contaminants in paper and paperboard into water through polyethylene coating layer”, Food Additives and Contaminants, 19(12), 2002, 1200–1206, https://doi.org/10.1080/02652030210151877

[26] Hammer IMS, “Plastic film thickness measurement

guide", Hammer IMS, 2026, https://feeds.hammer-ims.com/blog/plastic-thickness-measurement

[27] M. J. Galotto, A. Torres, A. Guarda, N. Moraga, J. Romero, "Experimental and theoretical study of LDPE versus different concentrations of Irganox 1076 and different thickness," Food Research International, Vol. 44, No. 2, 2011, pp. 566–574, https://doi.org/10.1016/j.foodres.2010.12.009

[28] A. Goulas, "Overall migration from commercial coextruded food packaging multilayer films and plastics containers into official EU food simulants," European Food Research and Technology, Vol. 212, No. 5, 2001, pp. 597–602,212(5), 597–602. https://doi.org/10.1007/s002170000294

[29] C. Wehlack, W. Possart, J. K. Krüger, U. Müller, "Epoxy and polyurethane networks in thin films on metals—Formation, structure, properties," Soft Materials, Vol. 5, No. 2–3, 2007, pp. 87–134, https://doi.org/10.1080/15394450701554536

[30] M. S. Alamri, A. A. A. Qasem, A. A. Mohamed, S. Hussain, M. A. Ibraheem, G. Shamlan, H. A. Alqah, A. S. Qasha, "Food packaging's materials: A food safety perspective," Saudi Journal of Biological Sciences, Vol. 28, No. 8, 2021, pp. 4490–4499, https://doi.org/10.1016/j.sjbs.2021.04.047

[31] V. Guazzotti, A. Ebert, A. Gruner, F. Welle, "Migration from acrylonitrile butadiene styrene (ABS) polymer: Swelling effect of food simulants compared to real foods," Journal of Consumer Protection and Food Safety, Vol. 16, No. 1, 2021, pp. 19–33, https://doi.org/10.1007/s00003-020-01308-8

[32] C. Kirchkeszner, N. Petrovics, T. Tábi, N. Magyar, J. Kovács, B. S. Szabó, Z. Nyiri, Z. Eke, "Swelling as a promoter of migration of plastic additives in the interaction of fatty food simulants with polylactic acid- and polypropylene-based plastics," Food Control, Vol. 132, 2022, Art. 108354, https://doi.org/10.1016/j.foodcont.2021.108354

[33] R. Mincheva, J. Raquez, "The surface of polymers," in Surface Modification of Polymers, 1st ed., Wiley, 2019, pp. 1–30, https://doi.org/10.1002/9783527819249.ch1

[34] N. Seref, G. Cufaoglu, "Food packaging and chemical migration: A food safety perspective," Journal of Food Science, Vol. 90, No. 5, 2025, Art. e70265, https://doi.org/10.1111/1750-3841.70265

[35] D. Li, L. Zhou, X. Wang, L. He, X. Yang, "Effect of crystallinity of polyethylene with different densities on breakdown strength and conductance property," Materials, Vol. 12, No. 11, 2019, Art. 1746, https://doi.org/10.3390/ma12111746

2026 IMEKO Joint Conference
TC8 - TC11 - TC24
Manila, Philippines August 26-29, 2026

Research-Industry Partnerships for Food Packaging Safety in the Philippines: Case Studies from Two Local Manufacturers

Elyson Keith P. Encarnacion[1,2], Floridel V. Loberiano[1], April Star L. Canonizado[1], Harold E. Armario[1], Agaseve F. Del Rosario[1], Anne C. Alcantara[1], Winnie P. Alejandro[1], Rizel Marie S.M. Ting[1], Josefino Antonio T. Mendoza[1], David J. Alcarde Jr.[1], Theressa F. Aviles-Liclican[1], Kim Angelene R. Tagle[1], Daniela Marie D. Barredo[1], Jeric B. Bañadera[1], Ellaine R. Dioso[1], Abraham R. De Guzman[3,4]

[1] *Department of Science and Technology – Industrial Technology Development Institute, Taguig City, Philippines, 1631, ekpencarnacion@itdi.dost.gov.ph*
[2] *Technological University of the Philippines – College of Management and Multidisciplinary Studies, City of Manila, Philippines, 1000*
[3] *University of Western Australia – UWA Business School, Perth, Western Australia, 6009*
[4] *HORIBA Group – Horiba Manila Representative Office, Makati City, Philippines, 1226*

***Abstract* – A strong national quality infrastructure, supported by competent testing laboratories, plays a crucial role in ensuring food packaging safety, while strengthening the competitiveness of locally manufactured products in domestic and international markets. However, the absence of mandatory certification schemes in the Philippines limits systematic monitoring of food contact articles accessible to consumers. In this study, the Packaging Safety Laboratory partnered with two local manufacturers that provided selected products for exploratory research. Paper food packaging from Manufacturer X was analyzed for perfluoroalkyl substances (PFAS) using validated liquid chromatography tandem mass spectrometry. Highly bioaccumulative PFAS were detected including PFDA (3.04 µg/kg), PFUnA (0.46 µg/kg), PFTriA (0.22 µg/kg), and PFTA (0.51 µg/kg). Regulated and more mobile PFAS such as PFOS and PFHxS were not detected. However, their carboxylic acid counterparts, PFOA (5.65 µg/kg) and PFHxA (103 µg/kg) respectively were measured with PFHxA exceeding the 25 µg/kg individually targeted non-polymeric PFAS limit specified in the EU Packaging and Packaging Waste Regulation. Plastic food bags produced by Manufacturer Y were evaluated using a modified 21 CFR Part 177 migration approach with n-heptane as fatty food simulant and UV-Vis spectrophotometry. After extraction at 25 ± 3 °C for 30 minutes, replicates of pure low-density and high-density polyethylene films showed average absorbance values of 1.060 AU and 0.795 AU respectively, exceeding the 0.1 AU maximum allowable limit adopted by the FDA Philippines. Both manufacturers identified corrective actions to reduce contaminant levels. Retesting and follow-up investigations are essential to systematically evaluate the effectiveness of manufacturer-initiated interventions and ultimately, research-industry collaborations.**

I. INTRODUCTION

Food packaging safety has become an increasingly important global public health concern due to the potential migration of hazardous substances from the contact materials into food systems during storage, transport, and consumption [1-3]. As modern food supply chains continue to rely heavily on plastic, paper, and multilayer contact materials, the ability of countries to ensure packaging safety depends not only on toxicological knowledge and analytical capability, but also on the strength of their national quality infrastructure (NQI) [4-5]. An NQI is comprised of interconnected ecosystems of metrology, standardization, accreditation, conformity assessment, and market surveillance [6]. Robust NQI systems are widely recognized as critical enablers of local testing competency, industrial competitiveness, consumer protection, and international trade because testing services, harmonized standards, conformity assessment, and regulatory systems ensure that products consistently comply with technical and safety requirements [7,8].

Industry stakeholders play a central role in shaping and operationalizing the NQI because manufacturers generate the demand for reliable testing services, technical standards, metrological traceability, and conformity assessment systems necessary for production, innovation, and market access [9]. Effective collaboration among

industries, regulatory agencies, and research institutions is essential for translating scientific measurements into practical quality assurance mechanisms and evidence-based policies [10]. In developing economies such as the Philippines, partnerships between public research institutions and industries facilitate technology transfer, strengthen laboratory capabilities, and support the gradual establishment of quality-oriented production systems [11]. Such collaborations are particularly relevant in emerging areas such as packaging safety where the chemical complexity of food contact materials, the need to detect intentionally and non-intentionally added substances, and evolving regulatory expectations often exceed routine analytical and technical services available to many industries [5,12].

The Philippines has strengthened the legal an institutional basis of its food safety system through the Food Safety Act of 2013, which promotes science-based regulation and risk-oriented control measures [13,14]. However, unlike conventional food safety systems, packaging safety in the Philippines remains relatively underdeveloped despite the growing scientific evidence linking food packaging materials to chemical exposure risks [15,16]. Local studies have shown that food packaging may contain contaminants such as per- and polyfluoroalkyl substances (PFAS), phthalates, and benzophenone, many of which are associated with carcinogenicity, endocrine disruption, and developmental toxicity among others [17-19].

The limitations in local food contact article system reflect weaknesses across several pillars of the Philippine NQI. First, there is currently no comprehensive mandatory certification or conformity assessment framework specifically governing food contact article testing laboratories. Second, only a limited number of laboratories possess the technical competence and instrumentation necessary for migration testing, polymer characterization, and trace-level contaminant analysis. Third, the scarcity of certified reference materials, interlaboratory programs, and proficiency testing schemes for packaging contaminants constrains metrological traceability and measurement comparability, both of which are essential for generating reliable analytical data [20]. Finally, regulatory and policy frameworks governing contact article safety remain insufficient compared with more established international systems such as European Union Commission Regulation No. 10/2011 [21] and the United States 21 Code of Federal Regulations (CFR) Part 177 [22].

Recognizing these gaps, the Department of Science and Technology – Industrial Technology Development Institute (DOST-ITDI), through its Packaging Safety Laboratory (PSL), has initiated collaborative research efforts with local manufacturers to generate baseline scientific data on their respective products and, in a much larger scope, packaging safety in the Philippines. The present study demonstrates this approach through partnerships with two packaging manufacturers producing paper- and plastic-based food contact materials. Accordingly, this paper examines how two research-industry partnerships were established, what baseline analytical findings were generated from selected paper- and plastic-based food contact articles, and how post-testing consultations informed preliminary manufacturer actions. Through these case studies, the paper illustrates how competent research laboratories can contribute to the gradual development of testing capacity, industry awareness, and generation for food packaging safety in the Philippines.

II. MATERIALS AND METHODS

Stakeholder Identification

Data of stakeholders who inquired about packaging testing services from 2021 to 2025 were collected. Digital search of companies with accessible websites and social media accounts was also performed, and their corresponding details were documented. Several stakeholder engagements were organized, and relevant information were gathered through surveys, technical discussions, and feedback forms.

Upon evaluation of all records, personal communication through electronic mail and/or phone was conducted to invite interested stakeholders for a private physical meeting. The meeting served as a preliminary consultation mechanism to discuss the objectives of the research collaboration, roles and responsibilities of each participating party, confidentiality considerations, contaminants of concern, sample types and availability, testing requirements, expected use of analytical results, and most importantly, willingness to participate. This process led to the selection of one paper packaging manufacturer and one plastic packaging producer for case-study evaluation.

Realization of Partnerships

A technical service contract or a memorandum of agreement was drafted for the identified partners. Each agreement underwent iterative review and revision by the concerned parties until the scope of work, responsibilities, confidentiality provisions, data-use terms, and other legal and technical conditions were mutually acceptable. Representatives signed the contract or agreement prior to notarization.

Experimentation and Way Forward

For both manufacturers, selected products were purposively identified for exploratory or case-study evaluation based on the manufacturers' declared technical concerns, product relevance, and alignment with the laboratory's available optimized or validated methods. The sampling was not intended to represent the full production range of either manufacturer or the broader

Philippine packaging sector. The paper packaging manufacturer chose PFAS as the analyte of concern. Determination of PFAS in identified paper-based samples (i.e., wrapper, clamshell and cup) was conducted using a solid phase extraction (SPE) procedure and liquid chromatography tandem mass spectrometry (LC-MS/MS) method developed and optimized by the laboratory as described by Encarnacion et al. [15]. Quality control measures included external calibration, procedural blanks analysis, and recovery assessment using a second-source certified reference material (CRM) solution. Where available, calibration linearity, blank response, recovery performance, and limits of detection were evaluated against the laboratory's established method-performance criteria. Meanwhile, the plastic packaging manufacturer selected total UV-absorbing contaminants (TACs), a screening parameter for UV-absorbing extractives, as the parameter for evaluation. Determination of TACs migrating from specific plastic bags and films/sheets to fatty/oily foods was performed using extraction and UV-Vis spectrophotometry methods validated by the laboratory as detailed by Alejandro et al. [16]. Extraction was performed by subjecting 5 cm x 10 cm of each product to 100 mL n-heptane (as fatty/oily food simulant) at room temperature (25 ± 3 °C) for 30 minutes while spectrophotometric scanning was conducted with blank correction. Each product was tested in duplicate. After all experiments had been completed, a private post-experiment meeting for each manufacturer was facilitated to discuss the results, their implications, and possible follow through studies.

III. RESULTS AND DISCUSSION

Stakeholder Identification

Preliminary consultation with the paper packaging manufacturer revealed that it sources its raw materials across Asia and produces its final products locally. Having been established and in operation for more than three decades, the stakeholder (Manufacturer X) provides wrappers, clamshells, and cups to international quick service restaurants (QSRs). With PFAS guidelines being implemented in other countries, Manufacturer X would like to assess if the PFAS levels in its paper-based products will be able to penetrate regulated markets and meet established thresholds.

In a separate private meeting, the plastic packaging manufacturer disclosed that it sources its resins, additives, and colorants locally. Despite being relatively new to the packaging industry, the stakeholder (Manufacturer Y) provides bags and films/sheets to various Philippine-based brand owners (e.g., a QSR uses the bags to store raw chicken while a bakery chain utilizes the films/sheets as mats to display confectioneries in its shops). With the goal to expand local reach, Manufacturer Y intends to acquire the Food and Drug Administration (FDA) Philippines' voluntary certification for food contact articles (FCA).

Realization of Partnerships

Due to apprehensions by its top management, Manufacturer X's in-house laboratory formalized the partnership through a short-term technical service contract that aims to quantify several PFAS compounds in the wrappers, clamshells, and cups they produce.

Meanwhile, Manufacturer Y signed a long-term memorandum of agreement that will evaluate the company's plastic bags and films/sheets used as food contact articles, and will be used to develop interventions for improvement, if necessary.

Analysis of PFAS in Paper-based Packaging

Table 1 summarizes the PFAS compounds that were detected in Manufacturer X's tested products and their corresponding concentrations. Highly bioaccumulative PFAS such as perfluorononanoic acid (PFNA), perfluorodecanoic acid (PFDA), perfluoroundecanoic acid (PFUnA), perfluorotridecanoic acid (PFTriA) and perfluorotetradecanoic acid (PFTA) were detected but in trace amounts.

Table 1. Concentrations of PFAS in Manufacturer X's Tested Products

PFAS	Concentration, µg/kg		
	Wrapper (n=1)	Clamshell (n=1)	Cup (n=1)
PFHxA	103	1.34	1.29
PFHpA	8.76	0.22	0.25
PFOA	5.65	0.22	0.20
PFHxS	ND	ND	ND
PFNA	2.94	0.15	0.13
PFDA	3.04	0.77	0.37
PFOS	ND	ND	ND
PFUnA	0.46	ND	ND
PFTriA	ND	0.22	ND
PFTA	ND	0.51	ND

ND = Not Detected
Limit of Detection (LOD) Range = 0.02-0.08 µg/kg

Prior to the European Commission's Packaging and Packaging Waste Regulation (PPWR) [23], three mobile PFAS compounds have been explicitly banned: perfluorooctanesulfonic acid (PFOS) in 2019 [24], perfluorooctanoic acid (PFOA) in 2020 [25], and perfluorohexanesulfonic PFHxS (2023) [26]. Among the three, PFOA was still detected across Manufacturer X's tested samples with the highest concentration (5.65 µg/kg) found in paper used to wrap burgers and sandwiches. Meanwhile, only perfluorohexanoic acid (PFHxA) in wrapper was found to exceed the 25 µg/kg maximum allowable limit (MAL) for any single, non-polymeric PFAS [23]. The measured PFHxA concentration (103 µg/kg) in the tested product was approximately 4.12 times larger than the limit. Perfluoroheptanoic acid (PFHpA),

which has the second highest concentration in the wrapper, is still within the threshold but may require monitoring as it already exceeded one-third of the MAL. In summary, the findings warrant confirmatory batch testing and potential material or process intervention should Manufacturer X intend to supply the tested product for EU-regulated markets.

Analysis of TACs Migrating from Plastic Packaging to Fatty and Oily Foods

Through Differential Scanning Calorimetry (DSC) and Fourier transform Infrared (FTIR) Spectroscopy, Manufacturer Y's plastic samples were confirmed to be low density polyethylene (LDPE), high density polyethylene (HDPE) and polypropylene (PP) as declared. Table 2 summarizes the absorbance of the TACs that migrated from Manufacturer Y's selected plastic samples.

Table 2. Absorbance Units (AU) of TACs that Migrated from Manufacturer Y's Selected Products to Fatty/Oily Food Simulant

Selected Plastic Samples (n=2)	**TACs, AU (%RSD)**
Pure LDPE	1.060 (0.54%)
LDPE + Additive	0.925 (1.15%)
Pure HDPE	0.795 (1.16%)
Pure PP	0.284 (1.75%)
Pure PP + Additive	0.340 (0.42%)

The results indicate that none of Manufacturer Y's selected samples met the 0.10 AU level for extractives established by the US CFR [22] and adopted by FDA Philippines as current limit for FCA subject to n-heptane. These findings suggest potential compliance concerns for the selected samples and indicate the need for product improvement or confirmatory testing before regulatory certification is pursued.

Way Forward

During the post-experiment meeting, Manufacturer X noted that most measured PFAS concentrations were below the applicable individual PFAS threshold. However, the detection of PFOA and the elevated concentration of PFHxA were considered technical evidence for preliminary corrective actions. The discussion strengthened the company's confidence in working with PSL, leading to its intent to pursue a subsequent testing contract following planned reformulations of its coating system, which was presumed by the stakeholder as a possible contributor to PFAS occurrence in the tested paper products.

In contrast, the post-experiment consultation with Manufacturer Y focused on the potential limitations of its plastic food contact articles, particularly their suitability with fatty or oily food products. In response to the findings, the stakeholder indicated its intention to advise customers against using the tested plastic samples for application involving fatty or oily matrices, such as raw chicken and confectionery products, while exploring alternative resin sources. Manufacturer Y further expressed its intention to coordinate with the laboratory for retesting once reformulated or newly sourced materials become available.

IV. CONCLUSION

Consistent with the study objective, this exploratory case study demonstrated how research-industry partnerships can generate baseline analytical evidence for selected paper- and plastic-based food contact articles while providing a structured platform for technical discussion, risk communication, and manufacturer-led product improvement. The study further showed that analytical testing becomes more useful when results are discussed confidentially with manufacturers and translated into practical actions. Post-experiment consultations led manufacturers to identify preliminary interventions, including planned coating reformulation, evaluation of alternative resin sources, customer advisories, and future retesting. However, because the study involved only two manufacturers and purposively selected products, the findings should be interpreted as exploratory case-study evidence rather than representative estimates of food packaging safety across the Philippine market. Future work should include expanded industry participation, batch-to-batch monitoring, confirmatory testing after intervention, interlaboratory comparison, method harmonization, and proficiency testing.

Overall, the study supports the premise that research-industry partnerships can contribute meaningfully to the gradual establishment of food packaging safety systems in the Philippines. By generating local baseline data, identifying contaminants of concern, guiding manufacturers towards corrective actions, and demonstrating the role of competent research and testing laboratories, such partnerships can strengthen the national quality infrastructure for food contact article safety and provide scientific support for future standards, certification schemes, and evidence-based policies.

V. REFERENCES

[1] Q.Zhang, Y.Huo, Q.Yang, F.Zhao, M.Li, J.Ju, "Migration of chemical substances from packaging materials to food", Food Chem., vol.485, September 2025, doi: https://doi.org/10.1016/j.foodchem.2025.144544

[2] N.Seref, G.Cufaoglu, "Food Packaging and Chemical Migration: A Food Safety Perspective", J Food Sci., vol.90, no.5, May 2025, doi: https://doi.org/10.1111/1750-3841.70265

[3] R.K.Gupta, S.Pipilya, S.Karunanithi, G.M.EswaranU, S.Kumar, S.Mandilya, P.P.Srivastav, T.Suthar, A.M.Shakh, E.Harsanyi, B.Kovacs,

"Migration of Chemical Compounds from Packaging Materials into Packaged Foods: Interaction, Mechanism, Assessment, and Regulations", Foods, vol.13, no.19, p.3125, September 2024, doi: https://doi.org/10.3390/foods13193125

[4] K.Groh, T.backhaus, B.Carney-Almroth, B.Geuke, P.A.Inostroza, A.Lennquist, H.A.leslie, M.Maffini, D.Slunge, L.Trasande, A.M.Warhurst, J.Muncke, "Overview of known plastic packaging-associated chemicals and their hazards", Sci. Total Environ. vol.651, part 2, pp.3253-3268, February 2019, doi: https://doi.org/10.1016/j.scitotenv.2018.10.015

[5] B.Geueke, K.Groh, J.Muncke, "Food packaging in the circular economy: Overview of chemical safety aspects for commonly used materials", J. Clean Prod., vol.193, pp.491-505, August 2018, doi: https://doi.org/10.1016/j.jclepro.2018.05.005

[6] U.Harmes-Liedtke, A.S.Ramkissoon, C.Schoen, P.Grinsted, "The Evolution of Quality Infrastructure: Experiences and Prospects of Advanced Economies and Developing Countries", World Bank Group, Retrieved May 2026 from https://thedocs.worldbank.org/en/doc/e88b0ec71d550ef9cf0f3988342124af-0050062025/original/Ulrich-Harmes-Liedtke-Evolution-of-Quality.pdf

[7] K.Blind, P.Neuhäusler, T.Schubert, "The economic effects of the quality infrastructure", vol.84, March 2026, Technol. Soc. doi: https://doi.org/10.1016/j.techsoc.2025.103114

[8] K.Blind, "The role of the quality infrastructure within socio-technical transformations: A European perspective", Technol. Forecast. Soc. Change vol.199, February 2024, doi: https://doi.org/10.1016/j.techfore.2023.123019

[9] Y.Wu, H.J.de Vries, "Effects of participation in standardization on firm performance from a network perspective: Evidence from China", technol. Forecast. Soc. Change, vol.175, February 2022, doi: https://doi.org/10.1016/j.techfore.2021.121376

[10] G.Santoro, A.Ferraris, E.Giacoas, G.Giovando, "How SMEs Engage in open Innovation: a Survey", J. Knowl. Econ., vol.9, pp.561-574, January 2016, doi: https://doi.org/10.1007/s13132-015-0350-8

[11] S.Ankrah, O.AL-Tabbaa, "Universities-industry collaboration: A systematic review", Scand. J. Manag., vol.31, no.3, pp.387-408, September 2015, doi: https://doi.org/10.1016/j.scaman.2015.02.003

[12] J.Muncke, A.M.Andersson, T.Backhaus, S.M.Belcher, J.M.Boucher, B.C.Almroth, T.J.Collins, B.Geueke, K.J.Groh, J.J.Heindel, F.A.von Hippel, J.Legler, M.V.Maffini, O.V.Martin, J.P.Myers, A.Nadal, C.Nerin, A.M.Soto, L.trasande, L.N.Vandenberg, "A vision for safer food contact materials: Public health concerns as drivers for improved testing", Environ. Int., vol.180, October 2023, doi: https://doi.org/10.1016/j.envint.2023.108161

[13] A.S.Rustia, M.A.P.Tan, D.N.S.Guiriba, F.P.S.Magtibay, I.R.J.Bondoc, C.B.D.G.Mariano, D.H.Caincol, K.A.D.Bautista, B.F.R.Bulagao, V.C.L.De Guzman, A.C.Musni, A.M.T.Salem, J.E.B.BVillanueva, "Defining Risk in Food Safety in the Philippines", Curr. Res. Nutr. Food Sci., vol.9, no.1., 2021, doi: http://dx.doi.org/10.12944/CRNFSJ.9.1.23

[14] Fifteenth Congress of the Philippines, "RA No. 10611: Food Safety Act of 2013", July 2012, Retrieved May 2026 from https://lawphil.net/statutes/repacts/ra2013/ra_10611_2013.html

[15] E.K.P.Encarnacion, A.C.Alcantara, H.E.Armario, W.P.Alejandro, Z.Zhen, Z.Sun, N.Lin, "Preliminary Screening of Per- and Polyfluoroalkyl Substances (PFAS) in Philippine Fast Food Packaging Using Liquid Chromatography-Mass Spectrometry (LC-MS), Curr. Res. Nutr. Food Sci., vol.12, no.1., April 2024, doi: http://dx.doi.org/10.12944/CRNFSJ.12.1.34

[16] W.P.Alejandro, E.K.P.Encarnacion, A.C.Alcantara, D.J.Alcarde Jr., H.E.Armario, A.F.Del Rosario, R.M.S.M.Ting, "Assessment of Total UV-Absorbing Contaminants in LDPE Food Packaging from Philippine Markets", Curr. Res. Nutr. Food Sci., vol.13, no.2., May 2025, doi: http://dx.doi.org/10.12944/CRNFSJ.13.2.26

[17] A.F.Del Rosario, A.S.Canonizado, H.E.Armario, A.C.Alcantara, E.K.P.Encarnacion, "Determination of Selected Per- and Polyfluoroalkyl Substances (PFAS) in Locally Sourced Paper-based Food Contact Materials (FCMs)", 73rd Philippine Association for the Advancement of Science and Technology", September 2024, doi: https://doi.org/10.13140/RG.2.2.19749.51686

[18] A.C.Alcantara, E.K.P.Encarnacion, H.E.Armario, W.P.Alejandro, "Preliminary validation and Screening of Di(2-ethylhexyl) phthalate (DEHP) in Plastic-based Fast Food Packaging", 38th Philippine Chemistry Congress, July 2024, doi: https://doi.org/10.13140/RG.2.2.20526.11847

[19] D.J.Alcarde Jr., J.L.Diaz, E.K.P.Encarnacion, A.C.Alcantara, H.E.Armario, "Exposure Assessment of Filipino Consumers to Benzophenone Migrated From Paper and Paperboard Used as Packaging For Food and Beverages", 73rd Philippine Association for the Advancement of Science and Technology", September 2024, doi: https://doi.org/10.13140/RG.2.2.34364.04480

[20] H. Cantwell (ed.), "Eurachem Guide: the Fitness for Purpose of Analytical Methods—A Laboratory Guide to Method Validation and Related Topics", (3rd ed. 2025), Retrieved May 2026 from https://www.eurachem.org/images/stories/Guides/pd

f/MV_guide_3rd_ed_V1_EN.pdf
[21] Commission Regulation (EU), “EU No. 10/2011 of 14 January 2011 on plastic materials and articles intended to come into contact with food”, Retrieved May 2026 from https://eur-lex.europa.eu/legal-content/EN/TXT/PDF/?uri=CELEX:32011R0010
[22] US Food and Drug Administration – Department of Health and Human Services, “21 Code of Federal Regulations Part 177 – Indirect Food Additives: Polymers”, Retrieved May 2026 from https://www.ecfr.gov/current/title-21/chapter-I/subchapter-B/part-177?toc=1
[23] Commission Regulation (EU), “EU 2025/40 of 19 December 2024 on packaging and packaging waste, amending Regulation (EU) 2019/1020 and Directive (EU) 2019/904 and repealing Directive 94/62/EC”, 2025, Retrieved May 2026 from https://eur-lex.europa.eu/legal-content/EN/TXT/PDF/?uri=OJ:L_202500040
[24] Commission Regulation (EU), “EU 2019/1021 of the European Parliament and of the Council of 20 June 2019 on persistent organic pollutants (recast)”, 2019, Retrieved May 2026 from https://eur-lex.europa.eu/legal-content/EN/TXT/PDF/?uri=CELEX:32019R1021&qid=1778194111557
[25] Commission Delegated Regulation (EU), “EU 2020/784 of 8 April 2020 amending Annex I to Regulation (EU) 2019/1020 of the European Parliament and of the Council as regards the listing of perfluorooctanoic acid, its salts and PFOA-related compounds”, 2020, Retrieved May 2026 from https://eur-lex.europa.eu/legal-content/EN/TXT/PDF/?uri=CELEX:32020R0784
[26] Commission Regulation (EU), “EU 2023/1608 of 30 May 2023 amending Annex I to Regulation 2019/1021 of the European Parliament and of the Council as regards the listing of perfluorohexane sulfonic acid (PFHxS), its salts and PFHxS-related compounds”, 2023, Retrieved May 2026 from https://eur-lex.europa.eu/legal-content/EN/TXT/PDF/?uri=CELEX:32023R1608&qid=1778193886101

2026 IMEKO Joint Conference
TC8 - TC11 - TC24
Metro Manila, Philippines, August 26-29, 2026

Chemometric Evaluation of Total Reflection X-Ray Fluorescence (TXRF) Elemental Profiles of Milkfish *(Chanos chanos)* Tissue for Geographic Differentiation

Reno S. Bia[1], Kim Christopher C. Aganda[1], Anton John D. Rocha[1], Aldrin Jan E. Tabuso[1], John Kenneth C. Valerio[1]

[1]*Department of Science and Technology, Industrial Technology and Development Institute (DOST-ITDI), Bicutan, Taguig City, Philippines*

***Abstract* – This study evaluated the potential of Total Reflection X-Ray Fluorescence (TXRF)-based elemental fingerprinting combined with chemometric analysis for geographic differentiation of milkfish *(Chanos chanos)* gastrointestinal (GIT) tissues collected from selected fish landing sites across Luzon, Philippines. Elemental concentration and net peak area datasets generated from TXRF measurements were processed using a Python-based chemometric workflow. Principal Component Analysis (PCA) and Hierarchical Cluster Analysis (HCA) revealed discernible regional grouping tendencies and several distinct outlier samples, indicating variability in elemental composition potentially associated with localized environmental conditions. The concentration-based dataset produced improved clustering behavior, with the first three principal components explaining 73.2% of the total variance. The findings demonstrate the potential applicability of TXRF coupled with chemometric analysis as a rapid screening approach for exploratory seafood provenance studies and provide a preliminary framework for future large-scale traceability investigations.**

I. INTRODUCTION

Milkfish *(Chanos chanos)* is one of the most widely consumed aquaculture species in the Philippines and plays an important role in the country's fisheries and food sector. Due to its extensive commercial distribution across multiple fish landing sites in Luzon, verification of geographic origin has become increasingly challenging. Reliable analytical approaches for seafood traceability are therefore essential to support food authenticity, environmental monitoring, and supply chain transparency.

Seafood traceability has gained increasing attention due to concerns regarding product mislabeling, substitution, and the sustainability of aquatic resources [1,2]. Conventional traceability systems based primarily on documentation and supply chain records may be limited by incomplete reporting and product mixing, highlighting the need for analytical approaches capable of independently verifying product origin [3]. In this context, elemental fingerprinting has emerged as a promising strategy for food authentication because the elemental composition of biological tissues may reflect environmental conditions such as water chemistry, sediment interaction, and feeding behavior [4].

In fish, trace elements may accumulate through both dietary intake and environmental exposure, with certain tissues potentially preserving localized environmental signatures [5,6]. Gastrointestinal (GIT) tissue, in particular, may retain elemental characteristics associated with recently ingested materials and surrounding aquatic conditions, making it a potential matrix for investigating geographic variability without utilizing the edible portion of the fish. Such an approach also supports sustainable analytical practices through the utilization of non-edible biological materials.

Several elemental analysis techniques, including inductively coupled plasma mass spectrometry (ICP-MS) and atomic absorption spectrometry (AAS), have been widely employed for trace element determination. However, these techniques commonly require extensive sample preparation and longer analytical procedures. Total Reflection X-Ray Fluorescence (TXRF) offers an alternative multi-element analytical technique with advantages including minimal sample preparation, low sample consumption, rapid analysis, and simultaneous multi-element detection [7,8]. TXRF has been successfully applied in food analysis, environmental monitoring, and trace elemental screening of biological matrices, including fish samples [9,10].

The interpretation of complex multi-element datasets generated from elemental analysis requires robust multivariate statistical approaches capable of identifying relationships and clustering behavior among samples. Chemometric techniques such as Principal Component Analysis (PCA) and Hierarchical Cluster Analysis (HCA) are widely used for dimensionality reduction, visualization, classification, and exploratory analysis of chemical datasets [11,12]. These methods have been increasingly applied in food authentication studies to distinguish products according to geographic origin and compositional similarity.

Despite these developments, studies integrating TXRF-based elemental fingerprinting and chemometric analysis for geographic differentiation of milkfish remain limited, particularly using gastrointestinal tissue as the analytical matrix. Therefore, this study investigates the potential of TXRF-derived elemental profiles of milkfish GIT samples collected from selected fish landing sites across Luzon, Philippines. Principal Component Analysis (PCA) and Hierarchical Cluster Analysis (HCA) were employed to evaluate geographic variability and assess the applicability of TXRF-based chemometric fingerprinting for seafood traceability.

II. MATERIALS AND METHODS

A. Sampling Design and Matrix Selection

Milkfish (*Chanos chanos*) samples were collected from selected fish landing sites across Luzon, Philippines, representing multiple geographic regions and aquatic environments, including the National Capital Region (NCR), Region I (R1), Region III (R3), and Region IV-A (R4A).

The gastrointestinal tract (GIT) tissue was selected as the analytical matrix due to its potential to reflect recent dietary intake and environmental exposure, thereby preserving elemental signatures potentially associated with geographic origin and localized aquatic conditions. Compared with muscle tissue, the GIT matrix is expected to exhibit more pronounced elemental variability arising from environmental and feeding interactions, making it suitable for exploratory chemometric differentiation.

B. Reagents and Materials

Elemental analysis was performed using a Bruker S2 Picofox Total Reflection X-Ray Fluorescence (TXRF) spectrometer equipped with 30-mm quartz glass sample carriers. Prior to use, all glassware and quartz carriers were cleaned using a 5% RBS 50 detergent solution followed by immersion in 20% nitric acid solution to minimize possible elemental contamination.

A 1% (v/v) Triton X-100 solution (octylphenol ethoxylate) was used as dispersing medium during sample preparation to improve suspension stability and particle homogeneity. Yttrium (Y) standard solution (1000 mg/L) was used as the internal standard due to its absence in biological fish matrices and its analytical stability during TXRF measurement.

C. Sample Preparation

The sample preparation procedure was adapted from a previously validated TXRF method for biological fish tissue analysis.

Approximately 0.1 g of homogenized GIT tissue was accurately weighed using an analytical balance. Each sample was spiked with 10 µL of 1000 mg/L yttrium internal standard and diluted with 5 mL of 1% Triton X-100 solution.

To improve matrix homogeneity and reduce particle agglomeration, the suspensions were subjected to sonication in 5-minute intervals for at least three (3) cycles, with vortex mixing performed between sonication steps. Immediately prior to deposition, the suspensions were vortexed again to maintain uniform elemental distribution.

A 10 µL aliquot of the prepared suspension was deposited onto a pre-cleaned siliconized quartz carrier and allowed to air dry under ambient laboratory conditions until a thin and uniform residue approximately 1 cm in diameter was formed at the center of the carrier.

D. TXRF Measurement Conditions

Elemental measurements were performed using the Bruker S2 Picofox TXRF spectrometer operated under standardized analytical conditions. The instrument utilizes monochromatic molybdenum (Mo Kα) radiation at grazing incidence geometry to achieve total reflection conditions, thereby minimizing spectral background and enhancing trace elemental sensitivity.

The spectrometer was operated at an X-ray tube voltage of 50 kV and current of approximately 1000 µA. Acquisition times ranging from 1600 to 2000 seconds were employed to improve counting statistics and enhance trace-element detection.

Spectral deconvolution and elemental quantification were performed using the instrument's Bayesian fitting algorithm integrated within the TXRF software. The software automatically generated elemental concentration values and corresponding net peak areas for detected elements.

For chemometric processing, only elemental signals corresponding to the Kα (K12) emission lines were retained due to their stronger signal intensity and improved analytical reliability compared to weaker alternative emission lines. Signals corresponding to the yttrium internal standard were excluded from subsequent multivariate analyses to avoid artificial influence on clustering behavior.

E. Computational Workflow

Raw TXRF reports generated by the instrument software in portable document format (PDF) were processed using a Python-based workflow implemented in Google Colab. Elemental concentration values and corresponding net peak areas were extracted directly from the PDF reports using the *pdfplumber* Python library and compiled into structured sample-by-element matrices.

All data extraction, preprocessing, chemometric analysis, and figure generation procedures were performed in a Google Colab environment using Python scientific libraries including *NumPy, Pandas, Scikit-learn, SciPy,* and *Matplotlib.*

Table 1. Partial preview of the processed concentration-based elemental dataset used for chemometric analysis.

Sample	Element																		
	Na	P	S	Cl	K	Ca	Ti	V	Cr	Mn	Fe	Ni	Cu	Zn	As	Se	Br	Rb	Sr
G-NCR_Muntinlupa_Loc1	12.57	8.09	8.52	8.04	8.95	6.81	2.12	1.69	1.26	2.43	6.16	0.66	6.03	4.73	0.63	2.30	3.51	3.35	0.97
G-R3_Pampanga_Loc3	12.61	7.75	8.27	7.93	8.65	6.29	4.72	1.78	1.36	2.97	7.53	1.55	2.98	4.27	0.35	0.96	3.37	1.81	1.56
G-R4a_Quezon_Loc2	12.66	7.57	8.32	8.23	8.69	6.18	2.12	1.63	1.45	2.06	5.26	0.90	3.14	4.51	0.44	0.41	3.49	1.94	1.40
G-R4a_Quezon_Loc1	12.25	6.65	7.17	7.13	7.86	5.34	1.82	1.63	1.13	0.61	4.18	0.93	1.66	2.92	0.33	0.14	2.48	1.06	0.84
G-NCR_Muntinlupa_Loc3	12.58	6.80	7.40	7.32	8.19	4.89	2.47	1.63	1.35	1.82	5.40	0.76	3.19	3.33	0.89	0.86	2.85	2.37	0.46

III. Results and Discussions

A. Elemental Dataset Preprocessing and Signal Refinement

A full elemental scan was initially performed for all milkfish gastrointestinal (GIT) samples using TXRF in order to preserve the overall elemental fingerprint of each sample. Preliminary extraction of elemental concentration and net peak area datasets from the raw TXRF reports produced matrices containing twenty-six (26) elemental variables for both concentration and net area measurements.

Initial exploratory inspection of the raw datasets revealed substantial sparsity and inconsistent elemental detection frequencies among several variables. Certain elements exhibited frequent non-detection across the sampled regions, potentially introducing noise and instability during multivariate analysis. In addition, the concentration values displayed highly skewed distributions due to the large dynamic range between major and trace elemental concentrations.

To improve chemometric interpretability and reduce noise contribution, elemental variables detected in fewer than four (4) samples were excluded from the concentration-based dataset. This refinement step reduced the concentration matrix from twenty-six (26) to nineteen (19) retained elemental variables consisting of Na, P, S, Cl, K, Ca, Ti, V, Cr, Mn, Fe, Ni, Cu, Zn, As, Se, Br, Rb, and Sr. The net area dataset was retained in its complete form for comparative exploratory analysis.

Values reported as *"Not detected"* in the TXRF software output were treated as missing values *(NaN)* rather than numerical zeros to minimize artificial distortion of variance structures and inter-sample relationships. Remaining missing values were subsequently subjected to mean imputation on a per-element basis to preserve matrix continuity during multivariate processing.

Following imputation, logarithmic transformation using the *log1p* function was applied to reduce skewness arising from the large concentration differences among elemental variables and to stabilize variance across the dataset. The transformed datasets were then standardized through z-score normalization using the *StandardScaler* function from the Scikit-learn Python library to ensure equal contribution of all elemental variables during chemometric analysis.

Table 1 summarizes a partial preview of the processed concentration dataset used as the primary input matrix for subsequent chemometric analyses. The values shown correspond to log-transformed and standardized elemental concentration data after missing-value treatment, imputation, and z-score normalization. The complete processed dataset is provided as *Supplementary Table S1*.

Exploratory comparison between concentration-based and net-area-based datasets indicated that concentration-derived data produced improved clustering behavior and more interpretable multivariate separation patterns. Consequently, the concentration dataset was selected as the primary dataset for subsequent chemometric interpretation and visualization.

B. Principal Component Analysis of TXRF-Derived Elemental Profiles

Principal Component Analysis (PCA) was performed to evaluate multivariate relationships and regional clustering behavior among milkfish GIT samples based on TXRF-derived elemental profiles. PCA was applied to both concentration-based and net-area-based datasets in order to compare their respective chemometric performance and interpretability.

For the concentration-based dataset, the first three principal components (PC1–PC3) explained 73.2% of the total variance, with PC1 accounting for 44.5%, PC2 for 18.3%, and PC3 for 10.4%. In comparison, the net-area-based dataset explained 76.5% cumulative variance across the first three principal components, with PC1 contributing 55.9%, PC2 contributing 12.1%, and PC3 contributing 8.5%. Although both datasets demonstrated substantial variance capture, the concentration-derived dataset produced improved clustering behavior and more interpretable regional separation patterns. Consequently, the concentration-based dataset was selected as the primary basis for subsequent PCA interpretation and visualization.

Fig. 1 presents the scree plots illustrating the explained variance contribution of each principal component for both concentration-based and net-area-based datasets. The scree plots demonstrated that most dataset variance was concentrated within the first few principal components, particularly along PC1. However, PC3 still contributed meaningful explained variance in the concentration-based dataset (>10%), indicating that additional multivariate information relevant to sample differentiation remained beyond conventional two-dimensional visualization. This observation justified the inclusion of three-dimensional PCA visualization to further assess clustering tendencies and regional dispersion patterns among samples.

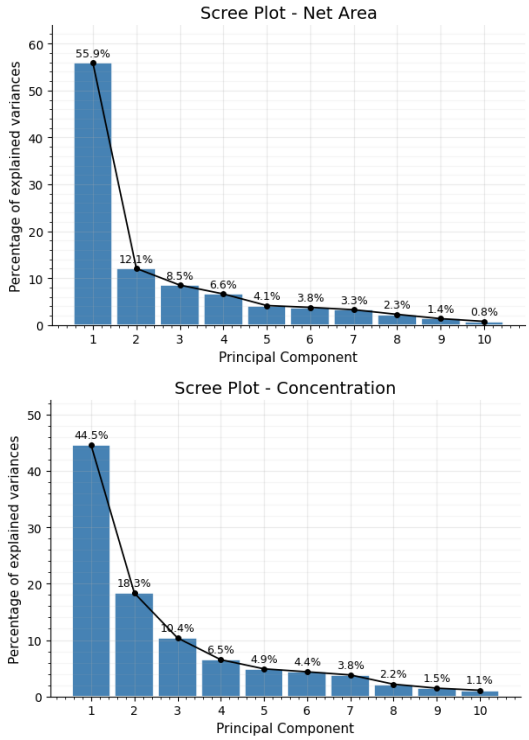


Fig. 1. Scree plots of concentration-based and net-area-based PCA datasets showing explained variance ratios across principal components.

Two-dimensional PCA score plots generated using the concentration-derived dataset revealed observable regional grouping tendencies among the milkfish samples. As shown in *Fig. 2*, partial overlap among several samples remained evident within the two-dimensional PCA space, particularly among samples originating from Region III and Region IV-A.

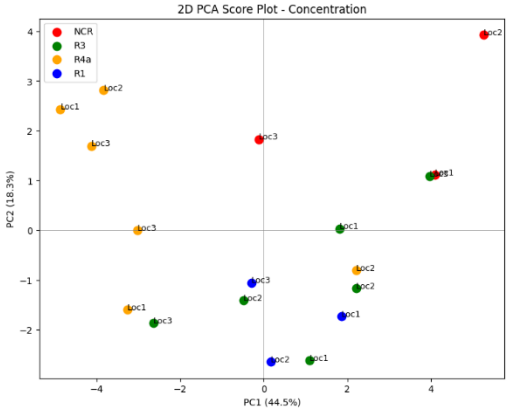


Fig. 2. Two-dimensional PCA score plot of concentration-derived elemental profiles of milkfish GIT samples.

To further improve visualization of multivariate relationships and clustering behavior, three-dimensional PCA score plots *(Fig. 3)* were subsequently generated using PC1, PC2, and PC3. Inclusion of the third principal component improved separation and visualization of several regional groupings that were less distinguishable in the two-dimensional projections. Region-specific clustering tendencies became more apparent when samples were color-coded according to geographic origin, with NCR samples generally occupying positive PC1 regions, while several Region IV-A samples were distributed toward negative PC1 values. Region III samples exhibited comparatively broader dispersion across the PCA space, suggesting greater internal elemental heterogeneity among sampling locations.

Partial overlap among regional clusters remained evident, indicating the influence of shared environmental conditions and localized variability.

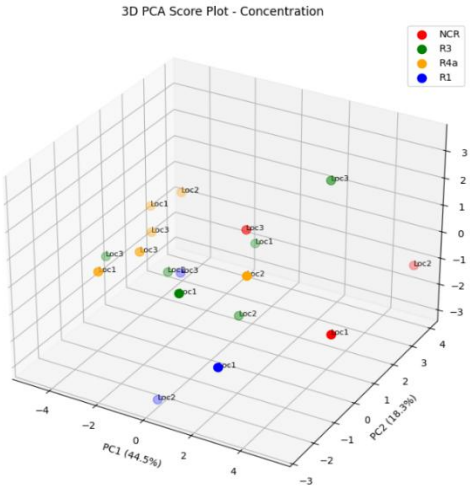


Fig. 3. Three-dimensional PCA score plot showing regional clustering behavior of milkfish GIT samples based on concentration-derived elemental profiles.

C. PCA Loading and Biplot Interpretation

To further investigate the elemental variables contributing to sample differentiation, PCA loading analysis and PCA biplot visualization were performed using the concentration-based dataset.

Fig. 4 presents the PCA biplot and loading behavior of the concentration-derived dataset. Several elemental variables contributed strongly to the observed clustering behavior and regional differentiation patterns. Major contributors to PC1 and PC2 included Na, K, Cl, Fe, Mn, Zn, Cu, Br, Rb, Se, and As, suggesting that both major mineral elements and trace metals influenced the elemental variability among milkfish samples.

Visualization of the PCA biplot revealed distinct elemental association tendencies among geographic regions. NCR samples were generally distributed toward the positive PC1 region and exhibited stronger association with elemental vectors corresponding to Fe, Mn, Cu, Se, and Rb, suggesting relatively elevated transition-metal and trace-element signatures potentially associated with urbanized aquatic environments.

Region I samples demonstrated clustering tendencies associated with K, P, S, Cl, and Br, indicating stronger contributions from mineral and ionic components. In contrast, several Region IV-A samples were distributed toward the negative PC1 region and exhibited moderate

association with As, V, and Se loading vectors, suggesting localized variability in trace elemental composition.

Among the evaluated regions, Region III samples exhibited comparatively broader dispersion across the PCA space and partially overlapped neighboring regional clusters, indicating greater internal elemental heterogeneity among sampling locations within the region.

Although regional grouping tendencies were evident, partial overlap among convex hull boundaries remained observable. Such overlap is expected in environmentally dynamic biological systems.

Consequently, the observed clustering behavior should be interpreted as exploratory geographic differentiation rather than absolute regional separation.

Overall, the PCA biplot demonstrated meaningful regional clustering tendencies and elemental association patterns among milkfish GIT samples.

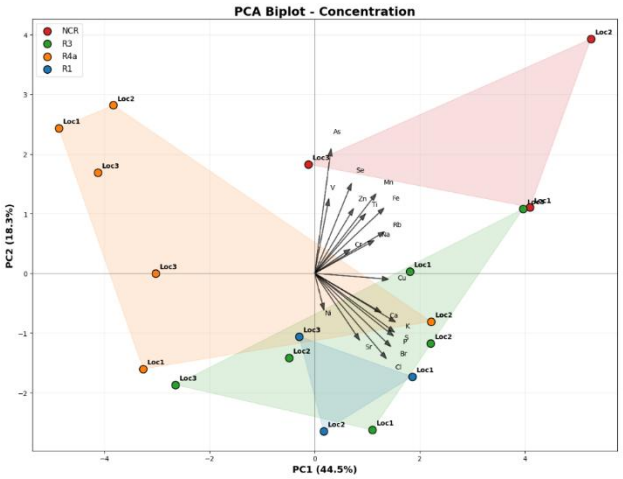


Fig. 4. PCA biplot of concentration-derived elemental profiles showing regional clustering tendencies and dominant elemental loading vectors among milkfish GIT samples.

D. Hierarchical Cluster Analysis (HCA)

Hierarchical Cluster Analysis (HCA) was performed to further evaluate similarity relationships and clustering behavior among the milkfish GIT samples. HCA was conducted using Euclidean distance metrics and Ward's linkage method to assess hierarchical grouping tendencies. The resulting HCA dendrogram generated from the concentration-based dataset is presented in *Fig. 5*.

The resulting HCA dendrogram demonstrated several regional grouping tendencies consistent with the PCA results. Samples originating from similar geographic regions generally exhibited shorter linkage distances and formed localized sub-clusters, indicating measurable similarities in elemental composition among selected sampling locations.

NCR samples generally exhibited closer clustering relationships associated with elevated trace-metal and mineral signatures, while Region I samples demonstrated partial grouping tendencies characterized by stronger association with mineral-related elemental components. In contrast, Region III samples displayed comparatively broader hierarchical dispersion and weaker clustering compactness, suggesting greater internal elemental heterogeneity among sampling locations within the region.

Several samples formed isolated branches, indicating potential outlier behavior consistent with PCA observations. These observations were consistent with the dispersion patterns previously identified in the PCA score plots and may reflect localized environmental exposure, differing aquatic conditions, or variable feeding interactions influencing elemental uptake.

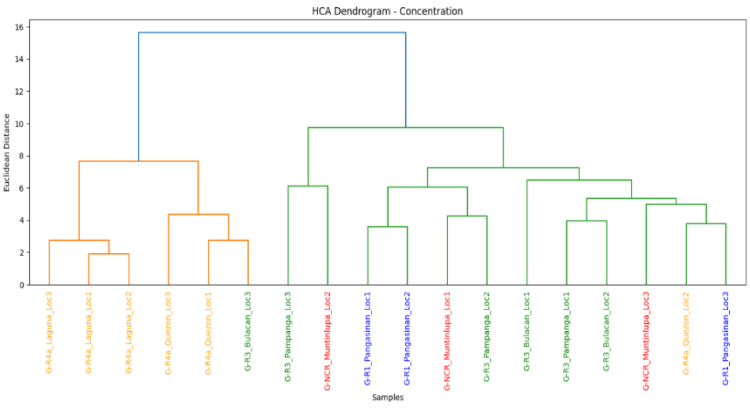


Fig. 5. HCA dendrogram of concentration-based elemental profiles of milkfish GIT samples.

Although distinct clustering tendencies were observed, complete separation among all geographic regions was not achieved. Partial overlap among clusters indicates that elemental signatures among the milkfish samples remain influenced by shared environmental conditions and interconnected aquatic systems. This behavior is expected in exploratory chemometric studies involving biological samples collected from environmentally dynamic aquatic environments.

Overall, the HCA results supported the PCA-derived clustering tendencies and demonstrated measurable hierarchical similarity relationships among milkfish samples. The combined PCA and HCA findings indicate that elemental fingerprinting coupled with chemometric analysis may serve as a promising exploratory approach for seafood provenance assessment and geographic differentiation studies.

IV. CONCLUSION

This study evaluated the applicability of Total Reflection X-Ray Fluorescence (TXRF)-based elemental fingerprinting combined with chemometric analysis for exploratory geographic differentiation of milkfish *(Chanos chanos)* gastrointestinal (GIT) tissues collected from selected fish landing sites across Luzon, Philippines.

TXRF analysis successfully generated multi-element datasets containing both major and trace elemental information from the milkfish GIT samples. Subsequent preprocessing and chemometric refinement using a Python-based workflow improved dataset interpretability

and enabled multivariate evaluation of regional variability. Among the evaluated datasets, concentration-derived elemental profiles produced improved clustering behavior and more interpretable chemometric patterns compared with raw net area datasets.

Principal Component Analysis (PCA) revealed discernible regional grouping tendencies and measurable elemental variability among samples originating from NCR, Region I, Region III, and Region IV-A. Three-dimensional PCA visualization further improved assessment of clustering behavior and sample dispersion, particularly due to the meaningful contribution of the third principal component. PCA loading and biplot analyses demonstrated that several elemental variables, including Na, K, Cl, Fe, Mn, Zn, Cu, Br, Rb, Se, and As, contributed significantly to regional differentiation patterns.

Hierarchical Cluster Analysis (HCA) produced clustering tendencies generally consistent with PCA observations and further demonstrated measurable hierarchical relationships among samples based on elemental composition. Although complete regional separation was not achieved, the observed clustering behavior indicates that TXRF-derived elemental fingerprints contain multivariate information potentially associated with geographic and localized environmental conditions.

Overall, the findings demonstrate the potential applicability of TXRF coupled with chemometric analysis as a rapid multi-element screening approach for exploratory seafood provenance assessment and geographic differentiation studies. As a proof-of-concept investigation, this work establishes a preliminary analytical and computational framework that may support future large-scale seafood traceability studies involving expanded sampling coverage, seasonal evaluation, and additional biological matrices.

REFERENCES

[1] Food and Agriculture Organization of the United Nations. 2018. *The State of World Fisheries and Aquaculture 2018: Meeting the Sustainable Development Goals.* FAO, Rome. https://openknowledge.fao.org/handle/20.500.14283/i9540en

[2] Galimberti, A., De Mattia, F., Losa, A., Bruni, I., Federici, S., Casiraghi, M., Martellos, S., & Labra, M. 2013. *DNA barcoding as a new tool for food traceability.* Food Research International, 50(1), 55–63. https://doi.org/10.1016/j.foodres.2012.09.036

[3] Kelly, S., Heaton, K., & Hoogewerff, J. 2005. *Tracing the geographical origin of food: The application of multi-element and multi-isotope analysis.* Trends in Food Science & Technology, 16(12), 555–567. https://doi.org/10.1016/j.tifs.2005.08.008

[4] Sturrock, A. M., Trueman, C. N., Darnaude, A. M., & Hunter, E. 2012. *Can otolith elemental chemistry retrospectively track migrations in fully marine fishes?* Journal of Fish Biology, 81(2), 766–795. https://doi.org/10.1111/j.1095-8649.2012.03372.x

[5] Burger, J., Gaines, K. F., Boring, C. S., Stephens, W. L., Snodgrass, J., Dixon, C., McMahon, M., Shukla, S., Shukla, T., & Gochfeld, M. 2002. *Metal levels in fish from the Savannah River: Potential hazards to fish and other receptors.* Environmental Research, 89(1), 85–97. https://doi.org/10.1006/enrs.2002.4330

[6] Yi, Y., Yang, Z., & Zhang, S. 2011. *Ecological risk assessment of heavy metals in sediment and human health risk assessment of heavy metals in fishes in the middle and lower reaches of the Yangtze River basin.* Environmental Pollution, 159(10), 2575–2585. https://doi.org/10.1016/j.envpol.2011.06.011

[7] Marguí, E., Van Grieken, R., & Queralt, I. 2008. *Total reflection X-ray fluorescence spectrometry and related techniques for trace element determination and speciation.* Analytical and Bioanalytical Chemistry, 390, 197–207. https://doi.org/10.1007/s00216-007-1693-5

[8] Borgese, L., Bilo, F., Dalipi, R., Bontempi, E., & Depero, L. E. 2015. *Total reflection X-ray fluorescence as a tool for food screening.* Spectrochimica Acta Part B: Atomic Spectroscopy, 113, 1–15. https://doi.org/10.1016/j.sab.2015.08.001

[9] Klockenkämper, R., & von Bohlen, A. 2014. *Total-Reflection X-Ray Fluorescence Analysis and Related Methods,* 2nd ed. John Wiley & Sons. https://doi.org/10.1002/9781118985953

[10] Gruber, A., Müller, R., Wagner, A., Colucci, S., Spasić, M. V., & Leopold, K. 2020. *Total reflection X-ray fluorescence spectrometry for trace determination of iron and some additional elements in biological samples.* Analytical and Bioanalytical Chemistry, 412, 6419–6429. https://doi.org/10.1007/s00216-020-02614-8

[11] Jolliffe, I. T., & Cadima, J. 2016. *Principal component analysis: A review and recent developments.* Philosophical Transactions of the Royal Society A: Mathematical, Physical and Engineering Sciences, 374(2065), 20150202. https://doi.org/10.1098/rsta.2015.0202

[12] Brereton, R. G. 2009. *Chemometrics for Pattern Recognition.* John Wiley & Sons. https://doi.org/10.1002/9780470746462

2026 IMEKO Joint Conference
TC8 - TC11 - TC24
Metro Manila, Philippines, August 26-29, 2026

Chemometric Evaluation of Total Reflection X-Ray Fluorescence (TXRF) Elemental Profiles of Milkfish (Chanos chanos) Tissue for Geographic Differentiation

Supplementary Table S1 - Concentration

Sample	Element								
	Na	P	S	Cl	K	Ca	Ti	V	Cr
G-NCR_Muntinlupa_Loc1	12.5658	8.0867	8.5230	8.0369	8.9542	6.8065	2.1163	1.6901	1.2613
G-R3_Pampanga_Loc3	12.6109	7.7480	8.2726	7.9334	8.6496	6.2899	4.7212	1.7766	1.3610
G-R4a_Quezon_Loc2	12.6575	7.5740	8.3187	8.2327	8.6861	6.1790	2.1163	1.6318	1.4516
G-R4a_Quezon_Loc1	12.2539	6.6516	7.1655	7.1294	7.8552	5.3366	1.8213	1.6318	1.1314
G-NCR_Muntinlupa_Loc3	12.5818	6.7968	7.4000	7.3159	8.1859	4.8873	2.4723	1.6318	1.3455
G-R3_Bulacan_Loc1	12.3104	8.0596	8.2058	8.1758	9.0531	5.9317	2.2844	0.7747	1.2413
G-R4a_Laguna_Loc1	12.3172	5.0370	5.4562	5.8822	7.0486	4.8660	1.3863	1.6318	1.0750
G-R1_Pangasinan_Loc3	12.4950	7.1115	7.4103	7.6985	8.1283	5.9444	2.2607	1.6318	1.3962
G-R4a_Laguna_Loc3	12.3754	5.2439	5.6595	6.2040	7.2919	4.9614	1.6174	1.6318	1.2060
G-R3_Bulacan_Loc3	12.3367	6.8066	7.0052	7.5214	7.7557	6.0749	1.5810	1.6318	1.2528
G-NCR_Muntinlupa_Loc2	12.5014	8.0665	8.4448	7.8880	8.9014	6.7731	4.3503	1.9081	1.2406
G-R3_Pampanga_Loc2	12.3234	8.1122	8.6761	8.2228	9.1355	6.0280	1.4207	1.7783	1.3002
G-R3_Pampanga_Loc1	12.5511	7.6449	8.0612	7.9628	8.5936	5.5405	4.3756	1.7317	1.3083
G-R1_Pangasinan_Loc1	12.5731	7.8740	8.1617	8.4598	8.6350	6.1414	1.4540	1.6318	1.0919
G-R4a_Laguna_Loc2	12.3345	5.3571	5.6237	6.0808	7.1894	5.1728	1.8066	1.6318	1.2470
G-R1_Pangasinan_Loc2	12.3314	7.4454	8.0756	8.2351	8.4442	6.9726	1.4656	1.6318	0.9746
G-R4a_Quezon_Loc3	12.1869	6.2603	6.7567	7.2023	7.5246	5.0714	2.3175	1.6318	1.0986
G-R3_Bulacan_Loc2	12.3896	7.5175	7.6774	7.5210	8.3025	5.4350	1.9727	1.3813	1.2208

2026 IMEKO Joint Conference
TC8 - TC11 - TC24
Metro Manila, Philippines, August 26-29, 2026

Chemometric Evaluation of Total Reflection X-Ray Fluorescence (TXRF) Elemental Profiles of Milkfish (Chanos chanos) Tissue for Geographic Differentiation

Supplementary Table S1 - Concentration

Sample	Element								
	Mn	Fe	Ni	Cu	Zn	As	Se	Br	Rb
G-NCR_Muntinlupa_Loc1	2.4257	6.1555	0.6627	6.0297	4.7258	0.6313	2.2976	3.5080	3.3457
G-R3_Pampanga_Loc3	2.9704	7.5310	1.5539	2.9760	4.2728	0.3528	0.9555	3.3663	1.8083
G-R4a_Quezon_Loc2	2.0563	5.2637	0.9002	3.1372	4.5070	0.4400	0.4055	3.4862	1.9430
G-R4a_Quezon_Loc1	0.6098	4.1765	0.9322	1.6582	2.9199	0.3257	0.1406	2.4816	1.0578
G-NCR_Muntinlupa_Loc3	1.8213	5.3982	0.7561	3.1897	3.3254	0.8945	0.8646	2.8513	2.3740
G-R3_Bulacan_Loc1	2.0055	4.8897	1.3002	2.2803	4.1078	0.2738	1.2361	3.5459	1.5810
G-R4a_Laguna_Loc1	1.5151	4.5115	0.8242	0.8629	4.2742	0.5140	1.3135	1.5021	1.0116
G-R1_Pangasinan_Loc3	1.2613	4.4738	0.6881	2.8154	3.1184	0.2422	0.6329	3.0022	1.6054
G-R4a_Laguna_Loc3	1.0818	4.3553	0.4762	0.6627	4.4585	0.4434	1.3135	1.7190	1.1694
G-R3_Bulacan_Loc3	0.3920	4.5301	1.2528	2.3165	3.4012	0.1856	0.1689	2.6448	0.9474
G-NCR_Muntinlupa_Loc2	3.5139	7.1805	0.5988	5.9165	4.5030	0.9322	2.4570	3.2422	3.1298
G-R3_Pampanga_Loc2	1.9359	5.5973	1.0716	3.5902	4.6033	0.2303	1.5777	3.7111	2.2214
G-R3_Pampanga_Loc1	1.5239	6.0022	1.0886	4.7794	4.4503	0.2799	1.2066	3.3520	1.6845
G-R1_Pangasinan_Loc1	1.4974	5.0888	0.4637	4.3187	4.2943	0.2799	1.0003	3.7479	2.0631
G-R4a_Laguna_Loc2	1.9199	4.9791	0.7467	0.7419	4.3988	0.5206	1.3135	1.6198	1.2528
G-R1_Pangasinan_Loc2	1.5581	4.2217	0.4886	3.6142	3.2858	0.2731	0.7821	3.4763	2.1342
G-R4a_Quezon_Loc3	2.0563	4.3012	0.9969	1.5539	3.0545	0.4756	1.3135	2.3341	0.8459
G-R3_Bulacan_Loc2	1.6409	5.8336	1.0508	4.8233	3.7250	0.1714	1.1706	2.7651	0.6081

2026 IMEKO Joint Conference
TC8 - TC11 - TC24
Metro Manila, Philippines, August 26-29, 2026

Chemometric Evaluation of Total Reflection X-Ray Fluorescence (TXRF) Elemental Profiles of Milkfish (Chanos chanos) Tissue for Geographic Differentiation

Supplementary Table S1 - Concentration

Sample	Element
	Sr
G-NCR_Muntinlupa_Loc1	0.9670
G-R3_Pampanga_Loc3	1.5644
G-R4a_Quezon_Loc2	1.4036
G-R4a_Quezon_Loc1	0.8416
G-NCR_Muntinlupa_Loc3	0.4574
G-R3_Bulacan_Loc1	1.3584
G-R4a_Laguna_Loc1	0.4947
G-R1_Pangasinan_Loc3	1.1787
G-R4a_Laguna_Loc3	1.0522
G-R3_Bulacan_Loc3	0.3243
G-NCR_Muntinlupa_Loc2	0.8713
G-R3_Pampanga_Loc2	1.0956
G-R3_Pampanga_Loc1	0.7419
G-R1_Pangasinan_Loc1	1.6639
G-R4a_Laguna_Loc2	0.3365
G-R1_Pangasinan_Loc2	1.2837
G-R4a_Quezon_Loc3	1.0522
G-R3_Bulacan_Loc2	0.9203

2026 IMEKO Joint Conference
TC8 - TC11 - TC24
Metro Manila, Philippines, August 26-29, 2026

Chemometric Evaluation of Total Reflection X-Ray Fluorescence (TXRF) Elemental Profiles of Milkfish (Chanos chanos) Tissue for Geographic Differentiation

Supplementary Table S2 - Net Area

Sample	Element									
	Na	Mg	Al	P	S	Cl	K	Ca	Sc	Ti
G-NCR_Muntinlupa_Loc1	9.8394	0.6780	1.3455	9.0911	9.0427	8.9809	9.7300	8.7305	0.6575	8.4915
G-R3_Pampanga_Loc3	9.9545	0.6931	9.2242	9.2235	9.1806	9.1246	9.7180	8.8899	0.8065	8.7538
G-R4a_Quezon_Loc2	10.4608	0.9517	1.7405	9.6116	9.5660	9.5072	9.8995	9.2709	0.8838	9.0181
G-R4a_Quezon_Loc1	10.6240	0.7275	1.4996	9.7549	9.7083	9.6508	9.9252	9.4302	0.8587	9.2116
G-NCR_Muntinlupa_Loc3	11.0242	0.9783	1.9782	10.1631	10.1174	10.0607	10.2903	9.8438	0.7930	9.6546
G-R3_Bulacan_Loc1	10.8735	0.7419	0.8879	10.0040	9.9585	9.9012	10.6609	9.6752	0.8629	9.4631
G-R4a_Laguna_Loc1	10.6023	1.3403	2.1247	9.6868	9.6320	9.5914	9.7509	9.4034	0.9282	9.2434
G-R1_Pangasinan_Loc3	10.9223	1.0438	1.1632	10.0360	9.9979	9.9498	10.3015	9.7713	0.9282	9.5845
G-R4a_Laguna_Loc3	10.4468	1.1151	2.0567	9.5399	9.4896	9.4404	9.6189	9.2754	0.6881	9.0388
G-R3_Bulacan_Loc3	11.1522	1.1346	1.2585	10.2622	10.2239	10.1756	10.5097	10.0008	0.8713	9.8091
G-NCR_Muntinlupa_Loc2	9.6795	0.6678	9.0076	8.9944	8.9460	8.8857	9.6042	8.6442	0.9555	8.4651
G-R3_Pampanga_Loc2	11.6047	1.2556	1.3661	10.7124	10.6707	10.6178	11.3386	10.4184	0.8961	10.2272
G-R3_Pampanga_Loc1	11.0795	1.0578	1.0367	10.1752	10.1347	10.0827	10.5592	9.8822	0.7655	9.7184
G-R1_Pangasinan_Loc1	10.8239	0.9555	1.3712	9.9857	9.9407	9.8844	10.4175	9.6674	0.9858	9.4442
G-R4a_Laguna_Loc2	10.5646	0.7701	1.5433	9.6704	9.6209	9.5832	9.7360	9.3636	0.7324	9.1526
G-R1_Pangasinan_Loc2	10.8817	0.7561	1.0152	10.0569	10.0152	9.9621	10.5853	9.9001	1.3813	9.5385
G-R4a_Quezon_Loc3	10.8593	1.0438	1.6487	9.9018	9.8771	9.8033	9.9537	9.5936	0.5306	9.3895
G-R3_Bulacan_Loc2	10.9594	1.0260	1.7967	10.1129	10.0727	10.0217	10.4526	9.8304	0.9783	9.6294

2026 IMEKO Joint Conference
TC8 - TC11 - TC24
Metro Manila, Philippines, August 26-29, 2026

Chemometric Evaluation of Total Reflection X-Ray Fluorescence (TXRF) Elemental Profiles of Milkfish (Chanos chanos) Tissue for Geographic Differentiation

Supplementary Table S2 - Net Area

Sample	Element									
	V	Cr	Mn	Fe	Co	Ni	Cu	Zn	Ge	As
G-NCR_Muntinlupa_Loc1	8.4189	8.3537	8.2646	8.4384	0.6152	8.2199	8.3040	8.2843	0.8065	8.0107
G-R3_Pampanga_Loc3	8.6618	8.6085	8.5502	8.9456	0.8459	8.3612	8.3217	8.3426	0.8416	8.2566
G-R4a_Quezon_Loc2	0.7031	8.9011	0.6831	8.7828	0.7885	8.6771	8.6583	8.6836	0.9858	0.8109
G-R4a_Quezon_Loc1	0.6152	9.0664	9.0136	8.9847	0.9243	8.8716	8.8664	8.8652	0.9517	8.8614
G-NCR_Muntinlupa_Loc3	0.4947	9.5116	9.4788	9.4740	0.7324	9.2988	9.2824	9.2669	0.7129	9.2413
G-R3_Bulacan_Loc1	9.3864	9.3165	9.2655	9.2874	0.8020	9.0866	9.1172	9.0811	0.7608	9.0722
G-R4a_Laguna_Loc1	0.3920	9.0965	9.0446	8.9943	0.7885	8.8799	8.8803	8.8537	0.6206	8.8476
G-R1_Pangasinan_Loc3	0.5653	9.4391	9.3867	9.3489	0.5306	9.2192	9.2041	9.1796	0.8416	9.1747
G-R4a_Laguna_Loc3	0.6152	8.8989	8.8349	8.8303	0.7839	8.7174	8.7609	8.8267	0.8671	8.6452
G-R3_Bulacan_Loc3	0.7178	9.6638	9.6135	9.6029	0.7608	9.4543	9.4601	9.4399	0.7975	9.4195
G-NCR_Muntinlupa_Loc2	8.3916	0.9478	8.2574	8.5796	0.9632	8.0469	8.1215	8.1011	0.7467	7.8865
G-R3_Pampanga_Loc2	10.1578	10.0939	10.0362	10.0839	1.2000	9.8961	9.8667	10.0855	0.8416	9.8299
G-R3_Pampanga_Loc1	9.6281	9.5528	9.5018	9.5784	0.7975	9.3336	9.3225	9.3445	1.0919	9.2222
G-R1_Pangasinan_Loc1	0.4886	9.3110	9.2399	9.2400	0.7561	9.0952	9.0937	9.1164	0.7275	8.9954
G-R4a_Laguna_Loc2	0.8242	9.0158	9.0098	9.0124	0.6152	8.8399	8.8317	8.8120	0.6627	8.7774
G-R1_Pangasinan_Loc2	1.0006	9.4015	9.3421	9.3142	0.6729	9.1970	9.1870	9.1767	0.7839	9.1543
G-R4a_Quezon_Loc3	0.7747	9.2625	0.6931	9.1597	1.2030	9.0585	9.0492	9.0433	0.6471	9.0608
G-R3_Bulacan_Loc2	9.5566	9.4850	9.4450	9.5074	0.9670	9.2739	9.2743	9.2938	0.9203	9.2056

2026 IMEKO Joint Conference
TC8 - TC11 - TC24
Metro Manila, Philippines, August 26-29, 2026

Chemometric Evaluation of Total Reflection X-Ray Fluorescence (TXRF) Elemental Profiles of Milkfish (Chanos chanos) Tissue for Geographic Differentiation

Supplementary Table S2 - Net Area

Sample	Element				
	Se	Br	Kr	Rb	Sr
G-NCR_Muntinlupa_Loc1	8.1306	8.3528	1.3686	9.2084	9.7746
G-R3_Pampanga_Loc3	8.3859	8.5228	8.9670	9.5474	10.3189
G-R4a_Quezon_Loc2	8.7100	8.9068	1.6034	9.8003	10.5599
G-R4a_Quezon_Loc1	9.0079	9.1364	0.5933	10.1251	10.7318
G-NCR_Muntinlupa_Loc3	9.3674	9.5974	0.5933	10.5055	11.1274
G-R3_Bulacan_Loc1	9.2236	9.4326	1.8500	10.3505	10.9824
G-R4a_Laguna_Loc1	0.8109	9.1083	0.8671	10.1302	10.7857
G-R1_Pangasinan_Loc3	9.3065	9.5347	1.6134	10.4007	11.0188
G-R4a_Laguna_Loc3	0.6627	8.8698	0.5423	9.8204	0.7275
G-R3_Bulacan_Loc3	9.5363	9.7534	0.7514	10.6701	11.4369
G-NCR_Muntinlupa_Loc2	8.0462	8.2385	1.6882	9.1324	9.8303
G-R3_Pampanga_Loc2	9.9791	10.1850	2.2597	11.0475	11.6481
G-R3_Pampanga_Loc1	9.3417	9.5707	1.8310	10.4526	11.0704
G-R1_Pangasinan_Loc1	9.1330	9.3917	1.6544	10.2706	10.8877
G-R4a_Laguna_Loc2	0.9632	8.9962	0.9163	9.9599	10.6092
G-R1_Pangasinan_Loc2	9.2996	9.5371	0.7419	10.4828	11.2946
G-R4a_Quezon_Loc3	0.7467	9.3151	1.3191	10.2456	0.7561
G-R3_Bulacan_Loc2	9.3338	9.5413	0.6419	10.4354	11.0598

2026 IMEKO Joint Conference
TC8 - TC11 - TC24
Metro Manila, Philippines, August 26-29, 2026

Evaluating Arsenic Removal from Natural Ore: A Treatability Study in Central Luzon

Maria Carmela Q. Capule, RCh, MPS, PhD[1]

[1] *CRL Environmental Corporation, Clark Freeport Zone, Pampanga, Philippines,*
mqcapule@gmail.com

***Abstract* – Arsenic is a naturally occurring metal associated with volcanic and geological materials. In the Philippines, pyroclastic deposits resulting from the eruption of Mount Pinatubo have been identified as potential sources of arsenic and other trace metals in the environment. Adsorption is recognized as one of the most effective and cost-efficient methods for removing arsenic from contaminated water. This study evaluated the adsorption potential of ore samples collected from Bulacan and Zambales, Philippines, for arsenic immobilization. Chemical characterization revealed that the Zambales ore contained chromium, iron, and nickel concentrations of 0.400%, 31.400%, and 0.477%, respectively, while arsenic was not detected. Bulacan ore contained arsenic, chromium, iron, and nickel at 0.00077%, 0.00083%, 11.10%, and 0.00047%, respectively. Based on the results of the analysis for Zambales ore, arsenic results were undetected at 1:1 from 24 to 72 hours of contact with the ore. In a 1:2 ratio, 24 hours showed traces of arsenic at 0.02 mg L^{-1}, while 48 to 72 hours of contact showed no detection. Bulacan ore, arsenic leached out in 48 to 72 hours of contact using a 1:2 ratio. Adsorption kinetics were evaluated using the Lagergren pseudo-first-order model. The 1:3 ratio exhibited the strongest correlation with the model, while the 1:2 ratio yielded a moderate fit ($R^2 = 0.75$), indicating reasonably favorable adsorption behavior. No significant correlation was observed at the 1:1 ratio. Overall, the findings demonstrate the potential applicability of adsorption using naturally occurring ore materials for environmental remediation and the immobilization of arsenic and other metal contaminants in water systems.**

I. INTRODUCTION

Arsenic is a naturally occurring metal found in the Earth's crust, but when it leaches into groundwater, it becomes a major public health hazard. Arsenic contamination of groundwater is a geogenic issue that arises from the dissolution of aquifer rocks. One source is the pyroclastic materials brought about by the volcanic eruption. Arsenic infiltrates groundwater as As(III) and As(V) through various mechanisms, including industrial activities, rock weathering, volcanic emissions, biological processes, and geochemical reactions (L. Hao, et.al, RSC Adv. 2018). A typical example is the Mount Pinatubo eruption that occurred in Region 3 in June 1991. There are several studies on arsenic presence in groundwater aquifers in selected municipalities nearby Mount Pinatubo, particularly focusing on the contamination levels resulting from the volcanic deposits brought about by the eruption.

There are several research studies on arsenic removal technologies. The adsorption method is one of the most effective and low-cost processes in removing arsenic from water. Leachability of arsenic by adsorption is based on the principle that arsenic ions in contaminated water can be immobilized by binding onto the surface of solid adsorbents, hence reducing their mobility and preventing leaching into groundwater. This method not only helps to improve water quality but also promotes sustainable practices by utilizing locally available resources.

There have been studies on the use of iron-based ores as adsorbents for the removal of arsenic (Mahamallik, P. and Swain, R., 2023; Zhang, W., 2004). Naturally occurring iron oxides are more effective for arsenic removal than the synthetic oxides (Zhang, W., et al., 2004), as they have a higher surface area and better adsorption properties, which enhance their ability to bind with arsenic in water.

Adsorption techniques use different adsorbents to absorb the arsenic ions on their surfaces or within their porous structures to remove arsenic from water. The specific surface area, pore structure, surface functional groups, and the desired operating conditions all play a role in the adsorbent selection process. (Makamallik, P. and Swain, R., 2023). The adsorption process is described using Langmuir and Freundlich isotherms and evaluated through kinetic models such as pseudo-first-order and pseudo-second-order kinetics. These models help explain the adsorption mechanism and capacity of the adsorbent material.

Iron ore in Bulacan is associated with magnetite–hematite deposits, recognized historically as one of the country's

significant iron-bearing regions alongside Samar and Camarines Norte (Pratt, 1916; Mines and Geosciences Bureau, Mineral Deposits of the Philippines). Laterite deposits, formed through tropical weathering, are enriched in iron oxyhydroxides such as goethite and hematite (Tardy, 1997; Eggleton, 2001). The deposits are located in Brgy. Camachin, Municipality of Doña Remedios Trinidad, Province of Bulacan.

The Camachin lateritic iron deposits represent a thick succession of intervening beds of volcanic flows and calcareous sediments. Iron rich mineralizing solutions from the intrusive diorite invaded these materials thus replacing the calcareous sediments by magnetite. The altered volcanic rocks and magnetite were later transported downslope and exposed to prolong weathering resulting to the formation of reddish-brown lateritic soil enriched with iron fine material and associated boulder to cobble size fragments of magnetite.

The Zambales nickel laterite deposit formed from the weathering of the ultramafic massif of the Zambales ophiolite complex (ZOC) Acoje block. Nickel mineralization in the deposit is associated with the low Nickel, high iron limonite zone and the extensive low-Fe, high-Ni saprolite zone. The nickel laterite profile is approximately 12 m high and composed of upper limonite zone (~7) m and a lower saprolite zone (~5m) as well as a thin transitional zone (~10cm), each characterized by a distinct set of physical, mineralogical, and geochemical properties. (Aquino, K. et.al, Minerals 2022).

Assessments at different optimum operating conditions such as the contact time and dosage were studied The effectiveness of the ore sample in adsorbing substances was evaluated to help reduce the costs of removing metals from the groundwater supply. Its potential application of the ore as a treatment medium for groundwater remediation was assessed. Leachability reduction once adsorbed, arsenic is less likely to leach into groundwater because it is immobilized on the adsorbent matrix. The findings could lead to more sustainable practices in groundwater remediation and potentially lower expenses for water treatment facilities.

II. METHODOLOGY

A. Materials and Methods

The ore samples used in this study were collected from Brgy. Camachin, Municipality of Doña Remedios Trinidad in Bulacan and Sta. Cruz, Zambales. Figure 1 presents the sampling locations of the ore samples taken in Bulacan and Zambales, Region 3, Philippines.

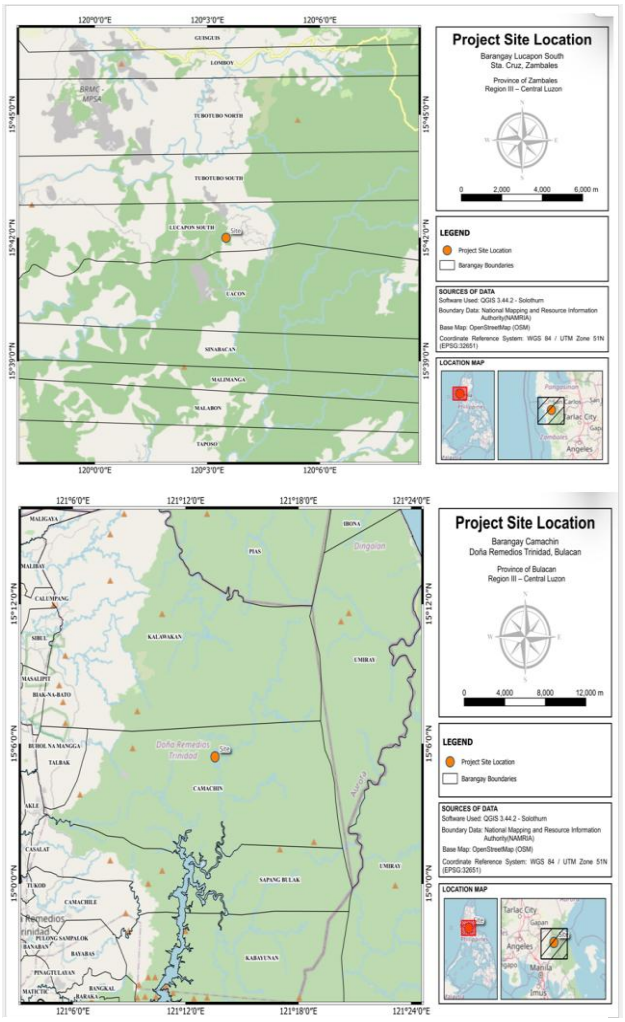


Fig. 1. Sampling locations of ores in Bulacan and Zambales, Philippines

B. Analytical Methodology

Analytical methodologies for pH, arsenic, chromium, iron and nickel in extracts/aqueous were based on the Standard Methods for the Examination of Water and Wastewater (SMEWW), 24th edition. For soil, USEPA Test Methods for Evaluating Solid Wastes, Volume 1A, 3rd Edition, were used for metals analyses. Table 1 presents the analytical methods and the corresponding test parameters. Metals are analyzed by Inductively Coupled Plasma – Optimal Emission Spectrometry (ICP-OES).

Table 1. Parameters and Analytical Methodologies

Parameter	Analytical Methodology
pH	Electrometric Method
Arsenic	ICP - OES
Chromium	ICP - OES
Iron	ICP - OES
Nickel	ICP - OES

Samples were air dried for at least two days. After air drying, samples were pulverized to fine particulates. Quartering was applied to ensure representativeness of samples to be weighed and tested Sample preparation and laboratory analyses were done in January 2026. For total metals determination in soil, 2 grams of sample is taken from representative sample. A 10 ml (1:1) nitric acid is added, heated to 95ºC and reflux for 10 to 15 minutes without boiling. Sample is cooled, added 5 ml of conc. nitric acid and reflux of additional 30 minutes. Two (2) ml of water and 3 ml of 30% hydrogen peroxide were added and digestion is continued until effervescence is minimal. Digestate is filtered using Whatman No. 41. Filtered digestate was analyzed by ICP-OES for arsenic, chromium, iron and nickel. The QA/QC sample undergoes the same sample preparation as the original sample.

Leachate determination is conducted through elutriate analysis. A total of twenty-two (22) ore samples were prepared and treated for treatability study. A representative aliquot of ore sample was weighed at different weight proportions based on Table 2. A known concentration of 100 ppb arsenic standard was dissolved in DI distilled water which was introduced to both ore samples using different ratios from 1:1, 1:2, and 1:3 as shown in table below. Ore samples were dissolved and mixed with distilled water with spiked arsenic solution. Samples were homogenized and mixed using homogenizer for thirty (30) minutes at 150 oscillation per minute. Samples were settled down at desired time. After 24, 48 and 72 hours of contact time, samples were filtered using Whatman #41 filter paper. For metals analyses, 100 ml of elutriate extract samples were digested in hotplate by adding 3ml nitric acid evaporating to a low volume ensuring samples do not boil and allowed to go dry. Cool, rinse down walls of beaker and watch glass and add 5ml conc. Nitric acid, cover and increase temperature of hot plate so gentle reflux action occurs. Continue heating until digestion is complete. Cool, add 10 ml (1+1) HCl and 15ml water per 100ml final volume. Cool and filter. Digestates were analyzed by ICP-OES (Agilent 5100) for metals using SMEWW 3120B and USEPA 6010B as reference.

Table 2. Sample Description and Target Analytes

Sample ID	Sample Description	Target Analyte
Zambales ore	400 gram sample, 400 ml DI water (1:1)	pH, Arsenic
Zambales ore	400 gram sample, 400 ml 100 ppb Arsenic Solution (1:1)	Arsenic, Chromium, Iron, Nickel
Zambales ore	200 gram sample, 400 ml 100 ppb Arsenic Solution (1:2)	Arsenic
Zambales ore	200 gram sample, 600 ml 100 ppb Arsenic Solution (1:3)	Arsenic
Bulacan ore	400 gram sample, 400 ml DI water (1:1)	pH, Arsenic
Bulacan ore	400 gram sample, 400 ml 100 ppb Arsenic Solution (1:1)	Arsenic, Chromium, Iron, Nickel
Bulacan ore	200 gram sample, 400 ml 100 ppb Arsenic Solution (1:2)	Arsenic
Bulacan ore	200 gram sample, 600 ml 100 ppb Arsenic Solution (1:3)	Arsenic

III. RESULTS AND DISCUSSION

Zambales ore samples contain total chromium, iron and nickel at 0.43%, 31.4%, and 0.477% respectively. Arsenic is not present in the sample investigated. On the other hand, Bulacan ore samples contain arsenic, chromium, iron and nickel at 0.00077%, 0.00083%, 11.10%, and 0.00047% respectively. The pH of Zambales ore was at 6.5 ±0.003 and Bulacan ore was at 6.3 ±0.003.

A known concentration of 100 ppb arsenic solution is introduced to determine its leachability properties. Zambales ore extracts showed no detection of arsenic when dissolved in distilled water. Leaching contact time started from 24 hours, 48 hours to 72 hours at a ratio of 1:1, 1:2, and 1:3.

Based on the results of the analysis from Zambales ore as shown in Figure 2, arsenic results at 1:1 were not detected (LOQ at 0.005 mg L^{-1}) from 24 to 72 hours of contact with the ore. The 1:2 treatment exhibited residual arsenic concentration of 0.02 ±0.00003 mg L^{-1} after 24 hours but achieved complete removal after 48 to 72 hours of contact time. The 1:3 treatment showed the highest residual concentration during the initial stage (0.03 mg L^{-1} at 24 hours). The presence of arsenic was observed until 48 hours at and 0.01 mg L^{-1}. In 72 hours at a 1:3 ratio, a complete removal of arsenic was achieved. Arsenic was not detected for the control sample in distilled water. For other metals, 0.061% chromium, 4.564% iron, and 0.064% nickel leached out in the ore sample based on a 1:1 ratio in 24 hours. This showed that 96% of other metals were adsorbed in the ore. Figure 2 also shows that the contact time (hr) is an ordered variable, which will show how arsenic concentration changes over time for the three ratios (1:1, 1:2, and 1:3). The results demonstrate progressive arsenic removal over time, with complete removal achieved after 72 hours for all treatment ratios. The 1:3 ratio starts with the highest arsenic concentration (0.03 mg L^{-1} at 24 hours) and decreases to zero by 72 hours. The 1:2 ratio decreases from 0.02 mg L^{-1} at 24 hours to zero by 48 hours, while the 1:1 ratio remains at zero throughout the

experiment. The adsorption performance improved with increasing adsorbent dosage. The 1:1 ratio consistently achieved the fastest removal, suggesting that higher adsorbent availability provided a greater number of active sites for arsenic binding. The slower removal observed at the 1:3 ratio may be attributed to limited adsorption capacity relative to the arsenic loading.

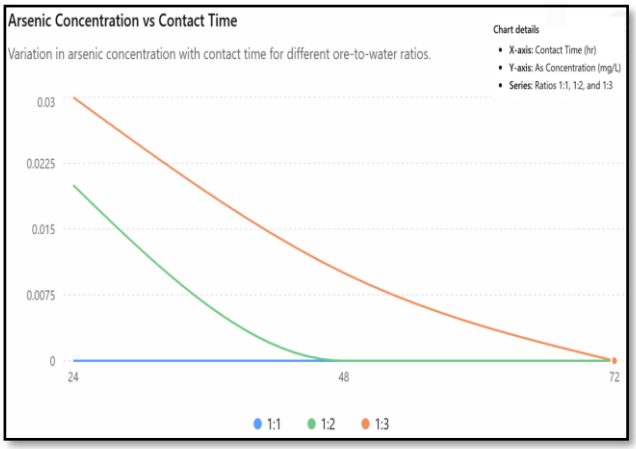


Fig. 2. Variation of arsenic (As) adsorption by Zambales ore with contact time (24–72 h) at different ore-to-water ratios (1:1, 1:2, and 1:3)

Bulacan ore extracts showed that the arsenic results were completely adsorbed in both 1:1 and 1:3 ratios from 24 to 72 hours of contact time, as shown in Figure 3. The 1:2 ratio exhibited a temporary increase in arsenic concentration at 48 h (0.04 mg L^{-}), followed by a slight decrease to 0.03 mg L^{-} at 72 h, whereas the 1:1 and 1:3 ratios remained at 0 mg/L throughout the experiment. The control sample in distilled water showed the presence of arsenic after 48 hours of contact time. This is evident since Bulacan ore has a background value of 7.7 ±0.00007 mg kg^{-1}. For the other metals, arsenic and nickel were not detected from the leachate (LOQ: As at 0.005 mg L^{-1} and Ni at 0.003 mg L^{-1}). Traces of chromium at 0.007 ±0.00003 mg L^{-1} and iron at 30 ±0.00003 mg L^{-1} were observed. Adsorption efficiency of these metals was more than 99%.

Figure 3 also shows the variation of arsenic concentrations in Bulacan ore samples with contact time for different mixing ratios. The arsenic concentration decreases with increasing contact time for the 1:2 and 1:3 ratios, reaching below detection limit (LOQ at 0.005 mg L^{-1}) at 72 hours, while the 1:1 ratio remains below the detection limit throughout the experiment.

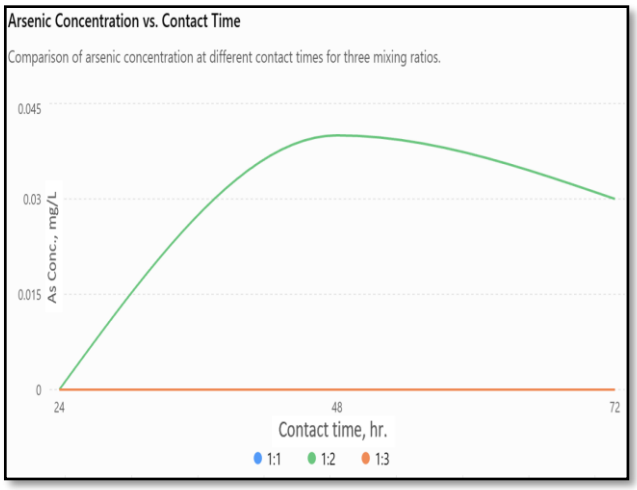


Fig. 3. Arsenic concentration (mg/L) by Bulacan ore as a function of contact time (24, 48, and 72 h) for different ore-to-solution ratios (1:1, 1:2, and 1:3)

The Lagergren pseudo-first-order is used to describe adsorption kinetics, especially the rate at which solutes such as arsenic are taken up by an adsorbent. It assumes that the rate of adsorption is proportional to the number of uncocupied sites. Equation below shows the adsorption time. Lagergren plot is evaluated based on the coefficient of determination. To plot the amount adsorbed (q_t) vs. time, first calculate q_t based on equation (1).

$$q_t = \frac{(C_i - C_e) \times V}{W} \quad (1)$$

Where C_i is initial concentration, C_e is concentration at time, V is volume, and W is adsorbent mass.

Figure 4a shows a strong correlation between the experimental data and the model predictions. The R^2 at 0.9471 implies that the adsorption process using a 1:3 ratio follows pseudo-first-order kinetics reasonably well.

Based on Figure 4b, R^2 (0.75) means that 75% of the variation in adsorption behavior is explained by the Lagergren model. It captures much of the adsorption trend but needs for improvement. An R^2 of 0.75 suggests that the pseudo-first-order model provides a reasonable but not perfect description of arsenic adsorption kinetics in a 1:2 ratio. This implies that the adsorption process may not be purely first-order. For arsenic adsorption, this often means the process involves stronger interactions (chemisorption) or multi-step diffusion mechanisms, which are better described by pseudo-second-order or diffusion-based models.

Figure 4c shows no correlation and the model explains none of the variation in the adsorption data at a 1:1 ratio. The model is unsuitable for describing the kinetics of

arsenic adsorption in this study. Other model is suggested such as the pseudo-second-order model which assumes chemisorption as the rate-limiting step, tends to fit arsenic adsorption better, the intraparticle diffusion model which checks if diffusion controls the rate.

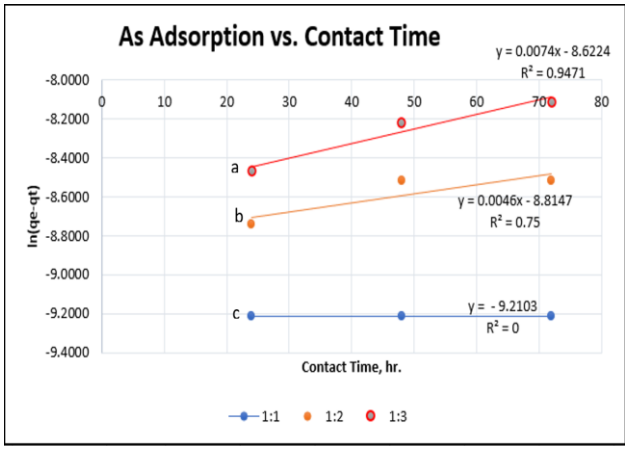


Fig. 4. Lagergren plot for Arsenic adsorption of ore vs. Contact time. Pseudo-first-order adsorption kinetics of arsenic for ore-to-water ratios of 1:1, 1:2, and 1:3. a) 1:3 ratio exhibited the strongest linear relationship ($R^2 = 0.9471$), suggesting a better fit to the pseudo-first-order kinetic model b) 1:2 ratio ($R^2 = 0.75$), c) 1:1 ratio showed no observable change in adsorption over the contact period ($R^2 = 0$).

In comparison of the two (2) ore samples, Bulacan ore showed better adsorption efficiency in metals investigated compared to Zambales ore.

This suggests that the Bulacan ore may possess unique properties that enhance its ability to bind with metals. Further studies could explore the underlying mechanisms that contribute to this increased efficiency.

IV. CONCLUSIONS

The adsorption method is effective without controlling the pH. Based on the results investigated, the ore from Zambales is most effective in removing arsenic in water compared to Bulacan. Among the ore/water ratios experimented with, one part of the sample to one part of water compared obtained the highest removal compared to the other ratios surveyed. For other metals such as chromium, iron, and nickel, other treatment methods to reduce these metals leaching out from the ore sample are suggested, including methods such as chemical precipitation, ion exchange, and membrane filtration, which have been shown to be effective in similar contexts.

For Bulacan ore samples, adsorption efficiency of metals was more than 99%. The high adsorption efficiency plays a crucial role in groundwater treatment that is contaminated with arsenic. The study demonstrates that adsorption is a viable treatment strategy for arsenic contaminated ore and associated water. The study also suggests a potential use of this method in environmental remediation efforts to immobilize metal contaminants. Arsenic removal from groundwater using local ore provides an opportunity to improve the water quality at low cost while minimizing environmental impact and communities which can benefit from safer drinking water.

It is recommended to conduct further studies for long-term stability of these adsorption processes and the possible mechanisms involved. Further studies may explore the scalability of these techniques for broader industrial applications, enhancing their practicality in environmental management.

REFERENCES

[1] C.Faulmino, A.Rola, "Arsenic in Philippine Groundwaters: Exploring Governance Limitations for Drinking Water Safety. Journal of Environmental Science and Management Special Issue, 2023, ISSN0119-1144, pp. 14-27.

[2] K.Aquino, C.Arcilla, C.Schardt, and C.Tupaz, "Mineralogical and Geochemical Characterization of the Sta. Cruz Nickel Laterite Deposit, Zambales, Philippines". MDPI Minerals, 2022, vol. 12, pp. 305.

[3] K.L.Solis, R.Macasieb, R.Parangal Jr., A.Resurreccion and J. Ocon, "A. Spatiotemporal Variation of Groundwater Arsenic in Pampanga, Philippines. Water 2020, vol. 12, 2366."

[4] L. Hao, M. Liu, N. Wang and G. Li. "A critical review on arsenic removal from water using iron-based adsorbents". Royal Society of Chemistry Advances, 2018, vol. 8, pp. 39545-39560.

[5] P. Mahamallik and R.Swain, "A mini-review on arsenic remediation techniques from water and future trends". Water Science & Technology, 2023, Vol. 87 No. 12, 3108.

[6] W.Zhang, P.Singh, E.Paling, S.Delides, "Arsenic removal from contaminated water by natural iron ores". Elsevier, Minerals Engineering, 2004, vol. 17, pp. 517-524.

2026 IMEKO Joint Conference
TC8 - TC11 - TC24
Metro Manila, Philippines, August 26-29, 2026

Method Validation of Total Reflection X-ray Fluorescence (TXRF) for Arsenic Screening in Milkfish (Chanos chanos)

Aldrin Jan E. Tabuso, Reno S. Bia, John Kenneth C. Valerio, Anton John D. Rocha, Alleni T. Junsay, and Kim Christopher C. Aganda

Department of Science and Technology, Industrial Technology and Development Institute (DOST-ITDI), Bicutan, Taguig City, Philippines

***Abstract* – Milkfish (Chanos chanos), one of the Philippines' most important aquaculture species, may accumulate arsenic (As) from natural and anthropogenic sources, which poses potential risks to consumers. This study validated a method for As determination in milkfish using Total Reflection X-ray Fluorescence (TXRF) with the use of Philippine Reference Material (PRM) 2002-As, Cd, Hg & Pb in milkfish. Validation results showed satisfactory performance, with recoveries ranging from 92–106% and relative standard deviations (RSD) below 10%, demonstrating acceptable accuracy and precision. The expanded uncertainty, estimated using the Nordtest approach, was 0.42 ppm. Method performance was further assessed through Levey–Jennings charts and Westgard rules, confirming analytical reliability. The findings indicate that TXRF is a rapid, reliable, and cost-effective technique for arsenic determination in milkfish, making it suitable for screening and routine monitoring of potential contamination to ensure seafood safety.**

I. INTRODUCTION

Milkfish *(Chanos chanos)* is one of the most important aquaculture species in the Philippines due to its wide production and adaptability to freshwater, brackish, and marine environments [1]. However, these same environments may serve as receiving systems for various contaminants, including toxic elements, which can be introduced through natural processes and anthropogenic activities. As a result, aquatic organisms such as milkfish are susceptible to accumulating trace elements, which may pose risks to human health when consumed.

Arsenic (As) is a naturally occurring metalloid widely distributed in the environment and is recognized as a significant contaminant in aquatic systems [2]. It can be introduced into water bodies through both anthropogenic sources, such as mining, industrial discharge, and agricultural activities, and geogenic processes, including the weathering of arsenic-bearing minerals and geothermal and volcanic activity [3,4]. Chronic exposure to arsenic has been associated with various adverse health effects, including skin lesions, cancer, cardiovascular diseases, and neurological disorders [2]. In aquatic environments, arsenic can undergo complex biogeochemical transformations, influencing its mobility, bioavailability, and eventual accumulation in aquatic organisms [3].

The Philippine setting provides an important environmental context for arsenic monitoring, as it lies within a geologically active region with numerous active volcanoes and geothermal systems. Volcanic emissions and geothermal discharges have been identified as natural contributors to the release of arsenic into surrounding soils and water bodies [4,5]. Studies have reported arsenic in groundwater systems in volcanic areas of the Philippines, including those surrounding Taal Volcano, indicating potential transport of arsenic into surface waters and aquaculture environments via runoff and hydrological interactions [5]. Consequently, monitoring arsenic in widely consumed fish species, such as milkfish, is essential for food safety and environmental assessment.

Conventional analytical techniques for trace-element determination in fish samples include inductively coupled plasma optical emission spectrometry (ICP-OES) and inductively coupled plasma mass spectrometry (ICP-MS), which provide high sensitivity and accuracy [6–7]. However, these techniques often require extensive sample preparation, including acid digestion, and involve higher operational costs and longer analysis times [8]. For routine screening purposes, there is a need for alternative analytical methods that are cost-effective, rapid, and require minimal sample preparation while maintaining acceptable analytical performance.

Total Reflection X-ray Fluorescence (TXRF) spectrometry has emerged as a suitable technique for multi-element analysis due to its advantages, including low sample requirement, minimal matrix effects, and the ability to achieve detection limits at the ppm to sub-ppb level [9–11]. TXRF has been successfully applied in the

analysis of trace elements in environmental and biological samples, including fish tissues [12]. However, determining arsenic using TXRF presents analytical challenges due to spectral overlap with other elements, such as lead (Pb), necessitating proper spectral deconvolution and method validation to ensure accuracy and reliability [13].

Despite the increasing use of TXRF in trace-element analysis, few validation studies focus on arsenic determination in milkfish in the Philippine context. Establishing a validated TXRF method using matrix-matched reference materials is therefore necessary to support reliable screening and monitoring of arsenic contamination in aquaculture products. In this study, TXRF analysis for arsenic determination in milkfish was validated using Philippine Reference Material (PRM) 2002-As, Cd, Hg & Pb in Milkfish. The method was evaluated for recovery, precision, and measurement uncertainty to assess its suitability as a rapid, cost-effective screening tool for arsenic in milkfish.

II. METHODOLOGY

A. Reagents and materials

The Bruker S2 PICOFOX is the TXRF used for the study. It is a compact and portable TXRF spectrometer for ultra-trace element analysis. It requires placing a small portion of the sample in a 30-mm-diameter quartz sample carrier. To ensure the cleanliness of the quartz sample carrier and other glassware used for analysis, they were cleaned by submerging them in a 5% RBS 50 solution, a special detergent for glass, and a 20% nitric acid bath.

The samples were prepared by suspending the solid sample particles in a liquid mixture containing Triton X100 (octylphenol ethoxylate) and a yttrium (Y) internal standard. The samples analyzed were PRM-2002, dried milkfish meat with added heavy metals, including arsenic, and DORM-5, a fish protein containing various elements.

B. Sample Preparation

Using an analytical balance, 0.1 g of the sample was weighed and suspended in a solution with 5 mL of 1% (v/v) Triton X-100 and 10 uL of 1000 mg/L yttrium standard. The suspension was mixed and agitated using a vortex shaker multiple times at 5-minute intervals to break clumps of the solid samples. Using a vortex shaker also kept the solids suspended right before transferring 10 uL of the sample to a siliconized quartz sample courier. The samples were air-dried until no liquid was visible, leaving a thin layer of the solid particles.

C. TXRF Parameters

Table 1 summarizes the different parameters used for the TXRF analysis.

Table 1. Parameters set for the analysis of PRM-2002 using TXRF.

Parameter	Unit	Value
X-ray voltage	kV	50
X-ray current	µA	1000
Duration of scan	s	2000
Amount of IS (Y)	µL	10
As sensitivity factor	-	0.52
Y sensitivity factor	-	1.780218

The scanning duration was set to 2000 seconds to improve quantification at low concentrations by increasing the count rate. The calibration constants, or sensitivities, for both arsenic, the target element, and yttrium, the internal standard, were also indicated.

III. RESULTS AND DISCUSSION

A. Calculation of concentration

During TXRF analysis, the Bruker S2 Picofox software automatically calculates elemental concentrations from the measured spectra. However, these reported concentrations do not account for potential background contamination introduced during sample preparation and handling. To address this limitation and ensure more reliable quantification in the present study, arsenic (As) concentrations were manually calculated from the net peak areas obtained from the TXRF spectra.

Each sample analysis was accompanied by a blank sample prepared using the same mixture (5 mL of 1% Triton X-100 solution and 10 µL of yttrium standard) but without the PRM-2002 sample. With this, any contamination reported in the blank samples will be attributed to the PRM-2002 samples. The deducted net area values will then be used to calculate the As concentration in the samples.

Figure 1 shows an example of the TXRF scans of a blank sample and a PRM-2002 sample. It can be observed that the graph for the PRM-2002 shows much higher peaks and overall counts than the blank samples, which could indicate that the PRM-2002 sample contains more elements; therefore, the scan also detected more material or signals. The figure also shows the PRM-2002 graph spike at 10.53 keV, the Kα peak of As, while the blank sample graph shows no peak in this energy range, indicating the absence of As in the blank sample.

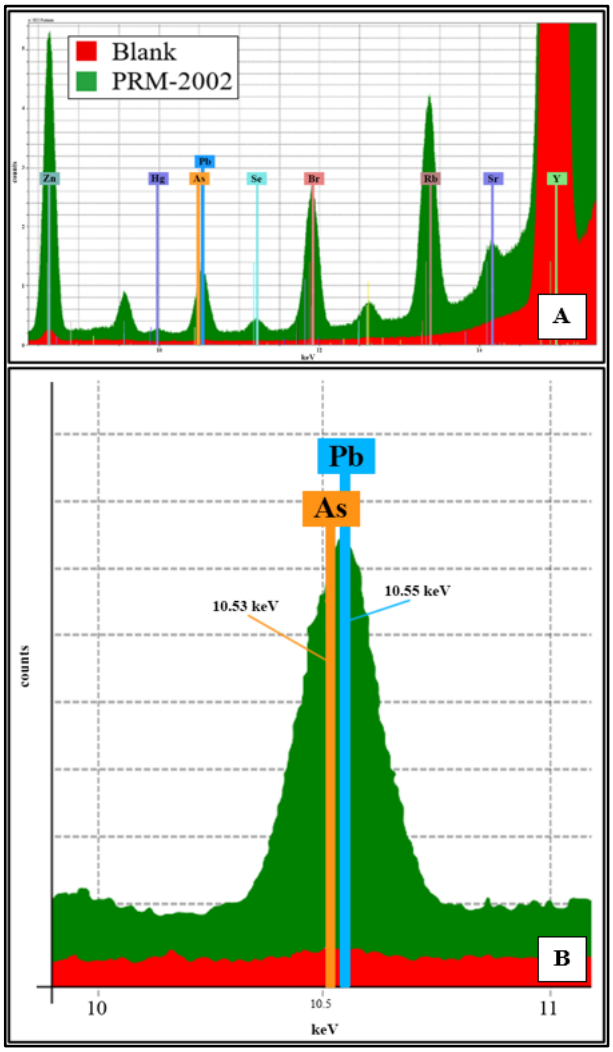


Fig. 1. TXRF spectra containing a blank sample and a PRM-2002 sample scan: (A) full spectra, (B) zoomed in on the peak of As.

Figure 1B focuses on the As Kα peak (10.53 keV), which overlaps with the lead (Pb) Lα peak (10.55 keV). The overlap of the peaks may cause interference when reporting the quantities of both elements, as existing TXRF systems cannot distinguish them as separate peaks, contributing to errors in the analysis. These errors are more evident when the concentration of Pb is much greater than that of As. The presence of both As and Pb with close concentrations in the PRM-2002 sample makes it a suitable reference material for method validation, as the measured counts for As and Pb are within a similar range, minimizing the likelihood of significant bias due to signal domination. For this analysis, the Bruker S2 Picofox software applied the SuperBayes deconvolution algorithm to identify and mathematically separate overlapping spectral peaks, thereby allowing more accurate determination of the individual peak intensities of each element. Longer scan time (2000s) was applied during the analysis to improve readability of secondary peaks (As Kβ and Pb Lβ) and to reduce statistical errors. Analyses were also performed in triplicate per sample to immediately observe deviations in the results. The resulting net peak area of As was recorded and used to calculate its concentration using Eq. (1).

Eq. (1) is used to calculate the concentration of the target heavy metal (C_{As}) using the following values reported by the TXRF:

A_{As} = net area of the As
S_{As} = sensitivity factor of As
C_Y = concentration of y std
A_Y = net area of y std
S_Y = sensitivity factor of y std

$$C_{As} = (C_Y \cdot A_{As} \cdot S_Y) / (A_Y \cdot S_{As}) \quad (1)$$

Table 2 shows the calculated average concentrations of As, expressed in ppm, along with the total recovery percentage, calculated using Eq. (2), where C_{ref} is the known concentration of the reference material.

$$\text{Total \% Recovery} = 100\ (C_{As} / C_{ref}) \quad (2)$$

The recovery percentages of the samples are within the 90-110% range, which is the acceptable mean recovery for amounts between 100 ppm and 100 ppb [14]. The differences in % recovery could be attributed to different factors, such as noise signals during the analysis, homogeneity of the samples during preparation and analysis, sample particle size, thickness of the thin-film on the quartz discs, and matrix effects.

Table 2. Calculated concentrations of As in multiple runs of PRM-2002 samples.

PRM Sample	As (ppm)	As Recovery (%)
1	2.175	92.161
2	2.324	98.475
3	2.461	104.280
4	2.451	103.856
5	2.210	93.644
6	2.272	96.271
7	2.350	99.576
8	2.428	102.881
9	2.494	105.678
10	2.421	102.585
Average	2.3586	99.941

The collected data points were also evaluated using the Westgard rules to check for errors. The Westgard rules are a set of statistical criteria used as a quality-control method for analytical data. It involves plotting the data into a Levey-Jennings chart, which shows limits up to three (3) times the standard deviation, denoted as ±3s. Figure 2 shows the Levey-Jennings chart for the TXRF analysis of As in the PRM-2002 samples. It can be observed that some data points exceeded only the ±1s limit, which is not a criterion for data rejection. Overall, the data points are acceptable within the Westgard rules.

B. Relative Standard Deviation

To evaluate the precision of the collected results, the relative standard deviation (RSD) was also calculated using Eq (3).

$$RSD = (sd / \bar{x}) \bullet 100\% \quad (3)$$

sd = Standard deviation
$\bar{x}$ = Mean

The calculated RSD is 4.70%, which suggests that the collected results have good precision. The study shows that the method can precisely detect and quantify low concentrations of As in milkfish samples.

C. Measurement Uncertainty

Measurement uncertainty was evaluated using the Nordtest approach, which involves a certified reference material (CRM). The Nordtest method is a top-down approach and does not require an uncertainty budget. Instead, the combined standard uncertainty is derived from two major sources: the uncertainty associated with random variations, denoted as u(Rw), and the uncertainty arising from systematic bias, denoted as u(bias). According to Nordtest TR 569, method bias and laboratory bias are incorporated into u(bias), whereas day-to-day variability and repeatability contribute to u(Rw) [15].

The u(Rw) was determined from the standard deviation of repeated PRM-2002 analyses performed over several months. Meanwhile, u(bias) was evaluated using the root-mean-square bias (RMS_{bias}) and the uncertainty of the certified reference value (u(Cref)).

The bias for each TXRF measurement was first calculated as the difference between the measured concentration (Clab) and the certified value (Cref), and then used to obtain RMS_{bias} using Eq. (5).

$$bias = C_{lab} - C_{ref} \quad (4)$$

$$RMS_{bias} = \sqrt{\frac{\Sigma(bias)^2}{n}} \quad (5)$$

The uncertainty of each certified reference value, $u(Cref_i)$, was then estimated from the corresponding standard deviation (s_i) and the number of replicate analyses (n_i) according to Eq. (6). These individual uncertainties were further combined to determine u(Cref) using Eq. (7). Because only one CRM was employed in the study, the calculated u(Cref) was equivalent to the standard uncertainty of that reference material.

$$\Sigma u(Cref_i)^2 = \frac{s_i}{\sqrt{n_i}} \quad (6)$$

$$u(Cref) = \sqrt{\frac{\Sigma u(Cref_i)^2}{n}} \quad (7)$$

After obtaining RMS_{bias} and u(Cref), these parameters were combined to estimate the bias uncertainty, u(bias), as given in Eq. (8).

$$u(bias) = \sqrt{RMS_{bias}{}^2 + \frac{s_{bias}^2}{n} + u(Cref)^2} \quad (8)$$

Equation (8) represents a modified form of the Nordtest bias uncertainty equation adapted for analyses involving a single CRM, where s_{bias} denotes the standard deviation of the calculated bias values.

Finally, the combined standard uncertainty (u_c) was obtained by integrating u(Rw) and u(bias) using Eq. (9).

$$u_c = \sqrt{u(Rw)^2 + u(bias)^2} \quad (9)$$

The expanded uncertainty (U) at a 95% confidence level was then calculated using a coverage factor of k=2:

$$U = u_c \bullet k \quad (10)$$

Table 3 summarizes the calculated uncertainty components, including u(Rw), u(bias), u_c, and U, all expressed in ppm.

Table 3. Nordtest method calculated uncertainty components ($u(Rw)$ and $u(bias)$), standard uncertainty (u_c), and expanded uncertainty (U) in ppm.

$u(Rw)$	$u(bias)$	u_c	U
0.111	0.179	0.211	0.421

Using the Nordtest method, the calculated expanded uncertainty was 2.36 ± 0.42 ppm.

D. Analysis of DORM-5

DORM-5 is a certified reference material (CRM) obtained from the National Research Council Canada. It is made from fish protein containing different concentrations of different elements. It is certified to have 13.3 ± 0.7 ppm of arsenic. Table 4 shows the As results obtained using the developed method, along with the recovery. The results from the analysis of DORM-5 samples show that the method can detect and quantify low concentrations of As with a recovery range of 97 - 102%

Table 4. DORM-5 sample TXRF spectroscopy calculated concentration and % recovery.

Sample	As (ppm)	As Recovery (%)
DORM-5 (1)	13.408	100.814
DORM-5 (2)	13.519	101.647
DORM-5 (3)	13.028	97.955
Average	13.318	100.139

IV. CONCLUSION

Exposure to arsenic at extended times or at high concentrations can affect a person's health in different ways, from getting skin lesions to developing neurological disorders. As a significant contaminant in aquatic systems, it could accumulate in aquatic organisms through continuous exposure. This bioaccumulation may affect humans through the consumption of contaminated aquatic organisms. Using TXRF as an alternative screening method to detect As in milkfish, a widely consumed fish species in the Philippines, can help prevent adverse human health effects from As. Using the PRM-2002, the method was optimized, yielding an average recovery of 99.941% for As in milkfish protein. The RSD was 4.70%, indicating good precision of the method. Using the Nordtest method, the measurement uncertainty was also calculated to be 2.36 ± 0.42 ppm. To verify the method, DORM-5, a fish protein CRM, was also analyzed, showing an As recovery of 100.139%. However, with the spectral overlap of Pb and As peaks, the method may not provide an accurate quantification, especially on samples where Pb has a significantly higher concentration than As. In this case, it is recommended to do confirmatory analysis using a more robust method such as ICP-MS and ICP-OES. Even with this limitation, TXRF analysis could be optimized for a cheap, quick, and green alternative for screening As in milkfish.

REFERENCES

[1] Yap, W. G., Villaluz, A. C., Soriano, M. G. G., & Santos, M. N. 2007. *Milkfish production and processing technologies in the Philippines.* Milkfish Project Publication Series No. 2, 96 pp. WorldFish Center / SEAFDEC Aquaculture Department.

[2] World Health Organization: WHO. 2022. *Arsenic.* WHO Fact Sheet. https://www.who.int/news-room/fact-sheets/detail/arsenic

[3] Wang, N., Xue, X.-M., Juhasz, A. L., Chang, Z., & Li, H.-B. 2023. *Arsenic occurrence and cycling in the aquatic environment.* Water, 15(1), 147. https://doi.org/10.3390/w15010147

[4] Smedley, P. L., & Kinniburgh, D. G. 2002. *A review of the source, behaviour and distribution of arsenic in natural waters.* Applied Geochemistry, 17(5), 517–568. https://doi.org/10.1016/S0883-2927(02)00018-5

[5] Apostol, G. L. C., Valenzuela, S., & Seposo, X. 2022. *Arsenic in groundwater sources from selected communities surrounding Taal Volcano, Philippines: An exploratory study.* Earth, 3(1), 448–459. https://doi.org/10.3390/earth3010027

[6] Leung, H. M., Leung, A. O. W., Wang, H. S., Ma, K. K., Liang, Y., Ho, K. C., Cheung, K. C., Tohidi, F., & Yung, K. K. L. 2014. *Assessment of heavy metals/metalloid (As, Pb, Cd, Ni, Zn, Cr, Cu, Mn) concentrations in edible fish species tissue in the Pearl River Delta (PRD), China.* Marine Pollution Bulletin, 78(1–2), 235–245. https://doi.org/10.1016/j.marpolbul.2013.10.028

[7] Mwakalapa, E. B., Simukoko, C. K., Mmochi, A. J., Mdegela, R. H., Berg, V., Müller, M. H. B., Lyche, J. L., & Polder, A. 2019. *Heavy metals in farmed and wild milkfish (Chanos chanos) and wild mullet (Mugil cephalus) along the coasts of Tanzania and associated health risk for humans and fish.* Chemosphere, 224, 176–186. https://doi.org/10.1016/j.chemosphere.2019.02.063

[8] Altundag, H., Yildirim, E., & Altintig, E. 2019. *Determination of some heavy metals by ICP-OES in edible parts of fish from Sapanca Lake and streams.* Journal of Chemical Metrology, 13(1), 7–13. https://doi.org/10.25135/jcm.24.19.03.1219

[9] Wobrauschek, P. 2007. *Total reflection X-ray fluorescence analysis—a review.* X-Ray Spectrometry, 36(5), 289–300. https://doi.org/10.1002/xrs.985

[10] Zarazúa, G., Girón-Romero, K., Tejeda, S., León, C. C.-D., & Ávila-Pérez, P. 2014. *Total Reflection X-Ray Fluorescence Analysis of Toxic Metals in Fish Tissues.* American Journal of Analytical Chemistry, 5, 805–811. https://doi.org/10.4236/ajac.2014.512089

[11] Beltrán, B. G., Ramos-Sanchez, V., Chávez-Flores, D., Rodríguez-Maese, R., & Palacio, E. 2020. *Total Reflection X-Ray Fluorescence Spectroscopy (TXRF) Method Validation: Determination of Heavy Metals in Dietary Supplements.* Journal of Chemistry, 2020, Article ID 8817393. https://doi.org/10.1155/2020/8817393

[12] Beltrán, B. G., Martínez-Serrano, I., Ramos-Sanchez, V., Chávez-Flores, D., Nevárez-Rodríguez, M. C., & Suárez-Domínguez, E. A. 2019. *Development and Validation of a New Method for Determination of Pb and Cr in Marine Organisms by Total Reflection X-Ray Fluorescence (TXRF) Spectroscopy.* Journal of Analytical Methods in Chemistry, 2019, Article ID 8150678. https://doi.org/10.1155/2019/8150678

[13] Moya-Riffo, A., Bennun, L., Sanhueza, V., & Santibañez, M. 2013. *A procedure for overlapping deconvolution and the determination of its confidence interval for arsenic and lead signals in TXRF spectral analysis.* X-Ray Spectrometry, 42(2), 93–99. https://doi.org/10.1002/xrs.2439

[14] Astuti, L. P., Warsa, A., Nurfiarini, A., & Tjahjo, D. W. 2021. *Bioaccumulation of non-essential heavy metals in fish in Ir H Djuanda Reservoir*, West Java. IOP Conference Series: Earth and Environmental Science, 744(1), 012004. https://doi.org/10.1088/1755-1315/744/1/012004

[15] Magnusson, B., Näykki, T., Hovind, H., Krysell,

M.,Sahlin, E. 2017. *Handbook for calculation of measurement uncertainty in environmental laboratories (NT TR 537 - Edition 4),* Denmark.

2026 IMEKO Joint Conference
TC8 - TC11 - TC24
Metro Manila, Philippines, August 26-29, 2026

Comparative Evaluation of Drinking-Water Supply Options in a Makati Office Using pH, Turbidity, and Uncertainty-Aware Cost-Based Decision-Making

Abraham R. De Guzman [1], Arvin Samson [2], Elyson Keith P. Encarnacion [3]

[1] *University of Western Australia, Holy Angel University, and HORIBA Instruments (Singapore) Pte Ltd., Manila Office, Philippines, ardeguzman3@student.hau.edu.ph, and apu.popoy@gmail.com*
[2] *HORIBA Instruments (Singapore) Pte Ltd., Manila Office, Philippines, arvin.samson@horiba.com*
[3] *Department of Science and Technology - Industrial Technology Development Institute, Philippines, ekpencarnacion@itdi.dost.gov.ph, and elysonencarnacion@ymail.com*

***Abstract* – This study compared externally supplied filtered water and an in-house point-of-use filtration machine in a Makati office using pH, turbidity, measurement uncertainty, and cost considerations. A total of 315 measurements collected from 18 March to 30 April 2026 were evaluated against the 2017 Philippine drinking-water limits of pH 6.5–8.5 and turbidity below 5 NTU. Measurements were performed using a HORIBA U-53G multiparameter water quality analyzer. Before each measurement day, the pH sensor was calibrated with HORIBA pH 4.01 standard solution and operated with automatic temperature compensation, while the turbidity sensor underwent four-point calibration. Externally supplied water had a mean pH of 6.053 with partial combined expanded uncertainty of 0.214 pH units, while the point-of-use system had a mean pH of 7.139 with partial combined expanded uncertainty of 0.073 pH units. Nonparametric bootstrap intervals were used for the zero-inflated, right-skewed turbidity data, giving 0–0.00429 NTU for supplied water and 0.00005–0.26921 NTU for the point-of-use system. Three point-of-use turbidity readings exceeded 5 NTU. Supplied water cost PHP 60 per container, including delivery. The point-of-use system was conditionally preferred, subject to turbidity control and verification of operating costs.**

I. INTRODUCTION

Urban offices commonly provide drinking water either through externally delivered filtered water or through point-of-use filtration systems installed within the workplace. Both options are usually treated as acceptable for routine consumption, but office decisions are often based on simple screening measurements without explicit treatment of measurement uncertainty. This creates a practical problem: a measured value near a drinking-water threshold may lead to unnecessary cost if over-interpreted, or to quality risk if under-interpreted.

In drinking-water monitoring, pH and turbidity are commonly used as rapid screening parameters because they are inexpensive, easy to measure, and useful for identifying changes in water chemistry, treatment performance, and aesthetic acceptability [1]-[4]. Turbidity is also a relevant operational indicator because it reflects suspended particles and can signal treatment or filtration problems [4], [5]. In buildings, final water quality can be affected by premise plumbing, stagnation, filter condition, flushing, and maintenance practice [6]-[10].

The Philippine National Standards for Drinking Water of 2017, issued under Department of Health Administrative Order No. 2017-0010, specify pH of 6.5-8.5 and turbidity below 5 NTU as mandatory drinking-water quality limits [27]. These values were used as the internal decision thresholds in this study.

This study compares the pH and turbidity performance of two office drinking-water supply options and relates the findings to operational and cost-sensitive decisions. It incorporates the HORIBA U-53G display resolution into the pH uncertainty model, documents automatic temperature compensation, daily pH calibration, and four-point turbidity calibration, and applies a non-negative bootstrap interval to turbidity data for which a symmetric interval would produce physically impossible negative limits. The cost analysis uses the known delivered-water price of PHP 60 per container and a break-even framework because verified maintenance and electricity costs for the point-of-use machine were not available.

II. MATERIALS AND METHODS

A. Study site and water supply options

The study was conducted in an office located in Makati City, Philippines. Two drinking-water supply options were evaluated:

Option A: Externally supplied filtered water. This refers to drinking water delivered to the office by an external supplier. The office depends on the delivery schedule, container availability, and supplier quality control.

Option B: Point-of-use filtration machine. This refers to a small filtration machine installed inside the office. The office is responsible for use, cleaning, filter condition, flushing, and maintenance coordination.

There were working days when delivery of externally supplied filtered water did not occur. Consequently, the number of sampled observations for externally supplied water was lower on some workdays than for the point-of-use filtration machine.

B. Measurement instrument, resolution, and temperature compensation

pH, turbidity, and temperature were measured using a HORIBA U-53G multiparameter water-quality meter. Per manufacturer specifications, the pH sensor uses the glass-electrode method, has a measurement range of pH 0-14, and displays pH at a resolution of 0.01 pH. The pH sensor provides automatic temperature compensation. Temperature is measured by a thermistor over -10 to 55 °C with a display resolution of 0.01 °C [31].

The U-53G turbidity sensor uses a tungsten-lamp source and 90° scattering method, with a measurement range of 0-1000 NTU. Because every turbidity observation in this study was between 0 and 8.78 NTU, the applicable display resolution for the complete dataset was 0.01 NTU.

Automatic temperature compensation adjusts the pH electrode response using the measured temperature during calibration and measurement. It compensates the temperature dependence of the electrode response; it does not eliminate the need to keep calibration standards and samples at comparable temperatures [33].

C. Daily pH and turbidity calibration

Before measurements on each sampling day, the U-53G pH sensor was automatically calibrated using HORIBA pH Standard Solution 100-4. This phthalate standard solution has a nominal pH value of 4.01 at 25 °C, and was used without dilution, consistent with the manufacturer's product instructions [32].

The daily pH procedure provided a one-point calibration or verification at pH 4.01. It checked instrument response near the acidic end of the observed sample range but did not independently determine electrode slope across the full drinking-water decision interval. Manufacturer technical guidance recommends calibration with at least two buffers that bracket the expected sample pH [33]. A pH 7.00 buffer should therefore be added in future monitoring to provide a two-point daily calibration spanning the principal sample range.

Before turbidity measurements, the instrument underwent four-point calibration in accordance with the manufacturer's calibration procedure [31]. This multipoint procedure verified the instrument response at four turbidity levels before the office-water measurements were performed.

Four-point turbidity calibration was completed, but the numerical certificate uncertainties of the pH and turbidity calibration standards were unavailable for propagation. These Type B contributions were therefore not included in the numerical uncertainty budget.

D. Measurement data

Dataset contained 315 usable repeated measurements collected during regular workdays from 18 March to 30 April 2026. Of these, 112 observations were from externally supplied filtered water and 203 observations were from the point-of-use filtration machine. pH was expressed in pH units and turbidity in nephelometric turbidity units (NTU).

E. Threshold values

The thresholds used in this paper were taken from the Philippine National Standards for Drinking Water of 2017.

Table 1. Decision thresholds used in the study.

Parameter	Threshold
pH	6.5-8.5
Turbidity	<5 NTU

F. Statistical estimation and pH uncertainty budget

For each water-supply option, the number of readings, arithmetic mean, sample standard deviation, and Type A standard uncertainty of the mean were calculated as follows:

$$\bar{x} = \frac{1}{n}\sum_{i=1}^{n} x_{\mathrm{i}} \quad (1)$$

$$s = \sqrt{\frac{\sum_{i=1}^{n}(x_i - \bar{x})^2}{n-1}} \quad (2)$$

$$u_A(\bar{x}) = \frac{s}{\sqrt{n}} \quad (3)$$

where $\bar{x}$ is the sample mean, x_i is an individual reading, n is the number of readings, s is the sample standard deviation, and $u_A(\bar{x})$ is the Type A standard uncertainty of the mean.

For pH, the 0.01 pH display increment, q_{pH}, was represented by a rectangular distribution. The associated standard uncertainty was:

$$u_{res} = \frac{q_{pH}}{\sqrt{12}} = \frac{0.01}{\sqrt{12}} = 0.00289\ pH \quad (4)$$

The Type A and resolution contributions were combined as:

$$u_c(\bar{x}) = \sqrt{u_A(\bar{x})^2 + u_{res}^2} \quad (5)$$

$$U_c = k u_c(\bar{x}), \qquad k = 2 \quad (6)$$

Here, $u_c(\bar{x})$ is the combined standard uncertainty of the mean and U_c is the combined expanded uncertainty at an approximate 95% coverage level. The model includes observed repeatability and display resolution but excludes calibration-standard uncertainty, longer-term drift, sampling effects, and handling effects because numerical estimates for these components were unavailable.

G. Turbidity interval estimation

Turbidity required a bounded statistical treatment because it is physically non-negative and the observed distributions were strongly zero-inflated and right-skewed. The applicable turbidity display increment is denoted by q_T; $q_T = 0.01\text{NTU}$ for all observed values because the complete dataset was within the 0–9.99 NTU resolution range. A symmetric $\bar{x} \pm U$ interval would extend below 0 NTU and would not provide a physically meaningful representation.

A nonparametric percentile-bootstrap procedure was therefore applied. For each water source, $B = 500{,}000$ samples of size n were drawn with replacement from the observed turbidity readings using a fixed random seed of 20260621. The mean of bootstrap sample b was calculated as:

$$\bar{x}^{*(b)} = \frac{1}{n}\sum_{i=1}^{n} x_i^{*(b)}, \qquad b = 1, \ldots, B \quad (7)$$

The 2.5th and 97.5th percentiles of the bootstrap distribution were reported as the 95% interval:

$$[L^*_{0.025}, U^*_{0.975}] \quad (8)$$

Here, $L^*_{0.025}$ and $U^*_{0.975}$ are the 2.5th and 97.5th percentiles, respectively, of the bootstrap distribution of the mean. Because all resampled readings were non-negative, the resulting interval was non-negative without post hoc truncation. The 0.01 NTU display resolution is disclosed as an instrument characteristic but was not convolved with the bootstrap distribution because a validated response model near the zero boundary and numerical calibration-standard uncertainty were unavailable. The interval therefore describes statistical uncertainty in the observed mean rather than a complete traceable measurement uncertainty [28]-[30].

H. Cost framework

The externally supplied water cost PHP 60 per container, inclusive of delivery. For N_c containers used during a selected decision period, the direct delivered-water cost is:

$$C_{delivered} = \text{PHP}60 N_c \quad (9)$$

No verified monetary data were available for point-of-use filter replacement, preventive maintenance, repair, or electricity. The point-of-use operating cost was therefore represented as:

$$C_{POU} = C_{maintenance} + C_{electricity} + C_{monitoring} + C_{corrective} \quad (10)$$

A numerical total-cost comparison was not made because $C_{maintenance}$ and $C_{electricity}$ were unknown. The point-of-use option is less costly on a direct operating basis only when $C_{POU} < \text{PHP}60 N_c$ for the same decision period and service demand.

I. Scenario-based decision analysis

A scenario-based decision framework was applied to connect measurement results with cost-sensitive office actions. Results clearly within limits were treated as suitable for continued use. Results close to thresholds or with uncertainty intervals overlapping thresholds were treated as retesting cases. Results clearly outside thresholds, or repeated individual exceedances, were assigned to corrective actions such as supplier inquiry, flushing, preventive maintenance, filter inspection, or temporary alternative supply.

This interpretation follows the broader view that water-quality monitoring should support risk-based operational

decisions rather than isolated pass/fail classification [11]-[14].

III. RESULTS

A. Sampling distribution

Table 2. Number of observations by water-supply option.

Water supply option	n	Percentage	Sampling dates
Externally supplied filtered water	112	35.6 %	18
Point-of-use filtration machine	203	64.4 %	19

The point-of-use filtration machine had more observations because it remained available when externally supplied water was not delivered. Supply continuity is operationally relevant because interruption can create emergency-purchase, staff-handling, and service-disruption costs.

B. pH results

Table 3. pH results and uncertainty.

Estimator or component	Symbol	Externally supplied water	Point-of-use machine
Number of readings	n	112	203
Arithmetic mean	$\bar{x}$	6.05348	7.13882
Sample standard deviation	s	1.13002	0.51657
Type A standard uncertainty	$u_A(\bar{x})$	0.10678	0.03626
Resolution standard uncertainty	u_{res}	0.00289	0.00289
Combined standard uncertainty	$u_c(\bar{x})$	0.10682	0.03637
Expanded uncertainty (k = 2)	U_c	0.21363	0.07274
Combined interval	$\bar{x} \pm U_c$	5.83985-6.26711	7.06608-7.21156
Minimum	*Min*	4.45	6.07
Maximum	*Max*	7.9	8.22
Readings below pH 6.5	-	52 (46.4%)	28 (13.8%)

Externally supplied filtered water had $\bar{x}$ = 6.05348 and U_c = 0.21363 pH units. The combined interval of 5.83985-6.26711 remained below the lower threshold of 6.5. In addition, 52 of 112 readings, or 46.4%, were below 6.5. These findings support confirmatory testing and supplier verification.

The point-of-use filtration machine had $\bar{x}$ = 7.13882 and U_c = 0.07274 pH units. Its combined interval of 7.06608-7.21156 was within the specified range, although 28 of 203 individual readings, or 13.8%, were below 6.5. The point-of-use source therefore performed better on mean pH but should not be described as uniformly conforming at the individual-reading level.

C. Turbidity results

Table 4. Turbidity results and physically bounded bootstrap intervals.

Estimator or statistic	Symbol	Externally supplied water	Point-of-use machine
Number of readings	n	112	203
Arithmetic mean (NTU)	$\bar{x}$	0.0014286	0.1173399
Median (NTU)	$\tilde{x}$	0	0
Sample standard deviation (NTU)	s	0.0151186	0.9640929
Applicable display resolution (NTU)	q_T	0.01	0.01
95% bootstrap interval (NTU)	$[L^*_{0.025}, U^*_{0.975}]$	0-0.0042857	0.0000493 - 0.2692118
Minimum (NTU)	*Min*	0	0
Maximum (NTU)	*Max*	0.16	8.78

Zero readings	-	111 (99.1%)	199 (98.0%)
Readings above 5 NTU	-	0	3 (1.48%)

Externally supplied filtered water had a mean turbidity of 0.0014286 NTU and a 95% bootstrap interval of 0-0.0042857 NTU. Only one reading was greater than zero, at 0.16 NTU, and all readings were below the 5 NTU threshold.

The point-of-use filtration machine had a mean turbidity of 0.1173399 NTU and a 95% bootstrap interval of 0.0000493-0.2692118 NTU. Of the 203 readings, 199 were 0 NTU. Four readings were greater than zero: 0.01, 7.01, 8.02, and 8.78 NTU. The three readings above 5 NTU occurred during the same monitoring event on 21 April 2026. The clustering indicates an isolated event rather than persistent high turbidity across the entire period, but it warrants flushing, equipment inspection, and immediate retesting.

D. Cost comparison

Table 5. Available cost information and comparison rule.

Cost item	**Externally supplied water**	**Point-of-use machine**
Known direct price	PHP 60 per container, including delivery	Not available
Maintenance cost	Not applicable to office equipment	Not available
Electricity cost	Not applicable	Not available
Period cost expression	$C_{delivered} = \text{PHP}60N_c$	$C_{POU} = C_{maintenance} + C_{electricity} + C_{monitoring} + C_{corrective}$
Decision rule	Use actual N_c for the selected period	Economically favorable only if $C_{POU} < \text{PHP}60N_c$

The delivered-water price provides a transparent variable cost: every additional container increases direct cost by PHP 60. A numerical cost advantage for the point-of-use machine cannot be demonstrated from the available information because maintenance and electricity costs were not recorded. Cost conclusions are therefore conditional and should be updated when these values become available.

IV. DISCUSSION

A. Comparative performance of the two supply options

The two water-supply options showed different quality profiles. Externally supplied filtered water performed better in turbidity, while the point-of-use filtration machine performed better in mean pH.

The main concern for externally supplied water was pH. Its mean and combined interval were below 6.5, and 46.4% of the readings were below the lower threshold. Daily pH calibration at pH 4.01 and automatic temperature compensation reduced two identifiable sources of measurement variation. However, the one-point pH calibration did not verify electrode slope across the pH 6.5–8.5 decision interval, and the calibration-solution certificate uncertainty was unavailable. Confirmatory pH testing using a two-point calibration and an accredited laboratory is therefore warranted before a definitive compliance conclusion is made.

The point-of-use machine showed acceptable mean pH but had three turbidity exceedances clustered during one monitoring event. This pattern supports a targeted maintenance response rather than immediate system replacement. Building-water studies show that plumbing conditions, stagnation, flushing, and maintenance activities can influence water quality at the point of use [6]-[10], [15]-[17].

B. Instrument resolution and pH uncertainty

The U-53G pH resolution contribution was small relative to the observed between-reading variability. For externally supplied water, $u_{res} = 0.00289$ pH compared with $u_A(\bar{x}) = 0.10678$ pH ; for the point-of-use machine, $u_{res} = 0.00289$ pH compared with $u_A(\bar{x}) = 0.03626$ pH. Incorporating display resolution changed the expanded uncertainties only slightly, from

approximately 0.21355 to 0.21363 pH for externally supplied water and from 0.07251 to 0.07274 pH for the point-of-use machine.

The small numerical effect does not make resolution irrelevant. Reporting it explicitly clarifies the instrument contribution and distinguishes a combined uncertainty estimate from a repeatability-only calculation. The uncertainty statement remains incomplete because the standard-solution uncertainty, electrode calibration slope, long-term drift, sample handling, and between-day effects were not quantified.

C. Automatic temperature compensation and calibration interpretation

Automatic temperature compensation uses the measured temperature to adjust the glass-electrode response during calibration and measurement. This is important because the theoretical pH electrode slope changes with temperature [33]. The U-53G temperature sensor has 0.01 °C resolution, which is sufficiently fine for the instrument's compensation calculation; however, temperature resolution alone does not establish the uncertainty of the compensated pH result.

The daily pH 4.01 calibration checks response at one point. Since the observed drinking-water values were principally around pH 6-8, a second buffer near pH 7 is needed to evaluate slope over the relevant interval. Future monitoring should use fresh pH 4.01 and pH 7.00 buffers that bracket the expected samples and should retain the calibration slope or acceptance record for each day.

D. Interpretation of turbidity uncertainty

The turbidity distributions were dominated by zero readings and contained only a few positive observations. Under these conditions, the standard deviation can be large relative to the mean, particularly when isolated excursions occur. A symmetric $\bar{x} \pm U$ interval is unsuitable because it extends below the physical lower bound of 0 NTU.

The percentile-bootstrap intervals provide a physically meaningful alternative. The externally supplied-water interval began at exactly 0 NTU, while the point-of-use interval remained non-negative. Four-point calibration of the instrument was performed before measurements, reducing the likelihood that the observed turbidity pattern resulted solely from an uncalibrated instrument response. However, a complete metrological interval would additionally require the numerical uncertainties of the calibration standards and a validated response model near zero. The bootstrap result therefore describes the uncertainty of the observed mean, while the maximum and exceedance count identify operational events. Both summaries are required for a sound decision.

E. Cost-sensitive decision implications

The known direct cost of externally supplied water is PHP 60 per container, including delivery. This cost increases linearly with consumption and can be calculated for any period once the number of containers is known. Additional external-supply costs may include storage, handling, emergency purchases, and disruption during missed deliveries.

For the point-of-use machine, relevant cost categories include filter replacement, preventive maintenance, electricity, cleaning, monitoring, and corrective action. Since maintenance and electricity costs were not available, assigning a numerical total would create an unsupported economic comparison. The appropriate present conclusion is a break-even rule: the point-of-use option is economically preferable only when its actual period cost is below PHP 60 multiplied by the number of delivered containers that it replaces.

The observed turbidity event also illustrates why maintenance decisions should be staged. Flushing, inspection, and retesting have lower immediate cost than premature equipment replacement. Filter replacement or more extensive servicing becomes justified when an exceedance is verified after flushing or recurs during subsequent monitoring.

Table 6. Measurement-based operational decision framework.

Measurement condition	Interpretation	Recommended action	Cost implication
Clearly within threshold	Low immediate concern	Continue use and routine monitoring	Lowest immediate cost
Near threshold or uncertain	Decision uncertainty	Repeat measurement; review calibration and temperature record	Low to moderate
Single verified exceedance	Event requiring investigation	Flush or resample; inspect source or equipment	Moderate
Clear nonconformity after verification	Corrective action required	Supplier inquiry or corrective maintenance	Moderate to high
Repeated verified nonconformity	Persistent problem	Supplier or maintenance review; consider alternative supply	Higher short-term cost, lower long-term risk

F. Practical decision outcome

On the available screening evidence, the point-of-use filtration machine is the conditionally preferred primary option because its mean pH was within the required range and it provided better supply continuity. This preference is conditional on an effective turbidity-control protocol comprising flushing, filter and outlet inspection, immediate retesting after an exceedance, preventive maintenance, and documented daily calibration.

Externally supplied water remains favorable for turbidity stability and may serve as an alternative or backup source, but its low-pH pattern requires confirmatory testing and supplier verification. A definitive economic preference cannot be stated until actual point-of-use maintenance and electricity costs are compared with PHP 60 times the number of delivered containers displaced.

V. CONCLUSIONS

This study evaluated 315 pH and turbidity readings from externally supplied filtered water and a point-of-use filtration machine in a Makati office. The externally supplied water had excellent turbidity performance but a mean pH of 6.053, with 46.4% of readings below 6.5. The point-of-use machine had a mean pH of 7.139, with 13.8% of readings below 6.5, and three turbidity exceedances clustered during one monitoring event.

The HORIBA U-53G provided 0.01 pH resolution, automatic temperature compensation, and 0.01 NTU turbidity resolution throughout the observed range. Incorporating pH display resolution produced partial combined expanded uncertainties of 0.21363 pH for externally supplied water and 0.07274 pH for the point-of-use machine. Daily pH calibration was performed with HORIBA 100-4 phthalate standard solution at nominal pH 4.01 and 25 °C, and turbidity sensor underwent four-point calibration before measurements.

For turbidity, nonparametric bootstrap intervals were used because the data were non-negative, zero-inflated, and right-skewed. This produced physically meaningful intervals of 0-0.00429 NTU for externally supplied water and 0.00005-0.26921 NTU for the point-of-use machine, without negative lower bounds.

Externally supplied water cost PHP 60 per container, including delivery. Because point-of-use maintenance and electricity costs were unavailable, the economic comparison was expressed as a break-even condition rather than a complete total-cost ranking. The point-of-use machine is conditionally preferred for primary office use based on mean pH and continuity, provided that turbidity excursions are controlled and its actual operating cost is subsequently verified.

VI. RECOMMENDATIONS

1. Conduct confirmatory pH testing of externally supplied filtered water through an accredited laboratory.

2. Request supplier documentation on treatment-process control, pH adjustment, and delivery-lot quality.

3. Use a two-point daily pH calibration with fresh buffers that bracket the expected sample range, including pH 4.01 and pH 7.00.

4. Retain daily calibration records for both sensors. For pH, record the date, standard-solution identification and lot, standard temperature, target value, observed response, and acceptance result. For turbidity, record the four calibration levels, standard identification and lot, observed responses, acceptance results, and operator.

5. Retain certificates or stated uncertainties for calibration standards so that their Type B contributions can be included in a complete uncertainty budget.

6. Apply flushing, outlet and filter inspection, and immediate retesting after any point-of-use turbidity reading above 5 NTU.

7. Replace or service the point-of-use filter if a verified turbidity exceedance recurs after flushing or if the prescribed maintenance interval has been reached.

8. Maintain a monitoring log containing date, time, source, sample temperature, pH, turbidity, calibration status, delivery status, filter status, and corrective action.

9. Record the number of delivered containers so that period cost can be calculated as $\mathrm{PHP}60 \times N_c$.

10. Record point-of-use maintenance, filter, electricity, monitoring, and corrective-action costs to permit a complete life-cycle cost comparison.

11. Future work should include microbiological indicators, conductivity, total dissolved solids, residual chlorine where applicable, independent sampling units, and a complete uncertainty budget.

VII. LIMITATIONS

The study was conducted at one office during one monitoring period. Repeated readings collected in short sequences may not be statistically independent. Daily pH calibration used a single pH 4.01 standard and therefore did not independently verify electrode slope across the full sample range. Although four-point turbidity calibration was performed before measurements, numerical certificate uncertainties for the pH and turbidity calibration standards, long-term drift, sample-handling effects, microbiological

indicators, and complete financial records were unavailable. Although display resolution was incorporated into the pH uncertainty model, the reported uncertainty is not a complete traceable GUM uncertainty budget. The delivered-water price was known, but the number of containers consumed and the maintenance and electricity costs of the point-of-use machine were not available for a full period-cost calculation. The findings should therefore be interpreted as an uncertainty-aware screening comparison and conditional operational decision, not as a complete potability assessment or life-cycle cost analysis.

REFERENCES

[1] M. Banna, S. A. Imran, A. Francisque, H. Najjaran, R. Sadiq, M. J. Rodriguez, and M. Hoorfar, "Online drinking water quality monitoring: Review on available and emerging technologies," Critical Reviews in Environmental Science and Technology, vol. 44, pp. 1370-1421, 2014. Available: https://www.tandfonline.com/doi/abs/10.1080/10643389.2013.781936

[2] J. Rahim, S. Sunarsih, and L. Budiati, "Online water quality monitoring: A case study in the Umbulan drinking water supply system, East Java, Indonesia," International Journal of Public Health Science, vol. 13, 2024. Available: https://ijphs.iaescore.com/index.php/IJPHS/article/view/23174

[3] M. Tariq, A. Siddiq, H. Irshad, M. Aman, and M. S. Khan, "An open source water quality measurement system for remote areas," Engineering Proceedings, 2021. Available: https://www.mdpi.com/2673-4591/12/1/50

[4] K. Hyde, "Turbidity measurement: Its application for water resource recycling in buildings," Process Safety and Environmental Protection, vol. 146, pp. 629-638, 2021. Available: https://www.sciencedirect.com/science/article/abs/pii/S0957582020318784

[5] A. D. De Roos, P. Gurian, L. Robinson, A. Rai, I. Zakeri, and M. Kondo, "Review of epidemiological studies of drinking-water turbidity in relation to acute gastrointestinal illness," Environmental Health Perspectives, vol. 125, 2017. Available: https://pubmed.ncbi.nlm.nih.gov/28886603/

[6] M. Yao, Y. Zhang, Z. Dai, A. Ren, J. Fang, X. Li, W. van der Meer, G. Medema, J. Rose, and G. Liu, "Building water quality deterioration during water supply restoration after interruption: Influences of premise plumbing configuration," Water Research, vol. 241, article 120149, 2023. Available: https://www.sciencedirect.com/science/article/pii/S0043135423005857

[7] R. Julien, E. A. Dreelin, A. Whelton, J. Lee, T. Aw, K. Dean, and J. Mitchell, "Knowledge gaps and risks associated with premise plumbing drinking water quality," AWWA Water Science, vol. 2, 2020. Available: https://awwa.onlinelibrary.wiley.com/doi/10.1002/aws2.1177

[8] K. Ra, C. R. Proctor, C. Ley, D. M. Angert, Y. Noh, T. O. Odimayomi, and A. Whelton, "Four buildings and a flush: Lessons from degraded water quality and recommendations on building water management," Environmental Science and Ecotechnology, vol. 18, 2023. Available: https://www.sciencedirect.com/science/article/pii/S2666498423000790

[9] P. Ji, J. L. Parks, M. Edwards, and A. Pruden, "Impact of water chemistry, pipe material and stagnation on the building plumbing microbiome," PLOS ONE, vol. 10, 2015. Available: https://journals.plos.org/plosone/article?id=10.1371/journal.pone.0141087

[10] M. A. Nisar, K. Ross, M. H. Brown, R. Bentham, and H. Whiley, "Water stagnation and flow obstruction reduces the quality of potable water and increases the risk of legionelloses," Frontiers in Environmental Science, vol. 8, 2020. Available: https://www.frontiersin.org/journals/environmental-science/articles/10.3389/fenvs.2020.611611/full

[11] I. Schmidt, B. Rickert, O. Schmoll, and T. Rapp, "Implementation and evaluation of the water safety plan approach for buildings," Journal of Water and Health, vol. 17, no. 6, pp. 870-883, 2019. Available: https://iwaponline.com/jwh/article/17/6/870/70401/Implementation-and-evaluation-of-the-water-safety

[12] L. Mogane, T. M. Masebe, T. Msagati, and E. Ncube, "A comprehensive review of water quality indices for lotic and lentic ecosystems," Environmental Monitoring and Assessment, vol. 195, 2023. Available: https://link.springer.com/article/10.1007/s10661-023-11512-2

[13] S. Joshi, R. Richard, D. Hogue, J. Brown, M. Cahill, V. Kotta, K. Call, N. Butzine, M. Marcos-Hernandez, J. Alja'fari, L. Voth-Gaeddert, T. H. Boyer, and K. A. Hamilton, "Water quality trade-offs for risk management interventions in a green building," Environmental Science: Water Research & Technology, vol. 10, no. 4, pp. 767-786, 2024. Available: https://pubs.rsc.org/en/content/articlelanding/2024/ew/d3ew00650f

[14] R. H. Lopes, C. R. D. V. Silva, P. T. C. O. Salvador, I. S. Silva, L. Heller, and S. A. Uchoa, "Surveillance of drinking water quality worldwide: Scoping review protocol," International Journal of Environmental Research and Public Health, vol. 19, 2022. Available: https://www.mdpi.com/1660-4601/19/15/8989

[15] H. Y. Buse and J. H. Mistry, "Microbial and

physicochemical water quality changes within distribution and premise plumbing systems during a chlorine conversion," PLOS Water, vol. 3, pp. 1-23, 2024. Available: https://journals.plos.org/water/article?id=10.1371/journal.pwat.0000181

[16] H. Y. Buse, J. Steenbock, S. Okum, N. Sojda, S. Kidney, J. Brossart, D. Elstun, E. Weaver, and S. Witt, "Impact of residential hot water heater type and water stagnation on drinking water quality within a full-scale premise plumbing system," Environmental Advances, vol. 18, 2024. Available: https://www.sciencedirect.com/science/article/pii/S2666765724001170

[17] C. Hayward, K. E. Ross, M. H. Brown, R. Bentham, M. A. Nisar, J. Hinds, J. Xi, and H. Whiley, "Microbial risks in drinking water systems: Persistence and public health implications of opportunistic premise plumbing pathogens," Frontiers in Microbiology, vol. 16, 2025. Available: https://www.frontiersin.org/journals/microbiology/articles/10.3389/fmicb.2025.1575789/full

[18] V. Fernandez Alvarez, D. Granada Salazar, C. Figueroa, J. Corrales, and J. F. Casanova, "Estimation of water turbidity in drinking water treatment plants using machine learning based on water and meteorological data," The 7th International Electronic Conference on Water Sciences, 2023. Available: https://www.mdpi.com/2673-4931/25/1/89

[19] G. Volf, I. Susanj Cule, N. Atanasova, S. Zorko, and N. Ozanic, "Explaining and predicting microbiological water quality for sustainable management of drinking water treatment facilities," Sustainability, 2025. Available: https://www.mdpi.com/2071-1050/17/15/6659

[20] C. Axiotidis, E. Konstantopoulou, and N. Sklavos, "A wireless sensor network IoT platform for consumption and quality monitoring of drinking water," Discover Applied Sciences, 2024. Available: https://link.springer.com/article/10.1007/s42452-024-06384-1

[21] R. J. Bayne, D. Pyle, K. Maguire, and R. Oosthuizen, "Examining water quality and transport implications of alternative supply during a drought in a South African municipality," Air and Water Components of the Environment Conference, 2024. Available: https://aerapa.conference.ubbcluj.ro/2024/pdf/221_241_Bayne_etal_AWC_2024.pdf

[22] C. Brocklehurst and T. Slaymaker, "Continuity in drinking water supply," PLOS Medicine, vol. 12, 2015. Available: https://journals.plos.org/plosmedicine/article?id=10.1371/journal.pmed.1001894

[23] M. Manga, T. G. Ngobi, L. O. Okeny, P. O. Acheng, H. Namakula, E. Kyaterekera, I. Nansubuga, and N. Kibwami, "The effect of household storage tanks/vessels and user practices on the quality of water: A systematic review of literature," Environmental Systems Research, vol. 10, pp. 1-26, 2021. Available: https://link.springer.com/article/10.1186/s40068-021-00221-9

[24] M. T. Ngcongo and M. Tekere, "WASH and drinking water quality considerations in schools in reflection of the sustainable development goals: A review," Journal of Water, Sanitation and Hygiene for Development, 2023. Available: https://iwaponline.com/washdev/article/13/8/566/96773/WASH-and-drinking-water-quality-considerations-in

[25] P. Gurian, S. Samuel, N. Yadav, M. Krieger, R. Singh, and T. Bartrand, "Impact of premise plumbing design, velocity, and operational factors on microbial activity during stagnation in pipes," AWWA Water Science, vol. 7, 2025. Available: https://awwa.onlinelibrary.wiley.com/doi/10.1002/aws2.70031

[26] H. Wang, E. Bedard, M. Prevost, A. Camper, V. Hill, and A. Pruden, "Methodological approaches for monitoring opportunistic pathogens in premise plumbing: A review," Water Research, vol. 117, pp. 68-86, 2017. Available: https://www.sciencedirect.com/science/article/abs/pii/S0043135417302300

[27] Department of Health, "Administrative Order No. 2017-0010: Philippine National Standards for Drinking Water of 2017," Republic of the Philippines, 2017. Available: https://www.fda.gov.ph/wp-content/uploads/2020/10/Administrative-Order-No.-2017-0010.pdf

[28] Joint Committee for Guides in Metrology, "Evaluation of measurement data - Guide to the expression of uncertainty in measurement," JCGM 100:2008, 2008.

[29] Joint Committee for Guides in Metrology, "Evaluation of measurement data - Supplement 1 to the Guide to the expression of uncertainty in measurement - Propagation of distributions using a Monte Carlo method," JCGM 101:2008, 2008.

[30] J. I. F. Slaets, H.-P. Piepho, P. Schmitter, T. Hilger, and G. Cadisch, "Quantifying uncertainty on sediment loads using bootstrap confidence intervals," Hydrology and Earth System Sciences, vol. 21, pp. 571-588, 2017.

[31] HORIBA, "Multi-parameter Water Quality Meters U-50 Series," Bulletin HRE-1930E, U-50 Series brochure, pp. 5-7.

[32] HORIBA Advanced Techno Co., Ltd., "pH Standard Solution 100-4," product specification: phthalate standard solution, pH 4.01 at 25 °C, 500 mL. Available: https://www.horiba.com/int/water-

quality/products/detail/action/show/Product/ph-standard-solution-100-4-1235/
[33] HORIBA, "Automatic Temperature Compensation in pH Measurement," Water Quality Technical Tips. Available: https://www.horiba.com/int/water-quality/support/technical-tips/bench-meters/automatic-temperature-compensation-in-ph-measurement/

2026 IMEKO Joint Conference
TC8 - TC11 - TC24
Metro Manila, Philippines, August 26-29, 2026

Multicriteria Selection of Candidate Substances for Density Certified Reference Materials Using the Analytic Hierarchy Process

César-Augusto Mata-Jiménez[1], Andrés Torres-Rocha[2], Maximo Hernández[2], José-de-Jesús Martínez-Díaz[2], Omar-Jair Purata-Sifuentes[2*]

[1] *Dirección de Termometría, Centro Nacional de Metrología, km 4.5 Carretera a Los Cues, Municipio El Marqués, Querétaro 76246, México, cmata@cenam.mx*
[2] *División de Ciencias Económico Administrativas, Departamento de Estudios Organizacionales, Universidad de Guanajuato, 36250, México, a.torresrocha@ugto.mx, mu.hernandezestrada@ugto.mx, jdj.martinezdiaz@ugto.mx, opurata@ugto.mx*

***Abstract* – This study addresses the selection of candidate substances for certified reference materials (CRM) used in density measurements, which are essential for metrological traceability and for the dissemination of density values across calibration and testing activities. The Analytic Hierarchy Process (AHP) is applied as a structured multicriteria framework to evaluate and rank candidates. Relevant physicochemical, practical, environmental and economic criteria are considered, including density, toxicity, viscosity, corrosivity, vapor pressure, surface tension, hygroscopicity, flammability, ignition point, thermal expansion, compressibility, purity, availability, and reactivity, in line with hydrostatic weighing and ISO 17034. Substances such as ethylene glycol, tetrachloroethylene, dodecane, FC-40, water-glycerin mixtures, dichlorotoluene, bromobenzene, dimethyl phthalate, and saline solutions were assessed via pairwise comparisons to derive priority weights and final ranking. Results show that AHP provides a structured approach for density CRM selection, balancing metrological requirements with practical considerations; the approach may also be extended to other reference-material development processes.**

I. INTRODUCTION

In metrology and science, the precision and reliability of measurements are paramount, particularly when it comes to density measurements, which are critical in various scientific and industrial applications [1], [2]. Certified Reference Materials (CRM) serve as essential tools in this context, providing the necessary benchmarks for ensuring measurement accuracy and traceability [3]. The significance of CRM extends to contribute to the dissemination of the unit with metrological traceability, complying with regulations beyond mere compliance with standards, like ISO 17034 [4]. They embody the foundation upon which the credibility of measurement systems rests. The selection of appropriate candidate substances for CRM is a complex, multicriteria process that requires a systematic approach to evaluating potential candidates across diverse facets [5]. This study employs the Analytic Hierarchy Process (AHP), a structured decision-making methodology [6], to support the ranking and selection of candidate substances based on their physicochemical properties, while also considering economic, practical, and environmental dimensions.

Density measurements are critical in numerous fields, including chemistry, physics, engineering, and environmental science, where they influence the characterization of materials and the assessment of their properties. The accuracy of these measurements relies heavily on the availability of high-quality CRM, which must possess specific characteristics that align with the measurement principles employed [7]. In hydrostatic weighing applications, substances with stable and well-defined density values are desirable as candidate certified reference materials for supporting calibration activities and ensuring comparability of density measurements. This demands a careful examination of various physicochemical properties, such as toxicity, viscosity, corrosivity, vapor pressure, surface tension, hygroscopicity, flammability, ignition point, thermal expansion, and compressibility coefficients. Moreover, the candidate substances' purity and reactivity must be assessed to ensure that they do not interfere with the measurement process or compromise the integrity of the results [8].

The initial selection criteria for candidate substances are extensive and interrelated, creating a complex landscape for decision-making. Each criterion must be weighed against the others to determine its significance in the context of density measurement. For instance, a substance with an ideal density value may be rendered unsuitable if it exhibits high toxicity or corrosivity, posing risks during

handling and measurement. Similarly, the ease of acquisition and the environmental impact of the substances must be factored into the decision-making process, highlighting the necessity for a holistic approach to CRM selection [9]. The ISO 17034:2016 standard establishes the requirements for the competence of reference material producers, emphasizing the importance of traceability and the need for rigorous evaluation of candidate substances [4].

The AHP methodology offers a robust framework for navigating this complexity by enabling decision-makers to conduct pairwise comparisons of the selection criteria. This structured approach allows for establishing priority weights for each criterion, reflecting their relative importance in the context of CRM selection. By evaluating each candidate substance against the established criteria, the AHP facilitates a systematic ranking process, culminating in a comprehensive assessment that guides the selection of the most suitable CRM [6].

In this study, a diverse set of candidate substances was considered, including ethylene glycol, tetrachloroethylene, dodecane, FC-40, saline solutions (brines), water-glycerin mixtures, dichlorotoluene, bromobenzene, and dimethyl phthalate. These substances present unique physicochemical properties that can influence their suitability as density CRM. For instance, ethylene glycol is known for its low toxicity and favorable density characteristics, while tetrachloroethylene is recognized for its stability but poses significant health risks. The evaluation of these candidates through the AHP framework highlights their strengths and weaknesses and provides insights into the trade-offs involved in the selection process.

This study's results underscore the AHP approach's effectiveness in providing a structured and objective framework for selecting suitable CRM for density measurements. By balancing metrological requirements with other relevant considerations, the AHP facilitates informed decision-making that aligns with accuracy, safety, and environmental sustainability goals. The findings contribute to developing certified reference materials at national density standard laboratories, reinforcing the laboratory's commitment to advancing metrological standards and practices. Moreover, as the demand for high-quality CRM continues to grow in various scientific and industrial fields [10], the insights gained from this study will play a pivotal role in enhancing the integrity of density measurements and supporting the advancement of metrology in general.

II. MATERIALS AND METHODS

The methodological framework employed in this study to evaluate and rank candidate substances for CRMs in density measurements integrates the AHP for multicriteria decision-making. This methodology encompasses the selection of criteria, candidate substances, the AHP process, and the evaluation of results.

A. Selection of criteria

The criteria were selected based on their relevance to hydrostatic weighing principles and compliance with the ISO 17034 standard for reference materials. The initial criteria include:

Density Value: The primary characteristic for CRMs in density measurements. The selected substances must exhibit well-defined and stable density values.

Toxicity: An assessment of the potential health risks associated with each substance. Lower toxicity is preferred to ensure safety in handling and use.

Viscosity: The fluidity of the substance at various temperatures, affecting the accuracy of density measurements.

Corrosivity: The potential of a substance to corrode materials, which can impact storage and measurement equipment.

Vapor Pressure: The tendency of a substance to evaporate, influencing its stability and handling.

Surface Tension: Affects the behavior of liquids in contact with other materials, impacting measurement accuracy.

Hygroscopicity: The ability of a substance to absorb moisture from the air, which can alter its density.

Flammability: The risk of fire associated with the substance, affecting safety during handling and storage.

Ignition Point: The temperature at which a substance ignites, contributing to safety considerations.

Thermal Expansion and *Compressibility Coefficients*: These properties influence density measurements under varying temperature and pressure conditions.

Purity: The degree of contamination or presence of impurities, which can affect density values.

Ease of Acquisition: The availability of the substance in sufficient quantities for use as a CRM.

Reactivity: The tendency of a substance to undergo chemical reactions, which can affect its stability and reliability as a CRM.

These criteria provided a comprehensive framework for evaluating potential candidate substances, balancing metrological requirements with practical and environmental considerations.

B. Selection of Candidate Substances

A preliminary list of candidate substances was compiled based on their physicochemical properties and relevance to density standards. The initial substances considered in this study include:

Ethylene Glycol: A common industrial chemical with a well-defined density.

Tetrachloroethylene: A solvent with stable properties, often used in density measurements.

Dodecane: A straight-chain alkane with known density characteristics.

FC-40: A fluorinated liquid known for its low toxicity and stable density.

Saline Solutions (Brines): Mixtures of water and salts with variable density.

Water-Glycerin Mixtures: Blends with adjustable density based on composition.

Dichlorotoluene: A solvent with specific density values and low volatility.

Bromobenzene: A dense aromatic compound with established properties.

Dimethyl Phthalate: An ester with defined density characteristics.

The selected candidate substances were evaluated against the criteria to determine their suitability as CRM for density measurements.

C. Analytic Hierarchy Process (AHP)

The Analytic Hierarchy Process (AHP) is a structured technique for organizing and analyzing complex decisions, based on mathematics and psychology. It allows decision-makers to model a complex problem in a hierarchical structure, enabling the evaluation of various alternatives against a set of criteria. The AHP involves the following steps:

1. *Define the problem and determine the goal*. The primary objective of this study is to identify and rank candidate substances that can serve as CRM for density measurements. This study aims to select the most suitable candidate substances for CRM in density measurements.
2. *Structure the hierarchy*. The hierarchy for this decision-making process is structured as follows: **Goal**: Selection of suitable CRM for density measurements. **Criteria**: for example: density value, toxicity, vapor pressure, surface tension, hygroscopicity, compressibility coefficient, etc. **Alternatives**: for example: ethylene glycol, tetrachloroethylene, dodecane, FC-40, etc.
3. *Conduct pairwise comparisons*. Pairwise comparisons were conducted for each criterion to determine their relative importance (or preference, or possibility). A scale of 1 to 9 was used, where: 1 = equal importance; 3 = moderate importance of one over another; 5 = strong importance; 7 = very strong importance; 9 = extreme importance. Intermediate values (2, 4, 6, 8) were used to express values between the judgments. The pairwise comparison matrix was constructed for the criteria, and the same process was applied to compare the candidate substances (alternatives) against each criterion.
4. *Calculate priority weights*. The priority weights for each criterion were calculated using the eigenvalue method. The following steps were taken to derive the weights: a) compute the sum of each column in the pairwise comparison matrix; b) normalize the matrix by dividing each entry by the sum of its column; c) calculate the average of each row (of the normalized matrix) to obtain the priority weights; d) check the consistency of the pairwise comparisons using the consistency ratio (*CR*). A *CR* lower than or equal to 0.1 indicates acceptable consistency.
5. *Aggregate the results*. The final ranking of the candidate substances was determined by aggregating the priority weights of each substance across all criteria. For each substance, the weighted sum was calculated by multiplying the priority weight of each criterion by the corresponding evaluation score of the substance against that criterion. The formula for the final score of each substance is as follows: Final score = Σ (W_{Ci} * $W_{Aj\text{-}Ci}$), where W_{Ci} is the weight of the i-th criterion, while $W_{Aj\text{-}Ci}$ is the weight of the j-th alternative concerning i-th criterion. The substances were ranked based on their final scores when summed over all criteria.

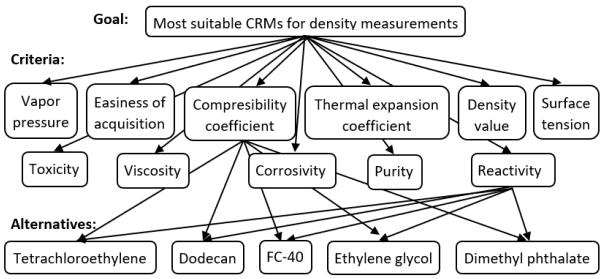


Fig. 1. Decision tree for CRMs hierarchy. Only two of the eleven criteria-alternatives connections are shown for clarity.

All calculations involved in the AHP methodology were performed using the free software SuperDecisions™, which has been validated [12] and is available free online [13]. However, some alternatives yield the same numerical results [14].

Among the authors, an expert specialist in density metrology and reference material development determined the importance of criteria and pairwise judgments. These were guided by [4] requirements, literature-reported properties, safety, handling, and practical use as density reference material. The CR ensured acceptable coherence of the comparisons.

III. RESULTS AND DISCUSSION

Using the methodological framework described in Section II, the following results were obtained.

A. Criteria weights

Some criteria were discarded due to their limited relevance to the selection process. For instance, factors related to material ignition were deemed less relevant for density measurements, resulting in the final retention of 11 criteria.

One goal, eleven criteria and five alternatives for the selection of density CRM are shown in Figure 1.

The retained criteria and their weights derived from the 55 pairwise comparisons are presented in Table 1. The AHP methodology yielded an inconsistency ratio (*CR*) of 3.18%, indicating a high level of consistency in the pairwise comparisons during the evaluation process. This low inconsistency ratio reinforces the reliability of the weights assigned to each criterion.

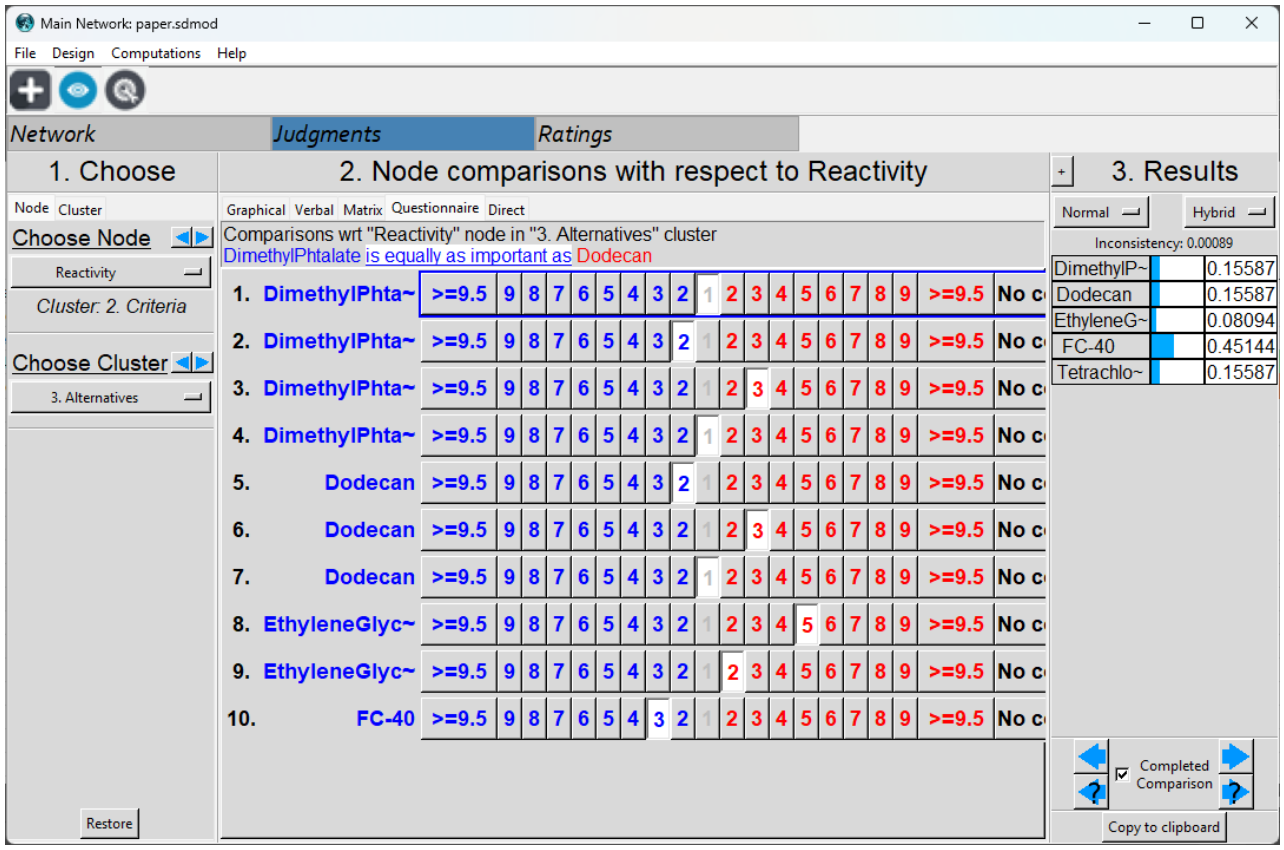


Fig. 2. SuperDecisions™ screenshoot. Ten pairwise comparisons of the five candidate substances with respect to the "Reactivity" criterion. The inconsistency value is shown in the upper-right area.

Table 1. Criterion weights for density CRM selection.

	Criterion	W_{Ci}
C1	Compressibility coefficient	0.062
C2	Corrosivity	0.064
C3	Density value	0.244
C4	Ease of acquisition	0.037
C5	Purity	0.156
C6	Reactivity	0.086
C7	Surface tension	0.035
C8	Thermal expansion	0.086
C9	Toxicity	0.115
C10	Vapor pressure	0.073
C11	Viscosity	0.043

The results highlight the importance of criteria such as density value, toxicity and purity as significant factors, reflecting the increasing emphasis on safety and quality in selecting CRM. Including economic and practical considerations, such as ease of acquisition, further enhances the relevance of the findings to real-world applications.

While not the most heavily weighted, the ease of acquisition criterion remains crucial in ensuring that selected CRM can be readily sourced and utilized in laboratory settings. This consideration is vital for laboratories facing budget, availability, and regulatory compliance constraints.

B. Candidate substances weights

The final list of candidate substances was reduced to five. Due to their inherent complexity, discarding mixtures (e.g., brine) was straightforward. The pairwise comparison matrices for each criterion were constructed to systematically evaluate how each substance performed relative to the others (see Figure 2).

Table 2 summarizes the pairwise comparison results, illustrating rankings across different criteria, in addition to the inconsistency ratio. Notably, the matrices revealed that certain substances consistently outperformed others in specific criteria, while in other cases, the rankings were reversed. This shows the complexity of the decision-making process, particularly when subjective criteria are involved (e.g., ease of acquisition).

Table 2. Alternatives' weights concerning each criterion, $W_{Aj\text{-}Ci}$. DMP = dimethyl phthalate, DCN = dodecane, EG = ethylene glycol, TCE = tetrachloroethylene, CR = inconsistency ratio (%).

	DMP	DCN	EG	FC-40	TCE	*CR*
C1	0.097	0.080	0.063	0.675	0.084	7.3
C2	0.120	0.212	0.141	0.422	0.106	2.6
C3	0.166	0.034	0.064	0.572	0.165	7.2
C4	0.231	0.231	0.231	0.077	0.231	0.0
C5	0.131	0.131	0.169	0.329	0.241	1.7
C6	0.156	0.156	0.081	0.451	0.156	0.1
C7	0.231	0.137	0.308	0.114	0.209	0.7
C8	0.231	0.164	0.262	0.123	0.197	1.2
C9	0.273	0.273	0.091	0.273	0.091	0.0
C10	0.297	0.297	0.297	0.083	0.024	9.5
C11	0.042	0.348	0.037	0.135	0.438	1.4

C. Ranking of candidate substances

The final step in the AHP evaluation was to calculate the overall weighting of each candidate substance. This was accomplished by summing the products of the normalized weights of each criterion and the respective performance scores of the substances in those criteria. The results of this analysis are presented in Table 3.

Table 3. Final hierarchy of candidate substances.

Substance	Preference
FC-40	0.359
Dimethyl phthalate	0.181
Tetrachloroethylene	0.167
Dodecane	0.160
Ethylen glycol	0.137

A short one-at-a-time sensitivity check was conducted in SuperDecisions to assess the robustness of the final ranking with respect to the criterion weights. For each retained criterion, its priority was varied over the interval 0.01–0.99, and the resulting priorities of the five candidate substances were observed. The sensitivity plots showed that FC-40 remained the highest-ranked alternative across the tested variations, indicating that the main conclusion is not driven by the particular value assigned to a single criterion weight. Thus, the final hierarchy can be considered robust within the explored range of weighting scenarios.

FC-40 emerged as the top-preferred substance, with almost 36 % preference over the other substances. This substance demonstrated superior performance across several key criteria, particularly in density value, purity, and reactivity, the most important criteria among the eleven considered.

IV. CONCLUSIONS

Applying the AHP methodology to select CRM for density measurements represents a significant advancement. By systematically evaluating candidate substances against a comprehensive set of criteria, this study provides a structured framework that balances metrological accuracy with economic, practical, and environmental considerations. The findings underscore the importance of a multifaceted approach to CRM selection, ensuring that the materials meet technical standards and align with broader safety and sustainability goals.

Including economic and practical aspects in the decision-making process is particularly noteworthy. Moreover, the practical applicability of the selected CRM cannot be overstated. Laboratories require materials that meet metrological standards and can be handled and stored without excessive risk. This study's findings serve as a reminder that selecting a CRM is not merely a technical exercise but also entails practical implications for laboratory operations. The criteria of toxicity, reactivity, and environmental impact should be integral to the decision-making process. The results of this study highlight the importance of considering these factors, as demonstrated by the comparative analysis of candidate substances.

While robust, the AHP methodology relies on experts' subjective judgments during pairwise comparisons. Future research could explore integrating additional decision-making frameworks or hybrid approaches that combine AHP with other methodologies, such as fuzzy logic or multi-objective optimization, to enhance the robustness of the decision-making process.

Additionally, expanding the candidate pool to include a broader range of substances could yield further insights into the comparative advantages and disadvantages of various materials. Future studies could also investigate the long-term stability and performance of the selected CRM in real-world applications, providing empirical data to support the research's theoretical findings.

REFERENCES

[1] K. Nishihashi, A. Waseda, Y. Kondo, Y. Bitou, N. Kuramoto, "Accurate density measurement of a small solid sample using a combination of hydrostatic weighing and pressure-of-flotation methods", Metrologia, 62, 2025, 015006.

[2] M-R. Ríos-Gutiérrez, O-J. Purata-Sifuentes, H-L.

González-Gómez, E. Funes-Rodríguez, H. López-Gutiérrez, “A study on the geometry of sinkers used for calibration of hydrometers with the ring method”, Journal of Physics: Conf. Series, 1065, 2018, 042056.

[3] M. McLinden, L. Bernardini, M. Richter, “A hydrostatic comparator for the density determination of solid objects”, Metrologia, 62, 2025, 025003.

[4] International Organization for Standardization, “ISO 17034:2016 General requirements for the competence of reference material producers”, ISO, 2016.

[5] M. Sargent, “The provision and use of traceability statements for reference materials”, Accreditation and Quality Assurance, vol. 25, 2020, pp. 367–372.

[6] T. L. Saaty, “How to make a decision: The Analytic Hierarchy Process”, European Journal of Operational Research, vol. 48, 1990, pp. 9-26.

[7] D. K. Aswal, S. Yadav, T. Takatsuji, P. Rachakonda, H. Kumar, “Handbook of Metrology and Applications”, Springer, 2023.

[8] J. S. Kane, The Use of Reference Materials: A Tutorial. Geostandards Newsletter, 25, 2001, pp.7-22. https://doi.org/10.1111/j.1751-908X.2001.tb00784.x

[9] B. King, “The selection and use of reference materials”, Accred. Qual. Assur., 8, 2003, pp. 429-433.

[10] F. Ulberth, “Certified reference materials for inorganic and organic contaminants in environmental matrices”, Anal. Bioanal. Chem., 386, 2006, pp. 1121-1136.

[11] J. K. Taylor, “Handbook for Standard Reference Materials Users”, NIST Special Publication 260-100, 1985.

[12] E. Mu, M. Pereyra-Rojas, “Practical decision making using super decisions v3: An introduction to the analytic hierarchy process”, Springer, 2017.

[13] R. W. Saaty, T. L. Saaty., "Super decisions. Software for Decision Making with Dependence and Feedback”, 2003, https://www.superdecisions.com/downloads/

[14] K. D. Goepel, “Implementation of an Online Software Tool for the Analytic Hierarchy Process (AHP-OS)”, International Journal of the Analytic Hierarchy Process, Vol. 10, Issue 3, 2018, pp. 469-487, https://doi.org/10.13033/ijahp.v10i3.590

2026 IMEKO Joint Conference
TC8 - TC11 - TC24
Metro Manila, Philippines, August 26-29, 2026

A Traceable Smart Meteorological Research Station for High-Accuracy Monitoring: Edge Computing, M2M Communication and Dynamic Data Science Models

Álvaro Silva Ribeiro[1], Catarina Simões[1], Gustavo Esteves Coelho[1], Luís Lages Martins[1]

[1] *National Laboratory for Civil Engineering (LNEC), Lisbon, Portugal*

***Abstract* – This paper presents a traceable smart meteorological research station developed at LNEC to support high-accuracy, long-term climate monitoring. The system integrates high-precision sensors with a calibration framework aligned with TIC principles to ensure metrological traceability and data quality. It combines edge computing and M2M communication for autonomous operation, high-frequency data acquisition, and efficient transmission. A dynamic data science framework enables real-time validation, anomaly detection, and adaptive quality control. The platform enhances reliability, scalability, and integration with environmental networks, strengthening climate research and supporting advanced analysis of atmospheric processes and extreme events.**

I. BACKGROUND AND SYSTEM CONCEPT

The increasing frequency and intensity of extreme weather events, such as heatwaves, intense precipitation, and urban flooding, are placing unprecedented pressure on cities and critical infrastructures. These phenomena, climate variability and change [1,2], require high-quality meteorological observations to support timely and informed decision-making [3,4]. In urban environments, where population density and infrastructure complexity amplify vulnerability, the availability of accurate, high-resolution, and traceable data becomes essential for risk assessment, early warning systems, and resilient planning strategies.

Traditional meteorological stations, while valuable, often present limitations in terms of spatial representativeness, temporal resolution, calibration consistency, and long-term data comparability [4,5]. These constraints hinder their effectiveness in supporting advanced applications such as real-time urban management, adaptive infrastructure design, and climate-responsive urban planning.

In the context of smart cities, the integration of sensing technologies, digital infrastructures, and data analytics enables a paradigm shift toward proactive and data-driven decision-making [6–8]. Smart urban systems rely on continuous environmental monitoring combined with automated processing and communication capabilities to enhance situational awareness and operational efficiency. Foundational work on wireless and environmental sensor networks supports this paradigm [9,10]. However, ensuring the reliability and scientific validity of such systems requires the incorporation of metrological traceability, robust data validation mechanisms, and scalable architectures [11,12].

This work introduces a traceable smart meteorological research station designed to address these challenges. The proposed system combines high-precision sensing, edge computing, and Machine-to-Machine (M2M) communication within a unified framework that supports high-frequency data acquisition and intelligent processing. By aligning metrological rigor with advanced digital technologies, the system aims to improve the quality, usability, and impact of meteorological data to support urban planning, infrastructure management, and climate resilience strategies in smart city environments.

II. SYSTEM ARCHITECTURE OF THE SMART METEOROLOGICAL STATION

The smart meteorological research station developed at LNEC is designed as a metrologically controlled infrastructure capable of delivering high-quality, traceable environmental data to support research in civil engineering and climate-related applications. The system architecture integrates sensing, acquisition, communication, and processing components, ensuring both measurement accuracy and operational autonomy.

Figure 1 illustrates the deployed station, which was conceived to address limitations in conventional meteorological networks, particularly regarding precipitation measurement [3,4]. The widespread use of tipping bucket rain gauges, although suitable for operational monitoring, often lacks the accuracy required for metrological research [13,15]. This limitation becomes

critical when analyzing short-duration, high-intensity precipitation events [1,2,16], which are increasingly relevant for hydrological modeling and urban flood risk assessment [17,18].



Fig. 1. LNEC research meteorological station.

At the core of the sensing layer is an SI-traceable gravimetric precipitation weighing gauge, based on the primary principle of mass measurement. This approach ensures direct traceability to the SI [11,12], enabling high-accuracy precipitation measurements. The station also includes complementary sensors for air temperature, relative humidity, atmospheric pressure, wind speed, and wind direction. These variables provide essential context for meteorological characterization and allow the assessment of external influence quantities affecting precipitation measurements, such as wind-induced under catch [15,19].

The data acquisition system operates at a high temporal resolution, with a sampling interval of 10 seconds. This enables the capture of fine-scale variability in precipitation dynamics, which is often lost in conventional systems using longer aggregation periods [17,18]. The high-frequency data stream supports detailed event characterization and enhances the detection of short, intense precipitation bursts.

From a system perspective, the architecture incorporates a Machine-to-Machine (M2M) communication layer that ensures continuous, reliable data transmission and interoperability with external platforms [8]. In parallel, edge computing capabilities enable local processing of the acquired data, supporting preliminary validation and efficient data handling before transmission [6,7,20].

The collected dataset is structured to preserve the native temporal resolution, ensuring consistency with the defined measurand and avoiding distortions associated with temporal aggregation. Extreme precipitation events are identified using a percentile-based approach, with the 95th percentile of 10-second accumulated precipitation values serving as a threshold. This method enables the detection of high-intensity precipitation events, which are critical for understanding urban drainage performance and flood risk in smart city environments.

Overall, the system architecture combines metrological rigor, high-resolution sensing, and intelligent data handling to provide a robust platform for advanced meteorological research and urban climate applications.

III. PRELIMINARY RESULTS FROM HIGH-INTENSITY PRECIPITATION EVENTS

To demonstrate the practical capabilities of the developed research station, preliminary measurements obtained during high-intensity precipitation events were analysed. Figure 2 presents a representative precipitation event recorded with the SI-traceable gravimetric weighing gauge operating at a sampling interval of 10 s. The event illustrates the capability of the system to capture rapid variations in precipitation intensity while maintaining high temporal resolution and metrological traceability.

The measurements reveal successive precipitation bursts with intensities exceeding the threshold adopted for extreme-event identification (95th percentile of the local distribution). Such high-frequency observations are particularly relevant for urban hydrology, where short-duration precipitation peaks strongly influence runoff generation and drainage system performance.

The results also demonstrate the stability of the weighing principle during rapidly varying precipitation conditions, providing continuous measurements without the discretization errors typically associated with tipping-bucket systems.

The research station obtained a full year of data in 2024, and applied to the full time series, considering only wet days with daily precipitation greater than 1 mm. From this data set, two samples wer extracted (see Figure 2), one (on the left) showing regular (non-extreme) precipitation and the other (on the right) related with the observation of an extreme precipitation event. The 95th percentile of precipitation intensity was calculated as 0,122 mm and used as the threshold for intense precipitation episodes.

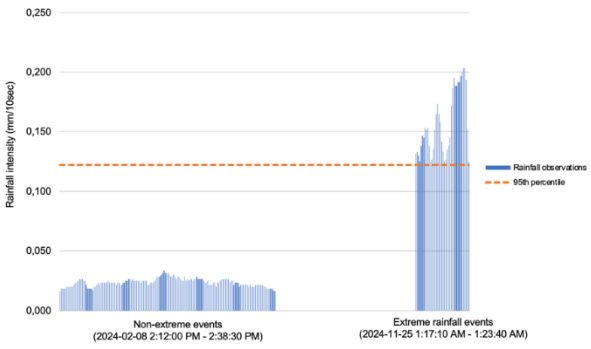


Fig. 2. Precipitation intensity events obsserved by LNEC research meteorological station showing a set of data of regular precipitation and a set of data related to an extreme event of precipitation

These preliminary results demonstrate the capability of the proposed SI-traceable gravimetric research station to discriminate precipitation dynamics with a level of detail

that is difficult to achieve using conventional monitoring systems. The combination of high temporal resolution (10 s sampling), continuous gravimetric measurement, and metrological traceability enables the clear identification and characterization of short-duration precipitation bursts associated with extreme precipitation events.

IV. METROLOGICAL TRACEABILITY AND DATA MANAGEMENT FRAMEWORK

This section presents the metrological foundations and data management strategies that ensure the reliability, accuracy, and long-term usability of the measurements from the LNEC meteorological station. The system uses a rigorous traceability framework. All measurements are linked to the International System of Units (SI) with well-defined calibration procedures and reference standards [11,12]. This aligns with Testing, Inspection, and Certification (TIC) principles.

A central component of this framework is calibrating the gravimetric precipitation weighing gauge using a dedicated method developed at LNEC (Figures 3 and 4). This approach relies on controlled gravimetric measurements. Known masses of water are applied under laboratory conditions to establish a direct, traceable relationship between the measured signal and accumulated precipitation. The method enables high-accuracy calibration across a range of intensities, including conditions representative of extreme events.

In parallel, wind speed and direction sensors are calibrated in a controlled wind tunnel facility (Figure 5 and Figure 6), also at LNEC. This allows precise characterization of sensor response under known flow conditions. These procedures reduced measurement uncertainty and improved confidence in the observed data, especially for variables that influence precipitation measurement accuracy, such as wind-induced effects [19].

The traceability chain is complemented by systematic uncertainty evaluation [11] and hydrological uncertainty frameworks [21], periodic recalibration, and continuous monitoring of sensor stability. These practices are essential to maintain the comparability and consistency of long-term datasets, which are critical for climate studies and infrastructure design [1,2].

From a data management perspective, the system supports high-frequency data acquisition with synchronized measurements at a 10-second interval. Data streams are structured to preserve temporal integrity and are enriched with metadata describing sensor status, calibration history, and environmental conditions. Storage and transmission protocols are designed to ensure data integrity and accessibility.

Edge computing enables real-time implementation of several complementary anomaly detection algorithms and quality control [6,7,20]. Range validation verifies compliance with physically admissible limits defined by WMO recommendations. Temporal consistency tests identify abrupt changes using moving-window statistics and z-score analysis. Multivariate consistency is evaluated through correlation analysis between precipitation, wind speed, humidity and atmospheric pressure. Isolation Forest and Density-Based Spatial Clustering will be used for unsupervised identification of abnormal sensor behaviour and unexpected environmental patterns. These algorithms operate locally at the edge device, allowing suspicious observations to be flagged before transmission while preserving the original measurements for traceability purposes [5,22].

Finally, a data science layer is implemented to enhance data usability and scientific value. Dynamic modeling techniques are applied to process high-frequency meteorological data, supporting data filtering, fusion of multiple variables, and automated quality assurance [23]. These methods improve dataset consistency, enable robust detection of extreme events, and facilitate advanced analyses relevant to urban climate applications. Together, the integration of metrological rigor and intelligent data processing establishes a reliable, scalable framework for high-quality environmental monitoring.

Table 1. Accuracy for main quantities measured by the multiparametric sation and precipitation weighing gauge.

Measuring instruments	Quantities	Accuracy
Multiparametric station	Atmospheric pressure	± 0,5 hPa at 0 °C until + 30 °C ± 1 hPa at − 52 °C until + 60 °C
	Air Temperature	± 0,3 °C
	Relative Humidity	± 3 % rh at 0 % rh until 90 % rh ± 5 % rh at 90 % rh until 100 %rh
	Wind speed	± 3 % at 10 m/s
	Wind direction	± 3,0 ° at 10 m/s
	Precipitation intensity	Better than 5 %, weather-dependent
Precipitation weighing gauge	Precipitation intensity	± 0,1 mm/min
	Accumulated precipitation	± 0,1 mm

Table 2 summarizes an example of the main contributors to an uncertainty budget of the gravimetric precipitation measurement. The dominant components arise from the calibration of the weighing system and repeatability during laboratory calibration. The combined uncertainty was evaluated according to the GUM methodology.

Table 2. Example of an uncertainty budget for accumulated precipitation measurement

Source of uncertainty	Estimate	PDF & type
Load cell calibration	0.03 mm	Normal (type B)
Resolution	0.02 mm	Uniform (type B)
Water density correction	0.01 mm	Normal (type B)
Collection area calibration	0.02 mm	Normal (type B)
Temperature effects	0.02 mm	Normal (type B)
Repeatability	0.03 mm	Type A
Combined standard uncertainty	0.06 mm	—
Expanded uncertainty (k=2)	0.12 mm	—



Fig. 3. Mass calibration of a precipitation weighinh gauge.

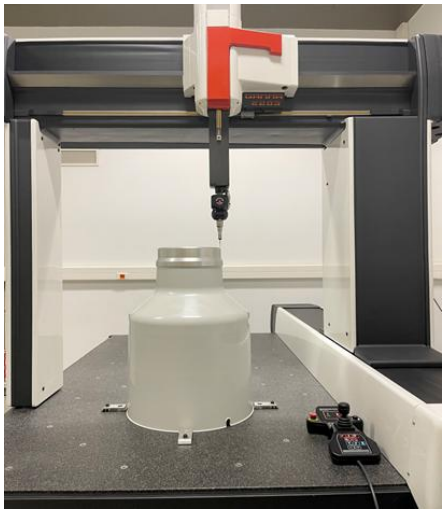


Fig. 4. Calibration of the cylinder collection diameter using a CMM 3D at LNEC.



Fig. 5. LNEC's Wind Tunnel no. 1 calibration area.



Fig. 6. Calibration of the multiparametric station in LNEC's wind tunnel no. 1.

V. R&DI MANAGEMENT, SCALABILITY, AND INTEGRATION

The developed meteorological station is not only a measurement system but also a strategic research and innovation (R&DI) infrastructure designed to support experimental development, methodological validation, and multidisciplinary collaboration. Its implementation at LNEC provides a controlled and traceable environment where new sensing technologies, calibration methods, and data processing approaches can be systematically tested and validated under both laboratory and real-world conditions.

From an R&DI perspective, the infrastructure enables continuous improvement of measurement methodologies, particularly in high-resolution precipitation monitoring and the characterization of extreme events. The integration of metrological traceability with advanced digital technologies creates a platform that directly innovates sensing, calibration, and data analytics [6,7,20] into

improved measurement practices and more reliable datasets. This is particularly relevant for supporting research in urban hydrology, climate modelling, and resilience planning [1,2,23].

Scalability is a key design feature of the system. The modular architecture enables the integration of additional sensors, expansion into distributed monitoring networks, and adaptation to diverse environmental contexts [3,23]. This flexibility supports the deployment of similar traceable stations in other locations, enabling the creation of harmonized observation networks that produce comparable, high-quality datasets across different regions. Such scalability is essential for addressing spatial variability in extreme weather phenomena and for supporting large-scale climate studies.

Interoperability is ensured through standardized communication protocols and data structures, facilitating integration with external platforms, environmental databases, and smart city infrastructure. The M2M communication framework enables seamless data exchange with other systems [8], while the structured metadata approach supports data discoverability, reuse, and long-term curation. This connectivity enhances the station's role within broader environmental observation ecosystems.

From a management standpoint, the infrastructure supports long-term sustainability through systematic calibration, data governance practices, and clear operational procedures. It enables efficient coordination among multidisciplinary teams, including experts in metrology, meteorology, data science, and engineering. Furthermore, the availability of high-quality, traceable datasets strengthens institutional capacity for evidence-based decision-making and supports collaboration with external stakeholders, including public authorities and urban planners.

Overall, the infrastructure represents a scalable, integrated platform that bridges measurement science and digital innovation, advancing reliable environmental monitoring systems and supporting the development of resilient, data-driven smart city strategies.

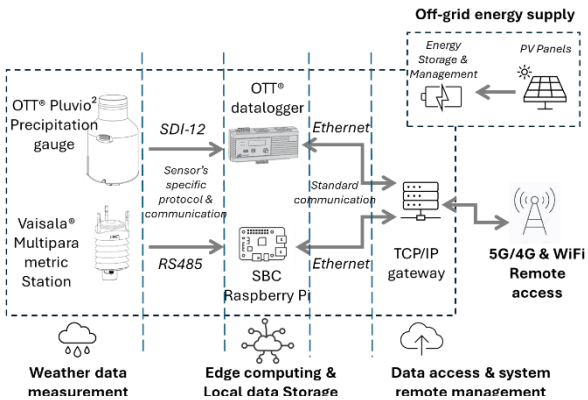


Fig. 6. Smart meteorological station system for remote real-time weather monitoring.

VI. CONCLUSIONS AND FUTURE WORK

This work presented a traceable smart meteorological research station designed to address current challenges in high-accuracy environmental monitoring, particularly in the context of extreme events and data-driven decision-making. The main contributions lie in integrating metrological traceability, high-resolution sensing, and intelligent data processing within a unified and scalable infrastructure. The implementation of SI-traceable calibration procedures, including advanced gravimetric methods for precipitation and controlled wind tunnel calibration for airflow measurements, significantly enhances measurement accuracy, reliability, and long-term comparability.

The proposed system demonstrates the advantages of combining sensing technologies with edge computing and Machine-to-Machine (M2M) communication to enable autonomous operation, real-time data validation, and efficient handling of high-frequency datasets. The incorporation of data science techniques further improves data consistency and usability, supporting robust identification of extreme events and enhancing the overall scientific value of the measurements.

Preliminary experimental observations obtained during intense precipitation events confirm the capability of the proposed station to acquire stable, high-frequency precipitation measurements while preserving metrological traceability. The results demonstrate the practical applicability of the developed infrastructure for monitoring short-duration extreme precipitation events and provide a foundation for future AI-assisted analysis and predictive environmental monitoring. These features are particularly relevant for applications in urban climate analysis, flood risk assessment, and smart city management, where timely and trustworthy data are essential.

Future work will focus on extending the system's capabilities by integrating advanced artificial intelligence-based models for predictive analytics and anomaly detection. Additional efforts will be directed toward further automation of calibration procedures, reducing operational effort while maintaining metrological rigor. The expansion of the infrastructure into distributed sensor networks will also be explored, enabling broader spatial coverage and supporting large-scale environmental monitoring initiatives. Finally, alignment with emerging international standards and interoperability frameworks will be pursued to facilitate data sharing, comparability, and integration within global observation systems.

REFERENCES

[1] IPCC (2021). *Climate Change 2021: The Physical Science Basis. Working Group I Contribution to the IPCC Sixth Assessment Report*

[2] Fowler, H. J., et al. (2021). Anthropogenic climate change and extreme precipitation. *Nature Reviews Earth & Environment*, ***2(2)**, 107-122.*
[3] WMO (2018). *Guide to Instruments and Methods of Observation. Volume V – Quality Assurance and Management of Observing Systems*. Geneva, Switzerland, World Meteorological Organization, 121pp.
[4] Michelson, D. B. (2004). Systematic correction of precipitation gauge observations using analysed meteorological variables. *Journal of Hydrology*, ***290(3–4)**, 161–177.*
[5] Durre, I., et al. (2010). Comprehensive automated quality assurance of daily surface observations. *Journal of Applied Meteorology and Climatology. **49(8)**, 1615-1633.*
[6] Satyanarayanan, M. (2017). The emergence of edge computing. *Computer, **50**, 30-39.*
[7] Shi, W., et al. (2016). Edge computing: Vision and challenges. *IEEE Internet of Things Journal, **3(5)**, 637-646.*
[8] Li, S., Da Xu, L., & Zhao, S. (2019). 5G Internet of Things: A survey. *IEEE Internet of Things Journal, **5(3)**, 1649–1663.*
[9] Akyildiz, I. F., et al. (2002). Wireless sensor networks: A Survey. *Computer Networks, **38**, 393-422.*
[10] Hart, J. K., & Martinez, K. (2006). Environmental Sensor Networks: A Revolution in the Earth System Science? *Earth-Science Reviews*, ***78**, 177-191.*
[11] JCGM 100:2008. *Evaluation of Measurement Data—Guide to the Expression of Uncertainty in Measurement (GUM).* Joint Committee for Guides in Metrology.
[12] JCGM 200:2012. *International vocabulary of metrology (VIM).* Joint Committee for Guides in Metrology.
[13] Habib, E., Krajewski, W. F., & Kruger, A. (2012). Performance evaluation of tipping-bucket rain gauges under different precipitation intensities. *Journal of Hydrology, **430–431**, 77–90.*
[14] Ciach, G. J. (2003). Local random errors in tipping-bucket rain gauge measurements. *Journal of Atmospheric and Oceanic Technology, **20(5)**, 752–759.*
[15] Pollock, M. D. et al. (2018). Quantifying and mitigating wind-induced undercatch in precipitation measurements. *Water Resources Research, **54**(6), 3863–3875.*
[16] Sevruk, B., & Hamon, W. R. (1984). International comparison of national precipitation gauges. *World Meteorological Organization (WMO), Instruments and Observing Methods Report No. 17, WMO/TD-No. 38.*
[17]. Goodison, B. E., Sevruk, B., Klemm, S., & Metcalfe, J. R. (1998). WMO solid precipitation measurement intercomparison: Final report. *World Meteorological Organization (WMO), Instruments and Observing Methods Report No. 67, WMO/TD-No. 872.*
[18] Villarini, G., & Krajewski, W. F. (2010). Review of the different sources of uncertainty in single-polarization radar-based estimates of precipitation. *Surveys in Geophysics**, 31(1)**, 107–129.*
[19] Ochoa-Rodríguez et al. (2015). Impact of spatial and temporal resolution of precipitation inputs on urban hydrological modelling outputs: A Multi-Catchment Investigation. *Journal of Hidrology**, 531**, 389–407.*
[20] Cristiano, E., ten Veldhuis, J. A. E., & van de Giesen, N. (2017). Spatial and temporal variability of precipitation and their effects on urban drainage systems. *Journal of Hydrology**, 547**, 489–498.*
[21] Kochendorfer, J., Rasmussen, R., Thériault, J. M., Becker, N., Menounos, B., & Rodell, M. (2017). The quantification and correction of wind-induced precipitation measurement errors. *Water Resources Research**, 53**, 3895–3927.*
[22] Beven, K. J., & Westerberg, I. (2011). On the problem of comparing model predictions and observational data in hydrology. *Hydrological Processes, **25**(23), 3407–3417.*
[23] McMillan, H. K., Krueger, T., & Freer, J. (2012). Benchmarking observational uncertainties for hydrology: Precipitation, river discharge and water quality. *Hydrology and Earth System Sciences, **16**, 1225–1238.*

2026 IMEKO Joint Conference
TC8 - TC11 - TC24
Metro Manila, Philippines, August 26-29, 2026

Prioritization of Packaging Safety Testing Services through Stakeholder Demand Analysis in the Philippine Packaging Industry

Harold E. Armario[1], Elyson Keith P. Encarnacion[1], Anne C. Alcantara[1], David J. Alcarde Jr.[1], Agaseve F. Del Rosario[1], Winnie P. Alejandro[1], Rizel Marie S.M. Ting[1], April Star L. Canonizado[1], Theressa A. Liclican[1]

[1] Department of Science and Technology, Industrial Technology Development Institute, Standards and Testing Division, Gen. Santos Avenue, Bicutan Taguig City, Metro Manila, Philippines
hearmario@itdi.dost.gov.ph

***Abstract* – The development of testing laboratories for the packaging industry requires alignment with stakeholder needs to ensure relevance and sustainability. This study evaluated the priorities of 75 stakeholders for local technical services related to food contact article safety through a structured survey involving packaging manufacturers and food and beverage brand owners. Plastic packaging was the most frequently handled material (46.0%), followed by paper packaging (25.0%). Despite broad recognition of packaging safety testing, routine laboratory engagement remained limited, with 53.3% of respondents conducting chemical testing only once per year. Testing was primarily driven by quality assurance and control (41.1%), customer requirements (33.1%), and regulatory compliance (25.8%). Migration testing (32.3%), heavy metal determination (16.7%), and barrier property evaluation (12.5%) emerged as priority analytical services. These findings reveal a gap between testing awareness and utilization, highlighting the need to strengthen laboratory capability and packaging safety infrastructure in the Philippines.**

Keywords: industry survey, packaging safety, regulatory compliance, stakeholder demand, sustainability

I. INTRODUCTION

The packaging industry plays a critical role in food safety, product quality, and regulatory compliance. Packaging acts as a barrier against contamination and helps preserve physicochemical and sensory properties, extending shelf life and reducing food loss [1–4]. However, food contact materials (FCMs), particularly polymer-based materials such as polyethylene (PE), polypropylene (PP), and multilayer laminates, can also be sources of chemical contamination due to the migration of additives, monomers, degradation products, and non-intentionally added substances (NIAS) into food [5–7]. Consequently, strict regulatory frameworks have been established to ensure that such migration does not pose risks to human health [8].

The increasing complexity of modern packaging systems has intensified the need for robust analytical methods and regulatory oversight. Studies report that common polymers can release micro- and nanoplastics, although the lack of harmonized analytical protocols limits reliable risk assessment [9]. Similarly, current methods often rely on non-specific migration measurements, particularly for organic contaminants, highlighting the need for standardized and more comprehensive analytical approaches [10]. The presence of largely unidentified NIAS, especially in PE, PP, and multilayer materials, further complicates risk evaluation and necessitates advanced analytical techniques [11,12]. This challenge is exacerbated by the growing use of recycled and emerging materials, which exhibit higher contamination levels, variability, and distinct chemical profiles [13–16].

In the Philippines, regulatory efforts such as FDA Administrative Order No. 2022-011 promote the safety evaluation of FCMs and alignment with international standards, including US 21 CFR and EU Regulation No. 10/2011 [17–19]. Despite these developments, local testing capacity remains underutilized. A survey by Del Rosario et al. Revealed substantial gaps between desired and actual testing practices among packaging-related companies, largely driven by cost constraints, limited accessibility, and limited awareness [20]. Testing is often conducted on an as-needed basis rather than as part of systematic quality assurance, indicating that the adoption of packaging safety testing services is still at an early stage.

Addressing these gaps requires aligning laboratory capabilities with industry needs through demand-driven prioritization. In this context, this study assesses stakeholder demand for packaging safety testing services in the Philippines by identifying priority analyses, evaluating current practices, and determining gaps between perceived importance and actual utilization. The findings aim to support strategic laboratory development, strengthen regulatory implementation, and enhance the national packaging safety framework.

II. MATERIALS AND METHODS

A. Study Design.

This study employed a cross-sectional descriptive survey to assess stakeholder demand for packaging safety testing services in the Philippine packaging industry, capturing current practices, testing needs, and perceived gaps in laboratory services.

B. Respondents and Sampling

A total of 75 stakeholders from packaging-related sectors participated, representing industries such as packaging manufacturing, food and beverage production, distribution and supply chains, and other packaging-dependent sectors. Participants were selected through purposive sampling, targeting companies actively involved in the production, use, or supply of packaging materials, ensuring responses from stakeholders directly engaged in packaging safety and testing activities.

C. Survey Instrument Development and Data Collection

A structured questionnaire was developed to collect quantitative and qualitative data on packaging safety testing, informed by regulatory requirements for food contact materials, common laboratory testing services, and prior industry engagements. It covered company profile, packaging materials, current testing practices, desired testing services, drivers and benefits of testing, and perceived barriers. The inclusion of both closed- and open-ended questions enabled a comprehensive assessment of stakeholder demand while capturing nuanced insights beyond predefined responses.

Data were collected through an online survey via Google Forms, enabling efficient distribution to packaging industry stakeholders. Participation was voluntary, with respondents informed of the study's purpose, and all responses were treated with strict confidentiality for research use only. Data were reviewed for completeness and consistency, and duplicate entries from the same organization were screened to ensure only relevant responses were included in the final dataset.

D. Data Analysis

Descriptive statistics were used to summarize survey responses and identify patterns in stakeholder practices, preferences, and testing needs. Frequency counts and percentage distributions described key variables such as packaging materials, testing practices, and drivers of testing. Analytical services were prioritized based on the proportion of respondents selecting each test, while comparative analysis of drivers (e.g., quality assurance, customer requirements, regulatory compliance) assessed their relative influence. This approach provided a quantitative basis for identifying priority testing areas and aligning laboratory capabilities with stakeholder needs.

III. RESULTS AND DISCUSSION

A. Demographics

As shown in Figure 1, most respondents were from the manufacturing/production sector, followed by academe and distribution, with smaller representation from brand owners, government, and other stakeholders.

The dominance of manufacturing respondents indicates that the survey captured key industry perspectives directly involved in material selection, processing, and quality assurance. They are primary users of packaging testing services responsible for safety and regulatory compliance. Participation from academe adds insights on research and method development, while distributors reflect supply chain considerations. As brand owners (e.g., food and beverage manufacturers) are also immediate users of packaging, there is a need to increase their population and participation in the survey to better capture the packaging testing landscape.

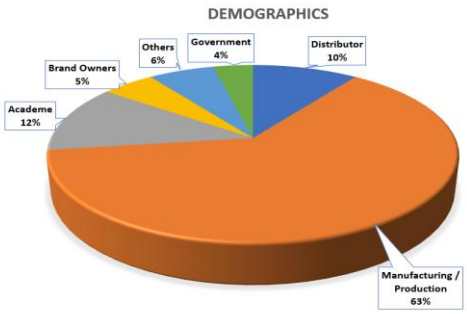


Fig. 1. Respondents Distribution Demographics

B. Packaging Materials Handled

Plastic packaging materials dominated the responses, followed by paper-based and metal packaging, with smaller contributions from glass, other materials, and rubber. This trend reflects the widespread use of plastics due to their versatility, cost-effectiveness, and functional performance [21], and indicates that stakeholders are primarily engaged with polymer-based systems. Supporting this observation, the study reported by Alejandro et.al. that a substantial proportion of LDPE food packaging samples in the Philippine market exhibited detectable levels of total UV-absorbing contaminants, with more than half exceeding regulatory limits [22].These materials also present more complex safety challenges, particularly in terms of chemical migration and non-intentionally added substances (NIAS), thereby driving demand for analytical testing services to address their diverse composition and potential for human exposure [23], as shown in Figure 2.

Paper-based materials account for a significant share, reflecting their continued relevance in sustainable packaging due to renewable sourcing, biodegradability, and higher recycling rates compared to plastics [24,25], as well as their growing role as plastic alternatives [26].

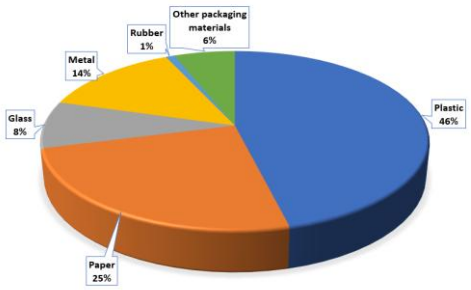


Fig. 2. Packaging Materials Handled

The presence of metal and glass further highlights material diversity, each with distinct safety considerations. Metal packaging may require protective coatings due to potential migration of substances such as bisphenol A and heavy metals [27,28], while glass, although generally stable, can still leach ions that require evaluation [29,30]. The smaller share of rubber and other materials suggests niche applications but underscores the need for broad analytical capabilities to address material-specific risks.

C. Frequency of Testing

Most respondents conduct packaging-related testing on an annual basis, followed by those performing it semiannually, monthly, or weekly, with only a few reporting irregular or uncertain practices. This pattern suggests that testing is largely compliance-driven and periodic rather than integrated into routine quality assurance.

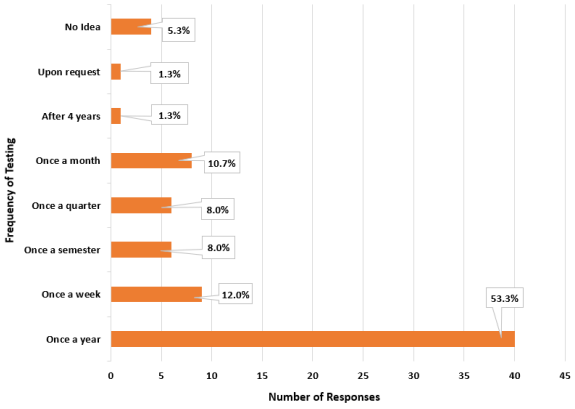


Fig. 3. Frequency of Testing

Although some stakeholders conduct more frequent testing, likely reflecting higher operational demands or stricter quality systems, these practices remain limited. Irregular and uncertain responses further highlight variability in testing behavior, likely influenced by cost, limited access to laboratory services, and gaps in technical awareness, as shown in Figure 3.

D. Drivers for Packaging Safety Testing

Consumer and regulatory concerns regarding chemical migration from food contact materials into food have driven the development of testing priorities that support risk management and regulatory control. Regulatory frameworks influence testing approaches across regions, with the European Union relying on migration limits and positive lists, the United States using premarket notifications and material specifications, and many Asian countries adopting less harmonized positive- or negative-list systems [31].

In contrast, Figure 4 shows that packaging safety testing is driven primarily by company quality assurance and control, followed by customer requirements, while regulatory requirements are cited least frequently. This suggests that testing practices are influenced more by internal quality systems and market expectations than by formal regulatory pressure. The limited role of regulation may reflect gaps in enforcement or awareness, highlighting the need to strengthen regulatory engagement and better align laboratory services with industry and policy requirements.



Fig. 4. Drivers for Packaging Safety Testing

E. Priority Testing Services

Testing Practices:

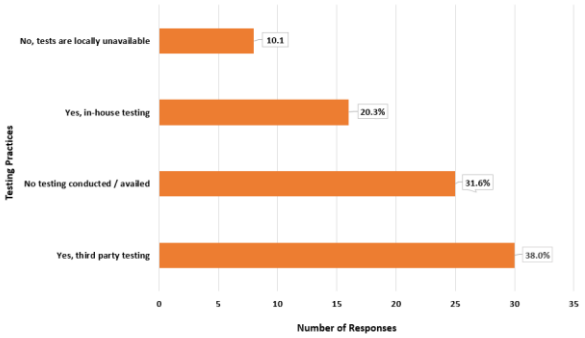


Fig. 5. Testing Practices

Stakeholders were asked how chemical testing is conducted for packaging products. As shown in Figure 5, most respondents rely on third-party laboratories, followed

by those who do not conduct testing. A smaller proportion perform in-house testing, while some reported that required tests are not locally available. These findings indicate strong dependence on external laboratories and limited local accessibility for routine packaging safety evaluation.

Among respondents conducting testing, either in-house or through third-party laboratories, overall migration testing was identified as the most commonly performed analysis (Figure 6), consistent with FDA Philippines requirements and its role as a general screening tool for material safety and regulatory conformity.

If Yes, Type(s) of Tests Conducted or Availed for Identified Packaging Products	
Physical Test (Burst, Edge Crush, Tensile)	8
Overall Migration Test	17
Barrier Properties (OTR / WVTR)	2
Heavy Metal Test	6
ROHS	1
Perfluoroalkyl Substances (PFAS)	1
Bisphenol A	1
Mineral Oils (MOSH/MOAH)	1
Other tests	5

Fig. 6. Conducted or Availed Tests for Packaging Products

Globally, testing priorities vary by jurisdiction. Phthalates and bisphenols are recognized as priority chemicals due to their endocrine-disrupting properties and migration risks. Europe has identified numerous high-priority substances used in packaging-related inks and adhesives [32], while Canada prioritizes contaminants such as phthalate esters, brominated flame retardants, and chloroparaffins [33]. These approaches highlight the growing emphasis on targeted contaminant testing beyond general migration assessments.

If No, Type(s) of Tests Desired for Identified Packaging Products	
Heavy and other Trace Metals e.g. Pb, Cd, Hg, Sb	16
UV Stabilizers	4
Overall Migration (Single Extraction)	21
Overall Migration (Multiple Extraction)	10
Alcohols e.g. Bisphenol A (BPA), Nonylphenol	6
Substances of Very High Concerns (SVHCs)	2
Volatile Organic Compounds e.g. Toluene	3
Barrier Properties (OTR / WVTR)	12
REACH	3
Halal testing	1
Esters e.g. Phthalates	2
Plasticizers	6
Organometallics	2
Non-Intentionally Added Substances (NIAS)	2
Aldehydes	2
Polyaromatic Hydrocarbons (PAH)	2
Mineral Oils (MOSH/MOAH)	2

Fig. 7. Desired test for Packaging Products

Among respondents not currently conducting testing, some reported that required analyses are not locally available. Despite this, strong demand exists for overall migration, heavy and trace metals, barrier properties, plasticizers, bisphenol A, and UV stabilizers, as well as advanced analyses such as NIAS, SVHCs, VOCs, and PAHs as shown in Figure 7.

The results show a clear gap between current testing practices and stakeholder demand. Testing is largely limited to overall migration and reliant on third-party laboratories, while many respondents report that required analyses are not locally available. Despite this, there is strong demand for both routine and advanced tests, highlighting limited local capacity and the need to expand accessible and comprehensive packaging safety testing.

Stakeholders were also asked about the perceived effects of packaging testing. As shown in Figure 8, packaging testing is primarily viewed as a tool for quality assurance and compliance, with improvements in product quality and regulatory conformance identified as the most recognized benefits. Business-related gains, such as increased customers and sales, were also noted, suggesting that testing enhances product credibility and market acceptance. However, market access benefits were less emphasized, indicating that testing is not yet fully leveraged for entry into regulated or export markets.

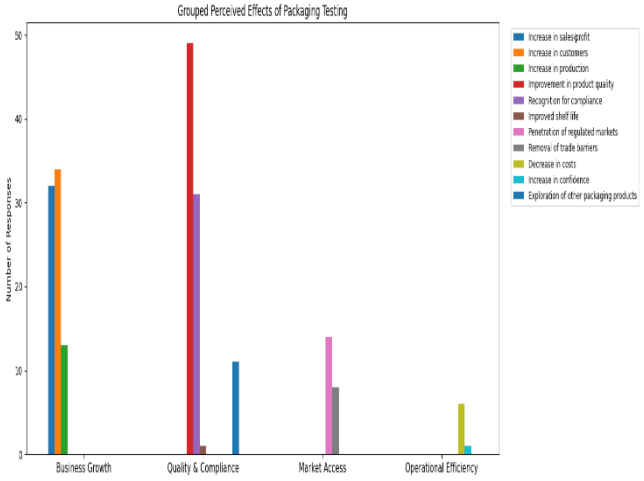


Fig. 8. Perceived Effects of Packaging Testing

The lowest perception is observed in operational efficiency, where responses suggest uncertainty on whether testing reduces costs or adds to operational burden. Overall, the results reinforce the previously identified gap: while stakeholders recognize the value of testing, limited access to comprehensive and advanced analyses constrains its full utilization for market expansion and process optimization.

F. Cost-benefit or Willingness-to-pay Analysis

To complement the stakeholder demand analysis, a preliminary economic assessment was conducted using the Packaging Safety Laboratory's (PSL) valuation model developed for packaging safety testing services. The model considers personnel services, supplies and reagents, equipment utilization, calibration, and utility costs to estimate the appropriate service fee for migration and other packaging-related analyses. This framework may likewise be applied to other priority testing services, including overall and specific migration analysis, OTR, WVTR, and other tests.

As an illustrative example, the estimated in-house service fee for PFAS analysis based on the valuation model is approximately Php 27,800.00 per test or sample. In comparison, an external laboratory quotation for the determination of PFOA and total PFAS content in three plastic samples amounts to Php 147,308.00, inclusive of service charges and value-added tax. While the two estimates are not directly equivalent in analytical scope and sample preparation, the comparison provides an indication that establishing in-house analytical capability may reduce testing costs and dependence on external laboratories, particularly when supported by sufficient testing demand. The results suggest that integrating stakeholder demand with preliminary economic considerations can provide a more practical basis for prioritizing investments in packaging safety laboratory infrastructure. Nevertheless, a comprehensive cost-benefit or willingness-to-pay analysis incorporating capital investment, annual operating costs, expected testing volume, and projected revenue is recommended for future studies.

IV. CONCLUSION

In conclusion, the findings show that while stakeholders in the Philippine packaging industry recognize the importance of packaging safety testing, it is not yet consistently integrated into routine quality practices. This gap between awareness and actual implementation may be linked to challenges such as limited access to local testing services, reliance on external laboratories, and the lack of structured testing programs within organizations.

The demand for both routine and advanced analytical services suggests that stakeholders are becoming more aware of regulatory expectations and the potential risks associated with increasingly complex packaging materials. This trend highlights the need for laboratories to expand beyond conventional testing and develop broader analytical capabilities.

To address these gaps, efforts should focus on strengthening local laboratory infrastructure, improving access to specialized services, and increasing stakeholder engagement through capacity building and regulatory support. Future surveys would also benefit from greater participation of brand owners, particularly food and beverage manufacturers, to better reflect packaging testing practices and industry needs. A demand-driven approach to laboratory development can help strengthen packaging safety systems and support the competitiveness of the Philippine packaging industry.

V. REFERENCES

[1] Rusu, O.-R., Borș, A., Floriștean, V.-C., & Vlad, G. (2024). The critical role of packaging in enhancing food safety, shelf life, and market competitiveness. *Scientific Papers. Series Veterinary Medicine, 67*(1). https://doi.org/10.61900/SPJVS.2024.01.16

[2] Kim, M. (2025). Review of recent issues in food safety of packaging materials: Regulatory concerns and scientific findings. *Korean Journal of Packaging Science & Technology, 31*(1), 11–27. https://doi.org/10.20909/kopast.2025.31.1.11

[3] Opara, U. L., & Mditshwa, A. (2013). A review on the role of packaging in securing food system: Adding value to food products and reducing losses and waste. *African Journal of Agricultural Research, 8*(22), 2621–2630. https://doi.org/10.5897/AJAR2013.6931

[4] Vasile, C.; Baican, M. Progresses in Food Packaging, Food Quality, and Safety—Controlled-Release Antioxidant and/or Antimicrobial Packaging. Molecules 2021, 26, 1263. https://doi.org/10.3390/molecules26051263

[5] Khokhar, P., & Pawar, K. (2025). Chemical migration from packaging materials into consumable food matrices: A mini review. *International Journal of Agriculture and Food Science, 7*(1), 21–25. https://doi.org/10.33545/2664844X.2025.v7.i1a.233

[6] Ong, H. T., Samsudin, H., & Soto-Valdez, H. (2022). Migration of endocrine-disrupting chemicals into food from plastic packaging materials: an overview of chemical risk assessment, techniques to monitor migration, and international regulations. *Critical Reviews in Food Science and Nutrition*, *62*(4), 957–979. https://doi.org/10.1080/10408398.2020.1830747

[7] García Ibarra, V., Rodríguez Bernaldo de Quirós, A., Paseiro Losada, P. *et al.* Identification of intentionally and non-intentionally added substances in plastic packaging materials and their migration into food products. *Anal Bioanal Chem* 410, 3789–3803 (2018). https://doi.org/10.1007/s00216-018-1058-y

[8] Carvalho OT, Tietz T, Zellmet S, Ebner I and Merkel S, 2022. Risk Assessment of Food Contact Materials. EFSA Journal 2022;20(S2):e200920, 10 pp. https://doi.org/10.2903/j.efsa.2022.e200920

[9] Čapla, J., Zajác, P., Čurlej, J., Fikselová, M., &

Kunová, S. (2025). Micro- and nanoplastics in food contact materials: A comprehensive synthesis of release mechanisms, analytical evidence, and risk implications. *Scifood, 19*, 596–611. https://doi.org/10.5219/scifood.80

[10] Ansari, M. D. I., Principato, L., De Nardo, L., & Punta, C. (2026). Nanomaterials in food packaging: An overview of regulatory frameworks and migration assessment. *Food Control, 151*, 111707. https://doi.org/10.1016/j.foodcont.2023.111707

[11] Kato, L.S.; Conte-Junior, C.A. Safety of Plastic Food Packaging: The Challenges about Non-Intentionally Added Substances (NIAS) Discovery, Identification and Risk Assessment. Polymers 2021, 13, 2077. https://doi.org/10.3390/polym13132077

[12] Gupta, R.K.; Pipliya, S.; Karunanithi, S.; Eswaran U, G.M.; Kumar, S.; Mandliya, S.; Srivastav, P.P.; Suthar, T.; Shaikh, A.M.; Harsányi, E.; et al. Migration of Chemical Compounds from Packaging Materials into Packaged Foods: Interaction, Mechanism, Assessment, and Regulations. Foods 2024, 13, 3125. https://doi.org/10.3390/foods13193125

[13] Biant, L., Nguyen, P. M., Hayert, M., Domenek, S., & Vitrac, O. (2025). Characterizing the heterogeneous contamination of commercial paper and board food packaging at different scales. *Food Additives & Contaminants: Part A*, *42*(3), 382–403. https://doi.org/10.1080/19440049.2025.2451639

[14] Miralles, P.; Fuentes-Ferragud, E.; Socas-Hernandez, C.; Coscollà, C. Recent Trends and Challenges on the Non-Targeted Analysis and Risk Assessment of Migrant Non-Intentionally Added Substances from Plastic Food Contact Materials. Toxics 2025, 13, 543. https://doi.org/10.3390/toxics13070543

[15] Geueke, B., Groh, K., & Muncke, J. (2018). Food packaging in the circular economy: Overview of chemical safety aspects for commonly used materials. *Journal of Cleaner Production, 193*, 491–505. https://doi.org/10.1016/j.jclepro.2018.05.005

[16] Karmaus, A. L., Osborn, R., & Krishan, M. (2018). Scientific advances and challenges in safety evaluation of food packaging materials: Workshop proceedings. *Regulatory Toxicology and Pharmacology, 98*, 80–87. https://doi.org/10.1016/j.yrtph.2018.07.006

[17] Food and Drug Administration. (2022). *Guidelines on the application and issuance of voluntary certification of food contact articles (FCA) used for prepackaged processed food products* (FDA Circular No. 2022-011). Department of Health, Philippines.

[18] US Food and Drug Administration. (2023). Title 21 Food and Drugs. Chapter 1 Food and Drug Administration, Department of Health and Human Services. Subchapter B Food for Human Consumption. Part 170-180

[19] European Commission. (2011). *Commission Regulation (EU) No 10/2011 of 14 January 2011 on plastic materials and articles intended to come into contact with food. Official Journal of the European Union, L 12*, 1–89. https://eur-lex.europa.eu/legalcontent/EN/TXT/?uri=CELEX%3A32011R0010

[20] Del Rosario, A. F., Encarnacion, E. K. P., Alcantara, A. C., Armario, H. E., Alcarde Jr., D. J., Ting, R. M. S., Alejandro, W. P., & Canonizado, A. S. L. (2026). A preliminary survey on the demand for oxygen and water vapor transmission rate testing of food packaging in the Philippines. *Multidisciplinary Science Journal*, *8*(7), 2026448. https://doi.org/10.31893/multiscience.2026448

[21] Fasake, V., Shelake, P. S., Srivastava, A., & Dashora, K. (2021). Characteristics of different plastic materials, properties and their role in food packaging. *Current Nutrition & Food Science, 17*(9), e050521193156. https://doi.org/10.2174/1573401317666210505100139

[22] Alejandro, W. P., Encarnacion, E. K. P., Alcantara, A. C., Alcarde, D. J. A., Armario, H. E., Del Rosario, A. F., & Ting, R. M. S. (2025). *Assessment of total UV-absorbing contaminants in LDPE food packaging from Philippine markets*. Current Research in Nutrition and Food Science, 13(2), 913–925. https://doi.org/10.12944/CRNFSJ.13.2.26

[23] Sogut, O., Seydim, A. C., & Atli, B. (2024). Migration from plastic food packaging materials: A review of chemical contaminants and analytical

approaches. *Food Chemistry, 439*, 138111. https://doi.org/10.1016/j.foodchem.2023.138111

[24] Jasmani, L., Ainun, Z.M.A., Adnan, S., Ibrahim, R., Sapuan, S.M. and Ilyas, R.A. (2021). Sustainable Paper-Based Packaging. In Bio-based Packaging (eds S.M. Sapuan and R.A. Ilyas). https://doi.org/10.1002/9781119381228.ch13

[25] Stark, N. M., & Matuana, L. M. (2021). Trends in sustainable biobased packaging materials: A mini review. *Materials Today Sustainability, 15*, 100084. https://doi.org/10.1016/j.mtsust.2021.100084

[26] Jieying, S., Tingting, L., Caie, W., Dandan, Z., Gongjian, F., & Xiaojing, L. (2024). Paper-based material with hydrophobic and antimicrobial properties: Advanced packaging materials for food applications. Comprehensive Reviews in Food Science and Food Safety, 23, e13373. https://doi.org/10.1111/1541-4337.13373

[27] Deshwal, G. K., & Panjagari, N. R. (2020). Review on metal packaging: Materials, forms, food applications, safety and recyclability. *Journal of Food Science and Technology, 57*(7), 2377–2392. https://doi.org/10.1007/s13197-019-04172-z

[28] Montanari, A. (2015). Inorganic Contaminants of Food as a Function of Packaging Features. In: Food Packaging Hygiene. SpringerBriefs in Molecular Science(). Springer, Cham. https://doi.org/10.1007/978-3-319-14827-4_2

[29] Lv, Y., Liu, N., Chen, C., Cai, Z., & Li, J. (2025). Pharmaceutical packaging materials and medication safety: A mini-review. *Safety, 11*(3), 69. https://doi.org/10.3390/safety11030069

[30] Jenke DR, Stults CL, Paskiet DM, Ball DJ, Nagao LM. Materials in Manufacturing and Packaging Systems as Sources of Elemental Impurities in Packaged Drug Products: A Literature Review. PDA J Pharm Sci Technol. 2015 1/2;69(1):1-48. doi: 10.5731/pdajpst.2015.01005. PMID: 25691713.

[31] Angela Störmer, & Keun Lee. (2017). Food package testing authorities and regulations. In *Food Packaging Materials* (pp. 303–332). CRC Press. https://doi.org/10.4324/9781315374390-12

[32] Khairun Tumu, Keith Vorst, & Greg Curtzwiler. (2023). Endocrine modulating chemicals in food packaging: A review of phthalates and bisphenols. *Comprehensive Reviews in Food Science and Food Safety*. https://doi.org/10.1111/1541-4337.13113

[33] J. Takala. (1996). Chemical safety information for developing countries. *Science of the Total Environment, 188*(Supplement), S112–S129. https://doi.org/10.1016/0048-9697(96)05283-7

2026 IMEKO Joint Conference
TC8 - TC11 - TC24
Metro Manila, Philippines, August 26-29, 2026

Assessment of methods for analytical testing of soluble sulphates in construction materials: integrating measurement uncertainty and proficiency testing

Michael S. Lagmay[1], Christy S. Daniel[1], Johanna Andrea C. Valdueza[1], Ruth L. Damian[1], Admer Rey C. Dablio[1]

[1]*Standards and Testing Division, Industrial Technology Development Institute, Department of Science and Technology, Bicutan, Taguig City, 1631, Philippines, mslagmay@itdi.dost.gov.ph*

***Abstract* – Accurate quantification of soluble sulphates in construction materials is essential for demonstrating compliance with relevant standards. This study presents a comprehensive assessment of method performance for acid- and water-soluble sulphate determination through method validation, measurement uncertainty (MU) evaluation, and proficiency testing (PT) participation. MU was estimated using hybrid bottom-up/top-down approach, identifying calibration, precision, and trueness as the major contributors to uncertainty for both methods. The results indicate that targeted improvements in calibration procedures, precision, and recovery would provide the greatest reduction in overall MU and further enhance measurement quality. To verify analytical performance externally, the laboratory participated in two PT schemes organized by DRRR GmbH in 2025. Satisfactory z'-scores were achieved, demonstrating acceptable performance and comparability with peer laboratories. The integration of method validation, MU evaluation, and PT participation provides a strong quality assurance framework, ensuring that soluble sulphate determinations are accurate, reliable, fit-for-purpose, and metrologically traceable for industry applications.**

I. INTRODUCTION

The assessment of chemical constituents in construction materials is central to ensuring both the safety and longevity of concrete structures. Sulphate is of particular concern as their presence in excessive concentrations can trigger chemical reactions with other chemical species in hydrated cement phases, leading to cracking, spalling, and eventual structural disintegration, a phenomenon collectively referred to as sulphate attack [1-3]. With this, national and international regulations have set maximum permissible levels of sulphate in cement and aggregates. This entails the need for chemical testing laboratories to adopt validated analytical methods that can generate reliable and accurate measurement results [4-6].

The individual quantification of acid-soluble sulphate and water-soluble sulphate is important because it provides insight into the immediate availability of sulphates and hence their potential long-term impacts within the cementitious matrix. Acid-soluble sulphate represents the total sulphate content accessible under aggressive chemical conditions, while water-soluble sulphate indicates the portion readily available to the environment. The differentiation between these two fractions establishes a more accurate understanding of sulphate behavior in concrete and provides critical data for durability assessment and compliance with standard specifications [7-9].

Despite the establishment of validated analytical methods for sulphate determination, the reliability of reported results is inevitably influenced by uncertainties arising from different sources along the stages of the measurement process. Measurement uncertainty (MU) sources include sampling, sample preparation steps, instrumental limitations, calibration processes, and analyst's competence, among others. Consequently, the evaluation of measurement uncertainty has become an essential practice by testing laboratories to quantitatively express the level of confidence in their generated test results. This requirement is stipulated in ISO/IEC 17025:2017 standard which is used to evaluate the competence of testing and calibration laboratories [10]. For this purpose, the ISO/IEC Guide 98-3:2008 Guide to the Expression of Uncertainty in Measurement (GUM) [11] and the Eurachem/CITAC Guide CG 4 [12] have been widely adopted for the identification, quantification, and combination of both random and systematic sources of uncertainty into a single, comprehensive statement of measurement quality.

However, assessment of MU, along with in-house validation of methods, address only the internal part of quality assurance. While rigorous, they handle only internal checks but do not fully account for the laboratory's

performance relative to other laboratories. Therefore, external comparison is required. Proficiency testing (PT) schemes have been established internationally as a mechanism for independent performance evaluation of testing laboratories. Participation in PT allows laboratories to compare their results against those of peer institutions under controlled conditions. This identifies potential biases, confirms analytical accuracy, ensures consistency with widely used standards, and determines areas for improvement [13-14]. In addition, laboratories seeking accreditation for a specific scope should demonstrate their competence through PT participation [10].

In this context, this study conducted a comprehensive method performance assessment for soluble sulphates determination in concrete and related materials through method validation, MU evaluation, and PT participation. These measures address quality assurance from both internal and external perspectives, ensuring that the validated methods for sulphate determination are accurate and reliable. Such practices enhance confidence in test results, which are essential for conformity assessment of structural durability and materials quality in the construction industry.

II. METHODS AND PROCEDURES

A. Method Validation

The experimental procedure and method validation approach have been described in detail in the authors' previous work [15]. The in-house validated method is summarized as follows: acid-soluble sulphate is extracted using a modified ASTM C114 method by digesting 1.000 g of sample with water and hydrochloric acid, followed by heating, filtration, washing, and dilution to 100.00 mL [16]. Sulphate is determined using a UV–Vis spectrophotometer (Shimadzu UV-1900i) by turbidimetric method based on US EPA 9038, in which the sample is reacted with barium chloride, allowed to develop turbidity, and measured at 420 nm using a 1 cm cuvette [17]. Meanwhile, water-soluble sulphate is determined following a modified ASTM C1580 method using a reduced but proportionally maintained sample-to-extractant ratio, where 12.000 g of concrete sample is mixed with 100.00 mL of Type 1 water, stirred at 500 rpm for 1 hour, filtered, and an aliquot is further diluted prior to analysis [18]. It is then quantified using ion chromatography (Dionex ICS-1000), with suppressed conductivity detection.

A single-laboratory method validation was conducted by following the internationally recognized guides from Eurachem [19] and IUPAC [20]. Linearity and working range, repeatability, intermediate precision, and trueness by spike recovery and bias, were assessed for the suitability of the method. The evaluation of results and the acceptance criteria were based on the laboratory's in-house protocol for method validation.

B. Measurement Uncertainty Evaluation

Measurement uncertainty was estimated using the hybrid bottom-up/top-down approach in accordance with the ISO/IEC Guide 98-3:2008 [11] and Eurachem/CITAC guide [12,21]. The bottom-up approach builds uncertainty by identifying and combining individual sources, whereas the top-down approach derives overall uncertainty from method performance evaluation data such as validation, quality control, or PT results.

Identification of MU Sources

The measurands are the concentrations of acid-soluble sulphate and water-soluble sulphate in concrete, expressed in percent (% w/w). The uncertainty sources were identified using the cause-and-effect diagram, as illustrated in Fig. 1. Both Type A and Type B sources of uncertainty were considered.

Quantification of Uncertainty Components (Type A)

Uncertainty components under Type A evaluations were the concentration of sulphate in the sample solution, method trueness, and method precision. Uncertainty arising from the determination of sulphate concentration in the sample solution, $u(C_{x,soln})$, was calculated using equation 1:

$$\boldsymbol{u\left(C_{x,soln}\right) = \frac{S}{B_1}\sqrt{\frac{1}{p}+\frac{1}{n}+\frac{(c_o-\bar{c})^2}{S_{xx}}}} \qquad (1)$$

where S is the residual standard deviation, p is the number of replicate measurements to determine c_o, n is the number of calibration data points, c_o is the determined concentration of sulphate using the calibration curve, $\bar{c}$ is the mean value of the different calibration standards, and S_{xx} is the residual sum of squares, the values of which were derived from the calibration curve [12].

The uncertainty contribution of method trueness for acid-soluble sulphate was evaluated using NCS DC 62102g Cement CRM and equation 2 was applied [12,19]:

$$\boldsymbol{\%u_{bias} = \sqrt{(\%bias)^2 + \left(\frac{s_{bias}}{\sqrt{n}}\right)^2 + u\left(c_{ref}\right)^2}} \qquad (2)$$

where $\%u_{bias}$ is the uncertainty due to bias in percent, s_{bias} is the percent relative standard deviation of the replicate results, $u(c_{ref})$ is the percent relative uncertainty of the certified value, and n is the number of measurements.

Meanwhile, for water-soluble sulphate, the results of spiking recovery studies during method validation were used. The recovery for the spiked samples was calculated using equation 3:

$$\boldsymbol{R = \frac{C_1 - \bar{C}_0}{C_2}} \qquad (3)$$

where C_1 is the concentration of the spiked sample with native analyte, $\bar{C}_0$ is the mean concentration of the unspiked samples (native concentration), and C_2 is the concentration added to the spiked sample. The standard un-

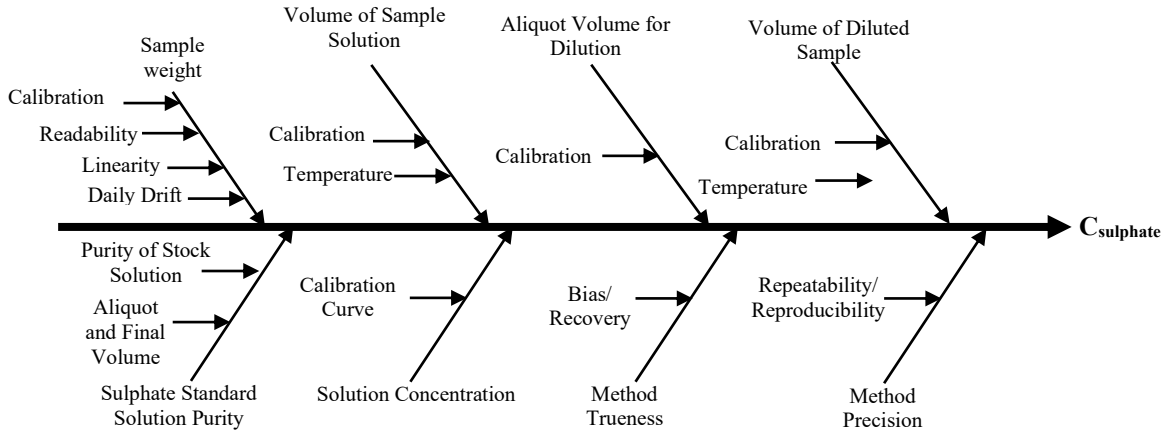


Fig. 1. Cause-and-effect diagram for soluble sulphates.

certainty associated with the mean recovery, *u(R)*, is represented by equation 4 [21]:

$$u(\bar{R})^2 = \sum_{i=1}^{N} \left\{ \left(\frac{\bar{c}_{1i} - \bar{c}_{0i}}{c_{2i}} \right)^2 \left[\frac{\frac{s^2(c_{1i})}{n_i} + \frac{s^2(c_{0i})}{m_i}}{(\bar{c}_{1i} - \bar{c}_{0i})^2} + \left(\frac{u(c_2)}{c_2} \right)^2 \right] \right\} \Big/ N \quad (4)$$

The uncertainty contribution of method precision, $u_{precision}$, for both measurands were taken from the intermediate precision method validation data. It was calculated using equation 5 [21]:

$$\boldsymbol{u_{precision}} = \sqrt{\frac{\boldsymbol{s_I^2}}{\boldsymbol{p}} + \frac{\boldsymbol{s_r^2(1-n)}}{\boldsymbol{np}}} \quad (5)$$

where s_I is the intermediate precision standard deviation, s_r is the repeatability standard deviation, n is the number of replicate measurements, and p is the number of data set.

Quantification of Uncertainty Components (Type B)

Type B evaluations were based on calibration certificates, certificates of analysis, and manufacturer specifications. Standard uncertainties were derived using assumed probability distributions (normal, triangular, or rectangular). When a confidence level was provided, expanded uncertainty was converted to standard uncertainty using the stated coverage factor; otherwise, appropriate distributions (triangular or rectangular) were assumed based on the available information. This approach ensures that all documentary-based uncertainties are consistently expressed in terms of standard uncertainties, making them compatible with subsequent combination and propagation in the overall MU budget.

Combined Uncertainty and Expanded Uncertainty

The overall combined uncertainty (u_c) was calculated using the model equations below [12]. For models involving a sum or difference of quantities, the equation used was:

$$\boldsymbol{u_c}\,(\boldsymbol{x}(\boldsymbol{p},\boldsymbol{q},\boldsymbol{r},\ldots)) = \sqrt{\boldsymbol{u(p)^2} + \boldsymbol{u(q)^2} + \boldsymbol{u(r)^2} + \cdots} \quad (6)$$

where *u(p)*, *u(q)*, and *u(r)* are the individual standard uncertainty of the uncertainty budget components. For models involving product or quotient, the equation used was:

$$\boldsymbol{u_c(x)} = \boldsymbol{x}\sqrt{\left(\frac{\boldsymbol{u(p)}}{\boldsymbol{p}}\right)^2 + \left(\frac{\boldsymbol{u(q)}}{\boldsymbol{q}}\right)^2 + \left(\frac{\boldsymbol{u(r)}}{\boldsymbol{r}}\right)^2 + \cdots} \quad (7)$$

where x is the value of the measurand, and *u(p)/p*, *u(q)/q*, and *u(r)/r* are the individual relative standard uncertainty of the components. The expanded uncertainty (U) was determined by multiplying the overall combined uncertainty by a coverage factor (k=2), signifying an approximate 95% confidence interval.

C. Proficiency Testing Participation

Deutsches Referenzbüro für Ringversuche und Referenzmaterialien (DRRR GmbH), an ISO/IEC 17043 accredited proficiency testing provider based in Germany, supplied the two PT schemes participated by the laboratory: (1) RVEP 240916, "Total sulfur content, Acid soluble sulphates EN 1744-1, No. 2010583" for aggregates, and (2) RVEP 240909, "Total sulphate content EN 196-2, No. 2010569" for cement. Only acid-soluble sulphate PT schemes were available. The PT samples were processed according to the protocol provided by the DRRR and were subjected to analysis using the validated method. Laboratory performance was evaluated using z'-scores.

III. RESULTS AND DISCUSSION

A. Method Validation

The validation protocols and results are comprehensively documented in the authors' earlier publication [15]. The study validated a UV-Vis turbidimetric method as a more efficient alternative to traditional gravimetry for determining acid-soluble sulphate in construction materials. While the conventional gravimetric approach is simple and requires no specialized instrumentation, it is limited by its tedious nature, susceptibility to errors during ignition, and low sensitivity. In contrast, the validated

spectrophotometric method demonstrated good linearity (r=0.9987) over the range of 5-25 mg/L SO_4^{2-}. Satisfactory repeatability was obtained with %RSD of 3.33 at 0.795 % w/w SO_4^{2-} (n=7). Acceptable intermediate precision was achieved with %RSD of 5.92 at 0.853 % w/w SO_4^{2-} (n=6), equivalent to HorRat of 1.36. Furthermore, trueness was confirmed with spike recoveries between 92.7% and 110.3%. An additional trueness by bias assessment using NCS DC 62102g Cement CRM obtained recoveries of 90.7-95.6%.

Meanwhile, method validation for water-soluble sulphate in concrete demonstrated satisfactory performance across all evaluated parameters as well. Linearity was confirmed over a working range of 0.25-8.00 mg/L (r=0.9998). Precision assessments yielded satisfactory results, with a repeatability %RSD of 4.1 (mean=0.137 %w/w SO_4^{2-}, n=6). Intermediate precision across different analysts also met acceptance criteria with a HorRat of 1.06, falling within the accepted < 2.0. Trueness was verified via spike recovery, achieving a mean recovery of 101.8% (ranging from 96.7 to 107.7%, n=7), which is within the 90-110% acceptance criteria. Overall, the results indicate that the methods are fit for the intended purpose in the analytical testing of acid-soluble and water-soluble sulphate in concrete and related materials. The method validation results are summarized in Table 1.

Table 1. Summary of method validation results.

Parameter	Acceptance Criteria	Acid-soluble sulphate	Water-soluble sulphate
Linearity and working range	r>0.9950; residuals are randomly distributed to zero	5-25 mg/L; r=0.9987; residual plot passed	0.25-8.0 mg/L; r=0.9998; residual plot passed
Repeatability	%RSD < 5	3.30	4.11
Intermediate Precision	HorRat < 2.0	1.36 (%RSD=5.92)	1.06 (%RSD=5.76)
Trueness by spiking	% Recovery = 90-110	92.7 - 110.3	96.7 - 107.7

B. Measurement Uncertainty Evaluation

While method validation confirms that the method is fit for its intended purpose under defined conditions, it does not fully capture the variability associated with routine application. This is where MU becomes essential. It enables results to be expressed with a quantified level of confidence rather than as exact values, effectively bridging the gap between method capability and result interpretation by translating performance into a clear and practical statement of confidence that supports more informed and sound decision-making [22].

Table 2 summarizes the calculated relative standard uncertainty of each identified component. For sample weighing, the expanded uncertainty from the balance calibration certificate (U=±0.00043 g, k = 2) was converted to standard uncertainty and combined with other factors such as linearity, readability, drift, and repeatability. Uncertainty in volumetric measurements was derived from glassware calibration and temperature effects (if applicable). The standard uncertainty of the sulphate standard purity was obtained from its certificate (U=±5 mg/L, k=2), and that of the volumetric wares used in the preparation. Uncertainty associated with the calibration curve was evaluated using linear regression parameters. Method trueness and method precision were taken from the validation data.

Table 2. Uncertainty budget.

Uncertainty Component	Relative Standard Uncertainty	
	Acid-soluble sulphate	Water-soluble sulphate
Sample weighing	0.0011	0.00002
Sample volume after extraction	0.0010	0.0010
Sample aliquot volume	0.0033	0.0029
Diluted sample volume	0.0006	0.0013
Sulphate standard solution purity	0.0025	0.0028
Calibration	0.0435	0.0197
Method trueness	0.0055	0.0438
Method precision	0.0398	0.0347

Fig. 2 illustrates the relative contributions of different measurement uncertainty sources associated with the determination of acid-soluble sulphate in concrete. Based on the analysis, the largest contributor is calibration (44.7%), followed by method precision (40.9%), and then by method trueness (5.6%) with a moderate but still significant contribution. These three sources alone already account for more than 91% of the total uncertainty budget, underscoring their critical role in ensuring the reliability of analytical results.

Other contributors, including the sample aliquot for dilution (3.4%), sulphate standard solution purity (2.6%), sample weight (1.2%), volume of sample solution after extraction (1.0%), and diluted sample volume (0.6%), are considered relatively minor uncertainty contributors. These results suggest that gravimetric (weighing) and volumetric operations (use of volumetric wares), while important, have been effectively controlled within the analytical workflow and provided limited influence on the overall uncertainty.

Meanwhile, for water-soluble sulphate determination, as shown in Fig. 3, the uncertainty budget is largely dominated by method trueness (spike recovery) (42.1%). This indicates that the accuracy of the method in completely recovering sulphate from the matrix is the most critical factor influencing the reliability of the results. This

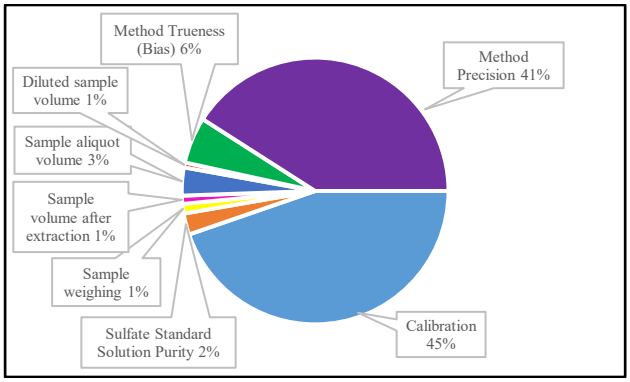


Fig. 2. %Contribution of MU components (acid-soluble sulphate).

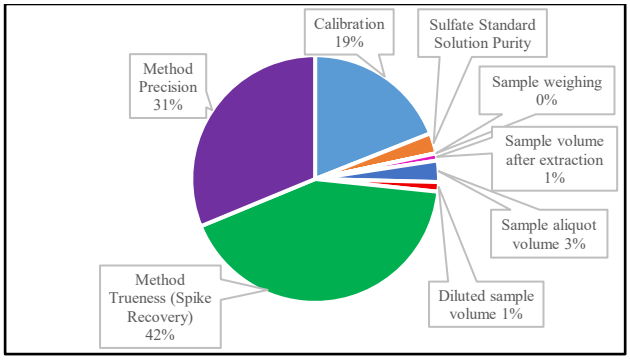


Fig. 3. %Contribution of MU components (water-soluble sulphate).

is followed by method precision (31.2%), then by calibration (19.0%). The other components are deemed minor contributors.

Calibration dominates the uncertainty budget which suggests that the consistency, stability, and accuracy of the calibration curve used for the quantification is an influential factor in the analytical process. This emphasizes the importance of employing metrologically traceable standards and verifying instrument performance regularly based on established protocols. To reduce the impact of calibration on overall measurement uncertainty, several practical strategies can be applied: preparing multiple independent calibration sets, performing replicate measurements of calibration standards, adjusting sample dilution so the response falls near the midpoint of the calibration range where uncertainty is typically lower, and increasing replicate measurements of the sample. These measures directly address the terms in equation 1 which is used to estimate the calibration contribution, and when applied properly, will mathematically reduce that contribution.

Uncertainty due to method precision originates from random error which is caused by the unpredictable variations in repeated observations of the measurand. Unlike systematic errors, random errors cannot be corrected, but it can generally be reduced by increasing the number of replicate measurements. Implementation of standardized analytical protocols, employing strict laboratory practices, and continuous analyst training are some of the approaches that can further minimize random errors [12].

Uncertainty arising from method trueness reflects systematic deviations caused by factors such as matrix effects, method and instrument limitations, and analyst competence. This underscores the importance of bias evaluation through the use of CRMs or sample spiking during routine analysis. Additional internal quality control measures may also be implemented, while external quality assurance can be strengthened through participation in interlaboratory comparisons or PT.

In general, for the two measurands, the results indicate that targeted improvements in calibration procedures and method performance would yield the greatest reduction in overall measurement uncertainty. This is in line with the recommendations of the ISO GUM [11] and the Eurachem CITAC Guide [12], which emphasize the prioritization of dominant sources when refining analytical methods.

Table 3 presents the obtained combined and expanded uncertainties for the two measurands. In the context of decision rules for conformity assessment, the expanded uncertainty provides an indication of how much risk is introduced when comparing results with specification limits. As described in the Eurachem/CITAC guide, there is no established or universally accepted percentage threshold for expanded uncertainty relative to the mean [23]. Its acceptability depends on the intended use of the data and whether it meets any defined target uncertainty or decision requirements. Decision rules describe how MU is taken into account to avoid incorrect acceptance or rejection of a product or sample [23].

Table 3. Combined and expanded uncertainty.

Parameter	**Acid-soluble sulphate in concrete**	**Water-soluble sulphate in concrete**
Mass Fraction, % w/w	0.887	0.130
Combined Uncertainty (u_c), % w/w	0.053	0.006
Expanded Uncertainty (U), % w/w (k=2)	0.105	0.015
Percentage of Uncertainty to Mass Fraction, %	11.87	11.88

MU plays a critical role in the reliability and defensibility of conformity assessment decisions. Lower uncertainty increases confidence that a measured value accurately represents the true value and reduces the likelihood that uncertainty will alter a pass/fail decision. For both measurands evaluated, the expanded uncertainties constitute a significant but reasonable proportion of the reported results. Consequently, uncertainty can meaningfully influence conformity assessment outcomes,

particularly when measured values are close to specification limits. In these borderline cases, materials may be incorrectly accepted as compliant (false acceptance) or rejected as non-compliant (false rejection) if uncertainty is not adequately considered.

Such decision errors can have important technical, economic, and regulatory consequences, including compromised material performance, unnecessary product rejection, increased costs, contractual disputes, and non-compliance with specifications. These findings highlight the need to incorporate MU into compliance evaluations rather than relying solely on reported test results. The application of predefined decision rules, such as guard bands, provides a structured approach for managing decision risk and supporting transparent, consistent, and technically defensible conformity assessments.

C. Proficiency Testing Participation

While in-house validation demonstrates that a method is fit for its intended purpose and MU evaluation describes the reliability of results, PT provides an external and independent assessment of the method's accuracy and reliability under routine conditions. Participation in a PT scheme is an important aspect of quality assurance which enables the laboratory to benchmark its analytical performance against other laboratories. This enables mutual recognition of test methods, facilitating compliance with technical and regulatory requirements across multiple countries, and reducing trade barriers in the construction industry by promoting acceptance of materials and products in international markets.

In the PT exercise organized by DRRR GmbH, the total sulphate content in aggregates (RVEP 240916), was determined using the acid-soluble sulphate method and was reported as sulfur trioxide (% w/w SO_3) in accordance with the PT provider's reporting requirements. An appropriate gravimetric factor was used to convert sulphate to SO_3. A total of twelve laboratories participated, with nine laboratories coming from the European Union (EU) and two laboratories from other regions.

For the total sulphate content determination (RVEP 240909), two laboratories were from Germany, and four laboratories were from non-EU countries. Table 4 summarizes the results, showing the assigned values, laboratory-reported values, and calculated z'-scores. The reported % w/w SO_3 and SO_4^{2-} were within the acceptable z'-score range of ± 2.0, indicating satisfactory performance as defined by ISO 13528:2022 [24]. This demonstrates that the laboratory-developed method for acid-soluble sulphate determination in construction materials has maintained its accuracy and reliability under actual testing conditions. The satisfactory PT performance not only provided an additional method performance verification but also enhances the credibility of the laboratory test results, providing confidence in third-party evaluations relevant to international construction material testing protocols. Moreover, it provides evidence of laboratory's competence and fulfilment of one of the accreditation requirements, as the laboratory prepares for formal recognition under ISO/IEC 17025:2017.

Table 4. Results of PT participation.

PT ID	Sample	Analyte	Reported Value, % w/w	Assigned Value, % w/w	z'-score
RVEP 240916	Aggregates (Blast furnace slag)	Acid-soluble sulphate (as SO_3)	0.45	0.40	0.43
RVEP 240909	Cement	Total Sulphate content (as SO_4^{2-})	2.77	2.70	0.99

IV. CONCLUSION

The study showed that sulphate determination in construction materials can be carried out reliably through a comprehensive quality assurance approach involving method validation, MU evaluation, and PT participation. Method validation confirmed that the methods are suitable for their intended use, with satisfactory performance in terms of linearity, precision, and trueness for both acid-soluble and water-soluble sulphate. Measurement uncertainty then provided a clearer understanding of the reliability of the results by quantifying the overall effect of different sources of variation, giving a practical measure of confidence in the reported values. To further support this, proficiency testing offered an external check by comparing results with those from other laboratories, showing that the methods perform consistently under routine conditions. These three components collectively demonstrate that the methods produce reliable, accurate, and metrologically traceable sulphate measurements, supporting their applicability for quality assurance and conformity assessment of construction materials.

ACKNOWLEDGEMENT

This work was supported by the DOST-ITDI under the GAA Project, "Development and Validation of an Ion Chromatographic Method for the Determination of Water-Soluble Anions in Concrete and Cement."

The authors would like to express their sincere gratitude for the project implementation guidance provided by the ITDI. The authors also acknowledge the dedicated service and valuable assistance provided by the staff of the Inorganic Chemistry Section of STD: Jan-Ervin Guerrero, Theressa Aviles-Liclican, Leonard Montero, Andrea Tero, Mark Nicholas Yow, Mark Anthony Principe, Glenn Levi Solis, and Arvi Jane.

REFERENCES

[1] J. P. Ingham, *Geomaterials under the Microscope*. Academic Press, 2013.

[2] N. Klein, E. Gomez, G. Duffó, and S. Farina, “Effect of sulphate on the corrosion of reinforcing steel in concrete,” *Construction and Building Materials*, vol. 354, 2022, doi: 10.1016/j.conbuildmat.2022.12924.

[3] J. Bai, Durability of Sustainable Construction Materials, Elsevier eBooks, 2016, pp. 397–414, doi: 10.1016/b978-0-08-100370-1.00016-0.

[4] European Committee for Standardization, *EN 197-1: Cement—Part 1: Composition, specifications and conformity criteria for common cements*, 2011.

[5] Bureau of Philippine Standards, *Philippine National Standard PNS 07:2018: Portland Cement Specification*. Department of Trade and Industry, 2018.

[6] European Committee for Standardization, *EN 1744-1:2010: Tests for chemical properties of aggregatess*, 2010.

[7] F. Agrela, M. Cabrera, A. P. Galvín, A. Barbudo, and A. Ramírez, “Influence of the sulphate content of recycled aggregatess on the properties of cement-treated granular materials,” *Construction and Building Materials*, vol. 68, pp. 127–134, 2014.

[8] C. Zhang *et al*., “Mechanism and performance control methods of sulphate attack on cementitious materials,” *International Journal*, 2024.

[9] TRL (Transport Research Laboratory), “Sulphate specification for structural backfills,” U.K. technical report.

[10] International Organization for Standardization (ISO), *ISO/IEC 17025:2017: General requirements for the competence of testing and calibration laboratories*, 2017.

[11] ISO, *ISO/IEC Guide 98-3:2008: Uncertainty of measurement—Part 3: Guide to the expression of uncertainty in measurement (GUM:1995)*, 2008.

[12] S. L. R. Ellison and A. Williams (eds.), *Eurachem/CITAC guide: Quantifying uncertainty in analytical measurement*, 3rd ed., ISBN 978-0-948926-30-3, 2012.

[13] ISO, *ISO/IEC 17043:2010: Conformity assessment—General requirements for proficiency testing*, 2010.

[14] B. Brookman and I. Mann, eds., *Eurachem Guide: Selection, Use and Interpretation of Proficiency Testing (PT) Schemes by Laboratories*, 3rd ed., Eurachem, 2021.

[15] C. Daniel, A. R. Dablio, M. Lagmay, et al., “Development and validation of methods for the determination of water-soluble and acid-soluble sulphate in concrete,” *Measurement Sensors*, vol. 38, 2025, doi:10.1016/j.measen.2024.101618.

[16] *Standard Test Methods for Chemical Analysis of Hydraulic Cement*, ASTM C114-24, ASTM International, West Conshohocken, PA, USA, 2024.

[17] U.S. Environmental Protection Agency, “Method 9038: Sulphate (Turbidimetric),” Washington, DC, USA, Sep. 1986.

[18] *Standard Test Method for Water-Soluble Sulphate in Soil*, ASTM C1580-20, ASTM International, West Conshohocken, PA, USA, 2020.

[19] H. Cantwell (ed.). Eurachem Guide: The Fitness for Purpose of Analytical Methods – A Laboratory Guide to Method Validation and Related Topics. 2025;(3rd ed).

[20] International Union of Pure and Applied Chemistry, “Harmonized guidelines for single-laboratory validation of methods of analysis,” Pure and Applied Chemistry, vol. 74, no. 5, pp. 835–855, 2002.

[21] R. Bettencourt da Silva (ed.), Eurachem/CITAC Guide: Evaluation of measurement uncertainty from in-house precision and recovery data. First Edition, ISBN 978-972-9348-30-3, 2026.

[22] JCGM 100:2008, *Evaluation of Measurement Data—Guide to the Expression of Uncertainty in Measurement (GUM)*, Joint Committee for Guides in Metrology, 2008.

[23] R. J. N. Bettencourt da Silva and A. Williams, eds., Eurachem/CITAC Guide: Setting and Using Target Uncertainty in Chemical Measurement, 1st ed. Eurachem, 2015.

[24] ISO, *ISO 13528:2022 – Statistical methods for use in proficiency testing by interlaboratory comparison, Geneva, Switzerland: ISO*, 2022.

2026 IMEKO Joint Conference
TC8 - TC11 - TC24
Metro Manila, Philippines, August 26-29, 2026

Application of Statistical Process Control (SPC) for Monitoring Stability and Variability in Perfluorooctane Sulfonate (PFOS) and Perfluorooctanesulfonic Acid (PFOA) Migration Measurements

David Jaucian Alcarde Jr.[1], Elyson Keith P. Encarnacion[2], Anne C. Alcantara[3], Harold E. Armario[4], April Star L. Canonizado[5], Agaseve F. Del Rosario[6], Winnie P. Alejandro[7], Rizel Marie S.M. Ting[8], Kim Angelene R. Tagle[9], Daniela Marie D. Barredo[10], Jeric B. Bañadera[11], Josefino Antonio T. Mendoza[12]

[1,2,3,6,7,8,9,10,11,12] *Packaging Technology Division, Industrial Technolgy Development Institute, Department of Science and Technology (DOST-ITDI), Bicutan, Taguig, Metro Manila, Philippines 1631*

[4] *Standards and Testing Division, Industrial Technolgy Development Institute, Department of Science and Technology (DOST-ITDI), Bicutan, Taguig, Metro Manila, Philippines 1631*

[5] *National Metrology Division, Industrial Technolgy Development Institute, Department of Science and Technology (DOST-ITDI), Bicutan, Taguig, Metro Manila, Philippines 1631*

Corresponding email: da6914@rit.edu

Abstract **– Reliable quantification of per- and polyfluoroalkyl substances (PFAS) in food-contact materials requires stable and consistent measurement performance. This study applies statistical process control (SPC) techniques to evaluate the stability and variability of perfluorooctane sulfonate (PFOS) and perfluorooctanoic acid (PFOA) migration measurements obtained from multi-analyst replicate datasets across low, medium, and high concentration levels. X-bar and range (R) control charts were used to assess subgroup means and within-subgroup variability. Several subgroup means exceeded X-bar control limits for both analytes; however, these deviations were primarily associated with systematic differences in concentration levels rather than process instability. R charts indicated stable variability for PFOS and a single out-of-control subgroup for PFOA. The results demonstrate that SPC is an effective tool for interpreting variability and supporting quality assurance in PFAS migration analysis..**

I. INTRODUCTION

Per- and polyfluoroalkyl substances (PFAS), including perfluorooctane sulfonate (PFOS) and perfluorooctanoic acid (PFOA), are persistent environmental contaminants widely detected in food-contact materials [1]–[4]. Their potential to migrate into food and beverages has raised increasing concerns regarding human exposure and safety [5]–[7]. Consequently, reliable measurement of PFAS migration is essential for regulatory compliance, exposure assessment, and risk evaluation [8], [9]. Analytical determination of PFOS and PFOA migration typically involves low-level concentration measurements performed under controlled experimental conditions [10], [11]. However, these measurements are inherently subject to variability arising from multiple sources, including sample preparation, instrumental response, and operator-dependent effects [12], [13]. In the context of laboratory quality systems, particularly those aligned with ISO/IEC 17025, it is critical to ensure that measurement processes are both stable and capable of producing consistent results over time and across analysts [14], [15].

Statistical process control (SPC) provides a well-

established framework for monitoring process performance and identifying sources of variability [16]. Originally developed for industrial quality control, SPC techniques—such as X-bar and range (R) control charts—have been increasingly applied in laboratory settings to assess analytical performance. These tools enable the detection of out-of-control conditions, systematic shifts, and abnormal variability patterns, thereby supporting continuous quality assurance and improvement.

Despite their potential, the application of SPC in chemical migration studies remains limited, particularly for emerging contaminants such as PFAS [17], [18]. In many cases, variability in migration measurements may be influenced not only by analytical factors but also by structured experimental conditions, such as concentration levels [19]. Distinguishing between variability arising from controlled experimental design and variability indicative of measurement instability is therefore essential for accurate interpretation of results. This study applies SPC techniques to PFOS and PFOA migration measurements obtained from multi-analyst replicate datasets across different concentration levels. X-bar and R control charts are used to evaluate measurement stability and within-subgroup variability, while identifying potential out-of-control conditions. The objective is to assess the extent to which observed variability reflects systematic experimental factors versus measurement-related effects, and to demonstrate the usefulness of SPC as a diagnostic tool for enhancing quality assurance in PFAS migration analysis.

II. MATERIALS AND DATA DESCRIPTION

A. Measurement context and measurand definition

The dataset analyzed in this study consists of laboratory-generated measurements of the surface migration of perfluorooctane sulfonate (PFOS) and perfluorooctanoic acid (PFOA) from food-contact materials. The measurand is defined as the mass of analyte per unit contact area, expressed in ng/100 cm², determined under controlled experimental conditions representative of routine migration testing. Each reported value represents the outcome of a measurement process influenced by multiple sources of variability, including analyte-specific behavior, sample preparation, instrumental response, and analyst-dependent effects. Within the context of laboratory quality systems, such measurements are interpreted as realizations of a stochastic process, where observed variability reflects both controlled experimental factors and inherent measurement uncertainty.

B. Dataset structure and experimental factors

The dataset comprises 48 individual measurements structured across multiple experimental factors relevant to laboratory variability. These include the analyte (PFOS and PFOA), the analyst (three operators: ASLC, HEA, and WPA), and the concentration regime, categorized into low (L), medium (M), and high (H) levels. Within each analyte–concentration combination, replicate measurements were performed, typically in triplicate, to evaluate repeatability under controlled conditions. Each observation is associated with a sample code (e.g., L1, M2, H3), which encodes the concentration level and replicate index. The dataset exhibits a partially balanced structure. Low-level measurements are available for two analysts (ASLC and HEA), whereas medium- and high-level measurements are available for all three analysts. Despite this imbalance, the dataset remains suitable for assessing variability across concentration levels and for evaluating potential analyst-related effects within a statistical process control framework.

C. Summary of dataset characteristics

A summary of the dataset structure and experimental factors is presented in Table 1.

Table 1. Summary of Data Structure for PFOS and PFOA Migration Measurements

Variable	Description
Analytes	PFOS, PFOA
Concentration Level	Low (L), Medium (M), High (H)
Analysts	Multiple analysts
Replicates	Repeated measurements per condition
Response Variable	Concentration (ng/100 cm²)
Data Structure	Paired PFOS–PFOA observations per replicate

D. Relevance for Statistical Process Control Analysis

The structured nature of the dataset enables its interpretation within a statistical process control (SPC) framework. Replicate measurements within each analyte–concentration combination form subgroups that can be used to evaluate both central tendency and within-group variability. This structure supports the application of X-bar and range (R) control charts to assess measurement stability and repeatability. From a measurement perspective, the dataset provides a practical representation of routine laboratory data, where variability arises from both controlled experimental conditions and operational factors. This makes it well-suited for evaluating the effectiveness of SPC techniques in distinguishing systematic variation from potential measurement inconsistencies.

III. METHODS

A. Data Structure and Experimental Design

The dataset analyzed in this study consists of migration measurements of perfluorooctane sulfonate (PFOS) and perfluorooctanoic acid (PFOA) obtained from controlled laboratory experiments. Measurements were generated across three concentration levels—low (L), medium (M), and high (H)—to capture variability under different analytical conditions. For each concentration level, replicate measurements were performed by multiple analysts, enabling the assessment of both within-group variability and operator-related effects. Each observation corresponds to a single measurement result expressed as concentration in ng/100 cm² and is associated with an analyte identifier (PFOS or PFOA), analyst, concentration level, and replicate index. The dataset structure allows grouping of observations into subgroups defined by analyte and concentration level, with replicates within each subgroup used to evaluate measurement consistency.

B. Statistical Process Control Framework

Statistical Process Control (SPC) techniques were applied to evaluate the stability and variability of the measurement process. Specifically, X-bar (mean) and range (R) control charts were constructed for each analyte to monitor subgroup central tendency and within-subgroup dispersion, respectively. Subgroups were defined based on replicate measurements within each concentration level for a given analyte. For each subgroup, the sample mean ($\bar{X}$) and range (R) were calculated. The range is defined as the difference between the maximum and minimum values within a subgroup:

$$R = \max(x_i) - \min(x_i) \quad (1)$$

Where x_i represents the individual measurements within the subgroup. The average range ($\bar{R}$) was then computed across all subgroups as:

$$\bar{R} = \frac{\sum_{i=1}^{n} R_i}{n} \quad (2)$$

Where R_i is the range of subgroup i, and n is the total number of subgroups. The quantity $\bar{R}$ provides an estimate of typical within-subgroup variability and is used in the construction of control limits for both X-bar and R-charts. The overall mean of subgroup means ($\bar{\bar{X}}$) and the average range ($\bar{R}$) were then used to establish control limits.

C. Construction of Control Charts

The X-bar control chart was constructed using the following control limits:

Upper Control Limit	$UCL_X = \bar{\bar{X}} + A_2 \cdot \bar{R}$	(3)
Center Line	$CL_X = \bar{\bar{X}}$	(4)
Lower Control Limit	$LCL_X = \bar{\bar{X}} - A_2 \cdot \bar{R}$	(5)

The R chart was constructed as:

Upper Control Limit	$UCL_R = D_4 \cdot \bar{R}$	(6)
Center Line	$CL_R = \bar{R}$	(7)
Lower Control Limit	$LCL_R = D_3 \cdot \bar{R}$	(8)

where A_2, D_3, and D_4 are control chart constants determined by subgroup size. For this study, the subgroup size was $n = 3$, corresponding to triplicate measurements within each condition. The constants were therefore specified as $A_2 = 1.023$, $D_3 = 0$, and $D_4 = 2.574$, based on standard SPC reference tables. Control charts were used to identify out-of-control conditions, defined as points falling outside the control limits. Such points were interpreted as indications of atypical behavior requiring further investigation.

D. Evaluation of Measurement Stability and Variability

Measurement stability was assessed using the X-bar charts by examining the distribution of subgroup means relative to the control limits. Subgroups exceeding control limits were evaluated to determine whether deviations were associated with systematic experimental factors, such as concentration levels, or indicative of potential instability in the measurement process. Within-subgroup variability was assessed using R charts, which provide insight into repeatability under controlled conditions. Elevated range values or points exceeding the upper control limit were interpreted as indicators of increased variability, potentially arising from analytical or procedural factors.

E. Computational Tools

All statistical analyses and control chart constructions were performed using Python. Standard scientific computing libraries were used for data processing and visualization. Control limits were calculated based on established SPC formulations, and graphical outputs were generated to produce publication-quality control charts.

IV. RESULTS AND DISCUSSIONS

A. Control Chart Parameters and Overall Variability

The computed control chart parameters for PFOS and PFOA migration measurements are summarized in Table 2.

Table 2. Summary of Control Chart Parameters for PFOS and PFOA

	Analyte	
	PFOS	PFOA
$\bar{\bar{X}}(ng/100cm^2)$	270.77	299.94
$\bar{R}(ng/100cm^2)$	32.34	45.43
$UCL_x(ng/100cm^2)$	303.85	346.41
$LCL_x(ng/100cm^2)$	237.69	253.46

$UCL_R(ng/100cm^2)$	83.24	116.94
$LCL_R(ng/100cm^2)$	0	0

The results show that PFOA exhibits a higher average range ($\bar{R}$ =45.43 ng/100 cm²) compared to PFOS ($\bar{R}$ =32.34 ng/100 cm²), indicating greater within-subgroup variability. This suggests that PFOA measurements are subject to slightly higher dispersion under the same experimental conditions, reflecting differences in analytical behavior between the two analytes. To further interpret how this variability manifests in the measurement process, control charts were constructed to evaluate both subgroup means and within-subgroup dispersion.

B. X-bar Chart Analysis: Measurement Stability

To assess measurement stability across analytes and concentration levels, X-bar control charts were constructed to examine the behavior of subgroup means relative to established control limits. The X-bar charts for PFOS and PFOA are shown in Figures 1 and 2.

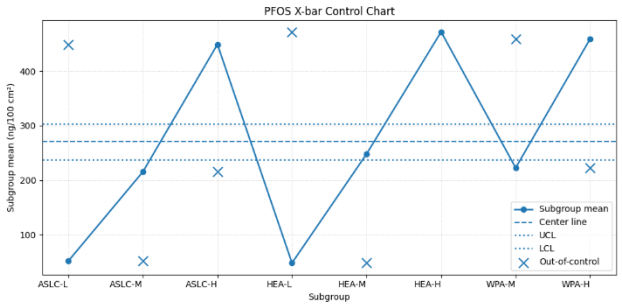


Figure 1. PFOS X-bar control chart

The PFOS X-bar chart shows several subgroup means falling outside the control limits. These out-of-control points are primarily associated with different concentration levels, where low-level measurements fall below the lower control limit and high-level measurements exceed the upper control limit. This pattern indicates that the observed deviations are not random but instead reflect systematic shifts in subgroup means due to concentration differences. Consequently, the apparent lack of statistical control is attributable to the inclusion of multiple concentration regimes within a single control chart, rather than instability in the measurement process itself. Having established the behavior for PFOS, a similar analysis was performed for PFOA as shown in Figure 2 to determine whether comparable patterns are observed across analytes.

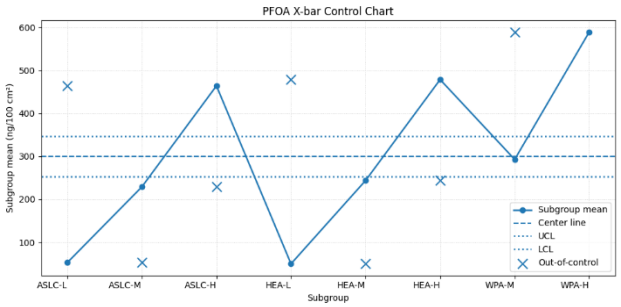


Figure 2. PFOA X-bar control chart

A similar pattern is observed for PFOA, where multiple subgroup means exceed the control limits. As with PFOS, these deviations correspond closely to concentration levels, indicating that concentration-driven variability dominates the behavior of subgroup means. Notably, seven subgroups for PFOA fall outside the X-bar control limits, consistent with the results reported for PFOS. This reinforces the conclusion that the X-bar chart is capturing structured experimental variation rather than true process instability. While the X-bar charts provide insight into the stability of subgroup means, further evaluation of measurement performance requires examination of within-subgroup variability using R charts.

C. R-Chart Analysis: Within-Subgroup Variability

To complement the evaluation of subgroup means, R charts were used to assess within-subgroup variability and provide insight into the repeatability of the measurement process. Figure 3 shows the R control chart for PFOS.

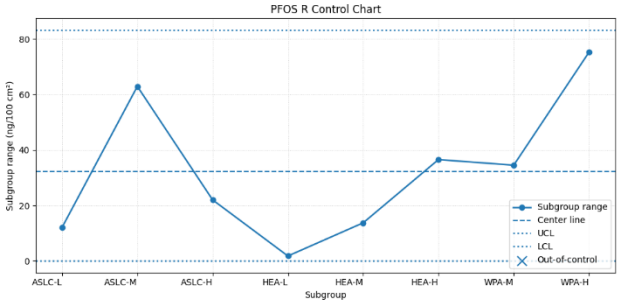


Figure 3. PFOS R control chart

The PFOS R chart shows that all subgroup ranges fall within the control limits, indicating stable within-subgroup variability across all measurement conditions. This suggests that the analytical method demonstrates consistent repeatability for PFOS measurements. The absence of out-of-control points in the R chart supports the interpretation that the variability observed in the X-bar chart is not due to random measurement fluctuations but rather to systematic differences in concentration levels. In contrast, the behavior of PFOA was examined to identify whether similar stability in within-subgroup variability is

maintained. To determine whether this stability is consistently maintained across analytes, the within-subgroup variability of PFOA measurements was examined using the corresponding R chart.

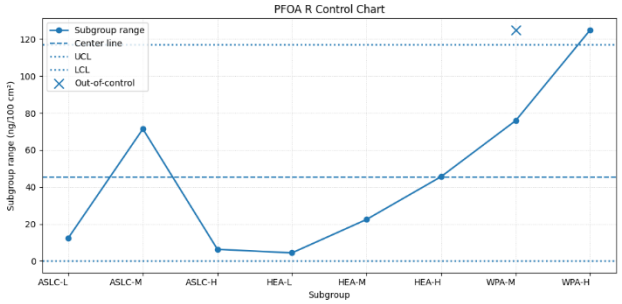


Figure 4. PFOA R control chart

The PFOA R chart exhibits one subgroup exceeding the upper control limit, indicating localized variability within that subgroup. This suggests the presence of a specific measurement condition where repeatability was reduced, potentially due to procedural or instrumental factors. Despite this isolated deviation, the majority of subgroup ranges remain within control limits, indicating that overall measurement variability for PFOA remains largely stable. Taken together, the X-bar and R chart results provide a comprehensive view of both systematic and random components of variability.

D. Influence of Concentration Level on Variability

Across both analytes, variability is strongly influenced by concentration level. The systematic separation of subgroup means observed in the X-bar charts confirms that concentration is the dominant driver of variability. At the same time, within-subgroup variability, as reflected in the R charts, remains relatively stable. This concentration-dependent behavior highlights an important consideration in the interpretation of SPC results for chemical measurements. When multiple concentration regimes are analyzed within a single control chart, systematic differences between groups may be incorrectly interpreted as out-of-control conditions. Therefore, SPC signals must be interpreted in the context of the experimental design to avoid misclassification of expected variation as measurement instability.

E. Implications for Measurement Stability and SPC Application

The combined interpretation of X-bar and R charts demonstrates that the measurement process is generally stable, with variability primarily driven by structured experimental factors rather than uncontrolled analytical effects. From a metrological perspective, this distinction is critical for ensuring accurate interpretation of measurement data. The results emphasize that SPC techniques, while powerful, must be applied with consideration of underlying experimental conditions. In the present case, the apparent lack of control observed in X-bar charts reflects concentration-driven variation rather than true process instability, while R charts confirm consistent repeatability. In summary, these findings demonstrate that SPC provides a valuable diagnostic framework for monitoring measurement performance, identifying atypical behavior, and supporting quality assurance in PFAS migration analysis.

V. CONCLUSIONS

This study applied statistical process control (SPC) techniques to evaluate the stability and variability of PFOS and PFOA migration measurements obtained from multi-analyst replicate datasets. The X-bar control charts indicated multiple out-of-control subgroup means for both analytes; however, these deviations were primarily associated with systematic differences across concentration levels rather than intrinsic instability of the measurement process. In contrast, the R charts demonstrated generally stable within-subgroup variability, with PFOS exhibiting fully controlled behavior and PFOA showing only a single out-of-control subgroup, indicating localized variability.

These findings highlight that the dominant source of variability in the dataset is structured and concentration-driven, while the measurement process itself exhibits good repeatability. From a metrological perspective, the results emphasize the importance of interpreting SPC outputs within the context of experimental design to avoid misclassification of expected variation as process instability. Overall, SPC is shown to be an effective diagnostic tool for monitoring analytical performance in PFAS migration studies. Its integration into routine laboratory workflows can enhance quality assurance, support ISO/IEC 17025 compliance, and improve confidence in measurement results for emerging contaminants.

REFERENCES

[1] M. Chang *et al.*, “Perfluorooctane Sulfonate (PFOS) and Perfluorooctanoic Acid (PFOA) in the Surface Waters of China: A Meta-Analysis,” *Water*, vol. 17, no. 9. p. 1275, 2025. doi: 10.3390/w17091275.

[2] V. Polychronidou and R. Nag, “Human health risk assessment of Per- and polyfluoroalkyl substances (PFAS),” *Sci. Total Environ.*, vol. 1000, p. 180428, 2025, doi: https://doi.org/10.1016/j.scitotenv.2025.180428.

[3] C. G. Eze *et al.*, “Emerging contaminants in food matrices: An overview of the occurrence,

pathways, impacts and detection techniques of per- and polyfluoroalkyl substances," *Toxicol. Reports*, vol. 12, pp. 436–447, 2024, doi: https://doi.org/10.1016/j.toxrep.2024.03.012.

[4] M. C. O. Souza and J. L. Domingo, "Levels of per- and polyfluoroalkyl substances (PFAS) in foodstuffs: a review of dietary exposure, health risks, and regulatory challenges," *Food Res. Int.*, vol. 221, p. 117494, 2025, doi: https://doi.org/10.1016/j.foodres.2025.117494.

[5] R. Li *et al.*, "Per- and polyfluoroalkyl substances in food contact materials: Migration, health risks and sustainable alternatives," *Trends Food Sci. Technol.*, vol. 172, p. 105667, 2026, doi: https://doi.org/10.1016/j.tifs.2026.105667.

[6] S. Y. Wee and A. Z. Aris, "Environmental impacts, exposure pathways, and health effects of PFOA and PFOS," *Ecotoxicol. Environ. Saf.*, vol. 267, p. 115663, 2023, doi: https://doi.org/10.1016/j.ecoenv.2023.115663.

[7] S.-H. You and C.-C. Yu, "Health Risk Exposure Assessment of Migration of Perfluorooctane Sulfonate and Perfluorooctanoic Acid from Paper and Cardboard in Contact with Food under Temperature Variations," *Foods*, vol. 12, no. 9. p. 1764, 2023. doi: 10.3390/foods12091764.

[8] M. Y. D. Alazaiza, T. M. Alzghoul, M. B. Ramu, S. S. Abu Amr, and M. F. M. Abushammala, "PFAS contamination and mitigation: A comprehensive analysis of research trends and global contributions," *Case Stud. Chem. Environ. Eng.*, vol. 11, p. 101127, 2025, doi: https://doi.org/10.1016/j.cscee.2025.101127.

[9] S. Berlinski, B. Calder, and D. Paustenbach, "An evaluation and risk assessment of children's exposures to water-soluble per- and polyfluoroalkyl substances through winter gloves.," *Toxicol. reports*, vol. 15, p. 102095, Dec. 2025, doi: 10.1016/j.toxrep.2025.102095.

[10] P. Vera, E. Canellas, N. Dreolin, J. Goshawk, and C. Nerín, "The analysis of the migration of per and poly fluoroalkyl substances (PFAS) from food contact materials using ultrahigh performance liquid chromatography coupled to ion-mobility quadrupole time-of-flight mass spectrometry (UPLC- IMS-QTOF)," *Talanta*, vol. 266, p. 124999, 2024, doi: https://doi.org/10.1016/j.talanta.2023.124999.

[11] M. Sadia, L. W. Y. Yeung, and H. Fiedler, "Trace level analyses of selected perfluoroalkyl acids in food: Method development and data generation," *Environ. Pollut.*, vol. 263, p. 113721, 2020, doi: https://doi.org/10.1016/j.envpol.2019.113721.

[12] Z. Zahra, M. Song, Z. Habib, and S. Ikram, "Advances in per- and polyfluoroalkyl substances (PFAS) detection and removal techniques from drinking water, their limitations, and future outlooks," *Emerg. Contam.*, vol. 11, no. 1, p. 100434, 2025, doi: https://doi.org/10.1016/j.emcon.2024.100434.

[13] G. Briassoulis, S. Ilia, and E. Briassouli, "Exposure to Per- and Polyfluoroalkyl Substances (PFASs) in Healthcare: Environmental and Clinical Insights.," *Life (Basel, Switzerland)*, vol. 15, no. 7, Jul. 2025, doi: 10.3390/life15071057.

[14] F. S. H. Krismastuti and M. H. Habibie, "Complying with the resource requirements of ISO/IEC 17025:2017 in Indonesian calibration and testing laboratories: current challenges and future directions.," *Accredit. Qual. Assur. J. Qual. Comp. Reliab. Chem. Meas.*, vol. 27, no. 6, pp. 359–367, 2022, doi: 10.1007/s00769-022-01523-w.

[15] M. Outaki *et al.*, "Quality approach towards ISO/IEC 17025 accreditation at the center of analysis and characterization of Marrakesh Cadi Ayyad University: metrology stakes," *Int. J. Metrol. Qual. Eng.*, vol. 15, no. 22, 2024, doi: https://doi.org/10.1051/ijmqe/2024019.

[16] G. J. da Silva and A. C. Borges, "Statistical Process Control in the Environmental Monitoring of Water Quality and Wastewaters: A Review," *Water*, vol. 17, no. 9. p. 1281, 2025. doi: 10.3390/w17091281.

[17] X. Li, X. Shen, W. Jiang, Y. Xi, and S. Li, "Comprehensive review of emerging contaminants: Detection technologies, environmental impact, and management strategies," *Ecotoxicol. Environ. Saf.*, vol. 278, p. 116420, 2024, doi: https://doi.org/10.1016/j.ecoenv.2024.116420.

[18] M. J. K. Bashir and A. Mojiri, "Recent Developments in Emerging Contaminants Determination and Treatment Technologies," *Separations*, vol. 9, no. 12. p. 434, 2022. doi: 10.3390/separations9120434.

[19] E. K. P. Encarnacion *et al.*, "Preliminary Screening of Per- and Polyfluoroalkyl Substances (PFAS) in Philippine Fast Food Packaging Using Liquid Chromatography–Mass Spectrometry (LC-MS)," *Currrent Res. Nutr. Food Sci.*, vol. 12, no. 1, 2024, doi: http://dx.doi.org/10.12944/CRNFSJ.12.1.34.

2026 IMEKO Joint Conference
TC8 - TC11 - TC24
Metro Manila, Philippines, August 26-29, 2026

Measurement Capability of TXRF for Trace Heavy Metal Detection in Epoxy-Based Die Attach Adhesives

Tabuso, Aldrin Jan E.[1], Rocha, Anton John D.[1], Mendoza, Charisse M.[1], Santillan, Abegail I.[1], Martin, Zamantha Nadir Z.[1], Cortes, Edna Linda M.[1], and Bauca, Marianne Therese A.[1]

[1] *Industrial Technology Development Institute, DOST Compound, Bicutan, Taguig, Metro Manila, Philippines, aldrinjantabuso@gmail.com*

Abstract **- The detection and quantification of hazardous substances in electronic materials are essential for compliance with the Restriction on Hazardous Substances (RoHS) directive and for minimizing environmental and health risks associated with electronic waste. This study presents a method for heavy metal analysis in epoxy-based die-attach adhesives using Total Reflection X-Ray Fluorescence (TXRF) spectroscopy. Acetone was selected as the optimal solvent for sample preparation due to effective dilution and lower safety risks. Calibration using 30 ppm and 100 ppm standards for Br, Cr, Hg, Pb, and Cd yielded measured concentrations that closely matched the expected values. Signal stabilization was achieved at approximately 1200 seconds. Measured concentrations in epoxy samples were below 100 ppm for Cd, and below 1000 ppm for other elements, meeting RoHS limits. The method demonstrated high repeatability and reproducibility, confirming its robustness for industrial use, and offers a fast, reliable screening tool for ensuring material compliance.**

I. INTRODUCTION

The rapid advancement of information technology has led to a significant increase in e-waste, driven by the frequent replacement of electronic devices prior to their end-of-life. In many developing countries, inadequate regulatory enforcement leads to improper disposal practices, such as landfilling and incineration, posing risks of environmental contamination from hazardous substances present in electronic materials [1][2].

To mitigate these risks, international regulations such as the Restriction on Hazardous Substances (RoHS) directive limit the presence of toxic elements, including lead (Pb), mercury (Hg), cadmium (Cd), chromium (Cr), and bromine (Br) in electronic products. Compliance with these regulations requires reliable and accessible analytical methods, particularly in the semiconductor and electronics (S&E) industry, which plays a major role in the Philippine economy [3][4].

Total Reflection X-Ray Fluorescence (TXRF) is a promising technique for trace element analysis due to its high sensitivity, minimal sample preparation, and capability for multi-element detection. It has been widely used in environmental, industrial, and semiconductor applications to monitor trace contaminants [5][6].

This study aims to develop a TXRF-based method to detect trace heavy metals in epoxy-based die-attach adhesives. The work focuses on optimizing sample preparation and measurement conditions and evaluating the method's performance for potential use as a rapid screening tool to support regulatory compliance in local industries.

II. MATERIALS AND METHOD

A. *Preparation of samples*

Five (5) die-attach (DA) epoxy adhesives were obtained from local semiconductor manufacturers as primary samples. These samples were production-used materials representative of industrial formulations. A commercial epoxy adhesive, Epo-Tek H70E, was procured via standard purchase request and used as a reference material.

A total of six (6) conductive epoxy adhesives were evaluated: CRM 1084A, Atrox 800HT2V-P1, Epo-Tek H20E, Atrox 850HT1, Ablebond 84-1LMI, and Epo-Tek H70E. All samples are silver-filled conductive epoxies designed for die attachment applications.

B. *Solvent selection for TRXF sample preparation*

Due to their high viscosity and metallic filler content, epoxy adhesives were not directly suitable for TXRF analysis, which requires uniform thin films (<100 μm). Solvent screening was conducted to identify a medium capable of reducing viscosity and dispersing silver fillers.

Tested solvents included boiling distilled water, nitric acid (20% and 65%), sulfuric acid (1N and 98%), dichloromethane (DCM), and acetone, as reported in the literature by Epoxy Technology Inc. [7].

For each test, 100 mg epoxy was mixed with 3 mL solvent in sealed vials and gently agitated. Dissolution performance was evaluated based on polymer matrix

breakdown, with successful dissolution defined as complete removal of the epoxy matrix and sedimentation of metallic fillers.

C. *Determination of TXRF sensitivity factors*

Elemental quantification in TXRF was performed using internal standardization with yttrium (Y). Sensitivity factors were established for Br, Cd, Cr, Pb, and Hg using certified reference solutions. Low (30 ppm) and high (100 ppm) standard solutions were prepared from certified materials obtained from Industrial Technology Development Institute - NMD and STD laboratories. Each 3 mL solution contained 10 µL yttrium internal standard (IS).

Ten (10) quartz discs per concentration were prepared by depositing 10 µL aliquots and air-drying them to form thin films (~100 µm thick). Samples were analyzed using a 2000-second acquisition time. Sensitivity factors were calculated from intensity ratios of analyte peaks relative to yttrium using Equation (1), enabling conversion of fluorescence intensities to concentrations.

$$\%conc_{element} = \frac{conc_{IS} \times A_{element} \times sf_{IS}}{A_{IS} \times sf_{element}} \quad (1)$$

where:

$A_{element}$ = adjusted net area under the peak of element
A_{IS} = net area under the peak of internal standard
$sf_{element}$ = sensitivity factor of the element
sf_{IS} = sensitivity factor of the internal standard

D. *Optimization of analysis time*

The optimal TXRF acquisition time was determined using time-dependent signal stability experiments. Epoxy samples (100 mg) were dissolved in 3 mL of acetone and 2 mL of Triton X-100 solution, with 10 µL yttrium added as an internal standard. Triton X-100 enhanced the dispersion of silver fillers.

Ten (10) replicate discs were prepared and analyzed at acquisition times ranging from 600 to 2000 s in 200 s intervals. Silver (Ag) peak intensity was used as the response indicator. The optimal time was selected based on signal stability and precision across replicates.

E. *Verification of reagent purity*

All reagents (acetone, Triton X-100, and yttrium standard solution) were evaluated for contamination with Pb, Hg, Cd, Cr, and Br in accordance with IEC 62321-3-1 requirements.

Each reagent was analyzed using TXRF under optimized conditions. Five (5) replicate measurements were performed, and average trace metal contents were recorded to confirm suitability for ultra-trace analysis.

F. *TXRF analysis of epoxy DA samples*

All epoxy samples were weighed to obtain a 100 mg sample, which was dissolved in the optimized solvent system and homogenized before deposition. Thirty (30) quartz disc replicates were prepared per sample to ensure statistical reliability. TXRF measurements were conducted using established sensitivity factors and optimized analysis time. Elemental identification and quantification were derived from spectral peak intensities.

Table 1 summarizes the different parameters used for the TXRF analysis.

Table 1. Parameters set for the analysis of PRM-2002 using TXRF.

Parameter	Unit	Value
X-ray voltage	kV	50
X-ray current	µA	1000
Filter		none
Amount of IS (Y)	µL	10
Y sensitivity factor	-	1.780218

G. *Repeatability and Reproducibility*

Method precision was evaluated in accordance with IEC 62321-3-1. For repeatability, four analysts each analyzed ten (10) samples in triplicate, with randomized sample order. For reproducibility, a single analyst performed four (4) independent runs of ten (10) samples, each in triplicate, with samples randomized within each run.

The method was considered acceptable if no more than 5% of paired results exceeded repeatability and reproducibility limits, ensuring both instrumental and operator variability remained within IEC-defined statistical thresholds.

III. RESULTS AND DISCUSSION

A. *Solvent Selection*

The dissolution experiment was done in a controlled laboratory with an ambient temperature of 20-25°C and a relative humidity of 40-60%. Table 2 summarizes the solvents used and their capability to dissolve the epoxy samples.

Table 2. Results of the dissolution experiment

Solvent	Epoxy dissolution
boiling distilled water	Negative
warm nitric acid (20 v/v)	Negative
warm nitric acid (65 v/v)	Negative

warm sulfuric acid (1N)	Negative
warm sulfuric acid (98%)	Positive
dichloromethane (DCM)	Positive
acetone	Positive

Among the three reagents that dissolved the epoxy, acetone was chosen as the solvent for the sample preparation because it has a lower corrosive tendency and, therefore, is the safest reagent to handle.

B. *Determination of the sensitivity factor*

The sensitivity factors were determined using standard solutions of the target elements Br, Cr, Hg, Pb, and Cd. This step ensures that the TXRF readings were, in a way, calibrated to the target elements. Two (2) concentrations of each element were analyzed, 30 and 100 ppm. Across multiple scans, the standard samples show high precision but inaccurate values. Therefore, the sensitivity factors were adjusted to ensure that the analysis of the actual epoxy samples would produce accurate results. Table 3 shows the determined sensitivity factors for the epoxy samples.

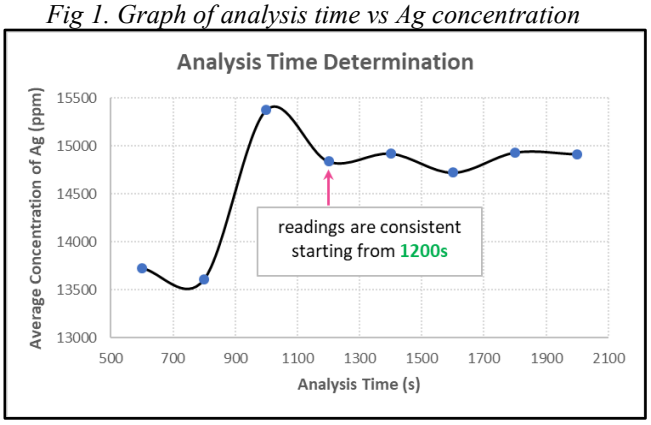
Table 3. Determined sensitivity factors for TXRF analysis

Element	Sensitivity factor
Br	1.271
Cr	0.5845
Hg	0.0515
Pb	0.892
Cd	0.04

C. *Determination of analysis time (duration)*

Determining the optimal duration of analysis prevents unnecessary analysis time that no longer contributes to the results. To determine the optimal time, an epoxy sample was prepared and analyzed at different time points. The epoxy sample used for the analysis contains Ag; therefore, it was the element considered for determining the optimal analysis time. In Figure 1, the concentration readings stabilize after around 1200 seconds of analysis time. Based on this observation, the analysis time was determined to be 1200 seconds.

Fig 1. Graph of analysis time vs Ag concentration



D. *Checking of reagent purity*

Contamination could come from various sources. One of which is the reagents used themselves. The main reagents used for sample preparation were each analyzed using the Bruker S2 Picofoc TXRF spectrometer, and Table 4 summarizes the results. It shows that the reagents have minimal heavy-metal content and do not significantly contribute to the epoxy samples' results.

Table 4. TXRF analysis of reagents (in ppm)

Element	Triton X-100	Acetone	Y Internal Standard
Br	3.8	5.473	0
Cr	2.577	0.306	0
Hg	0	0	0
Pb	1.416	4.941	0.001
Cd	0	0	0

E. *Analysis of epoxy samples*

A total of six (6) epoxy samples were analyzed using the developed method. Five (5) of the samples were acquired from local semiconductor assembly plants, and one (1) is a commercial epoxy.

The TXRF results include the net area values of each detected element from the spectra. For the analysis, the net area values were recorded and used to calculate concentrations using Eq. (1).

Table 5 shows the concentration of heavy metals in all six (6) epoxy samples.

Table 5. TXRF analysis of epoxy samples (in ppm)

Epoxy sample	Br	Cr	Hg	Pb	Cd
CRM1084A	0.000	0.000	0.001	0.065	2.847
ATROX 850HT1	0.000	0.010	0.001	0.010	50.019

Epo-Tek H20E	0.000	0.013	0.001	0.042	50.888
Ablebond 84-1LMI	0.000	0.014	0.000	0.022	59.365
ATROX 800HT2V-P1	0.000	0.012	0.001	0.097	58.760
Epo-Tek H70E	0.000	0.002	0.021	0.030	0.238

It appears that some of the epoxy samples contain very small amounts of heavy metals. Despite the presence of heavy metals, the results are considered good since they are below the RoHS limit, as listed in Table 6.

Table 6. TXRF analysis of epoxy samples (in ppm)

Element	RoHS limit (ppm)
Br	1000
Cr	1000
Hg	100
Pb	1000
Cd	1000

F. *Repeatability and reproducibility analysis*

As per IEC 62321-3-1 standards, the absolute difference between two test results obtained must not exceed the calculated repeatability/reproducibility limit r/R in more than 5% of the cases. Using formulas (1) to (5), the limits were calculated, and the absolute differences of individual measurements were compared against these limits. Table 7 summarizes the detected occurrences of exceeding the calculated limits.

Table 7. Repeatability and reproducibility results

Element	% Occurrence of exceeding the limit	
	Repeatability	Reproducibility
Br	4.17	1.25
Cr	1.67	0.00
Hg	0.83	1.25
Pb	1.67	0.00
Cd	2.50	1.25

The results show that the occurrence of exceeding the repeatability and reproducibility limits was never more than 5%. Thus, the new test method for the detection and quantification of heavy metals in epoxy-based epoxies passes the repeatability and reproducibility requirements stipulated in IEC 62321-3-1.

IV. CONCLUSION

A method for the detection and quantification of the five RoHS-regulated heavy metals (Cr, Br, Cd, Hg, and Pb) in epoxy-based die-attach adhesives was developed using Total Reflectance X-Ray Fluorescence Spectroscopy (TXRF) with the Bruker S2 Picofox 400.

The accuracy of element quantification was achieved by determining the sensitivity factor for each heavy metal, which was then incorporated into the method. The optimum analysis time was also identified to make the method as productive as possible without unnecessarily damaging the sample, thus enabling multiple scans for each prepared sample. The method achieved good results in the repeatability and reproducibility assessments, which speaks to its consistency across different conditions and equipment users.

The TXRF analyses of the different epoxy samples also showed compliance with the RoHS limits, with Cd less than 100 ppm and Br, Cr, Hg, and Pb all less than 1000 ppm.

REFERENCES

[1] Lancaster, S.T., Sahlin, E., et.al., “Evaluation of X-ray fluorescence for analysing critical elements in three electronic waste matrices: A comprehensive comparison of analytical techniques”, Waste Management, 2024, 190 pp. 496–505.

[2] Kumar, A., Thorbole, A., Gupta, R.K., “Sustaining the future: Semiconductor materials and their recovery”, Materials Science in Semiconductor Processing, 2005, 185, p.108943.

[3] RoHS directive - environment - European Commission. (n.d.). https://environment.ec.europa.eu/topics/waste-and-recycling/rohs-directive_en

[4] SEIPI. About the Industry – SEIPI, September 2024, https://seipi.org.ph/about-the-industry/

[5] Margui, E., Zawisza, B., Sitko, R., “Trace and ultratrace analysis of liquid samples by X-ray fluorescence spectrometry”, Trends in Analytical Chemistry, 2014, 53, pp.73–83.

[6] Klockenkämper, R. & von Bohlen, A., “Total-Reflection X-Ray Fluorescence Analysis and Related Methods”, Second Edition, John Wiley & Sons, Inc., New Jersey, USA, 2015.

[7] Epoxy Technology Inc., “Reworking, Removing and Decapsulating Cured Epoxies”, 2015, Tech Tip, 8, Epoxy Technology Inc., USA, Accessed online: www.epotek.com

2026 IMEKO Joint Conference
TC8 - TC11 - TC24
Meto Manila, Philippines, 26-29 August 2026

Chemometric Characterization of Arsenic Speciation and Geochemical Drivers of Arsenic Toxicity in the Molawin Creek-Maahas River System, Los Baños, Laguna, Philippines

John Ray G. Gaspar[1], Val Jason G. Lagrada[1], Joshua L. Maligalig[2], Shaira C. Javier[2], Rejaynil M. Valdez[2]

[1] *Institute of Chemistry, College of Arts and Sciences, University of the Philippines Los Baños, College, Laguna, ichem.uplb@up.edu.ph*
[2] *Laboratory and Experimental Services Division, Ecosystem Research and Development Bureau, Department of Environment and Natural Resources, College, Los Baños, Laguna, erdb@denr.gov.ph*

***Abstract* – Molawin Creek within the Makiling Forest Reserve is a domestic water source connected to the Maahas River and Laguna de Bay. Due to the area's volcanic geology, arsenic (As) naturally occurs in the system, but factors affecting its speciation and toxicity remain poorly understood. This study investigated As occurrence across five sampling points and applied chemometric analyses to identify the geochemical drivers of toxicity. Results showed that total As concentrations from midstream to downstream exceeded the 10 µg/L limit for Class B waters under DAO 2016-08. Spearman correlation and PCA indicated that As mobility is associated with geogenic weathering, anthropogenic inputs, and temperature. Kruskal-Wallis analysis revealed significant spatial variability for total As ($\chi^2 = 13.03$, $\rho = 0.011$) and the As(III):As(V) ratio ($\chi^2 = 13.50$, $\rho = 0.009$). Oxidation-reduction potential strongly influences the As(III):As(V) ratio ($\rho = -0.63$), while pH stabilizes speciation. The Convergence point showed the highest As(III):As(V) ratio, suggesting it as a possible toxicity hotspot.**

I. Introduction

Arsenic (As) contamination in aquatic environments is a concern because its mobility and toxicity depend on geochemical conditions and its chemical form. In natural waters, As may originate from rock weathering, geothermal and volcanic processes, sediment-water interaction, and biological activity, with additional inputs from mining, agriculture, industrial discharge, and domestic wastewater [1]. Once released, As is redistributed among water, sediments, soils, and organisms through adsorption, desorption, precipitation, dissolution, oxidation-reduction, and microbial transformation [2]. Thus, As risk is controlled not only by concentration but also by the physicochemical conditions that affect its mobility and speciation.

The Molawin Creek–Maahas River System is located within the Makiling Forest Reserve in Los Baños, Laguna, an area influenced by the volcanic geology of Mt. Makiling. Volcanic and geothermal settings may release As into connected groundwater and surface waters through weathering and leaching [1], [2]. Philippine studies have emphasized the need to examine As in geologically influenced water sources near Mt. Makiling and other groundwater systems, where As poses an emerging drinking-water safety concern [3], [4]. Since Molawin Creek serves as a domestic water source and drains toward the Maahas River and Laguna de Bay, As occurrence in this system has potential implications for local water safety and downstream aquatic environments.

The risk posed by As depends strongly on speciation. In freshwater, inorganic As mainly occurs as arsenite [As(III)] and arsenate [As(V)], with As(III) generally considered more toxic and mobile than As(V) [3], [5]. Because these species differ in toxicity, mobility, and behavior, total As alone may not adequately represent ecological or public health risk [5]. As speciation is influenced by oxidation-reduction potential, pH, salinity, temperature, microbial activity, organic matter, and interactions with iron and manganese oxides [1], [2], [6]. These factors can shift As between less toxic and more toxic forms, making the As(III):As(V) ratio useful for assessing toxicity.

In the Philippines, DAO 2016-08 sets a 10 µg/L limit for As in Class B waters [7]. While this threshold is important for regulatory compliance, it does not account for As speciation. This is a limitation in dynamic river systems where pH, redox conditions, dissolved ions, and organic

inputs may influence the release, conversion, or persistence of toxic As species.

Chemometric analysis provides a practical approach for interpreting complex water quality datasets by identifying relationships, reducing data complexity, and supporting environmental assessment [8], [9]. Techniques such as Principal Component Analysis (PCA) and correlation analysis have been used to evaluate spatial variability, identify possible pollution sources, and determine physicochemical drivers of contaminant behavior [8]–[10]. This study therefore investigated the spatial distribution of total As and As species in the Molawin Creek–Maahas River System, evaluated the As(III):As(V) ratio as a toxicity indicator, and applied statistical and chemometric analyses to identify the geochemical drivers influencing As mobility, speciation, and toxicity.

II. Materials and Methods

A. *Selection of sampling points*

Five sampling points were selected along the Molawin Creek-Maahas River System to represent different hydrologic sections and surrounding land-use conditions. The upstream station was located within the Makiling Botanical Garden at the upper campus of the University of the Philippines Los Baños (UPLB), representing the forested headwater section of the system. Two midstream pointss were selected to represent the more urbanized section of the river corridor. Midstream I was located near the lower UPLB campus in Barangay San Antonio, while Midstream II was located near residential areas in Barangay Maahas. The downstream station was located near residential and agricultural-use areas. The Convergence station was selected at the junction of Molawin Creek and Bay River to represent the mixing zone between the two water systems. Site descriptions, observed local activities, and geographic coordinates are summarized in Table 1.

Table 1. Description, local activities, and geographic coordinates of the selected sampling points along the Molawin Creek–Maahas River system.

Site	Description	Coordinates
Upstream (U)	Protected forest	14°09'24"N 121°14'02"E
Midstream I (M1)	Easy access point to other sampling sites	14°10'13"N 121°15'08"E
Midstream II (M2)	Vegetated midstream used for bathing	14°10'54"N 121°15'03"E
Downstream (D)	Adjacent to residential areas	14°11'14"N 121°15'33"E
Convergence (C)	Junction of Molawin Creek and Bay River	14°11'15"N 121°15'34"E

B. *Physico-chemical analysis*

In situ physicochemical parameters, including temperature, pH, dissolved oxygen (DO), electrical conductivity (EC), total dissolved solids (TDS), and oxidation-reduction potential (ORP), were measured using a calibrated Horiba U-53G multiparameter water quality meter (HORIBA Ltd., Kyoto, Japan). Levels of chloride were determined by the argentometric method following SMEWW 4500-Cl B. Nitrate was analyzed using the colorimetric brucine-sulfanilic acid method based on US EPA Method 352.1. Orthophosphate was determined using the ascorbic acid method following SMEWW 4500-P E. Chemical oxygen demand (COD) was analyzed using the potassium permanganate oxidation method described by Goh and Lim [11]. Iron was quantified by flame atomic absorption spectrophotometry (FAAS) using a Shimadzu AA-7000 atomic absorption spectrophotometer (Shimadzu Corp., Kyoto, Japan) following SMEWW 3111B. All analyses were performed in triplicate for each sampling point, and results were summarized as point means.

C. *Total arsenic and arsenic speciation analysis*

Total As and As species were analyzed following SMEWW 3114B using a Shimadzu AA-7000 atomic absorption spectrophotometer coupled with an HVG-1 hydride vapor generator (Shimadzu Corp., Kyoto, Japan), following the Shimadzu HVG-1 arsenic analysis procedure. For total As determination, water samples were acid-digested and treated with potassium iodide (KI) and ascorbic acid to reduce As(V) to As(III) prior to hydride generation atomic absorption spectrophotometry (HVG-AAS). The measured concentration represented total As. For As(III) determination, acid-digested samples were analyzed directly by HVG-AAS without the KI–ascorbic acid reduction step. As(V) was calculated as the difference between total As and As(III):

$$\text{As(V)} = \text{Total As} - \text{As(III)} \quad (1)$$

The As(III):As(V) ratio was computed to evaluate the relative dominance of arsenite in the water samples.

D. *Chemometric and statistical analysis*

Chemometric and statistical analyses were performed in

R using RStudio [12], [13]. Descriptive statistics were used to summarize As behavior at each sampling point. Spatial differences in total As and the As(III): As(V) ratio were evaluated using the Kruskal–Wallis test, while Spearman rank correlation was used to assess associations among arsenic species, speciation ratios, and physicochemical parameters. PCA was performed on standardized variables using z-score scaling to minimize the influence of differences in units and variable ranges. Correlation matrices and PCA outputs were visualized using the Hmisc, corrplot, factoextra, ggplot2, and tidyverse packages [12], [13].

E. *Hazard mapping*

A hazard map was generated using the geographic coordinates of the sampling points and the measured As parameters. Total As concentration and the As(III):As(V) ratio were used as hazard indicators to represent arsenic occurrence and relative toxicity across the Molawin Creek–Maahas River system. Sites were classified as low hazard when total As was ≤10 µg/L and the As(III):As(V) ratio was <0.40; moderate hazard when total As was >10 µg/L or the As(III):As(V) ratio was 0.40–0.69, but not both high; and high hazard when total As was >10 µg/L and the As(III):As(V) ratio was ≥0.70. The 10 µg/L threshold was based on the Class B arsenic limit under DAO 2016-08 [7]. Graduated point maps were prepared in R using ggplot2 and ggrepel [12], [13], where point size represented total As concentration and point color represented the assigned hazard class.

III. Results and Discussion

A. *Spatial variation of arsenic and water quality parameters*

The measured As species and selected water quality parameters showed distinct spatial differences across the Molawin Creek–Maahas River system. The pattern generally shifted from lower As and less chemically altered conditions at the Upstream to greater As enrichment and stronger geochemical alteration at the Downstream and Convergence points. Among all sites, the Convergence point represented the most critical condition, where elevated As, higher Fe, higher PO_4 and COD, and low DO occurred together. This indicates that the Convergence functions not only as a hydrologic mixing point but also as a site where conditions favorable to arsenic mobility and toxicity are concentrated.

Total As increased from 2.42 µg/L Upstream to 25.14 µg/L at Convergence, exceeding the 10 µg/L Class B limit under DAO 2016-08 at all points except Upstream [7]. This indicates that As enrichment begins beyond the forested headwater section and persists toward the lower reaches. The highest total As at Convergence may reflect the combined influence of geogenic inputs, sediment-water interaction, and local mixing processes, since As mobility is affected by weathering, redox-sensitive release, and sediment-associated transport [1], [2].

Table 2. Average As concentrations, in µg/L, *and toxicity indicators across sampling points. Values are point means based on three replicate measurements.*

Site	As(III)	As(V)	Total As	As(III): As(V)
U	0.57	1.85	2.42	0.31
M1	2.14	12.37	14.51	0.17
M2	2.58	9.35	11.93	0.28
D	2.55	12.84	15.39	0.20
C	11.01	14.13	25.14	0.79
Limit	-	-	10.00	-

Convergence also recorded the highest Fe (4.78 mg/L), exceeding the 1.0 mg/L guideline [7]. Since Fe-bearing phases can regulate As retention and release, the co-occurrence of elevated Fe and total As suggests that Fe-associated processes may contribute to arsenic accumulation at this site [1], [6]. Low DO (3.53 mg/L) and mildly acidic pH (6.05) further indicate conditions that may favor arsenic mobility and species transformation [1], [2].

PO_4 and COD also reached their highest levels at Convergence, suggesting nutrient and organic enrichment that may influence microbial and redox processes involved in arsenic transformation [1], [2]. Speciation results confirmed Convergence as the primary toxicity hotspot: As(III) reached 11.01 µg/L, and the As(III):As(V) ratio was highest at 0.79. Since As(III) is generally more toxic and mobile than As(V), the site represents the highest-risk area in the system [3], [5].

B. *Chemometric identification of geochemical drivers*

Kruskal–Wallis analysis confirmed significant spatial variability in total As and As toxicity ratio. Total As differed significantly among sampling points ($\chi^2 = 13.03$, $p = 0.011$), and the As(III):As(V) ratio also showed significant spatial variation ($\chi^2 = 13.50$, $p = 0.009$). These results indicate that both As enrichment and As speciation were site-dependent. Similar applications of multivariate and nonparametric approaches in water quality studies have shown that spatial differences in contaminants are often controlled by local hydrologic conditions, land use, and physicochemical gradients [8], [9], [10].

Spearman correlation analysis (Fig. 1) showed that total As was strongly correlated with COD ($\rho = 0.97$) and with EC, Fe, PO_4, TDS, TSS, and temperature ($\rho = 0.90$). Total As was negatively correlated with pH ($\rho = -0.90$) and DO ($\rho = -0.70$). These relationships indicate that As enrichment was associated with dissolved-ion enrichment, Fe, nutrient and organic indicators, higher temperature,

lower oxygen, and lower pH. The strong association between As and Fe supports the role of Fe-bearing phases in As retention and release, while the relationship with COD and PO_4 suggests that organic and nutrient inputs may influence redox processes and sorption competition [1], [2], [6].

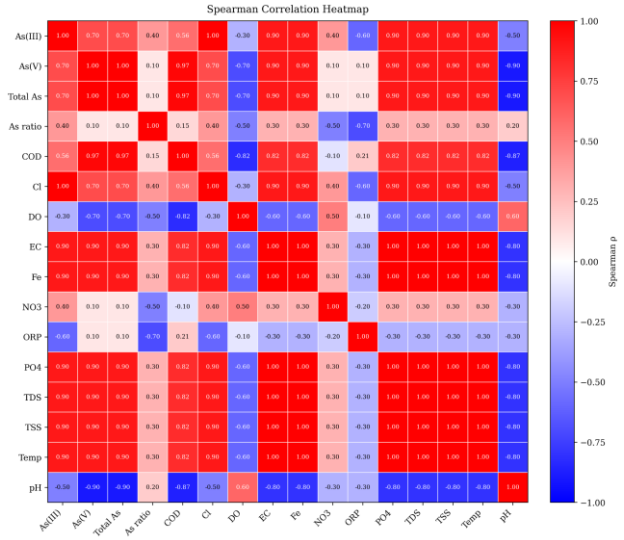


Fig. 1. Spearman correlation heatmap showing relationships among arsenic species, toxicity ratio, and physicochemical parameters.

The As(III):As(V) ratio was most strongly and negatively correlated with ORP ($\rho = -0.63$), suggesting that lower redox potential favored the relative dominance of As(III). This result is consistent with the known redox sensitivity of arsenic species, where reducing conditions may favor arsenite persistence and increase toxicity risk [1], [2], [5]. This distinction is important because total As and arsenic toxicity were not controlled by exactly the same factors. Total As was more closely related to chemical loading and Fe-associated enrichment, while the As(III):As(V) ratio was more closely related to redox condition.

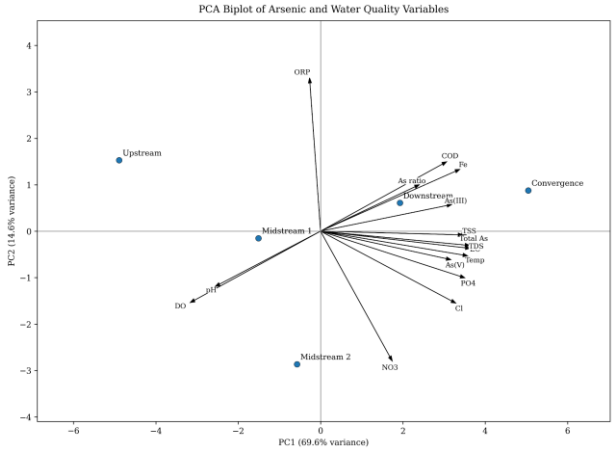


Fig. 2. PCA biplot showing major geochemical gradients among sampling points.

The PCA biplot (Fig. 2) supported the correlation results. PC1 explained 69.6% of the variance and represented an enrichment gradient associated with total As, As species, Fe, EC, TDS, TSS, PO_4, Cl, COD, and temperature. The Convergence point was positioned farthest along this gradient, confirming its high arsenic and chemical loading. PC2 explained 14.6% of the variance and reflected redox- and oxygen-related variables, particularly ORP, DO, and pH. Together, PC1 and PC2 explained 84.2% of dataset variability, showing that arsenic mobility and toxicity were influenced by overlapping mineralization, Fe-related, nutrient-organic, and redox gradients.

C. *Hazard mapping and monitoring implications*

The hazard-class map integrated total As concentration and the As(III):As(V) ratio to identify priority monitoring points (Fig. 3). Upstream was classified as low hazard because total As was below the 10 µg/L Class B limit and the As(III):As(V) ratio was <0.40. Midstream 1, Midstream 2, and Downstream were classified as moderate hazard because total As exceeded the limit, although their As(III):As(V) ratios remained below 0.40.

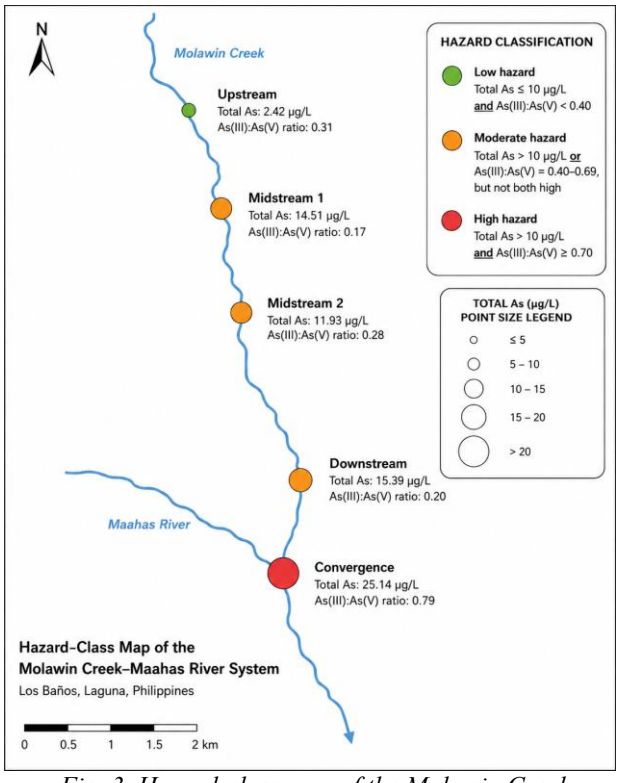


Fig. 3. Hazard-class map of the Molawin Creek–Maahas River system showing total As concentration and As(III):As(V) ratio across sampling points.

Convergence was classified as high hazard because it

had both the highest total As concentration (25.14 µg/L) and the highest As(III):As(V) ratio (0.79), indicating the greatest dominance of the more toxic As(III) species. This confirms that total As exceedance alone does not fully describe toxicity risk. The Convergence station should therefore be prioritized for monitoring, followed by Downstream. Future monitoring should include total As, As(III), As(V), ORP, pH, DO, Fe, COD, PO_4, and dissolved-ion indicators to track changes in arsenic toxicity and guide site-specific mitigation.

IV. Conclusion

This study demonstrated that integrating chemometric techniques with As speciation analysis provides a more informative approach for assessing water quality and toxicity risk in the Molawin Creek–Maahas River system. Total As exceeded the 10 µg/L Class B limit under DAO 2016-08 at all points except Upstream, showing arsenic enrichment beyond the forested headwater section. However, total As alone was insufficient to describe toxicity because risk depended on the relative dominance of As(III). The Convergence point was identified as the primary toxicity hotspot, with the highest total As, As(III), and As(III):As(V) ratio, along with elevated Fe, COD, PO_4, and low DO. Chemometric analysis showed that total As was associated with Fe, nutrient and organic indicators, dissolved-ion enrichment, temperature, lower DO, and lower pH, while the As(III):As(V) ratio was most strongly related to ORP. These findings recommend the use of chemometric analysis as a decision-support tool for distinguishing concentration-based exceedance from speciation-based risk and for guiding targeted monitoring strategies for environmental and public health protection.

V. Data availability

The raw replicate-level dataset may be provided by the authors upon reasonable request.

References

[1] N.Wang, Z.Ye, L.Huang, C.Zhang, Y.Guo, W.Zhang, “Arsenic Occurrence and Cycling in the Aquatic Environment: A Comparison between Freshwater and Seawater”, Water, vol.15, 2023, pp.147.

[2] S.Martínez López, A.Banegas García, C.Pérez Sirvent, M.J.Martínez Sánchez, M.A.Esteban Abad, “The Arsenic Biogeochemical Cycle: A Review”, Advances in Environmental and Engineering Research, vol.4, no.4, 2023, pp.1–30.

[3] M.L.Magalona, M.M.Peralta, M.S.Lacsamana, V.C.Sabularse, A.B.Pelegrina, C.C.de Guzman, “Analysis of Inorganic Arsenic (As(III) and Total As) and Some Physicochemical Parameters in Groundwater Samples from Selected Areas in Bulacan, Batangas, and Laguna, Philippines”, KIMIKA, vol.30, no.2, 2019, pp.28–38.

[4] C.J.P.Faulmino, A.C.Rola, “Arsenic in Philippine Groundwaters: Exploring Governance Limitations for Drinking Water Safety”, Journal of Environmental Science and Management, Special Issue 1, 2023, pp.14–27.

[5] Y.Tanaka, K.Matsuhashi, Y.Ogra, “Analytical techniques for arsenic speciation”, Analytical Sciences, vol.41, 2025, pp.317–321.

[6] A.Hechavarría-Hernández, J.L.M.Viana, L.Barbiero, A.T.Rezende-Filho, C.R.Montes, A.J.Melfi, A.H.Fostier, “Spatial and seasonal variation of arsenic speciation in Pantanal soda lakes”, Chemosphere, vol.329, 2023, pp.138672.

[7] Department of Environment and Natural Resources, “Water Quality Guidelines and General Effluent Standards of 2016 (DAO 2016-08)”, Philippines, 2016.

[8] S.M.Haque, Y.Umar, A.Kabir, “Advanced Chemometric Techniques for Environmental Pollution Monitoring and Assessment: A Review”, Chemosensors, vol.13, no.7, 2025, pp. 1-35.

[9] A.Inobeme, V.Nayak, T.J.Mathew, S.Okonkwo, L.Ekwoba, A.I.Ajai, E.Bernard, J.Inobeme, M.M.Agbugui, K.R.B.Singh, “Chemometric approach in environmental pollution analysis: A critical review”, Journal of Environmental Management, vol.309, 2022, pp. 1-18.

[10] H.Juahir, S.M.Zain, A.Z.Aris, M.K.Yusoff, M.B.Mokhtar, “Spatial assessment of Langat river water quality using chemometrics”, Journal of Environmental Monitoring, vol.12, 2010, pp.287–295.

[11] C.P.Goh, P.E.Lim, “Potassium permanganate as oxidant in the COD test for saline water samples”, ASEAN Journal on Science and Technology for Development, vol.25, no.2, 2017, Article 23, pp.383–393.

[12] R Core Team, “R: A language and environment for statistical computing”, R Foundation for Statistical Computing, Vienna, Austria, 2020.

[13] RStudio Team, “RStudio: Integrated Development for R”, RStudio, Inc., Boston, MA, USA, 2019.

2026 IMEKO Joint Conference
TC8 - TC11 - TC24
Metro Manila, Philippines, August 26-29, 2026

Corrosion Inhibition and Mechanical Performance of Epoxy-Polyaniline Composite Coating

Key Simfroso[1*], Gina Catalan[1], Joey Pangilinan[1], Marvin Louise Carpena[1], Chelsea Mae Escutin[1], Alistaire Kerwin Acma[1], Abbey Nicole Franco[2], Dharmatov Rahula Albano[2,3,4]

[1]*Department of Science and Technology - Metals Industry Research and Development Center (DOST-MIRDC), Gen. Santos Ave., Bicutan, Taguig City 1631 Philippines;*
**ktsimfroso@mirdc.dost.gov.ph, gacatalan@mirdc.dost.gov.ph, jgpangilinan@mirdc.dost.gov.ph, chelseamaeescutin07@gmail.com, carpenamarvin02@gmail.com, akacma@mirdc.dost.gov.ph*
[2]*The Graduate School, University of Santo Tomas, España, Manila 1015 Philippines;*
abbeynicole.franco.gs@ust.edu.ph, dbalbano@ust.edu.ph
[3]*Research Center for the Natural Sciences and Applied Sciences, University of Santo Tomas, España, Manila 1015 Philippines*
[4]*Department of Chemistry, College of Science, University of Santo Tomas, España, Manila 1015 Philippines*

***Abstract* – Epoxy-polyaniline (EP) coating was synthesized and evaluated for its combined corrosion inhibition and mechanical performances. Polyaniline (Pani) fillers were prepared via oxidative polymerization of aniline using ammonium peroxydisulfate, and subsequently dispersed in an epoxy matrix. The coating was deposited on mild steel via silk-screen printing. The results confirmed the successful formation of semicrystalline, thermally stable, organic Pani. SEM analysis revealed a dense, uniform, and low-porosity coating structure, indicative of effective barrier properties. The cyclic voltammogram of EP-coated metal presented a decrease in current density, achieving a corrosion inhibition efficiency of 97.52%, outperforming the neat epoxy coating. The microhardness measurement revealed an average hardness of 5.2 HV, less than that of the neat epoxy coating (9.4 HV), attributed to the softening effect of Pani while bend test confirmed retained flexibility.**

I. INTRODUCTION

In the realm of metal anti-corrosion, epoxy coatings remain one of the most widely used systems for corrosion protection due to their strong adhesion, chemical resistance, and structural stability [1, 2, 3]. However, despite these advantages, cured epoxy networks are susceptible to the formation of structural discontinuities such as microdefects and internal stresses, which may facilitate the ingress of moisture and aggressive ions over time [4]. These limitations can reduce long-term coating reliability, particularly in mechanically demanding environments.

To address these challenges, the incorporation of fillers has been widely explored. Among these, conductive polymers such as polyaniline (Pani) have attracted significant attention due to their adaptability, ease of synthesis, and advantageous properties, including good chemical and environmental stability, safety, and cost-effectiveness [5]. Previous studies have shown that epoxy-Pani composites exhibit improved corrosion resistance, with Pani acting as a barrier-forming filler that also promotes surface passivation [6, 7, 8]. Corrosive species (e.g., Cl^-, O_2, H_2O) penetrating a poorly protective epoxy coating reach the metal surface which leads to low impedance and rapid steel corrosion. Incorporating Pani significantly increases the charge transfer resistance and overall impedance. Its conductive nature facilitates electron transfer, promoting redox reactions that separate anodic and cathodic processes and form a protective iron oxide passive layer, which plays a vital role in corrosion prevention [9, 10].

Although the enhanced corrosion resistance of epoxy-Pani coatings is well documented, systematic evaluation of their mechanical properties remains limited [11, 12]. Equal attention to mechanical performance is essential, as corrosion-resistant coatings are often subjected to deformation, impact, and other external stresses. Once defects develop in the coating, its effectiveness as an anticorrosive barrier is compromised.

This study aims to evaluate an epoxy-Pani coating to determine strategies for improving the protective performance of epoxy-based systems in harsh, corrosive environments. The coating is assessed through a combined analysis of corrosion inhibition and mechanical performance. Electrochemical measurement was conducted using cyclic voltammetry (CV) to determine inhibition efficiency, while selected mechanical tests,

including microhardness and bending, were performed to evaluate structural integrity. This integrated evaluation approach provides a practical framework for developing more durable and effective protective coatings. Ultimately, the work contributes to the advancement of sustainable, high-performance solutions for metal protection in demanding service conditions, supporting improved reliability in corrosion-prone environments.

II. METHODOLOGY

A. *Synthesis of Pani*

Pani was synthesized via oxidative polymerization technique using two (2) solution mixtures: (i) a 0.2 M hydrochlroic acid (HCl) was added to a 5.71 g ammonium peroxydisulfate (APS, TPC India 30203) and a 50 mL clear solution was obtained; and (ii) an HCl of the same molarity was also added to a 1.83 mL aniline (99.5%, AR, TPC India 38151) in a 150 mL beaker, obtaining another 50 mL mixture. The two mixtures were stirred separately using a magnetic stirrer at 360 rpm without heating. After 30 minutes, the two mixtures were mixed and the final solution was oxidatively polymerized. Through this process, the resulting mixture turned into a dark green Pani.

The mixed solution was filtrated, and the obtained particles were washed with deionized (DI) water and ethanol five (5) times. In the end, the dark green Pani was obtained through filtration and dried in a vacuum oven. The final dried Pani product was also pulverized using an agate mortar and pestle.

B. *Mild Steel Substrate Preparation*

Mild steel substrates were prepared according to the specific requirements of each characterization and test. Surface preparation included sequential grinding with 120- and 400-grit abrasive papers and polishing using a 3 μm diamond paste. The samples were then ultrasonically cleaned in ethanol, dried, and stored prior to coating application.

C. *Preparation of Epoxy-Pani-Coated Specimen*

To fabricate the epoxy-Pani coating, epoxy resin and curing agent (J. Spencer Technologies Corp., Quezon City, Philippines) were mixed at a mass ratio of 2:1, after which a portion of Pani powder was added. The mixture was thoroughly mixed by manual stirring until a homogeneous dispersion was obtained. For comparison, a pure epoxy resin coating, labelled 'ER', was also prepared as a control. The resulting mixture was applied onto the prepared mild steel substrates via manual brushing and allowed to cure under ambient conditions for 48 h.

D. *Sample Characterizations and Tests*

Scanning electron microscopy-energy dispersive X-ray spectroscopy (SEM-EDX) analysis was used to examine the morphology of Pani fillers and the cross-sectional structure of the EP coating. Images were acquired at acceleration voltages of 20.0 kV for Pani fillers and 15.0 kV for coating cross-sections, with working distances of 43.7 mm and 6.0-7.1 mm, respectively.

The crystallinity of the Pani fillers was determined via X-ray diffraction (XRD) using Cu Kα radiation at 20 mA and 30 kV. Patterns were collected from 10° to 90° 2θ at 2°/min scan speed and 22.1°C temperature.

In addition, Pani fillers were evaluated by differential thermal analysis-thermogravimetry (DTA-TG) using an STA200RV simultaneous thermal analyzer from 25°C to 900°C at a rate of 10°C/min under nitrogen flow of 50 mL/min. This evaluated the thermal profile of the powder and its potential as an epoxy filler for enhancing composite thermal properties.

The corrosion inhibition of both coatings was evaluated using cyclic voltammetry (CV). The samples were immersed in 10mM potassium ferricyanide ($K_3[Fe(CN)_6]$) in 0.1M potassium nitrate (KNO_3). The potential was varied from -1000 mV to +1000 mV at a scan rate of 500 mV/s. To quantify the protective capability of each coating, the corrosion inhibition efficiency (IE%) was calculated using the following equation [13, 14]:

$$IE\% = [(i_{bare} - i_{coated})/i_{bare}] \times 100 \qquad (1)$$

where i_{bare} is the peak current of the unprotected mild steel and i_{coated} is the peak current of the coated specimen.

For mechanical tests, microhardness and bending test were performed on the coated specimen. Microhardness tests were performed on coated samples in accordance with ASTM E384-17. A load of 10 g was applied for each indentation. Five (5) indentation points were made on the surface of each coating. The bend test was conducted using a universal testing machine (UTM) with 50 kN capacity. Specimens were tested using a laboratory bend jig with a three-point bend setup. The loading pin used has a diameter of 12.7 mm.

III. RESULTS AND DISCUSSION

A. *Characterization Results for Pani Fillers*

The oxidative polymerization technique led to the formation of precipitates that became more compact upon drying. Subsequent grinding produced significantly finer particles, although some degree of agglomeration remained, as observed in the SEM micrograph in Fig. 1. The surface morphology exhibits a fibrous texture in its agglomerated state; these features, together with the finer particle fraction, are expected to enhance coating compactness by promoting improved filler dispersion and

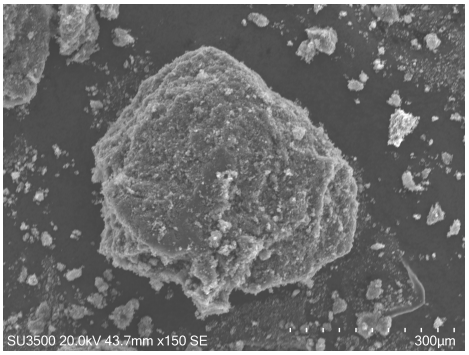


Fig. 1. SEM image of Pani in 150× magnification. The scale bar shows 300 µm.

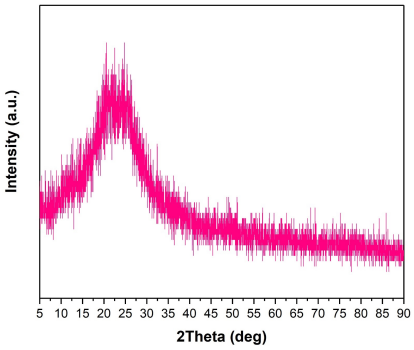


Fig. 2. X-ray diffraction pattern of Pani.

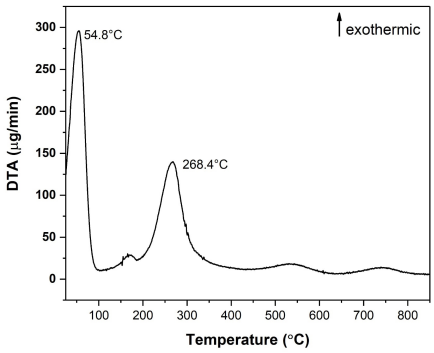


Fig. 3. DTA graph for Pani powder heated between 24°C and 900°C.

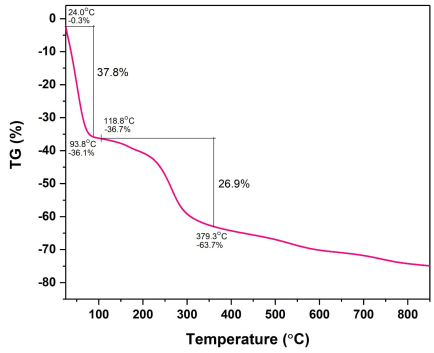


Fig. 4. The corresponding TG graph for Pani powder.

increasing the tortuosity of possible diffusion pathways.

The XRD pattern shown in Fig. 2 exhibits a semi-crystalline nature, characterized by broad yet distinguishable diffraction peaks. The three most prominent peaks appear at $2\theta \approx 20.4°$, $21.08°$, and $25.48°$, with the latter attributed to (200) plane which is consistent with the value reported in the literature [15], confirming that it is indeed a Pani. The broadness of these peaks suggests a limited crystallite size, which confirms that Pani retains a semi-crystalline structure rather than a fully crystalline phase. These structural characteristics, along with the morphology of Pani, are expected to enhance interfacial bonding and increase tortuosity within the coating, attributes that are beneficial for enhancing barrier performance.

The thermal decomposition profile of Pani fillers is presented through DTA and TG plots in Fig. 3 and 4. There are two major exothermic reactions that correspond to two major weight losses for Pani fillers. In the first stage, a sharp exothermic peak at 54.8°C in the DTA curve is the result of evaporation of adsorbed moisture and residual low-molecular-weight volatiles [16], which corresponds to the initial loss of 35.8% mass from 24.0-93.8°C. An exothermic peak at 268.4°C occurred in the second stage corresponding to Pani deprotonation and partial degradation of side chains [17]. It is revealed that the synthesized Pani is in the form of emeraldine salt (ES). The second exothermic reaction is accompanied by a subsequent 26.9% mass loss between 118.8-379.3°C. The mass loss then proceeds more gradually, reflecting carbonization and progressive structural breakdown at elevated temperatures. These observations confirm that the filler is an organic Pani.

B. Coating Characterization and Test Results

Fig. 5 presents cross-sectional images of the ER and EP coatings to elucidate their microstructural characteristics, internal structures, and substrate-coating interfaces. Both coatings appear to be compact with no visible pores. Some agglomeration observed in EP coating may possibly be due to non-homogeneous mixing, epoxy-Pani attraction, and/or viscosity-limited flow during curing. These agglomerates can tend to become stress concentration areas, which can consequently reduce toughness if the

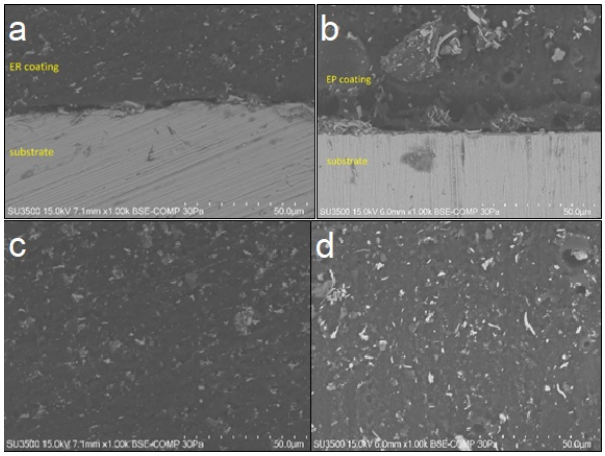


Fig. 5. SEM images of (a) ER coating-mild steel interface, (b) ES coating-mild steel interface, and (c,d) the internal structures at other regions of the ER and EP coatings, respectively, all captured at 1000× magnification.

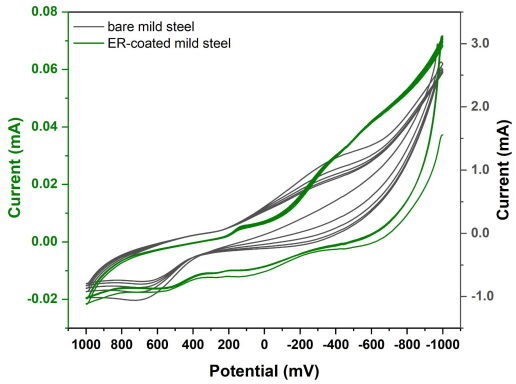


Fig. 6. Cyclic voltammogram of the ER-coated over the bare mild steel.

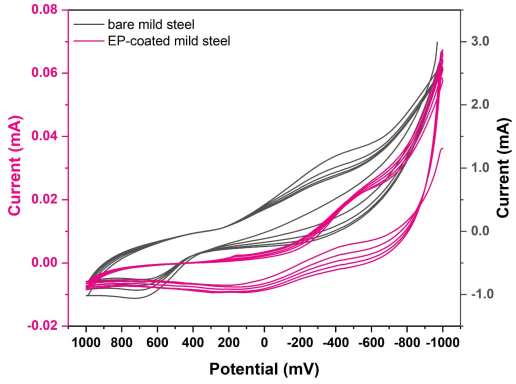


Fig. 7. Cyclic voltammogram of the EP-coated over the bare mild steel.

interfacial bonding with epoxy is weak [11, 18]. These photomicrographs also show the quality of interfacial adhesion of the substrate with the two types of coating. It can be observed that there is a wider gap between the substrate and the coating without Pani. The improved mechanical interlocking might be due to the addition of Pani and the proper preparation of the substrate surface.

The corrosion behavior of the EP coating was evaluated using CV. The cyclic voltammograms of the bare mild steel, ER- and EP-coated systems are illustrated in Fig. 6 and 7. The bare mild steel exhibited an active electrochemical profile characterized by significant redox activity, with a peak current reaching 2.71 mA. This indicates a high rate of electron transfer and susceptibility to corrosive attack in the electrolyte medium. The EP-coated sample provided superior protection with a corrosion inhibition efficiency IE% of 97.52% which is calculated from the peak current reaching 0.06695 mA compared to that of the ER-coated with an IE% of 97.36% from the peak current of 0.07156 mA. Both coatings maintain highly suppressed and stable CV loops, and remain highly effective barriers compared to the bare substrate.

Moreover, it is observed that during the anodic scan, no peak was observed in EP coating. In addition, a large passive region is observed. As seen, the current remains low and relatively constant in this region, despite a change in applied potential. It also shows that the onset potential, which is the point of the curve where the current starts to deviate from the baseline, is further delayed in comparison with the ER, indicating the initiation of a specific reduction-oxidation process. This behavior signifies that in the presence of Pani, there occurs a formation of a stable, protective region on the electrode surface that inhibits further oxidation and charge transfer showing the passivation ability of the conductive polymer.

Since the initial characterization confirmed the suitability of EP coating for corrosion protection, supported by its inherent nature and structure, subsequent mechanical tests were performed to further validate its potential for long-term performance.

Fig. 8 shows the surfaces of the ER and EP coatings with the five indentation marks used for the microhardness evaluation. The individual microhardness values and their average are also summarized in Table 1. The EP coating exhibits an average microhardness of 5.2 HV, which is considerably lower than that of ER. This is attributed to the presence of Pani fillers, which act as a relatively softer, functional, and conductive reinforcement. In polymer composites, Pani primarily contributes to functional and electrical enhancement rather than to purely mechanical strengthening. The low average microhardness measurement indicates that EP is softer

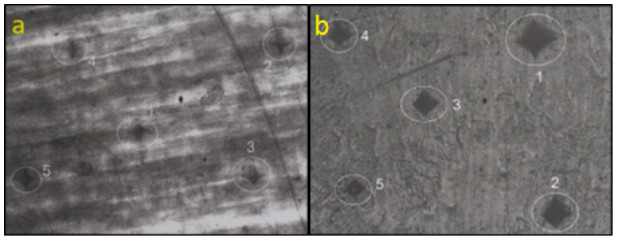


Fig. 8. Surface images of (a) ER and (b) EP coatings that underwent microhardness measurement.

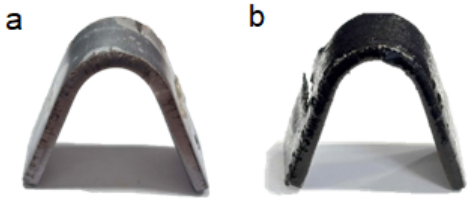


Fig. 9. Images of bended coated specimens: (a) ER- and (b) EP-coated mild steel.

than ER and that the incorporation of Pani reduced the overall hardness of the coating.

Table 1. Microhardness test results presenting point-by-point measurements and average value.

Coating	Hardness (HV)					
	1	2	3	4	5	Ave
ER	8	9	10	11	9	9.4
EP	3	4	5	6	8	5.2

Fig. 9 presents images of mild steel samples coated with ER and EP after the bend tests. Satisfactory resistance to deformation is observed as both coatings exhibit good flexibility, as evidenced by the absence of visible cracks along the outer radius of the bent region. Once crack occurs, the coating can no longer effectively function as a protective barrier against corrosion, as such defects serve as preferential pathways for the corrosive elements. The test is considered passed when the coated metal bends 180° and no crack is found.

Although the prepared EP coating demonstrated superior corrosion inhibition and effective crack suppression, its physical characteristics governing mechanical performance, particularly its susceptibility to delamination and relatively low hardness, still require further investigation and optimization. Improving these mechanical properties, while maintaining its corrosion inhibition performance, is essential for applications subjected to combined mechanical stresses and corrosive environments.

IV. CONCLUSION

A combined evaluation of the corrosion inhibition and mechanical performances of an epoxy-Pani composite coating was carried out. The coating was prepared through a straightforward addition of Pani synthesized via oxidative polymerization technique to an epoxy resin. The corrosion performance was evaluated using CV. The EP-coated mild steel showed a decrease in current density compared to the bare and ER-coated mild steel and a corrosion inhibition efficiency of 97.52%. Selected mechanical evaluations were also conducted to assess suitability for aggressive environments. Microhardness testing yielded an average hardness of 5.2 HV, less than that of the ER (9.4 HV), the reduction attributed to the softer reinforcement effect of Pani. The results of the bend test suggested a maintained flexibility of the epoxy matrix even with Pani-induced softening. To establish the applicability of the coating for both corrosive and mechanically demanding conditions, further experimental work is necessary, including the incorporation of dispersant or other processing aids and reinforcements to enhance its mechanical properties while preserving its corrosion inhibition performance.

REFERENCES

[1] A.R.Makhmetova, N.El-Sayed, D.T.Ainakulova, G.Yeligbayeva, J.M.Khatib, “An Overview of Epoxy Resins as coating to protect metals from corrosion”, Compl. Use of Min. Resour., 2024, vol.328, no.1, pp.20-32.

[2] T.Ramakrishnan, K.Raja Karthikeyan, V.Tamilselvan, S.Sivakumar, D.Gangodkar, H.R.Radha, A.N.Singh, Y.A.Waji, “Study of Various Epoxy-Based Surface Coating Techniques for Anticorrosion Properties”, Adv. Mater. Sci. Eng., 2022, 5285919, pp.1-8.

[3] I.M.Barańska, K.Antosz, “Epoxy Adhesive Materials as Protective Coatings: Strength Property Analysis Using Machine Learning Algorithms”, Materials, 2025, vol.18, No.12, 2803.

[4] X.Shi, S.G.Croll, “Recovery of surface defects on epoxy coatings and implications for the use of accelerated weathering”, Prog. Org. Coat., 2010, vol.68, No.1-2, pp.79-87.

[5] M.Beygisangchin, S.A.Rashid, S.Shafie, A.R.Sadrolhosseini, H.N.Lim, “Preparations, Properties, and Applications of Polyaniline and Polyaniline Thin Films—A Review”, Polymers, 2021, vol.13, No.12, 2003.

[6] N.B.Panah, M.Payehghadr, I.Danaee, H.Nourkojouri, M.Sharbatdaran, “Investigation of corrosion performance of epoxy coating containing polyaniline nanoparticles”, Iran Polym. J., 2012, vol.21, pp.747-754.

[7] T.Siva, K.Kamaraj, S.Sathiyanarayanan, “Epoxy

curing by polyaniline (PANI)—Characterization and self-healing evaluation", Prog. Org. Coat., 2014, vol.77, Issue 6, pp.1095-1103.

[8] Y.Wang, X.Jing, "Preparation of an Epoxy/Polyaniline Composite Coating and Its Passivation Effect on Cold Rolled Steel", Polymer Journal, 2004, vol.36, pp.374-379.

[9] R.N.Goswami, P.Mourya, B.Behera, O.P.Khatri, A.Ray, "Graphene-polyaniline nanocomposite based coatings: Role of convertible forms of polyaniline to mitigate steel corrosion", Appl. Surf. Sci., 2022, vol.599, 153939.

[10] H.Wang, Q.Qi, Y.Zhang, S.Chen, B.Dong, S.Zhu, Q.Hu, Z.Guo, "Anticorrosive Epoxy Nanocomposite Coatings Filled with Polyaniline-functionalized Silicon Nitride Particles", Ind. Eng. Chem. Res., 2020, vol.59, pp.16649-16659.

[11] M.A.Tarawneh, S.A.Saraireh, R.S.Chen, S.H.Ahmad, M.A.M.Al-Tarawni, L.J.Yu, B.O.Alsobhi, D.Hui, "Mechanical reinforcement with enhanced electrical and heat conduction of epoxy resin by polyaniline and graphene nanoplatelets", Nanotechnol. Rev. 2020, vol.9, pp.1550-1561.

[12] U.A.Samad, M.A.Alam, A.Chafidz, S.M.Al-Zahrani, N.H.Alharthi, "Enhancing mechanical properties of epoxy/polyaniline coating with addition of ZnO nanoparticles: Nanoindentation characterization", Prog. Org. Coat., 2018, vol.119, pp.109-115.

[13] A.M. Fathi, E.H.Anouar, A.O.Ahmed, M.I.Hegab, "Electrochemical, molecular dynamics, density functional theory, and corrosion inhibition studies of some chromeno-oxadithiin and chromeno disulfide derivatives for mild steel in 3.5% NaCl", J. Solid State Electrochem., 2023, vol.27, pp.3539-3555.

[14] M.B.Radovanović, Ž.Z.Tasić, M.B.Petrović Mihajlović, A.T.Simonović, M.M.Antonijević, "Electrochemical and DFT studies of brass corrosion inhibition in 3% NaCl in the presence of environmentally friendly compounds", Sci. Rep., 2019, vol.9, 16081.

[15] S.M.Ambalagi, M.Devendrappa, S.Nagaraja, B.Sannakki, "Dielectric Properties of PANI/CuO Nanocomposites", IOP Conf. Ser. Mater. Sci. Eng., 2018, vol.310, 012081.

[16] K.Luo, N.Shi, C.Sun, "Thermal transition of electrochemically synthesized polyaniline", Polym. Degrad. Stab., 2006, vol.91, pp.2660-2664.

[17] D.Yalcin, S.Bamford, M.Espiritu, N.Rigopoulos, I.Martinez-Botella, D. Alexander, Y.Gozukara, M.Greaves, E.A.Bruton, P.J.Kinlen, S.Howard, P.J.Pigram, B.W.Muir, T.M.Kohl, "New insight into degradation mechanisms of conductive and thermally resistant polyaniline films", Polym. Degrad. Stab., 2023, vol.215, 110427.

[18] M.Fuseini, M.M.Y.Zaghloul, D.Abakar, M.M.Y.Zaghloul, "Review of epoxy nano-filled hybrid nanocomposite coatings for tribological applications", FlatChem, 2025, vol.49, 100768.

2026 IMEKO Joint Conference
TC8 - TC11 - TC24
Metro Manila, Philippines, August 26-29, 2026

Influence of NaOH Concentration on the Quality and Electrochemical Behavior of Magnetite Film Formed by Blackening

Gina A. Catalan[1*], Key T. Simfroso[1], Marvin Louise B. Carpena[1], Joey G. Pangilinan[1], Alistaire Kerwin Acma[1], Abbey Nicole Franco[2], Dharmatov Rahula B. Albano[2,3,4]

[1]*Materials and Process Research Division, Department of Science and Technology-Metals Industry Research and Development Center (DOST-MIRDC), Taguig City, 1631, Philippines, *gacatalan@mirdc.dost.gov.ph, ktsimfroso@mirdc.dost.gov.ph, carpenamarvin02@gmail.com, jgpangilinan@mirdc.dost.gov.ph*

[2]*The Graduate School, University of Santo Tomas, España Blvd., Sampaloc, Manila, 1015, Metro Manila, Philippines, abbeynicole.franco.gs@ust.edu.ph, dbalbano@ust.edu.ph*

[3]*Department of Chemistry, College of Science, University of Santo Tomas, España Blvd., Sampaloc, Manila, 1015, Metro Manila, Philippines*

[4]*Research Center for the Natural Science and Applied Sciences, University of Santo Tomas, España Blvd., Sampaloc, Manila, 1015, Metro Manila, Philippines*

***Abstract* – This study investigates the influence of NaOH concentration on the formation, morphology, and corrosion performance of magnetite-like oxide films produced on low-carbon steel through alkaline blackening. Steel samples were treated in 20%, 40%, and 60% NaOH solutions with 2 wt% $NaNO_3$ at 130-135°C for 45 minutes and evaluated using oxalic acid spot testing, cyclic voltammetry, thickness and roughness measurements, and SEM-EDS. All treatments produced continuous iron oxide conversion layers and improved corrosion resistance relative to bare steel. Increasing the NaOH concentration increased the film thickness; however, the maximum thickness did not correspond to optimal protection. The 40% NaOH condition exhibited the most stable corrosion resistance, the lowest electrochemical activity, and the best overall film integrity, indicating superior passivation behavior. SEM-EDS confirmed thin iron oxide films with mixed or non-stoichiometric characteristics. The results demonstrate that the film continuity and electrochemical stability govern protective performance more strongly than thickness alone.**

I. INTRODUCTION

The hot alkaline nitrate blackening method is a long-established surface conversion process used to improve the corrosion resistance and appearance of ferrous materials through the formation of magnetite-rich (Fe_3O_4) or mixed iron oxide films [1]. This process is widely applied because it is simple, cost-effective, dimensionally stable and capable of providing moderate corrosion and wear resistance while preserving part tolerances. The protective behavior of black oxide films is primarily associated with the formation of compact oxide layers that act as diffusion barriers and alter electrochemical surface activity [2],[3]. However, film performance depends not only on oxide thickness, but also on film continuity, morphology, and phase composition, which are strongly influenced by bath chemistry and operating conditions [4],[5].

Numerous research studies have been carried out on the blackening treatment process. S. Kuśmierczak and M. Makovský conducted a study focusing on the cause of surface degradation of blackened steel parts [6]. The researchers used a machined steel throttle shaft that was further processed with blackening treatment. The blackened sample was analyzed for any presence of defects in size, color, appearance, and corrosion. To investigate this, light and electron microscopy methods were employed, along with a comprehensive analysis of the production workflow and technological conditions. The results revealed that degradation was closely linked to inadequate surface preparation. Improper pretreatment led to the localized formation of oxides. These oxides caused the surface layer to peel after the blackening process, ultimately compromising the quality of the final product.

Hanoz et al. conducted a surface characterization of black oxide coating on a low carbon steel surface [7]. They employed three different bath solutions, which included commercially available solutions at varying operating temperatures and immersion times. Their analysis included the surface morphology, corrosion resistance, and chemical composition of the oxide layers. The results of

their study showed that the morphology of the oxide layer was significantly influenced by the immersion time, while the temperature notably affected the homogeneity of the surface.

In addition, recent work by Riandadari et al. showed that increasing the temperature and treatment time enhance the thickness of the magnetite layer while reducing surface gloss, emphasizing the importance of controlled processing conditions [4].

This study aims to establish the relationship between NaOH concentration, oxide film characteristics, and corrosion behavior. By systematically evaluating the films obtained at 20%, 40%, and 60% NaOH, this work provides insights into optimizing a low-concentration alkaline blackening process.

II. METHODOLOGY

A. Materials and Sample Preparation

Low-carbon steel plates were used as substrates for the blackening experiments. The chemical composition of the steel shown in Table 1, was determined using a benchtop Spark Optical Emission Spectrometer (Spark-OES, SpectroMAXx, LMF07) according to ASTM E415-21. The plates were sectioned into coupons with dimensions of 60 mm × 20 mm × 2 mm, and a small hole was introduced at the upper edge to allow suspension during treatment, as shown in Fig. 1(a). Dimensional measurements were obtained using a digital caliper (Mitutoyo, 200 mm, 0.01 mm resolution), as presented in Fig. 1(b), and initial surface roughness was measured using a stylus profilometer (Mitutoyo, SJ 210).

Table 1. Chemical composition of low-carbon steel samples.

%Fe	%C	%Si	%Mn	%P
99.03	0.17± 0.013	0.17± 0.0089	0.36± 0.013	0.023± 0.0014
%S	%Cr	%Mo	%Ni	%Cu
0.0059± 0.00022	0.039± 0.0041	<0.0010± 0.00053	0.011± 0.0016	0.0084± 0.0010

B. Preparation of Blackening Treatment Solution

Alkaline blackening solutions were prepared using 20%, 40%, and 60% sodium hydroxide (NaOH) by weight, each containing 2 wt% sodium nitrate ($NaNO_3$) as the oxidizing agent. Sodium hydroxide flakes were gradually dissolved in cold DI water under continuous stirring to control heat generation. Sodium nitrate was subsequently added and the solutions were diluted to the required volume using DI water.

The pH of each solution was measured using a calibrated handheld pH meter (AZ, Model 8601). The measured pH values were 13.62, 13.72 and 13.88 for the 20%, 40%, and 60% NaOH solutions, respectively, which confirms strongly alkaline conditions.

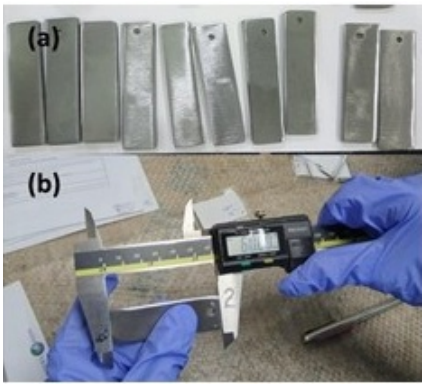


Fig. 1. (a) Prepared low-carbon steel coupons for blackening treatment; (b) dimensional measurement using a digital caliper.

C. Blackening Process

The alkaline blackening process was performed following the sequence illustrated in Fig. 2.

Pretreatment. Ground steel coupons were suspended using stainless steel wires and dipped in a warm diluted alkaline cleaning solution to remove surface contaminants. Samples exhibiting rust were reground prior to cleaning. After being cleaned, the coupons were rinsed sequentially with cold and boiling deionized (DI) water to ensure complete removal of residues and activate the surface for oxidation.

Blackening Treatment. The prepared blackening solutions were heated and maintained at 130-135∘C before immersion. The cleaned steel coupons were immersed in preheated solutions containing 20%, 40%, and 60% NaOH with 2 wt% $NaNO_3$, see Fig. 3. All treatments were conducted under identical operating conditions with a fixed immersion time of 45 minutes. The bath temperature was continuously monitored and maintained within the specified range throughout the process. Multiple samples were processed for each concentration to ensure reproducibility, and care was taken to maintain uniform immersion and avoid contact between samples.

Post-Treatment. After blackening, the samples were rinsed successively with warm, cold, and boiling DI water to remove residual chemicals. The coupons were then air-dried prior to characterization. No oil treatment was applied to the test coupons to prevent interference with subsequent analyses.

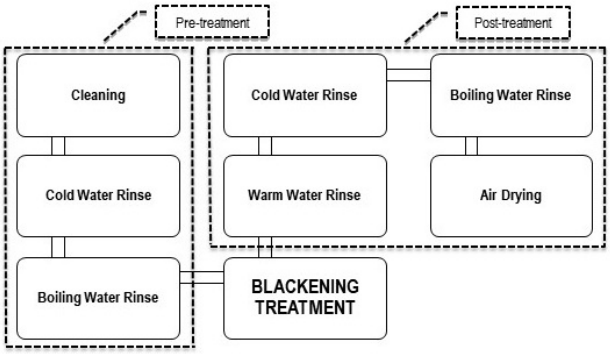


Fig. 2. Sequence of blackening treatment process.



Fig. 3. Steel samples immersed in 20% NaOH blackening solution.

D. Characterization of Magnetite Film

1. Oxalic Acid Spot Test

A qualitative oxalic acid spot test was conducted to assess the uniformity of the magnetite film. Drops of 5% oxalic acid solution were applied to the coated surface and allowed to react for a fixed duration. The resulting surface appearance was compared with reference images wherein a uniform and well-formed film retained a black to dark brown appearance, whereas poor or incomplete films exhibited a light gray or whitish discoloration.

2. Cyclic Voltammetry (CV)

Cyclic voltammetry was employed to evaluate the electrochemical behavior of the magnetite films and to assess their corrosion-related characteristics. This technique provides insight into the redox behavior and passivation properties of the coated surface, which are critical indicators of film stability and protective performance.

Electrochemical measurements were performed using a wireless potentiostat, Zensor ECWP100. The uncoated and magnetite-coated steel samples were used as working electrodes in an electrolyte consisting of 10 mM potassium ferricyanide prepared in 0.1 M potassium nitrate. The potential was swept from -1000 mV to +1000 mV at a scan rate of 500 mV/s. The corresponding current response was recorded to evaluate the electrochemical behavior and surface activity of the films.

3. Thickness Measurement

Film thickness was measured using a magnetic induction thickness gauge (Minitest 740, ElektroPhysik), which determines non-magnetic film thickness on ferromagnetic steel based on changes in magnetic flux. The instrument was calibrated prior to testing using standard shims of known thickness (5.8 μm and 11.4 μm) to ensure measurement accuracy.

4. Surface Roughness Measurement

Surface roughness was measured using a stylus profilometer, Mitutoyo, SJ 210. The instrument operates by traversing a diamond-tipped stylus across the sample surface, where vertical displacements caused by surface irregularities are recorded and converted into electrical signals. These signals are processed to generate a surface profile and determine the average roughness (Ra).

5. Scanning Electron Microscopy-Energy Dispersive X-ray Spectroscopy (SEM-EDS)

The surface morphology and elemental composition of the magnetite films were examined by SEM-EDS (Hitachi SU3500 with Bruker EDS detector); the electron beam was directed onto the sample surface to generate high-resolution micrographs, while characteristic X-ray emissions were analyzed to determine the elemental composition.

III. RESULTS AND DISCUSSION

A. Oxalic Acid Spot Test

The oxalic acid spot test (MIL-C-13924C) served as an initial qualitative assessment of oxide layer continuity and surface coverage. All treated samples (Fig. 4) passed the test, as no white spots or incomplete conversion rings were observed, indicating that alkaline blackening successfully produced continuous surface conversion layers at all NaOH concentrations [8]. Although this result confirms an acceptable oxide coverage, the test is limited to visual inspection and does not independently verify the specific formation of stoichiometric Fe_3O_4. Therefore, the oxalic acid test is best interpreted as evidence of successful surface conversion rather than definitive phase identification.

B. Cyclic Voltammetry

The results of cyclic voltammetry, as shown in Fig. 5, confirmed that alkaline blackening significantly altered the electrochemical behavior of low-carbon steel through oxide film formation. Compared with bare steel, all blackened samples exhibited modified redox behavior



Fig. 4. Oxalic acid spot test results at 20%, 40%, and 60%.

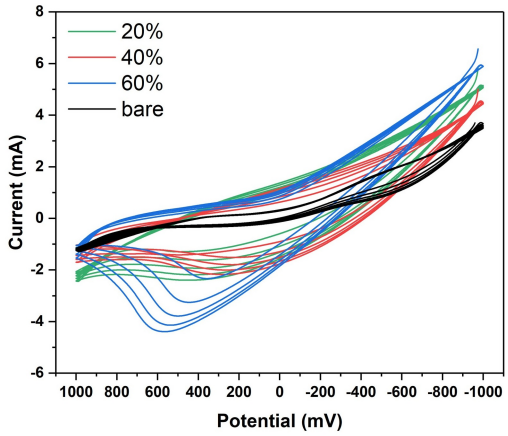


Fig. 5. Cyclic voltammograms for bare steel and samples treated at 20%, 40%, and 60% NaOH, illustrating decreased current density upon film and indicating improved passivation.

consistent with surface conversion and passivation.

Among coated conditions, the 40% NaOH sample demonstrated the most stable voltammetric profile with the lowest electrochemical activity and reduced hysteresis, indicating superior barrier performance and improved charge-transfer resistance. The 20% NaOH condition provided moderate passivation but showed comparatively higher electrochemical activity, suggesting a less compact oxide layer. In contrast, the 60% NaOH sample exhibited a higher current response, particularly under cathodic polarization, implying that excessive alkalinity may promote thicker but less protective oxide films due to structural heterogeneity or reduced compactness. CV analyses indicate that corrosion inhibition is more governed by oxide film stability and integrity than by thickness alone, with 40% NaOH providing the most effective electrochemical protection.

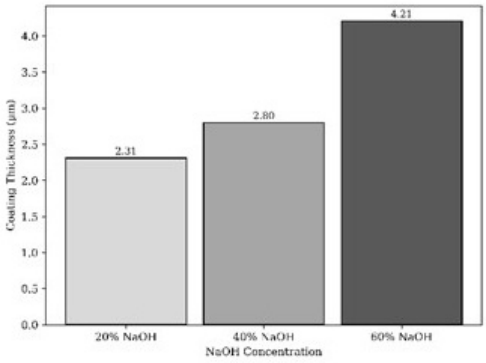


Fig. 6. Effect of NaOH concentration on the thickness of magnetite film formed on steel substrates.

C. Film Thickness

The thickness measurements of the magnetite films demonstrate a clear dependence on NaOH concentration, as shown in Fig. 6. Increasing the NaOH concentration from 20% to 60% resulted in a progressive increase in film thickness, from 2.31 μm to 4.21 μm, indicating that higher alkalinity promotes more rapid and sustained oxide layer formation [9].

D. Surface Roughness

Stylus profilometry results (Table 2) indicate that alkaline blackening produces concentration-dependent changes in surface roughness. At 20% NaOH, Ra increased slightly from 0.341 20% to 60%, resulting in a progressive increase in film thickness, from 2.31 μm to 4.21 m to 0.402 μm, suggesting minimal surface modification. A significant increase was observed at 40% NaOH, where Ra rose from 0.671 μm to 66 μm, indicating enhanced surface texture. In contrast, 60% NaOH resulted in a decrease in Ra from 0.197 μm to 0.166 μm, suggesting a surface smoothing effect, likely due to excessive alkaline dissolution. The results show that the moderate NaOH concentration (40%) promotes the greatest increase in surface roughness, while lower and higher concentrations produce limited or opposing effects.

Table 2. Surface roughness of steel before and after blackening treatment

NaOH concentration	Surface roughness before blackening, Ra_{ave} (μm)	Surface roughness after blackening, Ra_{ave} (μm)
20%	0.341	0.402
40%	0.671	1.66
60%	0.197	0.166

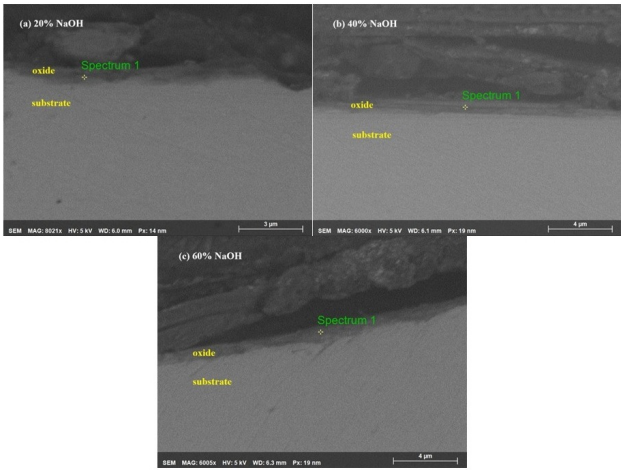


Fig. 7. SEM cross-sectional images of blackened steel surfaces (MAG: 6000-8021X, HV: 5 kV)

E. SEM-EDS

The Fe/O atomic ratios shown in Table 3 deviate from the theoretical value of Fe_3O_4, indicating oxygen-enriched surfaces, particularly at higher NaOH concentration. Thus, EDS alone cannot conclusively confirm magnetite formation. The deviation may be attributed to the semi-quantitative nature of EDS, limitations in oxygen quantification, and possible substrate signal contribution due to thin oxide films that lead to signal overlap and further distortion of the measured Fe/O ratios [10].

Table 3. EDS elemental composition (at.%) and Fe/O ratios of coated samples.

NaOH concentration	Atomic %		Fe/O ratio
	Fe	O	
20%	13.94	24.73	0.563
40%	24.38	34.51	0.706
60%	11.08	19.75	0.561

These results support the formation of iron oxide, but the confirmation of magnetite requires complementary phase analysis such as Raman and XRD [11].

All three blackened samples show continuous dark oxide coverage as shown in Fig. 7, but do not appear to be equally compact.

The 20% NaOH sample appears to have a relatively lighter and less homogeneous surface. The 40% NaOH sample exhibits the most visually consistent and uniform darkened surface, with a more even coverage and fewer apparent discontinuities, indicating a more compact and better-developed oxide film. In contrast, the 60% NaOH sample shows a darker overall oxidation but with more noticeable surface irregularity and non-uniform texture.

The SEM images suggest that while all treatments successfully formed oxide layers, 40% NaOH appears to produce the most uniform and visually compact film. Visual inspection alone cannot confirm density or phase composition, but it supports differences in film quality among the treatments.

IV. CONCLUSION

This study confirms that NaOH concentration is a critical process variable that influences oxide film formation, morphology, and corrosion performance during alkaline blackening of low-carbon steel. All treatment conditions successfully produced continuous iron oxide conversion layers that improved corrosion resistance compared to bare steel; however, protective effectiveness depended strongly on oxide film quality rather than the thickness alone.

Among the tested conditions, the 40% NaOH treatment demonstrated the best overall performance, exhibiting the most stable cyclic voltammetry response, improved passivation behavior, and the most visually uniform and compact oxide surface morphology. In contrast, while increasing NaOH concentration promoted greater oxide thickness, the 60% NaOH condition did not provide the highest corrosion protection, indicating that excessive alkalinity can produce thicker but less structurally optimized oxide layers. The 20% NaOH condition formed a protective film but showed comparatively lower uniformity and reduced electrochemical stability.

SEM-EDS results confirmed the formation of thin iron oxide conversion layers across all blackened samples, although Fe/O ratios and surface observations suggest that the films are more accurately described as magnetite-like or mixed iron oxide systems rather than pure stoichiometric Fe_3O_4. Collectively, the results demonstrate that film continuity, compactness, and electrochemical stability are more decisive in inhibiting corrosion than maximum oxide growth. Therefore, under the present processing conditions, 40% NaOH represents the optimal concentration to balance oxidation kinetics, film integrity, and protective performance in low-concentration alkaline blackening applications.

This work provides a practical framework for process optimization by emphasizing that effective blackening performance is governed by overall oxide quality rather than thickness alone.

REFERENCES

[1] C.H.Hager, R.D.Evans, “Friction and wear properties of black oxide surfaces in rollingsliding contacts”, Wear, vol.338-339, Sep. 2015, pp.221-231.

[2] W.E.O’Grady, “Mössbauer Study of the Passive Oxide Film on Iron“, Electrochemical Science and Technology, vol.127, no.3, March 1980, pp.555-563.

[3] M.Pourbaix, “Atlas of electrochemical equilibria in aqueous solutions“, 2nd edition, Houston, 1974.

[4] D.Riandadari, A.Sakti, F.Utama, F.Abdi, “Specimen Test Analysis of Different Forms in Process Blackening for Layer Thickness of Surface Coatings and Glossoness Level”, Proc. of the International Joint Conference on Science and Engineering 2022 H. P. Agustin, A. M. De Oliveira, Y. Anistyasari, K. Ueda, A. Wardhono, and I. A. T. Rahayu, Eds., Dordrecht: Atlantis Press International BV, 2022, pp.162-168.

[5] R.M.Cornell, U.Schwertmann, “The Iron Oxides: Structure, Properties, Reactions, Occurrences and Uses”, 1st ed. Wiley, 2003.

[6] S.Kuśmierczak, M.Makovský, “Problems of blackening of steel parts in technical practice”, MATEC Web Conf., vol.244, 2018, p.1012.

[7] D.Hanoz, A.G.Settimi, M.Dabalà, “Characterization of black coating on Fe360 steel obtained with immersion in aqueous solutions”, Surfaces and Interfaces, vol.26, Oct. 2021, p.101317.

[8] MIL-C-13924C Coating, Oxide, Black, for Ferrous Metals.

[9] R.W.Farrell, “Blackening of ferrous metals”, Metal Finishing, vol.100, Jan. 2002, pp.456-462.

[10] C.Puttichaem, G.P.Souza, K.C.Ruthe, K.Chainok, “Characterization of Ultra-Thin Diamond-Like Carbon Films by SEM/EDX”, Coatings, vol.11, no.6, Jun. 2021, p.729.

[11] S.Schwaminger, C.Syhr, S.Berensmeier, “Controlled Synthesis of Magnetic Iron Oxide Nanoparticles: Magnetite or Maghemite?”, Crystals, vol.10, no.3, March 2020, p.214.

2026 IMEKO Joint Conference
TC8 - TC11 - TC24
Metro Manila, Philippines, August 26-29, 2026

Analytical Testing of Nicotine Levels in Commercially Available E-cigarette Liquids in the Philippines using an HPLC-PDA Method

Harold E. Armario[1], Grace V. Amandy[1], Cherrylean B. Bembenuto[1], Marianne D. Pomarin[1], Anna Marie A. Umali[1], John Cyrus O. Alfaro[1], Cyril C. Ramil[1], Ma. Rachel V. Parcon[1]

[1] *Department of Science and Technology, Industrial Technology Development Institute, Standards and Testing Division, Gen. Santos Avenue, Bicutan Taguig City, Metro Manila, Philippines*
hearmario@itdi.dost.gov.ph

***Abstract* – Accurate nicotine quantification in e-liquids is essential for regulatory compliance, labeling transparency, and consumer protection. This study developed and validated a High-Performance Liquid Chromatography-Photodiode Array (HPLC–PDA) method for nicotine determination and applied it to 22 commercially available e-liquid products in the Philippines. The method demonstrated satisfactory analytical performance and fitness for purpose, with trueness evaluated using a certified reference material (CRM) ERM®-DZ002a. Measured nicotine concentrations ranged from 1.13 to 26.8 mg/mL and were consistently lower than declared values, showing absolute differences of 13–84%. Bland–Altman analysis indicated a systematic negative bias of approximately −9 mg/mL, suggesting widespread under-labeling. Products labeled at 24–50 mg/mL showed notably reduced measured concentrations. Although all samples complied with limits under Republic Act No. 11900, the discrepancies raise concerns regarding labeling accuracy, product consistency, and the need for stronger analytical verification and post-market surveillance.**

Keywords: consumer protection, electronic cigarette liquids, hplc-pda, method validation, nicotine.

I. INTRODUCTION

Electronic cigarettes (e-cigarettes), or electronic nicotine delivery systems (ENDS), are marketed as less harmful alternatives to conventional cigarettes [1]. They generate inhalable aerosols by heating liquids containing propylene glycol, glycerin, nicotine, and flavorings [2]. Nicotine, the primary addictive compound, drives dependence and associated toxicological risks [3]. Although combustion is absent, e-cigarettes can deliver nicotine at levels comparable to or exceeding traditional cigarettes [4]. Increasing evidence links their use to nicotine dependence, cardiovascular and respiratory effects, and exposure to harmful degradation products such as carbonyls and metals [5,6]. Product variability arising from device design and liquid composition contributes to inconsistent nicotine delivery and toxicant formation [7]. In addition, discrepancies between labeled and measured nicotine concentrations raise concerns regarding product quality and labeling accuracy [8,9]. These challenges are amplified in low and middle income countries, where regulatory frameworks and analytical monitoring remain limited. ENDS have rapidly expanded in these regions, often outpacing regulatory capacity, with many countries lacking specific policies or relying on conventional tobacco laws [10]. Although prevalence remains relatively low, increasing market penetration suggests rising exposure risks [11]. Limited local research and absence of predictive exposure models further constrain risk assessment in these settings [10].

In the Philippines, electronic cigarettes are regulated under Republic Act No. 11900 enacted in 2022, which governs product standards, labeling, and distribution [12]. The law permits nicotine concentrations of up to 65 mg per mL for vape liquids. However, standardized analytical protocols for nicotine verification are not specified, creating gaps in product quality assurance. Recent developments, including the country's first reported 2024 death linked to e-cigarette or vape-associated lung injury in a previously healthy young adult male, have heightened public health concerns [13]. Ongoing discussions on stricter regulations further reflect increasing concern [14].

The absence of mandatory laboratory verification may result in discrepancies between labeled and actual nicotine content. Thus, validated analytical methods and independent assessments are essential to ensure labeling accuracy and support regulatory enforcement. This study addresses these gaps by developing and validating a HPLC-PDA method for nicotine quantification and applying it to commercially available e-liquid products in

the Philippines. The findings aim to support evidence-based regulation, improve product surveillance, and strengthen public health protection in the context of emerging nicotine delivery systems.

II. MATERIALS AND METHODS

A. Materials and Reagents

Twenty-two commercially available e-liquid products were purchased from local retailers in Taguig City, Metro Manila. Samples were collected from August 2024 to July 2025 and were selected based on market availability to represent a variety of brands, flavors, and labeled nicotine concentrations encountered at the time of purchase. Only products sold in sealed packaging and bearing product information were included in the study. The labeled nicotine concentrations were recorded prior to analysis. Nicotine bitartrate dihydrate (PHR2532) was used for external calibration, while nicotine (N3876) was employed as the spiking standard for recovery studies. An Electronic Cigarette Liquid CRM (ERM®-DZ002a) was used to establish the trueness and metrological traceability of the method. Analysis was performed using a Shimadzu Nexera Lite LC-40D with a Shim-pack GIST C18 column. The mobile phase consisted of solvent A (10% acetonitrile (ACN) in 20 mM ammonium formate, pH 8.5) and solvent B (ACN), with 10% ACN used as diluent shown in Table 1.

B. Method Development and Validation

Chromatographic conditions for nicotine separation and detection were optimized based on the approach of Palazzolo et al. [15], including mobile phase composition, gradient program, flow rate, column temperature, and detection wavelength to achieve suitable peak shape, retention, and resolution. A photodiode array detector provided spectral confirmation of peak identity, while system suitability testing assessed repeatability, peak symmetry (tailing factor), column efficiency (theoretical plates), and retention factor (k′) within an acceptable range. Method validation was conducted in accordance with the Eurachem Guide [16] to demonstrate suitability for quantification of nicotine in e-cigarette liquids, with performance characteristics including linearity and working range, precision, and trueness.

C. Standard and Sample Solutions Preparation

A primary stock solution of nicotine bitartrate dihydrate (~1000 µg/mL) and a nicotine spike stock solution (~1370 µg/mL) were prepared in 10% ACN. Working standards (5.0–102.0 µg/mL as nicotine equivalents) were prepared by dilution, filtered through a 0.45 µm membrane, and transferred to HPLC vials for calibration. E-liquid samples from local retailers were coded as Sample 1–22, homogenized, diluted with 10% ACN to fit the calibration range, filtered, and transferred to HPLC vials. All preparations were performed in triplicate. For recovery studies, samples were spiked with nicotine standard, diluted, filtered, and analyzed in duplicate.

D. Statistical Analysis

Agreement between labeled and measured nicotine concentrations was evaluated using Bland–Altman analysis by plotting differences against their mean to assess bias and variability. The mean difference indicated systematic deviation, while the 95% limits of agreement (mean ± 1.96 x SD) identified under- or over-content. Analyses were performed in RStudio (R version 4.4.2).

III. RESULTS AND DISCUSSION

A. Method Development

The method development strategy was based on a mechanistic understanding of nicotine chemistry and reversed-phase chromatographic behavior.

Influence of mobile phase and physicochemical properties of nicotine:

Nicotine is a dibasic alkaloid (pKa_1 = 3.47, pKa_2 = 8.10; log P = 1.17), and its reversed-phase behavior depends on ionization state. Mobile phases at pH 7.0–9.0 effectively separate nicotine in C18 systems [17]. In this study, an alkaline mobile phase (pH 8.5) was employed under gradient elution conditions, consisting of 10% ACN in 20 mM ammonium formate (Solvent A) and ACN (Solvent B).

Table 1. HPLC-PDA Chromatographic Conditions

Parameters	Condition
Column	Shim-pack GIST C18 (150 x 4.6 mm, 3 µm)
Guard column	Shim-pack GIST C18 (10 x 4.0 mm, 3 µm)
Mobile phase composition	A - 10% ACN in 20 mM ammonium formate (pH 8.5) B - ACN
Flow rate	1.0 mL/min
Column Temperature	35 °C
Wavelength	259 nm

At this pH, nicotine remains largely non-ionized, reducing interaction with acidic silanol sites and improving hydrophobic retention. Basic analytes often exhibit peak tailing in silica-based columns due to residual silanol interactions [18,19]. Control of pH minimized these effects, while the optimized gradient system enabled efficient nicotine elution and separation from matrix components.

Chromatographic Efficiency and System Suitability:

As shown in Table 2, the optimized mobile phase improved retention, minimized silanol interactions, and produced near-ideal peak symmetry (T = 0.91). Reduced peak asymmetry improved quantitative accuracy by minimizing integration bias [20]. At 1.0 mL/min and 259 nm detection, nicotine was well resolved at 9.15 min with

a retention factor (k′) of 5.9, indicating adequate analyte retention and efficient interaction with the stationary phase. A high theoretical plate number (N ≈ 25,833) indicated efficient separation, while excellent injection repeatability (RSD 0.13%) confirmed autosampler stability and minimal carryover. The high resolution value (Rs = 44) demonstrated strong chromatographic separation. Consistent retention time at 35 °C further supported stable system performance, suggesting that variability in commercial samples was primarily sample-related rather than instrumental.

Table 2. System Suitability Performance Criteria

Criteria	Requirement	Results
Injection repeatability	RSD ≤ 2%	0.13
Tailing factor	T ≤ 2	0.91
Theoretical Plate Number	N ≥ 2000	25,833
Resolution (R_s)	$R_s \geq 2$	44
Retention factor (k′)	k' ≥ 2	5.9

B. Method Validation

The method for nicotine quantification in e-liquids was validated following the Eurachem guideline [16] for linearity, precision, and trueness, with performance characteristics summarized in Table 3.

Table 3. Summary of Method Validation Results

Performance Characteristics	Acceptance Criteria	Results
Linearity and Working Range	r ≥ 0.9950 residuals are randomly distributed to zero	0.9999 residuals are randomly distributed to zero Working range: 5-100 µg/mL
Repeatability	%RSD ≤ 2.0 HorRat ≤ 1.3	%RSD=0.43 HorRat=0.09
Intermediate Precision	HorRat ≤ 2.0	HorRat=0.15
Trueness by Reference Material	% Recovery = 90 - 110%	% Recovery = 99.3-100.5%

Linearity

The method showed excellent linearity over 5 to 100 µg/mL, with a correlation coefficient (r) of 0.9999 and randomly distributed residuals, indicating stable response. The range covers nicotine levels in commercial e-liquids, supporting single point external calibration. Minimal matrix effects were observed, as solvent composition did not significantly affect detector response.

Repeatability and Intermediate Precision

Results showed excellent repeatability and intermediate precision, with RSD values of 0.43% and 0.71%, respectively. Corresponding HorRat values of 0.09 and 0.15 were well below the Eurachem limit of 2, indicating superior precision and consistency with modern chromatographic methods [21]. This performance is attributed to stable chromatographic conditions, including symmetrical nicotine peaks, reproducible retention, consistent gradient formation, and minimal sample preparation variability [17,22]. The close agreement between repeatability and intermediate precision also suggests negligible variability from analysts, days, or routine operating conditions, supporting method ruggedness.

Trueness

Method trueness was evaluated using an e-cigarette liquid CRM (ERM®-DZ002), ensuring metrological traceability. Recoveries of 99.3%–100.5% demonstrated excellent agreement with certified values, indicating minimal systematic error, stable instrument response, and negligible matrix effects. As all results met the predefined acceptance criteria, the method demonstrates adequate performance for its intended purpose. Therefore, the method is considered fit for purpose and suitable for application under the specified analytical conditions.

C. Sample Analysis

Method applicability was demonstrated by analyzing commercial e-liquids and comparing measured nicotine concentrations with declared label values to evaluate labeling accuracy (Table 4).

Table 4. Results of Commercially Available E-liquids

Sample Code	Labeled (mg/mL)	Measured (mg/mL)	Absolute % Differences
Sample 1	10.00	8.66	13.4%
Sample 2	25.00	19.87	20.5%
Sample 3	10.00	6.24	37.6%
Sample 4	30.00	19.38	35.4%
Sample 5	30.00	13.59	54.7%
Sample 6	10.00	6.88	31.2%
Sample 7	10.00	6.42	35.8%
Sample 8	30.00	13.78	54.1%
Sample 9	24.00	3.95	83.5%
Sample 10	12.00	7.87	34.4%
Sample 11	9.00	4.92	45.3%
Sample 12	2.00	1.13	43.5%
Sample 13	12.00	8.41	29.9%
Sample 14	12.00	7.98	33.5%
Sample 15	2.00	1.26	37.0%
Sample 16	30.00	13.28	55.7%
Sample 17	30.00	8.67	71.1%
Sample 18	10.00	6.38	36.2%
Sample 19	24.00	9.63	59.9%

Sample 20	30.00	24.47	18.4%
Sample 21	50.00	26.84	46.3%
Sample 22	30.00	4.68	84.4%

The absolute %Differences is computed using the equation below:

$$Abs.\%Differences = \left|\frac{Cmeasured - Clabeled}{Clabeled}\right| x\ 100 \quad (1)$$

Most products showed substantial negative deviations between labeled and measured nicotine concentrations, indicating that actual nicotine levels were generally lower than those declared on the labels. Differences ranged from 13.4% to 84.4%, with most products exhibiting deviations between 30% and 60%. Similar labeling inaccuracies have been reported internationally. In the United States, Davis et al. (2015) found that 35 of 54 nicotine-containing refill fluids deviated by more than ±10% from their labeled nicotine concentrations [23], while Appleton et al. (2022) reported that 23 of 51 disposable e-cigarette products deviated by more than ±10%, with discrepancies ranging from −50.1% to +13.9% [24]. In South Korea, Kim et al. (2015) documented nicotine labeling differences ranging from −32.2% to +3.3% [25], and Goniewicz et al. (2015) reported significant discrepancies exceeding 20% in 19% of e-liquids marketed in the United States, South Korea, and Poland [26]. Similarly, in Europe, Bębenek et al. (2022) found that only 58.1% of 86 e-liquid products complied with a ±10% labeling accuracy criterion [27]. A global review by Taylor et al. (2021), covering 23 studies and 545 products, further demonstrated that nicotine concentrations were commonly mislabeled by 5–20%, with some products labeled as nicotine-free containing as much as 23.91 mg/mL nicotine [28]. These findings indicate that nicotine labeling inaccuracies remain a global concern, with the substantial negative deviations between labeled and measured nicotine concentrations observed in this study highlighting the need for stronger regulatory oversight and quality control in the Philippine market.

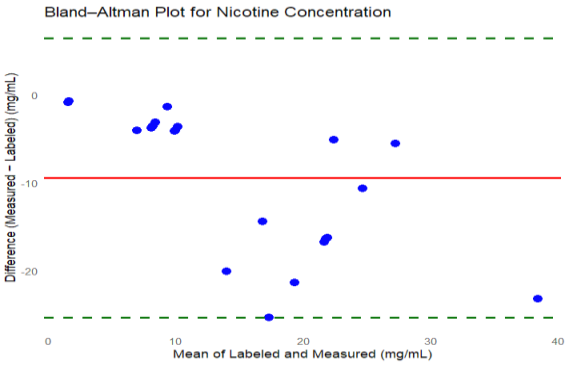


Fig. 1. Bland-Altman Analysis for Bias

Bland–Altman analysis (Figure 1) revealed a pronounced negative bias, with all values below the zero line and a mean difference of approximately −9 mg/mL, indicating systematically lower measured concentrations relative to the labeled claim. Some samples, particularly 9, 17, and 22, exhibited extreme deviations exceeding 70–80%. The wide limits of agreement further indicated variability, particularly at higher nicotine concentrations.

Given the demonstrated trueness and precision of the validated method, these discrepancies are unlikely due to analytical error and more likely reflect manufacturing variability, formulation complexity, and possible nicotine degradation. Overall, the findings demonstrate widespread labeling inconsistencies and emphasize the need for independent verification and strengthened post-market surveillance.

Plausible factors contributing to "below-label' nicotine results:

Manufacturing variability and filling accuracy:

Manufacturing variability likely explains the observed labeling discrepancies, as e-liquids are produced under heterogeneous quality control systems. Several studies report frequent nicotine deviations. Peace et al. (2016) found nicotine levels ranging from 45% to 131% of labeled values, with 67% exceeding ±10% variance [29], while Miller et al. (2020) reported that 48.3% of 574 samples deviated by more than 10% [30]. Raymond et al. (2017) observed deviations from 35% below to 52% above labeled values [31], and Davis et al. (2015) reported batch inconsistency [23]. However, strong quality control can reduce variability, as shown by Etter et al. (2017), where 82% of samples were within ±10% [9]. These findings highlight the importance of manufacturing and quality assurance practices.

Matrix Effects and Formulation Complexity:

Beyond manufacturing variability, formulation complexity also contributes to discrepancies between labeled and measured nicotine concentrations. E-liquids are multicomponent systems containing propylene glycol, vegetable glycerin, nicotine, and additives that influence nicotine distribution, stability, and measurement. Component interactions can produce synergistic or antagonistic effects, making nicotine behavior formulation dependent [32]. Flavor compounds may react with solvents and alter composition [33], while pH variation affects nicotine ionization and stability [34]. In addition, the propylene glycol–vegetable glycerin ratio influences mixing, homogeneity, and nicotine distribution [35]. These findings highlight e-liquids as chemically dynamic systems in which formulation characteristics contribute to nicotine variability.

Storage, Transport and Degradation Processes:

Post-manufacture storage and transport conditions may also contribute to discrepancies between labeled and measured nicotine concentrations. Nicotine degrades under light, oxygen, heat, and prolonged storage, reducing concentrations below labeled values. Ultraviolet exposure

can cause up to 16.9% nicotine loss over 48 hours, compared with 9% under visible light and 1.6% in dark conditions [36]. Elevated temperature and oxygen further accelerate oxidative and thermal degradation [37]. Stability also depends on formulation and storage duration, with salt-based products generally showing greater retention than free-base forms after prolonged storage [38]. These findings suggest that under-labeling may partly reflect degradation during storage and distribution, not manufacturing variability alone.

D. Regulatory Compliance Assessment

Under Republic Act No. 11900, the maximum allowable nicotine concentration for e-cigarette liquids is 65 mg/mL. All analyzed samples complied with this limit, with measured nicotine concentrations ranging from 1.13 to 26.84 mg/mL. However, substantial discrepancies between labeled and measured nicotine concentrations (13.4–84.4%) were observed, highlighting that regulatory compliance alone may not ensure accurate consumer information. Accurate nicotine labeling is essential because it influences user behavior, nicotine intake, and dependence potential. Products containing less nicotine than declared may encourage compensatory behaviors, such as increased puff frequency or consumption, to achieve the desired nicotine effect, potentially altering actual exposure patterns [39]. Conversely, inaccurate labeling may undermine consumer confidence and hinder informed product selection. Similar labeling discrepancies have been reported internationally, suggesting that nicotine mislabeling remains a persistent regulatory concern. These findings support the need for routine market surveillance, laboratory verification of nicotine content, and stricter enforcement of labeling requirements to enhance consumer protection and strengthen regulatory oversight of e-cigarette liquid products in the Philippines.

IV. CONCLUSION

This study provides analytically verified data to support stronger regulation of e-cigarette liquids in the Philippines. Effective oversight requires validated analytical methods that generate accurate, reproducible, and traceable measurements for compliance assessment and regulatory monitoring. As e-cigarette liquids diversify in formulation and nicotine strength, routine laboratory testing becomes essential for consumer protection and consistent enforcement. The validated method developed in this study can support nicotine monitoring, labeling verification, and science-based regulation.

V. REFERENCES

[1] Turfus, S., & Cooney, S. (2023). The science behind vaping. Drug Testing and Analysis, 15(10), 1054–1057. https://doi.org/10.1002/dta.3587

[2] Crotty Alexander, L. E., Vyas, A., Schraufnagel, D. E., & Malhotra, A. (2015). Electronic cigarettes: The new face of nicotine delivery and addiction. Journal of Thoracic Disease, 7(8), E248–E251. https://doi.org/10.3978/j.issn.2072-1439.2015.07.37

[3} Herman, M., & Tarran, R. (2020). E-cigarettes, nicotine, the lung and the brain: Multi-level cascading pathophysiology. The Journal of Physiology, 598(22), 5063–5071. https://doi.org/10.1113/JP279554

[4] Ramôa, C. P., Hiler, M. M., Spindle, T. R., Lopez, A. A., Karaoghlanian, N., Lipato, T., Breland, A. B., Shihadeh, A., & Eissenberg, T. (2016). Electronic cigarette nicotine delivery can exceed that of combustible cigarettes: A preliminary report. Tobacco Control, 25(e1), e6–e9. https://doi.org/10.1136/tobaccocontrol-2015-052447

[5] Buchanan, N. D., Grimmer, J. A., Tanwar, V., Schwieterman, N., Mohler, P. J., & Wold, L. E. (2020). Cardiovascular risk of electronic cigarettes: A review of preclinical and clinical studies. Cardiovascular Research, 116(1), 40–50. https://doi.org/10.1093/cvr/cvz256

[6] El-Hellani, A., Salman, R., El-Hage, R., Talih, S., Malek, N., Baalbaki, R., Karaoghlanian, N., Nakkash, R., Shihadeh, A., & Saliba, N. A. (2018). Nicotine and carbonyl emissions from popular electronic cigarette products: Correlation to liquid composition and design characteristics. Nicotine & Tobacco Research, 20(2), 215–223. https://doi.org/10.1093/ntr/ntw280

[7] Soule, E. K., Mayne, S., Snipes, W., Do, E. K., Theall, T., Höchsmann, C., Talih, S., Martin, C. K., Eissenberg, T., & Fuemmeler, B. F. (2023). Electronic cigarette nicotine flux, nicotine yield, and particulate matter emissions: Impact of device and liquid heterogeneity. Nicotine & Tobacco Research, 25(3), 412–420. https://doi.org/10.1093/ntr/ntac196

[8] Girvalaki C, Tzatzarakis M, Vardavas A, et al. Discrepancies in reported versus measured nicotine content of e-cigarette refill liquids across nine European countries before and after the implementation of the EU Tobacco Products Directive. Eur Respir J 2020; 55: 1900941 https://doi.org/ 10.1183/13993003.00941-2019

[9] Etter, J.-F., & Bugey, A. (2017). E-cigarette liquids: Constancy of content across batches and accuracy of labeling. Addictive Behaviors, 73, 137–143. https://doi.org/10.1016/j.addbeh.2017.05.012

[10] Kalan, M. E., Mejia, R., Egbe, C. O., Chopra, M., Bteddini, D., Jebai, R., Osibogun, O., Wilkinson, A. V., & Salloum, R. G. (2023). E-cigarette use in low-income and middle-income countries: Opportunity or challenge for global tobacco control. The Lancet Global Health, 11(12), e1855–e1856.

[11] Chandrashekhar T Sreeramareddy, Anusha Manoharan, Awareness About and E-Cigarette Use Among Adults in 15 Low- and Middle-Income Countries, 2014–2018 Estimates From Global Adult Tobacco Surveys, Nicotine & Tobacco Research, Volume 24, Issue 7, July 2022, Pages 1095–1103, https://doi.org/10.1093/ntr/ntab269

[12] Republic of the Philippines. (2022). Republic Act No. 11900: Vaporized Nicotine and Non-Nicotine Products Regulation Act. https://lawphil.net/statutes/repacts/ra2022/ra_11900_2022.html

[13] Perez, A. (2024). Philippines records first death due to vape-related lung injury. ABS-CBN News. https://www.abs-cbn.com/news/2024/5/31/ph-records-first-death-due-to-vape-related-lung-injury-1123

[14] Abanto, R. (2025). DOH floats total ban on vape. ABS-CBN News. https://www.abs-cbn.com/news/health-science/2025/11/24/doh-calls-for-total-ban-on-vape-1009

[15] Palazzolo, D., Nelson, J. M., & Hudson, Z. (2019). The use of HPLC-PDA in determining nicotine and nicotine-related alkaloids from e-liquids: A comparison of five e-liquid brands purchased locally. International Journal of Environmental Research and Public Health, 16(16), 3017. https://doi.org/10.3390/ijerph16163017

[16] Magnusson B, Örnemark U, eds. The Fitness for Purpose of Analytical Methods: A Laboratory Guide to Method Validation and Related Topics. Second Edition. Eurachem; 2014.

[17] Moisi, R.; Comănescu, M.-A.; Medvedovici, A.-V. ReversedPhase (RP) and Hydrophilic Interaction (HILIC) Separation Mechanisms for the Assay of Nicotine and E-Cigarette Liquids. Molecules 2025, 30, 3443. https://doi.org/10.3390/molecules30163443

[18] Mazzoccanti, G., Gasparrini, F., Calcaterra, A., Villani, C., & Ciogli, A. (2021). Static vs. dynamic electrostatic repulsion reversed phase liquid chromatography: Solutions for pharmaceutical and biopharmaceutical basic compounds. *Separations, 8*(5), 59. https://doi.org/10.3390/separations8050059

[19] Peris-García, E., Burgos-Gil, R., García-Alvarez-Coque, M. C., & Ruiz-Angel, M. J. (2020). Hydrophilic liquid chromatography versus reversed-phase liquid chromatography in the absence and the presence of 1-hexyl-3-methylimidazolium chloride for the analysis of basic compounds. *Separations, 7*(2), 30. https://doi.org/10.3390/separations7020030

[20] Komsta, Ł. (2018). Modeling of peak shape and asymmetry. In Ł. Komsta, Y. Vander Heyden, & J. Sherma (Eds.), *Chemometrics in chromatography* (1st ed.). CRC Press. https://doi.org/10.1201/9781315154404-12

[21] Ehling, S., Thompson, J., Schimpf, K. J., Pacquette, L. H., & Haselberger, P. A. (2025). A contemporary look at the precision of modern analytical methods in food analysis and the relevance of the Horwitz equation. *Journal of AOAC International, 108*(4), 566–571 https://doi.org/10.1093/jaoacint/qsaf026

[22] Gholap, V. V., Kosmider, L., & Halquist, M. S. (2018). A standardized approach to quantitative analysis of nicotine in e-liquids based on peak purity criteria using high-performance liquid chromatography. *Journal of Analytical Methods in Chemistry, 2018*, Article 1720375. https://doi.org/10.1155/2018/1720375

[23] Davis, B., Dang, M., Kim, J., & Talbot, P. (2014). Nicotine concentrations in electronic cigarette refill and do-it-yourself fluids. *Nicotine & Tobacco Research, 17*(2), 134–141. https://doi.org/10.1093/ntr/ntu080

[24] Appleton, S., Cyrus-Miller, H., Seltzer, R., Gilligan, K., & McKinney, W. (2022). Market survey of disposable e-cigarette nicotine content and e-liquid volume. *BMC Public Health, 22*, Article 1760. https://doi.org/10.1186/s12889-022-14152-2

[25] Kim, S., Goniewicz, M. L., Yu, S., Kim, B., & Gupta, R. (2015). Variations in label information and nicotine levels in electronic cigarette refill liquids in South Korea: Regulation challenges. *International Journal of Environmental Research and Public Health, 12*(5), 4859–4868. https://doi.org/10.3390/ijerph120504859

[26] Goniewicz, M. L., Gupta, R., Lee, Y. H., Reinhardt, S., Kim, S., Kim, B., Kosmider, L., & Sobczak, A. (2015). Nicotine levels in electronic cigarette refill solutions: A comparative analysis of products from the US, Korea, and Poland. *International Journal of Drug Policy, 26*(6), 583–588. https://doi.org/10.1016/j.drugpo.2015.01.020

[27] Bebenek, P.K.; Gholap, V.; Halquist, M.; Sobczak, A.; Ko´smider, L. E-Liquids from Seven European Countries–Warnings Analysis and Freebase Nicotine Content. Toxics **2022**, 10, 51. https://doi.org/10.3390/toxics10020051

[28] Taylor, A., Dunn, K., & Turfus, S. (2021). A review of nicotine-containing electronic cigarettes—Trends in use, effects, contents, labelling accuracy and detection methods. *Drug Testing and Analysis, 13*(2), 242–260. https://doi.org/10.1002/dta.2998

[29] Peace, M. R., Baird, T. R., Smith, N., Wolf, C. E., Poklis, J. L., & Poklis, A. (2016). Concentration of nicotine and glycols in 27 electronic cigarette formulations. *Journal of Analytical Toxicology, 40*(6), 403–407. https://doi.org/10.1093/jat/bkw037

[30] Miller, D. R., Buettner-Schmidt, K., Orr, M., Rykal, K., & Niewojna, E. (2021). A systematic review of refillable e-liquid nicotine content accuracy. *Journal of the American Pharmacists Association, 61*(1), 20–26. https://doi.org/10.1016/j.japh.2020.09.006

[31] Raymond, Barrett H. BSN, RN, FNP-S, NREMT-P; Collette-Merrill, Katreena PhD, RN; Harrison, Roger G. PhD; Jarvis, Sabrina DNP, FNP-BC, ACNP-BC, FAANP; Rasmussen, Ryan Jay MS, RN, FNP. The Nicotine Content of a Sample of E-cigarette Liquid Manufactured in the United States. Journal of Addiction Medicine 12(2):p 127-131, March/April 2018. | DOI: 10.1097/ADM.0000000000000376

[32] Goniewicz, M. L., Hajek, P., & McRobbie, H. (2014). Nicotine content of electronic cigarettes, its release in vapour and its consistency across batches: Regulatory implications. *Addiction, 109*(3), 500–507. https://doi.org/10.1111/add.12410

[33] Erythropel, H. C., Jabba, S. V., DeWinter, T. M., Mendizabal, M., Anastas, P. T., Jordt, S. E., & Zimmerman, J. B. (2019). Formation of flavorant–propylene glycol adducts with novel toxicological properties in chemically unstable e-cigarette liquids. *Nicotine & Tobacco Research, 21*(9), 1248–1258. https://doi.org/10.1093/ntr/nty192

[34] Lisko, J. G., Tran, H., Stanfill, S. B., Blount, B. C., & Watson, C. H. (2015). Chemical composition and evaluation of nicotine, tobacco alkaloids, pH, and selected flavors in e-cigarette cartridges and refill solutions. *Nicotine & Tobacco Research, 17*(10), 1270–1278. https://doi.org/10.1093/ntr/ntu279

[35] Vyshneva, V. (2022). Effect of propylene glycol and vegetable glycerine ratio in e-liquid on aerosol formation: Overview of relevant properties. *Adiktologie Journal, 22*, 118–125. https://doi.org/10.35198/01-2022-002-0005

[36] An, Y.-J., & Kim, Y.-H. (2023). Assessment of nicotine degradation in cigarette smoke under different storage conditions (light and duration). *Indoor Air, 2023*, Article 8814709. https://doi.org/10.1155/2023/8814709

[37] Asensio, J., Berenguer, D., Marcilla, A., & Beltrán, M. I. (2023). Nicotine fast pyrolysis under inert and air environments: Effect of catalysts. *Journal of Analytical and Applied Pyrolysis, 170*, 105899. https://doi.org/10.1016/j.jaap.2023.105899

[38] Kosarac, I., Katuri, G. P., Kubwabo, C., Siddique, S., & Mischki, T. K. (2023). Quantitation and stability of nicotine in Canadian vaping liquids. *Toxics, 11*(4), 378. https://doi.org/10.3390/toxics11040378

[39] White, C. M., Watson, C., Bravo Cardenas, R., Ngac, P., Valentin-Blasini, L., Blount, B. C., Koopmeiners, J. S., Denlinger-Apte, R. L., Pacek, L. R., Benowitz, N. L., Hatsukami, D. K., Donny, E. C., Carpenter, M. J., & Smith, T. T. (2022). Early changes in puffing intensity when exclusively using open-label very low nicotine content cigarettes. *Nicotine & Tobacco Research, 24*(11), 1798–1802. https://doi.org/10.1093/ntr/ntac118

2026 IMEKO Joint Conference
TC8 - TC11 - TC24
Metro Manila, Philippines, August 26-29, 2026

Digital Transformation of LNEC Laboratories: A Smart LIMS Architecture Integrating AI, M2M Communication and Automated Data Analytics

Álvaro Silva Ribeiro[1], Júlio Sousa Ribeiro[2], Catarina Martins[3]

[1] National Laboratory for Civil Engineering (LNEC), Lisbon, Portugal
[2] MASTERINSOFT – Intelligence in Software and Computing Engineering, Porto, Portugal
[3] National Laboratory for Civil Engineering (LNEC), Lisbon, Portuga[l]

***Abstract* – Laboratories complying with ISO/IEC 17025 face growing demands in data management, traceability, and digital integration, particularly within the TIC sector. This paper presents a smart Laboratory Information Management System (LIMS) developed for LNEC to support intelligent laboratory operations. The platform unifies quality management processes, including client services, method lifecycle, and metrological control, within a single digital framework. It incorporates AI tools for automated data validation, anomaly detection, and decision support, alongside Machine-to-Machine communication to reduce manual handling and improve data integrity. Digital Calibration Certificates and advanced analytics further enhance traceability and data interpretation. The proposed system advances laboratory efficiency, reliability, and integration within evolving digital ecosystems.**

I. INTRODUCTION

Laboratories operating under ISO/IEC 17025 increasingly face structural challenges associated with the exponential growth of data, the need for strict traceability, and the demand for higher efficiency in testing and calibration activities. Within the Testing, Inspection and Certification (TIC) sector, digital transformation is no longer optional but a necessary condition for ensuring competitiveness, reliability, and scalability of operations [1,2]. Traditional Laboratory Information Management Systems (LIMS) have typically been designed as passive repositories of information, lacking advanced capabilities for automation, interoperability, and intelligent data processing.

Recent developments in Artificial Intelligence (AI), Machine-to-Machine (M2M) communication, and digital metrology are reshaping laboratory environments. These technologies enable real-time data acquisition, automated validation, predictive analytics, and seamless integration between instruments and information systems [3–5]. In parallel, initiatives such as Digital Calibration Certificates (DCC) and Industry 4.0 frameworks are fostering interoperability and standardization across measurement infrastructures [6,7]. Digital Twin concepts are also emerging as important enablers for intelligent laboratory environments, supporting virtual representations of equipment and processes for predictive analysis and optimization [8].

This paper presents the conceptual design and development of a smart LIMS platform tailored to the needs of the National Laboratory for Civil Engineering (LNEC). The system is designed as a unified digital architecture that integrates three fundamental operational vectors: client interaction and service management, resources and quality management, and technical and operational data analysis. The proposed approach emphasizes compliance with ISO/IEC 17025, while leveraging AI and digital technologies to enhance measurement integrity and operational efficiency [1,9].

II. LNEC LABORATORY FRAMEWORK AND QUALITY MANAGEMENT SYSTEM

LNEC operates a complex and heterogeneous laboratory ecosystem comprising 32 laboratories distributed across multiple domains of civil engineering. The institution manages approximately 1200 test and calibration methods, of which around 300 are accredited under ISO/IEC 17025. The operational structure includes approximately 170 technical and scientific personnel, supporting more than 20,000 testing and calibration activities annually. The metrological infrastructure includes over 3,200 measurement standards and equipment units, ranging from high-precision instruments to large-scale experimental setups.

The Quality Management System (QMS) at LNEC is fully aligned with ISO/IEC 17025 and encompasses procedures for method validation, uncertainty evaluation, equipment calibration, and reporting [1,10]. It also integrates risk-based thinking, ensuring that potential sources of error or bias are systematically identified and mitigated. However, the current implementation relies on a combination of legacy systems, spreadsheets, and manual processes, resulting in fragmentation and limited interoperability.

The proposed digital LIMS aims to embed QMS principles

directly into the operational workflows. Risk assessment is incorporated into each stage of the testing lifecycle, allowing dynamic evaluation of potential deviations. Conformity assessment is supported through configurable decision rules that consider measurement uncertainty and specification limits [10]. Confidentiality is ensured through role-based access control and secure data management protocols, while transparency is achieved through complete audit trails and traceability chains.

A critical aspect of the system is the management of metrological traceability. Each measurement result is linked to calibration data, reference standards, and uncertainty budgets, ensuring compliance with international metrology standards [11]. The integration of Digital Calibration Certificates allows machine-readable representation of calibration data, facilitating automated validation and interoperability with external systems [6].

III. SMART LIMS ARCHITECTURE AND OPERATIONAL INTEGRATION

The proposed LIMS architecture is designed as a modular and scalable platform capable of supporting the diverse needs of LNEC laboratories. A central component is the client portal, which enables full digital interaction between clients and the laboratory. Service requests are submitted, managed, and tracked through a structured workflow, ensuring transparency and efficiency. Each request is associated with metadata describing the required methods, specifications, deadlines, and compliance criteria.

The management of services is fully digitized, including quotation, scheduling, execution, and reporting. The system integrates with external enterprise software for financial and organizational management, enabling automatic synchronization of billing, cost allocation, and resource planning. This integration ensures consistency between technical operations and administrative processes.A key innovation of the platform is the implementation of a resource management module that includes dynamic scheduling of human resources and critical instrumentation. The system supports the generation of Gantt charts for planning laboratory activities, considering constraints such as equipment availability, calibration status, and personnel qualifications. This functionality allows optimized allocation of resources and minimizes downtime or bottlenecks.

Datasets within the LIMS are structured to provide comprehensive descriptions of methods, including specifications, measurement ranges, uncertainty models, and validation data. Each method is associated with standardized metadata, enabling consistent execution across laboratories. The system also supports version control, ensuring that updates to methods are tracked and validated according to QMS requirements.

Dashboards play a central role in the platform, providing real-time visualization of key performance indicators (KPIs) at different levels of responsibility within LNEC. Laboratory managers, technical staff, and strategic decision-makers have access to customized views, enabling informed decision-making and continuous monitoring of performance.

In addition, the platform integrates an Electronic Laboratory Notebook (ELN) module that enables structured and collaborative documentation of experimental activities. This includes the registration of visual evidence, allowing images captured before, during, and after testing to be linked to each record, enhancing traceability and supporting objective validation. The system also incorporates automated reporting capabilities, where results are compiled into standardized reports and validated through hierarchical workflows involving authorized personnel. All actions are recorded, ensuring full auditability, accountability, and compliance with ISO/IEC 17025 requirements.

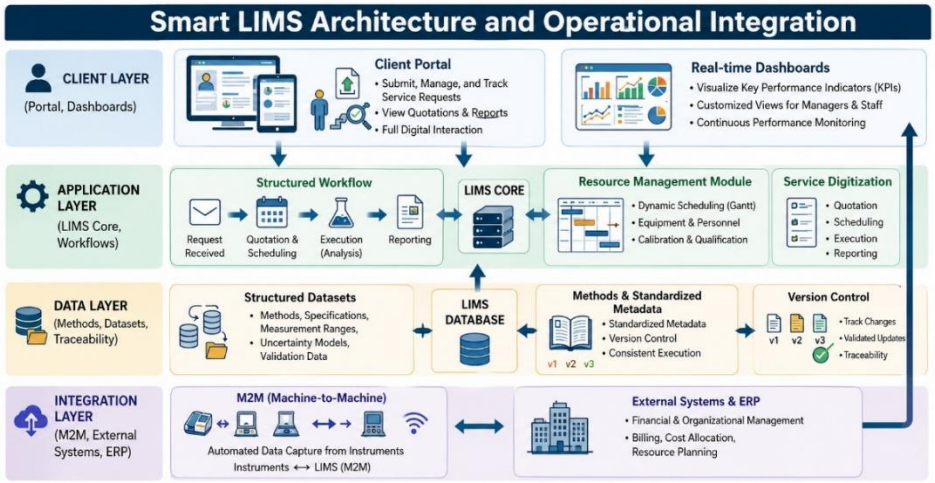


Fig. 1. Smart LIMS architecture integrating client interaction, resource management and data processing layers (created using Google Gemini)

IV. AI INTEGRATION, M2M COMMUNICATION AND DATA ANALYTICS

The integration of AI into the LIMS architecture enables the transition from data management to knowledge generation. AI algorithms are applied to automate data validation, detect anomalies, and support decision-making processes. Depending on the application, supervised and unsupervised machine learning techniques may be employed. For anomaly detection, algorithms such as Isolation Forest and Autoencoders can identify abnormal measurement patterns and detect possible equipment malfunction or procedural errors. Classification models, including Random Forest and Support Vector Machines, may support the automatic validation of test results against predefined quality criteria, while regression models can assist in predicting calibration drift and estimating maintenance intervals. These capabilities are complemented by collaborative validation workflows, where domain experts review and annotate AI-generated results, ensuring a human-in-the-loop approach to decision support consistent with ISO/IEC 17025 requirements. Machine learning models can therefore identify patterns in measurement data, supporting the early detection of deviations, improving measurement reliability, and contributing to the continuous improvement of laboratory processes [4,9]. Bayesian statistical methods may further support probabilistic decision-making and uncertainty-aware data interpretation within advanced analytics workflows [12].

M2M communication is implemented through standardized industrial communication interfaces that enable direct data exchange between laboratory instrumentation and the LIMS. Protocols include secure industrial interoperability, for lightweight event-driven communication, and APIs for integration with external information systems. Where required, legacy equipment can be connected through serial communication interfaces (RS-232/RS-485) using protocol converters or middleware. These mechanisms eliminate manual data entry, reduce transcription errors, improve data integrity, and facilitate interoperability between heterogeneous laboratory equipment. The system supports heterogeneous communication protocols, allowing integration of legacy and modern equipment [5].

Advanced data analytics modules provide capabilities for statistical analysis, uncertainty evaluation, and visualization of experimental results. Uncertainty propagation follows the principles established in the *Guide to the Expression of Uncertainty in Measurement* (GUM), combining uncertainty contributions associated with calibration data, reference standards, environmental conditions, instrument performance, and measurement repeatability [10]. The integration of Digital Calibration Certificates (DCC) enables uncertainty information to be automatically imported together with calibration metadata, allowing uncertainty budgets to be updated dynamically throughout the measurement chain. This approach reduces manual transcription errors, improves the consistency of uncertainty evaluation, and reinforces metrological traceability and compliance with ISO/IEC 17025 [6,11]. These tools also enable real-time monitoring of test execution and support the identification of trends and correlations in measurement data, contributing to more reliable decision-making and continuous improvement of laboratory performance.

The system also supports the development of digital tools aimed at improving efficiency across the three operational vectors. These include automated reporting, predictive maintenance of equipment, and optimization of testing workflows. By leveraging AI and data analytics, the platform enhances both operational performance and measurement reliability [3,13].

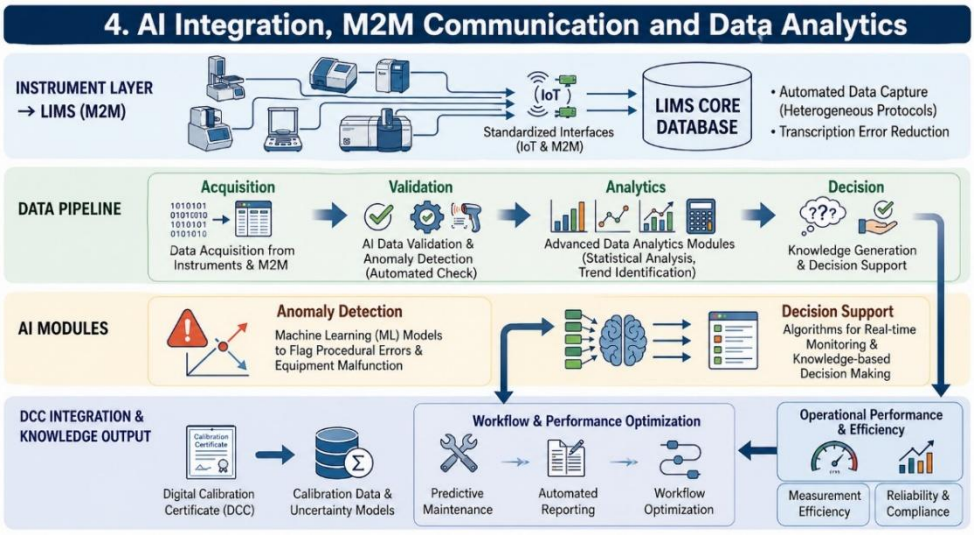


Fig. 2. Data flow architecture integrating M2M communication, AI-based analytics, and digital calibration certificates (created using Google Gemini)

V. DISCUSSION, STRATEGIC OBJECTIVES AND EXPECTED OUTCOMES

The digital transformation of LNEC laboratories is driven by strategic objectives aimed at enhancing efficiency, ensuring compliance, and strengthening integration within the TIC sector. The proposed LIMS platform contributes to these objectives by providing a unified and intelligent operational environment.

The expected added value includes improved data quality, reduced turnaround times, enhanced resource utilization, and increased transparency. The system also facilitates compliance with ISO/IEC 17025 by embedding quality requirements into digital workflows, simplifying audits and accreditation processes.

The interaction with ISO/IEC 17025 accreditation is particularly significant. The LIMS supports documentation control, traceability, and audit readiness, ensuring that all activities are performed in accordance with established procedures. Automated records and digital traceability chains provide evidence of compliance, reducing the administrative burden associated with audits. The KPI framework presented in Table 1 translates ISO/IEC 17025 requirements into measurable indicators aligned with operational, technical, and management processes. This mapping demonstrates that LIMS is not only an operational tool but also a digital enabler of compliance, transforming standard requirements into continuously monitored and auditable metrics.

Table 1. Expected Outcomes, KPI and Mapping to ISO/IEC 17025

Domain	KPI	Baseline	Expected Impact	ISO/IEC 17025 Clause(s)
Client Interaction	Service request volume (No./period)	Partial	Improved demand visibility and planning	7.1 (Review of requests, tenders and contracts)
	Response time to requests (time)	High	Faster client engagement	7.1, 8.2 (Management system documentation)
	Proposal acceptance rate (%)	Moderate	Increased competitiveness and conversion	7.1
	Customer satisfaction index (score)	Moderate	Enhanced trust and service quality	8.6 (Improvement), 7.9 (Complaints)
	Service tracking transparency (%)	Limited	Full transparency and traceability	7.5 (Technical records), 7.8 (Reporting)
Human Resources & Activity	Testing and calibration volume (No./period)	Partial	Increased operational throughput	7.2 (Selection, verification and validation of methods)
	Staff utilisation rate (%)	Moderate	Optimised workforce efficiency	6.2 (Personnel)
	Productivity per staff (No./person)	Variable	Higher productivity	6.2
	Average execution time per test (time)	High variability	Standardised and reduced execution time	7.2, 7.3 (Sampling), 7.4 (Handling of test items)
Critical Equipment	Equipment utilisation rate (%)	Moderate	Improved asset efficiency	6.4 (Equipment)
	Equipment downtime (time/%)	Significant	Reduced downtime and increased availability	6.4
	Equipment operational efficiency (%)	Moderate	Increased performance reliability	6.4, 7.7 (Ensuring validity of results)
Service Time Management	End-to-end service turnaround time (time)	High variability	Faster service delivery	7.1, 7.8
	On-time delivery rate (%)	Moderate	Improved reliability and planning	7.8 (Reporting of results)
Equipment Management	Equipment availability status (%)	Limited	Real-time monitoring and control	6.4
	Calibration compliance rate (%)	Partial	Full compliance with standards	6.4, 6.5 (Metrological traceability)
	Maintenance efficiency (time-based)	Reactive	Predictive and optimised maintenance	6.4
Methods & Services	Service distribution per method (No./%)	Limited	Improved method optimisation	7.2
	Accredited vs non-	Moderate	Increased accredited	5.3 (Scope of laboratory

	accredited activity (%)		activities	activities), 7.2
Service Origin	Internal vs external service ratio (%)	Unbalanced	Better strategic positioning	8.5 (Actions to address risks and opportunities)
Financial Performance	Revenue per laboratory (€)	Variable	Increased financial sustainability	8.5, 8.9 (Management reviews)
	Revenue per service (€)	Limited	Improved value generation	8.5
Quality & Compliance	Rework rate (%)	Moderate	Reduced errors and improved quality	7.10 (Nonconforming work), 8.7 (Corrective actions)
	Digital traceability coverage (%)	Partial	Full traceability and audit readiness	6.5, 7.5
Data & Analytics	Data automation level (%)	Low	Reduced manual intervention	7.11 (Control of data and information management)
	Dashboard usage rate (No./users)	Limited	Data-driven decision-making	8.4 (Control of records), 8.9

Although the platform is currently under implementation, preliminary performance targets have been established to support future validation of the proposed architecture. These include increasing digital traceability coverage to more than 95% of laboratory records, reducing manual data entry by approximately 80% through M2M integration, decreasing average service turnaround time by 20–30%, improving equipment utilisation by at least 15%, and achieving calibration compliance rates approaching 100%. These targets will serve as quantitative benchmarks during the operational evaluation of the LIMS.

The proposed KPI framework enables continuous monitoring of compliance, operational performance, and resource utilization, providing objective evidence for management reviews, continuous improvement, and accreditation activities. Cloud-enabled architectures facilitate scalable deployment of laboratory services, distributed data processing, and secure access to laboratory information across multiple organizational units [14].

Although the proposed architecture has been developed for testing and calibration laboratories operating under ISO/IEC 17025, several concepts, including digital traceability, AI-assisted workflows, and interoperable data management, are also consistent with the digital transformation trends observed in medical laboratories operating under ISO 15189 [15]

In conclusion, the proposed smart LIMS architecture represents a significant step toward the development of intelligent laboratory environments. By integrating AI, M2M communication, and digital metrology concepts, the system addresses critical challenges in data management, traceability, and operational efficiency. The implementation at LNEC demonstrates the feasibility and benefits of this approach, providing a model for other institutions seeking to modernize their laboratory infrastructures.

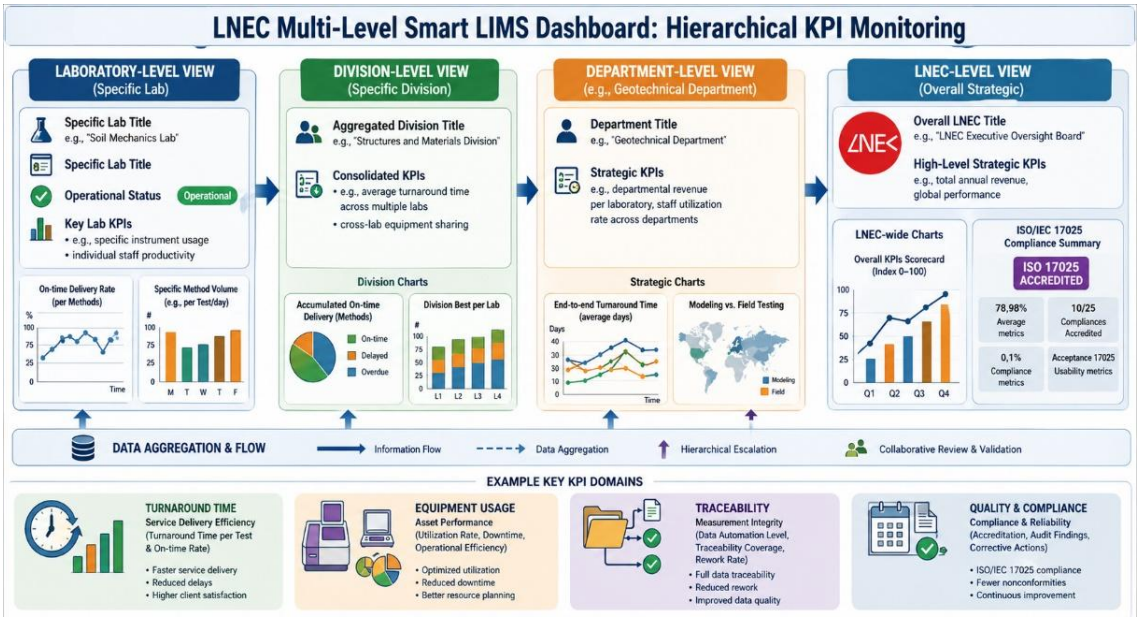


Fig. 3. Hierarchical KPI monitoring and dashboard structure for multi-level laboratory management. (created using Google Gemini)

REFERENCES

[1] ISO/IEC 17025:2017, *General requirements for the competence of testing and calibration laboratories*, ISO, Geneva, 2017.
[2] European Commission, *Digital Transformation of Industry*, Brussels, 2020.
[3] L. Wang, M. Törngren, M. Onori, Current status and advancement of cyber-physical systems in manufacturing, *Engineering* **2** (2016) 465–470.
[4] S. Yin, O. Kaynak, Big data for modern industry: challenges and trends, *Proc. IEEE* 103 (2015) 143–146.
[5] P. Leitão, J. Barbosa, Industrial cyber-physical systems, *Annu. Rev. Control* **47** (2019) 71–80.
[6] EURAMET, *Digital Calibration Certificate (DCC) – Concept and Implementation*, 2020.
[7] N. Jazdi, Cyber physical systems in Industry 4.0, *Automatisierungstechnik* **62** (2014) 706–715.
[8] M. Grieves, *Digital Twin: Manufacturing Excellence*, 2014.
[9] J. Lee, H.A. Kao, S. Yang, Service innovation and smart analytics, *Procedia CIRP* **16** (2014) 3–8.
[10] JCGM 100:2008, *Guide to the expression of uncertainty in measurement*, BIPM, 2008.
[11] BIPM, *The International System of Units (SI)*, 9th ed., 2019.
[12] A. Gelman et al., *Bayesian Data Analysis*, CRC Press, 2013.
[13] A. Kusiak, Smart manufacturing, *Int. J. Prod. Res.* **56** (2018) 508–517.
[14] J. Gao, L. Wang, X. Li, Cloud-enabled smart manufacturing, *J. Manuf. Syst.* **47** (2018) 64–75.
[15] ISO 15189:2022, *Medical laboratories – Requirements for quality and competence*, ISO, 2022.

Measurements System for the Characterization of Wetsuits Thermal Resistance

Cesare Svelto[1], Christian Laurano[2], Roberto Cantù[2], Gianluca Crotti[2]

[1] *Politecnico di Milano Dipartimento di Elettronica, Informazione e Bioingegneria (DEIB), Piazza Leonardo da Vinci 32 – 20133 Milano (IT), e-mail cesare.svelto@polimi.it christian.laurano@polimi.it*
[2] *Politecnico di Milano Dipartimento di Ingegneria Civile e Ambientale (DICA), Piazza Leonardo da Vinci 32 – 20133 Milano (IT), e-mail roberto.cantu@polimi.it gianluca.crotti@polimi.it*

***Abstract* – A custom measurement system, highly improved compared to its previous version, was developed and used for the measurement of neoprene wetsuit thermal resistance. The system can test the wetsuit thermal resistivity in water, under conditions like diving practice, by injecting a known quantity of thermal power within a custom-made cylindrical phantom enclosed by the wetsuit. The heat transfer from inner (warm) to outer (cold) water is measured by precise and distributed temperature measurements, allowing digital recording of all data and calculation of the thermal resistance of the wetsuit sample under test. A LabVIEW™ program was developed and used for the acquisition of the temperatures from 12 calibrated Pt-100 sensors and for the graphical and numerical data analysis during the experiments. The new measurement system is compliant with international regulations for assessing the thermal properties of wetsuit materials. Design of the system, experimental validation, wetsuits testing, and thermal resistance measurements are reported and discussed.**

Keywords: measurements system, thermal characterization, data acquisition system, wetsuit thermal resistivity, regulatory tests.

I. INTRODUCTION

Scuba diving wetsuits, whose invention dates to 1951 [1], are useful technical material [2] with a large worldwide market [3] and several applications to recreative and semi-professional human activities in seawater and freshwater environments. Wetsuits are typically made of neoprene [4, 5], a flexible and insulating material, providing both comfort and thermal insulation to the human body immersed in water. Various studies have investigated the insulation properties of neoprene wetsuits under different testing conditions [6-10].

In this work, we present the latest developments and improved performance of a custom measurement system designed and operated to test thermal resistance and thermal resistivity of scuba diving wetsuits [11]. In particular, the temperature measurement sensors have been significantly improved in terms of quality and number, allowing much better temperature gradient measurements across the wetsuit sample. A powerful water chiller is now used to keep stable the temperature of the water outside of the phantom and wetsuit under test. The custom LabVIEW™ program was expanded to acquire 12 different temperatures and to provide plots, averages, and general data analysis, also returning and saving the measured value of thermal resistance as a function of time. Experimental measurements are performed using 3 wetsuit samples of the same producer and thickness, as requested by the international wetsuit testing regulations [12]. The measurement system repeatability is being checked by repeating the test several times on the same wetsuit sample, after the same deep-drying conditions. Running long-term tests, it was observed that the wetsuit resistivity drops down with the wetting time even when working at standard atmospheric pressure (1 bar=1.013×10^5 Pa): this phenomenon is expected to significantly worsen when increasing the water pressure, i.e. the depth of the dive, posing some questions about the normative requirement of operating under stationary conditions, irrespective of the wetting time and wetsuit internal humidity conditions.

II. METHOD AND MEASUREMENT SYSTEM

The basic scheme and principle adopted for the assessment of thermal resistance of a wetsuit material, in accordance to [12], is theoretically quite simple and it is depicted in Fig. 1 A suitable anatomical phantom, in the shape of a cylinder e.g. also mimicking a human thigh, is inserted in a large water tank acting as a heat sink at controlled 'cold' temperature. The inner volume of the phantom is also filled with water which is continuously heated with thermal power P. When a steady-state condition is obtained, with T_{IN} the steady temperature within the phantom and T_{OUT} the steady temperature

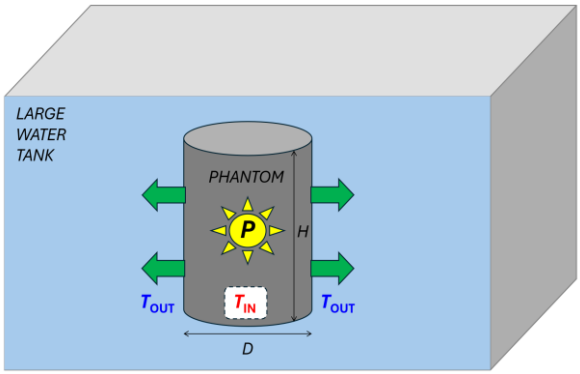


Fig. 1. Principle schematic with thermal power heat flow through the phantom cylindrical surface.

of the water in the tank, the thermal resistance of the phantom can be obtained by the equation of the steady-state heat flow $\dot{Q}$ through the phantom boundaries [13, 11], i.e.

$$R_T = \frac{\Delta T}{\dot{Q}} = \frac{\Delta T}{P} = \frac{T_{IN} - T_{OUT}}{P} \quad [K/W] \qquad (1)$$

where $\Delta T = T_{IN} - T_{OUT}$ is the temperature gradient between the inside and the outside of the phantom under steady-state thermal conditions.

Since the system operates with $T_{IN} > T_{OUT}$, the large green arrows in Fig. 1 indicate the heat flow from the inside to the outside of the phantom, through its cylindrical surface. As required by [12], the phantom's top and bottom circular surfaces must have equal diameters D=150 mm and provide high thermal insulation, while the cylindrical surface covered by the wetsuit must have height H=210 mm and allow the heat flow between the warm water inside the phantom and the cold water outside of it, i.e. toward the tank acting as the external heat sink. Under the assumption that the heat across the wetsuit is dominant with respect to the flow through the circular top and bottom surfaces of the phantom, Eq. (1) also provides a measurement of the thermal resistance of the wetsuit sample under test. With the given geometry [12], the area of the wetsuit enclosing the phantom is $A = \pi DH \cong 0.1$ m^2 and thus the thermal resistivity per unit area of the wetsuit material can be experimentally obtained by the simple practical formula

$$R_{T,A} = A\frac{\Delta T}{\dot{Q}} = AR_T = 0.1R_T \quad [m^2 \cdot K/W] \qquad (2)$$

Measurement results in terms of thermal resistivity values can be used to assess the wetsuit thermal performance class, in accordance with Table I of [12]. Accurate and high-resolution resistivity values can be used to compare wetsuits amongst each other much more finely than just by the corresponding classes. In particular, a high measurement resolution can assess if and how the wetsuit resistivity changes with time, use, and neoprene conditions (initial humidity, time of wetting, different pressure values, etc.).

The phantom empirical realization with the first experiments under medium- and long-term quasi-stationary thermal conditions are described in [11]. Here, we will discuss the main differences and improvements of the system regarding the temperature sensors quality and numerosity, the upgrade of the acquisition software, and the active temperature control of the water tank. This last achievement results in the capability of very-long-term measurements and analysis, with a water tank temperature substantially steady and independent of both the external room temperature and the input thermal power into the phantom.

III. EXPERIMENTAL APPARATUS

The old measurement system was implemented by two commercial NTC 10 kΩ temperature sensors (providing T_{IN} and T_{OUT} with no spatial averaging), connected to two 6½ digit Digital Multimeters (DMMs). The whole measurement chain was calibrated internally in our Laboratory by comparison to a precision digital thermometer, over 20 points in the temperature range 10-50 °C along the exponential resistance vs. temperature characteristic [11]. The temperature measurement system was cumbersome, inherently non-linear, and due to the availability of only two DMMs just one 'warm' temperature point inside the Phantom ($T_2 = T_{IN}$) was acquired together with just one 'cold' external temperature point ($T_1 = T_{OUT}$) from a second NTC sensor placed in the water tank in proximity to the wetsuit. For the new measurement system, we are using 12 independent platinum Resistance Temperature Detectors (RTDs), with 100 Ω nominal resistance at 25 °C (Pt-100), that were individually calibrated in an external calibration center. The reading of the 12 temperatures is accomplished by a precision industrial acquisition system, producing data rates typically at 1 Sa/s, in our experiments, and with 14-bit temperature resolution per each reading. The temperature measurements are acquired and processed by a dedicated LabVIEW™ program (Virtual Instrument, VI), also providing continuous data saving on the laboratory PC appending the data to an open TXT file, where all the measurement points and times can be accessed remotely at any time, during the test run as well. As required by [12] and explained in our description of the designed phantom [11], the 10 sensors are equally spaced in vertical distances (~1.8 cm one from the other) within the phantom cylindrical body, at a few millimeters from the wetsuit inner surface: these are the sensors reading the inner temperatures, now labeled T_1-T_{10}. Other 2 sensors are placed outside of the phantom, opposite diametrically to the cylinder structure and at heights of approximately ±8 cm from the central position: these are the sensors reading the outer temperatures, now labeled T_{11} and T_{12}. An image of the VI acquisition panel, showing the 12 temperatures measured in a steady state condition, is shown in Fig. 2a. The graph shows the plot of temperatures vs. time over an adjustable time window. Note that the wetsuits testing regulations [12]

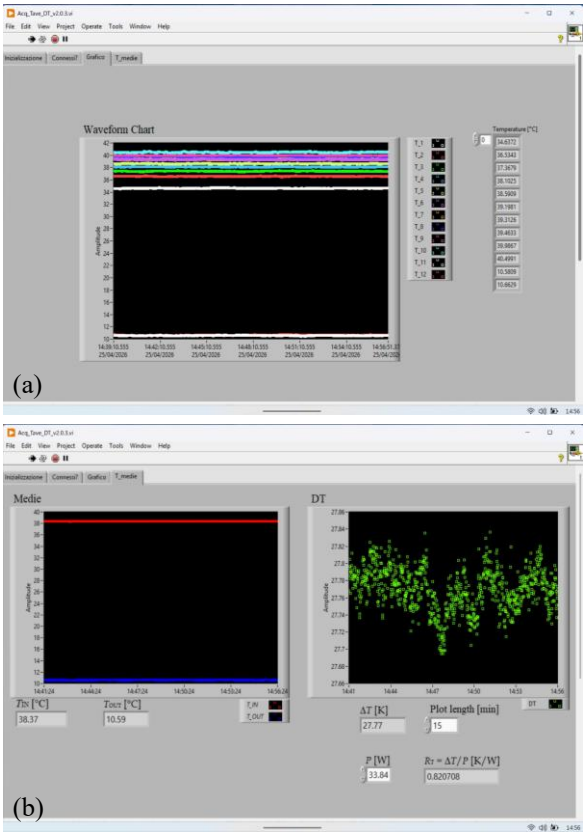


Fig. 2. (a) VI panel display showing the measured 12 temperatures, T_1-T_{12}. (b) VI panel display showing the average temperatures T_{IN} and T_{OUT} and the temperature gradient ΔT with the R_T value

require a stability interval of 15 min with a ΔT=T_{IN}-T_{OUT} stability of ±0.1 C. To monitor and record this situation, the average internal and external temperatures are evaluated, plotted, and recorded by the VI. The internal 'warm' temperature is T_{IN}=AVERAGE(T_1-T_{10}), corresponding to the red curve in Fig. 2b, while the external 'cold' temperature is T_{OUT}=AVERAGE(T_{11}, T_{12}) and corresponds to the blue curve in Fig. 2b. Also, the temperature gradient ΔT=T_{IN}-T_{OUT} is evaluated and plotted as the green curve in Fig. 2b. By inputting in the VI panel the value of the electrical and hence thermal power P [W] supplied to the phantom, the VI can also evaluate and display the measured thermal resistance, from (1) as R_T=ΔT/P.

A second major improvement to our test and measurement system is the use of a larger cylindrical iron tank to host the phantom during the tests (see Fig. 3). The new water tank has an internal volume of 460 L and is designed to be operated at absolute pressures ranging from 1 bar up to 6 bar. Within the tank, and placed around the phantom central vertical position, a copper pipe serpentine allows a coolant liquid to flow without direct contact to the water in the tank but providing efficient cooling of the external water volume also removing the heat that flows through the wetsuit from within the phantom toward the water tank. The external surface of the

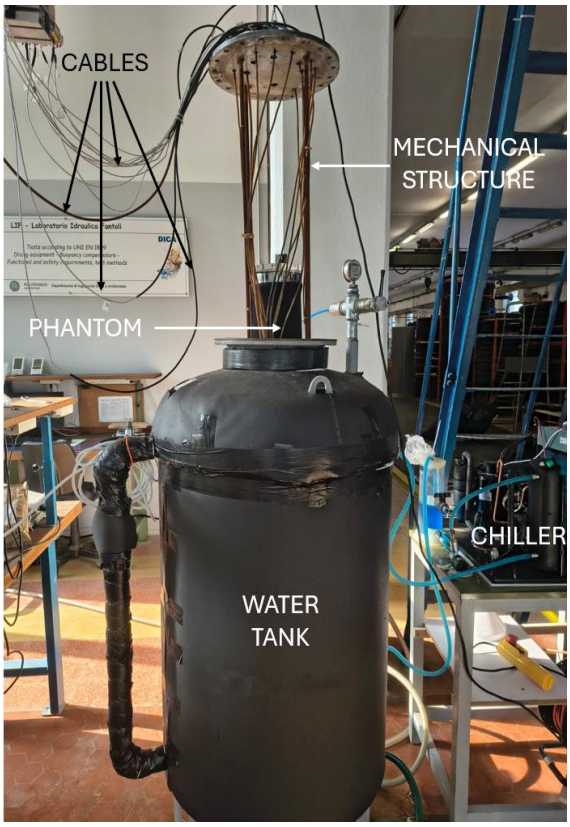


Fig. 3. Photo of the water tank covered by the insulating robber panel. On the top part and circular aperture of the tank is visible the mechanical structure used to immerse and extract the phantom in/from the water tank as well as the electrical cables used to drive the heater and read the temperature sensors. On the right side of the photo, the water chiller can be seen.

iron tank is covered by a 2 cm thick flexible insulating robber panel (black external layer covering the tank in Fig. 3), to thermally insulate the tank walls from the laboratory environmental temperature, which is not controlled. The coolant liquid is externally refrigerated by a commercial chiller with cooling power up to 1.8 kW. This cooling system allows very-long-term measurements with reduced sensitivity of the temperature of the water int tank, T_{OUT}, to the room temperature variations and, more significantly, also independently from the power level P that is input within the phantom. In the steady-state regime, all the power P flows from the phantom into the tank, from where the chiller is capable of continuously removing it, since the maximum power by which the phantom can be supplied the internal electric heater is 300 W. During the experiments, the temperature of the 'cold' water in the tank is typically maintained within a working range 10.5 °C≤T_{OUT}≤12.5 °C (since a cold-water external temperature within 10-15 °C is required [12]). When filling the tank and starting the tests, some 4 to 5 hours are needed from the switching on of the chiller to cool down the 460 L of tap water from its original

temperature down to the desired T_{OUT} working value. However, as is now proven in several tests, the chiller can be continuously left working day and night, also for weeks, producing stable T_{OUT} values in the water tank. The chiller is currently operated in cycles on-off, with a minimum off period Δt=10 min (the restart of the refrigerator machine compressor is prevented for 10 minutes after every switch-off), and it is automatically turning on when the coolant temperature increases over the set-point, T_{ON}, of the controller and automatically turning off when the temperature falls below switch-off threshold value, T_{OFF}. In our wetsuits testing, the chiller is typically operated with T_{ON}=11 °C and T_{OFF}=10 °C. It must be noted that for now the controller acts directly on the temperature of the coolant fluid and only indirectly on the temperature of the water in the tank.

IV. MEASUREMENT PROCEDURE AND RESULTS

Thermal tests on wetsuits samples are performed regularly in our laboratory and typically the steady-state measurement of R_T requires from ½ to 1 working day. The water in the tank can be prepared in advance, cooled and stable at the desired T_{OUT} value, by remotely turning on the chiller in the early morning (or by simply leaving it on for several days when tests are performed every day). The phantom, covered by the previously dry wetsuit, is inserted in the tank and the heater providing the required thermal power is switched on while starting the acquisition of all temperatures. One relatively long transient time, ranging from a few to several hours (depending on the wetsuit thermal resistance and hence on the thermal transient time constant, see [11]), must be waited until T_{IN} reaches exponentially its steady-state value starting from its original value. When the steady-state condition of ΔT is achieved, the corresponding thermal resistance is measured (1) and from it also the wetsuit resistivity value (2) and thermal class [12] are calculated.

Different neoprene wetsuit samples, having different thicknesses and coming from the same producer, for now, have been tested at 1 bar for assessing the thermal insulation of each wetsuit sample and its reproducibility between similar samples. For each of the 4 wetsuit thicknesses available (3.5 mm, 5 mm, 7.5 mm, and 9 mm), the thermal resistivity (2) obtained in the tests on 3 different neoprene wetsuits samples (M_1, M_2, M_3) of the same kind and nominally identical, is reported in Table I. As can be seen from Table I, the intra-sample (same wetsuit thickness) dispersion of thermal resistivity is within a few percent of the value, while the resistivity values increase significantly -as expected- with the wetsuit thickness. To establish an empirical model of resistivity vs. thickness, we wait for more data to be available and for the comparison also with other materials and thicknesses coming from some different producers. However, for the wetsuits tested in these experiments, the results of the average thermal resistivity as a function of wetsuit thickness, l, are reported in Figure 4 with a linear regression model of the data providing a slope $dR_{T,A}/dl$=13.5 (mK/W·m^2)/mm.

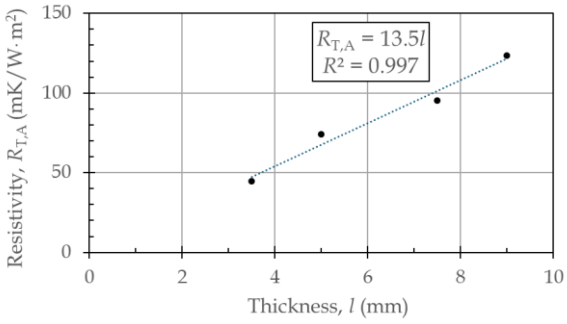


Fig. 4. Thermal resistivity as a function of the wetsuit thickness. The linear regression and the R^2 parameter are also shown.

Table 1. Thermal resistivity $R_{T,A}$ [m^2·K/W] of tested wetsuits samples. Average $\bar{R}_{T,A}$ values and relative sample standard deviation $s_{\%}(R_{T,A})$ for each thickness.

	3.5 mm	5 mm	7.5 mm	9 mm
M_1	0.0444	0.0745	0.1014	0.1213
M_2	0.0451	0.0738	0.0991	0.1249
M_3	0.0445	0.0747	0.0858	0.1250
$\bar{R}_{T,A}$	**0.0447**	**0.0743**	**0.0954**	**0.1237**
$s_{\%}(R_{T,A})$	**0.7%**	**0.5%**	**7%**	**1.4%**

V. REMARKS ON STATIONARY TESTS

During the experiments, we wanted to test how long-term stable the 'stationary' thermal gradient and wetsuit resistivity could remain, when the wetsuit sample was kept in water for a longer time than the typical duration of a test (see Fig. 5a). To this aim, we tested one 3.5 mm wetsuit, but also others, with a prolonged exposure of 1 day (or more) to the input thermal power and temperature gradient with respect to the stable external water temperature, kept at T_{OUT}≅11.5 °C . As shown in Fig. 5a, we recorded a slow but clear and continuous reduction of the thermal gradient ΔT in time, implying that R_T and $R_{T,A}$ are reducing as well. As can be seen from Fig. 5b, after reaching a peak ΔT value, the temperature gradient drifts down over the hours, even if the water tank temperature (T_{OUT}) is substantially stable: the internal water temperature (T_{IN}), keeps slowly reducing its value as in Fig. 5a (red curve). The observed temporal reduction of R_T shows how the wetsuit thermal insulation degrades with the wetting time, as depicted in the ΔT graph of Fig. 5b. The phenomenon is probably coming from a 'long-term' water infiltration in the neoprene material, but this effect happens in a way that can be measured and hence predicted and corrected over the few/several hours of the duration of a thermal resistivity test. Thus, a fully stationary ΔT condition cannot be

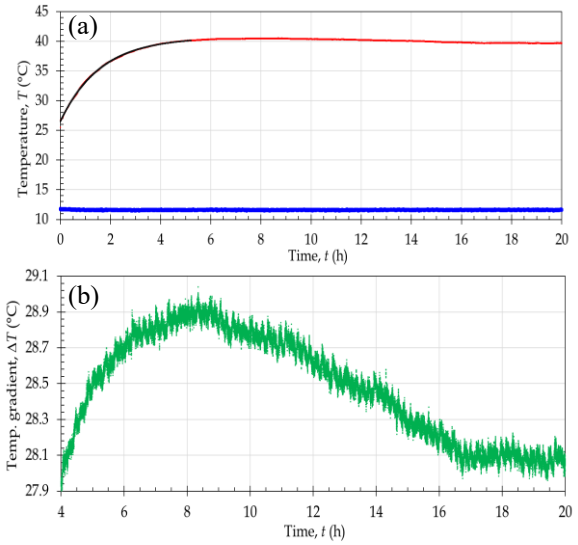


Fig. 5. Long-term measurement of the temperatures and effect of the wetting time on the thermal resistance. (a) T_{IN} (red trace) and its exponential fit (black trace) during the heating transient, T_{OUT} (blue trace). (b) Temperature gradient behavior (green trace) and thermal insulation degradation with time.

achieved in the wetsuit's characterization tests and, in addition, when the required ΔT stability [12] for the measurement is obtained, this condition typically happens after few/several hours of wetting time. In this case, the measured value of R_T is certainly lower, i.e. underestimated, with respect to the thermal insulation that the wetsuit can effectively offer to the scuba diver in the e.g. first hour of immersion. Moreover, although the testing times are expected to be reduced when exposing the wetsuit samples to higher water pressure, the effect of water infiltration within the neoprene material can happen much faster at higher pressures. This is expected to degrade the wetsuit performance, and the quality of its measurement. These phenomena will be further investigated, also at different water pressures, and a protocol to correct the thermal resistivity measurement as a function of the wetting time and pressure will be studied and proposed.

VI. CONCLUSIONS

An improved measurement system for the characterization of scuba diving wetsuits was developed and used to test neoprene wetsuits with different thickness. The measured thermal resistivity resulted in an intra-sample (same wetsuit thickness) dispersion of a few percent while it increases linearly with the wetsuit thickness. The stationarity of these thermal measurements comes to question since a worsening of the wetsuit resistivity with immersion time has been observed and the typical testing times can last from a few to several hours, depending on the neoprene sample thickness.

The system is now ready for studies of the dependency of the resistivity on the wetting time, for tests at higher water pressures, and for highlighting and compensating other (small?) non-idealities not yet considered.

REFERENCES

[1] C. Rainey, "Wet Suit Pursuit: Hugh Bradner's Development of the First Wet Suit," Archives of the Scripps Institution of Oceanography University of California, SIO Reference Number 98-16, 1998.

[2] A. VandeKerkhoff, L. Villanustre, C. Nam, "Rethinking Wetsuit Design: Enhancing Comfort, Fit, and Sustainability," Proc. of ITAA, 2025, #82, pp. 1–4.

[3] MARKET REPORT, "Diving Suits Market Size, Share, Trends and Forecast by Type, Price Range, Sales Channel, and Region, 2025-2033", 2025.

[4] J.K. Smith, "The Ten-Year Invention: Neoprene and Du Pont Research, 1930-1939", Technology and Culture, vol. 26, pp. 34-55, 1985.

[5] E.I. du Pont de Nemours & Company. Rubber Chemicals Division. "Neoprene A Remarkable Engineering Material." Wilmington, Delaware, 1943.

[6] V.M. Potocic Matkovic, I. Salopek Cubric, A. Pavko Cuden, "Dependence of Thermal Comfort of Diving Suit on Neoprene Properties and Diving Depth," in Polymers, vol. 17, pp. 1-13, 2025, Art no. 2820, doi: 10.3390/polym17212820.

[7] K.R. Kelly, L.J. Palombo, A.E. Jensen, J.R. Bernards, " Efficacy of Closed Cell Wet-Suit at Various Depths and Gas Mixtures for Thermoprotection during Military Training Dives," in Frontiers in Physiology, vol. 14, pp. 1-8, 2023, Art no. 1165196, doi: 10.3389/fphys.2023.1165196.

[8] H. Kim, Y. Bang, S. Lee, "Evaluation of Thermal Insulation and Characterization of Materials for Commercial Wetsuits for Surfers," in Textile Science and Engineering, vol. 53, pp. 229-240, 2016, doi: 10.12772/TSE.2016.53.229.

[9] M. Naebe, N. Robins, X. Wang, P. Collins, "Assessment of performance properties of wetsuits," in Proceedings of the Institution of Mechanical Engineers Part P: Journal of Sports Engineering and Technology, vol. 227, pp. 255-264, 2013, doi: 10.1177/1754337113481967.

[10] E. Bardy and J.C. Mollendorf, "Predicting the Thermal Conductivity of Foam Neoprene at Elevated Ambient Pressure," in Journal of Thermal Science and Engineering Applications, vol. 2, pp. 1-5, 2010, Art no. 014501, doi: 10.1115/1.4001937.

[11] G. Crotti, R. Cantù, S. Malavasi, G. Gatti, C. Laurano, C. Svelto, "Wetsuit Thermal Resistivity Measurements," in Sensors, vol. 24, pp. 1-19, 2024, Art no. 4561, doi: 10.3390/s24144561.

[12] CEN EN 14225-1:2017: "Diving suits – Part 1: Wetsuits – Requirements and test methods".
T.L. Bergman, A.S. Lavine, F.P. Incropera, D.P. DeWitt, "Fundamentals of Heat and Mass Transfer", 7th edition, John Wiley & Sons, Hoboken, NJ, USA, 2011.

2026 IMEKO Joint Conference
TC8 - TC11 - TC24
Meto Manila, Philippines, 26-29 August 2026

Advancing Metrology for Extreme Electrical Currents: Traceability, Uncertainty Analysis, and Conformity Assessment

Marija Cundeva-Blajer, Ilija Stojkovski, Kiril Demerdziev

Ss. Cyril and Methodius University in Skopje, Faculty of Electrical Engineering and Information Technologies, st. "Rugjer Boshkovikj"No.18, Skopje, Republic of North Macedonia
mcundeva@feit.ukim.edu.mk, ilijastojkovski996@gmail.com, kdemerdziev@feit.ukim.edu.mk

***Abstract* – The metrology infrastructure tends to enable measurement capabilities for extreme (very high or low) physical quantities not covered by existing laboratories, or to increase accuracy by decreasing uncertainty with improvement of already existing procedures. The calibration of instruments for extreme electrical currents is metrologically very challenging, due to factors like complex procedures to be validated, unestablished traceability chain to the SI units, and high number of uncertainty influential factors. After deep analysis of the CMCs in the area of very low electrical current at international level, the developed calibration procedure by the Laboratory for Electrical Measurements (LEM) is presented. The calibration results uncertainty are analysed with the GUM and the Monte Carlo approach, by using an original LEM made software MonteCalc Uncertainty Toolkit. Results are compared and discussed; conformity compliance assessment of calibration artefacts is conducted against Toolkit's embedded decision making rules.**

I. INTRODUCTION

For several decades, metrology has primarily functioned as a retrospective downstream process, focused on verifying product conformance and facilitating regulatory or contractual compliance. These verification protocols remain fundamental, but current paradigms in high-precision and regulated industries impose a shift in the applied metrology. In the contemporary industries, measurement data is changing role from a passive validation tool to an active strategic asset. Modern metrology trends emphasize the integration of real-time data acquisition to inform complex decision-making, mitigate operational risk, and optimize manufacturing performance through immediate feedback loops. In this context is the metrology infrastructure evolution, mostly in two relevant streams: 1) enabling measurement capabilities for extreme (very high or very low) physical quantities not covered by the existing laboratory facilities, or 2) increasing the accuracy through decreasing measurement uncertainty by innovation, improvement or modification of already existing protocols, [1]. One essential field for the contemporary industrial metrology is the measurements of low electrical currents, [2]. They are mainly applied in advanced electronics, material science, and nanotechnology, especially in testing semiconductors, photovoltaic devices, medical sensors, and insulation materials, where currents can be as small as picoamperes or even femtoamperes. Such tests are critical in devices' performance characterization, detecting leakage currents, and ensuring reliability in ultra-sensitive systems. The calibration of low electrical current instruments is a very challenging task, due to factors like complex measurement procedures needed to be validated, unestablished international measurement traceability chain for very low current values to the SI units, and high number of influential factors in the uncertainty budget. Therefore, various efforts for improvement of the calibration in field of low currents are made, [3]-[5].

In this paper, after conducting a thorough analysis of the current calibration and measurement capabilities (CMCs) in the area of low electrical current at international level, the developed calibration procedure for low electrical currents instruments by the Laboratory for Electrical Measurements (LEM) at the Ss. Cyril and Methodius University (UKIM) will be presented. The uncertainty of the calibration results will be analyzed by using the GUM approach and the advanced Monte Carlo methodology. For that purposes an original software MonteCalc Uncertainty Toolkit, [6], [7], developed in LabVIEW^{TM}, [8], by LEM will be applied. The results derived by the two methods will be compared and discussed by using experimental data. Based on the uncertainty propagation distribution gained by the two approaches, assessment of the conformity compliance of calibration artefacts will be conducted against prescribed decision making rules embedded in the MonteCalc Uncertainty Toolkit.

II. ANALYSIS OF CURRENT STATE IN THE FIELD OF LOW ELECTRICAL CURRENT METROLOGY

The establishment of an unbroken chain of international measurement traceability in the area of low currents is

rather challenging, [9], [1]. For appropriate needs assessment for expanding the metrology infrastructure, an analysis of the current-state-of-the-art is conducted. This is based on the published best CMCs of the some of the most relevant National Metrology Institutes (NMIs) in the Key Comparison Database (KCDB) of the International Bureau of Measures and Weights (BIPM), in the field of low currents, [10]. As a measurement point of interest the value of 10 nA DC current is selected. The best CMCs of 10 nA DC electrical current calibration at international level are displayed in Figure 1. The LEM at UKIM, provides calibration services mostly for the industry in South Eastern Europe. Therefore, a comparative analysis of the best CMCs of the NMIs established in the region of South Eastern Europe is conducted, shown in Figure 2.

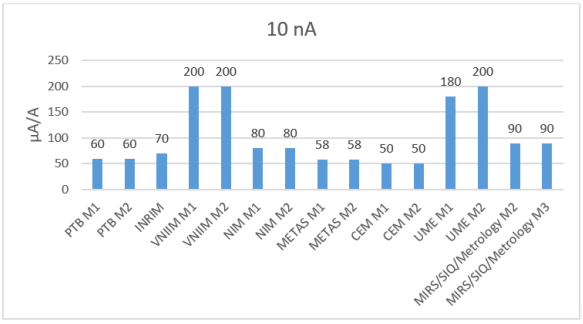


Figure 1. Expanded measurement uncertainties of DC electrical current of 10 nA at international level

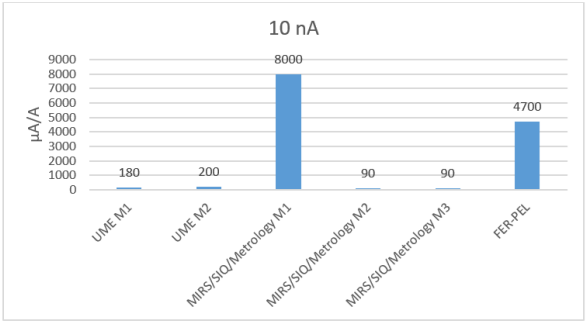


Figure 2. Expanded measurement uncertainties of DC electrical current of 10 nA in South Eastern Europe

III. CALIBRATION PROCEDURE OF INSTRUMENTS FOR LOW ELECTRICAL CURRENT DEVELOPED IN LEM

LEM has been an accredited calibration laboratory for electrical quantities instruments according to ISO 17025 since 2015, [11] and [12]. Recently, LEM has expanded its accredited scope for calibration of low current instruments down to 1 pA, DC current. A reference standard Transmille 4015 multifunction calibrator, with an adapter EA008 for calibration of instruments for low currents, has been acquired in LEM, with technical specification provided in [13], and established measurement traceability by the producer's accredited calibration laboratory with established traceability to national (NPL) and international primary reference standards (BIPM).



a) Calibration test set-up for low currents instruments



b) LEM reference standard-multifuntional calibrator with connected low currents adapter



c) Connections of the low currents adapter



d) Calibration of UUT- 8 ½ digit multimeter at low DC currents measurement range

Figure 5. LEM experimental configuration for calibration of instruments for low currents measurements

Based on the argumented needs, the LEM has developed a calibration procedure for low DC current instruments. The LEM's calibration configuration for this purpose is given in Figure 5 a). The calibrator [13] with the measuring adapter EA008, uses high DC voltage test signals, i.e. a measuring principle similar to the one usually

implemented in insulation testers, is shown in Fig. 5, b). The connections of the high resistance adapter EA008 are given in Figure 5 c). For validation of the established procedure, the unit under test (UUT) is an 8 ½ digit multimeter Agilent 3458A presented in Figure 5 d), with technical specification in [14].

IV. DIFFERENT APPROACHES IN CALIBRATION UNCERTAINTY ESTIMATION

Two procedures for uncertainty estimation are developed in LEM: 1) traditional evaluation as in Guide to the expression of uncertainty in measurement (GUM), [15] and 2) estimation by propagation of distributions by the Monte Carlo method, as in GUM Supplement 1, [16]. The calibration of low current instruments tends to extreme metrology, so proper approach selection for uncertainty estimation is a complex task, [17].

A. Uncertainty estimation by GUM methodology

The initial uncertainty analysis begins with the generally most adopted approach, the GUM protocol. To obtain the calibration results' uncertainty budget, data from a component of type A, as in the GUM, and components of type B are fused, following the GUM, and by using the original LEM data fusion concept, [18]. The type A uncertainty, u_A, is obtained by statistical processing of the experimental data, by the mean value, X_{mean}, and the measurements standard deviation, as:

$$u_A = \sqrt{\frac{1}{n-1}\sum_{i=1}^{n}(X_{icor} - X_{mean})^2} \quad (1)$$

where,
$$X_{mean} = \frac{1}{n}\sum_{i}^{n} X_{icor} \quad (2)$$

$$X_{icor} = X_i - X_{ref} \quad (3)$$

X_i is the measured value in the specific point, and X_{ref} is the value generated by the reference standard. The combined uncertainty of type B stands for:

$$u_B = \sqrt{u_{res_inst}^2 + u_{res_refst}^2 + u_{d_refst}^2 + u_{cal_refst}^2} \quad (4)$$

where the particular uncertainty input components are:
u_{res_instr} - from the resolution of the calibrated instrument,
u_{res_refst} - from the resolution of the reference standard,
u_{d_refst} – from the accuracy and the drift of the reference standard, and
u_{cal_refst} - from the calibration of the reference standard.

The total combined uncertainty is:

$$u_c = \sqrt{u_A^2 + u_B^2} \quad (5)$$

The expanded uncertainty, used in conformity statement decision process is:

$$U = 2 \cdot u_c \quad (6)$$

B. Uncertainty estimation by Monte Carlo approach

The GUM, enables harmonization in a broad scope of practical problems, and its traditional methodology is grounded in the Law of Propagation of Uncertainty (LPU). However, GUM's assumption on linearization and the approximations of the Student's t-distribution can be with restricted applicability. So, JCGM 101:2008, [16] proposes the Monte Carlo approach, propagating entire probability distributions, and not just some parameters. Various published studies highlight the effectiveness of Monte Carlo simulations in assessing measurement uncertainty, [19]. The Monte Carlo based on random selections, compensates the GUM constraints, in case of nonlinearities, or when a normal distribution is attributed to the probability density of the output quantity. However, if there are significant deviations from the normal distribution, which happens in certain cases of calibration of low current instruments, GUM will not provide an adequate representation. The Welch-Satterwhite method, [19] allows calculation of the effective degrees of freedom, defining the output distribution with a t-distribution; however, in real case scenarios evidently greater errors can be generated. Therefore, when one of the uncertainty contributions is significantly larger than the others, or when the order of magnitude of the output quantity is the same or close order to the uncertainty, the only reliable option is the Monte Carlo approach. The GUM Supplement 1 [16], suggests an algorithm on how to perform a Monte Carlo simulation. When executing the simulation, a certain number of trials need to be conducted. The number of trials is determined as:

$$M > \frac{10^4}{1-p} \quad (7)$$

where, M is the calculated number of trials, and p is the required probability. For coverage factor k=2, at probability of 95%, i.e. p=0.95, the minimal number of trials is 200000. With sufficient processing capacity, most applications perform 10^6 simulations.

The originally developed software package in LEM for Monte Carlo simulation entitled MonteCalc Uncertainty Toolkit, features functionalities described in [6]. The Toolkit is universal and can be applied to any case of testing/calibration uncertainty estimation, with no restrictions on the type of instrument, the physical quantity measured, the range, the type probability distribution etc. The Monte Carlo simulation is performed using a virtual instrument palette enabling generation of random numbers with an appropriate distribution. The distribution generation depends on the Type B parameters that are entered. For each Type B component, a distribution of random numbers is generated and summed together with the Type A component. From the resultant distribution, the uncertainty both by GUM and the Monte Carlo approach is calculated. The Toolkit has an incorporated complex evaluation module for conformity assessment against different prescribed decision-making rules in line with the Guideline ILAC G8:09/2019, [20]. The Toolkit's built-in decision rules are the binary rule, the binary rule with guard band, the non-binary rule with guard band and with measurement uncertainty, and other.

V. RESULTS AND DISCUSSION

The results presented in this contribution are only for a selected specific calibration point from the overall conducted calibration protocol, derived by the MonteCalc Uncertainty Toolkit. In Table 1 are the measurement uncertainties derived by the Toolkit, applying both GUM and Monte Carlo calculations, at the point of 10 nA DC electrical current, respectively.

Table 1. Comparison of extended calibration uncertainty derived by GUM and Monte Carlo at 10 nA, DC

DC current point		Expanded uncertainty	
Applied reference value	Measured value by low current instrument	Approach No. 1 GUM	Approach No. 2 Monte Carlo
(nA)	(nA)	(nA)	(nA)
10,0218	9,9978	0,0535	0,0520

In Figure 6 is the probability distribution gained at the calibration point of 10 nA in DC range, obtained by the MonteCalc Uncertainty Toolkit. In Figure 6, the x-axis presents the range of values that may be attributed to the measured quantity, therefore it is labeled as "Interval" in nA, while the y-axis corresponds to the number of repetitive results, regarding the performed Monte Carlo trials, and hence it is titled "Frequency".

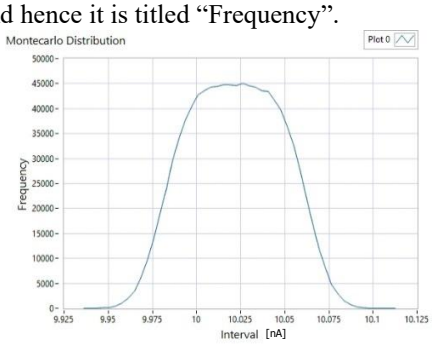


Fig. 6 Probability distribution from MonteCalc Uncertainty Toolkit at point of 10 nA in DC range

The derived calibration results with the accompanying uncertainty are subjected to conformity assessment by the built-in option of the MonteCalc Uncertainty Toolkit, against different decision making rules, as in [20].

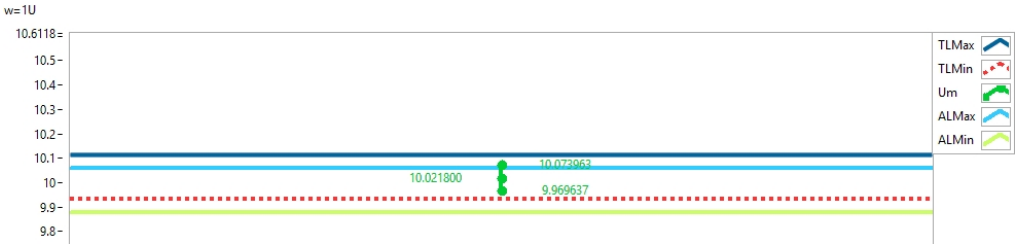


Fig. 7 Result at a calibration point of 10 nA at DC range with guard band w=U decision rule

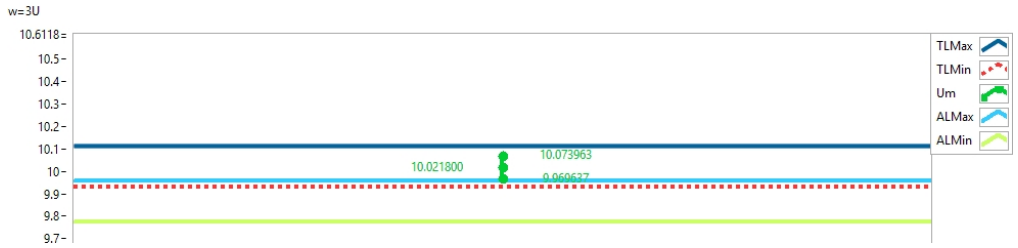


Fig. 8 Result at a calibration point of 10 nA at DC range with guard band w=3U Six-Sigma decision rule

The compliance graphs obtained by the Monte Carlo simulation method depending on the limit value set with an appropriate control for the particular decision making rule, i.e. guard band of one expanded uncertainty *w=U*, and of three expanded uncertainties *w=3U*, (the Six-Sigma rule), at the calibration point of 10 nA, DC are displayed in Figures 7 and 8, respectively. The values along the vertical axis in Figures 7 and 8, are the measured value of the current in nanoampere. The two methods yielded different uncertainty values. This is expected as the GUM assumes a normal distribution, an assumption that is not fully true in case of calibration at low currents values, and particularly in cases when the order of magnitude of the output quantity is the same or close to order of the uncertainty, as it is in this particular case study. In contrast, the Monte Carlo simulation accounts for the actual distribution by randomly generating variable values, providing more reliable conformity assessment decision.

In Table 2, the acceptance criteria are expressed, according to each decision making rule at the same calibration point. The following symbols are applied ✓ (accepted), ☑ (conditionally accepted), ☒ (conditionally rejected), and ✗ (rejected). From the outcomes presented in Table 2 it can be concluded that the conformity of the measurement results depends on the decision rule applied. As the calculated uncertainty is directly incorporated in the rule, its accurate estimation is of essential significance. So, the applied approach (GUM or Monte Carlo) directly impacts the final outcome of the decision making process.

Table 2 Declarations of UUT conformity at a calibration point of 10 nA DC according to different decision rules

Decision rule *w*	0,83*U*	*U*	1,5*U*	3*U*
Binary	✓	✓	✓	✓
Binary with guard band	✓	✓	✓	×
Non-binary with guard band	✓	✓	✓	☑
Non-binary with guard band & measurement uncertainty	✓	✓	✓	☒

VI. CONCLUSIONS

After a thorough international analysis of the up-to-date CMCs in area of low electrical currents and the needs confirmation for development of low current calibration infrastructure in South Eastern Europe, a traceable calibration procedure for low electrical currents instruments in LEM at UKIM is designed and accredited. The calibration results' uncertainty are analyzed by both GUM and Monte Carlo approach, with an original software MonteCalc Uncertainty Toolkit, made by LEM. The results derived by the two methods are compared and discussed by using experimental calibration data of a low current instrument-8 ½ digit multimeter. Based on the uncertainty propagation distribution from the two approaches, conformity assessment of the calibration artefact is conducted against prescribed decision rules. The results justify the developed approaches appropriateness.

ACKNOWLEDGEMENT

This work is supported by Ministry of Education and Science of North Macedonia, Grant No. 15-6171/25, from 7.08.2025.

REFERENCES

[1] M. Cundeva-Blajer, Gj. Dimitrovski, V. Sapundziev, K. Demerdziev, V. Dimcev, "Infrastructure Development for Extreme Electrical Metrology", Jour. of Electrical Engineering and Information Technologies 2022, Vol. 7, No. 2, pp. 101-109 UDC: 006.91:621.3.03-021.423, https://jeeit.feit.ukim.edu.mk/index.php/jeeit/article/view/348 (last access 30.04.2026).

[2] "Low Level Measurements Handbook- Precision DC Current, Voltage, and Resistance Measurements", Keithley Tektronics Company https://www.tek.com/en/documents/product-article/keithley-low-level-measurements-handbook---7th-edition (accessed on 1.05.2026)

[3] C. Krause and D. Drung, "High-Accuracy Current Amplifier for Small Electric Currents," 2024 Conf. on Precision Electromagnetic Measurements (CPEM), Denver, CO, USA, 2024, pp. 1-2, doi: 10.1109/CPEM61406.2024.10646011

[4] N.-H. Kaneko, T. Tanaka, Y. Okazaki "Perspectives of the generation and measurement of small electric currents", 2024 *Meas. Sci. Technol.* 35 011001 DOI 10.1088/1361-6501/ad03a2.

[5] I. Finardi and L. Callegaro, "Calibration system for low-current transresistance amplifiers with a low-frequency sinewave source," XXXII General Assembly and Scientific Symposium of the International Union of Radio Science (URSI GASS), Montreal, QC, Canada, 2017, pp. 1-2, doi: 10.23919/URSIGASS.2017.8105167

[6] M. Cundeva-Blajer, M. Nakova, K. Demerdziev, "Conformity Assessment of Impedance Parameters Meters by MonteCalc Uncertainty Toolkit", Proc. of TC8 – TC11 – TC24 IMEKO Joint Conf., 14-17 Sept. 2025, Turin, Italy.

[7] M. Cundeva-Blajer, G. Dimitrovski, M. Nakova, K. Demerdziev, "Calibration of High Frequency Instruments-Evaluation of Uncertainty by Monte Carlo Approach", Proc. of TC8 – TC11 – TC24 IMEKO Joint Conf., 14-17 Sept. 2025,Turin, Italy.

[8] "LabVIEW Programming Reference Manual", National Instruments Corporation, 2024

[9] M. Cundeva-Blajer, B. Iliev "Review and Contribution to the Best Measurement and Calibration Capabilities in the Field of Electrical Energy and Power", Int. Conf. on Information, Communication and Energy Systems and Technologies ICEST 2016, 2016, Ohrid, R. Macedonia.

[10] BIPM KCDB Key Comparison Database https://www.bipm.org/kcdb/ (last access 30.04.2026).

[11] Demerdziev K., Cundeva-Blajer M., Dimcev V., Srbinovska M., Kokolanski Z. "Improvement of the FEIT Laboratory of Electrical Measurements Best CMC Through Internationally Traceable Calibrations and Inter-Laboratory Comparisons", Int. Conf. ETAI 2018, Struga, R. Macedonia, 20-22 Sept. 2018 (ETAI 6-4)

[12] K. Demerdziev, M. Cundeva-Blajer, V. Dimchev, M. Srbinovska, Z. Kokolanski, "Defining an uncertainty budget in electrical power and energy reference standards calibration", 18th Int. Conf. on Smart Technologies IEEE EUROCON, 1-4 July 2019, Novi Sad, Serbia, pp. 1-6.

[13] "Transmille 4015 Multiproduct Calibrator Extended Specifications", Transmille, UK 2022, https://transmillecalibration.com/wp-content/uploads/2018/05/EA008-Extended-Specifications.pdf (retrieved on: 1.05.2026)

[14] Keysight "Multimeter 3458A Data Sheet", https://www.keysight.com/us/en/assets/7018-06796/data-sheets/5965-4971.pdf (accessed on 1.05.2026)

[15] JCGM 100 (BIPM and other member organizations), Evaluation of measurement data – Guide to the expression of uncertainty in measurement (GUM), 2008.

[16] JCGM 101 (BIPM and other member organizations), Supplement 1 to the Guide to the expression of uncertainty in measurement - Propagation of distributions using a Monte Carlo method, 2008.

[17] K. Demerdziev, M. Cundeva-Blajer, "Trans-conductance amplifier calibration protocol establishment – metrology ambiguities, constraints, and measurement uncertainty propagation analysis", ACTA IMEKO Sep. 2023, V. 12, No. 3, pp. 1-10, https://doi.org/10.21014/actaimeko.v12i3.1462

[18] M. Cundeva-Blajer "Data Fusion for Uncertainty Evaluation in Extreme Electrical Metrology", Proc. of Int. Cong. on Measurement, Quality and Data Science MQDS 2023, 5-7.06.2023, Bordeaux, France

[19] P. R. Guimaraes Couto, J. Carreteiro, and S. P. de Oliveir, 'Monte Carlo Simulations Applied to Uncertainty in Measurement', Theory and Applications of Monte Carlo Simulations. InTech, Mar. 06, 2013. doi: 10.5772/53014.

[20] ILAC-G8:09/2019 "Decision Rules and Statements of Conformity"

2026 IMEKO Joint Conference
TC8 - TC11 - TC24
Metro Manila, Philippines, August 26-29, 2026

Simultaneous Determination of Common Food Preservatives in Selected Sauce Products in the Philippine Market by HPLC-PDA Method

Cyril C. Ramil[1], Grace V. Amandy[1], Cherrylean B. Bembenuto[1], Ma. Rachel V. Parcon[1]
[1]*Standards and Testing Division, Industrial Technology Development Institute, Department of Science and Technology, Bicutan, Taguig City, 1631, Philippines*

Abstract

Food safety is a fundamental component of public health protection and international trade, requiring strict compliance with regulations on food additives. Benzoic acid, sorbic acid, and parabens are commonly used preservatives in sauces to prevent spoilage, though excessive levels may pose health risks. This study applied a validated HPLC-PDA method to simultaneously quantify benzoic acid, sorbic acid, methylparaben, and propylparaben in fifteen (15) selected sauce products from Metro Manila, Philippines. The method demonstrated detection limits of 0.01–0.17 mg/kg and quantification limits of 0.04–0.58 mg/kg, and showed metrological traceability to SI units using a certified reference material. Sodium benzoate was the most frequently detected preservative. Most samples met regulatory and labeling standards, although four contained undeclared benzoic acid within the maximum allowable limits. These demonstrate the method's fitness for routine testing and underscore the critical need for continuous market surveillance to ensure proper labeling and protect consumer health.

I. INTRODUCTION

The global food industry relies heavily on chemical preservatives to ensure the microbial stability and shelf life of processed foods. In the Philippines, condiments and sauces ranging from traditional soy sauce to unique local staples like banana ketchup are integral to the daily diet. To prevent spoilage caused by yeasts, molds, and bacteria, manufacturers commonly use preservatives such as benzoic acid, sorbic acid, and parabens (alkyl esters of p-hydroxybenzoic acid). While these additives are effective antimicrobial agents, their excessive consumption is linked to adverse health effects, including metabolic disruption, allergic reactions, and potential endocrine interference [1-3].

The regulatory landscape for food additives is governed by strict Maximum Allowable Limits (MAL) to protect consumer health. Internationally, the Codex Alimentarius Commission and the European Food Safety Authority (EFSA) provide guidelines for acceptable daily intakes (ADI) [4]. Locally, the Philippine Food and Drug Administration (FDA) enforces standards that align with these global benchmarks [5]. However, the complexity of food matrices, specifically the high sugar content in ketchups and high salinity in soy sauces, poses significant challenges for accurate quantification. Discrepancies between declared ingredients and actual chemical composition can arise, necessitating robust market surveillance.

From a metrological perspective, the reliability of analytical results depends on measurement traceability and method validation. Ensuring traceability to the International System of Units (SI) through the use of certified reference materials enhances the comparability and reliability of data, particularly for regulatory and enforcement purposes. The use of Certified Reference Materials (CRMs) is critical in this process, providing the necessary link to establish the accuracy and realize the "unbroken chain of comparisons" required in high-level metrology [6-7].

High-Performance Liquid Chromatography coupled with a Photodiode Array detector (HPLC-PDA) is widely recognized as a robust and reliable technique for the simultaneous determination of these compounds. Compared to Gas Chromatography, which often requires labor-intensive derivatization for polar compounds like parabens, HPLC-PDA enables direct, sensitive, and efficient analysis of multiple preservatives with varying polarities in a single run [8-9].

This study employed a validated HPLC-PDA method for the simultaneous quantification of benzoic acid, sorbic acid, methylparaben, and propylparaben in selected sauce products from Metro Manila, Philippines. The method demonstrates suitable detection and quantification limits and establishes metrological traceability to SI units using a certified reference material. Furthermore, this study evaluates the compliance of commercially available products with regulatory standards and labeling requirements, providing insight into the occurrence of declared and undeclared preservatives. The findings highlight the method’s suitability for routine analysis and underscore the importance of ongoing market surveillance

to ensure food safety and consumer protection.

II. MATERIALS AND METHODS

A. Chemicals and Materials

Analytical standards of benzoic acid, sorbic acid, methylparaben, and propylparaben (purity 99.0–99.9%) were obtained from the Health Sciences Authority (Singapore) and Sigma-Aldrich (USA). Additional related standards (≥99.0%) and sodium acetate anhydrous were also sourced from Sigma-Aldrich. A certified reference material (CRM HRM-1012A: Preservatives in soy sauce) was used to establish metrological traceability. Analytical-grade solvents, including glacial acetic acid (≥99.8%), ethanol (≥95%), methanol, acetonitrile, and 2-propanol, were obtained from RCI Labscan (Thailand) and J.T. Baker (USA).

B. Standard Solutions Preparation

Individual standard stock solutions (500 mg/L) were prepared by dissolving 25.0 mg of benzoic acid (BA), sorbic acid (SA), methylparaben (MP), and propylparaben (PP) in 50 mL of 70% ethanol using 50 mL volumetric flasks. The solution was freshly prepared for every analysis. An intermediate standard solution (20 mg/L) containing the four analytes was prepared by appropriately diluting an appropriate amount of the stock solution with 70% ethanol. At least 6 working standards were prepared for the calibration curve with 70% ethanol. All solutions were filtered through a 0.2 µm nylon syringe filter before HPLC injection.

C. Chromatographic analysis

Chromatographic separation was performed using a Shimadzu Prominence HPLC system equipped with an autosampler, quaternary pump, column oven, and photodiode array (PDA) detector. Separation was achieved using a Waters Sunfire C18 analytical column (150 mm × 4.6 mm, 3.5 µm). The mobile phase consisted of sodium acetate–acetic acid buffer (pH 4.8) as solvent A and acetonitrile as solvent B in an isocratic ratio of 65:35 (v/v). The column temperature was maintained at 35 °C, and the autosampler was set at 15 °C. The flow rate was 0.8 mL/min, and the injection volume was 10 µL. Detection was performed using a PDA detector at dual wavelengths: 254 nm for sorbic acid, methylparaben, and propylparaben, and 229 nm for benzoic acid (Table 1). Quantification was carried out using an external calibration method.

D. Sample collection and handling

Fifteen (15) commercial condiment samples were purchased from a local supermarket in Taguig, Philippines. The samples included tomato ketchup, banana ketchup, tomato sauce, chili sauce, pepper sauce, meat sauce, pizza sauce, spaghetti sauce, and sriracha ketchup. All samples were homogenized and stored at 4 °C prior to analysis.

Table 1. Chromatographic conditions.

Parameters	Optimized Conditions
Column	Waters Sunfire C18 analytical column (150 mm x 4.6 mm, 3.5 µm)
Mobile phase	65% Sodium acetate/acetic acid buffer (pH 4.8) and 35% ACN
Column temperature	35°C
Injection volume	10 µL
Flow rate	0.8 mL/min
PDA wavelength	254 nm (MP, PP, SA) 229 nm (BA)

E. Sample Analysis

Homogenized sauce sample (2.0 g) was weighed into a 25 mL volumetric flask, followed by the addition of 20 mL of 70% ethanol. The mixture was sonicated for 10 min and diluted to mark with 70% ethanol. The mixture was mixed thoroughly and transferred to 50 mL conical centrifuge tubes. Sample solutions were vortexed for 1 min and centrifuged at 3000 rpm for 10 min. Aliquot of the sample solution was transferred into a 25 mL volumetric flask without disturbing the precipitates at the bottom. The aliquot volume was adjusted to ensure that the final concentration fell within the working calibration range. The solution was then diluted to volume with 70% ethanol and mixed thoroughly. Prior to HPLC analysis, all sample solutions were filtered using a 0.2 µm nylon syringe filter.

F. Quality Control Procedures

Quality control procedures were implemented throughout the analytical process to ensure data reliability. Reagent blanks were included in each analytical batch to monitor contamination, while calibration verification standards were analyzed periodically to ensure instrument stability within ± 10% of expected response.

System suitability tests were performed prior to sample analysis to evaluate retention time stability, peak symmetry, and chromatographic resolution. For recovery studies, selected samples were spiked to assess matrix effects and accuracy, with acceptable recovery limits set at 80–120%. All samples were analyzed in triplicate (n=3), and quality control standards were injected intermittently to monitor instrumental drift throughout the analytical sequence.

III. RESULTS AND DISCUSSION

A. Overview of Method Performance (Validated HPLC-PDA Method)

The present study applied an in-house validated HPLC-PDA method for the simultaneous determination of benzoic acid (BA), sorbic acid (SA), methylparaben (MP), and propylparaben (PP) in commercial sauce products. The method validation confirmed that the analytical

procedure is suitable for routine food monitoring in complex matrices. As summarized in Table 2, the method exhibited excellent linearity ($r \geq 0.995$), satisfactory repeatability (HorRat ≤ 1.3) and intermediate precision (HorRat ≤ 2), and acceptable recoveries within the range of 90-110%. Sensitivity was adequate for trace-level detection, with LODs ranging from 0.01 to 0.17 mg/kg and LOQs from 0.04 to 0.58 mg/kg. These performance characteristics confirm the method's suitability for regulatory monitoring of preservatives in complex food matrices.

Table 2. Summary of Method Validation Data for Preservatives.

Performance Characteristics	BA	SA	MP	PP
Repeatability (HorRat ≤ 1.3)	0.10	0.09	0.05	0.07
Intermediate Precision (HorRat ≤ 2)	0.26	0.14	0.44	0.25
Trueness by Spiking (%Recovery)	95-99	95-102	95-104	96-103
LOD (mg/kg)	0.04	0.01	0.17	0.15
LOQ (mg/kg)	0.13	0.04	0.58	0.51

B. Quality Control Performance

Chromatographic Separation and System Suitability

Efficient chromatographic separation is essential for the simultaneous determination of benzoic acid (BA), sorbic acid (SA), methylparaben (MP), and propylparaben (PP). The optimized HPLC-PDA conditions achieved complete baseline resolution of all analytes under isocratic elution within a short run time. As shown in Figs. 1 and 2, well-resolved peaks were obtained with retention times of 2.98 min (BA), 3.59 min (SA), 5.47 min (PP), and 5.59 min (MP). Dual-wavelength PDA detection (229 nm for BA and 254 nm for SA, MP, and PP) enhanced selectivity and signal response while minimizing matrix interferences from complex sauce samples. The absence of co-eluting peaks and satisfactory peak symmetry confirmed adequate chromatographic selectivity for all target analytes.

System suitability testing was performed before each analytical batch to verify instrument performance and chromatographic stability. Evaluated parameters included retention time repeatability, peak symmetry (tailing factor), theoretical plate number (N), and resolution (Rs) between adjacent peaks. All system suitability criteria were fulfilled. Retention time and injection repeatability (%RSD ≤ 2%) indicated stable chromatographic performance, while tailing factors were within acceptable limits, confirming efficient column behavior and mass transfer. Theoretical plate numbers were above 2000, indicating higher column efficiency and better analyte separation. Resolution values exceeded 2 for all analyte pairs, ensuring baseline separation and reliable quantification. Overall, the system demonstrated robust chromatographic efficiency and suitability for routine quantitative analysis of preservatives in complex food matrices.

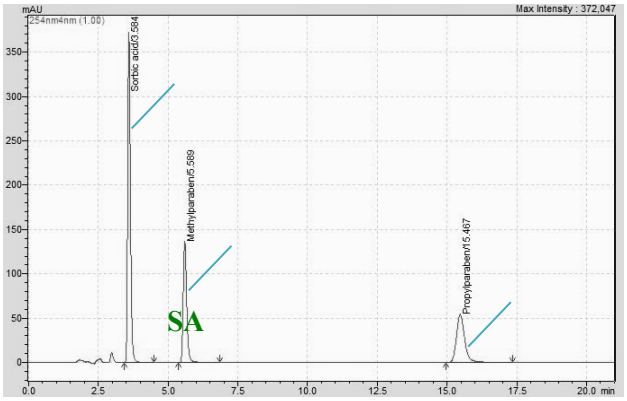


Fig. 1. Chromatogram of the standard mixture of four preservatives at 254 nm.

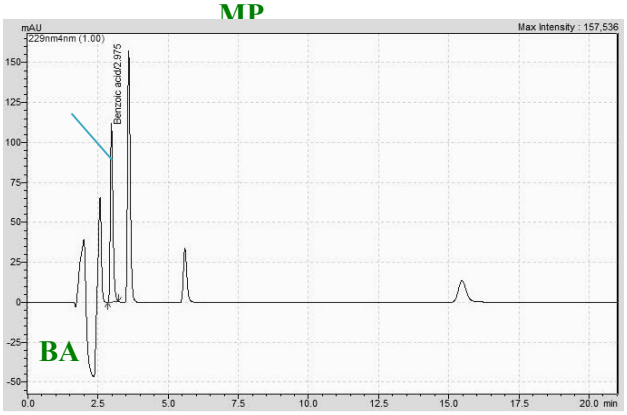


Fig. 2. Chromatogram of the standard mixture of four preservatives at 229 nm.

Calibration Verification and Instrument Stability

Calibration verification was performed throughout the analytical sequence to ensure the continued validity of the calibration model and stability of detector response. Verification standards analyzed at regular intervals remained within ± 10% of their nominal concentrations, demonstrating consistent instrument sensitivity and linear response over time [10,11]. No significant drift in peak area or retention time was observed, indicating stable pump performance, detector response, and column behavior. Such stability is essential for ensuring that external calibration remains valid across extended analytical runs, particularly in routine food analysis. These results confirm that the analytical system maintained consistent performance, supporting the reliability of quantitative results and their comparability with regulatory limits.

Accuracy and Matrix Effects (Recovery Studies)

Method accuracy was evaluated through recovery studies using spiked samples at multiple concentration levels. Recoveries were within the acceptable range of 80–

120%, meeting commonly accepted criteria for food analysis methods [11]. The satisfactory recoveries indicate that matrix effects from complex sauce compositions such as sugars, salts, and organic acids, did not significantly affect analyte extraction or detector response. Matrix effects are a well-recognized challenge in chromatographic analysis and can lead to signal suppression or enhancement if not properly controlled [12]. The recovery ranges obtained were 87–117% for benzoic acid, 87–106% for sorbic acid, 86–104% for methylparaben, and 81–105% for propylparaben (PP). These values fall strictly within the acceptable range of 80–120%, meeting established performance criteria for validating food analysis methods.

Blank Controls and Contamination Check

Reagent blanks were included in each analytical batch to monitor potential contamination and carry-over effects. No detectable peaks corresponding to the target analytes were observed in blank chromatograms, confirming the absence of background contamination from solvents, reagents, or sample preparation procedures. Additionally, no carryover was detected between injections, indicating effective system flushing and autosampler performance. This ensures that analyte signals in sample chromatograms originate solely from the samples themselves and are not influenced by residual analytes from previous injections.

The use of blank controls is essential for confirming method specificity and ensuring data integrity, particularly at concentrations near the detection limits. The absence of contamination further supports the reliability of trace-level measurements reported in this study.

C. Metrological Traceability

Metrological traceability was established using a certified reference material (CRM HRM-1012A: preservatives in soy sauce), ensuring that measurement results are directly linked to SI units. The average bias calculated for BA, MP, and PP were -58.05, -1.44, and 1.89, respectively. Bias values for all analytes were within their respective expanded uncertainties, confirming agreement between measured and certified values. This demonstrates that the analytical results are not only precise but also traceable and comparable to internationally recognized reference standards. Also, it ensures that the method generates reliable and internationally comparable results, in accordance with ISO/IEC 17025 principles and the International Vocabulary of Metrology (VIM) [13,14]. This is particularly important for food safety enforcement and supporting harmonized regulatory compliance across different jurisdictions.

D. Preservative Levels in Commercial Sauce Products

The in-house validated HPLC-PDA method was applied to fifteen (15) commercially available sauce products obtained from Metro Manila, Philippines, to evaluate preservative occurrence and regulatory compliance. The samples, analyzed in triplicate (n = 3), included tomato, banana, and sriracha ketchup, as well as various sauces (e.g., tomato, chili, spaghetti, pizza, meat, and cayenne pepper). The results are summarized in Table 3.

Table 3. Preservative content of various sauce products.

Sample Matrix	Code	BA, mg/kg	SA, mg/kg	MP, mg/kg	PP, mg/kg
Tomato ketchup	1	715	ND	ND	ND
Chili sauce	2	6	ND	ND	ND
Banana ketchup	3	998	ND	ND	ND
Banana ketchup	4	51	36	ND	ND
Sriracha ketchup	5	682	ND	ND	ND
Cayenne Pepper sauce	6	ND	ND	ND	ND
Tomato sauce	7	ND	ND	ND	ND
Tomato ketchup	8	0.8	ND	ND	ND
Chili sauce	9	645	ND	ND	ND
Spaghetti sauce	10	852	ND	ND	ND
Meat sauce	11	33	549	ND	ND
Tomato sauce	12	0.8	ND	ND	ND
Banana ketchup	13	885	ND	ND	ND
Tomato sauce	14	ND	ND	ND	ND
Pizza sauce	15	833	ND	ND	ND

ND - Not detected

Benzoic acid (or its salt, sodium benzoate) was the most frequently detected preservative, with concentrations ranging from trace levels (0.8 mg/kg) to 998 mg/kg. Higher concentrations were observed in banana ketchup samples (Samples 3 and 13), reflecting formulation requirements for high-sugar acidic products. The predominance of benzoic acid in the analyzed products can be attributed to its effectiveness in acidic environments (pH 2.5–4.0), antimicrobial activity against yeasts and molds, and favorable solubility and cost compared to alternative preservatives [15–18]. In contrast, the absence of preservatives in selected samples (e.g., cayenne pepper sauce and certain tomato sauces) indicates that product stability may be achieved through intrinsic factors such as low pH or thermal processing.

E. Regulatory Compliance Assessment

All samples complied with the maximum allowable limit (MAL) of 1000 mg/kg established by the Codex Alimentarius, indicating overall adherence to concentration-based regulatory standards. Despite

compliance in concentration, discrepancies in labeling were observed. Four samples (Samples 2, 8, 11, and 12) contained detectable levels of benzoic acid that were not declared on the product labels. Trace levels in Samples 8 and 12 may be attributed to the natural occurrence of benzoates in raw materials such as tomatoes [14]. However, the concentration detected in Sample 11 (33 mg/kg) suggests possible undeclared addition or cross-contamination during processing, indicating gaps in labeling transparency.

Sorbic acid was detected in only two samples and remained within permissible limits. Methylparaben and propylparaben were not detected in any of the analyzed products, suggesting a shift away from paraben-based preservatives, likely influenced by regulatory considerations and consumer preferences. Overall, these findings demonstrate that while preservative levels in commercial sauces generally comply with regulatory limits, inconsistencies in labeling persist. This underscores the importance of continuous market surveillance using validated analytical methods to ensure accurate labeling, protect consumer health, and support regulatory enforcement.

F. Food Safety Implication

Although all measured concentrations were within regulatory limits, the detection of undeclared preservatives raises concerns regarding cumulative exposure and consumer awareness. Benzoic acid, while widely used for microbial stability in acidic foods, may cause adverse reactions in sensitive individuals when consumed at elevated or repeated doses [19,20]. Therefore, even compliant levels require continuous monitoring, especially in commonly consumed products such as sauces. The absence of parabens may reduce potential endocrine-related risks, aligning with current international regulatory trends [21].

IV. CONCLUSION

An in-house validated HPLC-PDA method was successfully applied for the simultaneous determination of benzoic acid, sorbic acid, methylparaben, and propylparaben in commercial sauce products. The method demonstrated satisfactory analytical performance in terms of linearity, precision, trueness, sensitivity, and selectivity, and was supported by metrological traceability through the use of a certified reference material. These characteristics confirm its suitability for routine analysis of preservatives in complex food matrices.

Application of the method to fifteen commercially available sauces revealed that benzoic acid was the predominant preservative, while sorbic acid was less frequently detected, and parabens were absent in all samples. All products complied with established regulatory limits; however, the detection of undeclared benzoic acid in several samples highlights inconsistencies in labeling practices.

These findings underscore the importance of combining validated and traceable analytical methods with continuous market surveillance to ensure regulatory compliance, accurate labeling, and consumer protection. Furthermore, the study provides relevant data that may support regulatory agencies and the food industry in strengthening quality control systems and maintaining public confidence in food safety.

V. REFERENCES

[1] Islam, M. S., Zahan, N., Hossain, M. S., & Rouf, A. S. S. (2019). Determination of Preservatives in Fruit Juice Products Available in Bangladesh by a Validated RP HPLC Method. *Dhaka University Journal of Pharmaceutical Sciences*, *18*(2), 195–208. https://doi.org/10.3329/dujps.v18i2.43262.

[2] Maher, H. M., Alzoman, N. Z., Almeshal, M. A., Alotaibi, H. A., Alotaibi, N. N., & Al-Showiman, H. (2018). Quantitative screening of parabens in Ready-to-eat foodstuffs available in the Saudi market using high performance liquid chromatography with photodiode array detection. Arabian Journal of Chemistry, 13(1), 2897–2911. https://doi.org/10.1016/j.arabjc.2018.07.019.

[3] Lou, Z., Rahman, M. R. T., Zhang, J., et al. (2017). Determination of preservative residues and microbial contents of commercial Chinese duck neck meat. CyTA - Journal of Food, 15(3), 357–360. https://doi.org/10.1080/19476337.2016.1266390.

[4] Joint FAO/WHO Expert Committee on Food Additives. Meeting (67th: 2006: Rome, I., World Health Organization, & Food and Agriculture Organization of the United Nations. (2007). Evaluation of certain food additives and contaminants: sixty-seventh report of the Joint FAO/WHO Expert Committee on Food Additives. World Health Organization.

[5] Rustia, A. S., Tan, M. a. P., Guiriba, D. N. S., Magtibay, F. P. S., Bondoc, I. R. J., Mariano, C. B. D., Caincol, D. H., Bautista, K. a. D., Bulagao, B. F. R., De Guzman, V. C. L., Musni, A. C., Salem, A. M. T., & Villanueva, J. E. B. (2021). Defining risk in food safety in the Philippines. *Current Research in Nutrition and Food Science Journal*, *9*(1), 233–257. https://doi.org/10.12944/crnfsj.9.1.23.

[6] Bulska, E., et al. (2026). Metrological framework for the development of plant-based certified reference materials. Part I. Journal of Chemical Metrology, 20(1). https://doi.org/10.25135/jcm.2602.3803.

[7] Nelson, M. A., Waters, J. F., Toman, B., et al. (2018). A new realization of SI for organic chemical measurement: NIST PS1 primary standard for quantitative NMR (Benzoic Acid). Analytical Chemistry, 90(17), 10510–10517. https://doi.org/10.1021/acs.analchem.8b02575.

[8] Nasrollahi, S. S., Moosavi, N. S., & Yamini, Y. (2023).

Determination of parabens in different samples using green analytical chemistry approaches since 2015. TrAC - Trends in Analytical Chemistry, 166, 117163. https://doi.org/10.1016/j.trac.2023.117163

[9] Jain, R., Mudiam, M. K. R., Chauhan, A., Ch, R., Murthy, R., & Khan, H. A. (2013). Simultaneous derivatisation and preconcentration of parabens in food and other matrices by isobutyl chloroformate and dispersive liquid–liquid microextraction followed by gas chromatographic analysis. Food Chemistry, 141(1), 436–443. https://doi.org/10.1016/j.foodchem.2013.03.012

[10] EURACHEM / CITAC Guide to Quality in Analytical Chemistry Eurachem/CITAC Guide to Quality in Analytical Chemistry An Aid to Accreditation Third edition Acknowledgements. (n.d.). www.eurachem.org.

[11] Latimer, G.W. Jr., et al. Official Methods of Analysis of AOAC International, 22nd Ed. Association of Official Analytical Chemists (AOAC) International: Suite 500, 481 North Frederick Avenue, Gaithersburg, Maryland 20877-2417, USA, 2023.

[12] Rogatsky, E., & Stein, D. (2005). Evaluation of matrix effect and chromatography efficiency: new parameters for validation of method development. *Journal of the American Society for Mass Spectrometry*, *16*(11), 1757–1759. https://doi.org/10.1016/j.jasms.2005.07.012

[13] Barwick, V., & Wood, S. (2010). Achieving metrological traceability in chemical and bioanalytical measurement. *Journal of Analytical Atomic Spectrometry*, *25*(6), 785. https://doi.org/10.1039/b919885g

[14] Bianchi, F., Giannetto, M., & Careri, M. (2018). Analytical systems and metrological traceability of measurement data in food control assessment. *TrAC Trends in Analytical Chemistry*, *107*, 142–150. https://doi.org/10.1016/j.trac.2018.07.024

[15] Nehela, Y., Taha, N. A., Elzaawely, A. A., Xuan, T. D., Amin, M. A., Ahmed, M. E., & El-Nagar, A. (2021). Benzoic Acid and Its Hydroxylated Derivatives Suppress Early Blight of Tomato (Alternaria solani) via the Induction of Salicylic Acid Biosynthesis and Enzymatic and Nonenzymatic Antioxidant Defense Machinery. Journal of Fungi, 7(8), 663. https://doi.org/10.3390/jof7080663.

[16] Pereira, L. M., Della Betta, F., Seraglio, S. K. T., Schulz, M., Nehring, P., Gonzaga, L. V., Fett, R., & Costa, A. C. O. (2021). Assessment of sorbate and benzoate content in mustard, ketchup and tomato sauce by Sub-Minute Capillary Electrophoresis. Food Technology and Biotechnology, 59(3), 376–384. https://doi.org/10.17113/ftb.59.03.21.7095.

[17] Hazan, R., Levine, A., & Abeliovich, H. (2004). Benzoic Acid, a Weak Organic Acid Food Preservative, Exerts Specific Effects on Intracellular Membrane Trafficking Pathways in Saccharomyces cerevisiae. Applied and Environmental Microbiology, 70(8), 4449–4457. https://doi.org/10.1128/aem.70.8.4449-4457.2004.

[18] Quansah, J. K., & Saalia, F. K. (2024b). Chemistry of food additives: preservatives. In Food science and nutrition. https://doi.org/10.5772/intechopen.114887.

[19] Davidson, P. M., Sofos, J. N., & Branen, A. L. (2005). *Antimicrobials in food*. https://doi.org/10.1201/9781420028737.

[20] Chipley, J. R. (2020). *Sodium Benzoate and Benzoic Acid* (pp. 41–88). CRC Press. https://doi.org/10.1201/9780429058196-3.

[21] Soni, M., Carabin, I., & Burdock, G. (2005). Safety assessment of esters of p-hydroxybenzoic acid (parabens). *Food and Chemical Toxicology*, *43*(7), 985–1015. https://doi.org/10.1016/j.fct.2005.01.020.

2026 IMEKO Joint Conference
TC8 - TC11 - TC24
Manila, Philippines August 26-29, 2026

Assessment of a Direct Mercury Analyzer Method for Rapid Determination and Monitoring of Total Mercury in Harvested Fish

Elyson Keith P. Encarnacion[1,2], Benilda S. Ebravia[1,3], Evangeline C. Santiago[2], Mylene G. Cayetano[2,4]

[1] *Department of Science and Technology – Industrial Technology Development Institute, Taguig City, Philippines, 1631, ekpencarnacion@itdi.dost.gov.ph*
[2] *University of the Philippines Diliman – Institute of Environmental Science and Meteorology, Quezon City, Philippines, 1101*
[3] *University of Santo Tomas – Graduate School, Manila, Philippines, 1015*
[4] *Gwangju Institute of Science and Technology – International Environmental Research Institute, Gwangju, Republic of Korea, 61005*

***Abstract* – The Laguna Lake Development Authority (LLDA) is mandated to manage contaminants in Laguna de Bay. To strengthen LLDA's capacity for pollution monitoring, this study assessed a rapid method for determining total mercury in fish without requiring sample preparation. Using milkfish meat, the method exhibited a detection limit below 10% of Codex Alimentarius' maximum level for mercury in most fish. Linearity was established from 0.522 to 101 µg/kg. Trueness by bias was within the DORM-4 reference material's expanded uncertainty while trueness by recovery, evaluated using NIST SRM 3133 as spike, was within the 60-115% acceptable range. Repeatability at 2.76 µg/kg and 77.5 µg/kg yielded %RSDs below their corresponding thresholds. Uncertainty estimation identified reference material, calibration curve, and sample weight as major contributors. Overall, the method passed all performance characteristics evaluated using Eurachem procedures and AOAC criteria. Follow-through studies may include spatial and temporal analyses of harvested fish for monitoring applications.**

I. INTRODUCTION

Laguna de Bay is the Philippines' largest inland lake [1], and one of the country's most important freshwater resources [2]. The lake provides fisheries and aquaculture production [3], domestic and industrial water-related services [4], flood control [5], and transportation routes [6]. Among these multiple functions, fisheries and aquaculture are the most economically important [7].

Laguna de Bay has historically been used for open-water fisheries and enclosure-based aquaculture, with fish pens and cages becoming prominent features of lake utilization [7,8]. In the latter's production system, tilapia (*Oreochromis spp.*) and milkfish (*Chanos chanos*) have consistently been identified as among the major cultured aquatic commodities [9]. Their importance extends beyond livelihood generation at the lakeshore, because fish harvested from Laguna de Bay enters commercial distribution channels that supply consumers in Metro Manila and surrounding provinces [10]. Thus, the safety of aquatic produce from the lake is a regional safety issue with implications for a large consuming population [11].

Various contaminants have been detected in fish harvested from Laguna Lake [11,12,13]. Among these contaminants, mercury (Hg) is of particular concern because of its persistence, toxicity, and ability to undergo transformation into methylmercury ($MeHg^+$), the species most strongly associated with bioaccumulation and biomagnification in aquatic food webs [14]. Previous researchers have detected mercury in fish harvested from Laguna Lake since 1990, although the reported concentrations were below the applicable maximum permissible levels [15]. Accordingly, mercury is a contaminant of regulatory interest to the Laguna Lake Development Authority (LLDA).

LLDA, created under Republic Act No. 4850, is mandated to promote the sustainable development, management, and conservation of the Laguna de Bay region, protecting the lake against environmental degradation and pollution [16]. This legal mandate provides the institutional basis for contaminant monitoring intended to protect both the lake ecosystem and the communities that depend on its resources. In principle, effective lake governance should include the capacity to assess the contaminants in aquatic produce, particularly harvested fish intended for human consumption.

However, sustained mercury monitoring in fish appears operationally challenging. Traditional

instrumental methods which include Cold Vapor Atomic Absorption Spectrometry (CV-AAS) and Inductively Coupled Plasma Mass Spectrometry (ICP-MS) require high-order equipment, several chemicals for sample preparation, and lengthy time for analysis [17]. As a result, available evidence suggests that mercury data for Laguna de Bay fish are relatively limited and episodic [15,18].

Direct mercury analysis offers a promising alternative to more expensive and labor-intensive conventional methods. A Direct Mercury Analyzer (DMA) operates through thermal decomposition, amalgamation, and atomic absorption [19]—allowing total mercury determination without extensive wet chemical digestion or elaborate sample preparation [20]. In this regard, the current study aims to validate an existing DMA within the Department of Science and Technology – Industrial Technology Development Institute (DOST-ITDI) to assist LLDA as a third-party research and testing laboratory in conducting regular monitoring of mercury in harvested fish from Laguna de Bay.

II. MATERIALS AND METHODS

A. Sample Collection

Milkfish samples, intended as the method validation matrix, were randomly obtained from the harvests of fisherfolks from the West and East Bays of Laguna de Bay. Each fish was weighed using Shimadzu BX52KS top-loading balance, scaled and filleted. The fillet of each fish was homogenized using a commercial blender, placed in a resealable bag, labelled, and stored in a Biobase BDF-40V328 freezer at -40 °C until analysis.

B. Preliminary Screening

Prior to the conduct of each performance characteristic, homogenized fillets were removed from storage and allowed to equilibrate to room temperature. Each homogenized fillet was measured on a pre-weighed nickel boat using Mettler Toledo XPE206DR semi-microbalance. All samples were introduced into the Milestone DMA-80 Direct Mercury Analyzer for thermal combustion, amalgamation, and atomic absorption measurement. Mercury levels were determined to establish an initial concentration profile for the sample set. Samples appropriate for the assessment of selected performance characteristics were retained for method validation.

C. Method Validation (Eurachem)

Limits of Detection (LOD) and Quantification (LOQ): Ten (10) 19.1-52.3 mg portions of the sample with the lowest mercury concentration from the screening were analyzed.

Working Range and Linearity: Calibration solutions were gravimetrically prepared from Merck Certipur (950 ± 7 mg/kg Hg; traceable to NIST SRM 3133). Fifty (50) mg of each solution were introduced into the DMA to generate the calibration curve.

Trueness by Bias: Ten (10) independent analysis of 1.2-2.1 mg portions of the DORM-4 Fish Protein Certified Reference Material (CRM) for Trace Metals and other Constituents (412 ± 36 µg/kg Hg; traceable to NRC) were measured across ten (10) different days.

Trueness by Recovery: Ten (10) 24.1-47.0 mg portions of the sample with the highest mercury concentration from the screening were spiked with approximately 50 mg of 52.1 µg/kg Hg gravimetrically prepared from NIST SRM 3133 (10.004 ± 0.040 mg/g Hg). All spiked samples were analyzed.

Repeatability: Ten (10) 19.1-52.3 mg portions of the samples with the lowest and second highest (as the highest was already consumed) mercury concentration from the screening were analyzed.

III. RESULTS AND DISCUSSION

A. Sample Collection and Preliminary Screening

A total of 65 marketable-sized milkfish samples were obtained from Laguna de Bay. Whole fish weights ranged from 226 to 424 grams while corresponding homogenized fillets were within 87.1-195 grams. Mercury concentrations in the final samples varied from 2.60 to 97.9 µg/kg Hg.

B. Method Validation

The current maximum allowable limit (MAL) for methylmercury in the General Standard for Contaminants and Toxins in Food and Feed (GSCTFF) of the Codex Alimentarius is 500 µg/kg $MeHg^+$ for non-predatory fish [22]. This includes Laguna de Bay's cultured aquatic species such as tilapia and milkfish. Because methylmercury constitutes the predominant fraction of mercury in fish muscle tissue, typically accounting for approximately 75-90% [23], the total Hg measured in homogenized fillets using DMA may reasonably be used as a screening proxy for $MeHg^+$ but not as a direct substitute. Relative to the Codex maximum level, the calculated LOD (0.417 µg/kg Hg) and LOQ (1.39 µg/kg Hg) are approximately 1200-fold and 360-fold lower, respectively. Both values are substantially below 10% of the MAL and are therefore, acceptable [24,25]. This indicates that the method possesses sufficient analytical sensitivity for the determination of mercury in non-predatory fish, particularly in the context of regulatory monitoring and compliance assessment.

The validated working range was initially established at 0.522-101 µg/kg Hg with a correlation coefficient (r) of 1.000 (Figure 1), exceeding the minimum acceptance criterion of 0.995 [26]. This demonstrated an excellent linear relationship between mercury concentration and instrument response (peak height). Residual analysis across this range showed random dispersion of data points around zero (Figure 2), indicating no evident systematic deviation from linearity [27].

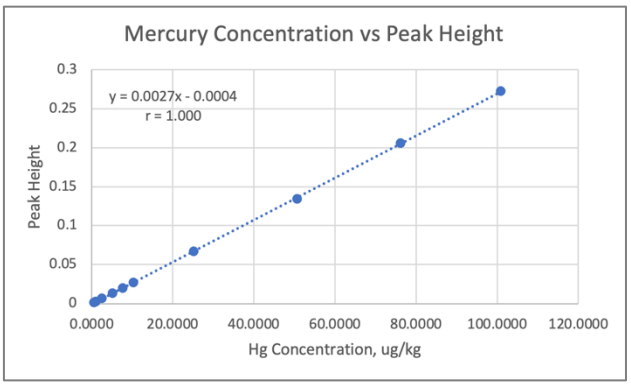


Figure 1. Working Range for the Determination of Mercury in Fish using DMA

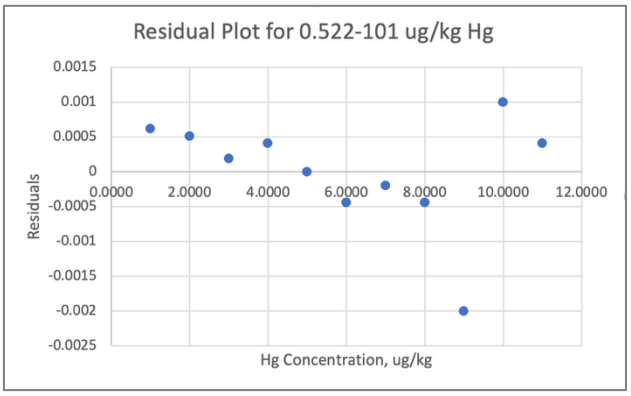


Figure 2. Residual Plot for 0.522-101 µg/kg Working Range for the Determination of Mercury in Fish using DMA

Nevertheless, because 96.9% of the samples analyzed fell within the lower portion of the calibration domain, a narrower linear range of 0.522-25.2 µg/kg Hg was selected for routine analysis to better reflect commonly encountered concentration levels. Within the reduced range, the calibration curve remained highly linear with r = 0.9999 and met predefined criterion [26].

Analysis of ten replicates of the DORM-4 CRM produced mercury concentrations ranging from 386 to 447 µg/kg Hg. All observed values fell within the expanded uncertainty (U) of the reference value (412 ± 36 µg/kg Hg), indicating satisfactory agreement between the measured and assigned concentrations. Meanwhile, recovery values ranged from 93.7 to 108%, demonstrating that the method performs well within the 80-110% accuracy limits established by the Association of Official Analytical Chemists (AOAC) [28]. The mean concentration was 415 ± 37 µg/kg Hg, corresponding to a recovery of 101%. Overall, these results suggest that the DMA method exhibits minimal systematic bias in the determination of mercury in fish samples.

In addition, analysis of spiked fish samples yielded recoveries ranging from 83.3 to 105%. These values fall well within the AOAC acceptable recovery criterion of 60-115% for analyte levels around 10 µg/kg Hg. Because the spike concentration (52.1 µg/kg Hg) lies approximately midway the two concentration levels, it may also be evaluated against the more stringent acceptance range of 80-110% typically applied at 100 µg/kg Hg. The mean recovery of 92.0% indicates satisfactory trueness of the method, particularly in view of the inherent complexity of the fish tissues matrix. When considered alongside the minimal bias indicated by CRM analysis, these findings support the use of DMA as an accurate and reliable method for the intended application.

Repeatability was successfully evaluated at both low and high mercury concentration levels. At the low level (2.76 µg/kg Hg), the method yielded a relative standard deviation (%RSD) of 5.04%, which is substantially below the AOAC acceptable repeatability criterion of 30% at 1 µg/kg Hg [28]. In contrast, at the high level (77.5 µg/kg Hg), the observed %RSD was 1.24%, likewise satisfying the corresponding repeatability criterion of 15% at 100 µg/kg Hg [28]. These results demonstrate that the DMA method exhibits excellent precision across a broad concentration range and yields repeatable mercury measurements in fish samples at both low and elevated ultratrace levels.

Table 1. Summary of Method Validation for the Determination of Mercury in Fish using DMA

Performance Characteristics	Values	Acceptance Criteria	Remarks
LOD	0.417 µg/kg	≤ 10% of MAL (500 µg/kg)	Passed
LOQ	1.39 µg/kg	-	-
Working Range and Linearity (0.522-101 µg/kg)	(r = 1.000, random residuals)	($r \geq 0.995$, random residuals)	Passed
Trueness by Bias	415 ± 37 µg/kg (101%)	412 ± 36 µg/kg (80-110%)	Passed
Trueness by Recovery	92.0%	60-115%	Passed
Repeatability at Low Level (2.76 µg/kg)	5.04%	≤ 30%	Passed
Repeatability at High Level (77.5 µg/kg)	1.24%	≤ 15%	Passed

Table 1 summarizes the minimum performance characteristics assessed for quantifying mercury in fish muscle tissues using DMA method. Overall, the method satisfied all evaluated performance criteria specified under the applied Eurachem and AOAC validation framework.

C. Uncertainty Estimation

Analysis of the procedure identified five contributors to the combined measurement uncertainty (Figure 3). The concentration of the CRM was the dominant source,

accounting for 90.8% of the total uncertainty budget. The second largest contributor was the calibration curve, which accounted for 8.54% of the total uncertainty. The remaining factors were comparatively minor and included sample weight (0.408%), bias (0.207%), and repeatability (0.030%). These results indicate that the overall uncertainty of the method was governed primarily by contributions associated with reference material and calibration performance, both of which are critical to metrological traceability and analytical accuracy. Meanwhile, other analytical factors had relatively negligible influence. Considering that the method is meant for regulatory evaluation and compliance assessment, there is a need to further reduce the uncertainty by incorporating ultratrace-level reference materials with narrower expanded uncertainties, and tighter quality controls for better calibration performance.

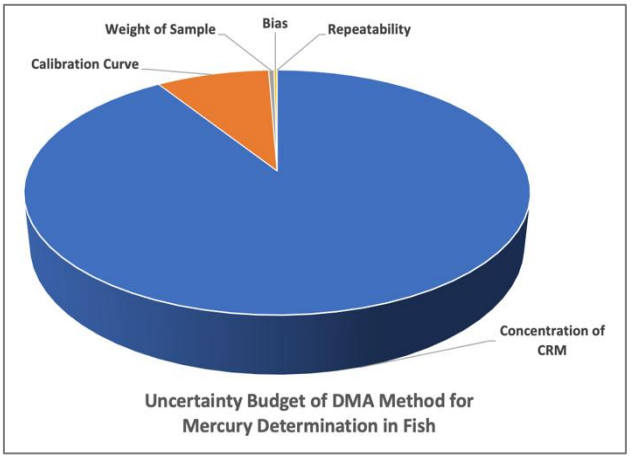


Figure 3. Uncertainty Budget for the Determination of Mercury in Fish using DMA

IV. CONCLUSION

The study successfully achieved its objective of establishing a rapid and fit-for-purpose analytical approach for total mercury determination in harvested fish using direct mercury analysis. This signifies a milestone in addressing an important capability needed by LLDA in monitoring the Laguna de Bay. Taken together, the validation results demonstrate that the method is not only technically sound but also operationally suitable for regulatory and surveillance contexts which require inexpensive, time-bound, and preparation-free analysis. Beyond method performance, the work also provides a practical pathway for strengthening institutional monitoring capacity by generating a validated procedure that can easily be adopted by LLDA should they choose to veer away from employing third party laboratory services and once the necessary instrumentation becomes available. In this sense, the study advances both analytical method development and environmental governance by linking laboratory validation to a concrete public sector monitoring application.

At the same time, several gaps remain that should be addressed before the method is used as a stand-alone basis for long-term regulatory decisions. First, the present assessment focused on fish and on total mercury determination under controlled validation conditions. Therefore, broader applicability to other relevant matrices and other commercially important species from Laguna de Bay still needs to be established. In addition, because direct mercury analysis measures total mercury rather than speciated methylmercury, future work should examine the relationship between total mercury and methylmercury in local fish tissues to strengthen interpretation against food safety benchmarks. Moreover, method comparison with a well-established confirmatory platform such as CV-AAS or ICP-MS would also further reinforce confidence in routine implementation. Moving forward, the validated method may serve as the analytical foundation for a spatially and temporally resolved mercury monitoring program for harvested fish in Laguna de Bay. This future endeavor could generate the historical dataset needed to support risk assessment, guide regulatory responses, and improve protection of both consumers and lake-dependent communities.

V. REFERENCES

[1] M.L.A.Cuvin-Aralar, “Impacts of aquaculture on fish biodiversity in the freshwater lake Laguna de Bay, Philippines”, Lakes Reserv. Res Manag., vol.21, pp.31-39, April 2016, doi: https://doi.org/10.1111/lre.12118.

[2] M.Tamayo-Zafaralla, R.A.V.Santos, R.P.Orozco, G.C.P.Elegado, “The ecological status of Lake Laguna de Bay, Philippines”, Aquat. Ecosyst. Health Manag, vol.5, no.2, pp.127-138, June 2002, doi: https://doi.org/10.1080/14634980290031820.

[3] R. Palanca-Tan. “Economic Vulnerabilities of Fishing-dependent Households around Laguna Lake, Philippines”, Philipp. J. Sci., vol.149, no.3A, pp.815-831, April 2020, doi: https://doi.org/10.56899/149.3A.10.

[4] R.R.Diwa, M.V.Elvira, C.C.Deocaris, M.Fukuyama, L.P.Bela, “Transport of toxic metals in the bottom sediments and health risk assessment of Corbicula fluminea (Asiatic clam) collected from laguna de Bay, Philippines”, Sci. Total Environ., vol.838, part 4, September 2022, doi: https://doi.org/10.1016/j.scitotenv.2022.156522.

[5] E.C.Herrera, K.Naito, “Hydrodynamic Invcestigation of Laguna Lake for Water Security and Flood Risk Management of Metro Manila”, Proc. IAHS, vol.386, pp.95-100, April 2024, doi: https://doi.org/10.5194/piahs-386-95-2024.

[6] V.Vargas-Nguyen, “Laguna de Bay, Philippines: Environmental Literacy”, July 2015, Retrieved April 2026 from https://ian.umces.edu/blog/laguna-de-bay-

philippines-environmental-literacy/.

[7] D.C.Israel, “The Current State of Agriculture in Laguna de Bay”, Philippine Institute for Development Studies, December 2007, Retrieved April 2026 from https://pidswebs.pids.gov.ph/CDN/PUBLICATIONS/ris-old-backups/dps/pidsdps0720.pdf.

[8] A.Santos-Borja, D.N.Nepomuceno, “Laguna de Bay: Institutional development and change for lake basin management”, Lakes Reserv. Res. Manag., vol.11, pp.257-269, doi: https://doi.org/10.1111/j.1440-1770.2006.00310.x.

[9] R.Palanca-Tan, “Benefits from Laguna Lake: Perspective of Small Fisher Households”, J. Manag. Glob. Sustain., vol.8, no.2, December 2020, doi: https://doi.org/10.13185/2244-6893.1120.

[10] S.Chakraborty, R.Avtar, R.Raj, H.V.Thu Minh, “Village Level Positioning Ecosystem Services and their Values to local Communities in the Peri-Urban Areas of Manila, The Philippines”, Land, vol.8, no.2, p.177, doi: https://doi.org/10.3390/land8120177.

[11] C.J.G.Mercado-Dy, L.M.Atienza, C.B.Juanico, D.P.T.Depositario, W.A.Hurtada, “Bioaccumulation and Non-Carcinogenic Health Risk Assessment of Heavy Metals in Selected Fish Species from South Bay of Laguna Lake”, Acta Med. Philipp., vol.55, no.7, November 2023, doi: https://doi.org/10.47895/amp.vi0.3031.

[12] M.E.P.Revilleza, S.E.A.Salamat, M.G.V.Paraso, “Antibacterial Residues in Cultured Nile Tilapia (Oreochromis niloticus) in the Lakeshore Barangays of Los Baños, Laguna, Philippines”, Philipp. J. Vet. Med., vol.58, no.2, pp.231-238, January 2022, Retrieved April 2026 from https://www.researchgate.net/publication/358109674_Antibacterial_Residues_in_Cultured_Nile_Tilapia_Oreochromis_niloticus_in_the_Lakeshore_Barangays_of_Los_Banos_Laguna_Philippines.

[13] C.M.Bajet, A.Kumar, M.N.Calingacion, T.C.Narvacan, “Toxicological Assessment of pesticides used in the Pagsanjan-Lumban catchment to selected non-target aquatic organisms in Laguna Lake Philippines”, Agric. Water Manag., vol.106, pp.42-49, September 2024, doi: https://doi.org/10.1016/j.agwat.2012.01.009.

[14] B.Brodziak-Dopierata, A.Fischer, “Analysis of the Mercury Content in Fish for Human Consumption in Poland”, Toxics, vol.11, no.8, p.717, August 2021, doi: https://doi.org/10.3390/toxics11080717.

[15] M.L.A.Cuvin-Aralar, “Mercury levels in the sediment, water, and selected finfishes of Laguna Lake, The Philippines”, Aquaculture, vol.84, no.3-4, pp.277-288, February 1990, doi: https://doi.org/10.1016/0044-8486(90)90093-3.

[16] Philippine Congress, “Republic Act No. 4850, Laguna Lake Development Authority Act of 1966”, Retrieved April 2026 from https://elibrary.judiciary.gov.ph/thebookshelf/showdocs/2/6885.

[17] O.G.N.Neto, S.R.Dias, F.E.A.Albuquerque, M.Miranda, M.Lopez-Alonso, R.B.Oliveira, D.Pinto, A.H.H.Minervino, “Comparative analysis between mercury levels in fish tissues evaluated using direct mercury analyzer and inductively plasma-coupled mass spectrometer”, Chemosphere, 351, January 2024, Retrieved April 2026 from https://repositorio.cuc.edu.co/server/api/core/bitstreams/c0d55a05-084c-4307-8fa5-25acf6ecb2a3/content.

[18] V.B.Molina, “Health Risk Assessment of Heavy Metals Bioaccumulation in Laguna de Bay Fish Products”, 14th World Lake Conference, July 2011, Retrieved April 2026 from https://www.pref.ibaraki.jp/soshiki/seikatsukankyo/kasumigauraesc/04_kenkyu/kaigi/docments/kosyou/14/2011wlc_victoriob.molina.pdf.

[19] S.L.CFerreira, C.S.A.Felix, S.V.A.Dantas, L.S.G.Teixeira, V.A.Lemos, A.C.deSouza, L.A.Mendes, C.C.Windmöller, “Speciation, fractionation, and determination of mercury using the direct mercury analyzers – A review”, Microchem. J., vol.217, October 2025, doi: https://doi.org/10.1016/j.microc.2025.115076.

[20] N.A.Panichev, S.E.Panicheva “Determiantion of total mercury in fish and sea products by direct thermal decomposition atomic absorption”, Food Chem., vol.166, pp.432-441, January 2015, doi: https://doi.org/10.1016/j.foodchem.2014.06.032.

[21] H. Cantwell (ed.), “Eurachem Guide: the Fitness for Purpose of Analytical Methods—A Laboratory Guide to Method Validation and Related Topics”, (3rd ed. 2025), Retrieved May 2026 from https://www.eurachem.org/images/stories/Guides/pdf/MV_guide_3rd_ed_V1_EN.pdf

[22] Joint FAO/WHO, “Discussion Paper on Maximum Levels for Methylmercury Fish”, Codex Alimentarius, April 2017, Retrieved May 2026 from https://www.fao.org/fao-who-codexalimentarius/sh-proxy/es/?lnk=1&url=https%253A%252F%252Fworkspace.fao.org%252Fsites%252Fcodex%252FMeetings%252FCX-735-11%252FWD%252Fcf11_12e.pdf

[23] K.R.Mahaffey, “Fish and shellfish as dietary source of methylmercury and the ω-3 fatty acids, eicosahexaenoic acid and docosahexaenoic acid: risks and benefits”, Environ. Res., vol.95, no.3, pp.414-428, July 2004, doi: https://doi.org/10.1016/j.envres.2004.02.006

[24] European Committee for Standardization (CEN) Technical Committee, “Handling and reporting of concentrations below Limit of Detection or Limit of Quantification regarding European Standards

CEN/TC 264, stationary source emissions), January 2019, Retrieved May 2026 from https://www.vdi.de/fileadmin/pages/vdi_de/redakteure/ueber_uns/fachgesellschaften/KRdL/dateien/CEN-TC264_TFE_-_Limit_of_Detection_and_Limit_of_Quantification__Status-_January_2019_.pdf

[25] A.K.M.Carlos, G.J.M.Manalo, E.K.P.Encarnacion, A.F.DelRosario, JATmendoza, ACAlcantara, WPAlejandro, RMSMTing, "Profiling of Total Residual Contaminants Migrating from Philippine-based Polyethylene Packaging to Fermented and Alcoholic Foods, Curr. Res. Nutr. Food Sci. J., vol.14, no.1, doi: http://dx.doi.org/10.12944/CRNFSJ.14.1.32

[26] R.R.J.Reddy, S.K.Kolli, S.Salakolusu, S.D.M.Kallam, J.K.Raghupathi, N.K.Katari, "Characterization and Analytical Method Validation for Potential Impurities of a Merchantability Drug Substance Fluoxetine HCl", vol.39, no.2, January 2025, doi: https://doi.org/10.1002/bmc.6069

[27] M.Law, D.Jackson, "Residual plots for linear regression models with censored outcome data: A refined method for visualizing residual uncertainty", Commun. Stat. Simul. Comput., vol.46, no.4, pp.3159-3171, doi: https://doi.org/10.1080/03610918.2015.1076470

[28] Association of Official Analytical Chemists, "Appendix F: Guidance for Standard Method Performance Requirements", Retrieved May 2026 from https://www.aoac.org/wp-content/uploads/2019/08/app_f.pdf

2026 IMEKO Joint Conference
TC8 - TC11 - TC24
Metro Manila, Philippines, August 26-29, 2026

Evaluation of Laboratory Performance in Food Nutrient Measurements: Proficiency Testing of Infant Formula (2011-2024)

Michael C. Pelagio[1], Leah C. Dajay[1], Jolly C. Cotara, Jennifer C. Laurea[1], Mylene B. Martin, and Joan C. Duldulao[1]

[1] *Department of Science and Technology – Food and Nutrition Research Institute (DOST-FNRI), DOST Compound, Gen. Santos Ave., Bicutan, Taguig City, Philippines,* lightmichael13@gmail.com

***Abstract* – Precise and consistent measurements are the foundation of both quality assurance and regulation, especially for complex food matrices such as infant formula. In the Philippines, infant formulas are strictly regulated and vary in composition, thus, reliable nutrient analysis is critical. The Department of Science and Technology–Food and Nutrition Research Institute (DOST-FNRI) as the country's sole ISO 17043-accredited provider of proficiency testing (PT) for food nutrients, routinely offers PT on infant formula.**

This study assessed laboratory performance across four PT rounds for infant formula conducted in 2011, 2016, 2021, and 2024. The evaluations encompassed proximate components—moisture, fat, protein, and ash—as well as selected minerals, specifically iron, calcium, sodium, potassium, and zinc. The participants varied from 15 to 38 laboratories, representing government, industry, and private sectors. To ensure comparability, standardized evaluation was employed, utilizing consensus values derived from participant results and z' /z-scores ($|z'/z| \leqslant 2$ indicating satisfactory performance).

Results indicate an upward trend, with improved satisfactory performance for fat and ash, and protein increasing from 71% in 2011 to 100% in 2024. Minerals content, particularly calcium, sodium and zinc, showed improvement. These trends are indicative of both improved laboratory capabilities and inherent difficulties associated with complex matrices and methodological variations.

The PT program underscores the nation's advancing proficiency in nutrient assessment, identifies areas necessitating harmonization efforts, and facilitates regulation. As a recommendation for future rounds, additional parameters such as vitamins, fatty acids, and other minerals should be incorporated to expand analytical coverage and further strengthen the measurement comparability and traceability.

I. INTRODUCTION

Measurement comparability is a core principle of metrology and underpins confidence in analytical results used for regulatory and quality assurance purposes. In food analysis, this is particularly critical for infant formula, where nutrient composition directly affects infant health, product compliance, and labeling accuracy. Even small deviations in some reported nutrient levels may have significant implications for both public health and regulatory enforcement.

In the Philippines, infant formula products are subject to stringent regulatory requirements; however, their formulations are often distinct from those in other countries. Variations may arise from differences in regulatory limits, fortification practices, ingredient sourcing, and adaptation to local nutritional needs. For instance, national regulations and guidance aligned with the Food and Agriculture Organization (FAO) and World Health Organization (WHO) frameworks allow flexibility for countries to establish nutrient levels appropriate to their population context [1]. As a result, commercially available infant formulas in the Philippines may differ in composition—particularly in micronutrient fortification—from those used in international proficiency testing schemes.

This variability highlights a critical challenge: the use of non-representative PT materials may not adequately reflect the analytical difficulties encountered by local laboratories. Matrix effects, analyte interactions, and concentration ranges can significantly influence measurement accuracy, especially in complex products like infant formula. The AOAC International emphasizes that analytical methods must be validated within the context of the specific food matrix to ensure reliable results [2].

Proficiency testing (PT), as defined by the International

Organization for Standardization under ISO/IEC 17043, plays a vital role in assessing laboratory competence and ensuring comparability of results across laboratories [3]. However, for PT to be effective, the test materials must be commutable, and representative of routine samples analyzed by participating laboratories.

As the sole ISO/IEC 17043-accredited PT provider for food nutrients in the Philippines, DOST-FNRI plays a critical role in addressing this gap by developing PT schemes based on locally relevant matrices [4,5]. This study evaluates laboratory performance across four PT rounds for infant formula conducted between 2011 and 2024, with the objective of assessing trends in measurement comparability and identifying areas for improvement.

II. MATERIALS AND METHODS

A. PT Design and Preparation of Test Items

The DOST-FNRI Proficiency Testing Laboratory (FNRI-PTL) regularly organizes proficiency testing (PT) schemes for food nutrient analysis in accordance with international standard. Infant formula was selected as one of the PT matrices due to its nutritional importance and analytical complexity. This study evaluated four PT rounds for infant formula conducted in 2011, 2016, 2021, and 2024. The measurands for the first PT round consist of proximate (moisture, fat, protein, and ash) and minerals (iron, calcium, and sodium). Potassium and zinc were eventually added on the succeeding PT rounds. These analytes are routinely included in infant formula nutritional labeling and are critical for ensuring compliance with national and international regulations. [6]

Representative samples of commercially available infant formula, representative of those distributed in the Philippine market. were purchased directly from retail outlets. The test materials were prepared following the established standard operating procedures of FNRI-PTL [4,5] The samples were mixed for homogeneity, divided into individual units, packed and sealed in pre-labelled laminated aluminum foil packets. The amount of material per packet was based on the estimated quantity required to perform duplicate analyses, including allowance for repeat testing when necessary.

Systematic sampling was performed to allocate units for homogeneity testing, stability testing, contingency purposes, and selection of PT items distributed to participants. Candidate PT items were stored under conditions determined during preliminary trial runs to maintain analyte stability throughout the PT cycle [7,8]

B. Homogeneity and Stability Assessment

Homogeneity and stability studies were conducted prior to distribution of PT items in accordance with ISO 13528 [9] and established FNRI-PTL procedures [4,5].

For homogeneity assessment, ten randomly selected PT units were analyzed randomly in duplicate for all relevant measurands by subcontracted laboratories with demonstrated analytical competence through ISO/IEC 17025 accreditation or satisfactory performance in relevant PT schemes [10]. Statistical evaluation of homogeneity was performed following ISO 13528 [9] and the approach described by Fearn and Thompson [11].

Homogeniety assessment was done for all measurands in the first PT round in 2011. In succeeding PT round for 2016, only selected measurands were assessed for homogeneity such as moisture, fat, potassium and zinc [5]. For the rest of the PT rounds in 2021 and 2024, only moisture, fat and iron were assessed for homogeneity.

For stability assessment, selected PT units stored under prescribed conditions were analyzed at predetermined intervals to evaluate possible changes in analyte concentration during storage and transport. Analyses were conducted under the same experimental conditions used in the homogeneity study. Transport stability assessment was also performed to ensure that analyte integrity was maintained during shipment to participants.

C. Participation and Distribution of PT Items

Participation in the PT rounds was open to local government laboratories, private commercial laboratories, quality assurance and quality control (QA/QC) laboratories of food manufacturers and academic institutions involved in food nutrient analysis. Across the four PT rounds, participation ranged from 15 to 38 laboratories.

Each participating laboratory received one PT item together with supporting documents such as instructions to participants, sample receipt forms, method details forms, and result reporting sheets. Laboratories were assigned unique identification codes to ensure confidentiality of reported results and performance evaluations. PT items were distributed through courier or express delivery services under conditions appropriate for the stability requirements of the matrix.

D. Statistical Evaluation

Assigned values and statistical evaluations were established in accordance with the FNRI Proficiency Testing Supplement on Statistical Procedures and based on the principles described in ISO 13528 [9] and the IUPAC Harmonized Protocol [12]. Robust statistical methods were applied to minimize the influence of outlying results.

Laboratory performance was evaluated using z-scores or z'-scores, depending on the availability and significance of uncertainty associated with the assigned value:

$$z\ score = \frac{\mathrm{x} - x_{pt}}{\sigma_{pt}} \quad (1)$$

$$z'\ score = \frac{\mathrm{x} - x_{pt}}{\sqrt{u^2(x_{pt}) + \sigma_{pt}^2}} \quad (2)$$

The use of z′-scores, as presented in Eq. (2), incorporated the standard uncertainty of the assigned value ($u(x_{pt})$), which includes contributions arising from material inhomogeneity, transport conditions, and potential instability of the proficiency test item.

The calculated z or z' scores were interpreted as follows:

- $|z \text{ or } z'| \leq 2.00$: "Satisfactory" (S) performance
- $2.00 < |z \text{ or } z'| < 3.00$: "Warning" (W) signal
- $|z \text{ or } z'| \geq 3.00$: "Action" (A) signal

III. RESULTS AND DISCUSSIONS

A. Homogeneity and Stability of PT Items

All conducted PT rounds for infant formula satisfied the homogeneity criteria prior to distribution to participants. Statistical evaluation conducted in accordance with ISO 13528 demonstrated that between-unit variability was relatively small to the standard deviation for proficiency assessment. This confirmed that the prepared PT items were sufficiently homogeneous for interlaboratory comparison.

For the first PT round in 2011, the stability for minerals failed which can be due to incosistent analytical reproducibility of the methods used by the subcontracted laboratory. Stability studies for the rest of the measurands in the succeeding PT rounds likewise showed no significant changes in analyte concentrations within the established storage and transport periods. These findings verified that the assigned values remained valid throughout the duration of the PT rounds. Similar to homogeneity testing, not all measurands were analyzed for stability in succeeding PT rounds. All measurands were tested for their stability in 2011 while only moisture, fat, potassium and zinc for 2016. For 2021, only moisture was analyzed and for 2024, moisture, fat and iron. The tested measurands were subsequently reduced to only include the identified critical parameters at the discretion of technical experts and laboratory head at that time.

B. Assigned Values and Performance Evaluation

All PT rounds utilized concensus to determine the assigned value of each measurand. For 2011 and 2021 PT rounds, the robust average of PT participants' results calculated using Algorithm A based on ISO 13528 guidelines [5]. In PT round for 2016, the median of the participants' result was used due to limited number of participants for zinc while mean of participant's results was used for the potassium and zinc in 2024 PT round. The rest of the assigned values were derived from the robust average of the participants' results in 2024 PT rounds using Algorithm A. Due to high variation of results for moisture and protein in 2011 PT Round, provisional z scores were given to participants. It indicates that the scores are for evaluative purpose and for information only [4,5]. In PT rounds beyond 2016, z' score were issued if uncertainty of participants' result is not negligible: $u(x_{pt}) > 0.3\sigma_{pt}$. For 2016, z' was issued in moisture, fat, iron, calcium, potassium and zinc. In 2021 PT round, z scores were only issued on protein and potassium while the rest were evaluated using z'scores. As for the latest PT round of infant formula in 2024, z' scores were given to fat, protein, calcium, sodium and zinc.

Table 1: Summary of statistics of PT rounds for infant formula

PT Round	N	Measurand	n	X_{pt}	σ_{pt} (%)	Satisfactory Performance (%)
2011	38	Moisture	33	2.32	12%	79%
		Fat	30	22.09	5%	80%
		Protein	31	9.70	2%	71%
		Ash	34	2.51	2%	88%
2016	28	Moisture	24	2.42	12%	83%
		Fat	22	23.73	5%	82%
		Protein	21	10.14	3%	71%
		Ash	24	2.66	2%	83%
		Iron	20	6.17	15%	70%
		Calcium	19	377	10%	79%
		Sodium	21	155	12%	67%
		Potassium	19	573	10%	89%
		Zinc	17	4.17	15%	82%
2021	15	Moisture	13	2.15	12%	92%
		Fat	10	25.00	5%	80%
		Protein	10	10.48	3%	90%
		Ash	13	3.12	2%	77%
		Iron	8	5.68	15%	88%
		Calcium	8	509	10%	75%
		Sodium	6	214	12%	83%
		Potassium	7	615	10%	86%
		Zinc	8	4.80	14%	75%
2024	21	Moisture	18	2.08	12%	83%
		Fat	15	26.16	5%	87%
		Protein	14	10.45	3%	100%
		Ash	18	2.95	2%	89%
		Iron	13	5.48	15%	85%
		Calcium	15	478	10%	93%
		Sodium	14	180	12%	86%
		Potassium	11	594	10%	82%
		Zinc	12	4.20	15%	92%

C. Performance Trends in Proximate Analysis

As shown in Figure 2 and Table 1, improvement in laboratory performance was observed across the PT rounds for proximate analyses. Moisture analysis achieved satisfactory performance rates of 79%, 83%, 92%, and 83% for PT rounds conducted in 2011, 2016, 2021, and 2024, respectively. The high level of satisfactory performance indicates that moisture determination methods used by participating laboratories were generally well established and based on AOAC methods.

Fat analysis also demonstrated consistent improvement as shown in Figure 1, with satisfactory results increasing from 80% in 2011 to 87% in 2024. The gradual improvement may be attributed to better implementation of standardized extraction procedures, improved analyst

competency, and increased use of validated methods. The use of acid hydrolysis prior to solvent extraction by most laboratories especially in 2024 PT rounds, may also have improved extraction efficiency in complex infant formula matrices.

Among the proximate parameters, protein analysis showed the most significant improvement as evident in Figure 1. Satisfactory performance increased from 71% in 2011 and 2016 to 90% in 2021 and eventually reached 100% in 2024. This trend suggests substantial enhancement in laboratory capability for nitrogen determination, likely associated with improved implementation of Kjeldahl and Dumas methods, better calibration practices, and increased compliance with laboratory quality management systems.

Ash analysis exhibited relatively high satisfactory performance throughout the PT rounds, ranging from 77% to 89%. The lower satisfactory performance observed in 2021 shown in Figure 1 may be associated with relatively low number of participating laboratories

Overall, the observed improvement in proximate analysis reflects the positive impact of continuous PT participation on laboratory performance. Repeated participation allows laboratories to identify analytical weaknesses, implement corrective actions, and improve analytical consistency over time.

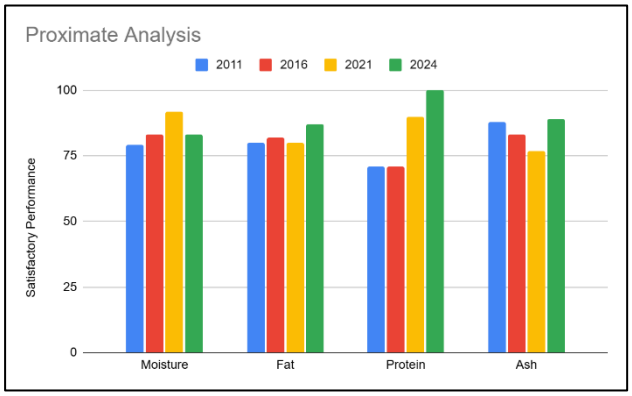


Figure 1: Summary of trends in satisfcatory perfomance in proximate analysis across 4 PT rounds.

D. Performance Trends in Minerals Analysis

Compared with proximate analysis, mineral determinations exhibited greater variability among laboratories. Iron analysis showed satisfactory performance levels of 70%, 88%, and 85% for the 2016, 2021, and 2024 PT rounds, respectively. The substantial improvement from 2016 to 2021 shown in Figure 2 suggests enhanced competency in trace mineral analysis and increased adoption and improvement in sample digestions and instrumental techniques

As shown in Figure 2, calcium analysis demonstrated progressive improvement over time, increasing from 79% satisfactory performance in 2016 to 93% in 2024. This improvement may be associated with improved digestion procedures, better calibration strategies, and increased awareness of matrix effects.

Sodium determination consistently exhibited greater variability compared with other mineral analytes. Satisfactory performance increased from 67% in 2016 to 86% in 2024 as can be observed in Figure 2; however, sodium remained among the most challenging parameters for participating laboratories. Several factors may have contributed to this variability, including contamination during sample preparation, matrix interferences, and instrumental sensitivity.

Potassium and zinc analyses generally showed acceptable performance as evident in the trends shown illustrated in Figure 2. Potassium achieved satisfactory performance rates of 89%, 86%, and 82% across the 2016, 2021, and 2024 PT rounds, respectively, while zinc improved from 75% in 2021 to 92% in 2024. The increasing performance for zinc may reflect improved trace element handling procedures and increased use of matrix-matched calibration.

The variability observed in mineral analysis highlights the continuing analytical challenges associated with trace element determination in complex matrix of infant formula. Matrix interactions, digestion efficiency, and contamination control remain critical factors influencing measurement comparability.

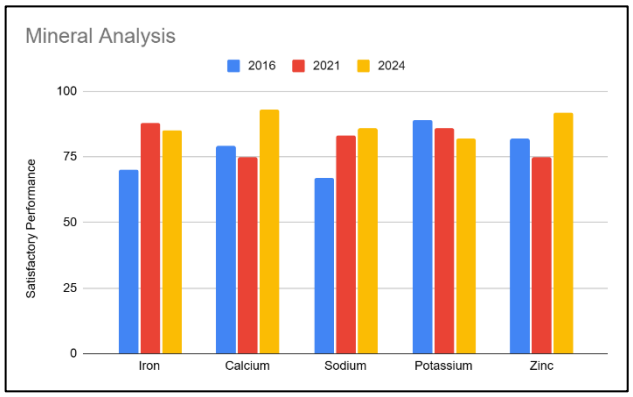


Figure 2: Summary of trends in satisfcatory performance in mineral analysis across 3 PT rounds.

E. Influence of Matrix Complexity on Laboratory Performance

Infant formula is a highly complex matrix composed of proteins, lipids, carbohydrates, vitamins, and minerals that may interact during sample preparation and instrumental analysis. Such complexity can affect extraction efficiency, analyte recovery, and matrix interference, particularly for mineral determination [13].

Unlike some international PT schemes that use matrices not commonly encountered in the Philippine market, the PT items used in this study were representative of locally available infant formula. This increased the relevance of

the PT scheme to routine laboratory analysis and provided a more realistic assessment of laboratory capability.

The observed variability in selected analytes, particularly sodium and iron, demonstrates the influence of matrix effects and methodological differences on analytical performance. Laboratories using different digestion methods, calibration standards, and instrumentation may obtain significantly different results despite analyzing the same PT material.

These findings emphasize the importance of matrix-specific method validation, appropriate quality control measures, and continued participation in PT schemes to improve measurement comparability.

F. Measurement Comparability and Metrological Significance

The improvements in laboratory performance observed from 2011 to 2024 reflects the strengthening of measurement comparability within the Philippine food testing sector. The use of harmonized statistical evaluation procedures based on ISO 13528 and the IUPAC Harmonized Protocol enabled standardized interpretation of laboratory performance across PT rounds.

The implementation of z′-scores further strengthened the reliability of performance assessment by incorporating uncertainty contributions arising from homogeneity, transport, and stability of the PT materials. This approach aligns with metrological principles emphasizing the importance of uncertainty evaluation in ensuring comparability of measurement results.

The findings demonstrate that PT serves not only as an external quality assurance tool but also as a mechanism for strengthening national measurement infrastructure. Through continued participation in PT schemes, laboratories can benchmark performance, identify sources of error, and improve analytical reliability.

The increasing satisfactory performance rates observed in this study indicate that local laboratories are continuously improving their capability to generate reliable nutrient measurements for infant formula. This is particularly important in supporting regulatory enforcement, product quality assurance, and consumer protection.

G. Future Directions

Although significant improvements were observed across the PT rounds, challenges remain in achieving consistent comparability for selected mineral analytes. Continued efforts in method harmonization, analyst training, contamination control, and uncertainty estimation are therefore recommended.

Future PT rounds may expand the analytical scope to include vitamins, fatty acids, and additional minerals to address evolving regulatory requirements and industry needs. The inclusion of these parameters would further strengthen analytical capability and support comprehensive nutrient measurement in infant formula and related food matrices.

IV. CONCLUSION

This study evaluated laboratory performance across four proficiency testing rounds for infant formula conducted between 2011 and 2024 by the DOST-FNRI Proficiency Testing Laboratory. The results demonstrated progressive improvement in laboratory capability for both proximate and mineral analyses.

Among the proximate parameters, protein analysis showed the greatest improvement, reaching 100% satisfactory performance in 2024. Fat and ash analyses also exhibited increasing satisfactory performance across PT rounds. Mineral determinations generally improved over time, particularly for calcium and zinc, although variability remained for sodium.

The findings highlight the important role of proficiency testing in strengthening laboratory competence, measurement comparability, and traceability in food nutrient analysis. The use of locally representative infant formula matrices provided a more realistic assessment of laboratory performance under Philippine testing conditions.

As a recommendation, future PT rounds should include additional parameters such as vitamins, fatty acids, and other minerals to further strengthen analytical coverage and support evolving regulatory and industry requirements.

V. REFERENCES

[1]. Codex Alimentarius Commission, Standard for Infant Formula and Formulas for Special Medical Purposes Intended for Infants (CXS 72-1981), 2007

[2] AOAC International “Official Methods of Analysis of AOAC INTERNATIONAL (22nd ed.)”. Rockville, MD, USA: AOAC International 2003.

[3] ISO, “IEC 17043:2023 Conformity Assessment – General Requirements for Proficiency Testing” 2023. International Organization for Standardization (ISO), Geneva.

[4] Portugal, T.R., Udarbe, M.A., Ardeña, J.G., Castillo L.N., Mendez, S.T. “Provision of proficiency test (PT) scheme on proximate and mineral analyses: Philippine experience.” Journal of Food Composition Analysis, 2011, 24:656-662.

[5] Dajay, L.C., Portugal, T.R., Climaco, J.C., Parcon, M.R.V., Udarbe, M.A., Placio, R.E.E., Adona, P.E. Jr. “Establishment of proficiency testing progrmans in the Philippines. , 2019, Accred Qual Assur 24:65–71.

[6] World Health Organization. International code of marketing of breast-milk substitutes. World Health Organization; 1981.

[7] Portugal, T.R., Parcon, M.R.V., Udarbe, M.A. (2013) “Proficiency test on total dietary fiber in wheat flour” 2013, Int J Chem Eng Appl 4(2):82–87.

[8] Cotara, J.C., Dajay, L.C., Guerra, M.O., Martin, M.B., Laurea, J.C., Adona, P.E., Parcarey, M.G., Capili, C.Z. “Provision of chemical proficiency testing round on corn ‑ based snack food for laboratories in the Asia-Pacific”, 2022, Accred Qual Assur 27:165-179.

[9] International Organization for Standardization (ISO), “ISO 13528:2022, Statistical Methods for Use in Proficiency Testing by Interlaboratory Comparison”, 2022. Geneva, Switzerland.

[10] International Organization for Standardization (ISO). “ISO/IEC 17025:2017 — General requirements for the competence of testing and calibration laboratories” 2022. Geneva, Switzerland.

[11] Fearn, T. and Thompson, M., “A New Test for ‘Sufficient Homogeneity’,”.,Analyst, 2001, vol. 126, pp. 1414–1417.

[12] Thompson, M., Ellison, S.L.R., Wood, R. “The International harmonized protocol for the proficiency testing of analytical chemistry laboratories (IUPAC Technical Report)” 2006, Pure Appl Chem 78(1):145–196

[13] Luo, G., Zhu, Y., Ni, D., Chen, J.,Zhang, W., Mu, W., “Infant formula – Key components, nutritional value, and new perspectives” 2023. Food Chemistry, Volume 424.

2026 IMEKO Joint Conference
TC8 - TC11 - TC24
Metro Manila, Philippines, August 26-29, 2026

Forward and inverse risk geometry in conformity assessment: linking acceptance probability and conformance probability

Omar-Jair Purata-Sifuentes

Departamento de Estudios Organizacionales, Universidad de Guanajuato, Fraccionamiento 1, Colonia El Establo, Guanajuato 36250, México, opurata@ugto.mx

***Abstract* – Conformity assessment under measurement uncertainty can be viewed from two complementary perspectives. The forward view uses the acceptance probability $P_a(x)=P(Y_m \in A \mid X=x)$, conditioned on the true value x, whereas the inverse view, consistent with JCGM 106, uses the posterior conformity probability $p_c(y)=P(X \in C \mid Y_m=y)$, conditioned on the measured value y. This paper presents a compact dual framework linking both quantities through the joint model of production and measurement. For additive measurement error, $P_a(x)$ is shown to be a sliding-window finite-difference transform of the error cumulative distribution function, yielding a simple geometric interpretation of its extrema. In the normal-normal case, closed-form expressions are obtained for both $P_a(x)$ and $p_c(y)$. A guard-band example shows that the maximum of forward acceptance probability and posterior conformity probability need no coincide exactly, because they condition on different variables and incorporate different information. The framework thus provides a valuable conceptual link for risk-based conformity assessment.**

I. INTRODUCTION

Conformity assessment under measurement uncertainty is primarily a decision-making process. A measured value is compared to an acceptance interval, while the true value of the measurand is assessed against a tolerance interval. Since the true value cannot be directly observed, any decision to accept or reject an item is subject to the risk of making a false decision. This issue has been widely examined in metrology literature and formalized in risk-based approaches to decision rules [1-4].

A notably influential approach is provided by JCGM 106, which frames conformity assessment in probabilistic terms and develops decision rules that account for measurement uncertainty, acceptance intervals, and the risks associated with false decisions. Even when the framework remains foundational, recent work shows that the topic is still active and evolving. For example, Ramebäck et al. [5] showed that, even when a decision rule is fixed, the chosen uncertainty-evaluation method can materially affect conformity decisions when results lie near specification limits. Likewise, Orsay et al. [6] used guard-band methodology to establish acceptance limits in custody-transfer applications, emphasizing the practical importance of uncertainty-informed decision rules in high-consequence industrial settings.

In that *inverse* perspective, the key quantity is the posterior probability of conformity, and the specific risks for the consumer and producer are naturally derived from it. However, there is another equally valid perspective where one may instead condition on the true value of the item and ask for the probability that the decision rule will accept it. This *forward* probability of acceptance is common in operating characteristic reasoning, yet it is not always explicitly connected to the posterior viewpoint used in the JCGM framework [1].

The current work presents a concise dual interpretation of these two perspectives. The first quantity, $P_a(x) = P(Y_m \in A \mid X=x)$, is a forward acceptance probability conditioned on the true value. The second, $p_c(y) = P(X \in \mathrm{T} \mid Y_m=y)$, is an inverse conformity probability conditioned on the measured value. Although both quantities originate from the same joint model of production and measurement, they imply different geometries, various extrema, distinct interpretations of risk, and they induce different but related geometries of conformity assessment [5].

The objectives of this paper are threefold. First, to establish a concise dual framework linking $P_a(x)$ and $p_c(y)$. Second, to demonstrate that, in the additive-error case, the forward acceptance probability can be viewed as a simple geometric interpretation through a sliding-window finite-difference transform of the error cumulative distribution function. Third, to show that, under guard banding in the normal-normal scenario, the locations that maximize $P_a(x)$ and $p_c(y)$ may not precisely coincide. This paper aims to clarify the relationship between the JCGM 106:2012 approach with a forward formulation that is often implicitly used in risk-based analysis of decision rules [7].

II. NOTATION FOR CONFORMITY ASSESSMENT SETTING

Let X denote the true value of a scalar measurand associated with an item and let Y_m denote the corresponding measured value. Let the tolerance interval be $T = [T_L, T_U]$, so that an item is truly conforming if and only if $X \in T$. Let the acceptance interval be $A = [A_L, A_U]$, so that an item is accepted if and only if $Y_m \in A$. In general, A and T need not coincide but the use of guard bands generally leads to the case $A \subset T$.

Let $g_0(x)$ denote the process distribution of the true value X, and let $h(y \mid x)$ denote the conditional probability density of the measured value Y_m given $X = x$. The joint density of X and Y_m is therefore

$$f_{X,Y}(x, y) = g_0(x)h(y|x). \quad (1)$$

The marginal density of Y_m is

$$h_0(y) = \int_{-\infty}^{\infty} g_0(\xi)h(y|\xi)d\xi. \quad (2)$$

Whenever $h_0(y) > 0$, the posterior density of X given $Y_m = y$ is

$$g(x|y) = \frac{g_0(x)h(y|x)}{h_0(y)}. \quad (3)$$

Within this setting, two conditional probabilities are of special interest. The first is the probability of acceptance for an item with true value x:

$$P_a(x) = P(Y_m \in A|X = x) = \int_A h(y|x)dy. \quad (4)$$

The second is the posterior probability of conformity for an item with measured value y:

$$p_c(y) = P(X \in T|Y_m = y) = \int_T g(x|y)dx. \quad (5)$$

These two quantities are the core objects of this paper. Figure 1 illustrates both.

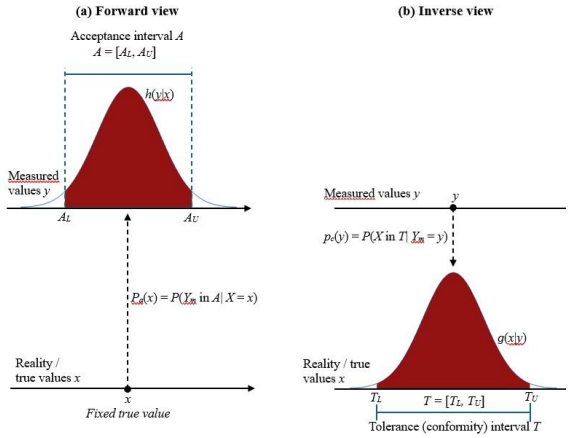


Fig. 1. Dual representation of conformity assessment.

III. THE DUAL FRAMEWORK

$P_a(x)$ and $p_c(y)$ originate from the same joint model, but they address different questions. The forward quantity $P_a(x)$ asks: if the true value was x, what is the probability that the decision rule would accept the item? The inverse quantity $p_c(y)$ asks: if the measured value was y, what is the probability that the item is truly conforming? This distinction is not just formal because it shapes the conditioning structure and the geometry of the problem. The forward formulation conditions on the true value and carries measurement uncertainty to the decision. Conversely, the inverse formulation conditions on the measurement result and gradually propagates process and measurement information backwards to the probability of conformity.

A. Premise 1

Define $P_a(x)$ and $p_c(y)$ by equations (4) and (5), respectively, combining equations (2) and (3) we get

$$g(x|y) = \frac{g_0(x)h(y|x)}{\int_{-\infty}^{\infty} g_0(\xi)h(y|\xi)d\xi}. \quad (6)$$

Then $P_a(x)$ is a forward acceptance operator and $p_c(y)$ is an inverse conformity operator associated with the same joint model. This result follows directly from the double factorization of the joint density $f_{X,Y}(x,y)$, forwards as shown by equation (1), and inverse as $h_0(y)g(x|y)$ (by combining equations (1) and (3)).

The dual nature of these operators also highlights their relationship with risk. In the JCGM-style inverse formulation, specific consumer and producer risks are expressed through $p_c(y)$, while the forward quantity $P_a(x)$ naturally results in integral expressions for global risks.

B. Premise 2

The global consumer's risk and global producer's risk can be written as

$$R_C = \int_{x \notin T} g_0(x)P_a(x)dx, \quad (7)$$

and

$$R_P = \int_{x \in T} g_0(x)[1 - P_a(x)]dx. \quad (8)$$

The global consumer's risk is the probability that an item is truly non-conforming and nevertheless accepted. Therefore,

$$R_C = P(X \notin T, Y_m \in A) = \int_{x \notin T} \int_A g_0(x)h(y|x)dydx. \quad (9)$$

Since the inner integral is $P_a(x)$, the stated form follows. The second expression is derived analogously from the event $X \in T$, $Y_m \notin A$.

This result is particularly significant for the present paper because it demonstrates that the forward operator is not external to the JCGM logic; rather it operates at the level of global risk, not posterior item-specific risk.

IV. GEOMETRIC PERSPECTIVE ON THE FORWARD OPERATOR

The forward acceptance probability becomes especially transparent under an additive measurement-error model. Assume

$$Y_m = X + E, \quad (10)$$

where E is a measurement error random variable with cumulative distribution function (CDF) F_E and density f_E, when the latter exists. Then the event $Y_m \in A$ is equivalent,

for fixed $X = x$, to $A_L - x \le E \le A_U - x$.

Hence,

$$P_a(x) = F_E(A_U - x) - F_E(A_L - x). \quad (11)$$

This representation allows for the straightforward interpretation that for each fixed x, the interval $[A_L - x, A_U - x]$ forms a window of constant width in the error domain, and $Pa(x)$ sizes the probability mass within that window. As x changes, the window moves rigidly along the error axis.

C. Premise 3

Assume the additive measurement model in equation (10) with acceptance interval A. If $w = A_U - A_L$ and $z = A_U - x$, then equation (11) becomes

$$P_a(x) = F_E(z) - F_E(z - w), \quad (12)$$

That is, P_a is a sliding-window finite-difference transform of the error CDF. This sliding-window view yields an immediate criterion for extrema.

D. Premise 4

If the error density exists, then

$P'_a(x) = f_E(A_L - x) - f_E(A_U - x)$.

Therefore, every critical point inside A satisfies

$f_E(A_L - x) = f_E(A_U - x)$.

When f_E is symmetric and unimodal about zero, then $P_a(x)$ attains its maximum at

$$x^* = (A_L + A_U) / 2, \quad (13)$$

at which arrives when differentiate equation (12) wrt x. If f_E is symmetric and unimodal about zero, the two window boundaries reach equal heights when the window is centered at zero, which results in $x^* = (A_L + A_U) / 2$.

This premise describes the extrema of $P_a(x)$ purely in geometric terms, given that the slope of the forward acceptance probability depends on the difference between the error density at the left and right edges of the moving window.

V. CLOSED FORM SOLUTIONS FOR THE NORMAL-NORMAL MODEL

To obtain explicit expressions for both the forward and inverse quantities, consider the conjugate normal-normal scenario

$$X \sim N(\mu_0, \sigma^2), \qquad Y_m \mid X = x \sim N(x, u_m^2).$$

The forward acceptance probability follows immediately from the normal measurement model

E. Premise 5

Under normal-normal model above,

$$P_a(x) = \Phi\left(\frac{A_U - x}{u_m}\right) - \Phi\left(\frac{A_L - x}{u_m}\right). \quad (14)$$

The posterior distribution of X given $Y_m = y$ is

$X \mid Y_m = y \sim N(\mu_{post}(y), \sigma_{post}^2)$,

with

$$\sigma_{post}^2 = \left(\frac{1}{\sigma_0^2} + \frac{1}{u_m^2}\right)^{-1},$$

and

$$\mu_{post}(y) = \sigma_{post}^2 \left(\frac{\mu_0}{\sigma_0^2} + \frac{y}{u_m^2}\right).$$

Therefore,

$$p_c(y) = \Phi\left(\frac{T_U - \mu_{post}(y)}{\sigma_{post}}\right) - \Phi\left(\frac{T_L - \mu_{post}(y)}{\sigma_{post}}\right). \quad (15)$$

This case is especially illustrative because both $P_a(x)$ and $p_c(y)$ are expressed as differences of Gaussian cumulative distribution functions. However, they are centered differently. The forward quantity is centered on the acceptance interval and the measurement error model, while the inverse quantity is centered on the tolerance interval and the posterior mean, which depends on the measured value and the process distribution. window.

VI. EXAMPLE OF MAXIMA'S NON-COINCIDENCE

Here we present a numerical example showing that the maximizer of $P_a(x)$ need not coincide exactly with the maximizer of $p_c(y)$.

Let the tolerance interval be $T = [-1, 1]$, and let the acceptance interval be guard banded inwards as $A = [-0.8, 0.8]$. Assume the process model $X \sim N(0.15, 0.55^2)$, and the measurement model $Y_m \mid X = x \sim N(x, 0.25^2)$.

Because the acceptance interval is symmetric about zero, Premise 4 equation (13) implies that the forward acceptance probability is maximized at $x^* = (-0.8 + 0.8)/2 = 0$. Thus, the true value that maximizes the chance of acceptance is the center of the acceptance interval.

Now, the posterior mean is

$$\mu_{post}(y) = \sigma_{post}^2 \left(\frac{0.15}{0.55^2} + \frac{y}{0.25^2}\right),$$

the measured value maximizing the posterior conformity probability $p_c(y)$ is the value y^* for which the posterior mean is centered in the tolerance interval, that is $\mu_{post}(y^*) = 0$. Solving for y^* gives

$$y^* = -\mu_0 \frac{u_m^2}{\sigma_0^2} = -(0.15)\frac{0.25^2}{0.55^2} = -0.031.$$

Hence, the two maxima are not numerically aligned, that is $x^* \neq y^*$. This example shows a quantitatively small difference, but conceptually significant (see Figure 2). The forward maximum depends on the geometry of the acceptance interval and the measurement error model. In contrast, the inverse maximum is based on the geometry of the tolerance interval and the posterior distribution, which includes the process prior. The guard band emphasizes this difference because acceptance and conformity are based on different operational intervals.

Figure 2 illustrates the guard banded decision rule with $A \subset T$. The maximum of the forward acceptance probability is centered on the acceptance interval, whereas the maximum of the posterior conformity probability is centered on the measured value that centers the posterior distribution within the tolerance interval.

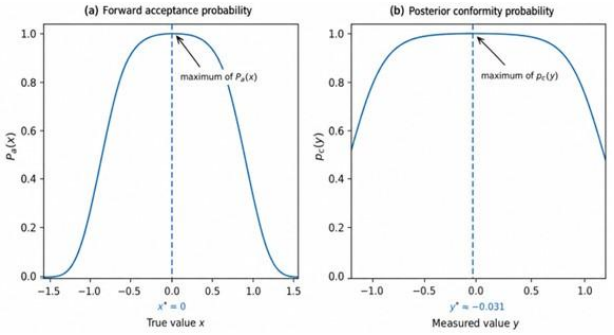


Fig. 2. Guardband comparison of maxima.

VII. DISCUSSION

The proposed framework facilitates reconciling two probability statements that are both common in conformity assessment but are conditioned on different variables. According to the JCGM 106 formulation, conformity assessment explicitly relies on tolerance limits, acceptance limits, and the associated risks of false acceptance and false rejection, with guarded acceptance and rejection considered as separate decision rules [1]. The guide also notes that reducing consumer's risk typically raises the producer's risk, so acceptance limits are set to balance these risks rather than minimize both at once [8].

From that perspective, the inverse quantity $p_c(y) = P(X \in \mathrm{T} \mid Y_m = y)$ is the suitable focus for item-specific post-measurement conformity statements. Conversely, the forward quantity $P_a(x) = P(Y_m \in A \mid X = x)$ is particularly useful when analyzing the operating behavior of a decision rule based on the true value or when calculating global risks by integrating over a production process. This distinction aligns with how JCGM 106 separates specific and global risks, utilizing the joint model of production and measurement to determine the latter [9].

Recent literature underscores the practical significance of this distinction. Orsay and de Oliveira's study on custody-transfer measurements demonstrate that guard-band methods continue to be crucial in high-stakes industrial environments, where uncertainty-based acceptance limits help minimize incorrect conformity judgments [10]. Their findings highlight that guard bands are practical tools, not just theoretical concepts, for enhancing decision accuracy in financially critical applications.

Recent application papers indicate that conformity-assessment behavior heavily relies on how uncertainty is modeled and propagated. For instance, Habibi et al. [11] demonstrate in a surface-metrology context that accounting for uncertainty in conformity assessment significantly influences decision outcomes, particularly when form deviation and uncertainty interact near specification limits. Likewise, Hernández-Vásquez et al. [12] show that incorporating additional uncertainty sources, like sampling, impacts the guard bands and consequently the final compliance decision. Martínez-Velázquez et al. [13] shows that conformity-assessment behavior, specifically global risks heavily depend on measurement traceability.

In this context, the dual formulation offers a valuable interpretive advantage. The forward quantity $P_a(x)$ is determined solely by the acceptance interval and measurement model, with its extrema influenced by the geometry of the sliding window over the error distribution. In contrast, the inverse quantity $p_c(y)$ depends not only on the tolerance interval but also on the posterior distribution, which includes prior or process information alongside measurement uncertainty. Therefore, the fact that the maxima do not align under guard banding is not contradictory; it stems from the two different conditioning structures. This view also aligns with ongoing discussions where acceptance limits and guard bands are seen as adjustable tools for managing decision risk, rather than being fixed by measurement uncertainty alone [10].

The guard-band example presented here is intentionally straightforward, yet it hints at several avenues for future exploration. Recent research has expanded conformity-assessment analysis into areas such as regression frameworks, performance metrics based on confusion matrices, and sector-specific optimization of acceptance limits. This progression indicates that the field is advancing toward more comprehensive models of risk and decision quality. Consequently, the dual forward/inverse approach introduced here can serve not only as a conceptual clarification but also as a foundation for future developments in analytical modeling, including asymmetric priors, non-Gaussian error models, and decision rules involving multiple parameters [10-13].

VIII. CONCLUSIONS

This paper presented a concise dual interpretation of conformity assessment under measurement uncertainty. The forward quantity $P_a(x)$ and the inverse quantity $p_c(y)$ are shown to be complementary operators based on the same joint model of production and measurement. In the case of additive errors, the forward acceptance probability can be understood geometrically as a sliding-window finite-difference transform of the error distribution. Specifically, in the normal-normal framework, both $P_a(x)$ and $p_c(y)$ have closed-form expressions, making their comparison straightforward. A numerical example with guard banding demonstrated that the value optimizing the forward acceptance probability might not align precisely with the value optimizing the posterior conformity probability. This discrepancy is expected, as it results from conditioning on different variables and using different sources of information. The suggested perspective could clarify the geometry of false decisions and serve as a helpful conceptual link between operating-characteristic reasoning and posterior conformance-based decision rules.

REFERENCES

[1] JCGM 106:2012, Evaluation of measurement data – the role of measurement uncertainty in conformity assessment (2012).

[2] A. Allard, N. Fischer, I. Smith, P. Harris, L. Pendrill, Risk calculations for conformity assessment in practice, Proc. of 19th Int. Congress of Metrology (2019) 16001. https://doi.org/10.1051/metrology/201916001

[3] G. Gómez, F.R. Lourenço, E.C. de Oliveira, Use of measurement uncertainty in conformity assessment and process capability indices in quality evaluation of pharmaceutical manufacturing processes, Chemometr. Intell. Lab. Syst. 264 (2025) 105470, http://dx.doi.org/10.1016/j.chemolab.2025.105470

[4] O.J. Purata-Sifuentes, F.J. Martínez-Velázquez, J.A. Báez-Macías, J.Y. Sánchez-Martínez, Decentered process effect on conformity assessment risks for manufacturing of non-automatic weighing instruments, Measurement 270 (2026). https://doi.org/10.1016/j.measurement.2026.120882

[5] H. Ramebäck, A. Tovedal, K. Norlin, On the significance of the measurement evaluation method in decision making: A synthesis of JCGM 101 and JCGM 106 applied to gross alpha and gross beta measurements using LSC, Applied Radiation and Isotopes 208 (2024). https://doi.org/10.1016/j.apradiso.2024.111282

[6] G.L. Orsay, R. Medeiros, E.C. de Oliveira, Conformity assessment applied to custody transfer in the oil and gas industry: A brief review, Acta IMEKO 14 (4) (2025) 1–8, http://dx.doi.org/10.21014/actaimeko.v14i4.2007

[7] Shirono, K., Takai, J., Tanaka, H. Economic optimisation of acceptance interval in conformity assessment for processes with known and unknown biases. Measurement 261 (2026). https://doi.org/10.1016/j.measurement.2025.119847

[8] L.R. Pendrill, Using measurement uncertainty in decision-making and conformity assessment, Metrologia 51 (2014) S206-S218. https://doi.org/10.1088/0026-1394/51/4/S206

[9] O.J. Purata-Sifuentes, E.A. Purata-Funes, G. Foyer, Overestimation of conformity assessment risks in legal requirements of weighing instruments, ACTA IMEKO 12 (2023). https://doi.org/10.21014/actaimeko.v12i3.1471

[10] Orsay, G. L., & de Oliveira, E. C. (2025). Robust approach connected to measurement uncertainty for establishing acceptance limits in custody transfer measurements within the oil and gas industry. Chemical Engineering Science, 318, 122248. https://doi.org/10.1016/j.ces.2025.122248

[11] Habibi, N., Jalid, A., Salih, A., Form Deviation Uncertainty and Conformity Assessment on a Coordinate Measuring Machine, Machines 12(10) (2024). https://doi.org/10.3390/machines12100704

[12] Hernández-Vasquez, J.D., de Oliveira, E.C., The Importance of Measurement Uncertainty Arising from the Sampling Process in Conformity Assessment: The Case of Fuel Quality, Metrology 5(1) pp.7 (2025). https://doi.org/10.3390/metrology5010007

[13] F.J. Martínez-Velázquez, J.A. Báez-Macías, J.Y. Sánchez-Martínez, O.J. Purata-Sifuentes, Consumer/producer risks for decentered NAWI's manufacturing processes, Measurement: Sensors 38 (2025) 101831. https://doi.org/10.1016/j.measen.2025.101831

2026 IMEKO Joint Conference
TC8 - TC11 - TC24
Metro Manila, Philippines, August 26-29, 2026

Validation of a Direct Saponification GC-FID Method for Cholesterol Determination in Foods

Michael C. Pelagio[1], Joan C. Duldulao[1], Sheryl O. Gulla[1], and Leah C. Dajay[1]

[1] *Department of Science and Technology – Food and Nutrition Research Institute (DOST-FNRI), DOST Compound, Gen. Santos Ave., Bicutan, Taguig City, Philippines,*
lightmichael13@gmail.com

***Abstract* – Accurate determination of cholesterol in foods supports public health protection by enabling informed, healthier dietary choices. It ensures accurate nutrition labeling and regulatory compliance in the Philippines. This study validated a gas chromatography–flame ionization detector (GC-FID) method for simplified cholesterol analysis across food matrices. The direct saponification technique enables a rapid and cost-efficient analysis in comparison to the traditional derivatization techniques.**

Method detection limit was established with LOD and LOQ values of 0.9930 mg/100g and 3.3100 mg/100g, respectively. Instrument-level sensitivity showed LOD and LOQ of 0.0077 mg/mL and 0.0081 mg/mL respectively. The method exhibited good linearity (r = 0.9949) across the calibration range (0.02-0.20 mg/mL). Accuracy was evaluated using NIST SRM 1869 and other quality control materials ranging from cereals, fish and meat-based matrices. Repeatability (6-8 replicates) results showed $\%RSD_r$ values from 1.66% to 4.66%, while intermediate precision (6-7 days) had acceptable $\%PRSD_R$ ranging from 2.78% to 5.40. Assessment of trueness demonstrated that all matrices are within respective acceptable ranges. The computed percentage of recoveries ranges from 95-104%. Method performance was further supported by satisfactory participation in BIPEA proficiency testing, with z-scores of −0.56 and -0.87 (Cordon Bleu 2024 and 2026 round), +0.32 (Butter Biscuits) and −1.25 and +0.60 (Clinical Nutrition Cream 2024 and 2026 round). Overall, the validated method demonstrated fitness for purpose, providing reliable and comparable cholesterol measurements across diverse food matrices. Continued participation in proficiency testing programs is recommended to further strengthen measurement comparability and long-term analytical performance.

I. INTRODUCTION

Cholesterol content in foods remains a critical parameter in evaluating dietary exposure to lipids associated with cardiovascular diseases [1]. Reliable analytical measurements are therefore necessary to support public health initiatives, food composition databases, regulatory monitoring, and product development. In the Philippine context, laboratories are expected to generate results that are not only accurate but also comparable across institutions, particularly for nutrition labeling and compliance assessment.

Gas chromatography with flame ionization detection (GC-FID) is widely used for cholesterol determination due to its sensitivity and robustness. However, many established methods rely on derivatization, which increases analytical complexity and may introduce additional variability [2]. Direct saponification without derivatization offers a simplified alternative by reducing sample preparation steps while maintaining analytical integrity [3,4].

From a metrological perspective, analytical methods must demonstrate fitness for purpose through validation of key performance characteristics such as detection capability, linearity, precision, and trueness [5,6]. The use of certified reference materials (CRMs) and quality control reference materials supports traceability, while proficiency testing (PT) provides evidence of interlaboratory comparability [7]. This study evaluates a direct saponification GC-FID method for cholesterol determination in wide variety of food matrices. Focusing primarily on analytical performance and its suitability for routine laboratory application..

II. MATERIALS AND METHODS

A. Preparation of Standards

A cholesterol stock solution (20 mg/mL) was prepared by accurately weighing 0.20 g of cholesterol standard (>99% purity) into a 10 mL volumetric flask and dissolving in toluene, followed by dilution to volume. Similarly, an internal standard stock solution of 5α-cholestane (10 mg/mL) was prepared by accurately weighing 0.10 g of 5α-cholestane (>99% purity) and diluting to 10 mL with toluene.

The preparation scheme for working and calibration

solutions was adapted from a previously reported method [4]. A mixed working solution (Standard A, 2.0 mg/mL) was prepared by combining 0.10 mL of the cholesterol stock solution and 0.01 mL of the 5α-cholestane stock solution, and diluting to 1 mL with toluene.

Two additional working solutions of the internal standard were prepared from the 5α-cholestane stock solution. Standard B (0.1 mg/mL) was used in the preparation of calibration standards, while Standard C (1.0 mg/mL) served as the internal standard solution for the sample. Calibration standards were prepared by combining varying volumes of Standard A and Standard B to achieve the desired concentration range, as summarized in Table 1.

Table 1. Preparation of calibration of standards

Concentration, mg/mL	Volume of Standard A, mL	Volume of Standard B, mL
0	0	1
0.02	0.01	0.99
0.04	0.02	0.98
0.06	0.03	0.97
0.08	0.04	0.96
0.10	0.05	0.95
0.12	0.06	0.94
0.14	0.07	0.93
0.16	0.08	0.92
0.18	0.09	0.91
0.20	0.10	0.90

B. Sample Preparation and Direct Saponification

A test portion of 0.2–0.3 g was used for reference materials (RMs) with medium to high cholesterol content while larger test portion of 0.5 g was used for low-cholesterol content reference materials, including selected RMs and nonfat milk, to ensure adequate analyte detectability. Samples were analyzed in triplicate to assess intermediate precision. Trueness was assessed using at least duplicate samples, whereas repeatability was established through 6-8 replicates. Each test portion was accurately weighed into 15 mL screw-capped tubes prior to the analysis. The method for direct saponification was adapted from a published research article where the method was validated for the analysis of milk and milk products [3]. The procedure commenced by adding 5 mL of freshly prepared 0.5 M methanolic KOH solution to each sample. The tubes were tightly sealed and incubated in a water bath maintained at 80 °C ± 2 °C for 15 minutes. To ensure uniform heat distribution and prevent the clumping of samples, the tubes were vigorously mixed for approximately 10 seconds at 5-minute intervals during incubation. After saponification, the samples were cooled in an ice bath for 15–20 minutes prior to extraction.

Extraction was performed by adding 1 mL of cold distilled water followed by 5 mL of n-hexane. The mixture was agitated for 1 minute using vortex mixer (5000 rpm) to facilitate analyte partitioning. The phases were allowed to separate, and the upper hexane layer was carefully collected into a vial containing a small amount of anhydrous sodium sulfate to remove residual moisture. The extraction step was repeated to ensure complete recovery of cholesterol. Eight (8) mL-portion of the combined extract were transferred to a 250-mL round bottom flask. It was then evaporated to dryness by using rotary evaporator set at 30℃. Reconstitute the dried extract using 2 mL of toluene then transfer to a dry vial and cap tightly.

An aliquot of 0.5–0.9 mL of the reconstituted extract was transferred into a high-recovery GC vial. The volume of aliquot depends on the expected cholesterol concentration of the reference material. Subsequently, 0.10 mL of Standard C (internal standard solution) was added, and the mixture was diluted to a final volume of 1 mL using toluene. The prepared samples were mixed thoroughly and analyzed immediately to minimize potential analyte degradation or variability.

C. GC-FID Parameters

Analysis of cholesterol in sample extracts were done using gas chromatography (Shimadzu GC-2014) equipped with flame ionization detector. The carrier gas was helium while the auxiliary gas was nitrogen. Table 2 shows the summary of the optimized parameters.

Table 2. Summary of optimized GC-FID parameters

Parameter	Settings
Capillary Column	Teknokroma (TRB-50, (50%) Diphenyl-(50%) dimethyl polysiloxane), 10 m x 0.1 mm x 0.1 μm
Injection Volume	2 μL
Injection Temperature	260℃
Detector Temperature	300℃
Oven Temperature Programming	Set initial temperature at 260 °C then hold for 1 minute, raise to 300 °C at a rate of 2 °C/min then hold for 4 minutes
Total Run Time	13 minutes
Split Ratio	1:250
Column Flow	0.55 mL/min

The performance of the instrument was checked by triplicate injections of 0.10 mg/mL of calibration standard. The %RSD of the averaged peak ratio and retention times of both standard and internal standard were established at <4% and <0.5% respectively. Routine performance check was regularly conducted after instrument start up to ensure that the entire system will correctly analyze the sample components. Reagent blanks were first loaded followed by calibration standards then the batches of samples. Two injections per replicate were made for all sample reference materials.

D. Results Calculation

The generated chromatograms for every run were processed to give the peak areas of 5α-cholestane and cholesterol. Peak ratio was calculated using the equation:

$$\text{peak ratio} = \frac{Peak\ Area\ Cholesterol}{Peak\ Area\ 5\alpha-cholestane} \quad (1)$$

The concentration of cholesterol (in mg/mL) was computed using the variables generated equation of the line:

$$\text{cholesterol (mg/mL)} = \frac{mean\ peak\ ratio - y\ intercept}{slope} \quad (2)$$

Finally, the amount cholesterol in mg/100 g of sample RMs can be determined by using the equation:

$$\text{mg/100g sample} = \frac{cholesterol\left(\frac{mg}{ml}\right) \times total\ volume}{sample\ weight \times DF} \times 100 \quad (3)$$

where DF was the overall dilution factor used throughout the analysis.

E. Experimental Design of the Method Validation

A range of certified reference materials (CRMs), and quality control reference materials were selected to represent diverse food matrices and cholesterol concentration levels as shown in Table 3.

Table 3. List of reference materials used in the validation

Reference Material	Cholesterol (mg/100 g)
SRM 1869 Infant/Adult Nutritional Formula	12.55 – 13.49
FAPAS Mixed Fat Spread T14285QC	90 - 126
FAPAS Biscuit Cookie T14266QC	25.2 – 35.1
BIPEA Fish	10.76 – 32.32
BIPEA Cordon Bleu	31.0 – 58.6
FNRI PT 23-01 Processed Meat	15.0 – 41.0
FNRI RM 19-01 Lyophilized Fish	139 - 233

The selection aimed to cover low- to high-fat matrices, processed foods, and complex compositions to evaluate method performance under realistic analytical conditions. Commercially available nonfat milk was used exclusively for the determination of method detection capability due to its low cholesterol.

Validation parameters included working range, linearity, limits of detection (LOD), limits of quantification (LOQ), precision, and accuracy. Working range was established from the lowest detectable concentration up to 10-times this level to ensure suitability for routine analysis as previously shown in Table 1. Linearity was assessed using calibration standards across the working range, with evaluation based on the correlation coefficient (r), slope, and intercept of the calibration curve. Detection capability was determined by analyzing 10 replicates of the lowest concentration calibration standard. The LOD and LOQ were calculated using signal-based approaches as follows:

$$\text{LOD} = \frac{(mean\ response + 3s_0') - intercept}{slope} \quad (4)$$

$$\text{LOQ} = \frac{(mean\ response + 10s_0') - intercept}{slope} \quad (5)$$

where s_0' represents the standard error of the response, calculated as the standard deviation of replicate measurements divided by the square root of the number of replicates (n).

In addition, method detection capability was evaluated using ten replicates of commercial nonfat milk as sample with low concentration of cholesterols. The method LOD and LOQ were calculated using:

$$LOD = 3 \times s_0' \quad (6)$$

$$LOQ = 10 \times s_0' \quad (7)$$

$$\text{where: } S_0' = \sqrt{1/n + 1/n_b} \quad (8)$$

n = number of replicates in routine analysis
n_b = number of blank observations

Precision was evaluated in terms of repeatability and intermediate precision. Repeatability was assessed by analyzing 7 replicate samples within a single day and expressed as percent relative standard deviation %RSDr:

$$\%RSD_r = \frac{Standard\ Deviation\ of\ Results}{Mean\ of\ Results} \times 100 \quad (9)$$

Intermediate precision was determined by analyzing triplicate samples over 6–8 days. The observed reproducibility was evaluated against the predicted relative standard deviation, $\%PRSD_R$ estimated using the Horwitz equation [7]:

$$\%PRSD_R = = 2C^{-015} \quad (10)$$

where C is the mass fraction of cholesterol in the sample. Acceptance criteria for precision were based on comparisons between observed $\%RSDR_r$ and predicted $\%PRSD_R$ values as summarized in Table 4. The values were based in AOAC [8].

Table 4. Summary of mass fraction and acceptance criteria for precision

Analyte, %	Mass Fraction (C)	$\%RSD_r$	$\%PRSD_R$	% Recovery
1	10^{-2}	2.7	4	97 - 103
0.1	10^{-3}	3.7	6	95 - 105
0.01	10^{-4}	5.3	8	90 - 107

Trueness was evaluated by comparing the average of measured values from at least 2 replicates with the assigned or certified values provided in the certificates of analysis of the reference materials and expressed as percent recovery. It was computed using the following equation:

$$\%\text{Recovery} = \frac{Mean\ of\ Results}{Reference\ Value} \times 100 \quad (11)$$

The validated method was further tested through participation in BIPEA proficiency testing schemes, providing independent evidence of method performance and interlaboratory comparability.

III. RESULTS AND DISCUSSIONS

A. System Performance and Chromatographic Behavior

System suitability tests demonstrated stable instrument performance, with %RSD values for peak area ratios below 4% and retention time variability within 0.5%, meeting commonly accepted criteria for GC-based quantitative methods [9,10]. Cholesterol and internal standard (5α-cholestane) were well-resolved under the optimized GC-FID conditions, with no observable co-eluting interferences as shown in Figures 1-2.

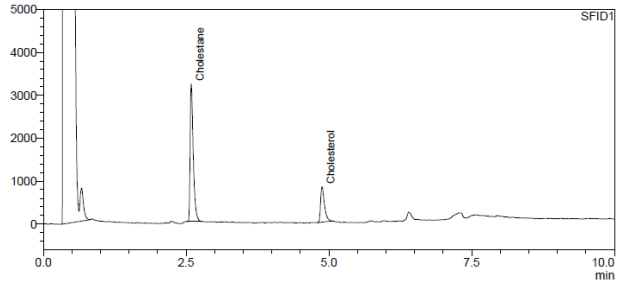


Fig. 1 Sample chromatogram of BIPEA Cordon Bleu showing medium concentration of cholesterols

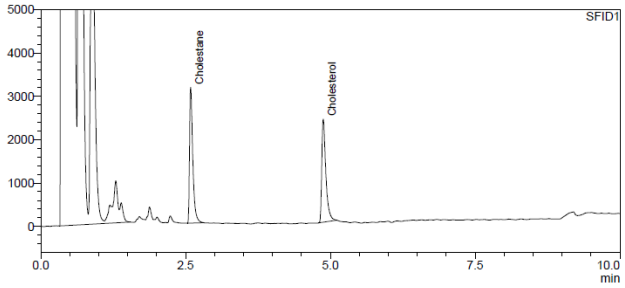


Fig. 2. Sample chromatogram from FNRI RM 19-01 Lyophilized Fish showing high concentration of cholesterols

This confirms the selectivity of the method despite the absence of derivatization, consistent with previous studies showing that direct saponification can yield clean chromatographic profiles for cholesterol analysis [3,4]. The relatively short analysis time (13 minutes) further supports the method's suitability for routine applications.

B. Linearity and Working Range

The method exhibited good linearity across the calibration range of 0.02 to 0.20 mg/mL. The averaged correlation coefficient (r = 0.9949) indicates an acceptable linear relationship between peak area ratio and analyte concentration.

The selected working range was found to be appropriate for the cholesterol levels encountered in the reference materials. This ensures that the method is suitable for both low- and high-cholesterol food matrices without requiring excessive dilution or concentration adjustments.

C. Detection Capability

The instrument detection limits (LOD = 0.0077 mg/mL; LOQ = 0.0081 mg/mL) demonstrate sufficient sensitivity for chromatographic detection. Method-level detection capability, evaluated using nonfat milk, yielded LOD and LOQ values of 0.9930 mg/100 g and 3.3100 mg/100 g, respectively.

These values are adequate for routine food analysis, particularly considering that most processed and animal-based food products contain cholesterol levels well above the method LOQ [11]. The use of a low-cholesterol matrix for method detection evaluation provides a realistic estimate of sensitivity under actual analytical conditions.

D. Precision

Repeatability results shown in Table 5 with ranging from %RSDr of 1.66 to 4.66% which fall within AOAC-recommended limits for analyte concentrations in the evaluated range [7]. These values indicate good short-term precision and reflect consistent sample preparation, extraction, and instrumental performance.

Intermediate precision reflects variability across

multiple days and analytical runs. All results derived from the Horwitz equation were within acceptable or expected ranges of $\%PRSD_R$. The Horwitz function is widely used as a benchmark for interlaboratory precision and provides a realistic expectation of variability in chemical measurements [5]. The observed agreement indicates that the method performs within established precision criteria for food analysis.

Table 5. Summary of mass fraction and acceptance criteria for precision (N= number of replicates)

Reference Material	$\%RSD_r$	$\%PRSD_R$	%Recovery
SRM 1869 Infant/Adult Nutritional Formula	1.66 (N=8)	5.40 (N=6)	102 (N=6)
FAPAS Mixed Fat Spread T14285QC	3.58 (N=7)	2.56 (N=6)	104 (N=6)
FAPAS Biscuit Cookie T14266QC	4.28 (N=7)	4.81 (N=7)	95 (N=7)
BIPEA Fish	4.66 (N=6)	5.00 (N=7)	104 (N=7)
BIPEA Cordon Bleu	2.45 (N=7)	4.49 (N=7)	101 (N=7)
FNRI PT 23-01 Processed Meat	4.19 (N=8)	4.71 (N=7)	102 (N=2)
FNRI RM 19-01 Lyophilized Fish	1.35 (N=7)	2.78 (N=6)	103 (N=6)

E. Trueness or Accuracy

Recoveries ranging from 95% to 104% as shown in Table 5, demonstrate acceptable trueness and compliance with AOAC criteria [8]. The close agreement between measured and certified values confirms the absence of significant systematic bias.

These results indicate that direct saponification effectively releases cholesterol without compromising accuracy, supporting findings from previous studies [1,2].

F. Measurement Comparability

Participation in BIPEA proficiency testing yielded satisfactory z-scores across similar food matrices as summarized in Table 6 which were all within the acceptable range ($|z| \leqslant 2$) defined in ISO 13528 [5]. These results confirm good agreement with consensus values and demonstrate interlaboratory comparability. Proficiency testing provides independent verification of analytical performance and is a critical component in ensuring measurement reliability and traceability [4,5].

Table 6. Summary of PT Participations from BIPEA

PT Round	z score	Adjectival Performance
Butter Biscuit (2023)	-0.56	Satisfactory
Cordon Bleu (2024)	+0.32	Satisfactory
Clinical Nutrition Cream (2024)	-1.25	Satisfactory
Clinical Nutrition Cream (2026)	+0.60	Satisfactory

IV. CONCLUSION

The direct saponification GC-FID method for cholesterol determination in foods has been demonstrated to be fit for purpose through a comprehensive validation approach. The method showed acceptable performance in terms of detection, linearity, precision, and trueness across a wide range of food matrices. The use of certified and quality control reference materials provided evidence of measurement traceability, while satisfactory results from proficiency testing confirmed interlaboratory comparability in accordance with ISO 13528.

The simplified analytical workflow, achieved through the elimination of derivatization, reduces labor intensive procedures and potential sources of variability without compromising measurement quality. This enhances the method's suitability for routine implementation in laboratories requiring reliable and efficient cholesterol analysis.

The findings of this study significantly strengthen the reliability of analytical data used for nutrition labeling, regulatory compliance, and food composition studies. The direct saponification method serves as a practical robust tool for advancing the reliability, comparability, and traceability of cholesterol analysis.

To ensure sustained method performance and international comparability, continued participation in local and global proficiency testing schemes is recommended. Additionally, future work may focus on expanding validation to a broader range of complex food matrices and refining measurement uncertainty estimation to further align with international metrological requirements.

V. REFERENCES

[1]. Carson, A., Lichtenstein, A.H., . Anderson, C.A.M., Appel, A.J., Kris-Etherton, P.M., Meyer, K.A.,

Petersen, K., Polonsky, T. and Van Horn, L. “Dietary cholesterol and cardiovascular Risk: a Science Advisory from the American Heart Association”, Circulation, 141, 2020, pp. E39-E53.

[2] Srigley, C. T., & Mossoba, M. M. “Current analytical methods for the determination of cholesterol in foods” Journal of AOAC International, 2007,100(2), 306–313.

[3] Fletouris, D. J., Botsoglou, N. A., Psomas, I. E., and Mantis, A. I. “Rapid determination of cholesterol in milk and milk products by direct saponification and capillary gas chromatography”. Journal of Dairy Science, 1998, 81(11), 2833–2840.

[4] Dinh, T.T.N., Thompson, L.D., Galyean, M.L. and Brooks, J.C. “Determination of Total Cholesterol in Meat and Poultry by Gas Chromatography: Single-Laboratory Validation”. Journal of AOAC International, 2012, 95(2), 472-488.

[5] International Organization for Standardization (ISO). (2017). ISO/IEC 17025:2017 — General requirements for the competence of testing and calibration laboratories.

[6] Eurachem. (2014). The Fitness for Purpose of Analytical Methods: A Laboratory Guide to Method Validation and Related Topics (2nd ed.).

[7] International Organization for Standardization (ISO). (2022). ISO 13528:2022 — Statistical methods for use in proficiency testing by interlaboratory comparison.

[8] AOAC International. (2023). Appendix F: Guidelines for Standard Method Performance Requirements. In: Official Methods of Analysis of AOAC INTERNATIONAL (22nd ed.). Rockville, MD, USA: AOAC International.

[9] United States Pharmacopeia (USP). General Chapter <621> Chromatography. Rockville, MD: United States Pharmacopeial Convention; 2021. Available at: USP Chromatography Chapter (PDF)

[10] Agilent Technologies. Evaluating System Suitability: CE, GC, LC and A/D ChemStation. Agilent Technologies; 2003. Available at: https://www.agilent.com/cs/library/support/documents/a10424.pdf

[11] Department of Science and Technology-Food and Nutrition Research Institute (DOST-FNRI). 2022. Philippine Food Composition Table (PhilFCT) Online Database. iFNRI Website. Retrieved April 27, 2026, from http://i.fnri.dost.gov.ph/fct/library

2026 IMEKO Joint Conference
TC8 - TC11 - TC24
Metro Manila, Philippines, August 26-29, 2026

Multivariate Analysis of PFOS and PFOA Migration Measurements Using Principal Component Analysis (PCA)

David Jaucian Alcarde Jr.[1], Elyson Keith P. Encarnacion[2], Anne C. Alcantara[3], Harold E. Armario[4], April Star L. Canonizado[5], Agaseve F. Del Rosario[6], Winnie P. Alejandro[7], Rizel Marie S.M. Ting[8], Kim Angelene R. Tagle[9], Daniela Marie D. Barredo[10], Jeric B. Bañadera[11], Josefino Antonio T. Mendoza[12]

[1,2,3,6,7,8,9,10,11,12]*Packaging Technology Division, Industrial Technolgy Development Institute, Department of Science and Technology (DOST-ITDI), Bicutan, Taguig, Metro Manila, Philippines 1631*

[4] *Standards and Testing Division, Industrial Technolgy Development Institute, Department of Science and Technology (DOST-ITDI), Bicutan, Taguig, Metro Manila, Philippines 1631*

[5] *National Metrology Division, Industrial Technolgy Development Institute, Department of Science and Technology (DOST-ITDI), Bicutan, Taguig, Metro Manila, Philippines 1631*

Corresponding email: da6914@rit.edu

***Abstract* – Understanding variability in chemical migration measurements is essential for ensuring data reliability in laboratory and regulatory contexts. This study applies Principal Component Analysis (PCA) to investigate the multivariate structure of perfluorooctane sulfonate (PFOS) and perfluorooctanoic acid (PFOA) migration data obtained from multi-analyst replicate measurements across low, medium, and high concentration levels. The first principal component (PC1) explained 98.79% of the total variance, indicating that variability is predominantly driven by concentration level. The second principal component (PC2) accounted for only 1.21%, reflecting minor residual variability. PCA score plots showed clear separation by concentration level, while slight analyst-related variation was observed along PC2, indicating minor operator-dependent effects relative to the dominant concentration-driven variability. These results demonstrate that variability is primarily systematic and that PCA provides an effective tool for interpreting measurement behavior in PFAS migration studies.**

I. INTRODUCTION

Per- and polyfluoroalkyl substances (PFAS), including perfluorooctane sulfonate (PFOS) and perfluorooctanoic acid (PFOA), are widely recognized as persistent environmental contaminants with potential risks to human health [1]–[4]. Their presence in food-contact materials has raised increasing concern due to the possibility of migration into food and beverages, thereby contributing to human exposure [5]–[8]. As a result, reliable measurement of PFAS migration is essential for regulatory compliance, exposure assessment, and risk evaluation. Analytical determination of PFOS and PFOA in migration studies typically involves low-level concentration measurements, often performed under controlled experimental conditions using standardized protocols [5], [9]–[11]. However, such measurements are subject to multiple sources of variability, including differences in concentration levels, analytical repeatability, and operator-related factors. Understanding the relative contributions of these sources is critical for ensuring the reliability and interpretability of analytical results, particularly in the context of regulatory decision-making.

Conventional approaches to evaluating measurement performance, such as univariate statistical analysis, may be limited in their ability to capture complex relationships among variables in multi-analyte datasets [12], [13]. In particular, when measurements are influenced by multiple factors—such as concentration levels and analyst variability—there is a need for analytical tools capable of simultaneously evaluating these effects. Multivariate statistical techniques provide a framework for exploring such relationships and identifying dominant patterns in the data.

Principal Component Analysis (PCA) is a widely used multivariate method for dimensionality reduction and

pattern recognition [14], [15]. By transforming correlated variables into a set of orthogonal principal components, PCA enables the identification of the main sources of variation within a dataset while preserving most of the original information. In chemical measurement contexts, PCA has been applied to evaluate analytical performance, detect anomalies, and interpret complex datasets where multiple factors influence measurement outcomes [16], [17]. In the context of PFAS migration analysis, the application of PCA offers an opportunity to distinguish between variability arising from experimental design—such as concentration levels—and variability associated with measurement processes [14]. Such differentiation is particularly important in metrological studies, where the ability to separate systematic variation from potential measurement inconsistencies is essential for ensuring data quality and traceability.

This study aims to apply Principal Component Analysis to PFOS and PFOA migration measurement data obtained from multi-analyst replicate experiments across different concentration levels. The objective is to characterize the multivariate structure of the dataset, identify the dominant sources of variability, and assess the extent to which measurement variability is influenced by concentration and operator effects. The findings are intended to provide insights into measurement behavior and to support improved interpretation of PFAS migration data in chemical testing laboratories.

II. MATERIALS AND DATA DESCRIPTION

A. Measurement context and measurand definition

The dataset analyzed in this study consists of laboratory-generated migration measurements of perfluorooctane sulfonate (PFOS) and perfluorooctanoic acid (PFOA) from paper-based food packaging materials. These materials were evaluated due to increasing concerns regarding the potential migration of per- and polyfluoroalkyl substances (PFAS) from food-contact packaging into food and beverages, which may contribute to human exposure. The measurand is defined as the surface migration level of PFOS and PFOA, expressed as mass per unit contact area (ng/100 cm²), determined under controlled laboratory conditions representative of routine migration testing for food-contact materials. Each reported value reflects the outcome of a measurement process influenced by multiple sources of variability, including analyte-specific behavior, sample preparation, instrument response, and analyst-dependent effects.

Migration measurements were obtained from paper-based food packaging materials under controlled laboratory testing conditions representative of routine PFAS migration analysis. Samples were prepared at low, medium, and high concentration levels and subjected to migration testing following standardized laboratory procedures. Quantification of PFOS and PFOA was performed using liquid chromatography–tandem mass spectrometry (LC-MS/MS). Migration levels were expressed as surface concentration in ng/100 cm². Measurements were performed independently by three analysts using the same analytical protocol and instrumentation. Replicate measurements were conducted for each condition to evaluate repeatability and analyst-dependent variability.

B. Dataset structure and experimental factors

The dataset comprises 48 migration measurements of perfluorooctane sulfonate (PFOS) and perfluorooctanoic acid (PFOA) obtained from paper-based food packaging materials under multiple experimental conditions. The experimental factors include the analyte (PFOS and PFOA), the analyst (three operators: ASLC, HEA, and WPA), and the concentration regime, categorized into low (L), medium (M), and high (H) levels. Within each analyte–regime combination, replicate measurements were performed, typically in triplicate, to assess repeatability. Each observation is associated with a sample code (e.g., L1, M2, H3), indicating the concentration regime and replicate index.

The dataset exhibits a partially balanced structure, with low-level measurements available for two analysts, while medium- and high-level measurements were available for all three analysts. For PCA, each observation was represented as a paired measurement consisting of PFOS and PFOA concentration values expressed in ng/100 cm². Although the dataset includes additional information such as analyst identity, concentration regime, sample code, and replicate number, these variables were not used as input variables in the PCA model. Instead, they were retained solely as descriptive metadata to support interpretation and visualization of clustering behavior in the PCA score plots.

C. PCA Input Matrix and Data Representation

To avoid ambiguity regarding the PCA computation, this section explicitly defines the structure of the input matrix and distinguishes the quantitative variables used in the analysis from the metadata used solely for interpretation. For Principal Component Analysis (PCA), the dataset was represented as a two-variable input matrix consisting exclusively of PFOS and PFOA concentration measurements. Each row of the matrix corresponds to a single observation obtained under a specific analyst, concentration regime, and replicate condition, while the two columns correspond to the measured concentrations of PFOS and PFOA expressed in ng/100 cm².

Prior to PCA, the concentration variables were standardized to remove scale effects and ensure equal contribution of both analytes to the model. Analyst identity, concentration regime, sample code, and replicate number were not included in the PCA computation. Instead, these variables were retained solely as descriptive

metadata to support post hoc labeling and interpretation of clustering patterns in the PCA score plots. A summary of the PCA input variables and associated metadata is presented in Table 1.

Table 1. Summary of PCA Input Variables and Metadata for PFOS and PFOA Migration Measurements

Category	Variable	Description
PCA input variable	PFOS	PFOS concentration (ng/100 cm^2)
PCA input variable	PFOA	PFOA concentration (ng/100 cm^2)
Metadata	Concentration level	Low (L), Medium (M), High (H)
Metadata	Analyst	ASLC, HEA, WPA
Metadata	Replicate	Repeated measurements per condition
Metadata	Sample code	Identifier (e.g. L1, M2, H3)

As shown in Table 1, only PFOS and PFOA concentration measurements were used as quantitative input variables for PCA, while all other variables served as descriptive metadata for interpretation of clustering patterns. This data representation provides the basis for the multivariate analysis and preprocessing procedures described in the following section.

III. METHODS

A. Data Preparation and Preprocessing

Prior to multivariate analysis, the dataset was prepared to ensure consistency and comparability between variables. Observations corresponding to PFOS and PFOA measurements obtained under the same experimental conditions (i.e., identical analyst, concentration regime, and replicate index) were paired and represented as joint variables within a single observation. Only complete paired observations were retained for subsequent analysis. To eliminate the influence of differences in measurement scale and magnitude between analytes, the data were standardized using z-score normalization. For each variable, the mean was subtracted and the result divided by the corresponding standard deviation. This transformation ensures that both PFOS and PFOA contribute equally to the multivariate analysis and prevents dominance of variables with larger numerical ranges

B. Principal Component Analysis

The first principal component (PC1) captures the maximum variance present in the dataset, while subsequent components (e.g., PC2) account for progressively smaller portions of the remaining variance. The PCA model was constructed using a covariance-based approach applied to the standardized data matrix. The analysis produced scores, representing the projection of each observation onto the principal components, and loadings, which describe the contribution of each original variable to the principal components. Explained variance ratios were computed to quantify the proportion of total variance captured by each principal component and to assess their relative importance in describing the dataset.

C. Visualization and Interpretation of Principal Components

The results of the PCA were examined through graphical visualization to facilitate interpretation of patterns and relationships within the dataset. Score plots of the first two principal components (PC1 versus PC2) were generated to evaluate clustering behavior and potential grouping of observations according to concentration regime and analyst. Separation of observations along PC1 was interpreted in relation to systematic variation associated with concentration levels, while dispersion along PC2 was examined to identify residual variability and potential secondary effects. Loading plots were used to assess the contribution and correlation of PFOS and PFOA to the principal components, with the direction and magnitude of loadings providing insight into the variables driving the observed patterns.

C. Computational Tools

All data processing and multivariate analyses were performed using Python. Standard scientific computing libraries were used for data manipulation, statistical analysis, and visualization. PCA was implemented using established numerical algorithms for eigenvalue decomposition of the covariance matrix, and graphical outputs were generated to produce publication-quality figures.

IV. RESULTS AND DISCUSSIONS

A. Principal Component Structure and Explained Variance

Principal Component Analysis (PCA) was applied to the standardized dataset to evaluate the dominant sources of variability in PFOS and PFOA migration measurements. The proportion of variance explained by each principal component is summarized in Table 2.

Table 2. Explained Variance and Interpretation of Principal Components

Principal Component	Explained Variance (%)	Interpretation

PC1	98.79	Dominant variability driven by concentration levels
PC2	1.21	Minor residual variability (secondary effects)

The results show that the first principal component (PC1) accounts for 98.79% of the total variance, while the second principal component (PC2) explains only 1.21%. This strong dominance of PC1 indicates that the multivariate structure of the dataset is effectively governed by a single underlying factor. From a measurement perspective, this suggests that the observed variability is primarily systematic rather than random, with most variation attributable to structured experimental conditions. To further investigate the nature of this dominant variability, the distribution of observations in the principal component space is examined through PCA score plots.

B. Interpretation of Principal Components

The PCA score plot colored by concentration level (Figure 1) provides direct insight into the dominant source of variability.

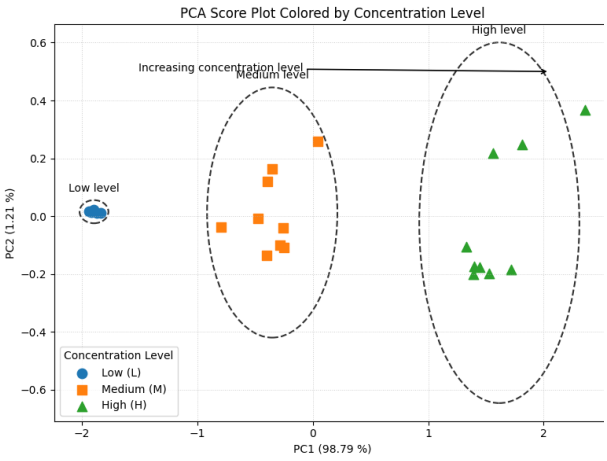


Figure 1. PCA Score Plot (Colored by Concentration Level).

Clear separation of low (L), medium (M), and high (H) concentration measurements is observed along PC1, which explains 98.79% of the total variance. As shown in Figure 1, observations corresponding to low, medium, and high concentration levels form well-separated clusters along PC1. This separation confirms that concentration level is the dominant source of variability in the dataset. The nearly linear ordering of clusters along PC1 further indicates that the principal component effectively represents a gradient of increasing concentration. In contrast, dispersion along PC2 is limited and does not exhibit systematic grouping, suggesting that residual variability is minimal and not strongly associated with any primary experimental factor. This observation reinforces the interpretation that variability is governed primarily by controlled experimental conditions rather than measurement instability.

C. Correlation Structure of PFOS and PFOA

To understand how individual variables contribute to the observed variability, the PCA loadings plot is examined in Figure 2.

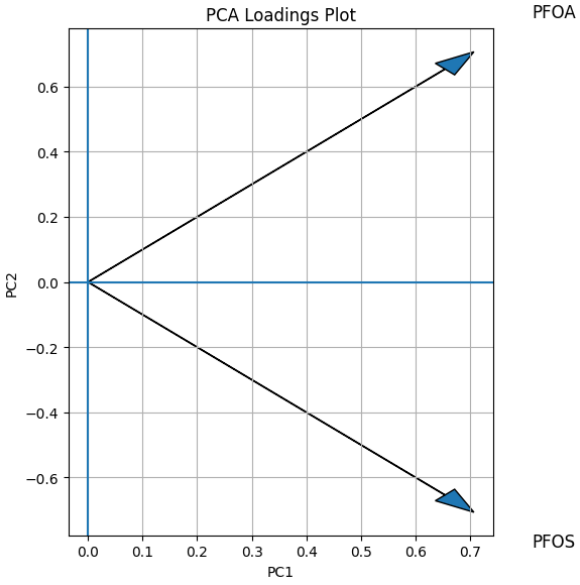


Figure 2. PCA Loadings Plot.

PFOS and PFOA exhibit strong positive loadings along PC1, indicating high correlation and shared variability driven by concentration. The loadings plot shows that both PFOS and PFOA have strong positive contributions to PC1 and are aligned in a similar direction. This indicates a high degree of correlation between the two analytes, reflecting their shared response to changes in concentration levels. The symmetric orientation of the loadings suggests that both variables contribute comparably to the dominant component. From an analytical perspective, this result confirms that PFOS and PFOA behave consistently across the dataset, and that the primary source of variability is not analyte-specific but rather driven by experimental conditions common to both.

D. Assessment of Analyst Influence

The potential influence of analyst-dependent variability was evaluated using the PCA score plot colored by analyst identity (Figure 2).

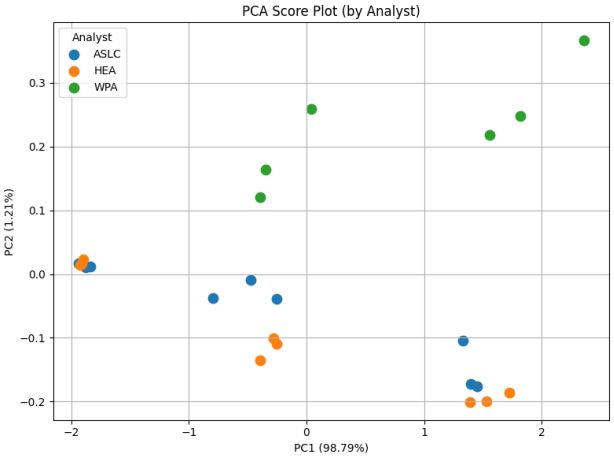


Figure 3. PCA Score Plot (Colored by Analyst). Concentration-based clustering remains dominant along PC1, while minor analyst-related separation is observed along PC2.

As shown in Figure 3, observations corresponding to different analysts remain distributed across the same concentration-based clusters along PC1, indicating that analyst identity does not substantially influence the dominant source of variability in the dataset. However, some separation associated with analyst WPA is observed along PC2, suggesting the presence of minor analyst-dependent effects within the residual variability. Since PC2 accounts for only 1.21% of the total variance, these operator-related differences are considerably smaller than the concentration-driven variability captured by PC1.

This finding suggests that the measurement process exhibits good intermediate precision, with consistent analytical performance across operators. The absence of systematic analyst clustering further supports the conclusion that the dataset is not significantly affected by operator bias.

E. Interpretation of Principal Components

The combined interpretation of Table 2 and Figures 1–3 provides a comprehensive understanding of the variability structure in the dataset. The overwhelming dominance of PC1, together with the clear clustering by concentration level, demonstrates that the variability is primarily governed by structured experimental factors rather than uncontrolled measurement effects.

The strong correlation between PFOS and PFOA further indicates that both analytes respond consistently to the same underlying conditions, reinforcing the robustness of the measurement system. Although concentration-driven variability dominates the dataset, minor analyst-dependent variation is observable along PC2. These secondary effects are relatively small compared with the dominant variability represented by PC1, indicating that operator-related variability contributes only modestly to the overall measurement structure. From a metrological perspective, these findings highlight the importance of distinguishing systematic variability associated with experimental design from potential measurement inconsistencies. The results demonstrate that PCA provides an effective framework for identifying dominant sources of variability and for supporting the interpretation of complex chemical measurement datasets.

V. CONCLUSIONS

This study applied Principal Component Analysis (PCA) to investigate the multivariate structure of PFOS and PFOA migration measurements obtained from multi-analyst replicate datasets. The results showed that the first principal component (PC1) accounted for 98.79% of the total variance, indicating that variability in the dataset is predominantly governed by a single dominant factor. Analysis of the PCA score plots confirmed that this dominant component corresponds to concentration level, with clear separation of low, medium, and high measurements along PC1.

The second principal component (PC2), which explained only 1.21% of the total variance, captured minor residual variability associated with secondary effects. While concentration-driven clustering remained dominant, slight analyst-related separation was observed along PC2, particularly for analyst WPA, suggesting the presence of minor operator-dependent variability. However, these effects were considerably smaller than the dominant concentration-driven variability represented by PC1. The strong alignment of PFOS and PFOA in the loading space further confirms that both analytes exhibit consistent behavior under the tested conditions.

From a measurement science perspective, these findings highlight the importance of distinguishing systematic variability arising from experimental design from secondary variability associated with measurement conditions. The results indicate that the observed variability in the dataset is largely structured and predictable, reflecting controlled changes in concentration rather than substantial instability in the measurement process.

In summary, this study demonstrates that PCA provides an effective and interpretable framework for analyzing variability in chemical migration datasets. By identifying dominant sources of variation and supporting improved interpretation of measurement behavior, PCA serves as a valuable complementary tool for laboratory quality assurance, metrological evaluation, and regulatory decision-making involving PFAS and other emerging contaminants.

REFERENCES

[1] M. A. Islam *et al.*, “Per- and polyfluoroalkyl substances (PFAS) contamination in agriculture

and its potential conflict with circular economy," *Environ. Pollut.*, vol. 385, p. 127036, 2025, doi: https://doi.org/10.1016/j.envpol.2025.127036.

[2] S. Y. Wee and A. Z. Aris, "Revisiting the 'forever chemicals', PFOA and PFOS exposure in drinking water," *npj Clean Water*, vol. 6, no. 1, p. 57, 2023, doi: 10.1038/s41545-023-00274-6.

[3] S. Y. Wee and A. Z. Aris, "Environmental impacts, exposure pathways, and health effects of PFOA and PFOS," *Ecotoxicol. Environ. Saf.*, vol. 267, p. 115663, 2023, doi: https://doi.org/10.1016/j.ecoenv.2023.115663.

[4] M. Chang *et al.*, "Perfluorooctane Sulfonate (PFOS) and Perfluorooctanoic Acid (PFOA) in the Surface Waters of China: A Meta-Analysis," *Water*, vol. 17, no. 9. p. 1275, 2025. doi: 10.3390/w17091275.

[5] R. Li *et al.*, "Per- and polyfluoroalkyl substances in food contact materials: Migration, health risks and sustainable alternatives," *Trends Food Sci. Technol.*, vol. 172, p. 105667, 2026, doi: https://doi.org/10.1016/j.tifs.2026.105667.

[6] A. Ramírez Carnero, A. Lestido-Cardama, P. Vazquez Loureiro, L. Barbosa-Pereira, A. Rodríguez Bernaldo de Quirós, and R. Sendón, "Presence of Perfluoroalkyl and Polyfluoroalkyl Substances (PFAS) in Food Contact Materials (FCM) and Its Migration to Food.," *Foods (Basel, Switzerland)*, vol. 10, no. 7, Jun. 2021, doi: 10.3390/foods10071443.

[7] E. P. on C. in the F. C. (EFSA C. Panel) *et al.*, "Risk to human health related to the presence of perfluoroalkyl substances in food," *EFSA J.*, vol. 18, no. 9, p. e06223, Sep. 2020, doi: https://doi.org/10.2903/j.efsa.2020.6223.

[8] D. W. Phelps, L. V. Parkinson, J. M. Boucher, J. Muncke, and B. Geueke, "Per- and Polyfluoroalkyl Substances in Food Packaging: Migration, Toxicity, and Management Strategies," *Environ. Sci. Technol.*, vol. 58, no. 13, 2024, doi: https://doi.org/10.1021/acs.est.3c03702.

[9] M. Surma, W. Wiczkowski, E. Cieślik, and H. Zieliński, "Method development for the determination of PFOA and PFOS in honey based on the dispersive Solid Phase Extraction (d-SPE) with micro-UHPLC–MS/MS system," *Microchem. J.*, vol. 121, pp. 150–156, 2015, doi: https://doi.org/10.1016/j.microc.2015.02.008.

[10] R. Loos *et al.*, "Analysis of perfluorooctanoate (PFOA) and other perfluorinated compounds (PFCs) in the River Po watershed in N-Italy," *Chemosphere*, vol. 71, no. 2, pp. 306–313, 2008, doi: https://doi.org/10.1016/j.chemosphere.2007.09.022.

[11] Tran Thi Lieu *et al.*, "Determination of perfluorooctanoic acid (PFOA) and perfluorooctane sulfonic acid (PFOS) in paper-based food packaging samples," *Vietnam J. Food Control*, vol. 5, no. 4, pp. 589–597, 2022, doi: https://doi.org/10.47866/2615-9252/vjfc.4006.

[12] H. Todorov, E. Searle-White, and S. Gerber, "Applying univariate vs. multivariate statistics to investigate therapeutic efficacy in (pre)clinical trials: A Monte Carlo simulation study on the example of a controlled preclinical neurotrauma trial.," *PLoS One*, vol. 15, no. 3, p. e0230798, 2020, doi: 10.1371/journal.pone.0230798.

[13] B. Percival, M. Gibson, J. Leenders, P. B. Wilson, and M. Grootveld, "Univariate and Multivariate Statistical Approaches to the Analysis and Interpretation of NMR-based Metabolomics Datasets of Increasing Complexity," in *Computational Techniques for Analytical Chemistry and Bioanalysis*, P. B. Wilson and M. Grootveld, Eds., The Royal Society of Chemistry, 2020, p. 0. doi: 10.1039/9781788015882-00001.

[14] I. T. Jolliffe and J. Cadima, "Principal component analysis: a review and recent developments.," *Philos. Trans. Ser. A, Math. Phys. Eng. Sci.*, vol. 374, no. 2065, p. 20150202, Apr. 2016, doi: 10.1098/rsta.2015.0202.

[15] T. Souza, "Principal Component Analysis (PCA) BT - Advanced Statistical Analysis for Soil Scientists," T. Souza, Ed., Cham: Springer Nature Switzerland, 2025, pp. 43–56. doi: 10.1007/978-3-031-88161-9_4.

[16] K. Kumar, "Principal component analysis: Most favourite tool in chemometrics," *Resonance*, vol. 22, no. 8, pp. 747–759, 2017, doi: 10.1007/s12045-017-0523-9.

[17] L. Shao, "Teaching Principal Component Analysis in the Course of Analytical Chemistry: A Q&A Based Heuristic Approach," *J. Chem. Educ.*, vol. 102, no. 1, pp. 155–163, 2025, doi: https://doi.org/10.1021/acs.jchemed.4c00818.

The Local Organizing Committee gratefully acknowledges the support of the below Conference Partners, Sponsors, and Exhibitors:

INSTITUTIONAL SUPPORT

SILVER SPONSOR

BRONZE SPONSORS

COPPER SPONSOR

EXHIBITORS

AD SPONSORS

CONFERENCE BAG SPONSOR

PHOTO WALL SPONSOR

BEST POSTER AWARD SPONSOR

This page is intentionally left blank.

IMEKO JOINT CONFERENCE
TC8-TC11-TC24
PHILIPPINES 2026

#imekomanila2026